CTSCo
Carbon Transport & Storage

A GLENCORE Company

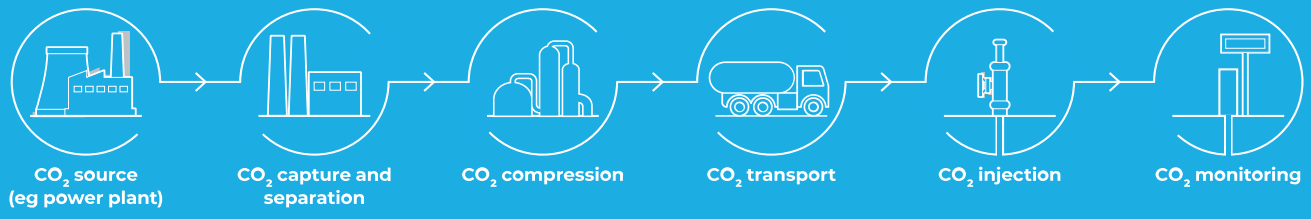

Surat Basin Carbon Capture and Storage Project

APPENDIX 9C: ANLEC PROJECT 7-0320-C323 FINAL REPORT, SOUTH SURAT METAL MOBILISATION AND FATE OF HEAVY METALS RELEASED

Table of contents

ANLEC Project 7-0320-C323 Final Report: South Surat metal mobilisation and fate of heavy metals released

Grant K. W. Dawson[1], Dirk M. Kirste[2], Julie K. Pearce[1,3], and Suzanne D. Golding[1]

[1]School of Earth and Environmental Sciences, University of Queensland, QLD 4072, Australia

[2] Department of Earth Sciences, Simon Fraser University, BC V5A 1S6, Canada

[3] Centre for Natural Gas, University of Queensland, QLD 4072, Australia

E-mail addresses: g.dawson@uq.edu.au (G.K.W. Dawson); s.golding1@uq.edu.au (S.D. Golding)

Submitted: 21 December 2022

Revised: 17 February 2023

ACKNOWLEDGEMENT

The authors wish to acknowledge financial assistance provided through Australian National Low Emissions Coal Research and Development. ANLEC R&D is supported by Low Emission Technology Australia (LETA) and the Australian Government through the Department of Industry, Science, Energy and Resources.

Part of this research was undertaken on the XFM beamline at the Australian Synchrotron, Victoria, Australia. Professor Gordon Southam and David Patterson are thanked for assistance with XFM data acquisition. The XFM work was supported by the Multi-modal Australian Science Imaging and Visualisation Environment (MASSIVE) (www.massive.org.au). We acknowledge travel funding provided by the International Synchrotron Access Program (ISAP) managed by the Australian Synchrotron and funded by the Australian Government.

The authors also acknowledge the facilities, and the scientific and technical assistance, of the Microscopy Australia Facility at the Centre for Microscopy and Microanalysis, The University of Queensland.

Executive Summary

ANLEC project 7-0320-C323 has undertaken an assessment of the trace metal content and potential for metal mobilisation from Precipice Sandstone and Moolayember Formation lithologies from the West Moonie 1 well in the southern Surat Basin to determine the likely groundwater impacts of greenhouse gas (GHG) stream injection into the Precipice Sandstone at the Carbon Storage and Transport Company's EPQ10 tenement. The southern Surat Basin is the preferred location for carbon storage trials as the Precipice Sandstone is deeper (>2000 m) and has higher salinity groundwater than in the northern Surat Basin. The project has combined geochemical reaction path and reaction transport modelling with mineralogical, geochemical and petrophysical analysis and laboratory batch reactor experiments of selected core samples and rock typing chips from the West Moonie 1 well in the EPQ10 tenement.

Whole-rock digestion ICP-OES and ICP-MS was used to determine the total major, minor and trace element content of Precipice Sandstone and Moolayember Formation samples from the West Moonie 1 well. These data provide a baseline for comparison with Precipice Sandstone and Moolayember Formation samples from the northern Surat Basin (former EPQ7) and help to determine the relative significance of element mobilisation during sequential extraction experiments. A three-stage sequential extraction process was used to investigate mineral-element associations and likely elemental behaviour under carbon storage conditions. Step 1 (pure water) extracted salts and weakly adsorbed elements. Step 2 (dilute acetic acid buffered at pH 5) extracted mostly calcite and ferroan carbonates, and strongly adsorbed elements. Step 3 (dilute acetic acid buffered at pH 3) extracted the remaining ferroan carbonates and acid-reactive silicates and sulfides. The sequential extractions also helped to constrain the types, quantity, and trace element content of carbonate minerals likely present but not necessarily detected by conventional means such as XRD. Based upon both absolute amounts and proportions that were acid-extracted, the elements that should be most closely monitored in lower Precipice Sandstone groundwater at EPQ10 include As, Co, Cu, Ni, Pb and Sb. Absolute amounts of the trace or ultra-trace elements Cd, P and S extracted from West Moonie 1 lower Precipice Sandstone are higher compared with the other sites investigated in the Surat Basin including EPQ7, but the absolute amounts of others are either lower (e.g., As, Co, Cu, Ni and Zn) or similar (e.g., Pb and Sb).

Completed batch reactions on twelve West Moonie 1 well core samples from the lower Precipice Sandstone and Moolayember Formation with a mixed gas stream, and four core samples with pure CO_2 are reported. In mixed gas experiments dissolved elements such as Ca, Mg, Mn, Sr, and Ba increased from reaction of trace amounts of carbonates in upper Precipice Sandstone samples and one Moolayember Formation sample, with stabilising trends in other experiments. The elements Fe, Pb, Mo, Cr, Se increased and subsequently decreased in concentration over time indicating subsequent adsorption or precipitation processes in the majority of experiments. Trace elements including Cr, As and Pb, however, increased over time from two lower Precipice Sandstone samples and a Moolayember Formation sample. Overall, the concentrations of As and Pb at the end of mixed gas experiments were below 30 µg/kg as the water to rock ratio in the batch reactor experiments was high. Nevertheless, these As concentrations were lower than those measured in experiments with West Wandoan 1 (EPQ7) lower Precipice Sandstone cores.

Reaction path modelling shows that carbonate minerals, chlorite and some K-feldspar are the main minerals reacting in the batch reactor experiments. In most cases the carbonate and chlorite mineral content was below detection of the XRD. The presence of O_2 in the mixed gas experiments and rapid Fe mobilisation from dissolution of siderite and chlorite results in the precipitation of $Fe(OH)_3$ and $Al(OH)_3$. The experiments and modelling were supported by sequential extraction, XRD, SEM-EDS and micro-XRF data to generate the mixed composition carbonates that would, on dissolution, mobilise trace elements and also establish some information on exchange/adsorption site content and occupancy. The reactions mobilised major, minor and trace elements and the rate of mobilisation and the mineral sources and sinks were incorporated into the geochemical models. The Fe oxyhydroxides act as a sink for Fe and deplete the O_2 content as well as providing new adsorption sites for sequestering some proportion of the trace metals mobilised through mineral dissolution and desorbed from or exchanged with the mineral $Fe(OH)_3$ as the fluid chemistry evolves.

Based on the well logs and examination of the core, 20 hydrostatic units (HSU) were identified that included 18 lower Precipice Sandstone HSU and 1 each for the Moolayember Formation and the upper Precipice Sandstone. Radial and 4 3D reactive transport models were generated that were populated by physical and chemical data obtained for the HSU. Injection over 3 years of a total of 330,000 tonnes of pure CO_2 and CO_2 with 400ppm O_2, 15 ppm NO and 5 ppm SO_2 was simulated in two different injection scenarios. The modelling used 2 different gridding methods, a radial and a 3-dimensional polygonal grid. The radial models are not able to represent stratigraphic structure that is dipping but require fewer cells and are thus less computationally demanding. The 3D models allow the incorporation of structural features including the topography of surfaces and regional dip or depth variations that can play an important role in the dynamics of multiphase and density dependent flow and transport. It was determined from the preliminary radial modelling that there was limited interaction between the lower Precipice Sandstone reservoir and both the underlying Moolayember Formation and the overlying upper Precipice Sandstone due to their very low permeabilities, so these were not included in the final models. In addition, the 3D model run was terminated at just over 10 years simulation time, but this was sufficient to show that a larger domain was required for the EPQ10 site.

Supercritical CO_2 migration was dominated by buoyancy, moving upward until encountering lower permeability HSU at which point lateral migration dominated. The trace gases SO_2, NO and O_2 were sequentially stripped out of the migrating supercritical CO_2 based on the trace gas solubility in the formation water. The migration of O_2 was considerably more extensive and contributed to the oxidation of Fe and precipitation of $Fe(OH)_3$. The primary pH control in and adjacent to the migrating supercritical CO_2 was the CO_2 content of the formation water. Dissolution of CO_2 into the formation water also led to increases in the formation water density and the onset of density driven convection. The low pH drove mineral dissolution reactions including carbonate mineral, chlorite, and K-feldspar dissolution. In the volume where O_2 migrated, dissolution of siderite and chlorite released Fe and precipitation of $Fe(OH)_3$ occurred. That precipitation maintained undersaturation with respect to siderite, so dissolution continued. Where O_2 was depleted within the volume where CO_2 migrated, siderite dissolution was very minor and saturation with respect to the carbonate mineral resulted in little to no dissolution. This had important implications for the mobilising of trace elements. The primary mechanism of trace element mobilisation was from carbonate mineral dissolution that led to elevated trace element concentrations; however, once the O_2 was depleted and, in any CO_2 impacted formation water where O_2 had not migrated, this mechanism no longer operated sufficiently to cause elevated trace element concentrations. The mobility of As, however, followed a different pattern. The low pH of the CO_2 impacted water caused As desorption from sites dominant in neutral pH, which resulted in an increase in As concentrations. Where the O_2 migrated, As was mobilised also from carbonate mineral dissolution; however, the newly formed $Fe(OH)_3$ provided additional adsorption capacity and the As, along with a proportion of the other trace elements was adsorbed. The As concentrations were very low (< 10 ppb); however, the concentrations of the other trace elements, Pb, Ba, Cd, Co, Cu, Mn, Ni, Sr and Zn, remained elevated but not as high as those observed in the experiments. This is mostly because modelled low (and finite) O_2 availability ultimately limits dissolution of siderite (a major host of trace elements), and many dissolved elements progressively get taken out of solution via adsorption over time.

The onset of density driven convection at approximately 8 years in the radial models resulted in increased dissolution of supercritical CO_2, as formation water with low CO_2 content came into contact with migrated and residually trapped CO_2. In the volume where O_2 did not migrate with the supercritical CO_2, As was liberated from the existing adsorption sites as the dense formation water migrated, but few of the other trace elements showed increases in concentration. For CO_2 impacted formation water migrating from within the volume where O_2 had migrated, the concentrations of the other trace elements were high and As was low. This contrast led to differences in the concentration profiles of As versus the other trace elements. In all cases, the important factors that contributed to decreasing concentrations of the trace elements were depletion in the source volumes, adsorption and advective mixing.

The potential for groundwater monitoring locations in the lower Precipice Sandstone was investigated and it was determined monitoring of EC, pH, Fe, K, Mg, and total alkalinity in addition to minor and trace elements would make useful tools for identifying migration and processes occurring along the migration pathway.

Contents

Table of Figures

Index of Tables

1. Introduction

The Carbon Transport and Storage Company (CTSCo) previously explored the suitability of the former EPQ7 Greenhouse Gas (GHG) exploration tenement at the Glenhaven site in the northern Surat Basin for carbon storage but has switched focus to the southern Surat Basin because of the potential environmental impacts of injection of a greenhouse gas (GHG) stream on the low salinity groundwater of EPQ7. The southern Surat Basin is generally distinguished here as being south of the town of Miles (Figure 1). The EPQ10 exploration tenement in the southern Surat Basin is the preferred location for carbon storage trials because the target storage reservoir, the Precipice Sandstone, is deeper (>2000 m) and has higher salinity groundwater than in the northern Surat Basin. The mineralogy, geochemistry and groundwater chemistry of the Evergreen Formation, Precipice Sandstone and Moolayember Formation are not well constrained in the southern Surat Basin, despite an improved understanding of the reservoir potential and regional hydrogeology arising from the Surat Deep Aquifer Appraisal Project (UQ-SDAAP) (Garnett et al., 2019; Pearce et al., 2019a) and the recent ANLEC R&D Project 7-0918-C316 Regional Hydrogeology of the Southern Surat Basin (Hofmann et al., 2021; Rodger et al., 2020), respectively. The sources, identities and fate of heavy metals and metalloids likely to be released through GHG stream-water-rock reactions at EPQ10 are largely unknown and should be understood to provide baseline data and allow an assessment of the potential groundwater geochemistry impacts of CO_2 storage in the southern Surat Basin.

Previous work on core from the northern Surat Basin has shown that trace metals mobilised through dissolution of carbonates and sulfides will later co-precipitate with carbonates and Fe oxides/oxyhydroxides, are adsorbed to Fe oxide/oxyhydroxide surfaces, or remain within the extent of the subsurface GHG plume (Dawson et al., 2019, 2020, 2021; Golding et al., 2019). Radial and 3D reactive transport modelling of the EPQ7 Glenhaven site also showed that trace metal mobilisation is largely limited to the mobile component of the CO_2 impacted volume and is dominated by density driven convection that is directed towards the bottom of the storage formation (Dawson et al., 2021). This results in the accumulation of trace elements in the dense fluid collecting at the bottom of the reservoir and a decrease in their content in the CO_2 impacted volume as time progresses and the sources become depleted. Therefore, the lateral and vertical extent of potentially elevated heavy metal concentration in Precipice Sandstone groundwater should not exceed the extent of the injected GHG plume. Nevertheless, site specific information for the southern Surat Basin EPQ10 tenement regarding the impact of GHG stream injection on reservoir and seal minerals and the processes that control trace element behaviour is essential to predict the likely changes to Precipice Sandstone groundwater geochemistry because of GHG stream-water-rock reactions.

The current ANLEC project 7-0320-C323 has undertaken an assessment of the trace metal content and reactivity of Precipice Sandstone, and Moolayember Formation lithologies from the West Moonie 1 well drilled by CTSCo using whole rock geochemistry, sequential extraction procedures and batch reactor experiments with a mixed gas (CO_2-SO_2-NO-O_2) and pure CO_2 under simulated *in situ* conditions. This was coupled with mineralogical analysis using X-ray diffraction (XRD) and scanning electron microscopy with energy dispersive spectroscopy spot and map analyses (SEM-EDS and MLA) to identify trace-metal bearing phases and the concentration range of labile metals present in these phases. Geochemical reaction path and reactive transport modelling have been used to predict the plume migration and likely groundwater impacts of GHG stream injection into the Precipice Sandstone at EPQ10.

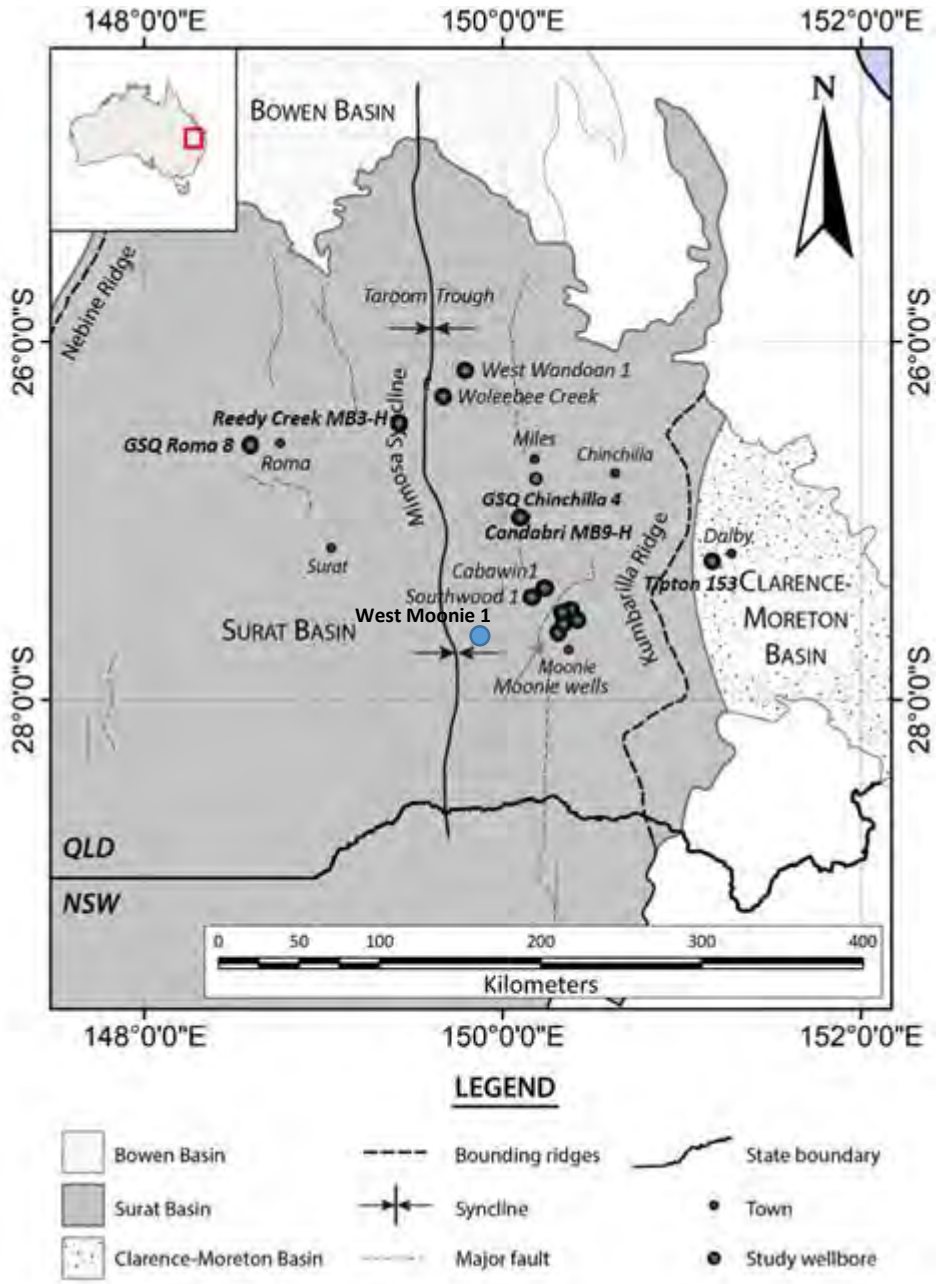

Figure 1: Map showing EQP10 West Moonie 1 (blue) and wells with core mineral characterisation data (green) modified from Pearce et al. (2019a). West Wandoan 1 is in the former EPQ7. Tipton 153 is likely in the Surat Basin given the appearance of the local stratigraphy; the exact boundary with the Clarence-Moreton Basin is uncertain, and likely gradational, near Dalby.

The CTSCo project has drilled two deep exploration wells in the EPQ10 tenement to evaluate the suitability of the tenement for GHG storage. The first well West Moonie 1 cored the entire Precipice Sandstone and parts of the underlying Moolayember Formation along with wireline logging evaluation of the reservoir-seal complex (Figure 2). We have used samples of core, as well as selected rock typing chips, from the Precipice Sandstone, lower Evergreen Formation, and Moolayember Formation from West Moonie 1 in the characterisation and rock reactivity experiments for this project. Some intervals of the Precipice Sandstone from this well, including the main baffle shale unit and part of the transition between the lower and upper Precipice Sandstone, were not made available to this project until near its end date. The second well, West Moonie 2, cored some 9 m of the uppermost Evergreen Formation primarily for rock mechanics testing of seal integrity (Figure 2).

This report summarizes the findings of ANLEC project 7-0320-C323 in respect to the whole rock geochemistry and chemical reactivity under low pH conditions in West Moonie 1. Reaction path modelling of the batch reactor experiments enabled determination of the carbonate mineral compositions and adsorption behaviour of the various hydrostratigraphic units that are essential inputs to the reaction transport models.

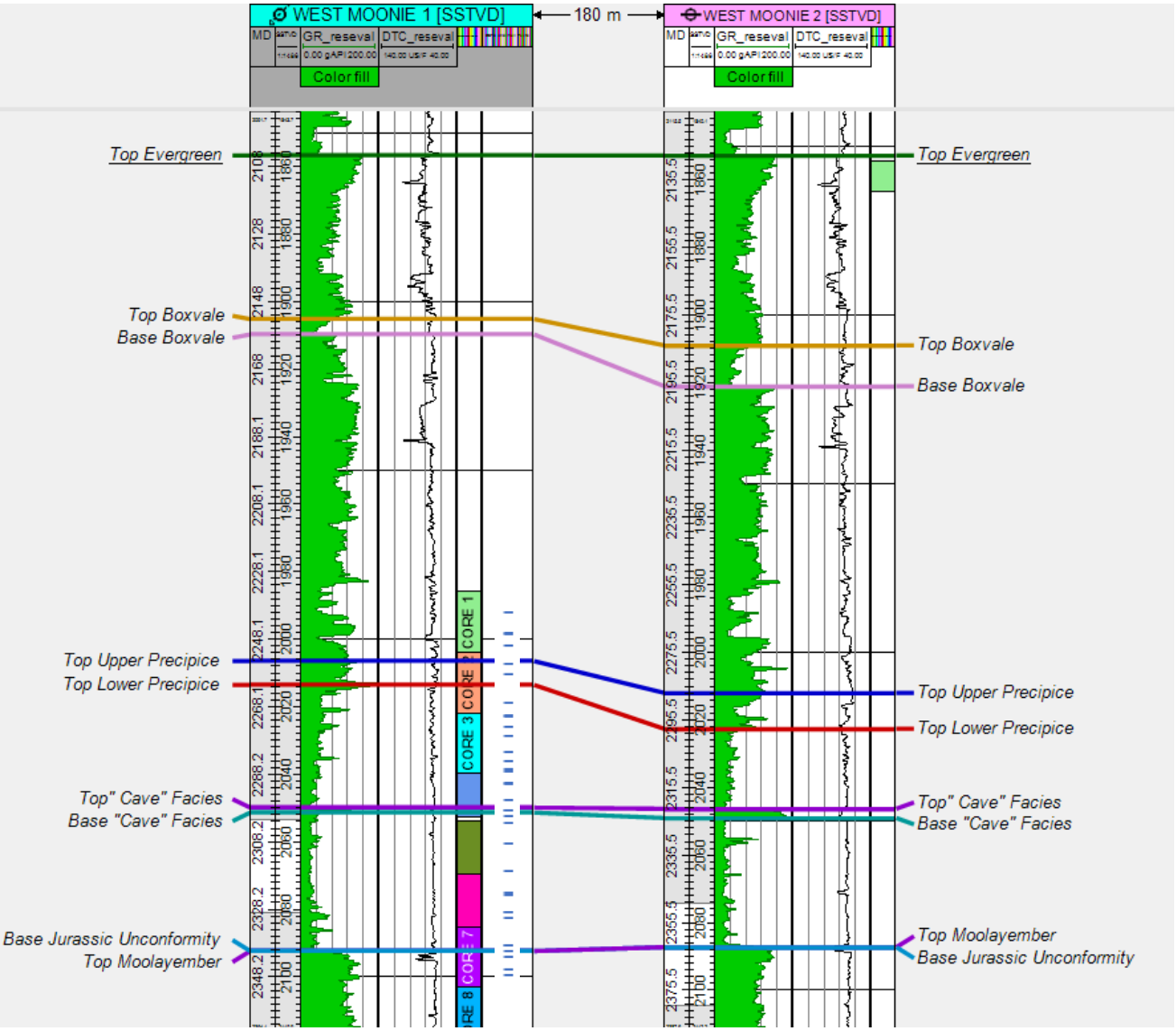

Figure 2: Well log for the recently drilled West Moonie 2 well compared to the West Moonie 1 well log. The cored intervals are shown as solid colour blocks on the right-hand side of the WM1 log, with the distribution of UQ core samples plotted (small blue dashes) just to the right of that. Image provided by CTSCo Pty Ltd.

2. Methods for rock analyses and experiments

2.1. Sampling strategy and preparation

This project focuses upon West Moonie 1 (WM1), the first well cored in the south Surat Basin EPQ10 tenement. We sampled cores and rock-typing chips from the reservoir-seal complex, i.e., the lower Evergreen Formation down to and including the top of the Moolayember Formation (Figure 3 and Table 1). The distinction between the 'upper Precipice Sandstone' and the base of the lower Evergreen Formation varies from well to well, as meandering river systems deposit either sandy or muddy sediments spatially. Regardless, the same major geological units (Table 1) present in wells sampled for previous ANLEC projects (e.g., 7-1115-0236 and 7-0919-0320) also occur in West Moonie 1, despite the distances between them. A "flow baffle" shale – lower Precipice Sandstone B – outcrops in Carnarvon Gorge (QLD) where it forms shallow caves and so is sometimes referred to as the "cave facies". The major geological units and subunits (upper Moolayember Formation, lower Precipice Sandstone A – D, upper Precipice Sandstone, and lower Evergreen Formation) were treated as discrete hydrostatic units (HSU # 0 – 6) during reactive transport modelling of previous studies. This was also the case for the rock characterisation and experimentation sections of this report, and initially for the reactive transport modelling as well; however, the most recent models split the rock package into 20 HSU to better represent the petrophysical and geochemical heterogeneity of the zone of interaction with CO_2.

Preparation of all samples for whole rock geochemistry and XRD was as follows:

1) Sample surfaces washed clean to remove visible drilling and cutting mud.
2) Depth-representative splits of samples cut for crushing. For core, this was an approx. 10 to 15 mm width of the entire core interval, preferably at least 5 mm from the outer core edge to reduce drilling-mud contamination; for chips, the split was as much material as could be spared.

Off-cuts were initially crushed to sand-size with agate wares that included a mortar and pestle (hand crushing) as well as a ring mill (< 30 seconds of operation at a time, to prevent over-crushing). For ten initial samples, a split of approximately 5 to 10 g of this material, crushed to pass through a 0.35 mm sieve, underwent both quantitative and clay-separates XRD analysis. Other samples have been assessed using semi-quantitative XRD analysis. The rest of the 'powder' underwent further crushing, with part then used for whole rock geochemistry; none of this material had been sieved or worked with metal crushers (comparisons with acid digests of the XRD splits showed 10 ppm copper contamination, among other elements, just due to hand-sieving).

Table 1: WM1 sampling intervals for this project.

Unit or Formation[1]		Core depth (mRT)	Brief description	Note
Lower Evergreen Formation		2235.81-2235.94	Fine- to medium-grained SANDSTONE with some micaceous laminations	
		2242.25	SILTSTONE with some laminations of fine-grained SANDSTONE	CTSCo core chip # 10
		2242.44-2242.54	Black muddy SILTSTONE with trace calcite	Batch reactor sample
		2245.63	Formation Boundary	Base of thick mudrock
Upper Precipice Sandstone		2246.14-2246.25	Medium- to coarse-grained SANDSTONE with some micaceous laminations	
		2251.71	Medium-grained SANDSTONE	CTSCo core chip # 20
		2254.94-2255.10	Fine- to medium-grained SANDSTONE with a black coal vitrain lens (4 mm)	Batch reactor sample from CTSCo core chip # 23 (2254.95 m)
		2263	Unit Boundary	Major lithological change
Lower Precipice Sandstone D		2263.61-2263.77	Weakly calcite cemented coarse- to very coarse-grained SANDSTONE with some pebbles	Batch reactor sample
		2267.71-2267.84	Interbedded micaceous black SILTSTONE and very fine- to fine-grained SANDSTONE	
		2267.84-2267.90	Fine-grained SANDSTONE with mud drapes	
		2268.26	Unit Boundary	Mudrock, then sandstone like below
Lower Precipice Sandstone C (switches from braided to meandering river)		2271.12	Pebbly very coarse-grained SANDSTONE	CTSCo core chip # 40
		2274.10-2274.18	Coarse- to very coarse-grained SANDSTONE with minor pebbles	Batch reactor sample. CTSCo core chip # 43 (2274.17 m)
		2278.90	Pebbly very coarse-grained SANDSTONE	CTSCo core chip # 48
		2281.82-2281.92	Medium- to coarse-grained SANDSTONE with some mica laminations	
		2284.13-2284.24	Medium- to very coarse-grained SANDSTONE with minor pebbles	Batch reactor sample from CTSCo core chip # 53 (2284.13 m)
		2285.05	Medium-grained SANDSTONE with some pebbles	CTSCo core chip # 54
		2288.49-2288.61	Medium- to very coarse-grained SANDSTONE	Batch reactor sample
		2288.90	Coarse-grained SANDSTONE	CTSCo core chip # 59
		2294	Weakly calcite cemented medium-grained SANDSTONE	CTSCo core chip # 65
		2296.97-2297.13	Poorly sorted medium to coarse-grained SANDSTONE, some mud drapes	
		2297.08	Unit Boundary	Major facies change
Lower Precipice Sandstone B (baffle carbonaceous sandstone with mudstone top)		2297.13-2297.19	Interlaminated micaceous black silty MUDSTONE and very fine-grained SANDSTONE	
		2298.92	Medium-grained SANDSTONE	CTSCo core chip # 70
		2299.45	Unit Boundary	Major facies change
Lower Precipice Sandstone A (braided river)	2	2301.09	Coarse-grained SANDSTONE	CTSCo core chip # 72
		2307.20	Medium- to coarse-grained SANDSTONE	Batch reactor sample from CTSCo core chip # 78 (2307.2 m)
		2315.77	Coarse-grained SANDSTONE	CTSCo core chip # 86
		2322.61-2322.73	Coarse- to very coarse-grained SANDSTONE	Batch reactor sample
		2323.25	Very coarse-grained SANDSTONE	CTSCo core chip # 93
		2328.54	Sub-unit Boundary	Defined in a related ANLEC project
	1	2328.54-2328.59	Grey micaceous SILTSTONE and very fine-grained SANDSTONE	Batch reactor sample
		2328.59-2328.68	White fine- to medium-grained SANDSTONE with micaceous laminations	
		2330.41-2330.55	Weakly calcite cemented fine- to coarse-grained SANDSTONE with some mica laminations	Batch reactor sample. CTSCo core chip # 99 (2330.55 m)
		2338.75-2338.85	Poorly sorted fine- to very coarse-grained SANDSTONE with pebble layers	
		2339	Triassic-Jurassic erosional unconformity and Formation Boundary	Seismic reflection boundary ~ 1.5 m deeper at thin coal and mudstone
Moolayember Formation		2339.00-2339.17	Fine- to medium-grained SANDSTONE with some coaly and micaceous layers	Batch reactor sample
		2340.54-2340.62	Black MUDSTONE with laminations of coalified seed ferns and trace calcite	
		2342.50	Siltstone with some very fine-grained SANDSTONE	CTSCo core chip # 112
		2346.40-2346.51	Weakly calcite cemented fine-grained SANDSTONE with some SILTSTONE interbeds and micaceous laminations	Batch reactor sample from CTSCo core chip # 116 (2346.5 m)
		2348.16-2348.30	Fine- to medium-grained SANDSTONE with pyrite nodules	
		2356.94-2357.06	Fine-grained SANDSTONE with some micaceous laminations	
		2359.90	Fine-grained SANDSTONE	CTSCo core chip # 130
		2362.90-2363.00	Black muddy SILTSTONE	
		2366.50-2366.61	Interlaminated fine-grained SANDSTONE and black muddy SILTSTONE	
		2367.41	SILTSTONE with some coal laminations	CTSCo core chip # 138
		2373.89-2373.99	Fine-grained SANDSTONE	
		2427.05	GRAINSTONE and very coarse-grained SANDSTONE	CTSCo core chip # 153
		2427.52-2427.74	Calcite cemented medium- to coarse-grained SANDSTONE with some pebbles and coal laminations	

1. The seven main units shown in this table were originally defined for the EPQ7 tenement in the northern Surat Basin in previous ANLEC projects 7-1115-0236 and 7-0919-0320.

2235.81-2235.94 m:

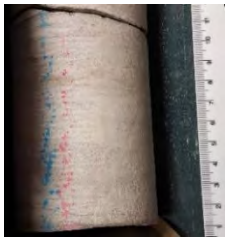

2242.44-2242.54 m:

2246.14-2246.25 m:

2254.94-2255.10 m:

2263.61-2263.77 m:

2267.71-2267.90 m:

2274.10-2274.18 m:

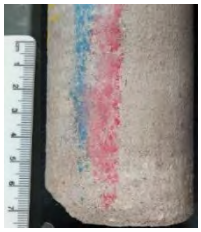

2281.82-2281.92 m:

2284.13-2284.24 m:

2288.49-2288.61 m:

2296.97-2297.19 m:

2297.40-2297.58 m:

2307.08-2307.20 m:

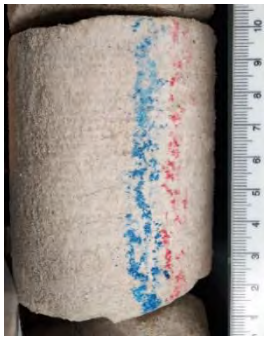

2322.61-2322.73 m:

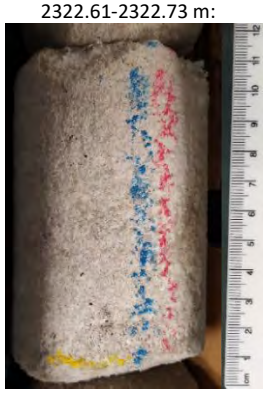

2328.54-2328.68 m:

2330.41-2330.55 m:

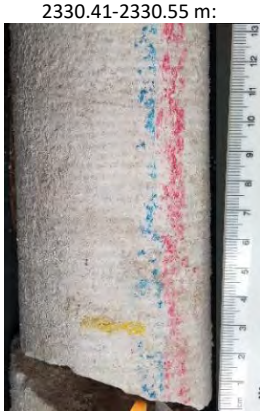

2338.75-2338.85 m:

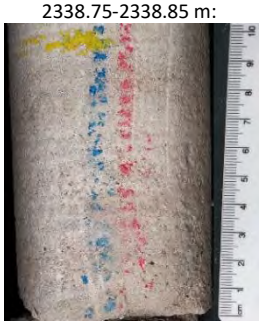

2339.00-2339.17 m:

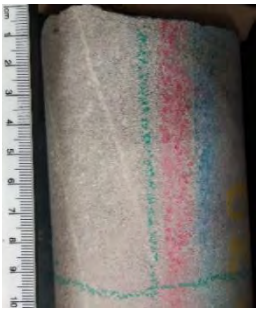

2340.54-2340.62 m:

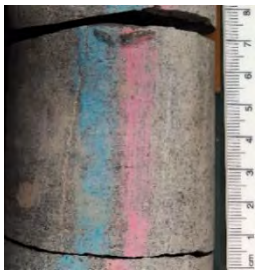

2346.40-2346.51 m:

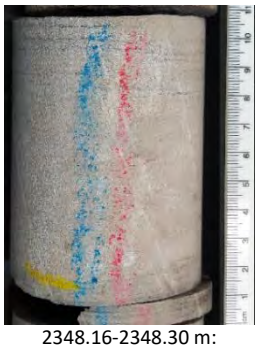

2348.16-2348.30 m:

2356.94-2357.06 m:

2362.90-2363.00 m:

2366.50-2366.61 m:

2373.89-2373.99 m:

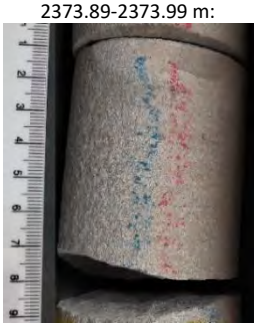

2427.52-2427.74 m:

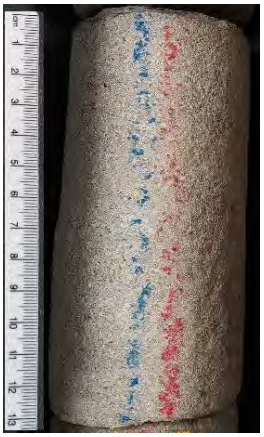

Figure 3: WM1 core samples.

2.2. Analytical methods

2.2.1. Whole-rock geochemistry procedures summary

Standard gravimetric analytical techniques (high precision ICP-OES and ICP-MS) were utilised at UQ to obtain concentration data for fifty-nine elements (including REE) within the rock samples. Rock powders have been prepared via clean crushing techniques using agate instead of metal tools to limit contamination and reduce element concentration backgrounds. Lithium metaborate fusion acid digest ICP-OES, coupled with weighing powdered rock samples before and after both oven drying and furnace ignition (Loss on Ignition - LOI), determined major elements content of the samples. A Teflon beaker acid digestion ICP-OES and ICP-MS method was used to determine minor and trace elements. Whole rock concentrations of the non-metals sulfur, phosphorous, selenium, and the metalloid boron may have greater analytical uncertainty (> 5 %) than other reported elements, due to factors such as ionisation energy, volatility, and mass/spectral interferences.

2.2.2. Sequential extraction procedure

There are three major steps in the procedure utilised for this study:

1) Water soluble, weakly adsorbed and exchangeable fractions:

Pure water with 0.01 mol/l ammonium acetate (near-neutral pH)

2) Strongly adsorbed elements and those bound to species that will dissolve at pH 5:

1 mol/l acetic acid buffered with ammonium-acetate at pH 5

3) Fraction that will easily dissolve at pH 3:

1 mol/l acetic acid buffered with ammonium-acetate at pH 3

We have generally followed the overall methodology of the modified (European) Community Bureau of Reference (BCR) Procedure in terms of sample powder mass, fluid volumes, fluid-rock ratios, reaction times, tube rotation rates, laboratory temperature, inter-step cleaning procedures, and use of acetic acid (a weak-acid like the carbonic acid produced by CO_2 dissolution in water) instead of a more aggressive strong-acid like HCl (e.g., Pueyo et al., 2008). Experiments sequentially extracting elements from 1 g of powder of each chosen sample took place in acid-cleaned 50 ml falcon tubes. Other complementary analyses such as whole rock geochemistry and XRD used the same powders, enabling direct comparison of the sequential extraction fluid chemistry results with the original element concentrations within the rock samples. Each of the extraction steps utilised generally the same methodology with only the extraction solution varying.

Each tube (plus powder) had approximately 40 ml of extraction solution added to it, with capped tubes then wrapped tightly with paraffin film to limit the potential for leakage during experiments. Tubes were rotated end-over-end at 30 rpm for 16 hours. Then tubes sat in a rack for a few minutes after rotation, prior to gentle internal washing and tapping to remove fine solids stuck to the sides or the inside of the lid. Centrifugation at 4000 rpm for 40 minutes further settled the fines. Clean 5 ml pipette tips were then used to carefully remove all but the last half-millilitre (or so) of fluid from each tube, stored in clean falcon tubes. Subsamples of this fluid were syringe filtered (0.11 µm) prior to analyses. Washing of the sample powders within tubes with 20 ml of pure water took place between each sequential extraction step, with this being discarded via pipetting following centrifugation.

Each weak-acid step has the same concentration, but different amounts of buffer to produce stable pH conditions that are less (pH 5) and more (pH 3) acidic. This is analogous to different concentrations of CO_2 producing variable pH conditions in groundwater. For the acid steps, it was necessary to first spend about 30 minutes manually agitating open tubes containing significant amounts of calcium carbonate minerals, to

limit build-up of gas produced by reactions that can cause sealed tubes to burst while being rotated end-over-end.

2.2.3. Batch reaction experiments

Batch experiments were performed using unstirred Parr® reactors with custom built thermoplastic vessel liners, sample holders and a dip tube assembly to avoid corrosion (Figure 4 and Pearce et al., 2015). Pressure and temperature of the vessels were monitored, with control and safety shutoff systems incorporated through a dedicated LabVIEW program. Vessels were maintained at 80 ± 1 °C with heating jackets and thermostats, and the vessel pressure monitored with pressure transducers. A fully contained pressurisation system utilised a Teledyne ISCO syringe pump (500HP) with vessel pressure at 20 MPa (3000 psi) to approximately replicate *in situ* conditions of the Precipice Sandstone-Moolayember Formation interface at the EPQ10 site in the Surat Basin.

The batch experiments use sister samples of intact rock instead of the powders used in the sequential extractions, and are targeted to examine specific lithologies, textures, and mineralogies. For a given reacted interval, SEM-EDS is performed on a surface of one sister sample, and directional permeability measurements obtained for another (approx. cubic) sample before and after experiments. Total dry rock mass is recorded before and after experiments. Fluid samples are taken incrementally during reactions. The data are then history-matched with modelling software to determine likely reactive surface areas of minerals and the specific mineral chemistries that appear to have reacted. This helps explain specific experimental results and provide input data for reactive transport modelling.

In the sets of experiments with CO_2-SO_2-NO-O_2 gas, rock core sub-sections (Table 2) were immersed in 125 ml of low salinity water approximating a simplified composition of Precipice Sandstone groundwater at the EQ10 site provided by CTSCo (632 mg/l Na, 11 mg/l Ca and K, 8 mg/l Fe, 7 mg/l Mg, 887 mg/l HCO_3^-, 325 mg/l Cl^-, 47 mg/l CO_3^{2-}, 14 mg/l SO_4^{2-}, and an initial pH of ~ 8.7). Reactor vessels were purged of residual air with a low pressure N_2 flush. They were subsequently pressurised to 20 ± 0.5 MPa, initially with N_2 gas at a temperature of 80 °C. A baseline water – rock reaction period with the inert N_2 gas was performed during which water samples were obtained to determine if any elements were released. The N_2 gas was subsequently replaced with a gas mixture of approximately 2 ppm SO_2, 11 ppm NO_x and 135 ppm O_2 in a balance of CO_2 using the syringe pump to achieve a pressure of 20 MPa. The water was periodically sampled (~ 5 ml) at in-situ temperature and pressure. Experiment lengths were generally about 3 months each, with exact timing depending on operational constraints. After terminating the experiment and depressurising, water was again sampled. Rock samples were oven dried for analyses. In addition, four experiments were performed on selected upper and lower Precipice Sandstone samples with pure CO_2 (instead of a mixed gas stream) to provide input data for the modelling (Table 2). These experiments were shorter in duration but more frequently sampled initially, to help characterize mineral reaction behaviour prior to onset of other processes such as adsorption and precipitation.

Solution pH and conductivity of sampled water was measured immediately *ex situ* with a TPS WP81 meter and probes. Water aliquots were diluted and acidified with pure HNO_3 for analyses. An ICP-OES (Perkin Elmer Optima 3300 DV ICP-OES) with an uncertainty of +/- 5 % was used to measure major elemental concentrations of aqueous species, particularly silicon, sulfur, and phosphorous that are not quantifiable using ICP-MS. Minor and trace element concentrations were measured by ICP-MS (Agilent 7900 ICP-MS with collision cell) with uncertainty of less than 5 %.

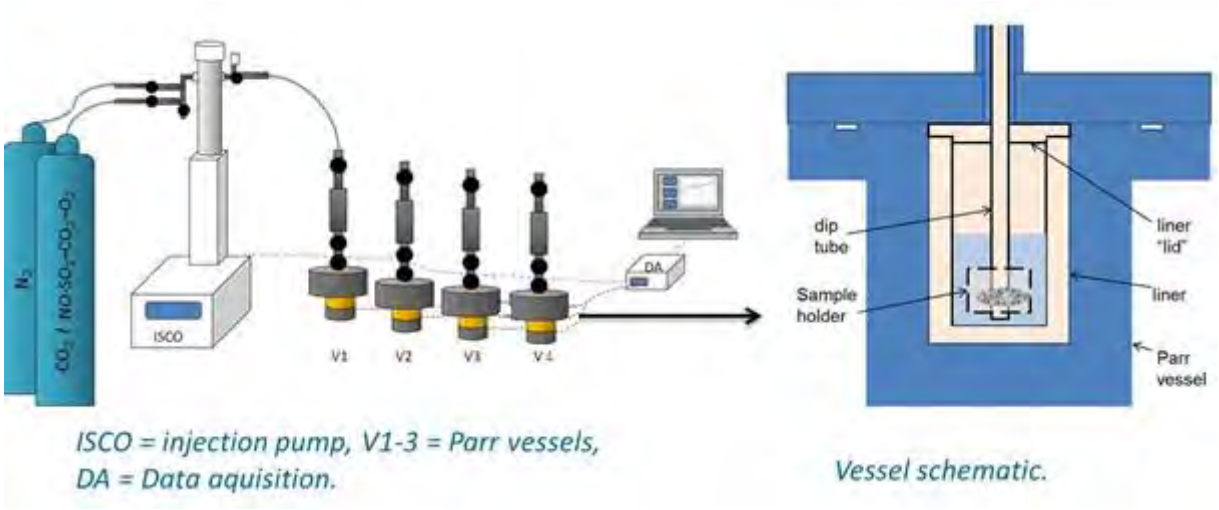

Figure 4: Schematic of the batch reactor system and the internal cross section of a Parr reactor.

Table 2: Batch reactor experimental samples reacted with mixed gas or pure CO_2.

Unit	Depth (mRT)	Brief description	Batch #	Mixed gas	Pure CO_2
Lower Evergreen Formation	2242.44-2242.54	Black muddy SILTSTONE	2	X	
Upper Precipice Sandstone	2254.94-2255.10	Fine- to medium-grained SANDSTONE with a black coal vitrain lens (4 mm)	1, 4	X	X
Lower Precipice Sandstone D	2263.61-2263.77	Coarse to very coarse sandstone with some pebbles	3, 4		X
Lower Precipice Sandstone C	2274.10-2274.18	Coarse to very coarse sandstone with minor pebbles	3	X	
	2284.13-2284.24	Medium- to very coarse-grained SANDSTONE with minor pebbles	1	X	X
	2288.49-2288.61	Calcite cemented medium- to very coarse-grained SANDSTONE	2, 4	X	
Lower Precipice Sandstone A	2307.20	Medium- to coarse-grained SANDSTONE	1, 4	X	X
	2328.54-2328.59	White fine- to medium-grained SANDSTONE with micaceous laminations	3	X	
	2322.61-2322.73	Coarse to very coarse sandstone	3	X	
	2330.41-2330.55	Calcite cemented fine- to coarse-grained SANDSTONE with some mica laminations	2	X	
Moolayember Formation	2339.00-2339.17	Fine- to medium-grained SANDSTONE with some coaly and micaceous layers	2	X	
	2346.40-2346.51	Fine-grained SANDSTONE with some SILTSTONE interbeds and micaceous laminations	1	X	

2.2.4. Mineral characterisation

A wide range of rock samples were characterised by X-ray diffraction (XRD) to determine major and minor minerals present. Batch reacted intervals also had mineralogy estimated by automated scanning Mineral Liberation Analysis (MLA), supplemental SEM-EDS surveys, and specialist clay separates XRD analysis (e.g., to discriminate between different clay phases).

2.2.5. Directional permeability analyses

A custom-built low pressure permeameter (Figure 5) at UQ was used to measure sample permeability, using the method of Dawson et al. (2015). Analysis of cubic samples enabled directional assessment of permeability, as the cubes were cut parallel to sedimentary bedding orientation, with two permeability measurements made along the bedding plane and one perpendicular to bedding (Figure 6). The apparatus can take up to 40 mm diameter samples, but the current experiments used 15 mm cubes required for the subsequent experiments with the batch reactor apparatus.

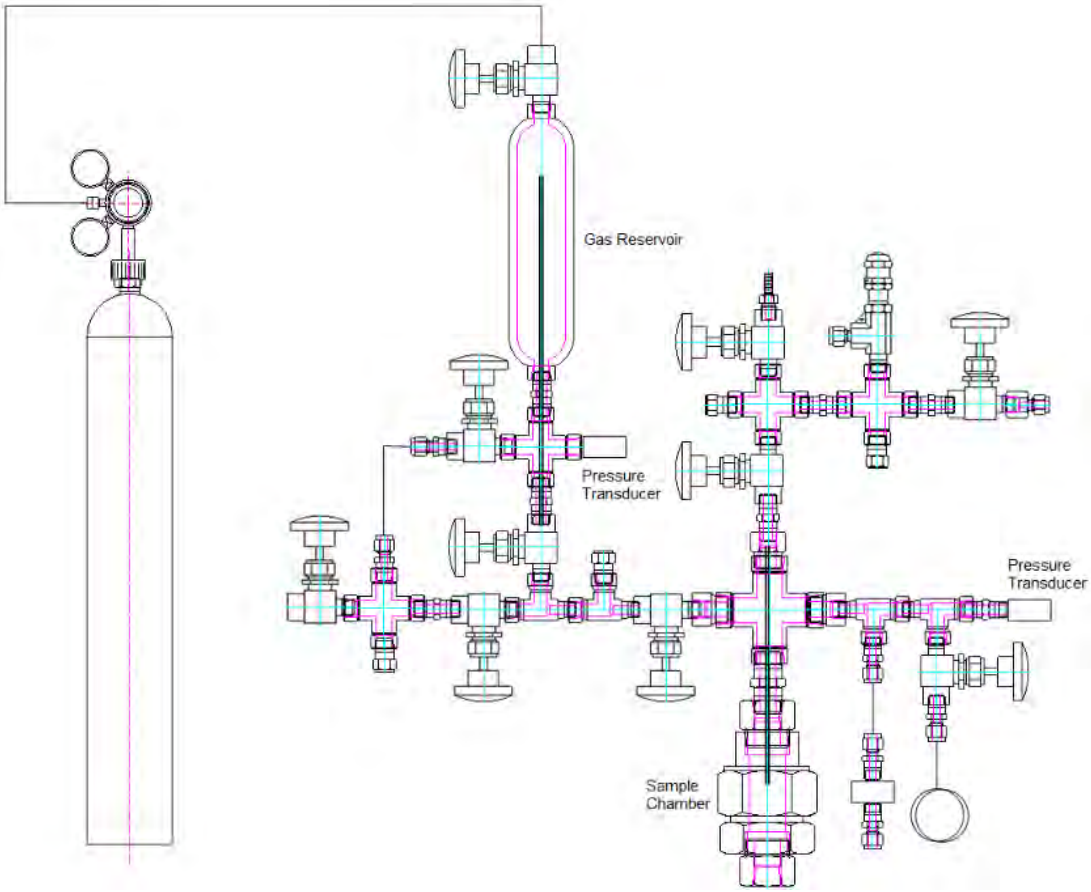

Figure 5: Low pressure permeameter (drawing not to scale).

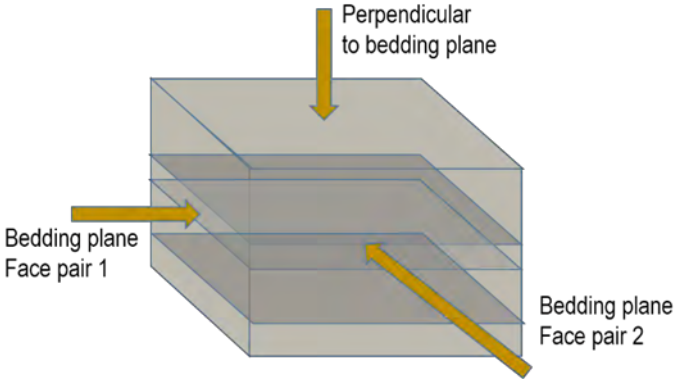

Figure 6: Directional permeability of a sedimentary rock.

3. Analytical and experimental results and discussion

3.1. Whole-rock geochemistry

Powdered rock sample elemental concentrations determined via acid digestion are shown in Table 3. Elements have been classified as major (> 1,000 mg/kg), minor (100 – 1,000 mg/kg), trace (10 – 100 mg/kg), and ultra-trace (< 10 mg/kg) based on median concentrations in West Moonie 1 (WM1) whole-rock assays. Chemically similar elements are grouped together in the tables, in accordance with the sets and groups of the periodic table. There is a table of element names and symbols in Appendix A, as well as individual rare earth element (REE) concentration data for the WM1 rock samples. Median element concentrations of West Moonie 1 (WM1) units are compared with our previous work (Dawson et al., 2019; Golding et al., 2019) involving sets of samples from other Surat Basin well cores; West Wandoan 1 (WW1), Woleebee Creek GW4 (WCG4), Chinchilla 4 (C4), and Tipton 153 (Tip153).

The siderite-associated elements Fe, Mg, and Mn have similar to slightly higher median concentrations in the lower Precipice Sandstone at both WM1 and the collective other locations. However, they are lower in both the WM1 upper Precipice Sandstone and the Moolayember Formation. Calcite-associated Ca median concentration is also consistently lower in WM1 units, as are Ni and Se. The WM1 Moolayember Formation may have less carbonate cement overall, based on our core results, or less carbonate veining and occurrence of siderite bands than in the other localities. The WM1 upper Precipice Sandstone samples may also be less carbonate cemented than elsewhere. However, some caution needs to be applied to comparisons of upper Precipice Sandstone samples from the various localities though, given that these are very small sample sets compared with those from the other units.

The WM1 lower Precipice Sandstone Al, Ba, Bi, Cd, P, W, and alkali metals median concentrations are significantly higher (>2x) than those of the collective other locations. The elements Be, Cr, Fe, Ga, Nb, Pb, Sc, Sr, V, and Y also have somewhat elevated medians (1.5x – 2x) too. Whereas Ca, Co, Cu, Ni, S, Sn, and Se are lower (<0.7x) and the rest of the element medians are similar. WM1 median Moolayember Formation Be, Cd, Sb, Sn, and Ta are significantly higher (>2x) than for other locations, whereas K is the only significantly elevated element in WM1 upper Precipice Sandstone samples. The magnitude of the differences between study sites likely falls within expected stratigraphic and regional geological variation, including the effects of post-depositional events such as tectonic activity and hydrothermal fluid migration.

The occurrence of several elements in WM1 core samples appears to be broadly correlated with each other (Figure 7), and we are interpreting this as largely being due to broad lithological controls upon element occurrence. Some elements may be syn-depositional in origin whereas others may have been at least partly introduced later during fluid migration events. Most of the elements are likely hosted within various minerals, though some such as Tl may be adsorbed within samples. The largely siderite-hosted elements Ca, Fe, Mg, and Mn correlate well with each other but no other elements (Figure 8). The few elements that don't correlate well with others include Mo, Na, Sb, and P, suggesting that there may be multiple hosts of these elements within the samples.

Table 3: Whole rock acid digestion concentrations of elements within WM1 core samples (mg element per kg rock), with reference to median values of previous projects' samples from other wells[1].

		Element Set	Alkali metals					Alkaline earth metals					Lanth.	Actinoids		Transition metals																						Post transition metals								Metalloids					Nonmetals			Volatiles	
		Element Group	1					2					3	3		3	4		5		6		7	8	9	10	11		12		13					14		15	13	14			15		15	16						
Unit		Depth (mRT)	Li	Na	K	Rb	Cs	Be	Mg	Ca	Sr	Ba	REE	Th	U	Sc	Y	Ti	Zr	Hf	V	Nb	Ta	Cr	Mo	W	Mn	Fe	Co	Ni	Cu	Ag	Zn	Cd	Al	Ga	Tl	Sn	Pb	Bi	B	Si	Ge	As	Sb	P	S	Se	Ads.H_2O	LOI
Lower Evergreen Formation		2235.81-2235.94	30	609	10,212	49	2	1	987	220	39	202	170	18	3	11	18	9,427	189	6	92	40	4	75	0.8	5	39	4,311	14	26	24	0.09	68	0.6	59,727	16	0.3	4	21	0.2	21	379,296	1	3	0.5	123	136	0.6	5,579	38,122
		2242.25	49	1,007	25,098	145	17	3	2,298	387	82	434	320	24	7	25	51	11,501	394	11	163	54	5	131	2	9	28	6,703	13	21	44	0.2	110	1	104,851	36	0.9	10	41	0.8	58	307,059	3	9	0.8	180	652	2	8,521	69,674
		2242.44-2242.54	91	1,257	22,163	139	21	4	2,739	408	78	398	222	18	4	20	32	7,557	257	8	159	41	4	97	2	6	41	8,928	29	63	35	0.2	127	0.9	120,748	33	0.8	6	34	0.8	41	289,355	2	6	0.7	217	506	1	11,740	88,047
Upper Precipice Sandstone		2246.14-2246.25	16	613	10,453	46	1	0.5	368	165	31	203	48	4	1	3	7	1,045	48	2	25	6	0.7	14	0.5	1	23	2,329	5	7	5	0.04	30	0.1	36,855	8	0.3	2	13	0.06	7	410,482	0.4	4	0.4	38	322	0.2	2,264	17,827
		2251.71	37	1,226	26,919	95	2	2	1,511	1,330	86	546	229	15	3	16	27	5,901	166	5	112	16	0.3	46	2	1	141	10,658	39	37	15	0.1	115	0.7	97,115	27	0.7	3	29	0.2	13	326,802	2	6	0.5	452	639	1	9,449	59,055
		2254.94-2255.10	14	850	24,398	82	1	0.9	1,025	727	62	443	134	6	1	7	15	3,538	74	2	40	7	0.5	17	0.3	2	152	10,511	11	8	14	0.06	73	0.3	65,518	14	0.6	3	16	0.06	7	383,702	2	5	0.3	244	405	0.7	3,028	38,450
Lower Precipice Sandstone D		2263.61-2263.77	8	674	15,082	49	1	0.4	228	90	22	169	26	3	0.7	2	7	774	61	2	10	5	0.6	10	0.2	1	13	1,251	5	6	8	0.04	14	0.2	20,851	4	0.3	3	9	0.04	34	441,409	0.2	3	0.4	<DL	188	0.1	1,882	10,824
		2267.71-2267.84	84	972	19,596	117	18	7	1,402	402	77	386	199	19	5	16	34	6,024	204	6	112	31	3	56	3	7	24	5,456	40	81	20	0.2	108	0.6	107,918	30	0.7	7	34	1	23	300,952	3	5	0.7	211	510	0.9	13,029	93,145
		2267.84-2267.90	33	875	19,159	92	6	2	770	266	68	309	109	8	2	8	22	3,391	117	4	57	17	2	32	1	4	15	2,526	12	23	8	0.09	80	0.4	72,092	16	0.6	4	20	0.3	11	361,964	2	4	0.7	183	280	0.5	8,640	50,291
Lower Precipice Sandstone C		2271.12	8	660	14,656	56	2	0.4	221	163	21	155	24	2	0.6	1	5	460	28	1	11	3	0.3	9	0.1	0.6	14	1,088	2	4	2	0.03	16	0.1	22,863	5	0.3	1	7	0.05	48	417,283	0.3	1	0.3	<DL	106	0.2	659	12,516
		2274.10-2274.18	7	470	12,271	54	2	0.4	191	128	28	158	27	2	0.6	1	6	538	29	1	12	4	0.6	11	0.5	0.8	81	3,992	5	8	9	0.04	20	0.09	20,873	4	0.4	2	10	0.1	8	443,796	0.5	4	0.4	36	1,228	0.1	<DL	12,097
		2274.17	7	647	14,823	48	1	0.3	187	143	25	146	27	2	0.5	1	5	561	25	0.9	12	3	0.3	10	0.2	0.9	102	4,383	4	7	3	0.04	17	0.09	20,863	4	0.3	0.8	9	0.08	13	399,200	0.3	3	0.4	73	1,117	0.2	2,673	12,918
		2278.90	8	555	10,250	42	1	0.5	317	124	32	128	49	3	0.7	2	6	925	33	1	22	5	0.5	20	0.1	1	27	1,687	2	6	6	0.04	36	0.1	26,427	7	0.2	1	9	0.09	11	403,948	0.5	1	0.3	104	119	0.3	1,804	16,595
		2281.82-2281.92	23	642	15,206	77	4	2	718	154	52	233	139	10	3	9	35	3,788	165	5	65	19	2	53	0.9	4	10	2,335	13	20	15	0.09	54	0.5	58,635	15	0.5	3	15	0.2	31	389,852	1	4	0.6	100	328	0.6	2,713	33,721
		2284.13-2284.24	8	130	2,216	10	0.7	0.4	171	49	22	44	30	2	0.5	2	6	825	25	0.9	14	2	0.3	10	0.3	0.7	5	611	7	11	18	0.04	21	0.08	21,142	5	0.1	3	8	0.1	5	437,173	0.3	3	0.5	<DL	87	0.1	1,783	16,488
		2285.05	55	1,627	20,998	130	18	6	1,954	347	78	327	213	16	5.0	19	34	9,121	276	8	168	39	3	130	2	8	19	6,077	26	47	45	0.22	160	1	97,206	29	0.7	9	41	0.6	44	318,634	2	6	1	674	809	1	6,635	72,613
		2288.49-2288.61	9	89	1,980	11	0.7	0.4	219	61	14	35	32	3	0.8	2	5	865	34	1	12	6	0.8	12	0.1	1	5	732	2	7	7	0.03	9	0.1	21,050	5	0.07	2	8	0.1	28	417,651	0.2	0.9	0.2	33	79	0.1	1,422	16,121
		2288.90	9	527	2,910	12	0.7	0.6	234	83	17	39	42	3	0.8	2	5	912	37	1	12	5	0.5	14	0.3	0.8	6	843	7	22	9	0.05	14	0.2	20,275	5	0.08	3	12	0.2	10	421,552	0.3	1	0.3	284	176	0.2	1,574	15,740
		2294	4	379	3,173	4	0.2	0.2	106	119	25	47	91	9	1.7	2	8	3,636	151	4	11	14	0.1	11	0.3	3	2	495	1	5	3	0.1	8	0.5	5,170	3	0.07	2	9	0.04	15	414,855	0.8	1	0.2	<DL	171	0.5	<DL	6,993
		2296.97-2297.13	5	<DL	1,673	7	0.5	0.5	155	170	55	65	294	28	3	2	21	3,254	184	5	15	15	2	13	0.4	3	39	1,925	2	2	5	0.07	14	0.4	16,822	9	0.08	3	14	0.1	14	439,705	4	2	0.4	178	104	0.8	3,923	13,606
Lower Precipice Sandstone B		2297.13-2297.19	106	879	17,672	144	26	8	2,154	6,534	184	396	294	31	6	20	35	7,425	261	7	133	55	6	113	2	9	27	7,680	33	73	41	0.1	134	0.8	139,279	39	1	7	37	0.7	43	264,337	3	18	2	393	1,471	1	12,881	114,673
		2298.92	8	504	3,026	8	0.5	0.3	136	96	18	52	38	2	0.5	1	3	947	33	1	12	5	0.5	15	0.4	0.9	4	537	1	5	4	0.03	13	0.1	20,177	5	0.05	2	7	0.05	5	414,649	0.4	0.6	0.2	327	91	0.2	404	14,949
Lower Precipice Sandstone A		2301.09	5	657	3,556	3	0.2	0.2	112	286	12	36	32	2	0.5	0.8	3	312	46	1	5	1	0.2	4	0.3	0.8	9	635	0.8	3	6	0.04	11	0.2	9,025	2	0.03	2	4	0.06	6	464,156	0.3	0.6	0.1	339	96	0.1	2,606	7,818
		2307.20	3	329	2,931	4	0.2	0.2	108	144	11	44	29	2	0.5	0.8	3	572	35	1	5	3	0.3	4	0.2	0.7	28	1,334	1	3	22	0.03	11	0.1	5,063	2	0.03	1	5	0.03	8	438,348	0.3	0.6	0.2	<DL	70	0.2	6,272	4,480
	2	2315.77	3	317	2,287	2	0.2	0.1	171	158	10	48	20	1	0.3	0.4	1	288	21	0.7	3	1	0.1	2	0.1	0.3	7	440	0.6	2	1	0.02	4	0.07	3,885	1	0.01	0.3	3	0.02	5	438,910	0.2	0.6	0.1	<DL	91	0.06	393	6,282
		2322.61-2322.73	3	131	1,202	4	0.3	0.2	72	82	12	52	34	3	0.7	1	4	785	70	2	5	5	0.5	8	0.1	0.9	9	524	0.6	1	12	0.04	2	0.2	5,008	2	0.04	2	4	0.02	6	451,211	0.4	0.4	0.1	<DL	29	0.1	1,493	5,473
		2323.25	3	534	2,090	2	0.2	0.07	61	151	9	43	19	1	0.3	0.5	2	406	20	0.6	3	2	0.2	3	0.2	0.5	10	593	0.4	2	1	0.02	7	0.1	3,443	1	0.02	2	3	0.02	3	435,599	0.2	0.4	0.1	359	48	0.07	<DL	4,894
		2328.54-2328.59	88	934	17,996	136	22	6	2,037	315	125	374	279	35	7	19	35	8,544	364	12	113	64	7	97	0.8	13	20	6,854	22	43	42	0.2	28	1	138,030	40	0.7	7	31	0.6	54	277,540	3	4	0.8	281	365	0.9	5,501	87,459
		2328.59-2328.68	12	221	3,464	18	2	0.6	268	55	27	99	75	7	2	3	8	2,127	100	3	23	14	2	18	0.2	3	5	870	2	5	5	0.06	15	0.3	34,056	7	0.1	2	11	0.07	16	425,150	0.5	0.8	0.2	57	58	0.2	2,301	24,390
	1	2330.41-2330.54	3	630	957	4	0.3	0.2	54	51	10	66	21	2	0.5	0.9	3	681	34	1	5	4	0.5	4	0.05	0.7	3	266	1	2	22	0.02	3	0.1	6,297	2	0.03	3	5	0.02	7	440,082	0.1	0.4	0.1	24	47	0.07	900	6,751
		2330.55	4	288	1,863	5	0.3	0.2	88	81	12	74	23	2	0.5	1	3	783	27	0.8	7	4	0.3	5	0.1	0.7	3	339	0.9	3	1	0.03	7	0.1	6,946	2	0.03	0.6	5	0.03	6	458,759	0.2	0.6	0.2	<DL	60	0.1	2,237	4,922
		2338.75-2338.85	5	168	1,521	7	0.5	0.4	126	45	17	49	43	3	0.6	1	4	1,003	34	1	12	5	0.7	10	0.1	1	3	436	1	3	11	0.02	8	0.1	11,671	4	0.07	2	6	0.09	6	440,591	0.4	0.7	0.2	352	39	0.1	<DL	8,929
Moolayember Formation		2339.00-2339.17	42	438	9,380	46	2	3	1,035	168	65	113	132	14	3	11	23	3,628	145	5	72	17	2	37	0.7	5	15	3,238	15	18	13	0.1	180	0.6	83,475	21	0.4	4	22	0.2	17	342,919	2	10	1	129	521	0.6	3,772	55,634
		2340.54-2340.62	47	944	21,902	126	17	2	3,380	612	56	327	143	14	3	17	27	4,486	141	5	102	18	2	47	0.4	4	184	18,672	19	26	32	0.2	96	0.6	92,677	21	0.6	7	24	0.5	28	315,292	1	6	0.7	739	278	0.7	8,422	70,479
		2342.5	50	1,974	28,567	151	7	3	3,521	844	79	557	188	14	4	13	29	4,474	173	5	94	16	2	48	0.7	4	160	15,319	7	14	25	0.2	101	0.7	88,295	23	0.7	6	24	0.5	21	315,141	2	7	1	492	219	1	9,878	52,211
		2346.40-2346.51	38	1,637	33,664	148	6	2	4,271	1,107	74	580	141	12	4	13	26	3,376	148	5	91	11	0.2	39	3	4	231	18,749	22	23	16	0.2	88	0.6	81,894	21	0.8	4	21	0.3	24	331,555	2	6	2	284	279	0.8	1,889	59,991
		2348.16-2348.30	18	1,381	28,002	105	3	1	4,131	2,516	77	465	114	10	2	7	18	2,887	102	3	47	11	1	23	6	3	651	41,935	12	18	8	0.2	51	0.7	53,947	13	0.9	6	14	0.1	16	341,227	1	43	2	854	10,842	0.7	5,315	61,304
		2356.94-2357.06	29	1,763	30,610	136	4	2	5,201	1,734	72	562	110	10	3	10	21	2,873	111	3	66	12	1	27	0.4	2	354	25,765	7	11	11	0.1	74	0.5	71,014	17	0.7	5	17	0.2	19	321,255	1	2	0.6	848	109	0.6	5,324	59,006
		2359.90	35	1,844	32,014	145	4	2	4,853	1,822	71	585	134	11	3	11	22	3,265	124	4	85	12	1	41	0.4	2	296	23,066	7	11	14	0.1	81	0.5	77,615	19	0.7	6	17	0.2	18	331,816	2	4	0.8	668	139	0.7	4,314	62,320
		2362.90-2363.00	87	1,763	29,038	162	19	3	6,509	791	79	553	162	14	4	15	29	3,860	136	4	99	14	1	38	0.6	4	281	25,479	12	18	23	0.2	95	0.6	86,774	23	0.8	4	28	0.6	32	308,228	2	3	1	130	128	1	10,209	55,925
		2366.50-2366.61	50	4,851	28,679	143	9	2	8,242	2,822	78	514	152	12	4	15	29	3,778	139	4	88	15	1	40	0.6	4	936	48,238	10	16	23	0.2	99	0.7	79,808	21	0.7	7	24	0.5	21	286,173	2	2	0.9	1,103	176	0.9	9,139	77,922
		2367.41	84	4,251	30,687	179	16	4	8,140	1,391	87	542	157	14	4	17	28	4,444	147	4	124	15	1	51	0.8	4	257	31,655	15	26	34	0.2	88	0.7	95,883	27	0.8	7	24	0.6	28	301,984	2	2	0.7	768	182	1	16,060	56,684
		2373.89-2373.99	22	8,040	31,577	139	4	1	5,234	2,663	63	546	99	9	2	9	17	2,329	87	3	53	10	0.9	22	0.3	2	299	22,647	7	10	9	0.08	69	0.4	62,848	15	0.7	2	17	0.2	19	349,977	1	3	0.8	273	98	0.6	5,353	32,603
		2427.05	18	5,921	24,537	109	3	1	3,522	2,078	64	530	104	8	2	7	16	1,597	69	2	43	7	0.7	18	0.4	2	442	20,262	10	12	9	0.1	34	0.3	48,856	12	0.6	2	14	0.1	14	363,969	1	8	1	149	190	0.6	4,867	24,336
		2427.52-2427.74	14	5,505	22,449	104	3	0.8	2,373	32,042	167	465	104	7	2	5	24	1,344	64	2	32	6	0.6	14	0.4	2	730	11,103	17	12	5	0.09	29	0.2	38,819	11	0.5	1	14	0.09	12	367,376	1	11	0.9	143	243	0.7	5,060	51,233
Median	Lower Evergreen Form.	WM1	49	1,007	22,163	139	17	3	2,298	387	78	398	222	18	4	20	32	9,427	257	8	159	41	4	97	2	6	39	6,703	14	26	35	0	110	1	104,851	33	1	6	34	1	41	307,059	2	6	1	180	506	1	8,521	69,674
		T153, WW1	29	811	14,528	64	2	1	2,945	37,390	125	410	151	12	3	10	21	3,487	138	4	92	9	2	34	0.5	0.7	495	17,371	11	15	11	0.09	75	0.2	74,343	20	0.5	2	26	0.2	36	304,791	1	4	0.4	402	463	2	6,393	100,031
	Upper Precipice SS	WM1	16	850	24,398	82	1	0.9	1,025	727	62	443	134	6	1	7	15	3,538	74	2	40	7	0.5	17	0.5	1	141	10,511	11	8	14	0.06	73	0.3	65,518	14	0.6	3	16	0.06	7	383,702	2	5	0.4	244	405	0.7	3,028	38,450
		C4, T153, WCG4, WW1	28	499	8,602	58	2	0.6	1,946	970	133	300	156	11	2	11	22	3,697	158	4	64	10	2	25	0.7	0.5	457	18,392	9	16	9	0.1	87	0.3	77,390	20	0.4	2	21	0.1	33	306,382	2	5	0.3	361	168	2	5,934	78,337
	Lower Precipice SS	WM1	8	531	3,318	12	0.7	0.4	189	135	22	70	36	3	0.7	2	6	889	36	1	12	5	0.5	11	0.3	1	10	979	2	5	8	0.04	14	0.2	20,857	5	0.09	2	9	0.08	11	423,351	0.4	1	0.3	87	105	0.2	1,843	13,262
		C4, T153, WCG4, WW1	3	293	1,041	4	0.2	<DL	131	266	13	36	32	2	0.4	0.6	3	706	35	1	7	3	1	6	0.2	0.3	9	661	3	7	14	0.03	14	0.06	9,319	3	0.04	3	5	0.01	29	449,584	0.3	0.5	0.2	42	209	1	1,123	7,814
	Moolayember Formation	WM1	38	1,844	28,679	139	4	2	4,271	1,734	74	542	134	12	3	11	24	3,376	136	4	85	12	1	38	0.6	4	296	22,647	12	16	14	0.2	88	0.6	79,808	21	0.7	5	21	0.2	19	331,555	2	6	0.9	492	190	0.7	5,324	56,684
		WCG4, WW1	34	999	17,027	74	3	1	7,079	4,243	111	299	134	9	2	16	26	4,683	116	3	145	13	0.5	70	0.8	3	852	40,434	18	33	33	0.1	88	0.3	87,138	20	0.4	2	15	0.2	19	287,090	2	6	0.4	578	538	2	7,929	93,884

Colour Legend	Major	Minor	Trace	Ultra-Trace	> 100,000	1,000 - 100,000	100 - 1,000	10 - 100	< 10

Ads. H2O is adsorbed water released at 105 °C, LOI is Loss On Ignition – the non-adsorbed volatile mass released at 1,000 °C.

1. Other wells studied in previous projects are Chinchilla 4 (C4), Tipton 153 (T153), Woleebee Creek Groundwater Bore 4 (WCG4), and West Wandoan 1 (WW1).

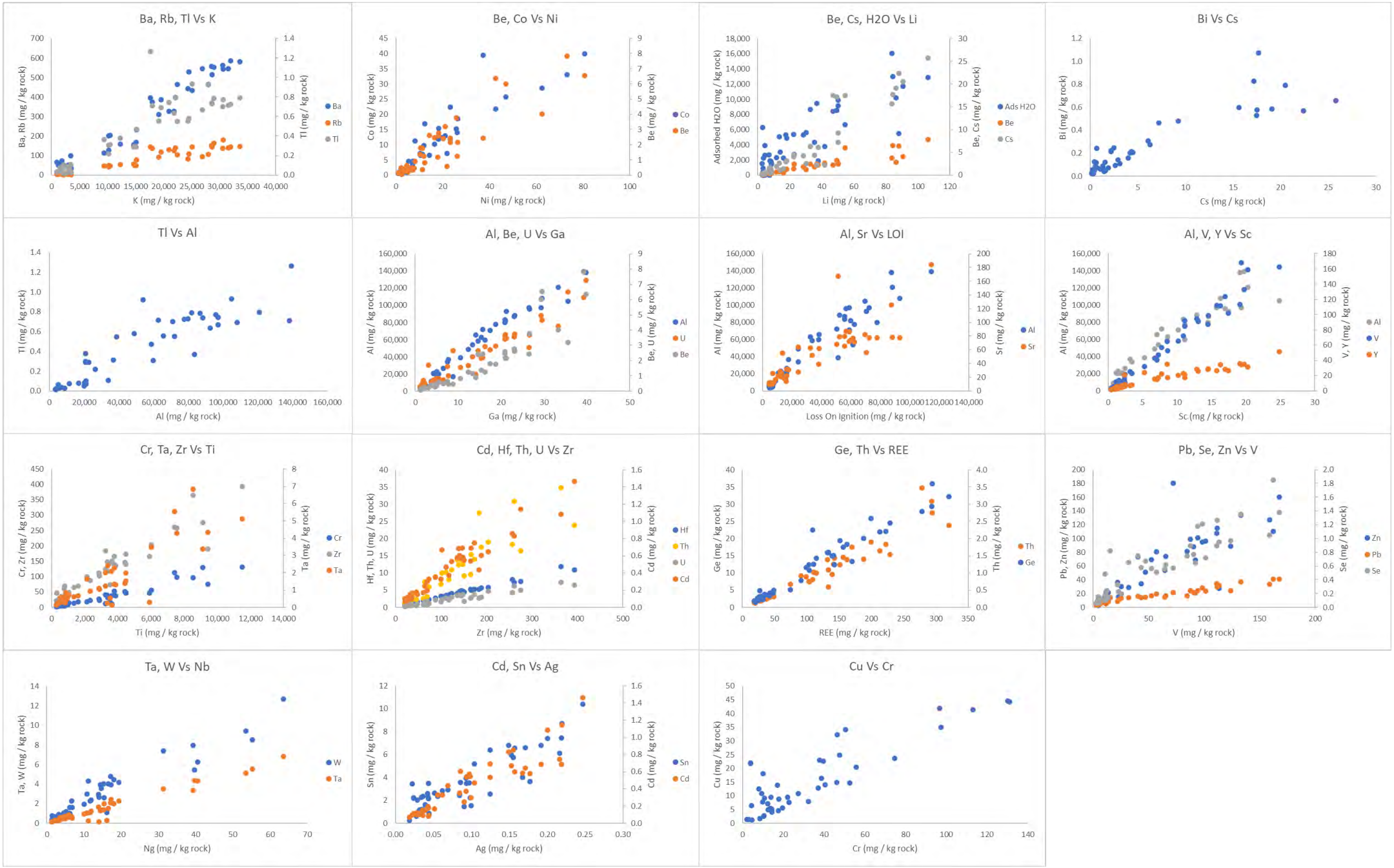

Figure 7: All these elements within WM1 rock samples appear to be intercorrelated, so may be subject to broad lithological and mineralogical controls. Several of these elements, including Ag, Al, Ba, Be, Cd, Co, Cr, Cu, Li, Ni, Pb, Se, Sr, Tl, U, V, and Zn, have defined quality threshold concentrations when dissolved in groundwater (Appendix B).

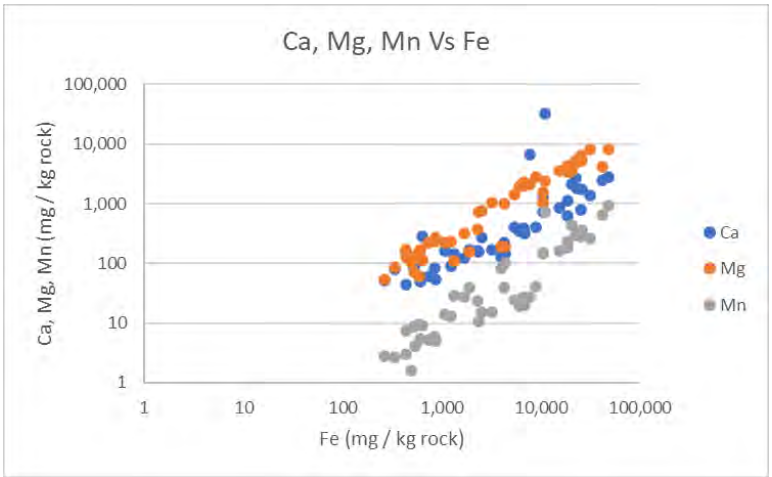

Figure 8: Siderite (iron carbonate) likely hosts most of the Ca, Fe, Mg, and Mn in the WM1 rock samples, with lesser amounts also probably present in other minerals too (carbonates like calcite, other types of minerals). Each of these elements have defined quality threshold concentrations when dissolved in groundwater (Appendix B).

3.2. Sequential extraction experiments

The intention of this procedure is to help isolate the mobility mechanisms and occurrences of elements in rocks, particularly elements extractable over a pH range of 3 – 7. For ease of reading, the tabulated data of this section only includes elements that were extracted in significant amounts from at least one major studied rock unit (upper Precipice Sandstone, lower Precipice Sandstone, Moolayember Formation) during at least one extraction step. The criteria for significant extraction are rock unit median extraction of a given element that is greater than 10 mg per kg of rock (substantially extracted), and/or greater than 10 % of the total concentration that was originally present within the rocks (readily extracted). Full tabulated WM1 data are available for reference in Appendix A.

When referring to the overall extraction of given elements from the sample sets during each step, we generally use major rock unit median values rather than averages that can be significantly biased by outlier samples (e.g., if there were 100 % extraction of an element from one sample but it was below detection for most other samples). We have included summary median results data from previous work (Dawson et al., 2019; Golding et al., 2019) involving sets of samples from other well cores for comparison with the current WM1 well core sequential extraction experiments; the other wells are West Wandoan 1 (WW1), Woleebee Creek Groundwater Bore 4 (WCG4), Chinchilla 4 (C4), and Tipton 153 (T153).

Elements have been classified as major (> 1,000 mg/kg), minor (100 – 1,000 mg/kg), trace (10 – 100 mg/kg), and ultra-trace (< 10 mg/kg) based on median concentrations in West Moonie 1 (WM1) whole-rock assays. Chemically similar elements are grouped together in the tables, in accordance with the sets and groups of the periodic table. When considering the results of this section, it is important to remember that powdered samples have significantly greater mineral surface area exposed to fluid than would generally occur in nature, and the fluid-rock ratios of the experiments are very high, which may result in faster and more complete mass transfer of susceptible elements into the fluid phase.

3.2.1. Elements extracted by water at pH 7

The extraction fluid of the first step was water with a trace amount of ammonium acetate to encourage desorption of weakly adsorbed ions. A large proportion of ionic compounds dissolved during this step were likely to have originally been present as dissolved salts within formation water. Mostly K, Na, Ca, and S were water-extracted from WM1 samples, along with a portion of Mg, Sr, and Si, as occurred in previous experiments with samples from other locations in the Surat Basin (Table 4). Mainly ionic compounds such as some chlorides and sulfates are expected to dissolve in water with near-neutral pH, and some elements and/or compounds weakly adsorbed to components such as clays or organic matter within rock samples may also desorb. Table 5 shows that over a quarter of all Na, Ca,

and S (likely mainly from salts), as well as over 10 % of Mo (probably desorbed), was extracted from some units during this step that essentially acts as a baseline for subsequent extractions with acidic fluids.

The greatest extraction of Na and Si occurred from the same samples, and these elements also correlate with water-extracted Ba, Cs, Li, Rb, and Sr (Figure 9). Extraction of Ni correlates with Co, and highest extraction of Cr correlates with REEs, Th, and Ti (Figure 10). There was greater median water extraction of some elements including As, K, Pb, and Zn from WM1 lower Precipice Sandstone compared with those from well core of other sites (including EPQ7 WW1) but less extraction of Na, Mg, S, and others (Table 4). For upper Precipice Sandstone samples, there was less extraction of Ca, Mg, Na, Si, and Sr than from well cores of other sites but more Cd, Co, K, Ni, Pb, and Zn from WM1. Moolayember Formation WM1 samples had substantially less median water extraction of Ca, Mg, Mn, and S, and more extraction of elements such as Co and Sb compared to cores from other well locations.

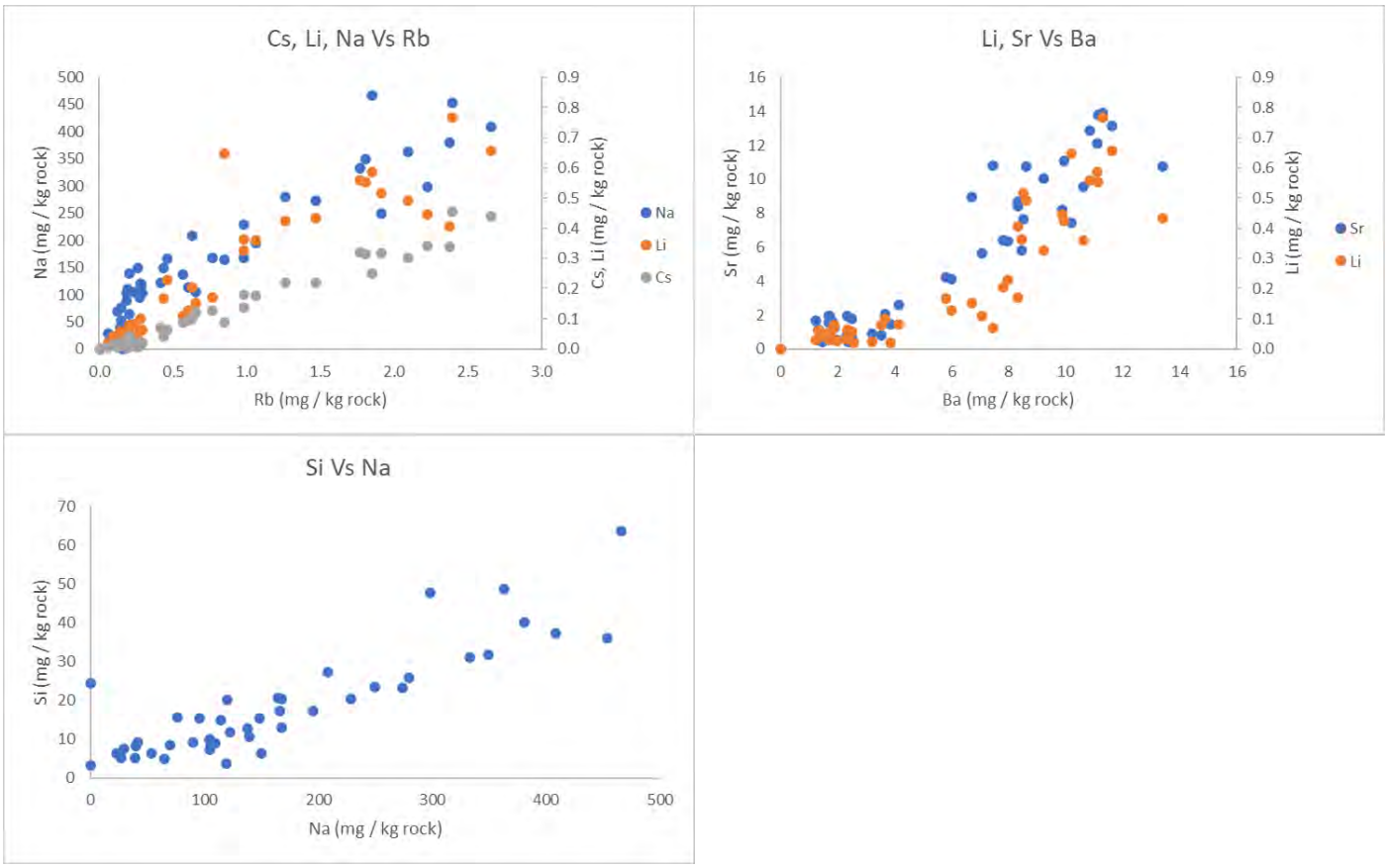

Figure 9: The pH 7 water-extracted elements Ba, Cs, Li, Na, Rb, and Si appear to correlate with each other (powdered WM1 well core samples).

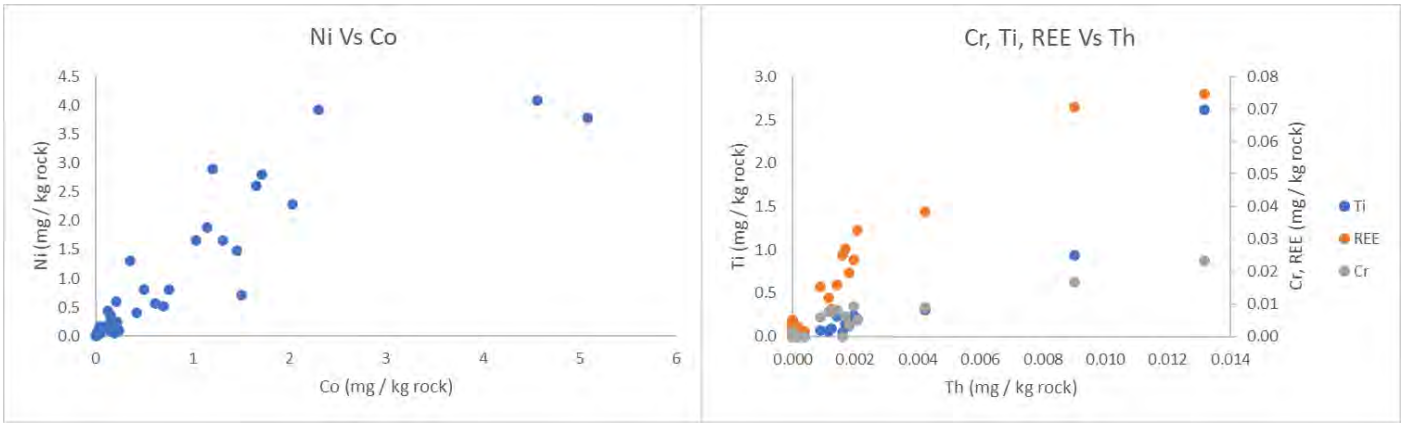

Figure 10: Other selected pH 7 water-extracted element correlations (powdered WM1 well core samples).

Table 4: Absolute amounts of selected[1] elements extracted by pH 7 water (mg element per kg rock powder) from WM1 core samples, with reference to median values of previous projects' samples from other wells[2].

		Element Set	Alkali metals		Alkaline earth metals					Transition Metals								Post transition metals			Metalloids				Nonmetals	
		Element Group	1		2					6	7	8	9	10	11	12		13	14	15	13	14	15		15	16
Unit		Depth (mRT)	Na	K	Be	Mg	Ca	Sr	Ba	Mo	Mn	Fe	Co	Ni	Cu	Zn	Cd	Al	Pb	Bi	B	Si	As	Sb	P	S
Lower Evergreen Formation		2235.81-2235.94	166	146	<DL	9.0	64	6.4	8.0	0.08	0.2	<DL	1.5	1.5	0.03	2.4	0.001	<DL	0.005	<DL	<DL	17	0.01	0.004	<DL	47
		2242.25	274	482	<DL	13	107	11	13	0.1	0.1	<DL	0.4	0.4	0.03	0.5	<DL	<DL	0.003	<DL	0.08	23	0.03	0.008	<DL	119
		2242.44-2242.54	363	194	<DL	15	106	11	8.6	0.3	<DL	<DL	0.4	1.3	0.006	0.02	<DL	<DL	0.004	<DL	0.1	49	0.05	0.02	<DL	31
Upper Precipice Sandstone		2246.14-2246.25	105	242	<DL	14	34	2.6	4.1	0.008	0.7	<DL	0.5	0.8	0.07	3.5	0.003	<DL	0.04	<DL	<DL	8.4	0.006	0.006	<DL	67
		2254.94-2255.10	148	206	0.001	13	47	4.3	5.8	0.02	0.8	<DL	1.5	0.7	0.003	2.5	0.003	<DL	0.004	<DL	<DL	15	0.006	0.007	<DL	61
Lower Precipice Sandstone D		2263.61-2263.77	39	176	<DL	4.3	11	0.7	2.3	0.005	0.9	<DL	1.2	1.9	0.8	3.0	0.002	<DL	0.06	<DL	<DL	5.1	0.01	0.005	<DL	44
		2267.71-2267.84	208	268	<DL	10	76	6.4	7.8	0.2	<DL	<DL	1.7	2.8	<DL	0.6	<DL	<DL	0.001	<DL	<DL	27	0.02	0.01	<DL	19
		2267.84-2267.90	466	347	<DL	18	122	12	11	0.4	<DL	<DL	2.3	3.9	<DL	<DL	<DL	<DL	<DL	<DL	<DL	64	0.02	0.02	<DL	28
Lower Precipice Sandstone C		2274.10-2274.18	26	136	0.002	4.0	11	0.5	2.0	0.002	2.9	<DL	1.0	1.7	0.8	2.7	0.002	<DL	0.02	<DL	<DL	5.0	0.01	0.01	<DL	42
		2281.82-2281.92	114	124	0.002	6.9	48	4.1	6.0	0.1	<DL	<DL	2.0	2.3	0.05	2.8	0.006	<DL	0.01	<DL	<DL	15	0.02	0.02	<DL	46
		2284.13-2284.24	39	153	0.0008	1.5	10	0.6	2.5	0.04	<DL	<DL	0.8	0.8	0.1	2.1	0.004	<DL	0.1	<DL	<DL	8.1	0.04	0.02	<DL	10
		2285.05	250	293	0.003	14	84	7.7	8.5	0.3	0.08	<DL	1.7	2.6	0.006	0.4	<DL	<DL	0.002	<DL	0.1	24	0.02	0.02	<DL	108
		2288.49-2288.61	22	152	<DL	1.0	9.7	0.4	1.5	0.01	<DL	<DL	0.2	0.6	0.4	0.6	<DL	<DL	0.08	<DL	<DL	6.3	0.01	0.008	<DL	7.0
		2294	150	1,389	0.001	4.7	48	1.9	1.7	0.09	<DL	0.09	0.2	0.4	0.05	0.5	<DL	<DL	0.12	<DL	<DL	6.3	0.05	0.01	<DL	38
		2296.97-2297.13	<DL	44	<DL	<DL	<DL	<DL	<DL	<DL	<DL	<DL	<DL	<DL	<DL	<DL	<DL	<DL	<DL	<DL	<DL	3.2	<DL	<DL	<DL	<DL
Lower Precipice Sandstone B		2297.13-2297.19	<DL	302	0.0009	3.1	25	1.5	3.9	0.1	<DL	<DL	0.2	0.2	<DL	0.07	<DL	4.8	0.002	<DL	<DL	24	0.01	0.01	<DL	<DL
		2298.92	89	1,004	0.001	2.7	31	1.2	1.3	0.04	0.1	<DL	0.05	0.1	0.04	0.8	<DL	<DL	0.06	<DL	<DL	9.2	0.02	0.006	<DL	17
Lower Precipice Sandstone A	2	2307.2	120	1,515	0.0008	6.6	68	2.0	3.7	0.05	0.7	0.2	0.05	0.1	0.2	0.4	<DL	<DL	0.02	<DL	0.1	20	0.01	0.005	<DL	22
		2315.77	104	1,095	<DL	3.9	67	1.7	1.2	0.06	0.5	0.2	0.03	0.09	0.03	0.2	<DL	<DL	0.01	<DL	<DL	7.2	0.03	0.006	<DL	22
		2322.61-2322.73	76	393	<DL	3.4	27	0.9	3.2	0.05	0.3	0.2	0.2	0.1	1.8	0.4	<DL	<DL	0.05	<DL	<DL	16	0.02	0.005	<DL	10
		2323.25	110	1,253	<DL	3.9	71	1.6	1.7	0.05	0.6	0.1	0.02	0.06	0.04	0.3	<DL	<DL	0.01	<DL	<DL	9.0	0.01	0.003	<DL	15
	1	2328.54-2328.59	298	250	0.001	23	100	8.2	10	0.07	<DL	<DL	0.1	0.4	0.04	<DL	<DL	<DL	0.0007	<DL	0.1	48	0.04	0.06	<DL	23
		2328.59-2328.68	42	171	0.0009	2.4	13	0.8	3.5	0.02	<DL	<DL	0.2	0.3	0.06	0.7	0.002	<DL	0.02	<DL	<DL	9.2	0.004	0.007	<DL	8.9
		2330.41-2330.54	29	112	<DL	1.2	16	0.4	2.6	0.01	0.09	<DL	0.2	0.1	4.4	0.2	<DL	<DL	0.04	<DL	<DL	7.4	0.02	0.004	<DL	5.4
		2338.75-2338.85	53	189	0.0008	1.8	7.8	0.4	2.4	0.02	<DL	<DL	0.1	0.09	1.0	2.0	0.001	<DL	0.009	<DL	<DL	6.3	0.005	0.007	<DL	8.5
Moolayember Formation		2339.00-2339.17	167	137	0.002	19	66	5.8	8.5	0.03	0.1	<DL	4.6	4.1	0.07	9.1	0.01	<DL	0.05	<DL	<DL	20	0.02	0.02	<DL	192
		2340.54-2340.62	381	312	<DL	24	94	8.4	8.3	0.03	0.1	<DL	0.02	0.06	0.0006	0.03	<DL	<DL	0.0007	<DL	0.1	40	0.08	0.01	<DL	24
		2346.40-2346.51	280	262	<DL	24	75	11	10	0.8	0.2	<DL	0.7	0.5	0.003	0.2	<DL	<DL	0.002	<DL	0.2	26	0.03	0.04	<DL	62
		2348.16-2348.30	104	175	<DL	117	259	8.9	6.7	0.3	3.8	<DL	0.6	0.6	0.002	0.07	<DL	0.4	0.003	<DL	0.09	10	0.004	0.03	<DL	350
		2356.94-2357.06	228	264	<DL	30	78	10	9.2	0.04	0.4	<DL	0.03	0.04	0.001	0.05	<DL	<DL	0.001	<DL	0.2	20	0.004	0.006	<DL	13
		2362.90-2363.00	453	464	<DL	22	85	14	11	0.1	<DL	<DL	0.02	0.03	0.003	0.02	<DL	<DL	0.003	<DL	0.3	36	0.02	0.03	<DL	18
		2366.50-2366.61	333	363	0.0009	28	87	13	11	0.09	0.3	<DL	0.02	0.03	0.0006	0.01	<DL	<DL	<DL	<DL	0.2	31	0.008	0.01	<DL	16
		2373.89-2373.99	167	358	<DL	61	222	8.7	8.3	0.05	0.8	<DL	0.02	0.03	0.002	0.002	<DL	<DL	0.0009	<DL	0.1	13	0.005	0.01	<DL	23
		2427.52-2427.74	123	460	<DL	14	1,038	11	7.5	0.07	10	<DL	0.2	0.06	0.009	0.004	<DL	<DL	0.001	<DL	0.09	12	0.3	0.04	2.2	76
Medians	Lower Evergreen Formation	WM1	274	194	<DL	13	106	11	8.6	0.1	0.1	<DL	0.4	1.3	0.03	0.5	<DL	<DL	0.004	<DL	0.1	23	0.03	0.008	<DL	47
		T153, WW1	217	169	<DL	51	916	8.6	6.4	0.02	0.5	<DL	0.05	0.04	<DL	0.005	0.0002	5.6	0.003	<DL	0.1	8.5	0.01	0.009	4.6	16
	Upper Precipice Sandstone	WM1	127	224	0.0006	13	40	3.4	5.0	0.02	0.8	<DL	1.0	0.8	0.04	3.0	0.003	<DL	0.02	<DL	<DL	12	0.006	0.006	<DL	64
		C4, T153, WCG4, WW1	174	179	<DL	51	156	6.1	4.1	0.04	0.8	<DL	0.02	0.03	<DL	<DL	0.0001	0.01	0.003	<DL	0.03	30	0.008	0.009	2.9	64
	Lower Precipice Sandstone	WM1	83	259	0.0008	3.9	29	1.3	2.5	0.05	<DL	<DL	0.2	0.3	0.05	0.5	<DL	<DL	0.02	<DL	<DL	9.1	0.02	0.008	<DL	18
		C4, T153, WCG4, WW1	136	173	<DL	11	33	1.0	1.6	0.03	0.3	<DL	0.2	0.2	<DL	0.08	0.0001	0.2	0.001	<DL	0.08	2.3	0.005	0.008	2.9	177
	Moolayember Formation	WM1	228	312	<DL	24	87	10	8.5	0.07	0.3	<DL	0.03	0.06	0.002	0.03	<DL	<DL	0.001	<DL	0.1	20	0.02	0.02	<DL	24
		WCG4, WW1	287	245	<DL	98	534	18	6.3	0.1	1.6	<DL	0.004	<DL	0.001	0.02	<DL	1.2	<DL	<DL	<DL	36	0.01	0.007	<DL	101
Colour Legend			Major	Minor	Trace	> 1,000	100 – 1,000		10 – 100		< 10															

1. Tabulated elements were > 10 mg/kg and/or > 10 % median extracted from at least one of the four major rock units (full WM1 data in Appendix A).
2. Other wells studied in previous projects are Chinchilla 4 (C4), Tipton 153 (T153), Woleebee Creek Groundwater Bore 4 (WCG4), and West Wandoan 1 (WW1).

Table 5: Proportions of selected[1] elements extracted by pH 7 water (percentage of total amount in rock powder) from WM1 core samples, with reference to median values of previous projects' samples from other wells[2].

		Element Set	Alkali metals		Alkaline earth metals					Transition Metals								Post transition metals			Metalloids				Nonmetals	
		Element Group	1		2					6	7	8	9	10	11	12		13	14	15	13	14	15		15	16
Unit		Depth (mRT)	Na	K	Be	Mg	Ca	Sr	Ba	Mo	Mn	Fe	Co	Ni	Cu	Zn	Cd	Al	Pb	Bi	B	Si	As	Sb	P	S
Lower Evergreen Formation		2235.81-2235.94	27.2	1.4	<DL	0.9	29.0	16.3	3.9	9.4	0.6	<DL	10.5	5.7	0.1	3.5	0.2	<DL	0.0	<DL	<DL	0.0	0.4	1.0	<DL	34.4
		2242.25	27.2	1.9	<DL	0.6	27.5	13.1	3.1	7.1	0.4	<DL	3.2	2.0	0.1	0.5	<DL	<DL	0.0	<DL	0.1	0.0	0.3	1.0	<DL	18.3
		2242.44-2242.54	28.9	0.9	<DL	0.5	25.8	13.7	2.2	10.9	<DL	<DL	1.2	2.1	0.0	0.0	<DL	<DL	0.0	<DL	0.2	0.0	0.8	2.9	<DL	6.0
Upper Precipice Sandstone		2246.14-2246.25	17.1	2.3	<DL	3.8	20.7	8.4	2.0	1.6	3.2	<DL	10.9	11.2	1.5	11.7	1.8	<DL	0.3	<DL	<DL	0.0	0.2	1.6	<DL	20.8
		2254.94-2255.10	17.5	0.8	0.1	1.2	6.4	6.8	1.3	7.5	0.5	<DL	13.3	8.8	0.0	3.4	0.8	<DL	0.0	<DL	<DL	0.0	0.1	2.2	<DL	15.1
Lower Precipice Sandstone D		2263.61-2263.77	5.8	1.2	<DL	1.9	12.3	3.4	1.4	1.9	7.0	<DL	25.1	34.1	10.5	20.7	1.1	<DL	0.6	<DL	<DL	0.0	0.3	1.2	<DL	23.7
		2267.71-2267.84	47.9	1.8	<DL	1.3	30.2	15.7	2.9	14.1	<DL	<DL	5.8	4.9	<DL	<DL	<DL	<DL	<DL	<DL	<DL	0.0	0.3	2.2	<DL	5.5
		2267.84-2267.90	23.8	1.4	<DL	1.3	28.4	9.4	2.5	19.0	<DL	<DL	14.4	12.1	<DL	0.8	<DL	<DL	0.0	<DL	<DL	0.0	0.5	1.9	<DL	6.8
Lower Precipice Sandstone C		2274.10-2274.18	5.6	1.1	0.3	2.1	8.6	1.8	1.3	0.4	3.6	<DL	22.6	21.3	9.3	13.9	1.9	<DL	0.2	<DL	<DL	0.0	0.2	2.3	<DL	3.4
		2281.82-2281.92	17.8	0.8	0.1	1.0	31.1	7.9	2.6	13.0	<DL	<DL	16.3	11.3	0.3	5.1	1.0	<DL	0.1	<DL	<DL	0.0	0.5	2.6	<DL	14.0
		2284.13-2284.24	30.3	6.9	0.2	0.9	20.9	2.9	5.6	13.9	<DL	<DL	11.0	7.2	0.6	10.0	4.8	<DL	1.5	<DL	<DL	0.0	1.5	4.6	<DL	11.3
		2285.05	15.3	1.4	0.0	0.7	24.3	9.9	2.6	12.1	0.4	<DL	6.4	5.5	0.0	0.3	<DL	<DL	0.0	<DL	0.2	0.0	0.3	1.7	<DL	13.4
		2288.49-2288.61	25.1	7.7	<DL	0.4	15.9	2.9	4.1	10.2	<DL	<DL	11.0	8.8	5.7	7.3	<DL	<DL	1.1	<DL	<DL	0.0	1.7	4.0	<DL	8.9
		2294	39.5	43.8	0.5	4.4	40.1	7.7	3.7	29.3	<DL	0.0	12.3	6.7	2.0	5.9	<DL	<DL	1.3	<DL	<DL	0.0	3.7	6.2	<DL	22.5
		2296.97-2297.13	<DL	18.1	0.2	2.0	14.5	2.6	5.9	25.3	<DL	<DL	8.9	7.7	<DL	0.5	<DL	0.0	0.0	<DL	<DL	0.0	0.6	2.3	<DL	<DL
Lower Precipice Sandstone B		2297.13-2297.19	<DL	0.2	<DL	<DL	<DL	<DL	<DL	<DL	<DL	<DL	<DL	<DL	<DL	<DL	<DL	<DL	<DL	<DL	<DL	0.0	<DL	<DL	<DL	<DL
		2298.92	17.8	33.2	0.3	2.0	32.6	6.4	2.5	10.1	3.3	<DL	5.2	2.9	1.0	6.3	<DL	<DL	0.9	<DL	<DL	0.0	2.9	3.9	<DL	18.3
Lower Precipice Sandstone A	2	2307.2	36.4	51.7	0.5	6.1	47.4	18.6	8.3	21.3	2.4	0.0	5.0	3.4	0.7	3.6	<DL	<DL	0.4	<DL	1.4	0.0	2.0	3.3	<DL	31.8
		2315.77	32.9	47.9	<DL	2.3	42.5	16.0	2.6	56.8	7.5	0.0	5.7	4.0	2.1	4.4	<DL	<DL	0.3	<DL	<DL	0.0	5.5	5.7	<DL	23.7
		2322.61-2322.73	57.9	32.7	<DL	4.8	32.8	7.5	6.2	38.3	3.3	0.0	38.7	9.4	14.7	18.2	<DL	<DL	1.3	<DL	<DL	0.0	5.4	4.0	<DL	34.3
		2323.25	20.5	59.9	<DL	6.4	47.0	16.8	3.9	28.5	6.0	0.0	4.6	2.5	3.2	4.4	<DL	<DL	0.4	<DL	<DL	0.0	3.4	3.1	<DL	30.7
	1	2328.54-2328.59	32.0	1.4	0.0	1.1	31.9	6.5	2.6	8.4	<DL	<DL	0.6	1.0	0.1	<DL	<DL	<DL	0.0	<DL	0.2	0.0	0.9	8.2	<DL	6.2
		2328.59-2328.68	18.7	4.9	0.1	0.9	23.6	3.0	3.6	13.1	<DL	<DL	7.9	6.3	1.3	4.3	0.5	<DL	0.2	<DL	<DL	0.0	0.5	4.1	<DL	15.4
		2330.41-2330.54	4.5	11.7	<DL	2.2	32.0	4.2	3.9	21.6	3.4	<DL	19.9	7.6	20.0	6.9	<DL	<DL	0.8	<DL	<DL	0.0	4.7	3.1	<DL	11.6
		2338.75-2338.85	31.8	12.4	0.2	1.5	17.6	2.6	4.9	15.7	<DL	<DL	10.2	3.0	8.9	24.5	1.1	<DL	0.2	<DL	<DL	0.0	0.7	3.9	<DL	22.0
Moolayember Formation		2339.00-2339.17	38.2	1.5	0.1	1.9	39.4	8.9	7.5	4.0	0.9	<DL	29.8	22.3	0.5	5.0	2.0	<DL	0.2	<DL	<DL	0.0	0.2	1.7	<DL	36.8
		2340.54-2340.62	40.3	1.4	<DL	0.7	15.3	15.1	2.5	7.4	0.1	<DL	0.1	0.2	0.0	0.0	<DL	<DL	0.0	<DL	0.4	0.0	1.3	1.9	<DL	8.6
		2346.40-2346.51	17.1	0.8	<DL	0.6	6.8	15.0	1.7	30.0	0.1	<DL	3.1	2.3	0.0	0.2	<DL	<DL	0.0	<DL	0.8	0.0	0.4	2.3	<DL	22.2
		2348.16-2348.30	7.6	0.6	<DL	2.8	10.3	11.6	1.4	4.6	0.6	<DL	5.1	3.1	0.0	0.1	<DL	0.0	0.0	<DL	0.6	0.0	0.0	1.1	<DL	3.2
		2356.94-2357.06	13.0	0.9	<DL	0.6	4.5	14.0	1.6	10.9	0.1	<DL	0.5	0.4	0.0	0.1	<DL	<DL	0.0	<DL	0.9	0.0	0.2	0.9	<DL	12.2
		2362.90-2363.00	25.7	1.6	<DL	0.3	10.7	17.5	2.0	22.1	<DL	<DL	0.2	0.2	0.0	0.0	<DL	<DL	0.0	<DL	0.8	0.0	0.7	2.7	<DL	14.3
		2366.50-2366.61	6.9	1.3	0.0	0.3	3.1	16.6	2.1	16.2	0.0	<DL	0.2	0.2	0.0	0.0	<DL	<DL	<DL	<DL	1.1	0.0	0.3	1.1	<DL	9.2
		2373.89-2373.99	2.1	1.1	<DL	1.2	8.3	13.8	1.5	15.5	0.3	<DL	0.3	0.3	0.0	0.0	<DL	<DL	0.0	<DL	0.7	0.0	0.1	1.2	<DL	23.6
		2427.52-2427.74	2.2	2.0	<DL	0.6	3.2	6.5	1.6	17.5	1.4	<DL	1.1	0.5	0.2	0.0	<DL	<DL	0.0	<DL	0.7	0.0	2.7	3.8	1.5	31.2
Unit Medians	Lower Evergreen Formation	WM1	27.2	1.4	<DL	0.6	27.5	13.7	3.1	9.4	0.4	<DL	3.2	2.1	0.1	0.5	<DL	<DL	0.0	<DL	0.1	0.0	0.4	1.0	<DL	18.3
		T153, WW1	24.6	1.5	<DL	1.7	5.2	8.6	1.3	5.5	0.1	<DL	0.5	0.2	<DL	0.0	0.1	0.0	0.0	<DL	0.4	0.0	0.3	3.4	1.2	5.0
	Upper Precipice Sandstone	WM1	17.3	1.6	0.1	2.5	13.5	7.6	1.7	4.5	1.8	<DL	12.1	10.0	0.7	7.6	1.3	<DL	0.2	<DL	<DL	0.0	0.1	1.9	<DL	17.9
		C4, T153, WCG4, WW1	16.5	1.7	<DL	2.7	5.6	3.1	1.3	5.7	0.2	<DL	0.1	0.2	<DL	<DL	0.1	0.0	0.0	<DL	<DL	0.0	0.1	1.7	1.1	23.5
	Lower Precipice Sandstone	WM1	22.1	7.3	0.0	1.7	29.3	6.5	3.2	14.0	<DL	<DL	9.6	6.5	1.1	4.8	<DL	<DL	0.3	<DL	<DL	0.0	0.8	3.2	<DL	13.7
		C4, T153, WCG4, WW1	30.7	14.3	<DL	3.9	7.4	5.1	2.4	9.3	3.1	<DL	2.5	1.6	<DL	0.1	0.1	0.0	0.0	<DL	<DL	0.0	<DL	3.1	3.1	41.6
	Moolayember Formation	WM1	13.0	1.3	<DL	0.6	8.3	14.0	1.7	15.5	0.1	<DL	0.5	0.4	0.0	0.0	<DL	<DL	0.0	<DL	0.7	0.0	0.3	1.7	<DL	14.3
		WCG4, WW1	23.2	1.6	<DL	1.6	9.6	14.8	2.4	11.3	0.1	<DL	0.0	<DL	0.0	0.0	<DL	0.0	<DL	<DL	<DL	0.0	0.2	1.7	<DL	23.4

Colour Legend	Major	Minor	Trace	Ultra-trace	> 75	50 – 75	25 – 50	5 – 25	< 5

1. Tabulated elements were > 10 mg/kg and/or > 10 % median extracted from at least one of the four major rock units (full WM1 data in Appendix A).
2. Other wells studied in previous projects are Chinchilla 4 (C4), Tipton 153 (T153), Woleebee Creek Groundwater Bore 4 (WCG4), and West Wandoan 1 (WW1).

3.2.2. Elements extracted by dilute acetic acid (a weak-acid analogous to carbonic acid)

Part A – Step 2 of procedure – 1 mol/L acetic acid buffered with ammonium acetate at pH 5

In this step, carbonates and some acid-reactive aluminosilicate minerals have at least partially reacted in most samples, possibly together with some trace-metal sulfides and related minerals. Any elements strongly adsorbed to minerals should have desorbed too. The elements Al, Fe, and Si were most substantially extracted from the lower Precipice Sandstone samples, though less so for WM1 than for other well core sets including EPQ7 WW1. Extraction of V correlates with Fe and Mg (Figure 11); both Fe and Mg could be siderite, chlorite, or mica hosted, whereas V most likely comes from mica. Extraction of the elements Al, Bi, Cs, Li, Rb, and Si correlates with each other (Figure 12), probably representing partial aluminosilicate dissolution. Extracted Ba and Se correlate with Sr, and as in the water-step Co and Ni are correlated (Figure 8).

Compared with median amounts of major and minor elements extracted from other well core sample sets including EPQ7 WW1, WM1 lower Precipice Sandstone samples had slightly higher extraction of elements such as P, Pb, and S, but generally lesser (e.g., As, Co, Cu, and Fe) or similar (e.g., Ca and Ni) median amounts of elements extracted (Table 6). Proportionally, median extraction of Cu and Pb at pH 5 from WM1 lower Precipice Sandstone samples was greater than 25 % of the total amounts present in the rocks, which was also the case for previously studied well cores including WW1 (Table 7). WM1 Moolayember Formation samples had significantly higher median extraction of Fe and Mg, despite having median total rock contents of Fe and Mg that were roughly half of those present in comparison well cores.

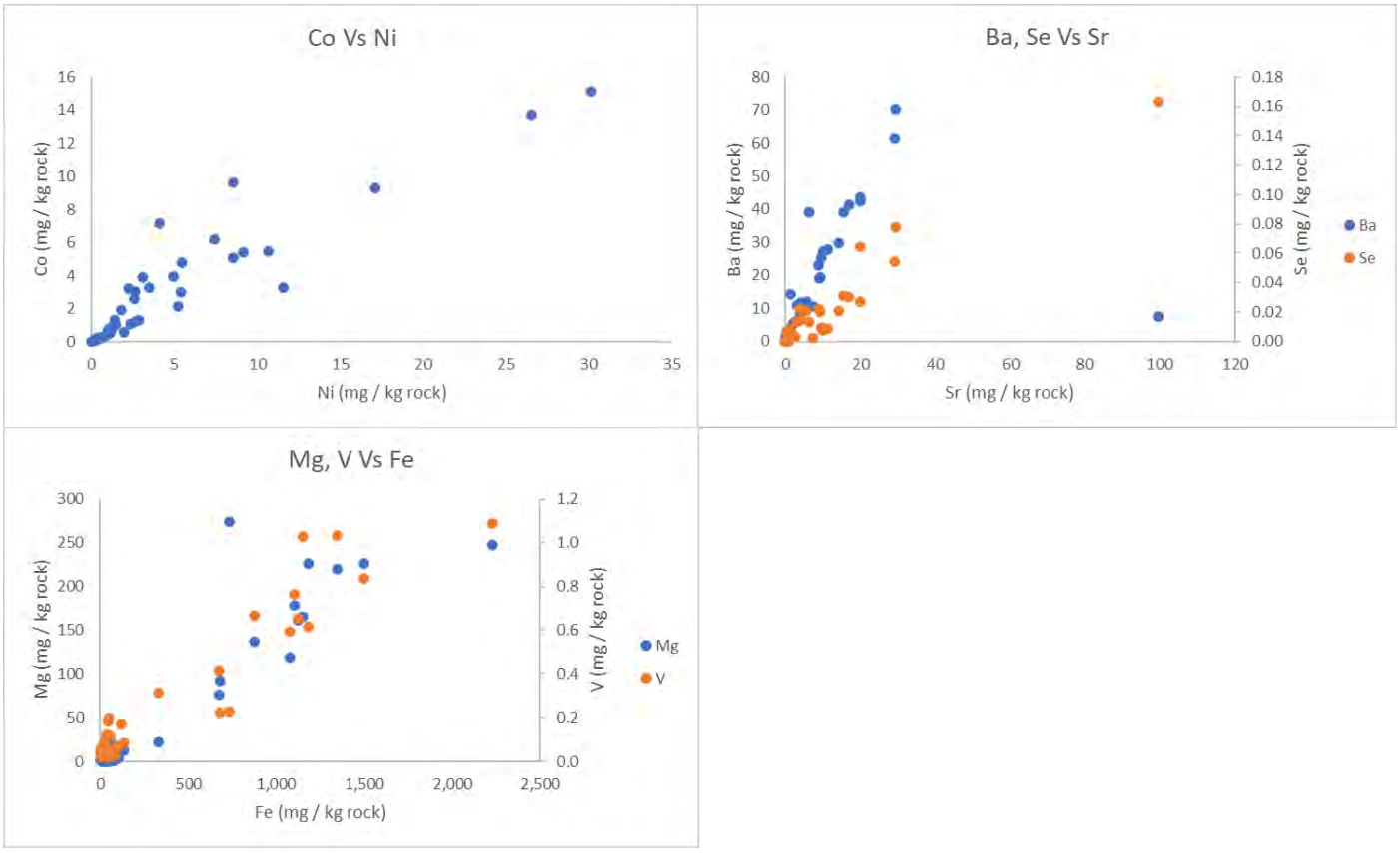

Figure 11: Selected pH 5 acid-extracted element correlations (powdered WM1 well core samples).

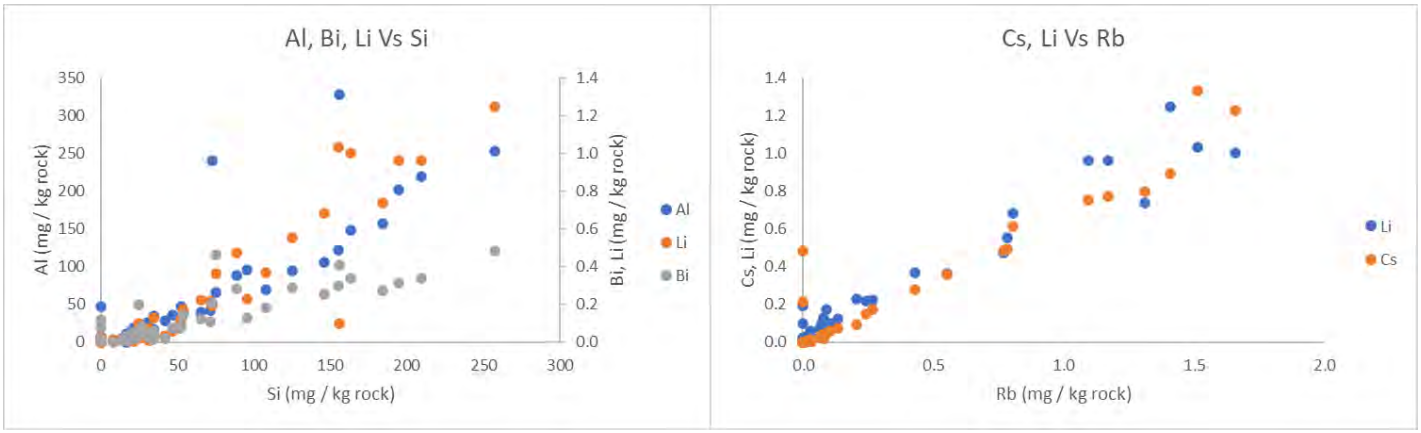

Figure 12: The pH 5 acid-extracted elements Al, Bi, Cs, Li, Rb, and Si correlate with each other (powdered WM1 well core samples).

Table 6: Absolute amounts of selected[1] elements extracted by pH 5 acid (mg element per kg rock powder) from WM1 core samples, with reference to median values of previous projects' samples from other wells[2].

		Element Set	Alkali metals		Alkaline earth metals					Transition Metals								Post transition metals			Metalloids				Nonmetals	
		Element Group	1		2					6	7	8	9	10	11	12		13	14	15	13	14	15		15	16
Unit		Depth (mRT)	Na	K	Be	Mg	Ca	Sr	Ba	Mo	Mn	Fe	Co	Ni	Cu	Zn	Cd	Al	Pb	Bi	B	Si	As	Sb	P	S
Lower Evergreen Formation		2235.81-2235.94	0.5	<DL	0.07	14	50	3.7	8.1	0.001	1.9	121	5.5	11	4.6	19	0.3	39	9.2	0.1	0.2	53	0.5	0.04	<DL	<DL
		2242.25	<DL	<DL	0.2	13	110	11	28	<DL	0.6	57	3.9	4.9	7.5	22	0.3	65	22	0.5	2.4	75	1.5	0.07	<DL	9.2
		2242.44-2242.54	10	<DL	0.2	25	156	17	41	0.06	<DL	56	14	27	5.6	14	0.3	253	12	0.5	1.0	257	1.0	0.07	3.3	38
Upper Precipice Sandstone		2246.14-2246.25	<DL	<DL	0.02	13	29	0.8	2.0	<DL	1.7	137	0.6	1.1	2.2	4.6	0.3	19	4.5	0.02	<DL	21	0.9	0.05	<DL	<DL
		2254.94-2255.10	<DL	<DL	0.1	22	51	2.7	5.8	0.002	5.6	329	3.2	2.3	0.8	15	0.3	34	5.8	0.04	2.2	34	1.0	0.04	0.9	<DL
Lower Precipice Sandstone D		2263.61-2263.77	<DL	<DL	0.02	1.6	18	0.2	0.8	<DL	<DL	29	0.7	1.0	3.6	1.4	0.004	13	3.0	0.01	<DL	34	0.8	0.03	28	17
		2267.71-2267.84	<DL	<DL	0.3	<DL	<DL	<DL	<DL	<DL	<DL	11	2.2	5.2	1.5	7.4	0.08	48	6.9	0.1	1.0	<DL	0.9	<DL	<DL	<DL
		2267.84-2267.90	<DL	<DL	0.7	4.8	81	6.3	39	0.05	0.7	47	15	30	3.3	7.0	0.08	329	14	0.4	1.1	156	0.6	<DL	<DL	<DL
Lower Precipice Sandstone C		2274.10-2274.18	<DL	<DL	0.03	1.4	6.8	0.2	0.9	<DL	1.5	58	0.7	1.0	4.7	1.8	0.004	11	2.6	0.08	0.4	27	1.1	0.07	12	47
		2281.82-2281.92	<DL	<DL	0.2	3.5	23	1.8	5.1	0.03	<DL	16	3.0	5.4	2.4	7.3	0.02	35	4.3	0.08	<DL	47	0.7	0.05	12	10
		2284.13-2284.24	0.06	<DL	0.04	0.9	3.2	0.2	1.0	0.05	<DL	7.6	1.3	2.9	1.8	2.7	0.006	17	4.8	0.03	<DL	35	1.2	0.04	8.2	<DL
		2285.05	<DL	<DL	0.8	12	88	8.8	23	0.05	<DL	31	9.3	17	4.0	19	0.3	88	18	0.3	0.5	89	1.1	0.1	<DL	10
		2288.49-2288.61	<DL	<DL	0.03	0.9	1.3	0.1	0.4	<DL	<DL	4.5	0.6	2.0	4.1	0.7	0.003	12	3.3	0.03	<DL	17	0.4	0.01	4.5	3.9
		2294	<DL	<DL	0.007	0.7	3.6	0.1	0.5	0.07	<DL	9.5	0.2	0.5	0.4	0.4	0.001	<DL	3.0	0.01	<DL	<DL	0.2	0.02	6.7	6.5
		2296.97-2297.13	<DL	<DL	0.7	<DL	<DL	1.3	14	<DL	0.3	51	6.2	7.4	6.7	9.0	0.09	241	10	0.2	1.1	72	3.3	0.1	<DL	<DL
Lower Precipice Sandstone B		2297.13-2297.19	<DL	<DL	0.03	<DL	<DL	<DL	<DL	<DL	0.8	28	<DL	<DL	2.0	2.0	0.06	6.8	4.2	0.08	1.0	<DL	0.05	<DL	<DL	<DL
		2298.92	<DL	<DL	0.02	0.7	2.1	0.2	0.7	0.04	<DL	6.4	0.2	0.5	0.6	2.4	0.001	6.3	2.3	0.02	<DL	<DL	0.09	0.008	15	2.3
Lower Precipice Sandstone A	2	2307.2	<DL	<DL	0.01	5.6	12	0.4	2.9	0.01	2.8	99	0.2	0.5	3.0	2.5	0.004	29	1.6	0.02	<DL	42	0.1	0.01	<DL	<DL
		2315.77	<DL	<DL	<DL	2.1	7.1	0.2	0.7	<DL	<DL	28	0.2	0.3	0.3	0.9	0.006	<DL	0.6	0.008	2.1	16	0.1	0.01	<DL	<DL
		2322.61-2322.73	<DL	<DL	0.008	2.0	3.8	0.1	1.5	<DL	1.3	48	0.1	0.2	8.0	0.3	0.002	4.3	1.2	0.01	<DL	14	0.06	0.005	3.3	3
		2323.25	<DL	<DL	<DL	1.5	8.2	0.2	1.1	<DL	0.6	27	0.07	0.2	0.4	1.5	0.005	1.7	0.6	<DL	<DL	8	0.05	0.004	5.7	5.7
	1	2328.54-2328.59	4.0	<DL	0.6	22	110	9.5	25	0.007	<DL	33	5.1	8.6	11	2.1	0.2	202	7.8	0.3	1.7	195	0.5	0.1	19	19
		2328.59-2328.68	<DL	<DL	0.05	1.8	9.7	0.2	1.6	<DL	<DL	6.7	0.4	0.9	2.0	2.8	0.3	26	4.3	0.03	1.1	30	0.1	0.01	<DL	<DL
		2330.41-2330.54	<DL	<DL	0.008	0.9	5.2	0.07	0.9	<DL	<DL	3.1	0.2	0.3	13	0.1	0.002	3.0	1.2	0.009	<DL	17	0.07	0.005	<DL	<DL
		2338.75-2338.85	0.3	<DL	0.03	1.6	4.7	0.1	1.1	<DL	<DL	4.5	0.2	0.3	7.1	1.9	0.004	9.4	2.0	0.06	<DL	35	0.1	0.01	<DL	<DL
Moolayember Formation		2339.00-2339.17	<DL	<DL	0.4	11	49	4.1	12	0.005	<DL	47	4.8	5.4	4.0	36	0.3	96	14	0.1	<DL	95	3.3	0.1	<DL	12
		2340.54-2340.62	7.7	<DL	0.2	76	173	16	39	<DL	9.4	673	1.3	2.7	8.7	16	0.3	157	11	0.3	1.3	184	0.7	0.05	<DL	<DL
		2346.40-2346.51	7.1	<DL	0.2	178	124	14	30	0.3	15	1,101	9.7	8.6	3.4	12	0.3	70	9.8	0.2	0.2	108	1.7	0.3	<DL	2.6
		2348.16-2348.30	3.2	<DL	0.1	275	834	7.3	11	0.2	20	734	3.3	3.5	1.3	4.3	0.4	26	6.8	0.07	1.6	51	1.1	0.2	11	34
		2356.94-2357.06	5.7	<DL	0.2	227	141	9.2	19	<DL	21	1,497	0.8	1.2	2.3	6.7	0.4	42	9.2	0.1	1.5	71	0.4	0.03	5.1	1.4
		2362.90-2363.00	12	59	0.3	162	200	29	61	0.003	11	1,125	3.9	3.1	4.7	8.1	0.3	122	11	0.3	2.1	155	0.2	0.09	<DL	<DL
		2366.50-2366.61	13	<DL	0.2	248	249	20	44	0.009	39	2,227	1.9	1.8	4.0	9.3	0.4	106	11	0.3	1.0	146	0.2	0.05	19	7.3
		2373.89-2373.99	<DL	<DL	0.1	226	659	5.7	12	<DL	19	1,182	1.3	1.4	1.5	4.7	0.4	47	7.7	0.09	<DL	52	0.8	0.06	12	13
		2427.52-2427.74	5.4	<DL	0.05	92	18,515	100	7.4	0.02	338	677	7.2	4.1	1.0	3.1	0.3	19	4.2	0.05	2.2	32	4.8	0.2	5.1	118
Unit Medians	Lower Evergreen Formation	WM1	0.5	<DL	0.2	14	110	11	28	0.001	0.6	57	5.5	11	5.6	19	0.3	65	12	0.5	1.0	75	1.0	0.07	<DL	9.2
		T153, WW1	22	52	0.09	376	28,087	47	20	0.004	166	1,599	1.7	1.1	1.2	16	0.03	734	10	0.07	<DL	328	0.8	0.02	<DL	<DL
	Upper Precipice Sandstone	WM1	<DL	<DL	0.07	17	40	1.7	3.9	0.001	3.6	233	1.9	1.7	1.5	10	0.3	26	5.2	0.03	1.1	28	1.0	0.05	0.5	<DL
		C4, T153, WCG4, WW1	15	21	0.09	65	220	8.4	19	0.01	12	373	1.0	0.8	1.5	12	0.005	370	6.3	0.04	<DL	131	0.6	0.03	<DL	<DL
	Lower Precipice Sandstone	WM1	<DL	<DL	0.03	1.6	6.0	0.2	1.1	<DL	<DL	27	0.5	1.0	3.2	2.0	0.005	12	3.1	0.03	<DL	28	0.3	0.01	6.0	1.2
		C4, T153, WCG4, WW1	4.1	10	0.01	3.4	7.6	0.4	3.1	0.02	0.5	54	0.9	0.9	6.4	3.1	<DL	278	1.8	0.01	<DL	96	0.5	0.02	<DL	<DL
	Moolayember Formation	WM1	5.7	<DL	0.2	178	200	14	19	0.005	19	1,101	3.3	3.1	3.4	8.1	0.3	70	10	0.1	1.3	95	0.8	0.09	5.1	7.3
		WCG4, WW1	0.7	1.8	0.05	10	234	1.3	1.1	0.02	9.1	75	2.4	3.7	6.2	7.3	<DL	221	5.3	0.08	<DL	4.3	0.5	0.05	<DL	1.2
Colour Legend			Major	Minor	Trace	> 1,000	100 – 1,000		10 – 100		< 10															

1. Tabulated elements were > 10 mg/kg and/or > 10 % median extracted from at least one of the four major rock units (full WM1 data in Appendix A).
2. Other wells studied in previous projects are Chinchilla 4 (C4), Tipton 153 (T153), Woleebee Creek Groundwater Bore 4 (WCG4), and West Wandoan 1 (WW1).

Table 7: Proportions of selected[1] elements extracted by pH 5 acid (percentage of total amount in rock powder) from WM1 core samples, with reference to median values of previous projects' samples from other wells[2].

		Element Set	Alkali metals		Alkaline earth metals					Transition Metals								Post transition metals			Metalloids				Nonmetals	
		Element Group	1		2					6	7	8	9	10	11	12		13	14	15	13	14	15		15	16
Unit		Depth (mRT)	Na	K	Be	Mg	Ca	Sr	Ba	Mo	Mn	Fe	Co	Ni	Cu	Zn	Cd	Al	Pb	Bi	B	Si	As	Sb	P	S
Lower Evergreen Formation		2235.81-2235.94	0.1	<DL	5.9	1.4	22.7	9.5	4.0	0.1	4.9	2.8	39.1	40.8	19.7	28.0	42.7	0.1	44.6	59.9	0.7	0.0	14.5	7.5	<DL	<DL
		2242.25	<DL	<DL	6.5	0.6	28.4	13.7	6.4	<DL	2.0	0.8	30.2	23.3	17.0	20.2	18.9	0.1	52.8	56.1	4.1	0.0	17.3	8.5	<DL	1.4
		2242.44-2242.54	0.8	<DL	6.1	0.9	38.3	21.6	10.4	2.4	<DL	0.6	47.6	42.5	16.0	11.2	34.2	0.2	36.2	60.8	2.5	0.1	16.4	9.1	1.5	7.4
Upper Precipice Sandstone		2246.14-2246.25	<DL	<DL	4.9	3.4	17.8	2.6	1.0	<DL	7.4	5.9	12.1	15.4	42.9	15.3	100	0.1	34.5	31.7	<DL	0.0	23.8	14.1	<DL	<DL
		2254.94-2255.10	<DL	<DL	13.1	2.2	7.1	4.3	1.3	0.7	3.7	3.1	28.4	28.1	5.5	19.9	91.5	0.1	35.7	59.9	29.5	0.0	22.0	14.0	0.4	<DL
Lower Precipice Sandstone D		2263.61-2263.77	<DL	<DL	6.7	0.7	20.5	0.9	0.5	<DL	<DL	2.3	15.0	18.0	45.3	10.0	2.4	0.1	32.7	34.8	<DL	0.0	26.2	7.1	WR<DL	9.1
		2267.71-2267.84	<DL	<DL	10.7	0.3	20.2	8.1	10.1	1.5	2.8	0.9	37.8	37.3	16.3	6.5	13.0	0.3	39.9	38.0	4.9	0.1	11.2	<DL	<DL	<DL
		2267.84-2267.90	<DL	<DL	11.7	<DL	<DL	<DL	<DL	<DL	<DL	0.4	18.0	22.4	19.3	9.2	21.2	0.1	34.7	43.2	9.2	<DL	19.7	<DL	<DL	<DL
Lower Precipice Sandstone C		2274.10-2274.18	<DL	<DL	7.1	0.7	5.3	0.7	0.6	<DL	1.8	1.5	15.7	13.4	52.1	9.0	4.4	0.1	24.6	69.4	5.4	0.0	27.5	16.6	31.8	3.8
		2281.82-2281.92	<DL	<DL	6.9	0.5	15.0	3.4	2.2	3.9	<DL	0.7	23.8	26.5	16.2	13.7	2.8	0.1	28.6	37.0	<DL	0.0	18.9	8.9	12.1	2.9
		2284.13-2284.24	0.0	<DL	11.0	0.5	6.5	0.8	2.3	17.3	<DL	1.2	19.3	25.5	10.2	12.5	7.9	0.1	61.4	22.6	<DL	0.0	41.0	9.5	WR<DL	<DL
		2285.05	<DL	<DL	13.2	0.6	25.4	11.3	7.0	2.0	<DL	0.5	36.1	36.3	9.0	11.6	23.5	0.1	43.3	48.8	1.2	0.0	19.3	9.6	<DL	1.3
		2288.49-2288.61	<DL	<DL	9.1	0.4	2.2	0.8	1.1	<DL	<DL	0.6	29.4	29.2	58.1	8.3	2.9	0.1	43.0	48.3	<DL	0.0	42.0	7.1	13.3	4.9
		2294	<DL	<DL	3.3	0.7	3.0	0.5	1.0	20.9	<DL	1.9	19.6	10.3	13.5	5.4	0.2	<DL	31.4	32.7	<DL	<DL	12.9	7.7	WR<DL	3.8
		2296.97-2297.13	<DL	<DL	6.4	<DL	<DL	<DL	<DL	<DL	2.0	1.5	<DL	<DL	40.4	14.3	13.8	0.0	30.4	65.6	7.5	<DL	2.2	<DL	<DL	<DL
Lower Precipice Sandstone B		2297.13-2297.19	<DL	<DL	9.5	<DL	<DL	0.7	3.6	<DL	1.1	0.7	18.7	10.1	16.1	6.7	10.3	0.2	27.2	32.0	2.5	0.0	18.4	5.1	<DL	<DL
		2298.92	<DL	<DL	5.3	0.5	2.1	1.0	1.3	8.8	<DL	1.2	16.7	9.2	14.5	18.3	0.9	0.0	32.8	33.9	<DL	<DL	13.3	4.6	4.5	2.5
Lower Precipice Sandstone A	2	2307.2	<DL	<DL	6.7	5.2	8.4	3.8	6.7	4.1	10.0	7.4	23.9	18.0	13.8	22.3	3.2	0.6	31.2	55.7	<DL	0.0	18.8	6.5	WR<DL	<DL
		2315.77	<DL	<DL	<DL	1.3	4.5	1.6	1.5	<DL	<DL	6.4	24.6	14.5	24.9	21.1	8.3	<DL	18.1	30.7	46.1	0.0	20.4	12.8	WR<DL	<DL
		2322.61-2322.73	<DL	<DL	5.2	2.8	4.6	1.1	3.0	<DL	14.8	9.1	22.4	18.3	64.6	14.9	1.2	0.1	32.8	41.6	<DL	0.0	14.9	3.6	WR<DL	11.6
		2323.25	<DL	<DL	<DL	2.5	5.5	1.8	2.5	<DL	6.4	4.5	20.6	8.5	27.2	21.5	4.8	0.0	18.8	<DL	<DL	0.0	12.1	3.9	0.5	11.7
	1	2328.54-2328.59	0.4	<DL	9.6	1.1	34.9	7.6	6.8	0.9	<DL	0.5	23.2	20.1	26.6	7.5	22.6	0.1	24.8	55.5	3.1	0.1	13.0	15.2	<DL	5.3
		2328.59-2328.68	<DL	<DL	7.7	0.7	17.7	0.9	1.6	<DL	<DL	0.8	21.1	20.0	44.7	18.0	81.5	0.1	39.4	42.5	6.4	0.0	13.8	7.6	6.5	<DL
		2330.41-2330.54	<DL	<DL	4.5	1.6	10.1	0.7	1.4	<DL	<DL	1.2	15.8	21.1	58.8	3.5	2.1	0.0	26.1	46.0	<DL	0.0	18.2	3.3	22.5	<DL
		2338.75-2338.85	0.2	<DL	7.0	1.3	10.5	0.9	2.2	<DL	<DL	1.0	15.8	11.2	65.5	23.4	3.9	0.1	36.5	69.2	<DL	0.0	17.8	7.3	2.9	<DL
Moolayember Formation		2339.00-2339.17	<DL	<DL	16.8	1.1	29.2	6.2	10.5	0.6	<DL	1.4	31.2	29.7	31.5	19.9	53.2	0.1	64.9	58.8	<DL	0.0	32.7	14.0	<DL	2.2
		2340.54-2340.62	0.8	<DL	10.7	2.3	28.3	28.0	12.0	<DL	5.1	3.6	6.9	10.2	26.8	16.3	51.8	0.2	48.6	52.1	4.7	0.1	12.2	7.2	<DL	<DL
		2346.40-2346.51	0.4	<DL	10.9	4.2	11.2	19.4	5.1	9.5	6.4	5.9	43.3	36.7	21.0	13.4	49.5	0.1	45.9	59.2	0.9	0.0	26.0	16.8	<DL	0.9
		2348.16-2348.30	0.2	<DL	9.5	6.6	33.1	9.5	2.3	2.9	3.0	1.8	27.5	19.6	17.7	8.5	54.6	0.0	46.8	53.2	10.0	0.0	2.6	9.2	1.2	0.3
		2356.94-2357.06	0.3	<DL	10.5	4.4	8.1	12.8	3.5	<DL	6.0	5.8	12.9	11.1	21.2	9.1	82.6	0.1	54.0	53.8	7.9	0.0	16.4	5.3	0.6	1.3
		2362.90-2363.00	0.7	0.2	11.4	2.5	25.3	36.8	11.1	0.6	3.8	4.4	32.6	16.8	20.6	8.5	48.8	0.1	39.9	51.2	6.6	0.1	6.7	9.1	<DL	<DL
		2366.50-2366.61	0.3	<DL	8.2	3.0	8.8	25.7	8.5	1.5	4.2	4.6	19.0	11.0	17.5	9.4	54.0	0.1	44.0	53.5	4.8	0.1	8.9	5.0	1.7	4.1
		2373.89-2373.99	<DL	<DL	7.8	4.3	24.8	9.0	2.2	<DL	6.2	5.2	18.0	13.3	16.0	6.8	100	0.1	45.3	57.1	<DL	0.0	23.1	8.0	4.3	13.2
		2427.52-2427.74	0.1	<DL	6.3	3.9	57.8	59.5	1.6	5.5	46.2	6.1	42.4	33.3	17.9	10.7	100	0.1	29.9	50.6	18.0	0.0	42.0	18.9	3.6	48.6
Unit Medians	Lower Evergreen Formation	WM1	0.1	<DL	6.1	0.9	28.4	13.7	6.4	0.1	2.0	0.8	39.1	40.8	17.0	20.2	34.2	0.1	44.6	59.9	2.5	0.0	16.4	8.5	<DL	1.4
		T153, WW1	3.0	0.5	11.2	11.8	47.8	31.5	5.3	1.2	22.7	9.0	15.7	7.8	11.5	21.4	9.0	1.5	37.0	38.6	<DL	0.1	17.2	7.5	<DL	<DL
	Upper Precipice Sandstone	WM1	<DL	<DL	9.0	2.8	12.4	3.4	1.1	0.4	5.5	4.5	20.2	21.7	24.2	17.6	96	0.1	35.1	45.8	14.7	0.0	22.9	14.1	0.2	<DL
		C4, T153, WCG4, WW1	1.1	0.3	10.0	4.0	21.1	4.4	3.9	1.7	4.4	2.4	12.5	7.4	19.2	14.6	1.4	0.3	33.6	27.8	<DL	0.0	14.6	6.5	<DL	<DL
	Lower Precipice Sandstone	WM1	<DL	<DL	7.0	0.7	6.0	0.9	1.9	<DL	<DL	1.2	20.1	18.2	25.7	12.1	4.6	0.1	32.1	42.0	<DL	0.0	18.3	7.1	<DL	0.6
		C4, T153, WCG4, WW1	1.0	0.5	2.3	1.4	3.4	2.5	5.8	8.4	1.9	4.8	27.8	10.2	35.4	19.3	<DL	1.4	30.8	14.2	<DL	0.0	1.4	6.1	<DL	<DL
	Moolayember Formation	WM1	0.3	<DL	10.5	3.9	25.3	19.4	5.1	0.6	5.1	4.6	27.5	16.8	20.6	9.4	54.0	0.1	45.9	53.5	4.8	0.0	16.4	9.1	0.6	1.3
		WCG4, WW1	0.1	0.0	5.2	0.1	1.8	1.1	0.4	2.5	0.5	0.1	15.4	12.1	20.4	8.1	<DL	0.3	32.4	36.3	<DL	0.0	6.8	16.8	<DL	0.1

Colour Legend	Major	Minor	Trace	Ultra-trace	> 75	50 – 75	25 – 50	5 – 25	< 5

1. Tabulated elements were > 10 mg/kg and/or > 10 % median extracted from at least one of the four major rock units (full WM1 data in Appendix A).
2. Other wells studied in previous projects are Chinchilla 4 (C4), Tipton 153 (T153), Woleebee Creek Groundwater Bore 4 (WCG4), and West Wandoan 1 (WW1).

Part B – Step 3 of procedure – 1 mol/L acetic acid buffered with ammonium acetate at pH 3

Overall, there was mostly less element extraction from lower Precipice Sandstone samples during this step compared with the previous (pH 5) acid step. Acid-reactive minerals (e.g., carbonates) continued to dissolve, and all strongly adsorbed elements should have desorbed from the samples in this step. There was much lower median extraction of elements such as Co, Cu, Ni, Pb, Sr, and Zn from WM1 lower Precipice Sandstone compared with other well cores including EPQ7 WW1 (Table 8). WM1 samples generally experienced less substantial median extraction of elements, excepting Moolayember Formation Fe, Mg, and Mn, compared with the medians for previous studies using well core samples from other localities including EPQ7 WW1 (Table 8).

Up to three times higher proportions of Fe, Mg, and Mn was extracted from WM1 Moolayember Formation samples (Table 9) compared with the median for other well cores including EPQ7 WW1. This is possibly indicative of more reactive siderite-cemented WM1 samples collected given that the rocks have much lower median concentrations of these elements. The specific composition of the siderite at the WM1 location may also make it more reactive. Carbonates, particularly iron-bearing minerals such as siderite, are important hosts of several weak-acid extractable elements within samples from all units. Extraction of several elements, including Ca, Ga, Ge, Mg, Mn, Se, Sr, REE, and Y, appears to broadly correlate with iron extraction (Figure 13). Other strong correlations between extracted elements include Cd and Pb Vs Zn, Co Vs Ni, Cs and Cu Vs Rb, Ba and Si Vs Al (Figure 14).

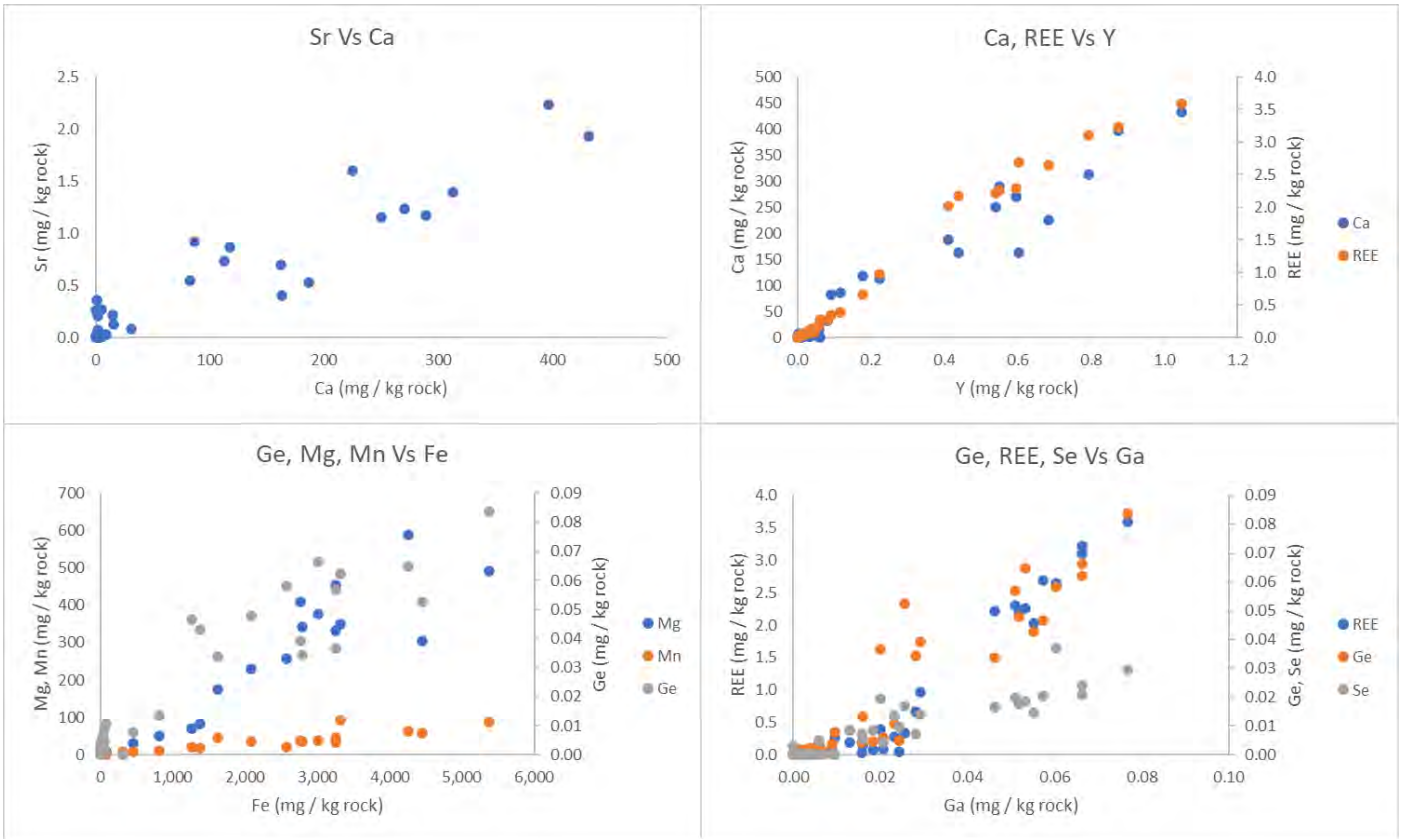

Figure 13: Potentially inter-related pH 3 acid-extracted element correlations (powdered WM1 well core samples).

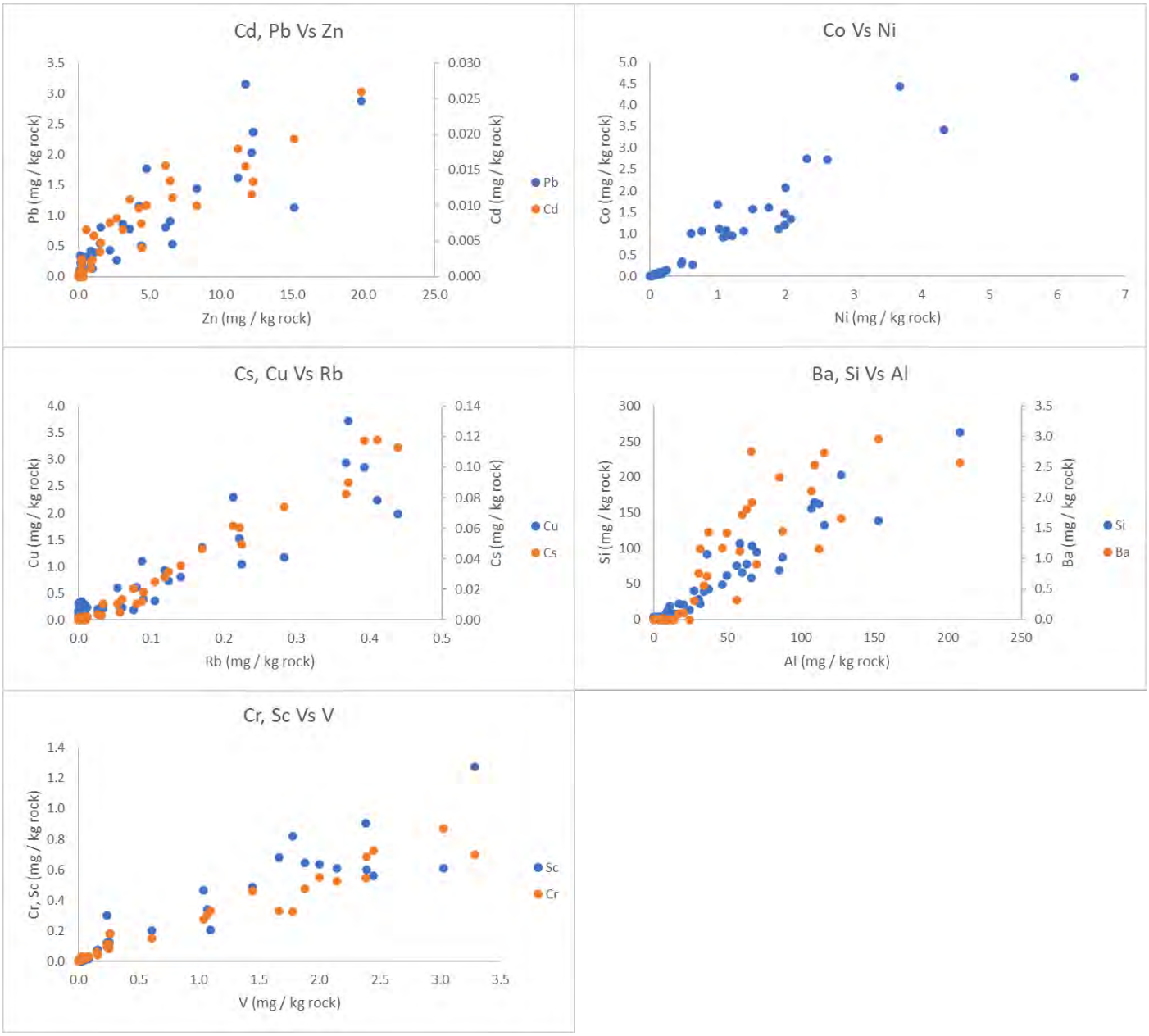

Figure 14: Other additional pH 3 acid-extracted element correlations (powdered WM1 well core samples).

Table 8: Absolute amounts of selected[1] elements extracted by pH 3 acid (mg element per kg rock powder) from WM1 core samples, with reference to median values of previous projects' samples from other wells[2].

		Element Set	Alkali metals		Alkaline earth metals					Transition Metals								Post transition metals			Metalloids				Nonmetals	
		Element Group	1		2					6	7	8	9	10	11	12		13	14	15	13	14	15		15	16
Unit		Depth (mRT)	Na	K	Be	Mg	Ca	Sr	Ba	Mo	Mn	Fe	Co	Ni	Cu	Zn	Cd	Al	Pb	Bi	B	Si	As	Sb	P	S
Lower Evergreen Formation		2235.81-2235.94	<DL	<DL	0.07	51	16	0.1	0.3	0.08	9.6	813	1.3	2.1	0.6	6.1	0.02	28	0.8	0.01	0.06	40	0.09	0.003	<DL	5.6
		2242.25	<DL	<DL	0.2	4.1	15	0.2	0.7	<DL	<DL	62	1.6	1.5	1.5	12	0.01	36	2.0	0.04	<DL	92	0.6	0.004	<DL	25
		2242.44-2242.54	0.7	<DL	0.1	9.1	0.8	0.4	1.7	<DL	<DL	80	4.7	6.3	2.0	12	0.01	127	2.4	0.06	0.1	203	0.2	0.004	<DL	22
Upper Precipice Sandstone		2246.14-2246.25	0.5	<DL	0.02	31	31	0.09	0.1	<DL	6.9	452	0.3	0.5	0.2	1.5	0.003	17	0.5	<DL	<DL	22	0.2	0.006	<DL	2.2
		2254.94-2255.10	1.2	<DL	0.1	70	163	0.4	0.6	<DL	19	1,263	1.0	0.6	0.2	6.6	0.01	34	0.5	<DL	<DL	39	0.3	0.006	124	4.7
Lower Precipice Sandstone D		2263.61-2263.77	0.005	<DL	<DL	1.6	5.6	0.0	<DL	<DL	<DL	32	0.06	0.09	0.3	0.2	<DL	6.1	0.2	<DL	<DL	1.7	0.09	0.004	<DL	1.3
		2267.71-2267.84	<DL	<DL	0.2	1.0	<DL	0.3	0.8	0.001	<DL	14	1.6	1.7	1.4	3.1	0.007	31	0.9	0.05	0.06	29	0.5	0.02	<DL	<DL
		2267.84-2267.90	<DL	<DL	0.03	4.2	1.7	0.05	3.0	0.0004	0.5	51	0.07	0.1	0.2	0.2	0.002	153	0.2	0.006	0.2	138	0.02	0.003	<DL	5.6
Lower Precipice Sandstone C		2274.10-2274.18	0.1	<DL	0.009	1.0	6.6	0.02	0.01	<DL	1.1	53	0.05	0.06	0.3	0.2	<DL	6.2	0.3	<DL	<DL	1.7	0.09	0.006	<DL	<DL
		2281.82-2281.92	<DL	<DL	0.09	0.5	2.2	0.03	<DL	0.005	<DL	4.4	0.3	0.5	0.2	0.9	0.001	9.6	0.2	<DL	<DL	13	0.07	0.002	<DL	1.1
		2284.13-2284.24	<DL	<DL	0.01	<DL	3.4	0.01	<DL	<DL	<DL	1.6	0.1	0.2	0.1	0.3	<DL	5.8	0.1	<DL	<DL	4.1	0.07	0.005	<DL	5.4
		2285.05	<DL	<DL	0.4	2.2	1.7	0.2	1.1	<DL	<DL	41	3.4	4.3	1.2	12	0.02	58	3.1	0.05	<DL	107	0.3	0.009	<DL	20
		2288.49-2288.61	<DL	<DL	0.009	0.2	2.4	0.009	<DL	<DL	<DL	1.4	0.05	0.2	0.2	0.1	<DL	3.5	0.1	<DL	<DL	3.5	0.03	0.002	<DL	<DL
		2294	<DL	<DL	<DL	0.3	<DL	0.02	<DL	<DL	<DL	2.5	0.04	0.09	0.04	0.2	<DL	<DL	0.1	<DL	<DL	<DL	0.02	0.003	<DL	2.6
		2296.97-2297.13	<DL	<DL	<DL	1.4	<DL	<DL	2.3	<DL	<DL	40	<DL	0.0004	0.0003	<DL	<DL	85	<DL	<DL	0.09	70	<DL	<DL	<DL	1.8
Lower Precipice Sandstone B		2297.13-2297.19	<DL	<DL	0.005	5.3	3.6	0.003	1.2	<DL	8.1	315	<DL	0.03	0.002	<DL	0.0002	31	0.001	0.0002	0.3	22	<DL	<DL	<DL	15
		2298.92	<DL	<DL	<DL	0.4	<DL	0.01	<DL	<DL	<DL	2.9	0.02	0.07	0.04	0.2	<DL	<DL	0.07	<DL	<DL	2.1	0.008	0.002	<DL	<DL
Lower Precipice Sandstone A	2	2307.2	0.3	<DL	0.008	2.0	4.9	0.03	<DL	<DL	0.7	38	0.03	0.09	0.2	0.2	<DL	25	0.07	<DL	<DL	13	0.01	0.002	57	<DL
		2315.77	<DL	<DL	0.008	1.3	3.7	0.007	<DL	<DL	<DL	24	0.05	0.09	0.05	0.2	<DL	<DL	0.03	<DL	<DL	3.1	0.02	0.003	<DL	0.8
		2322.61-2322.73	0.4	<DL	<DL	1.3	3.1	0.01	<DL	<DL	<DL	24	0.01	0.04	0.2	0.1	<DL	3.9	0.04	<DL	<DL	2.6	0.007	0.002	<DL	0.6
		2323.25	0.1	<DL	<DL	1.3	6.5	0.01	<DL	<DL	<DL	22	0.02	0.07	0.04	0.3	0.0008	<DL	0.03	<DL	<DL	4.3	0.007	0.002	<DL	7.3
	1	2328.54-2328.59	1.4	<DL	0.3	3.2	5.2	0.3	1.2	<DL	<DL	29	2.8	2.3	2.2	1.6	0.005	112	0.8	0.02	<DL	162	0.1	0.006	51	14
		2328.59-2328.68	0.7	<DL	0.03	0.8	3.0	0.04	0.1	<DL	<DL	3.9	0.1	0.2	0.2	0.6	0.007	20	0.3	<DL	<DL	21	0.01	0.003	53	<DL
		2330.41-2330.54	0.9	<DL	<DL	0.4	3.9	0.007	0.004	<DL	<DL	1.4	0.02	0.04	0.3	0.08	<DL	<DL	0.05	<DL	<DL	0.6	0.007	0.001	<DL	4.5
		2338.75-2338.85	<DL	<DL	0.02	0.7	1.2	0.01	<DL	<DL	<DL	2.0	0.02	0.03	0.3	0.2	0.0006	4.5	0.08	<DL	<DL	3.0	0.01	0.002	<DL	1.2
Moolayember Formation		2339.00-2339.17	1.9	<DL	0.2	1.5	2.1	0.07	0.3	<DL	<DL	48	1.0	0.8	1.1	20	0.03	57	2.9	0.02	<DL	75	1.1	0.02	<DL	19
		2340.54-2340.62	4.9	<DL	0.2	304	83	0.5	2.1	<DL	57	4,449	1.2	2.0	2.9	11	0.02	107	1.6	0.05	<DL	155	0.2	0.006	<DL	2.5
		2346.40-2346.51	4.1	<DL	0.2	410	113	0.7	1.8	0.04	37	2,762	2.7	2.6	0.8	6.4	0.01	63	0.9	0.02	0.05	77	0.8	0.06	60	11
		2348.16-2348.30	3.2	<DL	0.09	230	162	0.7	1.4	0.02	36	2,084	1.1	1.1	0.4	2.7	0.008	37	0.3	0.007	<DL	42	0.6	0.07	68	87
		2356.94-2357.06	2.3	<DL	0.2	590	289	1.2	1.7	<DL	62	4,258	1.1	1.4	0.7	4.4	0.007	60	0.5	0.009	<DL	66	0.1	0.008	98	6.7
		2362.90-2363.00	4.1	<DL	0.2	333	86	0.9	2.5	<DL	33	3,251	2.1	2.0	2.9	4.8	0.01	109	1.8	0.06	<DL	164	0.1	0.01	<DL	7.9
		2366.50-2366.61	7.2	<DL	0.2	493	432	1.9	2.7	<DL	88	5,382	0.9	1.1	2.3	3.6	0.01	116	0.8	0.02	<DL	132	0.08	0.009	71	<DL
		2373.89-2373.99	6.6	<DL	0.1	378	313	1.4	1.4	<DL	39	3,015	0.9	1.1	0.4	2.2	0.008	88	0.4	0.006	0.05	87	0.3	0.02	88	6.3
		2427.52-2427.74	7.0	<DL	0.05	174	251	1.1	1.2	0.003	45	1,626	1.7	1.0	0.2	1.1	0.006	47	0.4	<DL	0.1	49	1.5	0.04	71	15
Unit Medians	Lower Evergreen Formation	WM1	<DL	<DL	0.1	9.1	15	0.2	0.7	<DL	<DL	80	1.6	2.1	1.5	12	0.01	36	2.0	0.04	0.06	92	0.2	0.004	<DL	22
		T153, WW1	15	55	0.1	720	5,689	13	3.9	0.0003	69	2,654	1.4	1.3	0.7	6.3	0.009	1,086	2.0	0.02	<DL	682	0.6	0.01	35	<DL
	Upper Precipice Sandstone	WM1	0.9	<DL	0.06	50	97	0.2	0.3	<DL	13	857	0.6	0.5	0.2	4.1	0.007	26	0.5	<DL	<DL	30	0.3	0.006	62	3.5
		C4, T153, WCG4, WW1	8.0	14	0.1	112	109	1.0	1.6	0.001	35	1,732	1.2	1.1	0.7	5.0	0.004	415	2.3	0.02	<DL	190	0.6	0.01	12	<DL
	Lower Precipice Sandstone	WM1	<DL	<DL	0.008	1.2	3.0	0.02	<DL	<DL	<DL	23	0.05	0.09	0.2	0.2	<DL	6.2	0.1	<DL	<DL	4.2	0.02	0.003	<DL	1.3
		C4, T153, WCG4, WW1	6.1	6.5	0.01	2.6	1.8	0.09	0.3	<DL	0.2	29	0.3	0.6	1.0	1.2	0.002	211	0.6	0.009	<DL	57	0.04	0.003	<DL	<DL
	Moolayember Formation	WM1	4.1	<DL	0.2	333	162	0.9	1.7	<DL	39	3,015	1.1	1.1	0.8	4.4	0.01	63	0.8	0.02	<DL	77	0.3	0.02	68	7.9
		WCG4, WW1	42	15	0.08	164	730	2.0	2.1	0.006	29	1,490	1.4	2.2	2.8	3.5	0.005	214	0.7	0.01	<DL	123	0.3	0.01	<DL	<DL
Colour Legend			Major	Minor	Trace	> 1,000	100 – 1,000			10 – 100		< 10														

1. Tabulated elements were > 10 mg/kg and/or > 10 % median extracted from at least one of the four major rock units (full WM1 data in Appendix A).
2. Other wells studied in previous projects are Chinchilla 4 (C4), Tipton 153 (T153), Woleebee Creek Groundwater Bore 4 (WCG4), and West Wandoan 1 (WW1).

Table 9: Proportions of selected[1] elements extracted by pH 3 acid (percentage of total amount in rock powder) from WM1 core samples, with reference to median values of previous projects' samples from other wells[2].

		Element Set	Alkali metals		Alkaline earth metals					Transition Metals								Post transition metals			Metalloids				Nonmetals	
		Element Group	1		2					6	7	8	9	10	11	12		13	14	15	13	14	15		15	16
Unit		Depth (mRT)	Na	K	Be	Mg	Ca	Sr	Ba	Mo	Mn	Fe	Co	Ni	Cu	Zn	Cd	Al	Pb	Bi	B	Si	As	Sb	P	S
Lower Evergreen Formation		2235.81-2235.94	<DL	<DL	5.6	5.2	7.3	0.3	0.1	9.8	25.0	18.8	9.6	7.9	2.5	8.9	2.6	0.0	3.9	5.5	0.3	0.0	2.9	0.6	<DL	4.1
		2242.25	<DL	<DL	5.0	0.2	3.8	0.3	0.2	<DL	<DL	0.9	12.1	7.2	3.5	11.0	0.8	0.0	5.0	4.7	<DL	0.0	6.7	0.5	<DL	3.8
		2242.44-2242.54	0.1	<DL	3.1	0.3	0.2	0.5	0.4	<DL	<DL	0.9	16.2	10.0	5.7	9.6	1.6	0.1	7.0	7.9	0.3	0.1	3.9	0.5	<DL	4.4
Upper Precipice Sandstone		2246.14-2246.25	0.1	<DL	3.3	8.3	19.1	0.3	0.0	<DL	29.6	19.4	6.1	6.3	4.4	5.0	2.3	0.0	4.1	<DL	<DL	0.0	6.2	1.7	<DL	0.7
		2254.94-2255.10	0.1	<DL	11.2	6.9	22.5	0.7	0.1	<DL	12.8	12.0	8.9	7.5	1.8	9.1	3.4	0.1	3.2	<DL	<DL	0.0	7.1	2.1	50.7	1.2
Lower Precipice Sandstone D		2263.61-2263.77	0.0	<DL	<DL	0.7	6.3	0.1	<DL	<DL	<DL	2.5	1.3	1.6	3.3	1.1	<DL	0.0	2.8	<DL	<DL	0.0	3.0	1.1	<DL	0.7
		2267.71-2267.84	<DL	<DL	0.4	0.3	0.4	0.1	0.8	0.0	2.2	0.9	0.2	0.2	1.0	0.2	0.4	0.1	0.6	0.6	0.7	0.0	0.3	0.4	<DL	1.1
		2267.84-2267.90	<DL	<DL	7.4	0.1	<DL	0.4	0.2	0.1	<DL	0.5	13.5	7.5	17.1	3.9	1.8	0.0	4.4	16.6	0.6	0.0	11.9	3.6	<DL	<DL
Lower Precipice Sandstone C		2274.10-2274.18	0.0	<DL	2.0	0.5	5.1	0.1	0.0	<DL	1.4	1.3	1.1	0.8	3.1	0.8	<DL	0.0	3.3	<DL	<DL	0.0	2.2	1.3	<DL	<DL
		2281.82-2281.92	<DL	<DL	3.8	0.1	1.5	0.1	<DL	0.6	<DL	0.2	2.7	2.3	1.4	1.6	0.2	0.0	1.1	<DL	<DL	0.0	1.9	0.4	<DL	0.4
		2284.13-2284.24	<DL	<DL	3.8	<DL	6.9	0.1	<DL	<DL	<DL	0.3	1.6	1.7	0.5	1.6	<DL	0.0	1.7	<DL	<DL	0.0	2.3	1.0	<DL	6.2
		2285.05	<DL	<DL	7.3	0.1	0.5	0.3	0.3	<DL	<DL	0.7	13.3	9.2	2.6	7.3	1.4	0.1	7.7	8.2	<DL	0.0	5.7	0.8	<DL	2.4
		2288.49-2288.61	<DL	<DL	2.4	0.1	4.0	0.1	<DL	<DL	<DL	0.2	2.7	2.6	2.7	1.3	<DL	0.0	1.5	<DL	<DL	0.0	3.2	0.9	<DL	<DL
		2294	<DL	<DL	<DL	0.3	<DL	0.1	<DL	<DL	<DL	0.5	3.3	1.8	1.5	2.3	<DL	<DL	1.1	<DL	<DL	<DL	1.3	1.2	<DL	1.5
		2296.97-2297.13	<DL	<DL	1.0	3.4	2.1	0.0	1.8	<DL	20.6	16.4	<DL	1.4	0.0	<DL	0.0	0.2	0.0	0.1	2.1	0.0	<DL	<DL	<DL	14.7
Lower Precipice Sandstone B		2297.13-2297.19	<DL	<DL	<DL	0.1	<DL	<DL	0.6	<DL	<DL	0.5	<DL	0.0	0.0	<DL	<DL	0.1	<DL	<DL	0.2	0.0	<DL	<DL	<DL	0.1
		2298.92	<DL	<DL	<DL	0.3	<DL	0.1	<DL	<DL	<DL	0.5	1.9	1.5	1.1	1.5	<DL	<DL	1.0	<DL	<DL	0.0	1.3	1.4	<DL	<DL
Lower Precipice Sandstone A	2	2307.2	0.1	<DL	5.1	1.8	3.4	0.3	<DL	<DL	2.6	2.8	3.2	3.2	1.0	2.1	<DL	0.5	1.4	<DL	<DL	0.0	2.1	1.5	WR<DL	<DL
		2315.77	<DL	<DL	7.4	0.7	2.3	0.1	<DL	<DL	<DL	5.4	7.5	4.2	3.5	4.0	<DL	<DL	0.9	<DL	<DL	0.0	2.8	3.0	<DL	0.9
		2322.61-2322.73	0.3	<DL	<DL	1.8	3.8	0.1	<DL	<DL	<DL	4.6	2.2	4.0	1.5	4.4	<DL	0.1	1.1	<DL	<DL	0.0	1.7	1.5	<DL	2.1
		2323.25	0.0	<DL	<DL	2.1	4.3	0.1	<DL	<DL	<DL	3.8	4.3	2.7	3.1	3.8	0.7	<DL	0.9	<DL	<DL	0.0	1.8	2.1	<DL	15.0
	1	2328.54-2328.59	0.2	<DL	4.2	0.2	1.6	0.2	0.3	<DL	<DL	0.4	12.6	5.4	5.3	5.7	0.4	0.1	2.6	4.3	<DL	0.1	2.9	0.8	18.2	3.9
		2328.59-2328.68	0.3	<DL	3.9	0.3	5.4	0.1	0.1	<DL	<DL	0.5	7.8	5.3	4.7	3.7	2.0	0.1	2.9	<DL	<DL	0.0	1.3	1.8	93.9	<DL
		2330.41-2330.54	0.1	<DL	<DL	0.8	7.6	0.1	0.0	<DL	<DL	0.5	1.6	2.4	1.4	2.7	<DL	<DL	1.0	<DL	<DL	0.0	1.7	1.0	<DL	9.6
		2338.75-2338.85	<DL	<DL	3.6	0.5	2.7	0.1	<DL	<DL	<DL	0.5	1.6	1.2	3.2	2.4	0.5	0.0	1.5	<DL	<DL	0.0	1.5	1.2	<DL	3.2
Moolayember Formation		2339.00-2339.17	0.4	<DL	5.9	0.1	1.2	0.1	0.3	<DL	<DL	1.5	6.8	4.2	8.7	11.0	4.6	0.1	13.3	10.4	<DL	0.0	11.1	1.6	<DL	3.6
		2340.54-2340.62	0.5	<DL	8.8	9.0	13.5	1.0	0.6	<DL	31.1	23.8	6.4	7.5	9.1	11.6	3.0	0.1	6.9	8.6	<DL	0.0	3.4	0.9	<DL	0.9
		2346.40-2346.51	0.2	<DL	7.9	9.6	10.2	1.0	0.3	1.5	16.2	14.7	12.2	11.2	4.8	7.3	2.3	0.1	4.3	4.9	0.2	0.0	12.2	3.4	21.0	4.1
		2348.16-2348.30	0.2	<DL	8.1	5.6	6.4	0.9	0.3	0.3	5.6	5.0	8.8	6.3	5.2	5.2	1.2	0.1	1.9	4.7	<DL	0.0	1.4	2.8	7.9	0.8
		2356.94-2357.06	0.1	<DL	8.6	11.3	16.7	1.6	0.3	<DL	17.5	16.5	15.9	13.1	6.7	5.9	1.6	0.1	3.0	4.6	<DL	0.0	5.3	1.3	11.5	6.2
		2362.90-2363.00	0.2	<DL	8.2	5.1	10.9	1.2	0.5	<DL	11.7	12.8	17.5	10.9	12.5	5.1	1.7	0.1	6.3	10.1	<DL	0.1	4.6	1.3	<DL	6.2
		2366.50-2366.61	0.1	<DL	8.7	6.0	15.3	2.5	0.5	<DL	9.4	11.2	9.0	6.7	10.2	3.6	1.6	0.1	3.2	4.4	<DL	0.0	3.7	1.0	6.4	<DL
		2373.89-2373.99	0.1	<DL	7.3	7.2	11.8	2.2	0.3	<DL	13.1	13.3	12.6	10.3	3.8	3.3	2.1	0.1	2.5	3.7	0.2	0.0	7.5	2.1	32.3	6.4
		2427.52-2427.74	0.1	<DL	6.0	7.3	0.8	0.7	0.3	0.8	6.1	14.6	10.0	8.1	4.2	3.8	2.3	0.1	2.8	<DL	1.0	0.0	13.5	4.4	49.8	6.3
Unit Medians	Lower Evergreen Formation	WM1	<DL	<DL	5.0	0.3	3.8	0.3	0.2	<DL	<DL	0.9	12.1	7.9	3.5	9.6	1.6	0.0	5.0	5.5	0.3	0.0	3.9	0.5	<DL	4.1
		T153, WW1	2.1	0.5	13.7	22.5	15.1	8.0	1.2	0.0	12.5	15.1	12.5	9.0	9.1	8.6	3.3	2.2	9.5	15.3	<DL	0.2	13.4	3.0	8.7	<DL
	Upper Precipice Sandstone	WM1	0.1	<DL	7.3	7.6	20.8	0.5	0.1	<DL	21.2	15.7	7.5	6.9	3.1	7.1	2.9	0.0	3.7	<DL	<DL	0.0	6.7	1.9	25.3	0.9
		C4, T153, WCG4, WW1	0.9	0.2	11.4	4.9	7.8	0.6	0.6	0.1	8.9	8.0	8.9	6.2	7.1	7.6	2.3	0.4	8.1	11.7	<DL	0.1	9.4	1.6	3.4	<DL
	Lower Precipice Sandstone	WM1	<DL	<DL	2.2	0.3	2.5	0.1	<DL	<DL	<DL	0.5	2.5	2.4	2.1	2.2	<DL	0.0	1.3	<DL	<DL	0.0	1.8	1.1	<DL	1.0
		C4, T153, WCG4, WW1	1.4	0.3	0.8	1.0	0.1	0.5	0.8	<DL	1.5	5.2	7.9	5.6	7.2	5.3	0.9	1.6	6.7	6.2	<DL	0.0	<DL	0.9	<DL	<DL
	Moolayember Formation	WM1	0.2	<DL	8.1	7.2	10.9	1.0	0.3	<DL	11.7	13.3	10.0	8.1	6.7	5.2	2.1	0.1	3.2	4.7	<DL	0.0	5.3	1.6	7.9	4.1
		WCG4, WW1	3.6	0.1	8.6	3.0	10.4	1.7	0.7	0.7	4.4	3.5	10.0	7.3	7.6	4.3	2.5	0.3	4.9	5.4	<DL	0.1	7.3	2.8	<DL	<DL

Colour Legend	Major	Minor	Trace	Ultra-trace	> 75	50 – 75	25 – 50	5 – 25	< 5

1. Tabulated elements were > 10 mg/kg and/or > 10 % median extracted from at least one of the four major rock units (full WM1 data in Appendix A).
2. Other wells studied in previous projects are Chinchilla 4 (C4), Tipton 153 (T153), Woleebee Creek Groundwater Bore 4 (WCG4), and West Wandoan 1 (WW1).

Part C – Combined results of acidic extraction Steps 2 and 3

Overall, there was generally less substantive (i.e., less elements released at > 10 mg/kg) median acid-extraction of several elements (Table 10) from WM1 samples compared with the medians for the collective samples of other well cores including at EPQ7 that we have previously studied. The median amounts of lower Precipice Sandstone acid-extracted elements including Al, As, Ba, Co, Cu, Fe, K, Mg, Mn, Na, Ni, Si, Sr, and Zn were lower from WM1, others like Ca, Pb, and Sb were similar, whereas Cd (albeit very low magnitude), P, and S were higher for WM1. On the other hand, the median amounts of Fe and Mg extracted from WM1 Moolayember Formation samples were greater than those measured from well cores of other sites including EPQ7. Whereas for the limited number of upper Precipice Sandstone samples, median Fe and Mg were lower at WM1 than from other sites including EPQ7. Extraction of Mg correlates with Fe (likely mainly from siderite), Cr with V (micas), Se with Sr (clays?), Ga, Ge, and Y with REEs, and Co with Ni (Figure 15). Acid-extraction of Al, Ba, Bi, Cs, Li, Rb, and Si all appears to be intercorrelated (Figure 16). The elements with > 20 % median acid extraction from WM1 lower Precipice Sandstone are Bi, Co, Cu, Ni, and Pb (Table 11), which is broadly similar behaviour compared to other sites including EPQ7.

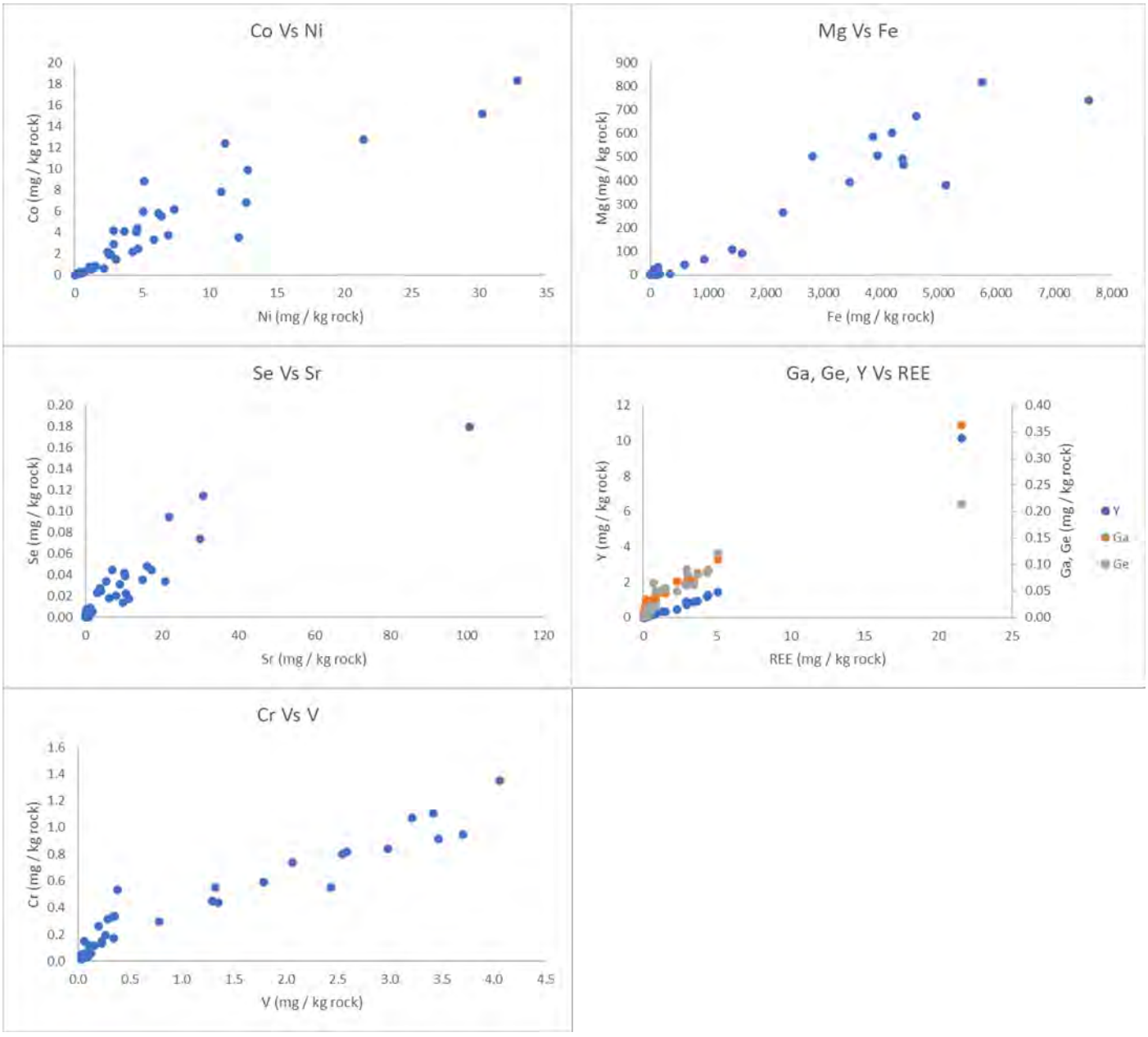

Figure 15: Selected total acid-extracted element correlations (summed data from Steps 2 and 3, powdered WM1 well core samples).

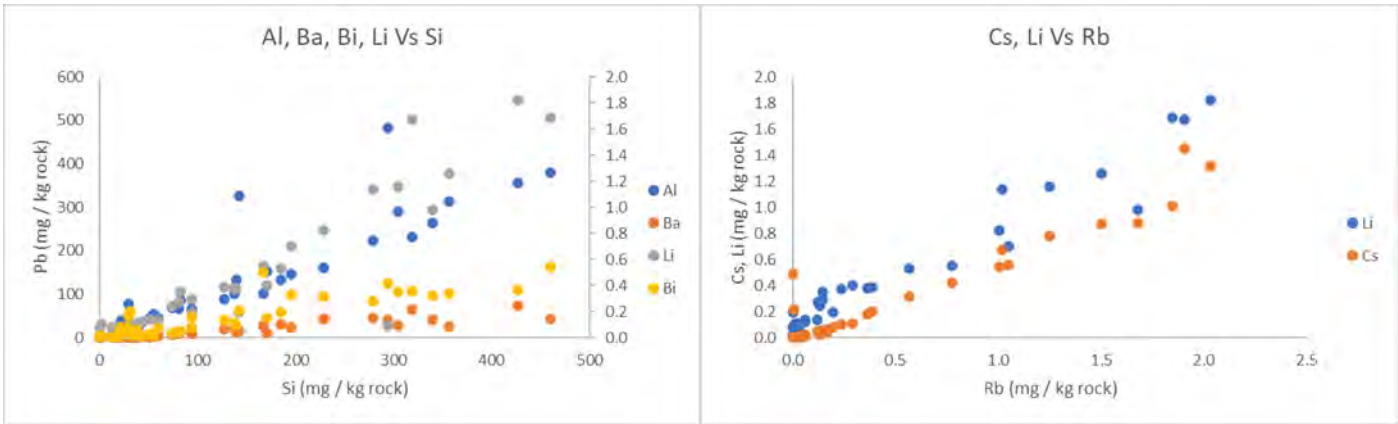

Figure 16: Total acid-extraction of these elements all appears to be correlated with each other (summed data from Steps 2 and 3, powdered WM1 well core samples).

Table 10: Absolute amounts of cumulative weak-acid extraction of selected[1] elements (mg element per kg rock powder) from WM1 core samples, with reference to median values of previous projects' samples from other wells[2].

		Element Set	Alkali metals		Alkaline earth metals					Transition Metals								Post transition metals			Metalloids				Nonmetals	
		Element Group	1		2					6	7	8	9	10	11	12		13	14	15	13	14	15		15	16
Unit		Depth (mRT)	Na	K	Be	Mg	Ca	Sr	Ba	Mo	Mn	Fe	Co	Ni	Cu	Zn	Cd	Al	Pb	Bi	B	Si	As	Sb	P	S
Lower Evergreen Formation		2235.81-2235.94	0.5	<DL	0.1	65	66	3.9	8.4	0.08	12	934	6.8	13	5.2	25	0.3	66	10	0.2	0.2	94	0.5	0.04	<DL	5.6
		2242.25	<DL	<DL	0.4	17	125	11	28	<DL	0.6	119	5.5	6.4	9.1	34	0.3	102	24	0.5	2.4	167	2.1	0.07	<DL	34
		2242.44-2242.54	11	<DL	0.4	34	157	17	43	0.06	<DL	137	18	33	7.6	27	0.3	380	15	0.5	1.1	460	1.2	0.07	3.3	60
Upper Precipice Sandstone		2246.14-2246.25	0.5	<DL	0.04	43	61	0.9	2.1	<DL	8.6	588	0.8	1.6	2.4	6.2	0.3	36	5.1	0.02	<DL	42	1.2	0.06	<DL	2.2
		2254.94-2255.10	1.2	<DL	0.2	92	215	3.1	6.3	0.002	25	1,592	4.2	2.9	1.0	21	0.3	69	6.3	0.04	2.2	74	1.3	0.05	125	4.7
Lower Precipice Sandstone D		2263.61-2263.77	0.005	<DL	0.02	3.2	24	0.2	0.8	<DL	<DL	61	0.7	1.1	3.8	1.6	0.004	19	3.2	0.01	<DL	35	0.9	0.03	28	18
		2267.71-2267.84	<DL	<DL	0.5	1.0	<DL	0.3	0.8	0.001	<DL	25	3.8	7.0	2.9	11	0.09	78	7.7	0.2	1.0	29	1.4	0.02	<DL	<DL
		2267.84-2267.90	<DL	<DL	0.7	9.0	83	6.3	42	0.05	1.2	98	15	30	3.5	7.3	0.09	482	14	0.4	1.3	294	0.6	0.003	<DL	5.6
Lower Precipice Sandstone C		2274.10-2274.18	0.1	<DL	0.04	2.5	13	0.2	0.9	<DL	2.6	111	0.8	1.1	5.0	1.9	0.004	18	2.9	0.08	0.4	28	1.2	0.08	12	47
		2281.82-2281.92	<DL	<DL	0.3	3.9	25	1.8	5.1	0.04	<DL	20	3.3	5.9	2.6	8.2	0.02	45	4.5	0.08	<DL	60	0.8	0.05	12	11
		2284.13-2284.24	0.06	<DL	0.06	0.9	6.5	0.2	1.0	0.05	<DL	9.2	1.4	3.1	1.9	3.0	0.006	23	4.9	0.03	<DL	39	1.3	0.05	8.2	5.4
		2285.05	<DL	<DL	1.2	14	90	9.0	24	0.05	<DL	72	13	21	5.2	30	0.3	147	21	0.3	0.5	195	1.4	0.1	<DL	30
		2288.49-2288.61	<DL	<DL	0.04	1.1	3.8	0.1	0.4	<DL	<DL	6.0	0.6	2.1	4.3	0.8	0.003	15	3.4	0.03	<DL	20	0.4	0.02	4.5	3.9
		2294	<DL	<DL	0.007	1.0	3.6	0.2	0.5	0.07	<DL	12	0.3	0.6	0.4	0.6	0.001	<DL	3.1	0.01	<DL	<DL	0.2	0.02	6.7	9.1
		2296.97-2297.13	<DL	<DL	0.7	1.4	<DL	1.3	17	<DL	0.3	91	6.2	7.4	6.7	9.0	0.09	326	10	0.2	1.2	142	3.3	0.1	<DL	1.8
Lower Precipice Sandstone B		2297.13-2297.19	<DL	<DL	0.03	5.3	3.6	0.003	1.2	<DL	8.9	343	<DL	0.03	2.0	2.0	0.06	38	4.2	0.08	1.3	22	0.05	<DL	<DL	15
		2298.92	<DL	<DL	0.02	1.1	2.1	0.2	0.7	0.04	<DL	9.2	0.2	0.5	0.6	2.6	0.001	6.3	2.4	0.02	<DL	2.1	0.09	0.01	15	2.3
Lower Precipice Sandstone A	2	2307.2	0.3	<DL	0.02	7.6	17	0.5	2.9	0.01	3.6	137	0.3	0.6	3.2	2.7	0.004	53	1.7	0.02	<DL	55	0.1	0.01	77	<DL
		2315.77	<DL	<DL	0.008	3.4	11	0.2	0.7	<DL	<DL	52	0.2	0.4	0.4	1.1	0.006	<DL	0.6	0.008	2.1	19	0.1	0.02	11	0.8
		2322.61-2322.73	0.4	<DL	0.008	3.2	6.9	0.1	1.5	<DL	1.3	72	0.2	0.2	8.2	0.5	0.002	8.2	1.3	0.01	<DL	16	0.07	0.007	14	3.9
		2323.25	0.1	<DL	<DL	2.8	15	0.2	1.1	<DL	0.6	49	0.09	0.3	0.4	1.7	0.006	1.7	0.7	<DL	<DL	12	0.05	0.006	1.7	13
	1	2328.54-2328.59	5.4	<DL	0.9	26	115	9.8	27	0.007	<DL	62	7.8	11	13	3.7	0.3	314	8.6	0.3	1.7	357	0.7	0.12	51	34
		2328.59-2328.68	0.7	<DL	0.07	2.5	13	0.3	1.7	<DL	<DL	11	0.6	1.2	2.2	3.3	0.3	47	4.7	0.03	1.1	51	0.1	0.02	57	<DL
		2330.41-2330.54	0.9	<DL	0.008	1.3	9.0	0.08	0.9	<DL	<DL	4.5	0.2	0.4	13	0.2	0.002	3.0	1.3	0.009	<DL	17	0.08	0.006	5.3	4.5
		2338.75-2338.85	0.3	<DL	0.04	2.2	5.9	0.2	1.1	<DL	<DL	6.5	0.3	0.4	7.4	2.1	0.005	14	2.1	0.06	<DL	38	0.1	0.01	10	1.2
Moolayember Formation		2339.00-2339.17	1.9	<DL	0.6	13	51	4.1	12	0.005	<DL	95	5.8	6.2	5.1	56	0.3	153	17	0.2	<DL	171	4.5	0.2	<DL	30
		2340.54-2340.62	13	<DL	0.4	381	256	16	41	<DL	67	5,122	2.5	4.7	12	27	0.3	265	13	0.3	1.3	339	1.0	0.06	<DL	2.5
		2346.40-2346.51	11	<DL	0.4	587	237	15	32	0.3	52	3,863	12	11	4.2	18	0.3	134	11	0.2	0.3	185	2.5	0.3	60	14
		2348.16-2348.30	6.4	<DL	0.2	504	996	8.0	12	0.2	56	2,818	4.4	4.6	1.7	7.0	0.4	64	7.1	0.08	1.6	94	1.7	0.3	78	121
		2356.94-2357.06	8.1	<DL	0.3	816	431	10	21	<DL	83	5,754	1.9	2.5	3.0	11	0.4	102	9.7	0.1	1.5	137	0.5	0.04	103	8.1
		2362.90-2363.00	16	59	0.5	494	287	30	64	0.003	44	4,376	5.9	5.1	7.6	13	0.3	232	13	0.4	2.1	319	0.3	0.1	<DL	7.9
		2366.50-2366.61	20	<DL	0.4	741	681	22	46	0.009	127	7,609	2.9	2.9	6.3	13	0.4	222	11	0.3	1.0	279	0.3	0.05	90	7.3
		2373.89-2373.99	6.6	<DL	0.2	604	972	7.1	13	<DL	58	4,197	2.2	2.5	1.9	6.9	0.4	134	8.1	0.1	0.05	139	1.1	0.08	100	19
		2427.52-2427.74	12	<DL	0.1	266	18,765	101	8.6	0.03	382	2,303	8.9	5.1	1.2	4.1	0.4	66	4.6	0.05	2.3	80	6.3	0.2	76	134
Unit Medians	Lower Evergreen Formation	WM1	0.5	<DL	0.4	34	125	11	28	0.06	0.6	137	6.8	13	7.6	27	0.3	102	15	0.5	1.1	167	1.2	0.07	<DL	34
		T153, WW1	36	106	0.2	1,095	33,776	61	24	0.004	235	4,253	3.1	2.4	2.0	23	0.04	1,820	12	0.09	<DL	1,010	1.4	0.03	35	<DL
	Upper Precipice Sandstone	WM1	0.9	<DL	0.1	68	138	2.0	4.2	0.001	17	1,090	2.5	2.2	1.7	14	0.3	52	5.7	0.03	1.1	58	1.3	0.05	62	3.5
		C4, T153, WCG4, WW1	27	35	0.2	174	329	9.4	21	0.02	47	2,688	2.2	1.7	2.1	18	0.01	786	8.6	0.06	<DL	328	1.1	0.04	12	<DL
	Lower Precipice Sandstone	WM1	0.002	<DL	0.04	2.7	10	0.2	1.1	<DL	<DL	51	0.6	1.1	3.4	2.4	0.006	21	3.3	0.03	<DL	32	0.3	0.02	9.2	5.0
		C4, T153, WCG4, WW1	10	12	0.02	6.9	14	0.5	3.3	0.02	0.6	89	1.2	1.5	8.6	5.4	0.003	547	2.7	0.02	<DL	148	0.6	0.02	1.1	<DL
	Moolayember Formation	WM1	11	<DL	0.4	504	431	15	21	0.005	58	4,197	4.4	4.7	4.2	13	0.4	134	11	0.2	1.3	171	1.1	0.1	76	14
		WCG4, WW1	44	21	0.1	223	930	3.7	4.7	0.03	45	1,732	3.9	5.8	8.1	11	0.006	462	5.9	0.09	<DL	148	1.0	0.06	<DL	1.3
Colour Legend			Major	Minor	Trace	> 1,000	100 – 1,000			10 – 100		< 10														

1. Tabulated elements were > 10 mg/kg and/or > 10 % median extracted from at least one of the four major rock units (full WM1 data in Appendix A).
2. Other wells studied in previous projects are Chinchilla 4 (C4), Tipton 153 (T153), Woleebee Creek Groundwater Bore 4 (WCG4), and West Wandoan 1 (WW1).

Table 11: Proportional cumulative weak-acid extraction of selected[1] elements (percentage of total amount in rock powder) from WM1 core samples, with reference to median values of previous projects' samples from other wells[2].

		Element Set	Alkali metals		Alkaline earth metals					Transition Metals								Post transition metals			Metalloids				Nonmetals	
		Element Group	1		2					6	7	8	9	10	11	12		13	14	15	13	14	15		15	16
Unit		Depth (mRT)	Na	K	Be	Mg	Ca	Sr	Ba	Mo	Mn	Fe	Co	Ni	Cu	Zn	Cd	Al	Pb	Bi	B	Si	As	Sb	P	S
Lower Evergreen Formation		2235.81-2235.94	0.1	<DL	11.5	6.5	30.0	9.9	4.2	9.9	29.9	21.7	48.7	48.7	22.2	37.0	45.3	0.1	48.5	65.4	1.0	0.0	17.4	8.1	<DL	4.1
		2242.25	<DL	<DL	11.4	0.7	32.2	13.9	6.6	<DL	2.0	1.8	42.3	30.5	20.5	31.2	19.7	0.1	57.8	60.8	4.1	0.1	24.0	8.9	<DL	5.2
		2242.44-2242.54	0.9	<DL	9.1	1.2	38.5	22.1	10.8	2.4	<DL	1.5	63.9	52.4	21.7	20.9	35.8	0.3	43.2	68.7	2.8	0.2	20.3	9.6	1.5	11.9
Upper Precipice Sandstone		2246.14-2246.25	0.1	<DL	8.3	11.7	36.8	2.8	1.0	<DL	37.0	25.3	18.2	21.7	47.3	20.4	100	0.1	38.6	31.7	<DL	0.0	30.1	15.9	<DL	0.7
		2254.94-2255.10	0.1	<DL	24.3	9.0	29.5	5.0	1.4	0.7	16.4	15.1	37.2	35.6	7.3	29.0	94.9	0.1	38.9	59.9	29.5	0.0	29.2	16.1	51.1	1.2
Lower Precipice Sandstone D		2263.61-2263.77	0.0	<DL	6.7	1.4	26.8	1.0	0.5	<DL	<DL	4.9	16.2	19.6	48.6	11.2	2.4	0.1	35.5	34.8	<DL	0.0	29.2	8.1	WR<DL	9.8
		2267.71-2267.84	<DL	<DL	11.1	0.6	20.6	8.2	10.9	1.5	5.0	1.8	37.9	37.5	17.3	6.8	13.3	0.4	40.6	38.6	5.6	0.1	11.5	0.4	<DL	1.1
		2267.84-2267.90	<DL	<DL	19.1	0.1	<DL	0.4	0.2	0.1	<DL	1.0	31.6	29.9	36.4	13.1	22.9	0.1	39.1	59.9	9.8	0.0	31.6	3.6	<DL	<DL
Lower Precipice Sandstone C		2274.10-2274.18	0.0	<DL	9.2	1.3	10.4	0.7	0.6	<DL	3.2	2.8	16.9	14.2	55.2	9.8	4.4	0.1	27.9	69.4	5.4	0.0	29.8	17.9	31.8	3.8
		2281.82-2281.92	<DL	<DL	10.7	0.5	16.5	3.4	2.2	4.5	<DL	0.9	26.4	28.8	17.6	15.3	3.1	0.1	29.7	37.0	<DL	0.0	20.7	9.3	12.1	3.3
		2284.13-2284.24	0.0	<DL	14.8	0.5	13.4	0.8	2.3	17.3	<DL	1.5	20.9	27.2	10.8	14.2	7.9	0.1	63.1	22.6	<DL	0.0	43.3	10.5	WR<DL	6.2
		2285.05	<DL	<DL	20.5	0.7	25.9	11.6	7.4	2.0	<DL	1.2	49.4	45.5	11.6	19.0	24.8	0.2	50.9	57.0	1.2	0.1	25.0	10.4	<DL	3.7
		2288.49-2288.61	<DL	<DL	11.5	0.5	6.2	0.8	1.1	<DL	<DL	0.8	32.1	31.8	60.8	9.6	2.9	0.1	44.5	48.3	<DL	0.0	45.2	8.0	13.3	4.9
		2294	<DL	<DL	3.3	0.9	3.0	0.6	1.0	20.9	<DL	2.4	22.9	12.1	15.0	7.7	0.2	<DL	32.5	32.7	<DL	<DL	14.2	8.9	WR<DL	5.3
		2296.97-2297.13	<DL	<DL	7.4	3.4	2.1	0.0	1.8	<DL	22.5	17.8	<DL	1.4	40.4	14.3	13.9	0.2	30.5	65.7	9.6	0.0	2.2	<DL	<DL	14.7
Lower Precipice Sandstone B		2297.13-2297.19	<DL	<DL	9.5	0.1	<DL	0.7	4.2	<DL	1.1	1.2	18.7	10.1	16.1	6.7	10.3	0.2	27.2	32.0	2.7	0.1	18.4	5.1	<DL	0.1
		2298.92	<DL	<DL	5.3	0.8	2.1	1.1	1.3	8.8	<DL	1.7	18.6	10.7	15.7	19.8	0.9	0.0	33.7	33.9	<DL	0.0	14.6	6.1	4.5	2.5
Lower Precipice Sandstone A	2	2307.2	0.1	<DL	11.8	7.0	11.8	4.1	6.7	4.1	12.6	10.3	27.1	21.3	14.8	24.4	3.2	1.1	32.6	55.7	<DL	0.0	20.9	8.0	WR<DL	<DL
		2315.77	<DL	<DL	7.4	2.0	6.8	1.7	1.5	<DL	<DL	11.8	32.1	18.7	28.4	25.1	8.3	<DL	19.0	30.7	46.1	0.0	23.2	15.8	WR<DL	0.9
		2322.61-2322.73	0.3	<DL	5.2	4.5	8.4	1.2	3.0	<DL	14.8	13.6	24.7	22.3	66.1	19.2	1.2	0.2	33.9	41.6	<DL	0.0	16.6	5.1	WR<DL	13.7
		2323.25	0.0	<DL	<DL	4.6	9.7	1.9	2.5	<DL	6.4	8.3	24.9	11.2	30.3	25.3	5.6	0.0	19.8	<DL	<DL	0.0	13.9	6.0	0.5	26.7
	1	2328.54-2328.59	0.6	<DL	13.8	1.3	36.6	7.8	7.1	0.9	<DL	0.9	35.8	25.5	31.9	13.2	23.1	0.2	27.4	59.8	3.1	0.1	15.9	16.0	18.2	9.2
		2328.59-2328.68	0.3	<DL	11.7	0.9	23.2	1.0	1.7	<DL	<DL	1.2	28.9	25.3	49.4	21.6	83.5	0.1	42.2	42.5	6.4	0.0	15.1	9.4	100	<DL
		2330.41-2330.54	0.1	<DL	4.5	2.4	17.6	0.7	1.4	<DL	<DL	1.7	17.4	23.5	60.2	6.1	2.1	0.0	27.1	46.0	<DL	0.0	20.0	4.3	22.5	9.6
		2338.75-2338.85	0.2	<DL	10.7	1.8	13.2	0.9	2.2	<DL	<DL	1.5	17.4	12.5	68.7	25.7	4.5	0.1	38.0	69.2	<DL	0.0	19.3	8.5	2.9	3.2
Moolayember Formation		2339.00-2339.17	0.4	<DL	22.6	1.2	30.5	6.3	10.7	0.6	<DL	2.9	38.0	33.9	40.1	30.9	57.8	0.2	78.2	69.2	<DL	0.0	43.8	15.6	<DL	5.8
		2340.54-2340.62	1.3	<DL	19.6	11.3	41.9	29.0	12.7	<DL	36.2	27.4	13.3	17.8	35.9	27.9	54.8	0.3	55.5	60.7	4.7	0.1	15.6	8.1	<DL	0.9
		2346.40-2346.51	0.7	<DL	18.9	13.8	21.4	20.4	5.4	11.0	22.6	20.6	55.5	48.0	25.8	20.7	51.8	0.2	50.2	64.1	1.1	0.1	38.3	20.2	21.0	5.0
		2348.16-2348.30	0.5	<DL	17.6	12.2	39.6	10.4	2.6	3.2	8.6	6.7	36.3	25.8	22.9	13.7	55.8	0.1	48.7	57.9	10.0	0.0	4.0	12.0	9.2	1.1
		2356.94-2357.06	0.5	<DL	19.1	15.7	24.8	14.4	3.8	<DL	23.5	22.3	28.8	24.2	27.9	15.1	84.2	0.1	57.0	58.4	7.9	0.0	21.7	6.6	12.1	7.4
		2362.90-2363.00	0.9	0.2	19.7	7.6	36.2	37.9	11.6	0.6	15.5	17.2	50.1	27.8	33.1	13.6	50.5	0.3	46.3	61.3	6.6	0.1	11.3	10.4	<DL	6.2
		2366.50-2366.61	0.4	<DL	16.9	9.0	24.1	28.2	9.0	1.5	13.6	15.8	28.1	17.7	27.6	13.0	55.6	0.3	47.2	57.9	4.8	0.1	12.6	6.0	8.1	4.1
		2373.89-2373.99	0.1	<DL	15.1	11.5	36.5	11.3	2.4	<DL	19.3	18.5	30.6	23.6	19.7	10.1	100	0.2	47.8	60.8	0.2	0.0	30.6	10.1	36.7	19.6
		2427.52-2427.74	0.2	<DL	12.2	11.2	58.6	60.2	1.8	6.3	52.3	20.7	52.4	41.4	22.1	14.4	100	0.2	32.6	50.6	19.0	0.0	55.5	23.3	53.4	54.9
Unit Medians	Lower Evergreen Formation	WM1	0.1	<DL	11.4	1.2	32.2	13.9	6.6	2.4	2.0	1.8	48.7	48.7	21.7	31.2	35.8	0.1	48.5	65.4	2.8	0.1	20.3	8.9	<DL	5.2
		T153, WW1	5.1	1.0	24.8	34.3	62.9	39.5	6.5	1.2	35.2	24.1	28.2	16.8	20.7	30.0	12.2	3.7	46.6	54.0	<DL	0.3	30.6	10.5	8.7	<DL
	Upper Precipice Sandstone	WM1	0.1	<DL	16.3	10.4	33.2	3.9	1.2	0.4	26.7	20.2	27.7	28.6	27.3	24.7	97	0.1	38.8	45.8	14.7	0.0	29.6	16.0	25.5	0.9
		C4, T153, WCG4, WW1	2.5	0.4	24.8	8.9	30.3	5.0	4.5	1.9	12.7	11.0	22.0	14.4	26.0	22.2	4.7	0.7	43.3	39.9	<DL	0.1	27.0	9.1	3.4	<DL
	Lower Precipice Sandstone	WM1	0.0	<DL	10.1	1.1	11.1	1.0	2.0	<DL	<DL	1.7	24.8	21.8	31.1	14.2	5.0	0.1	33.2	42.0	<DL	0.0	19.6	8.1	<DL	3.7
		C4, T153, WCG4, WW1	3.1	1.2	3.6	2.7	4.9	3.3	7.9	8.4	4.0	10.0	36.8	15.1	42.3	25.2	1.5	3.4	38.1	27.9	<DL	0.0	1.4	7.3	<DL	<DL
	Moolayember Formation	WM1	0.5	<DL	18.9	11.3	36.2	20.4	5.4	0.6	19.3	18.5	36.3	25.8	27.6	14.4	55.8	0.2	48.7	60.7	4.8	0.0	21.7	10.4	9.2	5.8
		WCG4, WW1	3.7	0.2	14.0	4.0	17.7	3.1	1.6	3.1	5.5	3.5	25.3	20.1	29.0	12.4	2.8	0.5	39.2	42.7	<DL	0.1	13.1	19.6	<DL	0.2
Colour Legend		Major / Minor	Trace	Ultra-trace	> 75		50 – 75			25 – 50			5 – 25				< 5									

1. Tabulated elements were > 10 mg/kg and/or > 10 % median extracted from at least one of the four major rock units (full WM1 data in Appendix A).
2. Other wells studied in previous projects are Chinchilla 4 (C4), Tipton 153 (T153), Woleebee Creek Groundwater Bore 4 (WCG4), and West Wandoan 1 (WW1).

3.3. Batch reaction experiments with mixed gas

Experiments were run soaking West Moonie 1 core samples with synthetic formation water and N_2 before adding CO_2 containing SO_2, NO and O_2. Experiments were run at 20 MPa and 80°C, to approximate in-situ reservoir PT conditions measured from well logs acquired at West Moonie, and waters were sampled periodically with a range of elements measured. The core samples reacted and discussed here are summarized in Table 12. The summary of three sets of mixed gas experiments is shown below, with figures for the third batch of experiments, together with additional mineralogy data (e.g., XRD), in Appendix C. The lines connecting data points in the batch reactor experiment figures are for visual aid only (to help distinguish between data of different samples) and have been modelled by curve-fitting algorithms in Microsoft Excel.

Table 12: Summary of three sets of batch reactor experiments on West Moonie 1 well core with mixed gas.

Unit	**Depth section (m)**	**label**	**plot colour**	**Summary of XRD minerals**
Upper Precipice Sandstone	2254.94-2255.10	2254.94 m	grey	66% quartz, kaolinite, K-feldspar, trace siderite
Lower Precipice Sandstone C	2284.13-2284.24	2284.13 m	blue	SS with 10% kaolinite and illite/mica
Lower Precipice Sandstone A	2307.20	2307. 20 m	orange	Quartz rich (98%) SS trace kaolinite, illite/mica, sylvite/KCl
Moolayember Formation	2346.40-2346.51	2346.40 m	yellow	44% quartz, with K-feldspar, kaolinite, illite/mica, minor smectite, siderite, calcite
Unit	**Depth section (m)**	**label**	**plot colour**	**Summary of XRD minerals**
Lower Evergreen Formation	2242.44-2242.54	2242.44 m	grey	57% quartz, kaolinite, illite/muscovite, K-feldspar, trace siderite, calcite, dolomite/ankerite
Lower Precipice Sandstone C	2288.49-2288.61	2288.49 m	blue	92% quartz, kaolinite, K-feldspar, trace ankerite
Lower Precipice Sandstone A	2330.41-2330.55	2330.40 m	orange	96% quartz, kaolinite, K-feldspar
Moolayember Formation	2339.00-2339.17	2339.07 m	yellow	74% quartz, kaolinite, trace muscovite/illite
Unit	**Depth section (m)**	**label**	**plot colour**	**Summary of XRD minerals**
Lower Precipice Sandstone D	2263.61-2263.77	2263.61 m	yellow	61% quartz, with K-feldspar, kaolinite, illite/mica, minor smectite, chlorite, siderite/ankerite, calcite
Lower Precipice Sandstone C	2274.10-2274.18	2274.10 m	grey	66% quartz, with K-feldspar, kaolinite, illite/mica, minor chlorite, siderite, ankerite
Lower Precipice Sandstone A	2322.61-2322.73	2322.61 m	blue	94% quartz, with kaolinite, illite/mica, minor K-feldspar, chlorite, siderite/ankerite, pyrite
Lower Precipice Sandstone A	2328.54-2328.59	2328.54 m	orange	37% quartz, 26% kaolinite, 35% illite/mica, minor ankerite

The ex-situ measured pH generally decreased with mixed gas addition (after time 0) and stabilised around pH 6, with electrical conductivity initially variable and mainly stabilising after ~60 days (Figure 17a, b, Figure 18a, b, and Appendix C). Dissolved Ca also generally stabilised from the lower Precipice Sandstone and Moolayember Formation samples; however, the concentrations increased from the upper Precipice Sandstone and lower Evergreen Formation samples (Figure 17c, Figure 18c). This is likely sourced from dissolution of the trace amounts of carbonate cements present. Dissolved Ba also increases from the lower Evergreen Formation and upper Precipice Sandstone samples, and one Moolayember Formation sample and may be sourced from substitution in the dissolving carbonates (Figure 17d, Figure 18d). In addition, Ba increases from a clay-rich lower Precipice Sandstone (along with Sr, Rb, U, Li, Appendix C Figure C1) potentially from reaction of clays. Mg also has an increasing trend from the lower Evergreen Formation and upper Precipice Sandstone samples and one Moolayember Formation sample, again likely sourced from the carbonates and it correlates with Ca from 2254.94 m (Figure 19a, C, Figure 20a). Mn also is likely from carbonates with increasing or initial increasing then decreasing trends from the lower Evergreen Formation

and upper Precipice Sandstone samples respectively (Figure 19b, d, Figure 20b). Mg and Mn increase in concentration from a lower Precipice Sandstone that contains trace ankerite and siderite and have stabilising trends from other lower Precipice Sandstones (Appendix C). Sr and Rb may be at least partly sourced from carbonates and show increases during experiments of Evergreen Formation and lower Precipice Sandstone containing trace carbonates (Figure 20c, d, Appendix C Figure C2). Dissolved K, Si, Al and Li show increasing or stabilising trends from the samples reacted, indicating reaction of silicates such as chlorite and feldspars (Figure 21, Figure 22, Appendix C Figure C3).

The dissolved Fe concentration generally decreased after mixed gas injection and subsequently increased and decreased, likely through precipitation of Fe(hydr)oxides (Figure 23, Figure 24, Appendix C Figure C4). Other elements such as Pb, Mo, Cr, Se also mainly show initially increasing and subsequently stabilising or decreasing trends indicating subsequent adsorption or co-precipitation (Figure 23, Figure 24, Figure 25, Figure 26, Appendix C). Chromium from lower Precipice Sandstone 2284.13 m, however, had an increasing trend, along with Co, Zn, Pb, Ni, As, and U from this sample (Figure 26 – Figure 28). Cu and Mo had increasing trends only from lower Precipice 2322.61 m that contained trace ankerite, pyrite and chlorite. Overall, in all experiments, Co and Zn had stabilising or increasing trends. Dissolved As from the two Moolayember Formation experiments had increasing trends, and apart from the 2284.13 m lower Precipice sample, As and Pb from other samples generally stabilised or decreased (Figure 25a, Figure 26a, Figure 27b, Figure 28b). Concentrations of Pb and As, however, remained below 30 µg/kg (30 ppb).

3.3.1. Comparison to EQP7 lower Precipice Sandstone mixed gas experiments

The dissolved concentration of elements such as Pb, Cu, Mo and Cd during EPQ 10 West Moonie 1 core lower Precipice Sandstone reactions with mixed gas are lower than or comparable with EPQ 7 (West Wandoan 1 and Woleebee Creek core) lower Precipice Sandstone experiments where increasing or stabilisation trends were observed (Golding et al., 2019). EPQ10 West Moonie 1 lower Precipice Sandstone samples mostly show initial increases and subsequent decreases in Pb concentrations, whereas 2284.13 m and 2288.51 m have a slightly increasing trend (along with a Moolayember sample). The Pb concentrations are overall lower or comparable to EPQ7 experiments where increasing and decreasing or stabilisation trends were observed. Mo concentrations are higher from West Moonie 1 core (compared to EPQ7); however, the initial increases trend to subsequent decreases in concentration. Cd concentrations are generally lower in West Moonie 1 experiments than West Wandoan 1 experiments. The concentration of U in EPQ 7 experiments was almost an order of magnitude higher than West Moonie 1 experiments, especially from quartz rich sandstones, in general though they were low overall, below 6 and 1.6 µg/kg respectively in EPQ7 and EPQ10. The West Moonie 1 experimental dissolved As trend is generally an initial increase and subsequent decrease, with an increasing concentration from two Moolayember, one lower Precipice Sandstone 2284.13 m, and increasing and stabilising trend from lower Precipice Sandstone 2263.61 m; however, concentrations remain below 30 µg/kg. EPQ 7 experiments had As concentrations with initial increases and subsequent decreases likely from adsorption to precipitated Fe-oxide/hydroxide, concentrations also remained below 30 µg/kg. Cr, Cu and Zn have increasing or stabilising trends in West Moonie 1 lower Precipice Sandstone experiments but have comparable concentrations to those from EPQ 7 experiments (Golding et al., 2019). The released concentrations of Ca, Mg, Mn, Sr, Zn, Ba have increasing trends from several samples that contain carbonates and are highest from West Moonie 1 upper Precipice Sandstone and Moolayember Formation, when compared to the lower Precipice Sandstone, consistent with a higher carbonate mineral content in the upper Precipice Sandstone. Quartz rich lower Precipice Sandstones from West Moonie 1 generally show stabilising concentrations of Ca, Mg, Mn, Sr, Ba, with increasing trends from one clay rich sample.

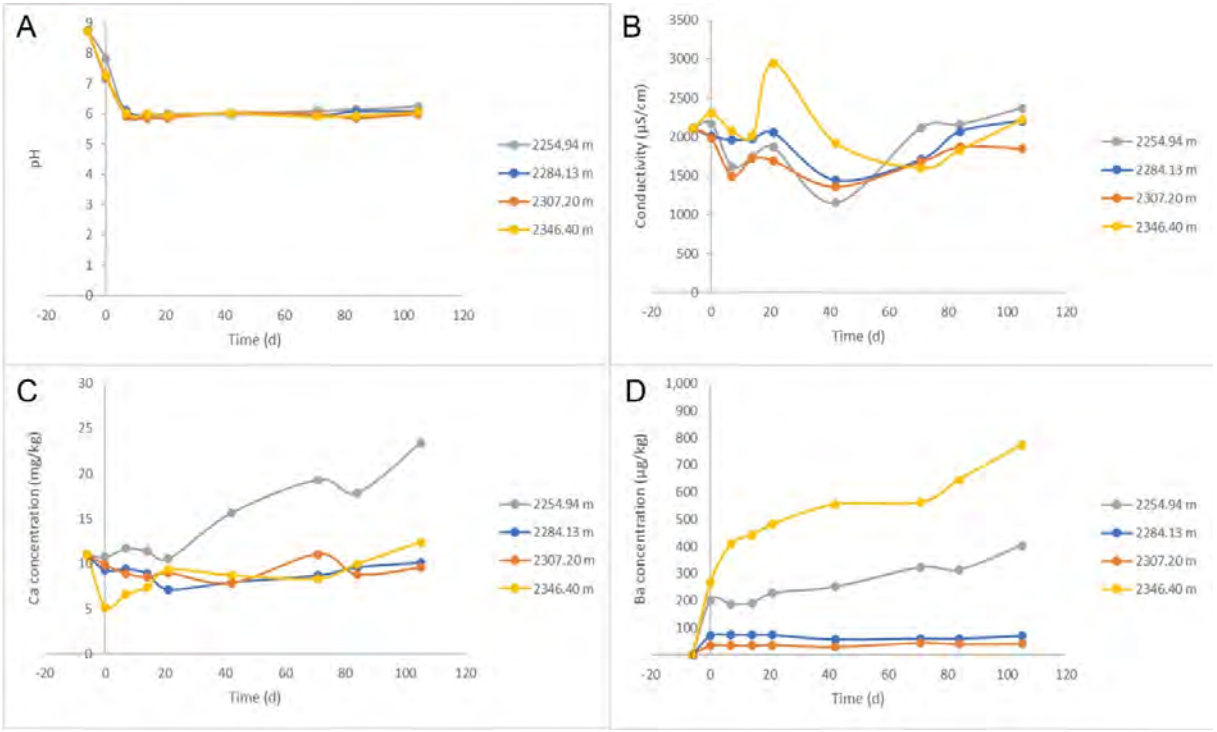

Figure 17: EPQ 10 West Moonie 1 core: a) Ex situ pH, b) electrical conductivity, c) dissolved Ca(mg/kg), and d) dissolved Ba concentration (µg/kg) during batch reaction of lower Precipice Sandstone, upper Precipice Sandstone and Moolayember Formation with O_2-NO-SO_2-CO_2. Negative time is the initial water composition and N_2 rock soak, after time zero mixed gas was added. The 2254.94 m in grey is upper Precipice Sandstone core, the two shown from 2284.13 m and 2307.20 m are lower Precipice Sandstone, the Moolayember Formation sample 2346.40 m is shown in yellow.

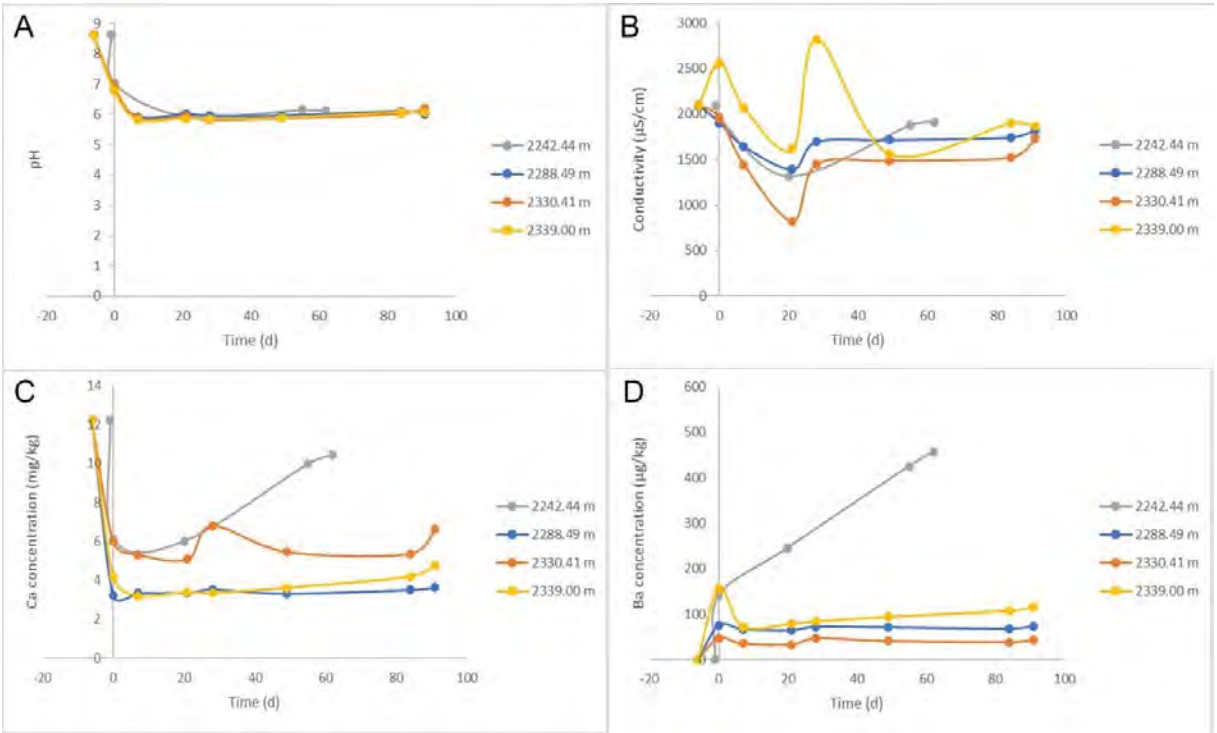

Figure 18: EPQ 10 West Moonie 1 core: a) Ex situ pH, b) electrical conductivity, c) dissolved Ca(mg/kg), and d) dissolved Ba concentration (µg/kg) during batch reaction of lower Precipice Sandstone, lower Evergreen Formation and Moolayember Formation samples with O_2-NO-SO_2-CO_2. Negative time is the initial water composition and N_2 rock soak, after time zero mixed gas was added. The 2242.44 m in grey is lower Evergreen Formation core, the two shown from 2288.49 m and 2330.41 m are lower Precipice Sandstone, the Moolayember Formation sample 2339.00 m is shown in yellow.

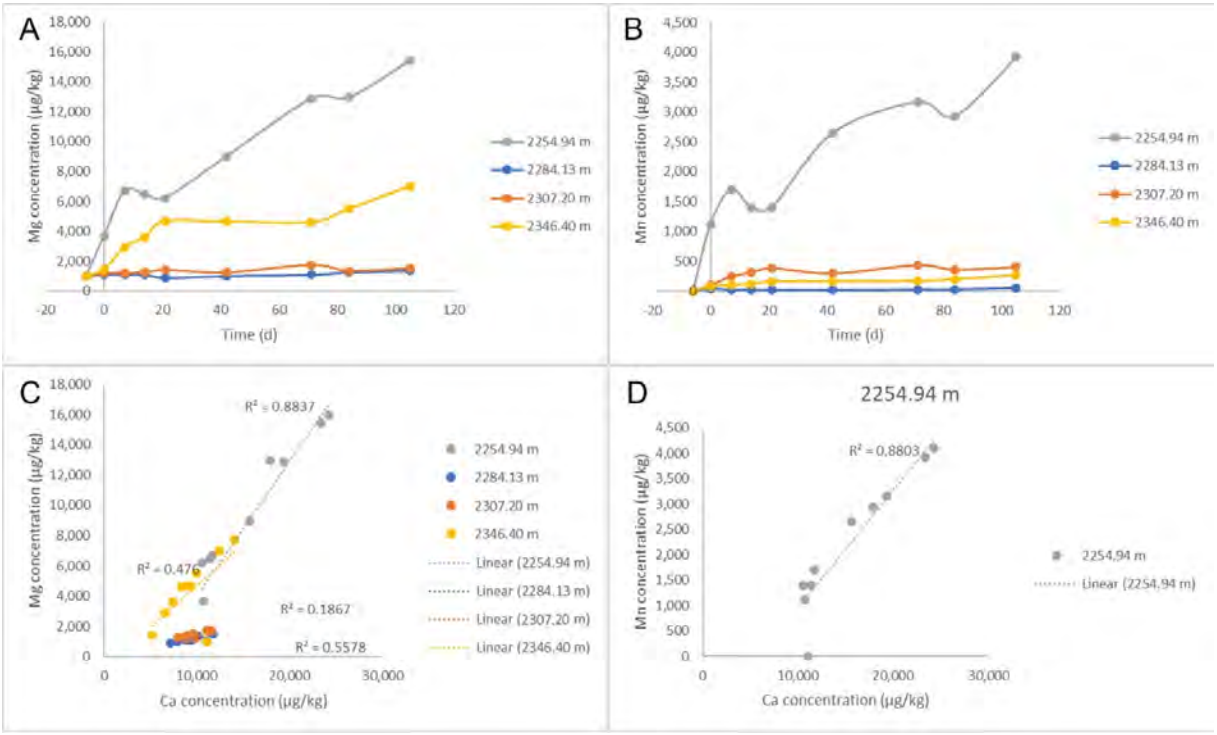

Figure 19: EPQ 10 West Moonie 1 core: Concentrations of a) dissolved Mg (µg/kg), b) dissolved Mn (µg/kg), c) dissolved Mg vs Ca, and d) dissolved Mn vs Ca, during batch reaction of lower Precipice Sandstone, upper Precipice Sandstone and Moolayember Formation with O_2-NO-SO_2-CO_2. Negative time is the initial water composition and N_2 rock soak, after time zero mixed gas was added. The 2254.94 m in grey is upper Precipice Sandstone core, the two shown from 2284.13 m and 2307.20 m are lower Precipice Sandstone, the Moolayember Formation sample 2346.40 m is shown in yellow.

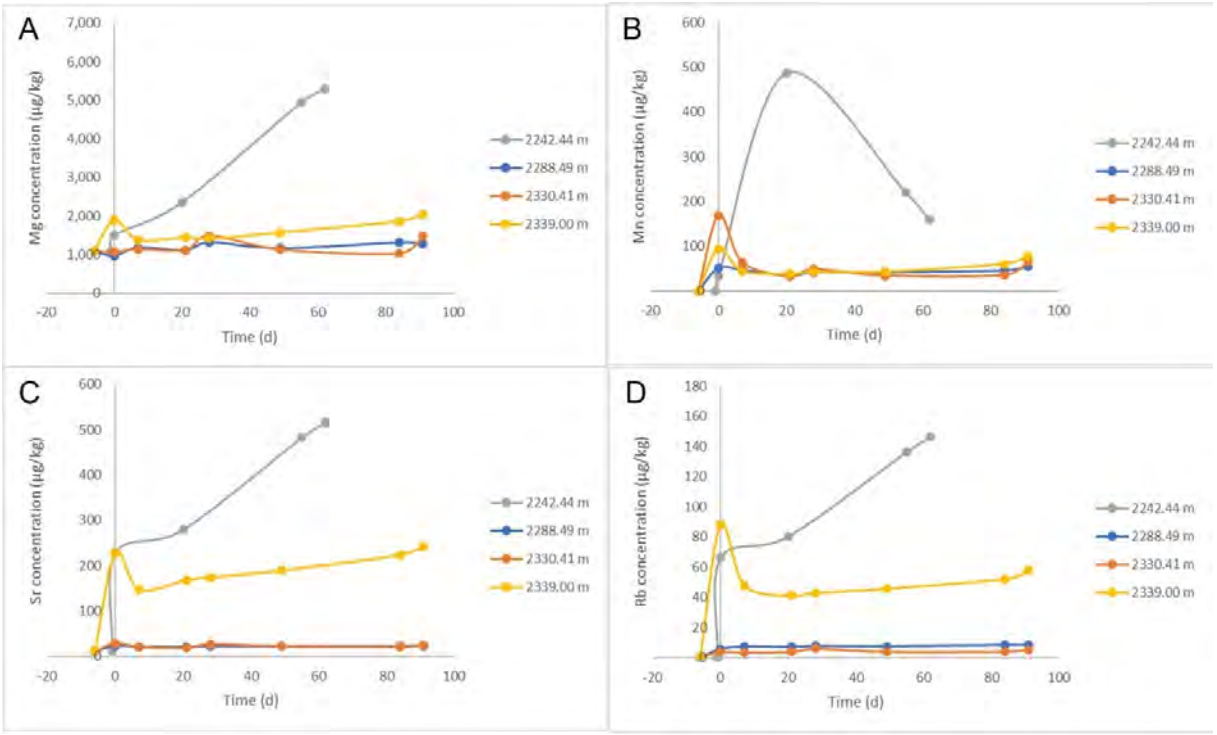

Figure 20: EPQ 10 West Moonie 1 core: Concentrations of a) dissolved Mg (µg/kg), b) dissolved Mn (µg/kg), c) dissolved Sr (µg /kg), and d) dissolved Rb concentration (µg/kg) during batch reaction of lower Precipice Sandstone, lower Evergreen Formation and Moolayember Formation samples with O_2-NO-SO_2-CO_2. Negative time is the initial water composition and N_2 rock soak, after time zero mixed gas was added. The 2242.44 m in grey is lower Evergreen Formation core, the two shown from 2288.49 m and 2330.41 m are lower Precipice Sandstone, the Moolayember Formation sample 2339.00 m is shown in yellow.

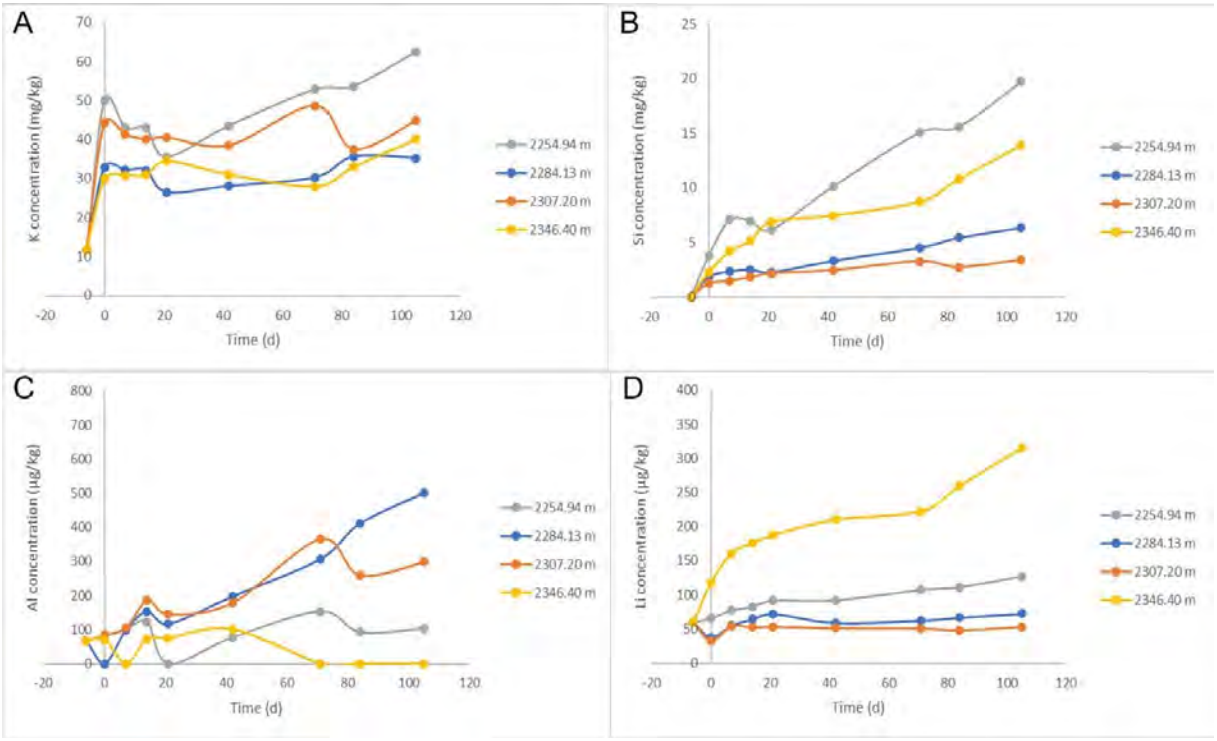

Figure 21: EPQ 10 West Moonie 1 core: Concentrations of a) dissolved K (mg/kg), b) dissolved Si (mg/kg), c) dissolved Al (µg /kg), and d) dissolved Li concentration (µg/kg) during batch reaction of lower Precipice Sandstone, upper Precipice Sandstone and Moolayember Formation with O_2-NO-SO_2-CO_2. Negative time is the initial water composition and N_2 rock soak, after time zero mixed gas was added. The 2254.94 m in grey is upper Precipice Sandstone core, the two shown from 2284.13 m and 2307.20 m are lower Precipice Sandstone, the Moolayember Formation sample 2346.40 m is shown in yellow.

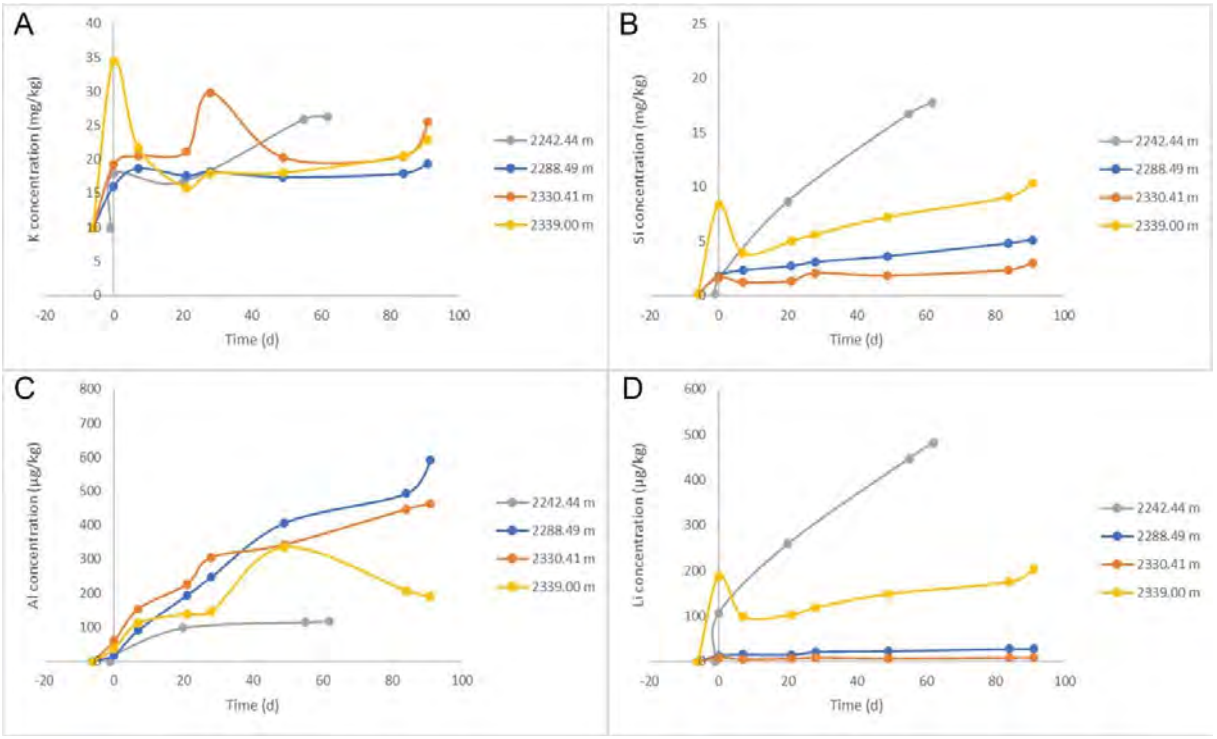

Figure 22: EPQ 10 West Moonie 1 core: Concentrations of a) dissolved K (mg/kg), b) dissolved Si (mg/kg), c) dissolved Al (µg /kg), and d) dissolved Li concentration (µg/kg) during batch reaction of lower Precipice Sandstone, lower Evergreen Formation and Moolayember Formation samples with O_2-NO-SO_2-CO_2. Negative time is the initial water composition and N_2 rock soak, after time zero mixed gas was added. The 2242.44 m in grey is lower Evergreen Formation core, the two shown from 2288.49 m and 2330.41 m are lower Precipice Sandstone, the Moolayember Formation sample 2339.00 m is shown in yellow.

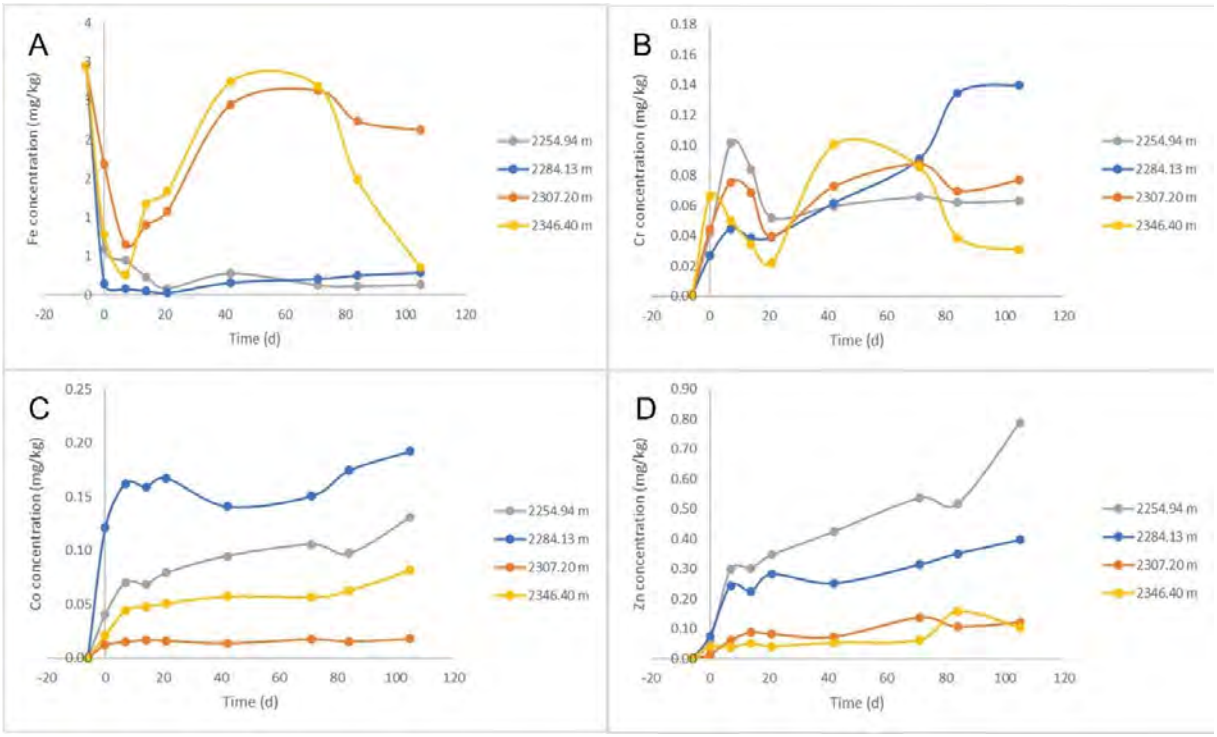

Figure 23: EPQ 10 West Moonie 1 core: Concentrations of a) dissolved Fe (mg/kg), b) dissolved Cr (mg/kg), c) dissolved Co (mg/kg), d) dissolved Zn (mg/kg), during batch reaction of lower Precipice Sandstone, upper Precipice Sandstone and Moolayember Formation with O_2-NO-SO_2-CO_2. Negative time is the initial water composition and N_2 rock soak, after time zero mixed gas was added. The 2254.94 m in grey is upper Precipice Sandstone core, the two shown from 2284.13 m and 2307.20 m are lower Precipice Sandstone, the Moolayember Formation sample 2346.40 m is shown in yellow.

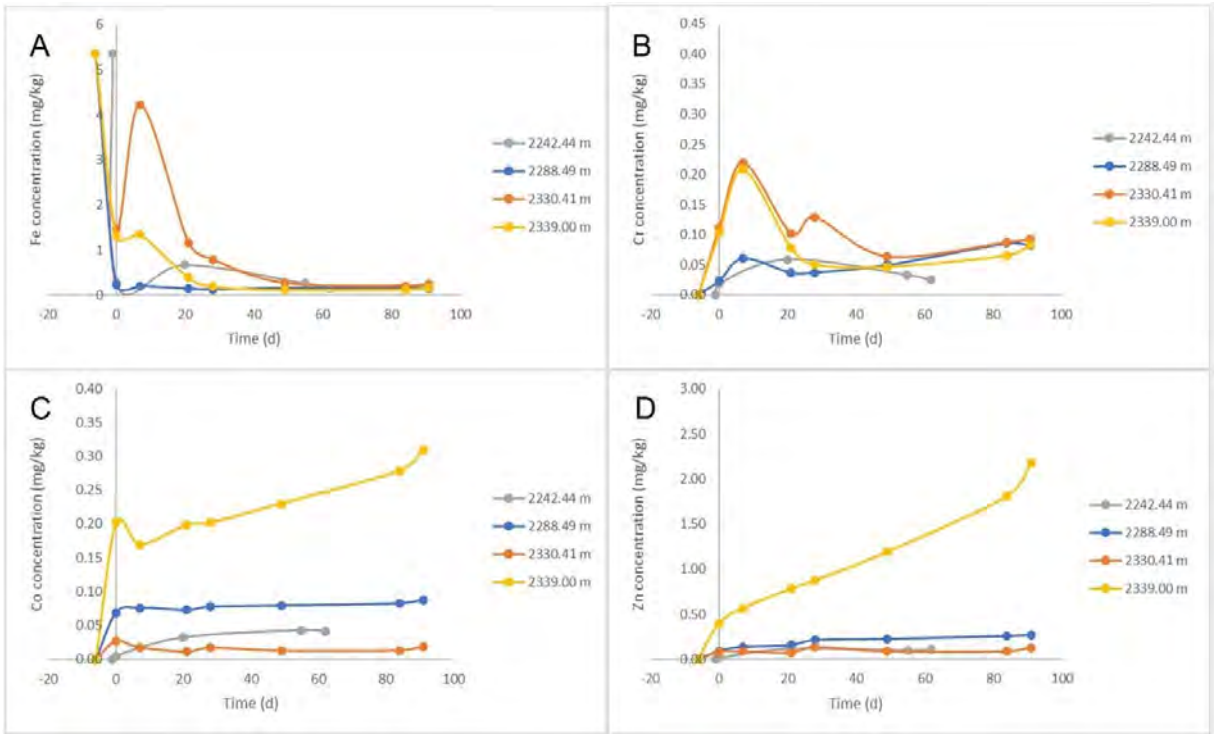

Figure 24: EPQ 10 West Moonie 1 core: Concentrations of a) dissolved Fe (mg/kg), b) dissolved Cr (mg/kg), c) dissolved Co (mg/kg), d) dissolved Zn (mg/kg) during batch reaction of lower Precipice Sandstone, lower Evergreen Formation and Moolayember Formation samples with O_2-NO-SO_2-CO_2. Negative time is the initial water composition and N_2 rock soak, after time zero mixed gas was added. The 2242.44 m in grey is lower Evergreen Formation core, the two shown from 2288.49 m and 2330.41 m are lower Precipice Sandstone, the Moolayember Formation sample 2339.00 m is shown in yellow.

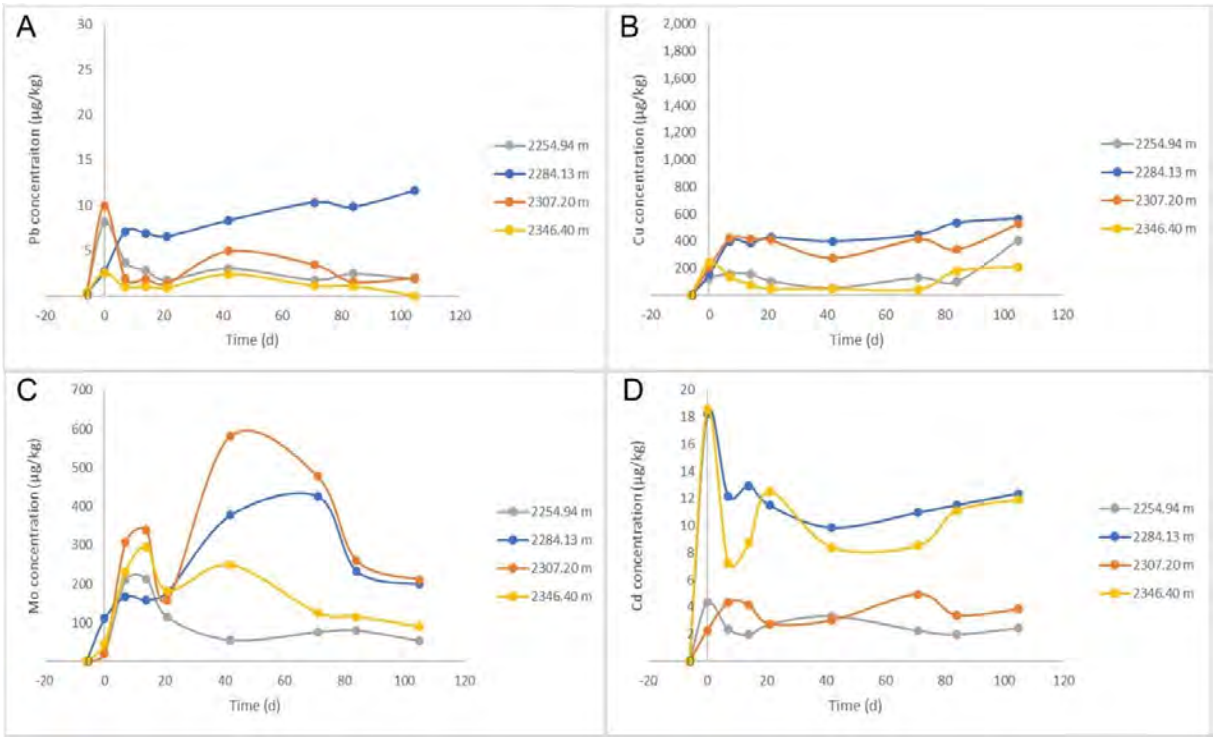

Figure 25: EPQ 10 West Moonie 1 core: Concentrations of a) dissolved Pb (µg/kg), b) dissolved Cu (µg/kg), c) dissolved Mo (µg/kg), d) dissolved Cd (µg/kg), during batch reaction of lower Precipice Sandstone, upper Precipice Sandstone and Moolayember Formation with O_2-NO-SO_2-CO_2. Negative time is the initial water composition and N_2 rock soak, after time zero mixed gas was added. The 2254.94 m in grey is upper Precipice Sandstone core, the two shown from 2284.13 m and 2307.20 m are lower Precipice Sandstone, the Moolayember Formation sample 2346.40 m is shown in yellow.

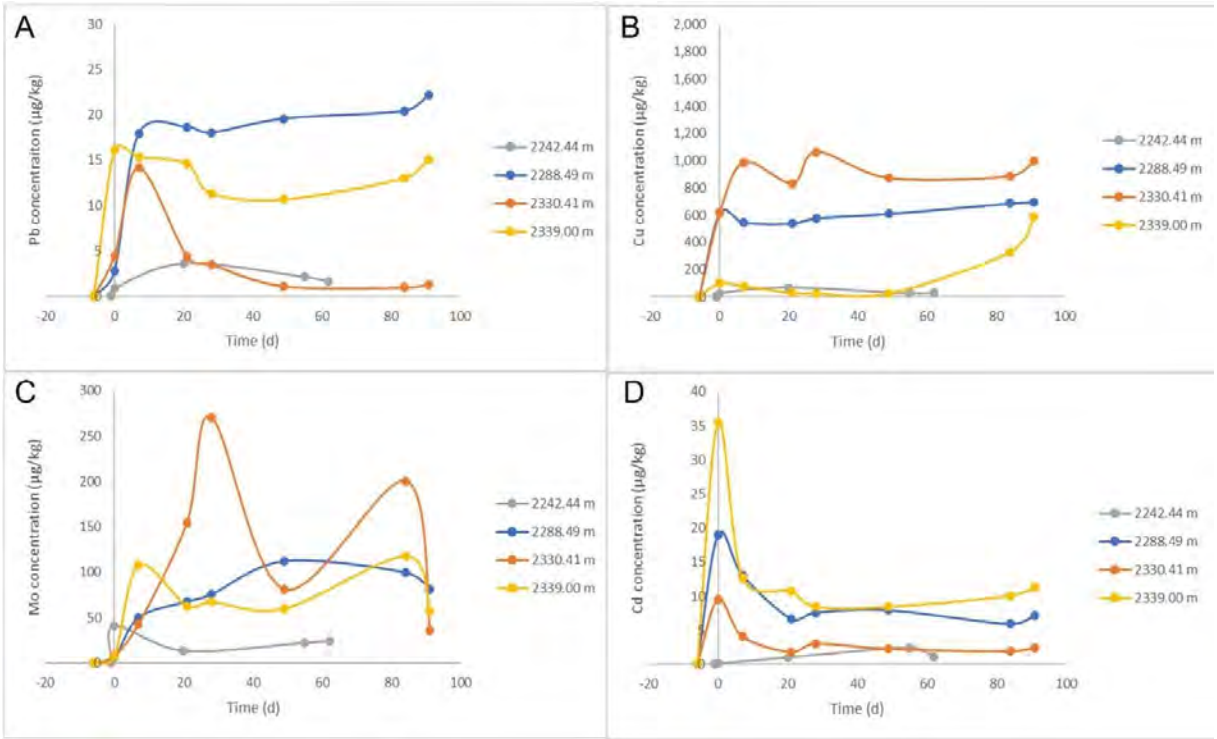

Figure 26: EPQ 10 West Moonie 1 core: Concentrations of a) dissolved Pb (µg/kg), b) dissolved Cu (µg/kg), c) dissolved Mo (µg/kg), d) dissolved Cd (µg/kg), during batch reaction of lower Precipice Sandstone, lower Evergreen Formation and Moolayember Formation samples with O_2-NO-SO_2-CO_2. Negative time is the initial water composition and N_2 rock soak, after time zero mixed gas was added. The 2242.44 m in grey is lower Evergreen Formation core, the two shown from 2288.49 m and 2330.41 m are lower Precipice Sandstone, the Moolayember Formation sample 2339.00 m is shown in yellow.

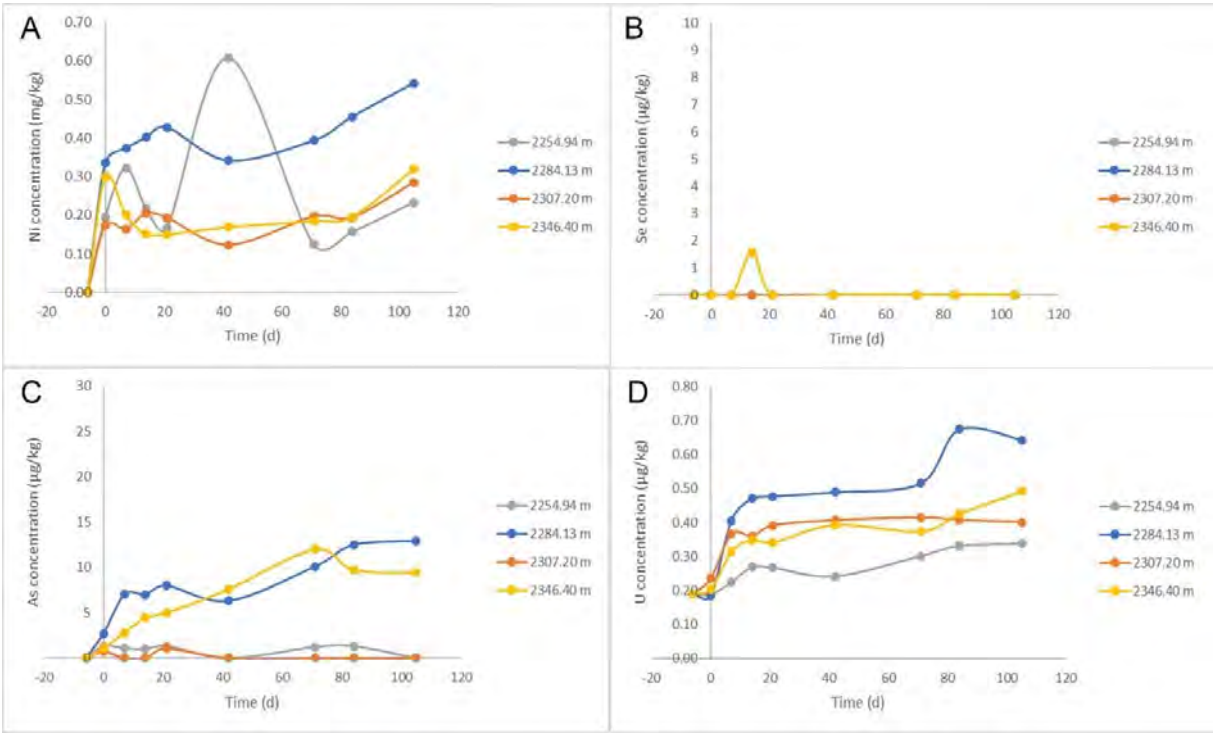

Figure 27: EPQ 10 West Moonie 1 core: Concentrations of a) dissolved Ni (mg/kg), b) dissolved Se (µg/kg), c) dissolved As (µg/kg), d) dissolved U (µg/kg), during batch reaction of lower Precipice Sandstone, upper Precipice Sandstone and Moolayember Formation with O_2-NO-SO_2-CO_2. Negative time is the initial water composition and N_2 rock soak, after time zero mixed gas was added. The 2254.94 m in grey is upper Precipice Sandstone core, the two shown from 2284.13 m and 2307.20 m are lower Precipice Sandstone, the Moolayember Formation sample 2346.40 m is shown in yellow.

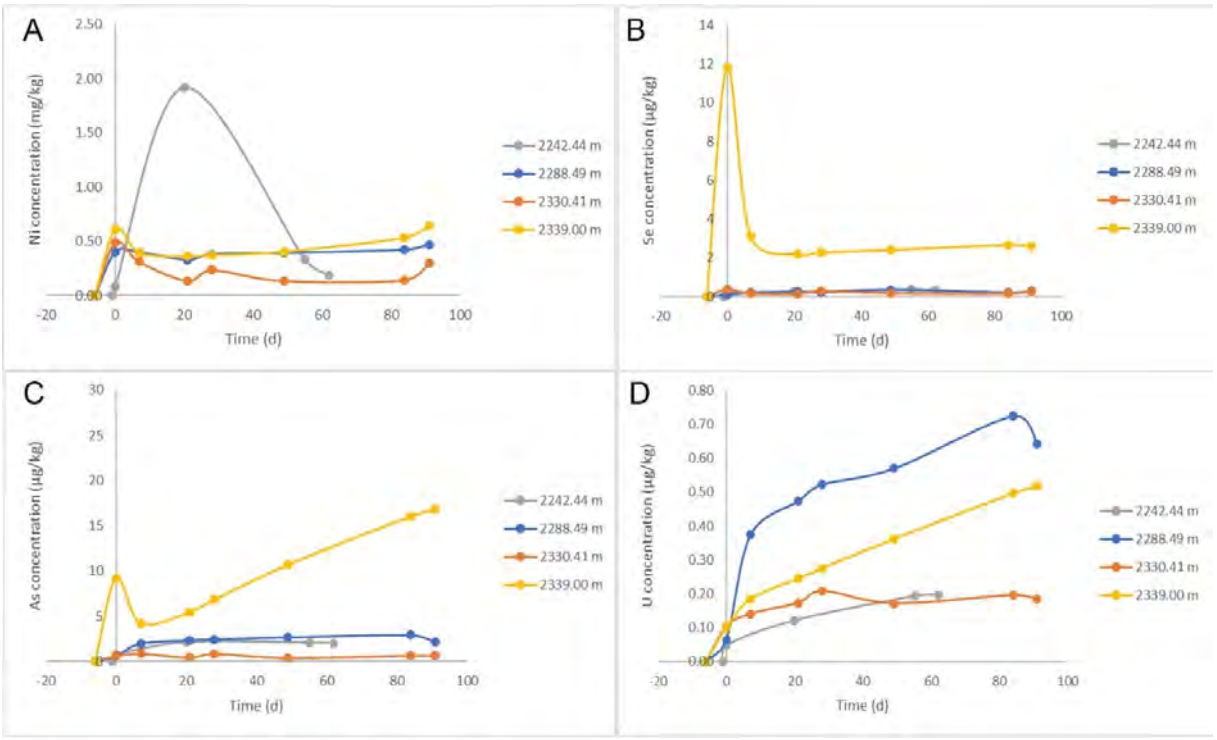

Figure 28: EPQ 10 West Moonie 1 core: Concentrations of a) dissolved Ni (mg/kg), b) dissolved Se (µg/kg), c) dissolved As (µg/kg), d) dissolved U (µg/kg), during batch reaction of lower Precipice Sandstone, lower Evergreen Formation and Moolayember Formation samples with O_2-NO-SO_2-CO_2. Negative time is the initial water composition and N_2 rock soak, after time zero mixed gas was added. The 2242.44 m in grey is lower Evergreen Formation core, the two shown from 2288.49 m and 2330.41 m are lower Precipice Sandstone, The Moolayember Formation sample 2339.00 m is shown in yellow.

3.4. Batch reaction experiments with pure CO_2

Four Precipice Sandstone samples were reacted with pure CO_2; this was vital for the geochemical model input data parameterisation described in later chapters. The three lower and one upper Precipice Sandstone samples reacted are summarised in Table 13.

Table 13: Summary of pure CO_2 batch experiments.

Unit	Depth section (m)	label	plot colour	Summary of XRD minerals
Upper Precipice Sandstone	2254.94-2255.10	2254.94 m	yellow	66% quartz, kaolinite, K-feldspar, trace siderite/ankerite
Lower Precipice Sandstone D	2263.61-2263.77	2263.61 m	grey	61% quartz, with K-feldspar, kaolinite, illite/mica, minor smectite, chlorite, siderite/ankerite, calcite
Lower Precipice Sandstone C	2288.49-2288.61	2288.49 m	blue	92% quartz, kaolinite, K-feldspar, trace ankerite
Lower Precipice Sandstone A	2307.20	2307. 20 m	orange	Quartz rich (98%) SS trace kaolinite, illite/mica, sylvite/KCl

Major elements and some minor elements from the lower Precipice Sandstones including Ca, Ba, Mg, Mn, Sr, Rb, Si, K, Li, and Cu initially increased in concentration and subsequently stabilised on reaction with pure CO_2 (Figures 29 to 33). Dissolved Ca, Ba, Mg, Mn, Sr, Rb, Si, K, Li, and Cu however generally increased through mineral dissolution from the upper Precipice Sandstone sample 2254.94 m that contained trace siderite/ankerite (Figures 29 to 33). Dissolved Al, Fe, Cr, Cd, Mo, Zn, Co, Ni, Se, U mainly increased initially and subsequently decreased or stabilised (Figures 29 to 34). The concentration of As initially increased before CO_2 injection likely from ion exchange (mainly from 2263.61 m and 2288.49 m) but subsequently decreased (Figure 32). Generally, Pb also increased before CO_2 injection, mainly again from 2263.61 m and 2288.49 m that contained trace carbonates (Figure 33). Generally, Pb subsequently decreased, however Pb, Ni, U, and Co from 2288.49 m gradually increased and subsequently stabilised. The maximum Pb released was higher in the 2263.61 m and 2288.49 m lower Precipice Sandstone pure CO_2 experiments compared to mixed gas experiments. The concentrations however decreased to below 10 µg/kg by the end of experiments. The formation of Fe-hydroxides in mixed gas experiments likely resulted in the overall lower Pb.

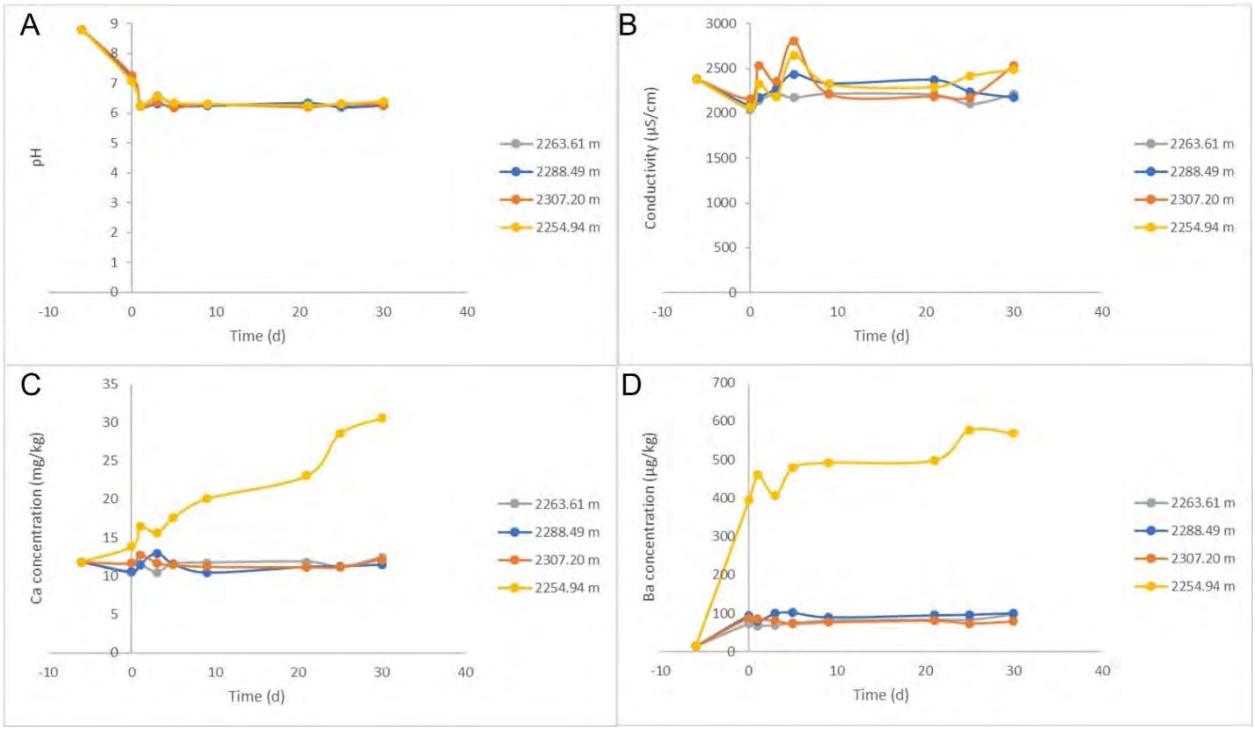

Figure 29: EPQ 10 West Moonie 1 core: a) Ex situ pH, b) electrical conductivity, c) dissolved Ca(mg/kg), and d) dissolved Ba concentration (µg/kg) during batch reaction of lower Precipice Sandstone and upper Precipice Sandstone with pure CO_2. Negative time is the initial water composition and N_2 rock soak, after time zero CO_2 gas was added. The 2254.94 m in yellow is upper Precipice Sandstone core, the other samples in grey, blue and orange are lower Precipice Sandstones.

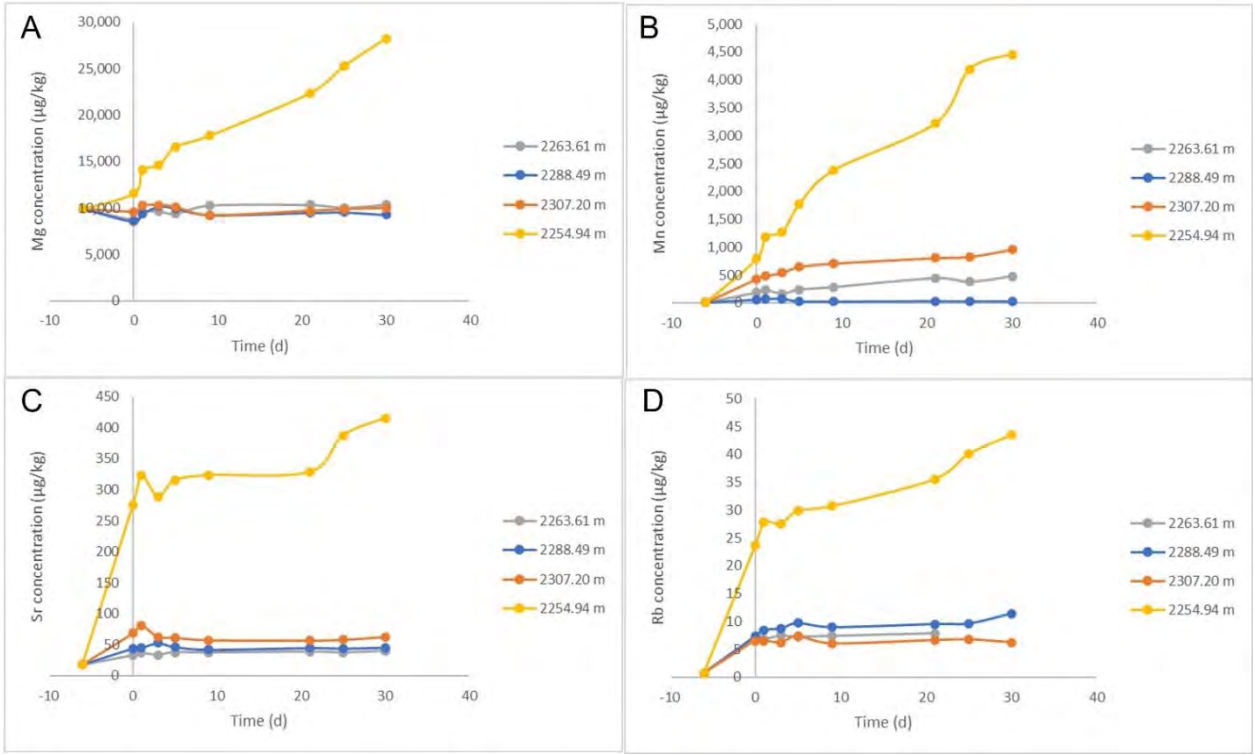

Figure 30: EPQ 10 West Moonie 1 core: Concentrations of a) dissolved Mg (µg/kg), b) dissolved Mn (µg/kg), c) dissolved Sr (µg/kg), and d) dissolved Rb (µg/kg), during batch reaction of lower Precipice Sandstone and upper Precipice Sandstone with pure CO_2. Negative time is the initial water composition and N_2 rock soak, after time zero CO_2 gas was added. The 2254.94 m in yellow is upper Precipice Sandstone core, the other samples in grey, blue and orange are lower Precipice Sandstones.

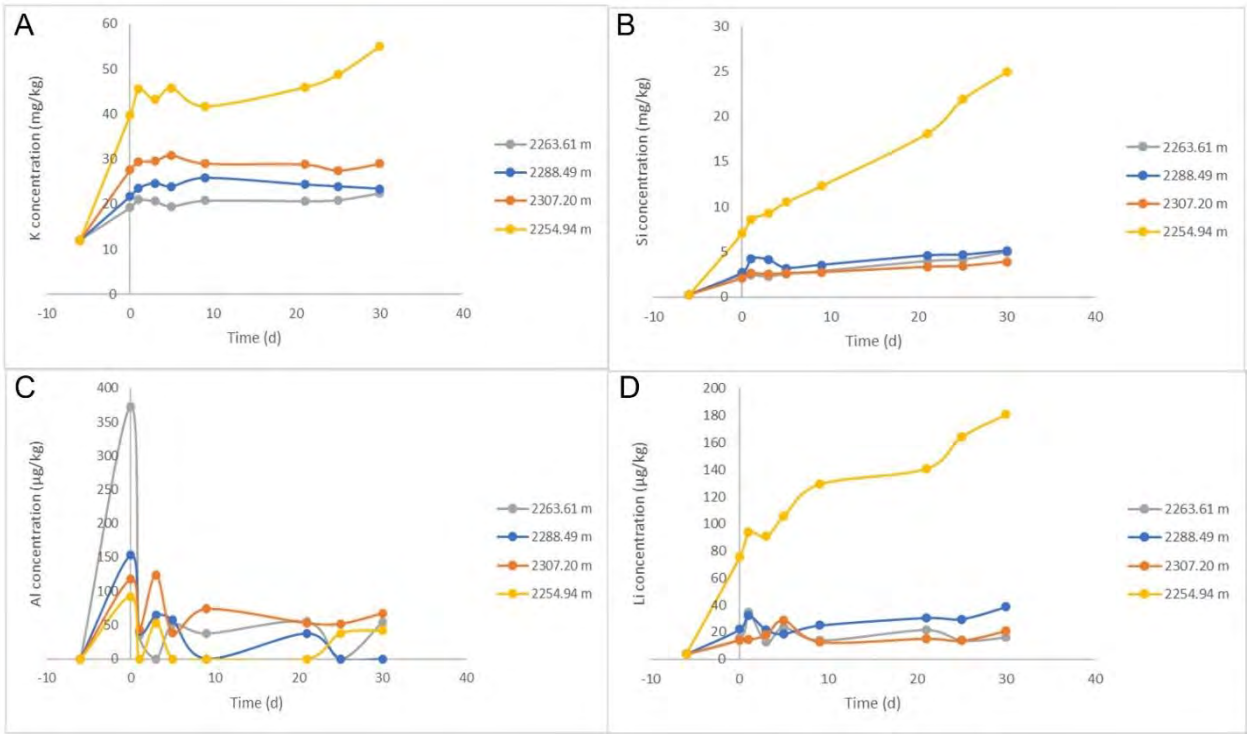

Figure 31: EPQ 10 West Moonie 1 core: Concentrations of a) dissolved K (mg/kg), b) dissolved Si (mg/kg), c) dissolved Al (µg /kg), and d) dissolved Li concentration (µg/kg) during batch reaction of lower Precipice Sandstone and upper Precipice Sandstone with pure CO_2. The 2254.94 m in yellow is upper Precipice Sandstone core, the other samples in grey, blue and orange are lower Precipice Sandstones.

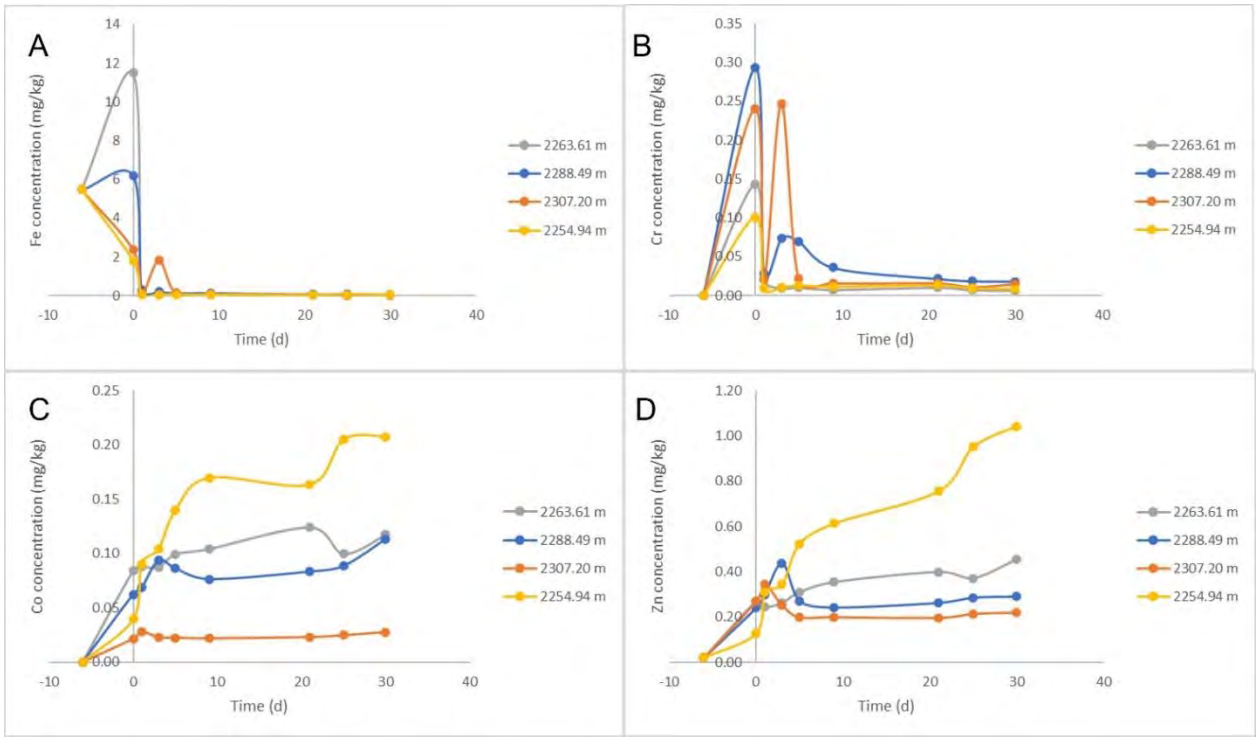

Figure 32: EPQ 10 West Moonie 1 core: Concentrations of a) dissolved Fe (mg/kg), b) dissolved Cr (mg/kg), c) dissolved Co (mg/kg), and d) dissolved Zn concentration (mg/kg) during batch reaction of lower Precipice Sandstone and upper Precipice Sandstone with pure CO_2. The 2254.94 m in yellow is upper Precipice Sandstone core, the other samples in grey, blue and orange are lower Precipice Sandstones.

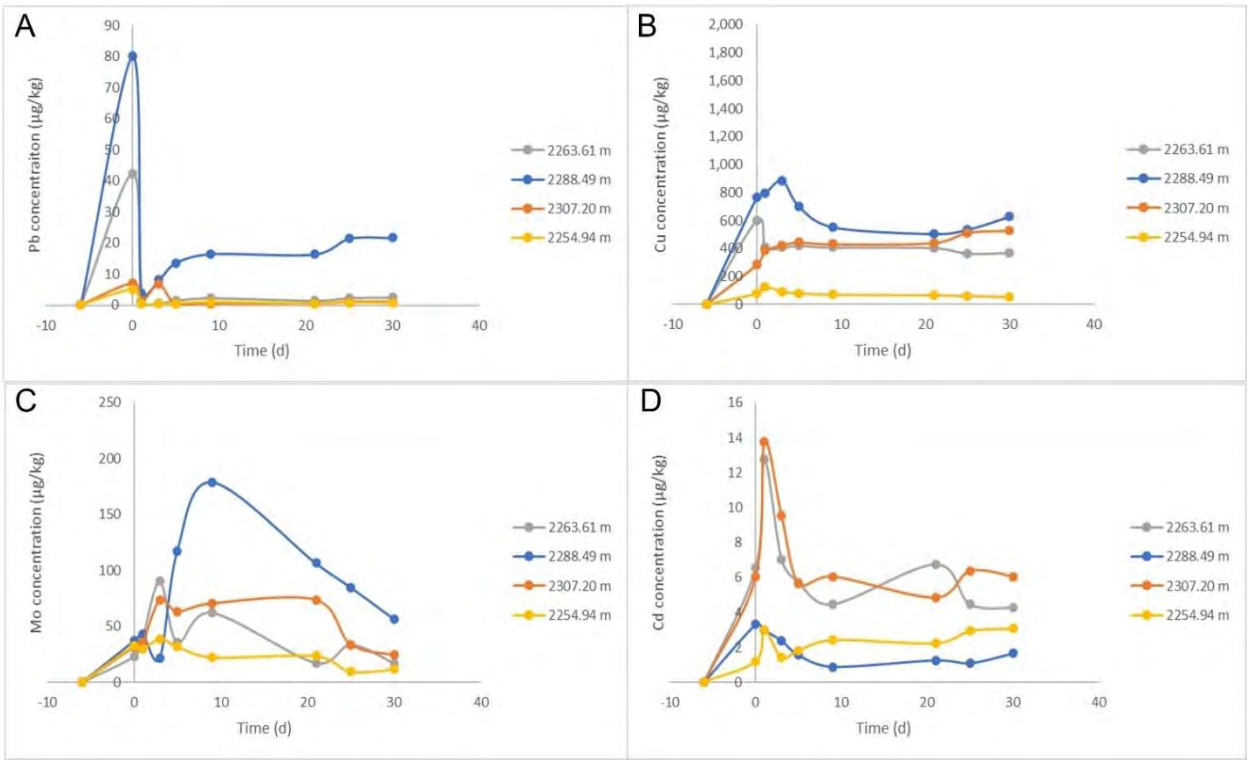

Figure 33: EPQ 10 West Moonie 1 core: Concentrations of a) dissolved Pb (µg/kg), b) dissolved Cu (µg/kg), c) dissolved Mo (µg/kg), and d) dissolved Cd concentration (µg/kg) during batch reaction of lower Precipice Sandstone and upper Precipice Sandstone with pure CO_2. The 2254.94 m in yellow is upper Precipice Sandstone core, the other samples in grey, blue and orange are lower Precipice Sandstones.

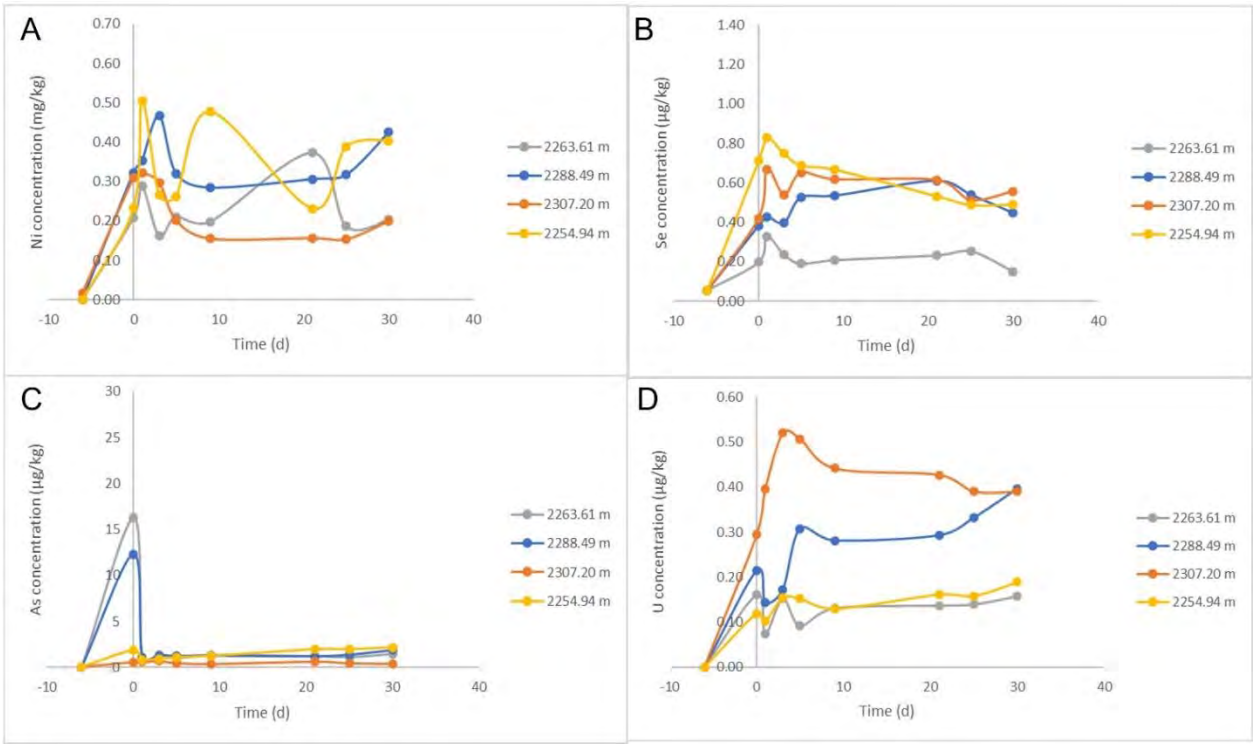

Figure 34: EPQ 10 West Moonie 1 core: Concentrations of a) dissolved Ni (mg/kg), b) dissolved Se (µg/kg), c) dissolved As (µg/kg), and d) dissolved U concentration (µg/kg) during batch reaction of lower Precipice Sandstone and upper Precipice Sandstone with pure CO_2. The 2254.94 m in yellow is upper Precipice Sandstone core, the other samples in grey, blue, and orange are lower Precipice Sandstones.

3.5. Directional permeability analyses of batch reacted and other key samples

The average permeabilities of the tested sandstone samples (Table 14), of both the upper and lower Precipice Sandstone, mostly exceed 1 Darcy (Darcy, 1856). However, the "vertical" permeability of the upper sample was lower than the average for sandstones from the lower Precipice Sandstone. The sandstone with the lowest measured permeability of those in the lower Precipice Sandstone is just above the mid-unit baffle siltstone, a thin and most likely regionally discontinuous unit that lies just above the primary injection interval. The Evergreen Formation caprock siltstone sample has very low permeability, with vertical being < 0.1 mD. The Moolayember Formation samples also have relatively low permeabilities, as expected. Sometimes permeability of samples increased following batch reactions, possibly due to dissolution of small amounts of pore-filing cement/s. In other cases, permeability decreased, which could be due to both mineral precipitation and fines migration blocking pores.

Table 14: Directional permeability within approximately 15 mm cubic pieces of WM1 rock samples (mD).

Formation / Unit	Core Box Depth Range (mRT)	Lithology	Pre/Post CO_2 Batch Reactor	Directional permeability of cubes (mD)			Kv / Kh (average)
				Bedding Plane 1	Bedding Plane 2	Perpendicular to **bedding ("vertical")**	
Evergreen Formation	2242.44 – 2242.54	Black SILTSTONE	Pre	0.90	0.36	0.048	0.08
			Post	1.7	1.4	0.070	0.05
Upper Precipice Sandstone	2254.95 (chip)	Medium SANDSTONE	Pre	1,252	1,608	607	0.42
			Post	1,739	2,150	492	0.25
Lower Precipice Sandstone D	2263.61 – 2263.77	Coarse to very coarse SANDSTONE	Pre	1,175	1,292	876	0.71
			Post	929	1,112	756	0.74
	2267.71-2267.84	Interbedded SILTSTONE and fine SANDSTONE	n/a	3.1	5.6	1.5	0.35
	2267.84-2267.90	Fine SANDSTONE	n/a	5.6	1.5	3.1	0.87
Lower Precipice Sandstone C	2274.10 – 2274.18	Coarse to very coarse SANDSTONE	Pre	1,420	1,539	2,220	1.50
			Post	1,405	1,440	1,982	1.39
	2284.13 (chip)	Medium to very coarse SANDSTONE	n/a	> 3,000 (Extremely permeable beyond measurement range)			n/a
	2288.49 – 2288.61	Medium to very coarse SANDSTONE	Pre	1,237	1,084	699	0.60
			Post	1,336	1,074	1,094	0.91
	2296.97-2297.13	Medium to coarse SANDSTONE	n/a	38	30	14	0.42
Lower Precipice Sandstone B	2297.13-2297.19	Interlaminated silty MUDSTONE and very fine SANDSTONE	n/a	0.05	(Very low)	0.30	5.93
Lower Precipice Sandstone A	2370.2 (chip)	Medium to coarse SANDSTONE	Pre	1,777	1,497	816	0.50
			Post	1,932	1,414	845	0.50
	2322.61 – 2322.73	Coarse to very coarse SANDSTONE	Pre	1,125	1,162	866	0.76
			Post	1,293	1,395	1,318	0.98
	2328.54 – 2328.59	Sandy SILTSTONE	Pre	(too thin - fissile)	(too thin - fissile)	0.36	n/a
			Post	(too thin - fissile)	(too thin - fissile)	0.02	n/a
	2330.41 – 2330.55	Fine to coarse SANDSTONE	Pre	1,559	1,301	1,613	1.13
			Post	1,546	1,574	2,132	1.37
Moolayember Formation	2339 – 2339.17	Fine to medium SANDSTONE	Pre	0.18	0.34	0.27	1.04
			Post	0.33	0.13	0.22	0.98
	2346.40 – 2346.51	Silty fine SANDSTONE	Pre	2.8	7.5	0.21	0.04
			Post	3.6	8.3	0.32	0.05

4. Reaction Path Modelling

4.1. Methodology

Geochemical modelling software was used to determine which reactions are occurring and their rates, as well as the actual chemical composition of variable composition mineral phases like carbonates and chlorite and the sources of trace elements mobilised by reaction. Reaction path modelling of the experiments was carried out using the Geochemist's Workbench (GWB) 12 Professional React module (Bethke et al., 2022). Detailed mineralogy, including the chemical composition of the minerals reacting, was required to be able to reactive transport model the chemical evolution of the system because of the injection of the CO_2 and trace gases.

The overall mineral content of the core samples used in the experiments was determined using X-ray diffraction (XRD), thin section analysis, scanning electron microscopy (SEM), and QEMSCAN. The major metal element composition (Ca, Fe, Mg, Na) of the individual mineral phases was derived for chlorite, plagioclase feldspar, pyrite and the carbonate minerals calcite, siderite and ankerite using SEM-EDS and XFM, as in Golding et al. (2017) and Dawson et al. (2021). The trace element content of minerals was estimated using several methods in conjunction with SEM-EDS and synchrotron X-ray fluorescence mapping (XFM) and physical characterisation data. The first was the use of sequential extraction data, with reference to whole rock geochemistry, to identify the specific phases with which the various trace elements could be associated and the amount that was mobilised. This allowed for the initial characterisation of mineral composition and adsorption site occupancy trends. The second source was using the P-T-X (batch) experiments to determine/confirm which trace elements were mobilised and the mechanism of mobilisation/demobilisation (e.g., mineral dissolution/precipitation, desorption/adsorption). The final step was completed by carrying out reaction path modelling using minerals that had solid solution compositions that included the trace elements to history match the water chemistry data of the experiments.

Reservoir pressure and temperature experiments with West Moonie 1 core, synthetic formation water and a pure CO_2 and a CO_2-NO-SO_2-O_2 gas mix (P-T-X experiments) were performed to provide changes in water chemistry including metal concentrations. Geochemical reaction path modelling was carried out on the P-T-X experiments using The Geochemist's Workbench (GWB) software. Reaction path models were constructed to history match the major and minor chemical composition of the water samples collected during the P-T-X experiments. Details of the set up for the reaction path and reactive transport modelling are provided below. Once a match of the major components was achieved, the trace element chemical compositions of the reacting mineral phases were adjusted based on the relationships determined from the sequential extractions and the mobilization of trace elements during the P-T-X experiments. The incorporation of trace elements in the minerals was carried out by developing regular and ideal mixing models for siderite, calcite, ankerite and pyrite solid solutions with equivalent carbonate minerals containing the trace elements (see below).

The proportion of the trace metal content associated with the steps of the sequential extraction limited the total content assigned to the specific mineral phases. The total amount of the mineral phase was limited by the measured mineral content (if detected) and the bulk chemistry including trace element contents. This ensured that neither major, minor, nor the trace element content of the rocks would be exceeded in the modelled minerals. The resultant mineralogies thus account for the mineral and chemical composition of the rocks and are thermodynamically defined so can be included in the reactive transport modelling.

Kinetically based reaction path and reactive transport geochemical modelling requires thermodynamic data and kinetic rate data to simulate changes in composition with time. The thermodynamic data for the aqueous species, gases and minerals is provided via an appropriate thermodynamic dataset while the kinetic data must be provided for the reactions of interest. The reaction rate equation is derived from the transition state theory that relates rate to the mineral reactive surface area, a reaction rate constant specific to that mineral at the correct

temperature, effects of inhibiting or catalysing species, and the proximity to equilibrium between the mineral and the solution (Lasaga, 1995).

$$r_{\bar{k}} = A_S k_+ \prod_j (a_j)^{P_i} \left(1 - \left(\frac{Q}{K}\right)^n\right)^m \quad \text{Eq. 1}$$

Where $r_{\bar{k}}$ is the reaction rate, A_S is the mineral surface area, k_+ is the rate constant, Q is the activity product, K is the equilibrium constant, a_j is the activity of the catalysing or inhibiting species and P_j is the power for species j, n and m are empirically derived power terms for a nonlinear rate law.

Most rate constant data are reported at 25°C and need to be re-calculated for higher temperatures. In addition, the pH dependence of mineral dissolution rates is incorporated using separate rate constants and activation energies for acidic, neutral, and basic mechanisms. Scripts, formulated for GWB, were used to establish dissolution rates (Eq. 1) using the following equation to calculate the rate constant at temperature and the given pH.

$$k = k_{25}^{nu} \exp\left[\frac{-E_a^{nu}}{R}\left(\frac{1}{T} - \frac{1}{T_0}\right)\right] + k_{25}^{H} \exp\left[\frac{-E_a^{H}}{R}\left(\frac{1}{T} - \frac{1}{T_0}\right)\right] a_H^{n_H} + k_{25}^{OH} \exp\left[\frac{-E_a^{OH}}{R}\left(\frac{1}{T} - \frac{1}{T_0}\right)\right] a_H^{n_{OH}} \quad \text{Eq. 2}$$

Where E_a is the apparent activation energy, R is the molar gas constant, T_0 is reference temperature (298.15 K), T is the temperature (K), *nu* is the neutral mechanism, *H* is the acid mechanism, *OH* is the base mechanism, a_H is the activity of H^+ and n is the power term.

Precipitation rates of mineral phases, especially alumino-silicate minerals, are poorly constrained. The common practice is to use the dissolution rates with values assigned to the nucleation site density or an initial volume ratio relative to the volume of solids if the mineral is not present in the system. For the experiments, a better match of the reaction path model to the data was found to be made when incorporating nucleation and crystal growth (Dawson et al., 2021; Golding et al., 2019; Pearce et al., 2015). The reaction path modelling precipitation rates (r_p) were generated based on modifications to the classical nucleation theory (Walton, 1967; Nielsen, 1983) and the non-linear portion of the *Burton-Cabrera-Frank* (BCF) crystal growth theory (Burton et al., 1951) described by Pham et al. (2011) and Hellevang et al. (2013).

$$r_P = A_S k_P (\frac{Q}{K} - 1)^2 - k_N \exp\left\{-\Gamma\left(\frac{1}{(T_K)^{\frac{3}{2}} \ln\left(\frac{Q}{K}\right)}\right)^2\right\} \quad \text{Eq. 3}$$

Where k_P is the precipitation rate constant, k_N is the nucleation rate constant, and Γ is the pre-exponential factor for nucleation. Other terms were defined for Eq. 1.

The nucleation and precipitation rate equation was written into GWB React scripts used for the modelling of the experiments. Pham et al. (2011) evaluated the sensitivity of the terms in the equation and found the results relatively insensitive to k_N and recommended a value of 1 be assigned to the nucleation rate constant. Equation 3 was successfully applied to experiments conducted on the Surat Basin mineralogies in Pearce et al. (2015) and the values used for the variables can be found in Table 15.

The initial mineral content (Table 16), initial fluid composition (Table 17) and changes in the fluid composition were used to produce reaction path models and determine the dissolving and precipitating mineral phases and modify the reaction rate parameters used. The Geochemist's Workbench React module was used with a thermodynamic database for mineral and aqueous species based on the EQ3/6 database (Wolery, 1992). Thermodynamic data for chlorite ($Fe_{0.75}Mg_{0.25}Al_2Si3O_{10}(OH)_8$ composition based on microprobe and P-T-X experiments for Surat Basin Precipice Sandstone samples in Pearce et al. (2015) were calculated using the methods of Blanc et al. (2015). In addition to the minerals initially present, potential product phases included

pyrite, siderite, magnesite, ankerite ($CaFe_{0.7}Mg_{0.3}(CO_3)_2$, dolomite, and the trace metal containing carbonate mineral phases cerussite, $NiCO_3$, otavite, rhodochrosite, smithsonite, sphaerocobaltite and strontianite. Kinetic rate data were sourced from the compilation of Palandri and Kharaka (2004), except for that of siderite and ankerite from Steefel (2001), that of illite from Kohler et al. (2003) and the chlorite data based on Lowson et al. (2007). Precipitation rates for the experiments were calculated using equation 3. Initial reactive surface areas were set to 70 cm^2/g for kaolinite and chlorite, 150 cm^2/g for smectite and illite and 10 cm^2/g for the remainder of the mineral phases. These values were calculated based on a tabular grain morphology for the clay minerals and spherical grain morphology for the framework grains and carbonates with an applied roughness factor of 7 and reservoir upscaling factor of 0.01 (Zhu et al., 2006). The reactive surface areas in the reaction path models were then adjusted to history match the chemical data from the experiments.

Table 15: Kinetic rate parameters for dissolution (Eq. 2) and precipitation (Eq. 3) where kd is the calculated dissolution rate constant from Eq. 2.

	$k_{25(H)}$ (mol/m²s)	$E_{a(H)}$ (kJ/mol)	n	$k_{25(nu)}$ (mol/m²s)	$E_{a(nu)}$ (kJ/mol)	k_p	Γ
Chalcedony				$3.98x10^{-14}$	90.9	k_d	$2x10^{+10}$
K-Feldspar	$8.7x10^{-11}$	40	0.5	$3.89x10^{-13}$	38	k_d	$2x10^{+10}$
Albite	$6.9x10^{-11}$	55	0.457	$2.75x10^{-13}$	69.8	k_d	$2x10^{+10}$
Illite	$1.92x10^{-12}$	46	0.6	$8.82x10^{-16}$	14	k_d	$2x10^{+10}$
Smectite	$1.05x10^{-11}$	35	0.34	$1.66x10^{-13}$	35	k_d	$3x10^{+10}$
$Al(OH)_3$	$2.24x10^{-8}$	47.5	0.992	$3.16x10^{-12}$	61.2	k_d	$2x10^{+10}$
Kaolinite	$4.9x10^{-12}$	65.9	0.777	$6.61x10^{-14}$	22.2	$k_d/10$	$2x10^{+10}$
Chlorite	$1.6218x10^{-10}$	94.3	0.49	$1.00x10^{-13}$	94.3	k_d	$2x10^{+10}$
Calcite	0.501	14.4	1	$1.55x10^{-06}$	23.5	k_d	$1x10^{+10}$
Dolomite	$6.46x10^{-04}$	36.1	0.7	$2.95x10^{-08}$	52.2	$k_d/100$	$3x10^{+10}$
Ankerite	$1.79x10^{-04}$	48	0.75	$2.24x10^{-09}$	48	$k_d/100$	$3x10^{+10}$
Siderite	$1.79x10^{-04}$	48	0.75	$2.24x10^{-09}$	48	$k_d/100$	$3x10^{+10}$
Pyrite*	$3.02x10^{-12}$	56.9	-0.5	$2.82x10^{-09}$	56.9	k_d	$2x10^{+10}$
$Fe(OH)_3$	$4.07x10^{-10}$	66.2	1	$2.51x10^{-15}$	66.2	k_d	$1x10^{+10}$

* includes activity of Fe and O_2 dependency terms n_{Fe}=0.5, n_{O2}=0.5

Table 16: Mineral masses (g) used in the reaction path modelling of the CO_2 with mixed gas experiments.

Sample ID	477	481	483	484	485	486	489	490B	492	495	497	500
Depth (m)	2346.5	2339.1	2330.5	2328.6	2322.7	2307.1	2288.6	2284.2	2274.1	2263.7	2255.0	2242.5
sample weight (g)	8.38	8.46	5.64	6.34	11.16	6.86	7.30	10.23	8.39	8.73	5.10	11.82
Quartz	3.99	6.63	5.40	2.90	10.67	6.74	6.41	8.34	5.80	6.51	3.45	7.22
Siderite 1	0.052	0.000	0.015	0.000	0.000	0.000	0.000	0.000	0.000	0.000	0.000	0.000
Siderite 2	0.000	0.016	0.000	0.013	0.033	0.016	0.013	0.016	0.031	0.026	0.023	0.158
Ankerite	0.000	0.000	0.000	0.000	0.000	0.000	0.000	0.000	0.001	0.000	0.000	0.000
Calcite	0.003	0.000	0.000	0.000	0.000	0.000	0.000	0.000	0.000	0.000	0.008	0.008
K-Feldspar	2.03	0.00	0.12	0.00	0.11	0.00	0.17	0.15	1.11	0.74	0.71	0.93
Kaolinite	1.20	1.62	0.10	1.65	0.16	0.07	0.38	0.87	0.61	0.60	0.77	2.44
Illite/mica	0.78	0.12	0.00	1.78	0.19	0.03	0.32	0.85	0.77	0.84	0.00	0.86
Chlorite	0.318	0.082	0.004	0.002	0.009	0.004	0.004	0.007	0.057	0.012	0.140	0.198
Smectite	0.00	0.00	0.00	0.00	0.00	0.00	0.00	0.00	0.00	0.00	0.00	0.00
Pyrite	0.00	0.00	0.00	0.00	0.00	0.00	0.00	0.00	0.00	0.00	0.00	0.00
Fe(OH)3	8.2E-7	8.3E-7	5.4E-7	6.2E-6	1.1E-6	6.8E-7	7.1E-7	9.9E-7	7.9E-7	1.0E-6	4.8E-6	1.1E-5
CEC[1] (meq)	1.5	1.5	0.15	1.3	1	0.5	0.15	0.85	0.5	0.5	0.85	0.15

1. CEC is Cation Exchange Capacity

Previous studies of the Precipice Sandstone and Moolayember Formation showed that iron-rich chlorite and carbonates like siderite, calcite and ankerite were present often in quantities below detection (Dawson et al., 2021; Golding et al., 2019; Pearce et al., 2015). However, those minerals proved to exert a significant influence on the chemical evolution of the fluid in the experiments. In the previous studies, the amount and composition of the carbonate minerals (if not detected) and the amount of chlorite (if not detected) were determined using the sequential extraction results, by applying a mass balance for elemental composition using the mineralogy and the bulk chemistry, from SEM-EDX and using mobilised element stoichiometry during the P-T-X experiments with pure CO_2 as the gas phase. Determining mineral amounts and composition was possible when pure CO_2 was used because there was little evidence of secondary phases like $Fe(OH)_3$ precipitating making the mobilised element stoichiometry directly related to the composition of the minerals dissolving. Addition of chlorite and siderite made it possible to history match the experiment data consistent with the previous modelling studies (Dawson et al., 2021; Golding et al., 2019; Pearce et al., 2015).

Table 17: Initial water chemistry for the P-T-X with trace gas experiments reported in ppb except Na and Cl in ppm and HCO_3- as total DIC in mol/kg.

Sample ID	477	481	483	484	485	486B	489	490B	492	495	497	500
Volume(ml)	125	125	125	125	125	125	125	125	125	125	125	125
T °C	80	80	80	80	80	80	80	80	80	80	80	80
pH*	4.25	3.98	3.86	4.17	4.27	4.21	4.02	4.25	4.06	4.18	4.25	4.17
Al	70.3	36.9	59.4	71.1	113.1	84.2	18.5	80.0	10.0	69.4	82.9	23.8
As	1.1	9.2	0.6	0.7	1.1	0.7	0.6	6.8	1.1	3.5	1.3	3.5
B	97.9	56.1	10.1	12.0	4.8	75.4	7.7	110.7	14.6	10.1	65.8	31.0
Ba	267.7	157.0	47.4	173.9	79.6	35.5	75.9	70.3	36.1	65.3	201.3	110.6
Ca	5218	4170	6007	7161	15730	9859	3249	9314	10697	3966	10758	2670
Cd	18.5	35.5	9.5	4.7	1.9	2.3	19.0	18.3	54.8	1.6	4.3	1.2
Co	21.1	202.2	27.2	24.1	12.1	12.4	69.0	121.1	41.3	56.3	40.7	5.3
Cr	66.3	103.0	111.4	19.9	14.8	44.4	23.2	26.8	10.4	16.1	41.7	28.5
Cu	244	102	620	467	3096	209	617	380	121	453	126	52
Fe	776	1323	1483	979	5918	1679	237	150	843	1281	587	389
K	29869	34467	19244	22980	31885	44372	16097	32884	18710	19049	50096	24602
Li	118.3	188.3	8.3	70.3	8.8	32.8	12.1	37.8	12.5	14.6	65.9	177.4
Mg	1427	1894	1068	1072	1238	1182	968	1121	1061	1289	3651	507
Mn	81.3	94.0	169.3	23.0	93.2	99.4	51.4	20.3	523.0	268.8	1121.6	63.3
Na	538	415	332	468	515	487	407	536	413	482	518	495
Ni	300	612	489	172	86	174	402	336	171	390	195	63
Pb	2.6	16.1	4.5	2.8	9.8	10.0	2.8	6.7	1.3	4.1	8.1	2.4
S	5828	38598	5291	6841	6011	5151	7700	9081	14021	10016	11212	8718
Si	2283	8339	1661	3378	2370	1239	1827	1822	2002	3137	3777	4004
Sr	340	228	28	206	53	42	23	57	27	23	136	159
Zn	42	399	82	27	277	16	97	200	65	91	60	25
Cl	325	325	325	325	325	325	325	325	325	325	325	325
HCO3-*	1.153	1.136	1.149	1.168	1.171	1.152	1.151	1.151	1.166	1.168	1.152	1.154

* pH and HCO_3^- calculated based on CO_2 saturation at given P/T conditions

Mixing models were constructed for the carbonate minerals calcite, siderite and ankerite (Table 18). The carbonate mixing models for Ca, Mg, Fe, Mn, Sr, Ba, Pb, Co, Cu, Zn, Cd, Ni and As were regular binary solution models for calcite-magnesite, calcite-rhodochrosite and calcite-strontianite, and ideal mixing models for the addition of -sphaerocobaltite, -smithsonite and -witherite. The siderite mixing model included siderite-calcite, siderite-magnesite and siderite-rhodochrosite regular binary solid solution terms and ideal mixing for the siderite -cerussite, -sphaerocobaltite, -smithsonite, -otavite, -$NiCO_3$, -$CuCO_3$, and ferrous arsenate. Ankerite thermodynamic data were calculated using ideal mixing ankerite -rhodochrosite, - strontianite, -sphaerocobaltite, -smithsonite and -witherite. Margules parameter terms for the regular solid solution models were sourced from Glynn (2000). In all cases, the molar volume and molecular weight were also calculated.

Table 18: Carbonate element composition in mol fraction metals.

	Calcite	Siderite 1	Siderite 2	Ankerite
Ca	0.667	0.00085	0.00085	0.4894
Mg	0.214	0.0205	0.0205	0.2447
Fe		0.9523	0.9518	0.2447
Sr	0.003			0.0006
Ba	0.003			0.0006
Mn	0.1	0.0009	0.0009	0.0172
As		0.0001	0.0001	
Cd			0.0001	
Co	0.003	0.0008	0.0008	0.0009
Cu		0.0069	0.0069	
Ni		0.0028	0.0028	
Pb			0.0004	
Zn	0.01	0.015	0.015	0.002

Adsorption was incorporated in the models using the modified two-layer formulation of Dzombak and Morel (1990). In the reaction path models, precipitation of $Fe(OH)_3$ and $Al(OH)_3$ results in the production of strong and weak adsorption sites with site densities of 0.2 mol for weak sites and 0.005 mol for strong sites per mol $Fe(OH)_3$ or $Al(OH)_3$. Site occupancy is determined based on fluid composition and the surface complexation constants in the thermodynamic database.

During the reaction path modelling it was determined that in some cases mineral dissolution and precipitation and adsorption did not sufficiently history match the experiment data. For those models, cation exchange was included in addition to adsorption. Modelling of cation exchange involves application of a cation exchange capacity and the use of a thermodynamic database containing mass action equations in the form of exchange reactions with selectivity coefficients. A database was compiled based on the selectivity coefficients from Appelo and Postma (2005) adhering to the Gaines-Thomas convention. Cation exchange capacities were assigned by iteratively modelling until a best fit was found.

Pure CO_2 models were run with the mineralogy shown in Table 19 and water chemistry shown in Table 20.

Table 19: Mineral masses (g) used in the modelling of the pure CO_2 experiments.

Sample ID	486	489	495	497
Depth	2307.1	2288.6	2263.7	2255
sample weight (g)	9.79	9.53	8.32	10.31
Quartz	9.62	8.37	6.20	6.97
Siderite 1	0.000	0.000	0.000	0.000
Siderite 2	0.022	0.016	0.025	0.047
Ankerite	0.000	0.000	0.000	0.000
Calcite	0.000	0.000	0.000	0.016
K-Feldspar	0.00	0.22	0.71	1.43
Kaolinite	0.10	0.50	0.57	1.57
Illite/mica	0.04	0.42	0.80	0.00
Chlorite	0.006	0.005	0.011	0.283
Smectite	0.00	0.00	0.00	0.00
Pyrite	0.00	0.00	0.00	0.00
Fe(OH)3	9.64E-07	9.29E-07	9.50E-07	9.71E-06

Table 20: Initial water chemistry (ppb except HCO_3^- given as total DIC in mol/kg) used in the pure CO_2 experiments.

Sample ID	486	489	495	497
Water Volume(ml)	125	125	125	125
Temperature	80	80	80	80
pH*	4.35	4.32	4.30	4.27
Al	10.0	152.0	315.3	84.3
As	0.1	12.3	2.3	1.9
B	8.0	14.9	12.9	24.9
Ba	70.7	93.2	72.2	394.1
Ca	11818	10504	10554	13814
Cd	0.1	3.3	6.6	1.2
Co	0.1	62.3	84.2	80.0
Cr	0.1	293.5	71.0	10.5
Cu	280	766	603	82
Fe	5471	6195	11485	1805
K	28016	21672	19223	39771
Li	9884.0	22.0	15.4	75.5
Mg	400	8535	8705	11580
Mn	3.9	62.0	188.0	794.7
Na	582233	567295	545130	532084
Ni	18	354	232	266
Pb	0.2	80.1	4.3	0.5
S	5188	6682	6967	15228
Si	2167	2710	2464	7046
Sr	65	44	32	275
Zn	20	243	269	300
Cl	325000	325000	325000	325000
HCO3-*	1.173	1.172	1.172	1.171

4.2. Results

The results of the reaction path modelling are presented for all of the experiments for the different HSU, including those with pure CO_2. Model outputs are presented beginning with the lower Precipice A Sandstone (483, 484, 485 and 486), then the lower Precipice C Sandstone (498, 490 and 492) including the transition zone (lower Precipice D Sandstone) between the lower Precipice and upper Precipice Sandstone (495), then the upper Precipice Sandstone (497 and 500) and the Moolayember Formation (477 and 481) experiments and finishing with the pure CO_2 experiments. For reference, Table 2 shows the major geological formations and units (e.g, lower Evergreen Formation, upper Precipice Sandstone, lower Precipice Sandstone A – D, and Moolayember Formation) in the context of their stratigraphic positions.

Samples 483, 484, 485 and 486 are all from the lower Precipice A Sandstone reservoir unit; however, 484 is from a finer grained facies. In the modelling, 483, 484 and 486 from the lower Precipice A unit show similar trends in the major, minor and trace element data (Figure 35). The matching to the SiO_2, Mg, Al and Fe data could only be achieved through the addition of chlorite and siderite. Cation exchange was included in both models to achieve a better fit to the trends of the major (Ca, Mg) and minor (Al) as well as some of the trace cations. Values for cation exchange capacity (CEC) in standard units are 2.7 meq/100 g for 483, 20.5 meq/100 g for 484, 9.0 meq/100 g for 485 and 7.3 meq/100 g for 486 provided the best fit to the data. The higher CEC for 484 coincides with higher kaolinite and illite/mica content relative to the other units. These CEC values are consistent with those determined for sedimentary rocks (Derkowski and Bristow, 2012). The SiO_2, Mg and Al data reflect the dissolution of chlorite and siderite (for Mg) and the small increases in Ca are the result of cation exchange. Precipitation of $Fe(OH)_3$ and $Al(OH)_3$ for 484 and 485 (Figure 36) predicted in the models results in similar Fe and Al trends to the experiment data.

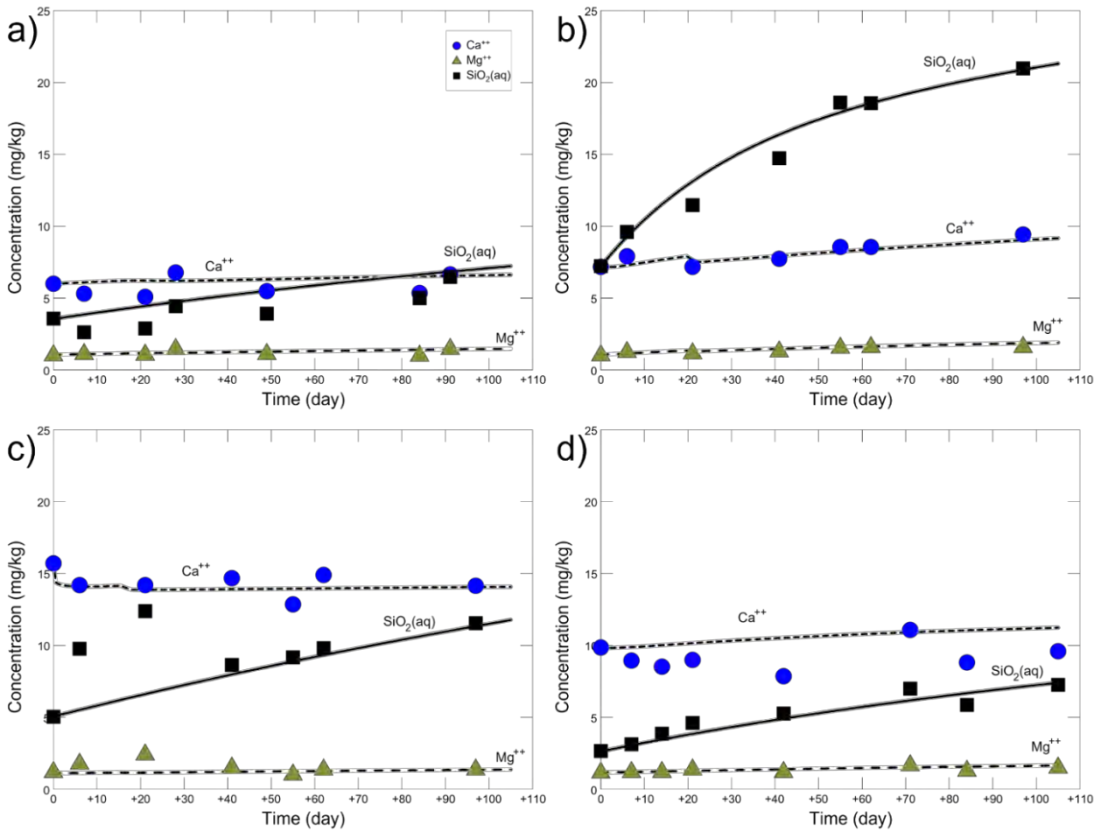

Figure 35: Lower Precipice A Sandstone experiment results for samples 483 (a), 484 (b), 485 (c), and 486 (d) with reaction path model traces for selected major elements in mg/kg.

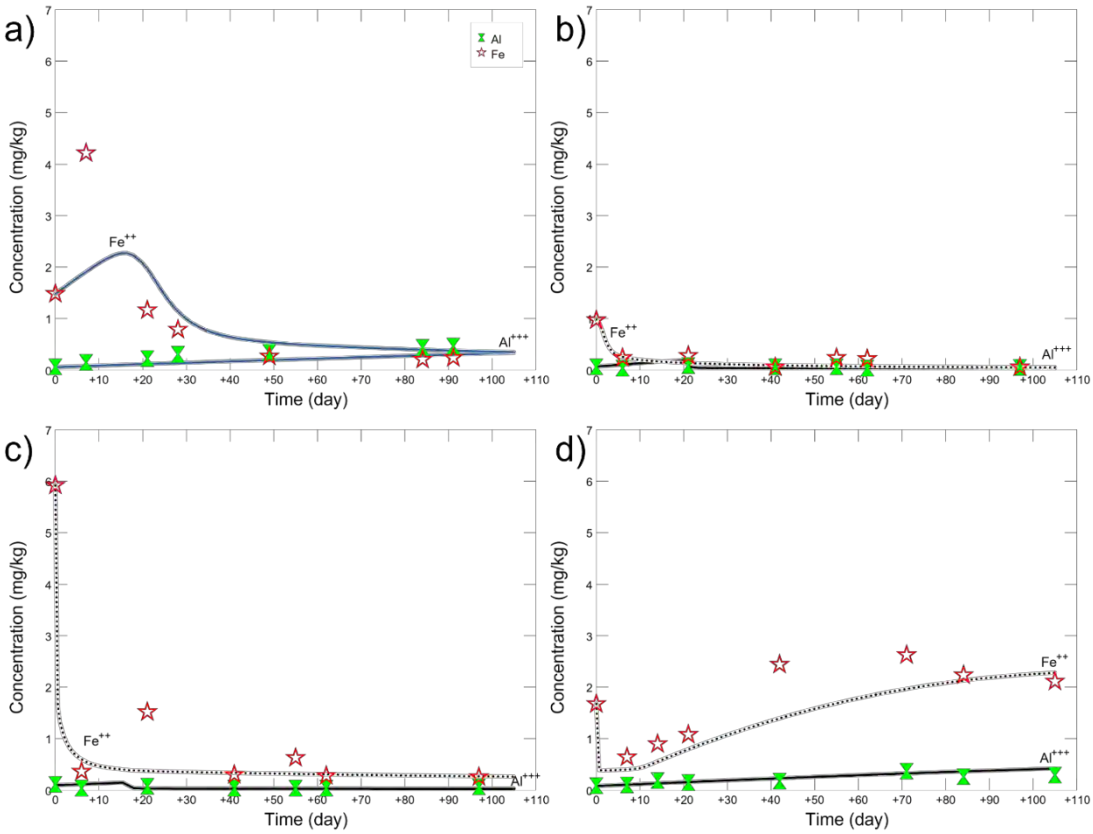

Figure 36: Lower Precipice A Sandstone experiment results for samples 483 (a), 484 (b), 485 (c), and 486 (d) with reaction path model traces for Al and Fe in mg/kg.

The minor and trace element model results are shown in Figure 37 and Figure 38. In many cases the models fit the trends of the experiment data but often the initial measured value is substantially higher or lower than the subsequent samples. This is commonly observed in batch type experiments and is typically the result of cation exchange and/or adsorption/desorption at the introduction of the CO_2 and the associated decrease in pH followed by rapid re-adsorption or desorption leading to the upward or downward shift in the concentrations (Lu et al., 2010; Varadharajan et al., 2013; Viswanathan et al., 2012; Zheng et al., 2009). The trends of the subsequent data are captured by the model, but the initial shift is difficult to model when using reaction path type modelling. For example, this is apparent in the modelled Cu trends vs the experiment data where the initial Cu is either lower or higher than the rest of the experiment values (Figure 37), yet the trend of the model is similar to the trend in the rest of the data.

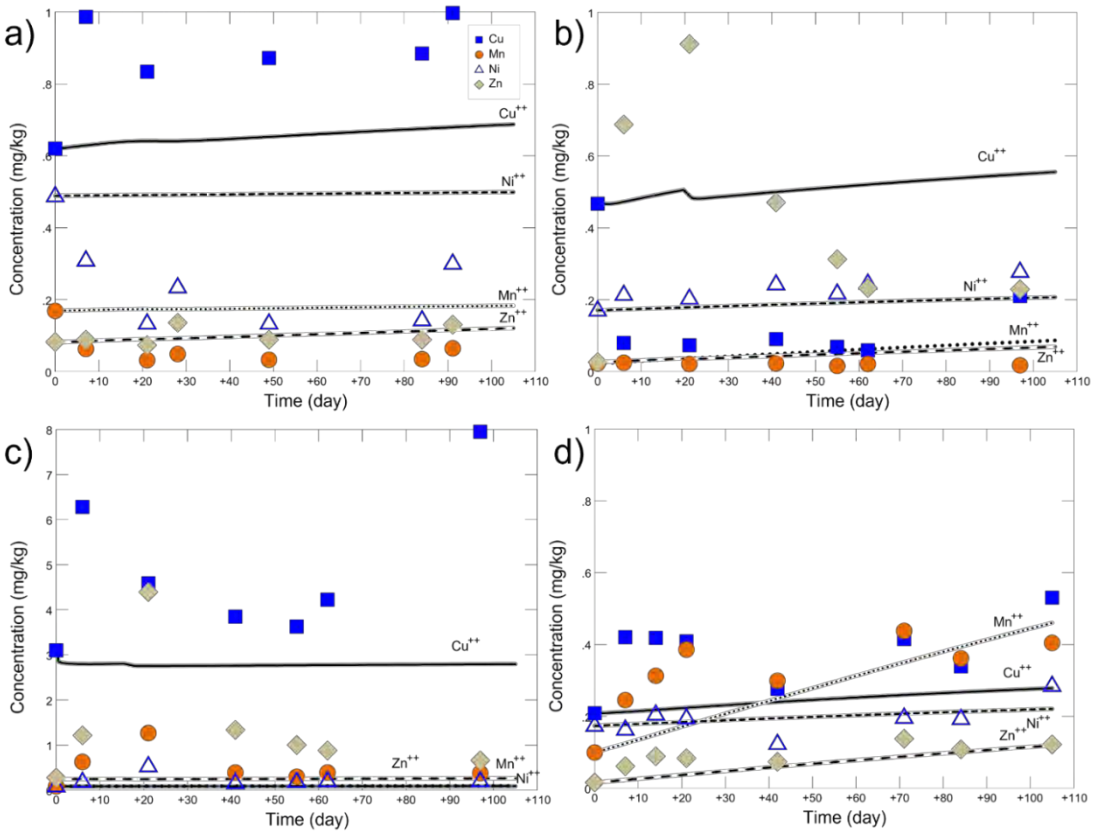

Figure 37: Lower Precipice A Sandstone experiment results for samples 483 (a), 484 (b), 485 (c), and 486 (d) with reaction path model traces for Cu, Mn, Ni and Zn in mg/kg.

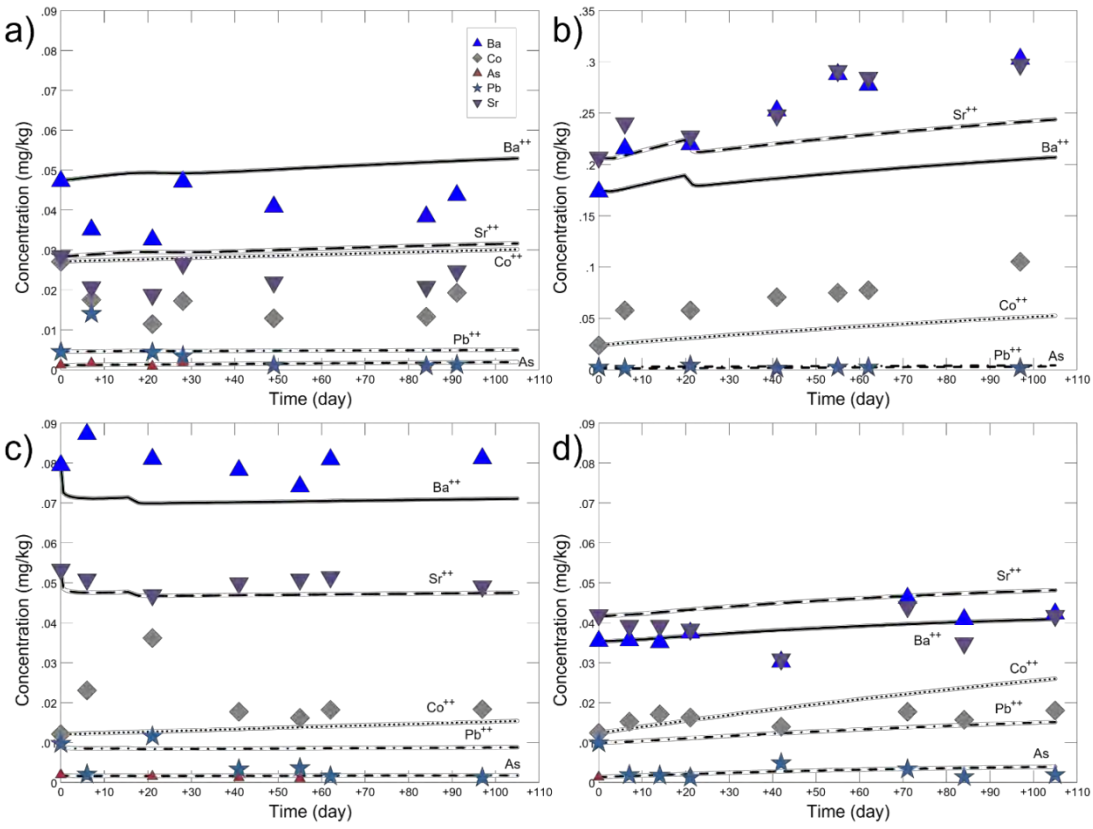

Figure 38: Lower Precipice A Sandstone experiment results for samples 483 (a), 484 (b), 485 (c), and 486 (d) with reaction path model traces for Ba, Co, As, Pb and Sr in mg/kg.

Figure 39 shows the change in mineral content from the modelling of samples 483 to 486. Dissolution of siderite and chlorite dominate with minor amounts of K-feldspar and chalcedony (SiO_2) predicted along with precipitation of $Fe(OH)_3$ and in $Al(OH)_3$ for 484 and 485. The siderite dissolution mobilizes trace elements and the production of adsorption sites through the precipitation of $Fe(OH)_3$ and $Al(OH)_3$ results in diminished, increasing or decreasing trends in the trace elements. The finer grained units, 484, show the greatest amount of reaction, consistent with the major element data. A small amount (0.001 g) of rhodochrosite $MnCO_3$) was included in the model to match the larger rise in Mn content. The rhodochrosite was not included in the reactive transport models as the apparent Mn increase also fits the previously described behaviour of Cu and the other trace elements.

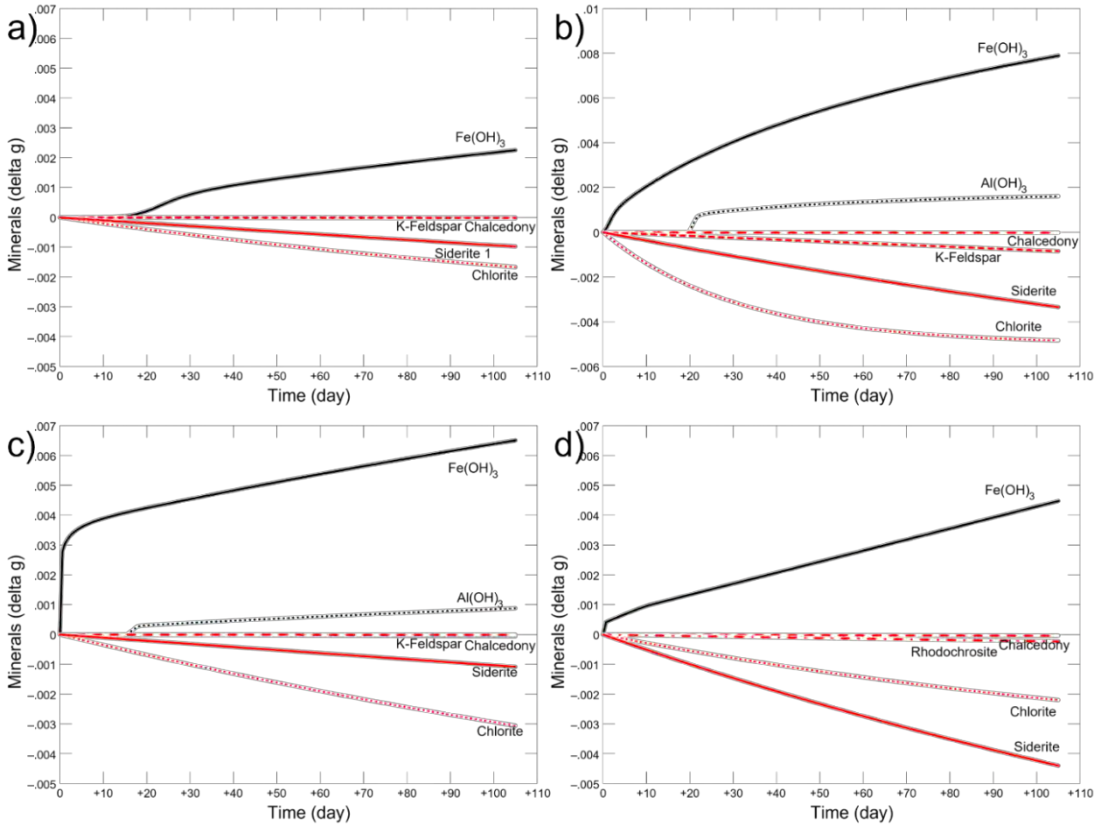

Figure 39: Changes in the mineral content (delta g) for samples 483 (a), 484 (b), 485 (c), and 486 (d) from the reaction path modelling.

The lower Precipice C Sandstone (samples 489, 490, 492 and 495) reaction path models for the major, minor and trace elements are show in Figures 40 to 43. Similar to the lower Precipice A Sandstone, the fit of the models to the data was best achieved with the addition of chlorite and siderite as well as including cation exchange and adsorption. The CEC values that resulted in the best fit were 2.1 meq/100 g for 489, 8.3 meq/100 g for 490, 6.0 meq/100 g for 492 and 5.7 meq/100 g for 497. These are again, similar to published values for sedimentary rocks, and the higher values coincide with higher kaolinite and illite/mica content. The modelled Fe content tracks the experiment reasonably well indicating the importance of precipitation of $Fe(OH)_3$ during the experiments. Precipitation of $Al(OH)_3$ in the models of 495 and 497 can account for the lower Al of the experiments (Figure 41).

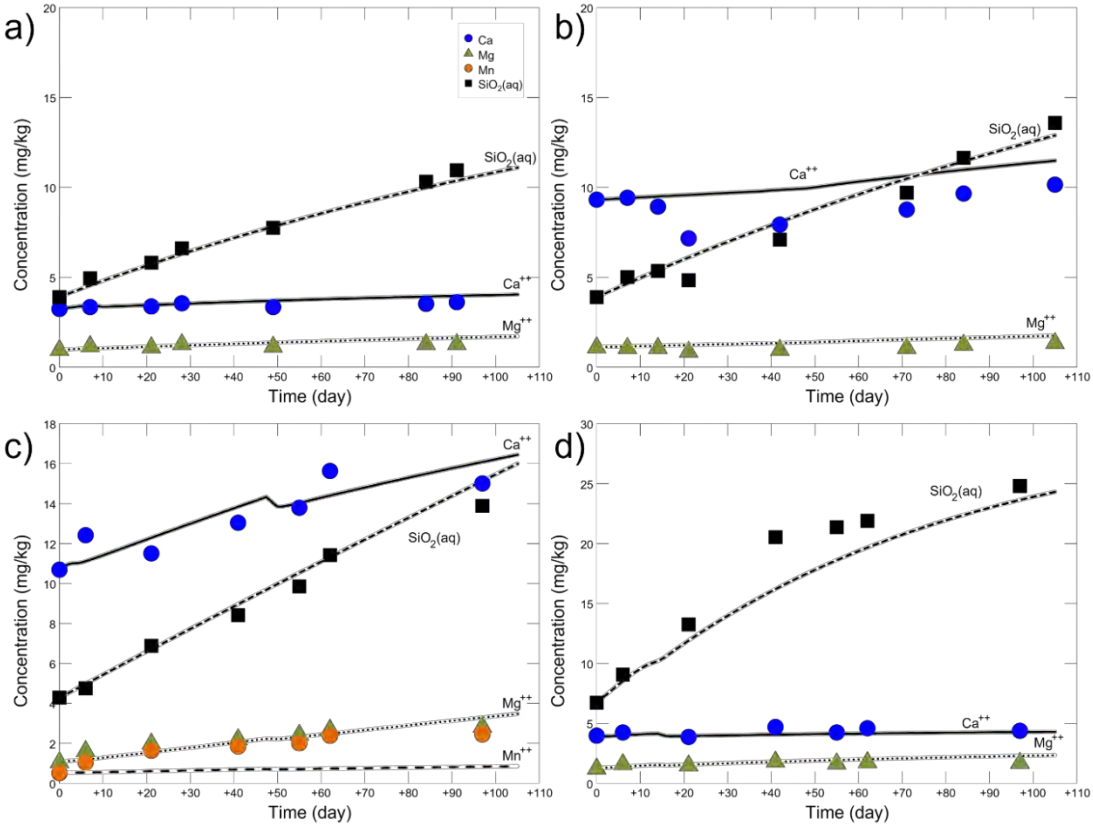

Figure 40: Lower Precipice C Sandstone experiments of samples 489 (a), 490 (b), 495 (c), and 497 (d) with reaction path model traces for selected major elements.

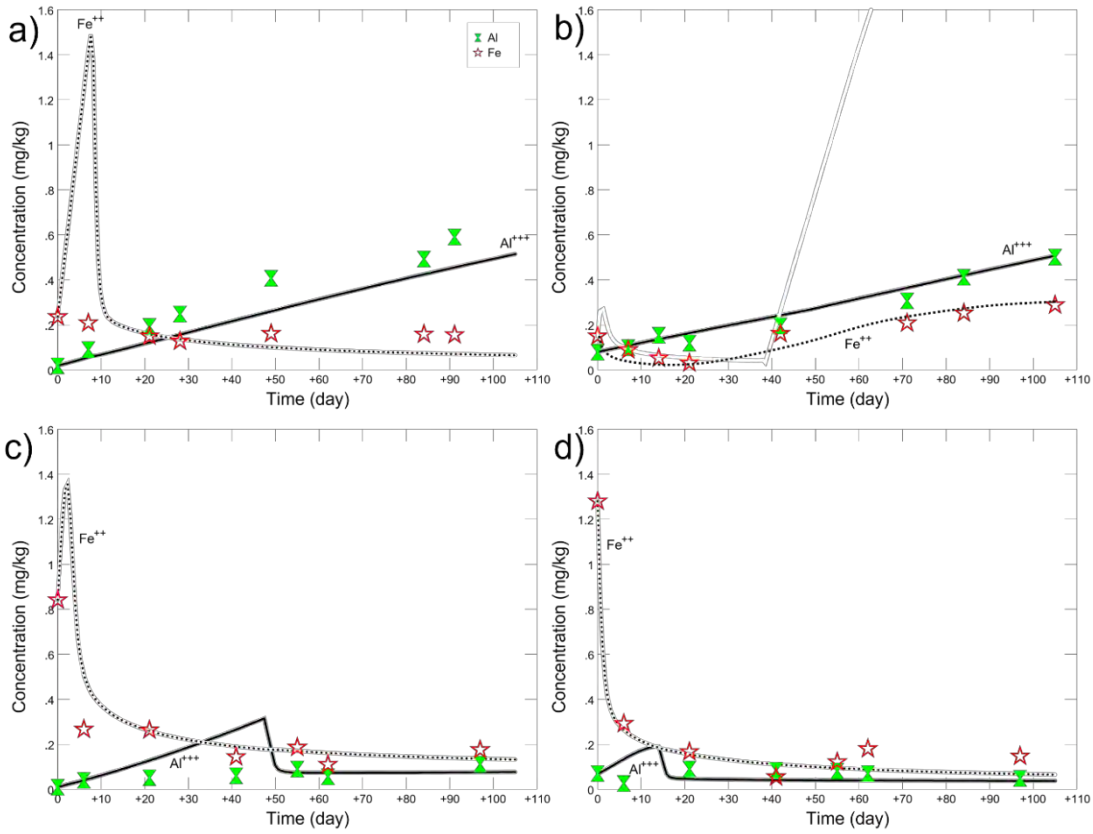

Figure 41: Lower Precipice C Sandstone experiments of samples 489 (a), 490 (b), 495 (c), and 497 (d) with reaction path model traces for Al and Fe content.

The minor and trace element model predictions along with the experiment data for the lower Precipice C Sandstone samples 489, 490, 492 and 497 are shown in Figure 42 and Figure 43. The model outputs show the same relationship as the lower Precipice A models to the experiment data. Some modelled elements track the data quite well while others track the data trends, but the initial composition is displaced relative to the subsequent data and results in misalignment. The models for samples 490 and 497 (Figure 42 b and d) show how the model output looks when the initial trace element content is set at a value more consistent with the remaining trend in the data, illustrating how the model tracks the data trends. The small displacement in the model trace for Cu and Mn in 489 and 497 (Figures 42 and 43 a and d) reflects the impact of cation exchange on the model output. The elevated Fe in these models displaces the Cu and Mn on the exchange sites so that they temporarily rise and then decrease as the Fe content lowers.

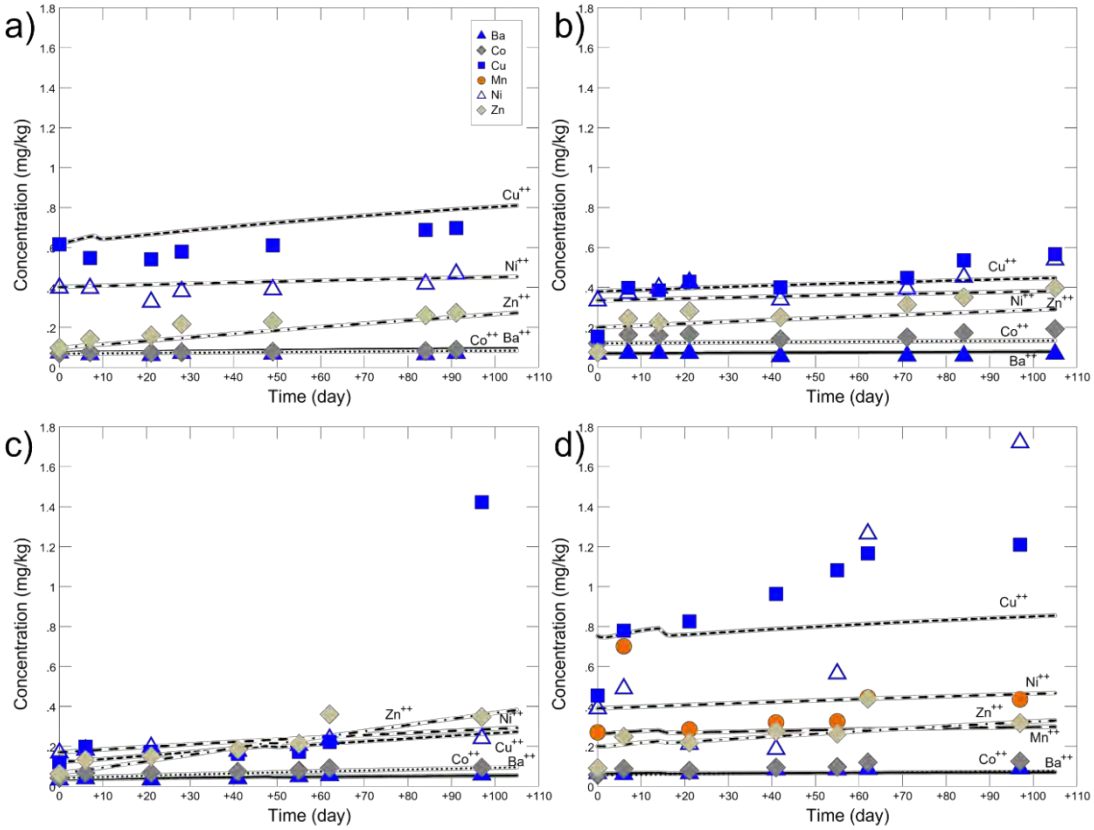

Figure 42: lower Precipice C Sandstone experiments of samples 489 (a), 490 (b), 495 (c), and 497 (d) with reaction path model traces for Ba, Co, Cu, Mn, Ni and Zn content.

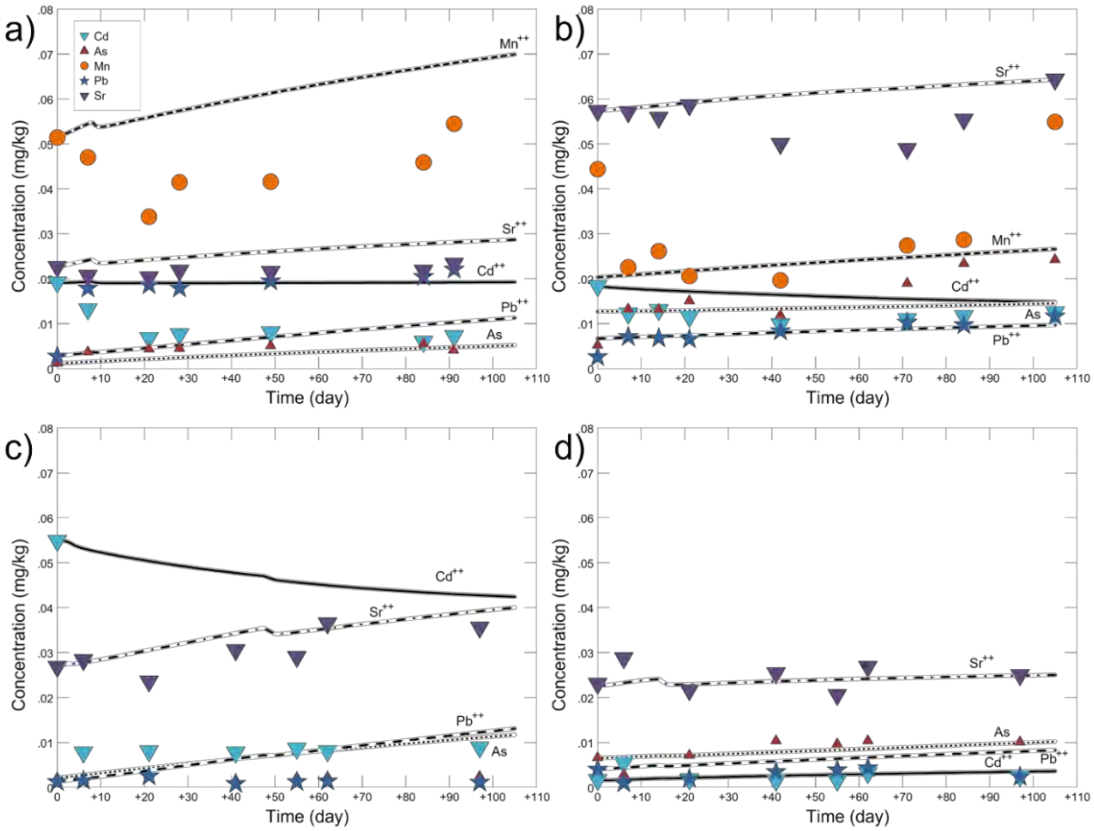

Figure 43: lower Precipice C Sandstone experiments of samples 489 (a), 490 (b), 495 (c), and 497 (d) with reaction path model traces for Cd, As, Mn, Pb and Sr content.

Dissolution of siderite and chlorite along with precipitation of $Fe(OH)_3$ dominate the changes in modelled mineral content for the lower Precipice C Sandstone (Figure 44) similar to those of the lower Precipice A Sandstone modelling. All display some minor K-feldspar and chalcedony (quartz) dissolution as well as minor amorphous $Al(OH)_3$ precipitation for sample 492 and 495. The $Fe(OH)_3$ and the $Al(OH)_3$ precipitation generates additional adsorption sites for trace elements in the models.

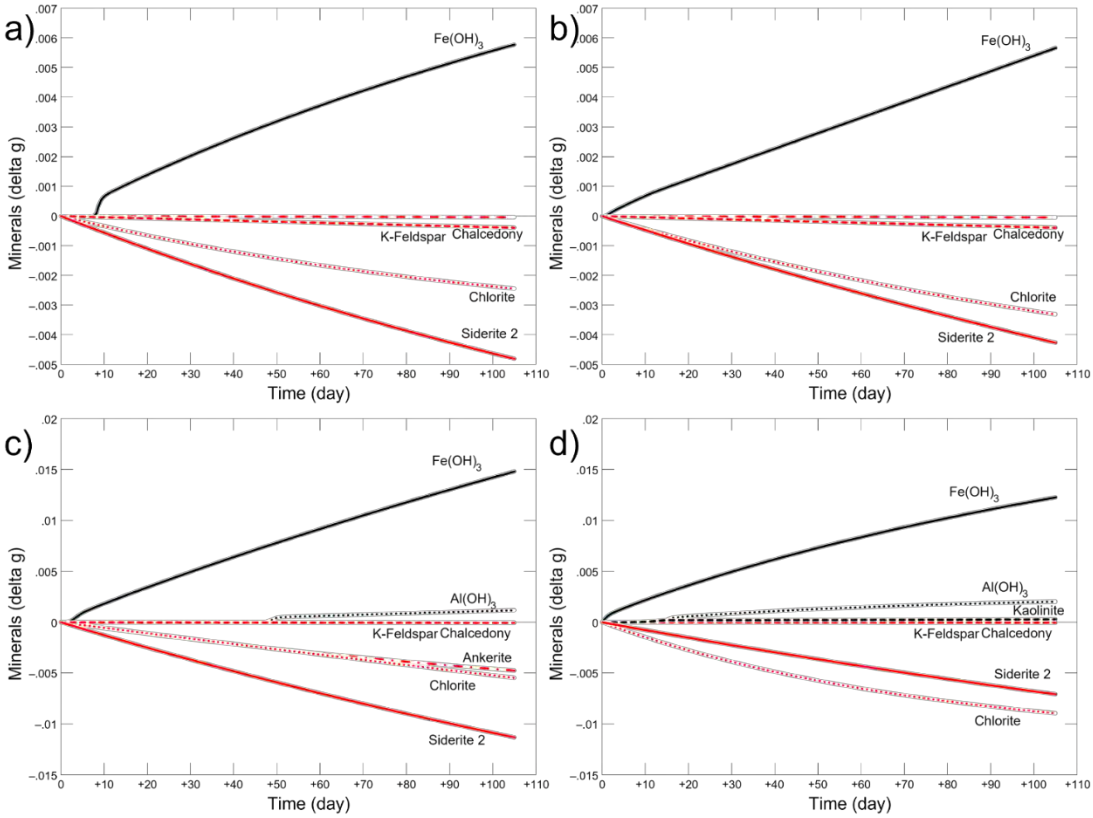

Figure 44: lower Precipice Sandstone C model results for 489 (a), 490 (b), 492 (c), and 495 (d) indicating predicted mineral dissolution and precipitation as changes in grams over the course of the experiment.

The upper Precipice Sandstone samples 497 and 500 reaction path model results superimposed on the experiment data are shown in Figure 45. The experiment for sample 500 was compromised by a leak detected on day 28 and the water was topped up while the vessel was resealed, and the experiment continued but there are some data inconsistencies from before and after the restart. Siderite and calcite were detected in XRD for both samples; however, chlorite was added to the models to achieve a better fit to the data. Interestingly, although these samples had the highest kaolinite and illite/mica content, cation exchange was not required to provide a better fit to the experiment data. The models fit the data reasonably well but will likely need refinement once the pure CO_2 data is modelled.

The fit of the models to the minor and trace element compositional evolution during the experiments on the upper Precipice Sandstone samples is shown in Figure 46. The Mn content was modelled with a high Mn calcite and fit the 497 model but only moderately to the data prior to the restart for sample 500 and not at all after the experiment restart. Only the Co and Cd appear to track well for sample 500. Pb is overestimated in the model and it appears that the Pb content of the carbonate minerals is likely too high; however, only one calcite and one siderite composition was used and overall, there is a reasonable fit for most of the minor and trace elements in the 497 model.

The best fit of the models to the major and minor element data for the upper Precipice Sandstone was achieved with dissolution of chlorite dominating over calcite and siderite and the precipitation of both $Fe(OH)_3$ and amorphous $Al(OH)_3$ (Figure 47). The models show significantly more reaction than for the lower Precipice Sandstone experiments. However, other than for Mn, the minor and trace element concentrations are not significantly different from the other Precipice experiments illustrating the role that adsorption plays in moderating metal concentrations and the ability of the models to capture this.

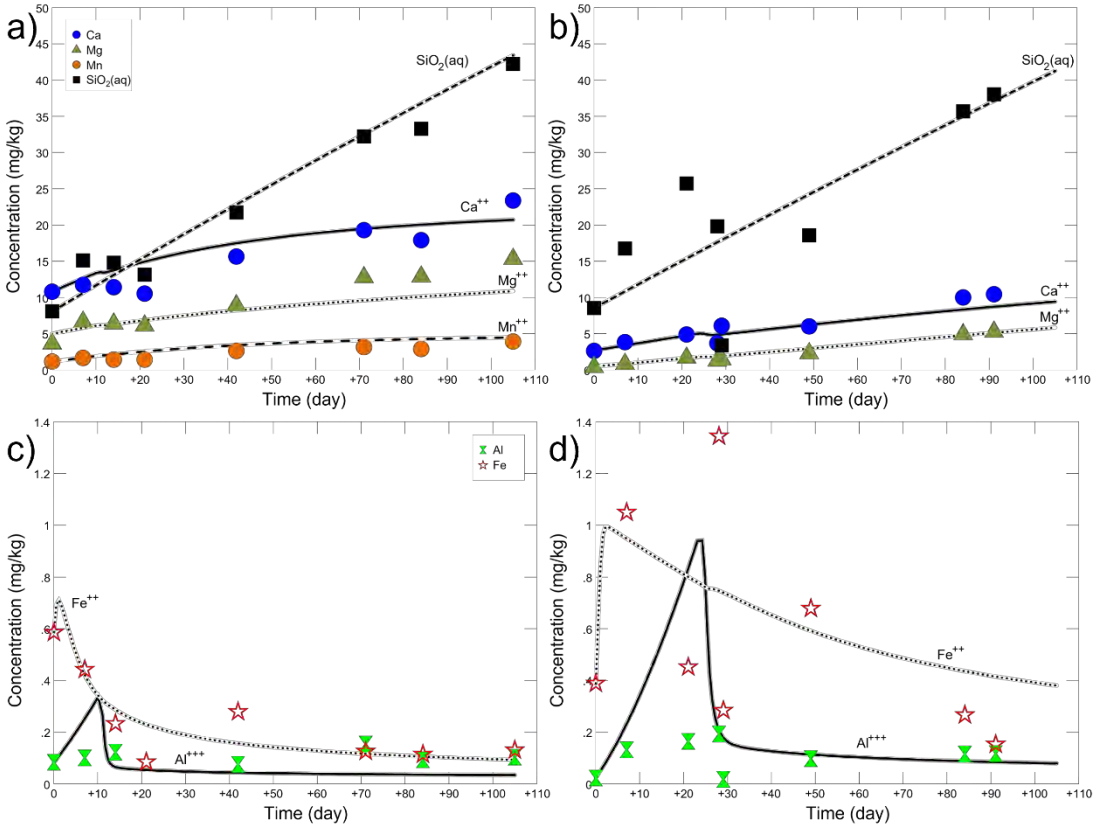

Figure 45: upper Precipice Sandstone experiments 497 (a and c) and 500 (b and d) with reaction path model traces for selected major (a and b) and minor (c and d) elements.

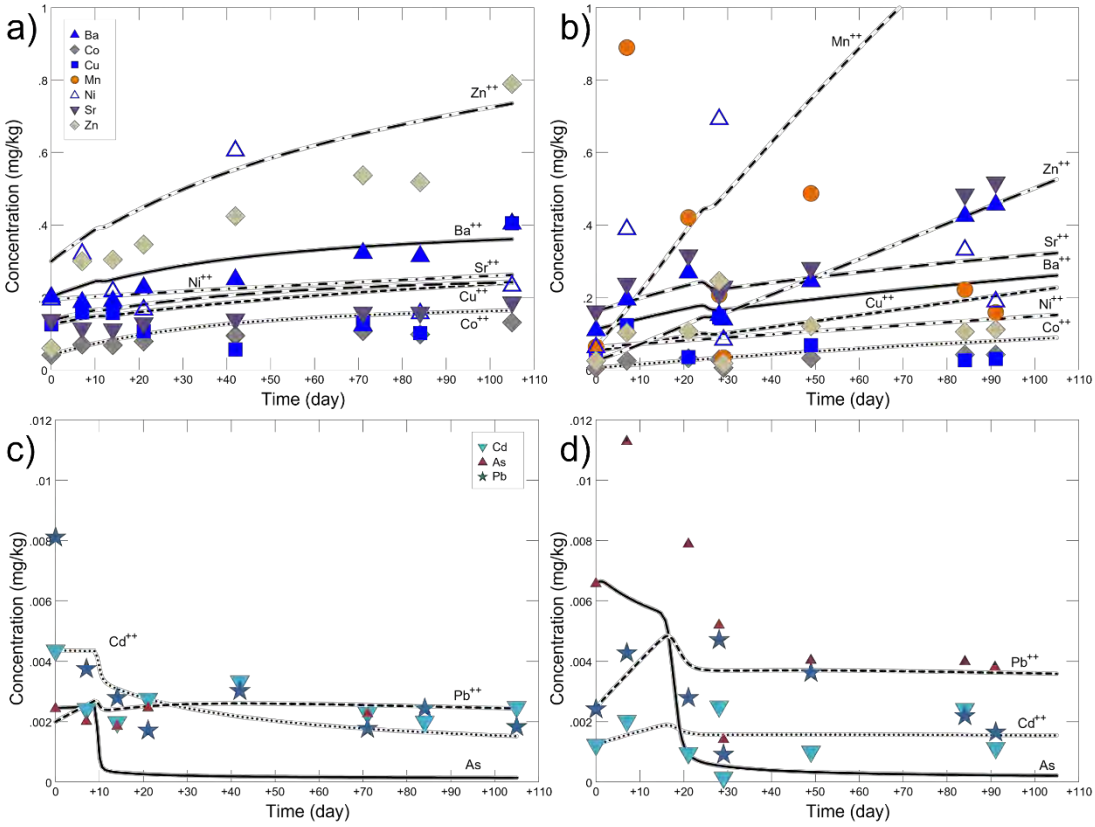

Figure 46: upper Precipice Sandstone experiments 497 (a and c) and 500 (b and d) with reaction path model traces for selected minor and trace elements in mg/kg.

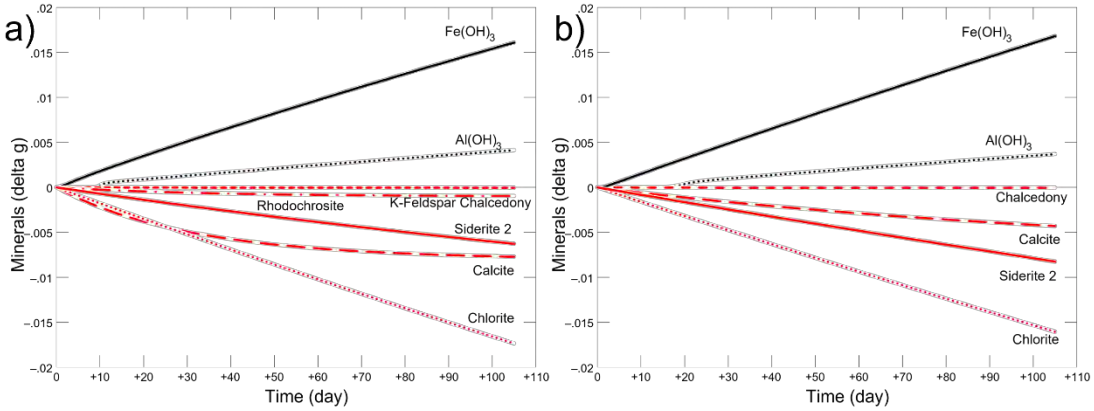

Figure 47: upper Precipice Sandstone model results for 497 (a) and 500 (b) indicating predicted mineral dissolution and precipitation as changes in grams over the course of the experiment.

Modelling of the experiments involving the Moolayember Formation samples is shown in Figure 48. Siderite, calcite and chlorite were detected in XRD of sample 477 while, for 481, siderite and chlorite were added to the model to achieve a better fit to the experiment data. Cation exchange was included in both models with CEC values of 17.9 meq/100 g for 477 and 17.7 meq/100 g for 481 being used. These CEC values are consistent with finer grained sedimentary rocks with high kaolinite content (Derkowski and Bristow, 2012; Revil and Leroy, 2004). For the modelling of 481, the initial water chemistry was adjusted for the SiO_2, Ca and Mg content to lower values to demonstrate how the modelled trend can fit the experiment if the initial displacement is ignored. Without the shift, it is not possible to fit the model to the experiment data without invoking very unlikely processes. In 481, the high Zn content was achieved through modelling sphalerite dissolution.

The model traces of the minor and trace element content overlain on the experiment data for the Moolayember Formation samples 477 and 481 are shown in the Figure 49. Similar to the previous models of the minor and trace elements, the models match the data reasonably well or match the data trends reasonably well if the initial composition is displaced or shifted to higher or lower values than the subsequent data.

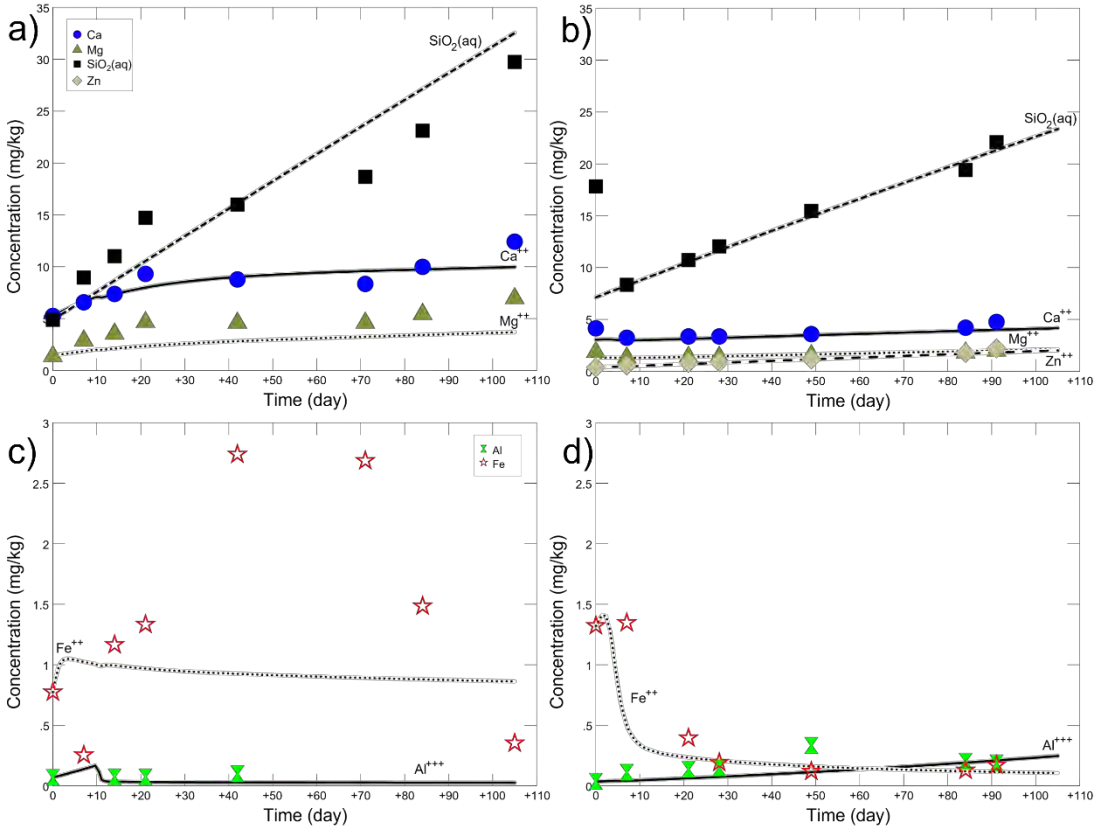

Figure 48: Moolayember Formation experiments 477 (a and c) and 481 (b and d) with reaction path model traces for selected major (a and b) and minor (c and d) elements.

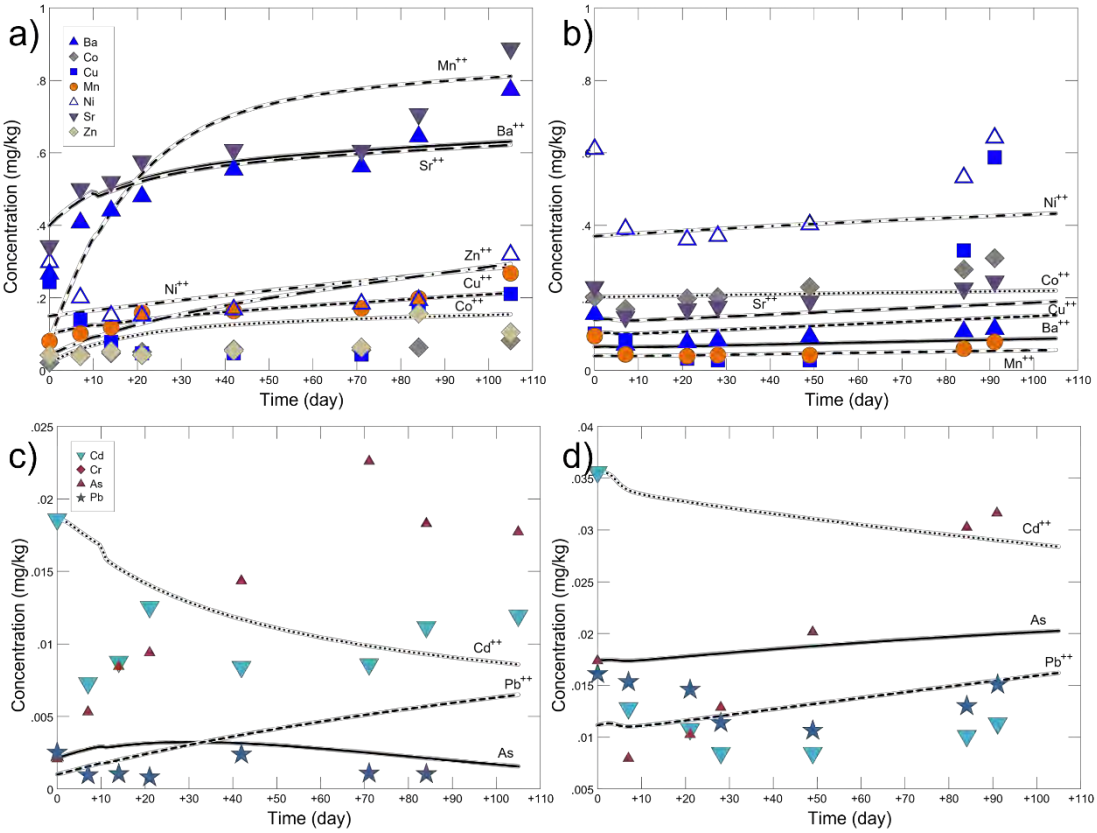

Figure 49: Moolayember Formation experiments 477 (a and c) and 481 (b and d) with reaction path model traces for selected minor and trace elements in mg/kg.

Changes in mineral content predicted by the Moolayember Formation models are shown in Figure 50. Dissolution of siderite, chlorite and calcite with minor amounts of chalcedony (quartz) and K-feldspar are predicted in the model of sample 477. The model of sample 481 shows that siderite and chlorite dissolution dominate, with some sphalerite and minor chalcedony dissolution taking place. $Fe(OH)_3$ precipitation takes place in both models and 477 also shows that some amorphous $Al(OH)_3$ precipitation occurs in order to get the best fit of the models to the data. The amount of $Fe(OH)_3$ precipitation in 477 is the highest and that is reflected in the trace element behaviour where decreases in Cd and As are modelled.

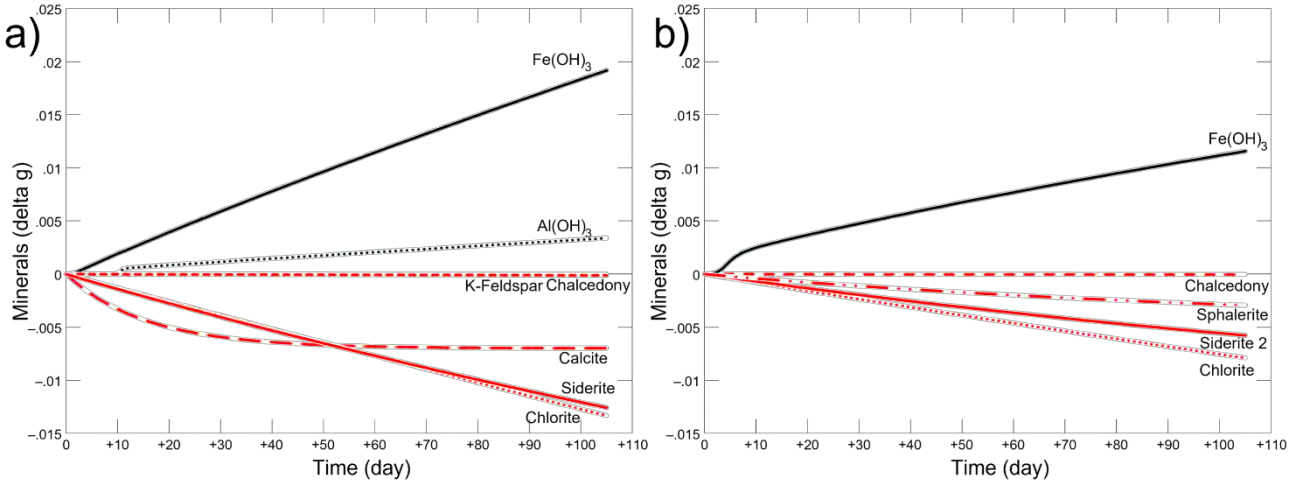

Figure 50: Moolayember Formation model results for 477 (a) and 481 (b) indicating predicted mineral dissolution and precipitation as changes in grams over the course of the experiment.

Experiments were run using pure CO_2 to evaluate the role of adsorption on newly formed sites from the precipitation of $Fe(OH)_3$ in the experiments with O_2 as a trace gas and to evaluate the consistency of the experimental results. With trace gases the precipitation of $Fe(OH)_3$ was expected to be much higher than without. The major ion chemistry of the pure CO_2 experiments was very similar to the results with trace gases for all of the samples (Figures 51 and 52). The minor and trace element relative amounts were also consistent between the experiments with and without trace gases (Figures 53 and 54), indicating that the experiments are repeatable, and the modelling is robust and capable of capturing the reactions and the rates. However, it was apparent that the pure CO_2 experiments contained some O_2 as precipitation of $Fe(OH)_3$ appeared to be controlling the Fe content. The model O_2 contents were orders of magnitude lower than those for the experiments with trace gases but none the less, $Fe(OH)_3$ precipitated (Figure 52 and Figure 55). The results of the experiments are not normalised to the amount of core initially present so the plots are in most cases not directly comparable since the amounts of the minerals impact the rates and extents of reactions. The shorter pure CO_2 experiments tend to have precipitation and dissolution rates and total amounts that are consistent with the experiments with trace gases but are higher in some cases. This may be the result of greater mass of sample used in the pure CO_2 experiments. There was also a requirement for Al mineral precipitation in order to get the model to history match the 489 experiment (Figure 52), which was not required in the experiment with the trace gases.

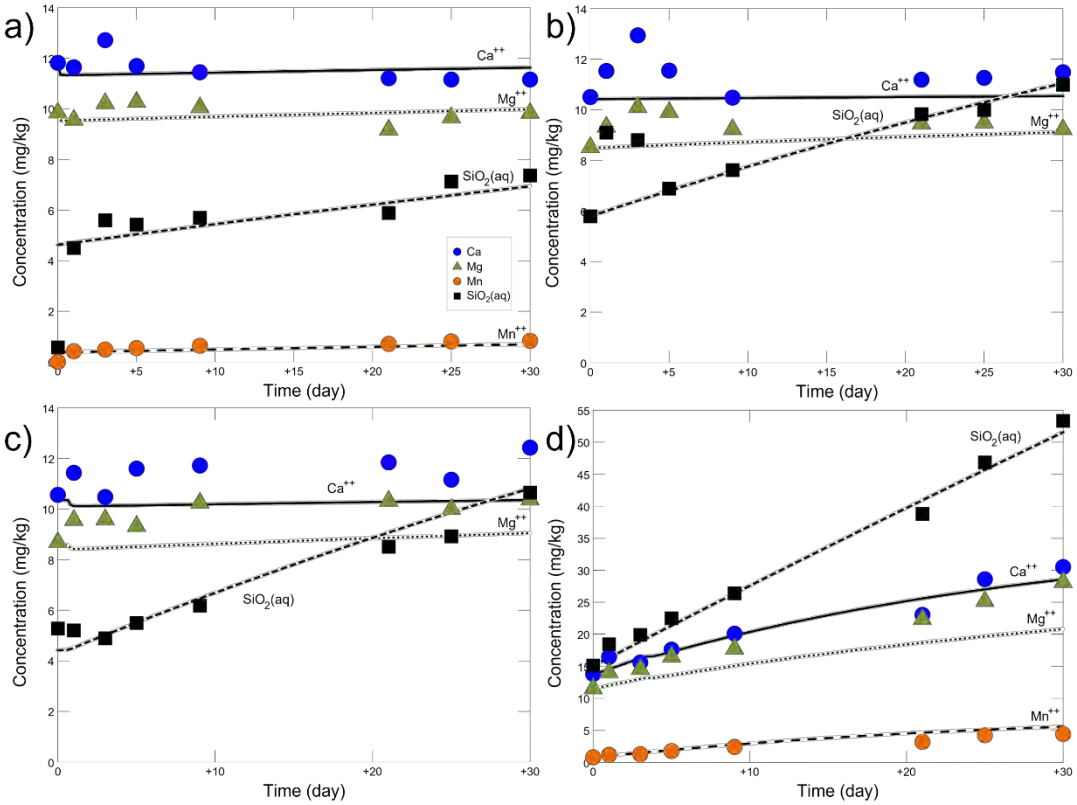

Figure 51: Precipice Sandstone pure CO_2 experiments of samples 486 (a), 489 (b), 495 (c), and 497 (d) with reaction path model traces for selected major elements in mg/kg.

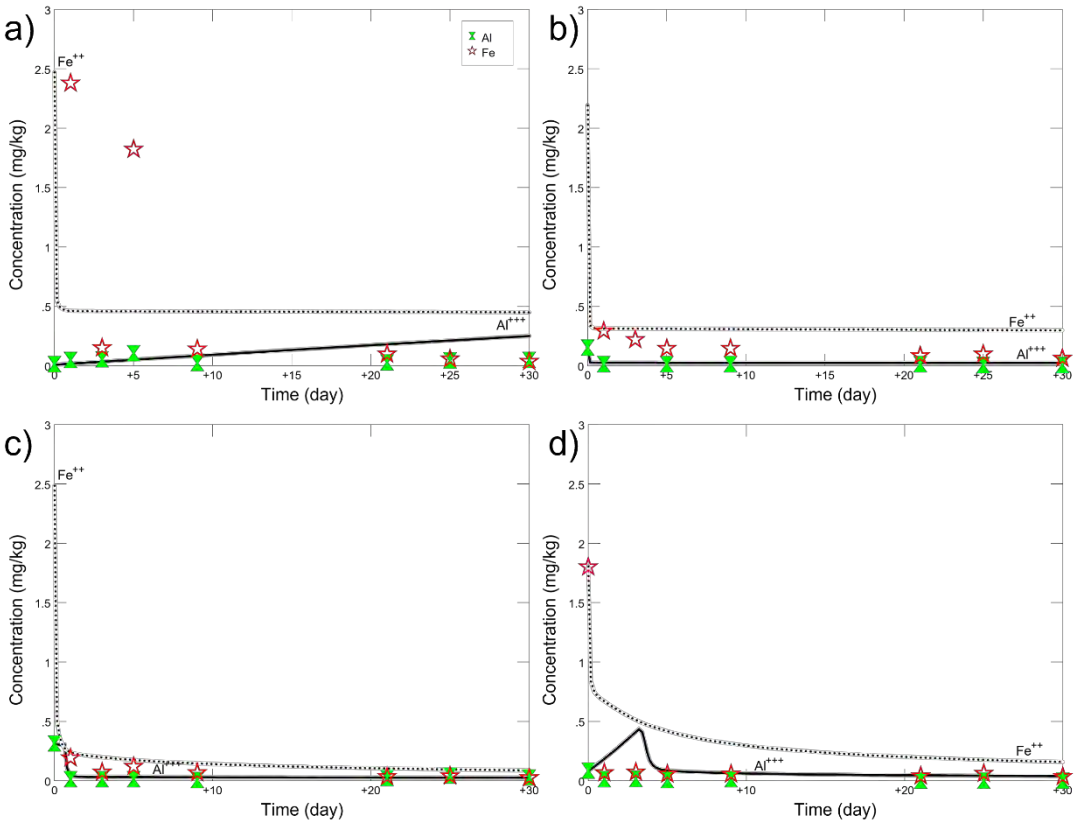

Figure 52: Precipice Sandstone pure CO_2 experiments of samples 486 (a), 489 (b), 495 (c), and 497 (d) with reaction path model traces for Al and Fe in mg/kg.

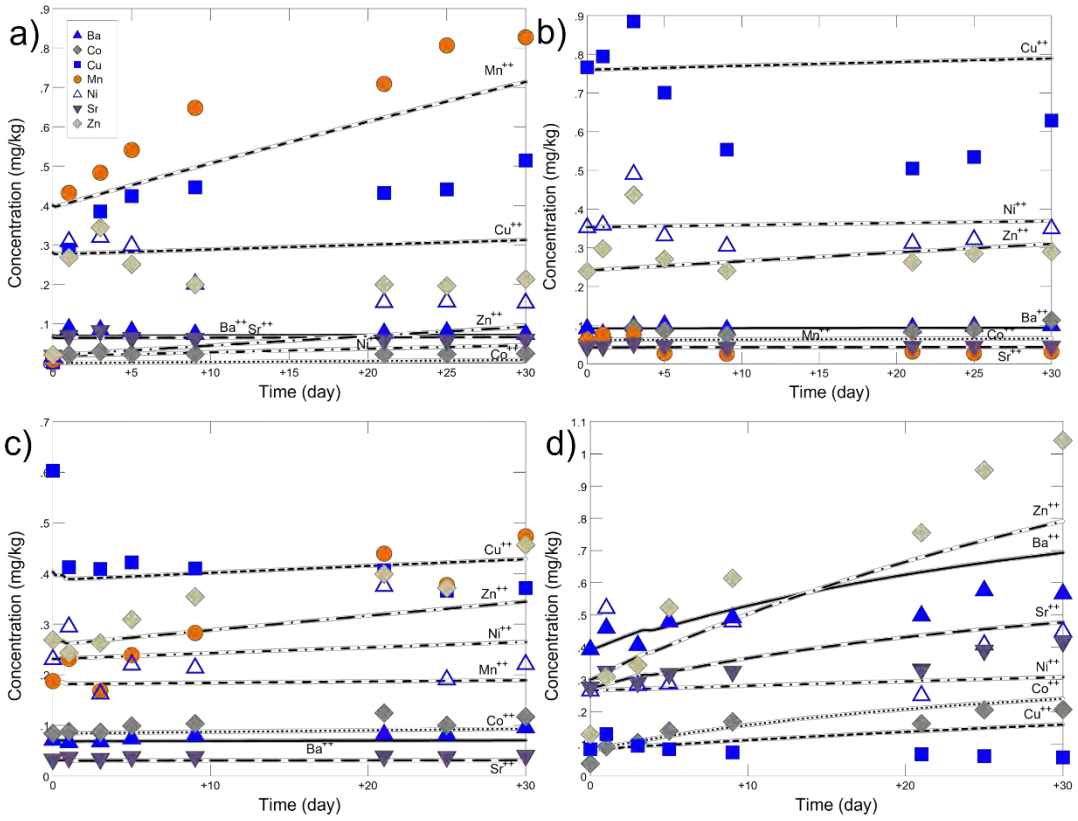

Figure 53: Precipice Sandstone pure CO_2 experiments of samples 486 (a), 489 (b), 495 (c), and 497 (d) with reaction path model traces for minor and trace elements Ba, Co, Cu, Mn, Ni, Sr and Zn in mg/kg.

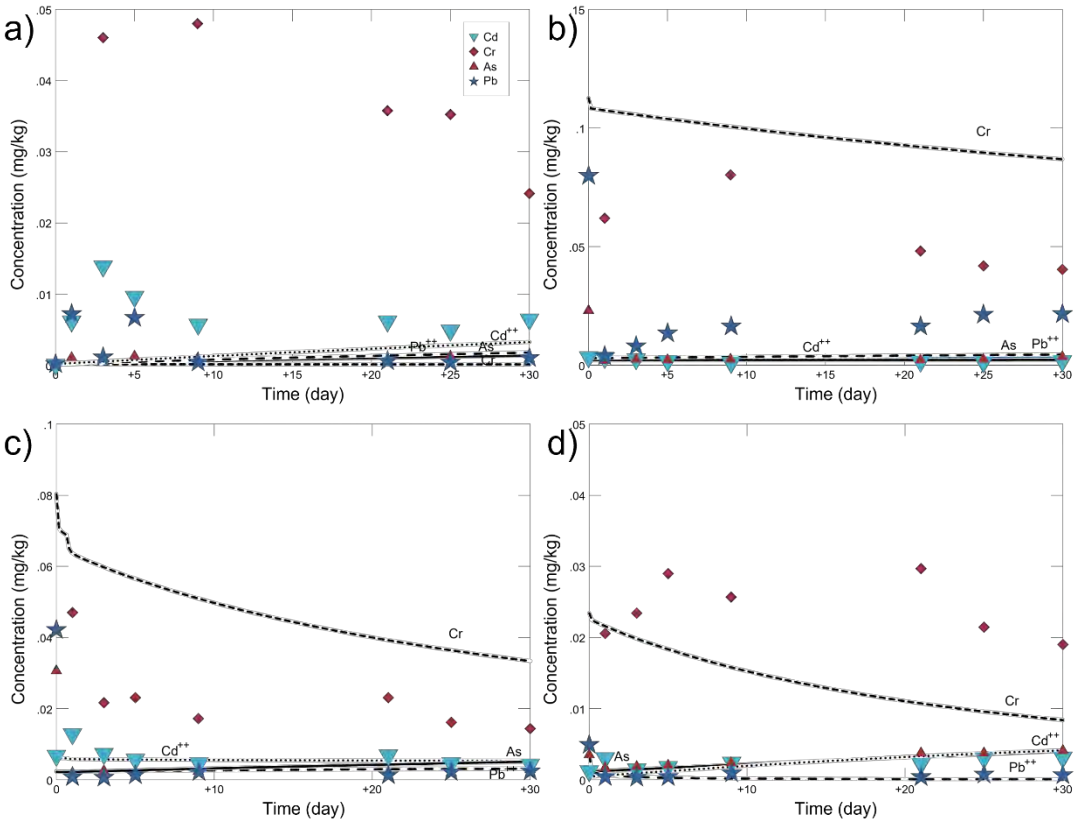

Figure 54: Precipice Sandstone pure CO_2 experiments of samples 486 (a), 489 (b), 495 (c), and 497 (d) with reaction path model traces for trace elements Cd, Cr, As and Pb in mg/kg.

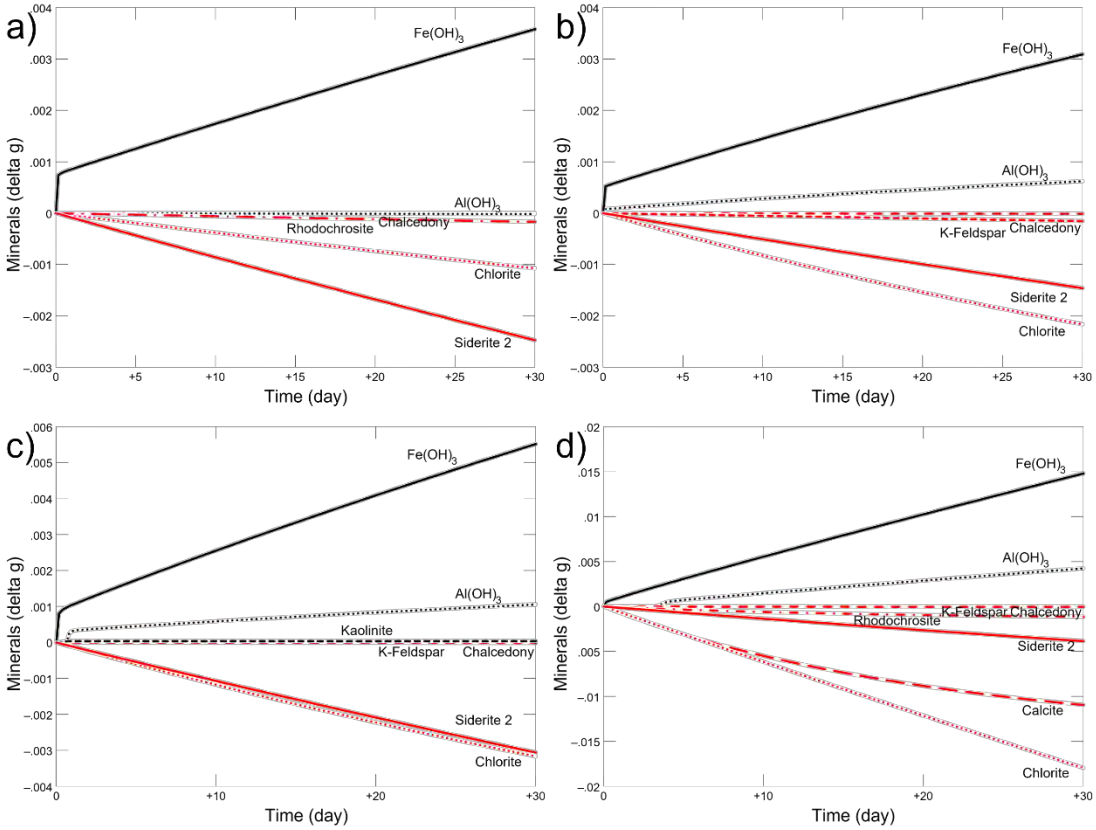

Figure 55: Precipice Sandstone pure CO_2 experiments of samples 486 (a), 489 (b), 495 (c), and 497 (d) with reaction path model traces for minerals.

4.3. Summary

The reaction path modelling shows that carbonate minerals and chlorite are the main minerals reacting in the experiments for all the different rock units. Precipitating minerals include $Fe(OH)_3$ and $Al(OH)_3$. Adsorption was modelled for $Fe(OH)_3$ and $Al(OH)_3$ precipitation. The mobilisation of trace metals is reasonably modelled using four different carbonate minerals that incorporate trace element content, along with cation exchange and adsorption on newly formed sites. Without cation exchange and adsorption, the models are less capable of history matching the data from the experiments. The modelling indicates that the experiments with and without trace gases are consistent.

5. Reaction Transport Modelling

5.1. Reactive Transport Model (RTM) Development

The reactive transport modelling was carried out using TOUGHREACT V3.0-OMP and V3.32-OMP (Sonnenthal et al., 2014) with the Equation of State (EOS) module ECO2N V1.0 (Pruess and Spycher, 2007). TOUGHREACT enables coupled multiphase fluid and heat flow, solute transport and chemical reactions. TOUGHREACT utilizes an integrated finite difference spatial discretization to solve flow and reactive-transport equations at each time step using the Newton-Raphson method. The code incorporates non-isothermal multiphase advection, diffusion, and dispersion, coupled with aqueous speciation and equilibrium and kinetically controlled solute-solute and solute-mineral reactions. TOUGHREACT assumes equilibrium between the gas phase constituents and the aqueous phase at the beginning of each time step. These versions of TOUGHREACT do not contain an EOS that specifically accounts for the effects of impurity gases on the flow and transport properties of CO_2, but they do allow for the inclusion of minor impurity gases in the CO_2 stream. The result is that for minor (<1%) impurity gases where there is little expected impact on CO_2 physical properties, the chemical behaviour is correct. In this report radial and 3D reactive transport models were produced that incorporate the injection of mixed gas (CO_2-O_2-NO-SO_2) into model domains populated by mixed mineralogy representative of the different hydrostratigraphic units in the study area. Dawson et al. (2021) evaluated the role of the Moolayember Formation and the overlying upper Precipice Sandstone on flow, transport and water quality impacts and determined limited penetration into, and flux out of, the upper Precipice Sandstone and the Moolayember Formation indicated that they could be ruled out as potential major sources of trace elements of concern to the Lower Precipice Sandstone reservoir. Radial models were run in this study to verify this observation and confirmed the low potential for fluxes into the lower Precipice Sandstone from the overlying upper Precipice Sandstone and the underlying Moolayember Formation. To save computational capacity, the radial and 3D models generated for this work did not include the Moolayember Formation or the upper Precipice Sandstone seal.

For both the reaction path and reactive transport models, in addition to mineral phases, adsorption sites were assigned. The data for the adsorption site behaviour is derived from the database of Dzombak and Morel (1990) and incorporated into the thermodynamic database. The Dzombak and Morel (1990) database is a compilation of many studies of adsorption on $Fe(OH)_3$ with the majority of these conducted at low temperatures. The database adsorption constants were adjusted to history match the batch experiments during which adsorption took place to better characterise the system at P and T. Geochemist's Workbench and TOUGHREACT allow modelling of adsorption by assigning specific sites to an existing mineral phase(s) and linking these to strong and weak sites defined in the basis species. For these simulations, sites were assigned to the $Fe(OH)_3$ defined in the mineral phases. The number of weak and strong sites was set at 0.577 and 1.44e-3 mol sites/mol $Fe(OH)_3$ based on the modelling of the batch experiments. The initial composition of elements occupying the sites is calculated by TOUGHREACT after the initial speciation as an equilibrium composition, so that the trace element content on the adsorption sites occur in addition to the defined aqueous composition. In the setup of these models, the equilibrated site occupation of trace elements never exceeded an approximately 20 ppm contribution of any given element to the bulk chemistry of the units.

In Dawson et al. (2021), models were also run with adsorption site amounts 10 times higher and 0.5 times and 10 times lower to evaluate sensitivity. With the higher adsorption site numbers, the trace element content of the initial equilibrated HSU generally exceeded the bulk chemistry trace element contents of many of the trace minerals. With the lowest site density, adsorption played an insignificant role in the trace element behaviour in the models. Because the adsorption site numbers were determined from the P-T-X experiments and were consistent for the majority of the modelling of those experiments regardless of what HSU were modelled, these site density numbers were determined to be the most appropriate.

Additional kinetic constraints were placed on the oxidation reaction of the dissolved gas species (O_2, SO_2, and NO) to limit the extent of numerical dispersion created proximal to the injector where highly soluble SO_2 tends to concentrate, and equilibrium assumptions between the gas phase and dissolved phase are compromised as well as to bring greater numerical stability to the system where very large changes in concentrations (up to 1e60) are expected due to reduction-oxidation (redox) reactions. Reaction rates were calculated using the transition state theory (TST) equation $r = k_i \prod(a_j^m)*(1-Q/K)$ where k_i is the rate, a_j^m is the activity of product term species j to its stoichiometric coefficient m, Q is the ion activity product and K is the reaction equilibrium constant. Precipitation rates in TOUGHREACT were calculated using equation 2 with the assumption that TST applies.

The following redox reactions were constrained by aqueous kinetics, product term species included HS^-, O_2(aq), SO_2(aq) and NO(aq) (Eqn. 4-6):

$$O_{2(aq)} + 0.5HS^- \leftrightarrow 0.5H^+ + 0.5SO_4^{-2}$$ Eq. 4 Rate = 8.55e-6 mol/s

$$SO_{2(aq)} + H_2O \leftrightarrow 1.75H^+ + 0.75SO_4^{-2} + 0.25HS^-$$ Eq. 5 Rate = 2.70e-5 mol/s

$$NO_{(aq)} + 0.75O_2 + 0.5H_2O \leftrightarrow H^+ + NO_3^-$$ Eq. 6 Rate = 8.40e-5 mol/s

5.2.1. Radial Model Setup

The initial full radial model domain is shown in Figure 56 and the set up used in the modelling, without the Moolayember Formation and the upper Precipice Sandstone seal, is shown in Figure 57. In this model there are 20 identified hydrostratigraphic units (HSU) from analysis of well logs and core, 18 in the lower Precipice Sandstone in addition to the Moolayember Formation and the upper Precipice Sandstone (Table 21 and Figure 58). The lower Precipice A Sandstone was modelled as 40 m thick and contained 9 HSU with one lower permeability hydrostatic unit at 5 m above the base and the low permeability lower Precipice B Sandstone ("Cave facies") at the top. Above the "Cave facies" the lower Precipice C Sandstone was 29 m thick and consisted of 7 HSU, with two low permeability HSU at 15 m and 23 m above the base of the lower Precipice C Sandstone. The radial model consists of a spatial domain represented by a 2D (X,Z) slice of a cylinder centred on the injection well (Figures 56 and 57). The full model domain has a 100 m thickness (Z) and 5000 m length (X) populated by porous-permeable media defined by the HSU porosity, permeability and mineralogy (Tables21 and 22) and the equilibrated formation water chemistry (Table 23). To replicate CTSCo's planned West Moonie test injection program, injection was 110,000 tonnes of CO_2 with 400 ppm O_2, 15 ppm NO(g) and 5 ppm SO_2(g) per year for 3 years into the bracketed bottom 28 m (-2064 to -2092 m) of the Precipice Sandstone model domain shown in Figure 56. This injection interval includes HSU 1-6 of Table 21. Additional simulations were run with pure CO_2 injection and a variation with a shorter injection interval that spanned only HSU 5 and 6 (18 m, -2064 to -2082 m)) to evaluate the impact of the vertical heterogeneity of the HSU at West Moonie 1. The model was discretised using a radial grid consisting of 150 cells in the X direction and 39 cells in the Z direction. Grid spacing was highly refined at the injection site placed at the left side. The full radial model included a 14 m thick section of the Moolayember Formation that was discretised into 4 layers and a 9 m thick section of the upper Precipice Sandstone discretised as 4 layers. The boundary conditions included no flow at the top and bottom of the model domain and a fixed head boundary in HSU 1, 6, 8, 11, 13 and 17 on the right-hand side of the model domain.

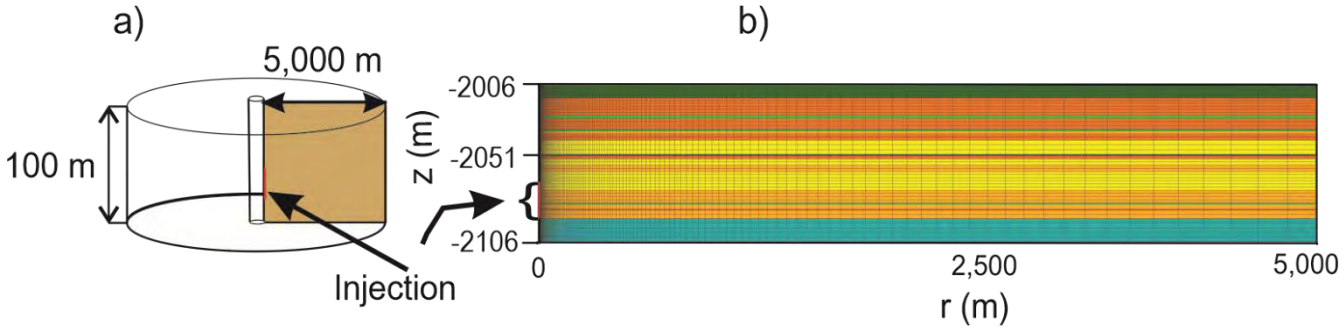

Figure 56: Full radial RTM model setup showing a) radial model with a slice indicating the Moolayember Formation and the lower and upper Precipice Sandstone hydrostratigraphic units (HSU). b) 2D slice of the radial model showing the injection interval and refinement of the gridding of the HSU. The Moolayember Formation is shown at the base (blue) and the upper Precipice at the top of the model (dark green). The yellow-coloured Precipice Sandstone HSU have the highest porosity and permeabilities, the brown HSU have intermediate porosities and permeabilities and the green have low porosities and permeabilities. (10 times vertical exaggeration).

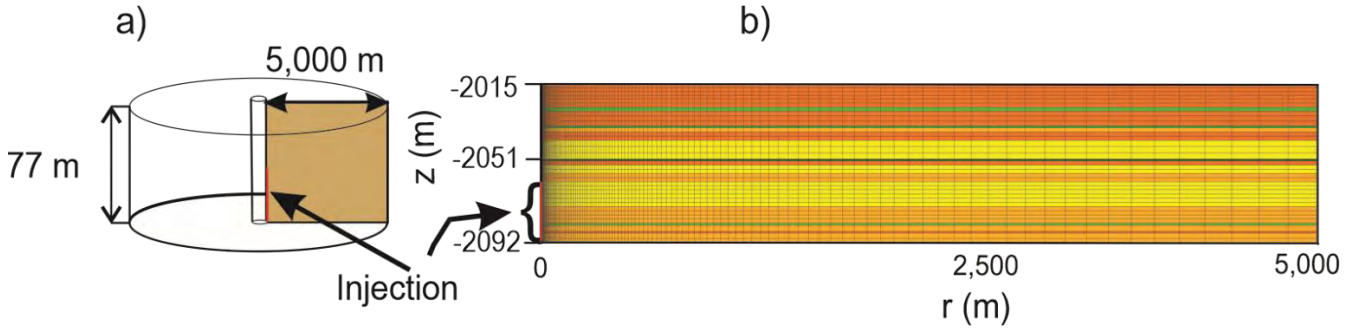

Figure 57: Radial model setup without the Moolayember Formation and upper Precipice Sandstone showing a) radial model with a slice indicating the lower Precipice Sandstone hydrostratigraphic units (HSU). b) 2D slice of the radial model showing the injection interval and refinement of the gridding of the HSU 1-18. The yellow-coloured HSU have the highest porosity and permeabilities, the brown HSU have intermediate porosities and permeabilities and the green have low porosities and permeabilities. (11 times vertical exaggeration).

Table 21: Mineralogy sample assignment, discretisation, hydrologic, and physical properties of the different hydrostratigraphic units used in the model[1].

	Moolayember	HSU 1	HSU 2	HSU 3	HSU 4	HSU 5	HSU 6	HSU 7	HSU 8	HSU 9	HSU 10	HSU 11	HSU 12	HSU 13	HSU 14	HSU 15	HSU 16	HSU 17	HSU 18	U. Precipice
Mineralogy	477	483	484	483	484	485	485	486	485	489	484	486	489	490	484	495	492	495	495	497
Thickness (m)	15	5	1	3	1	8	12	4	4	2	1	9	4	2	1	7	2	4	7	9
Top (m)	2092	2087	2086	2083	2082	2074	2062	2058	2054	2052	2051	2042	2038	2036	2035	2028	2026	2022	2015	2006
Cells (z)	5	2	1	1	1	4	6	2	2	1	2	3	2	1	1	3	1	2	4	4
Density (kg/m^3)	2600	2600	2600	2600	2600	2600	2600	2600	2600	2600	2600	2600	2600	2600	2600	2600	2600	2600	2600	2600
Porosity	0.06	0.18	0.14	0.18	0.1	0.18	0.18	0.18	0.18	0.14	0.1	0.18	0.14	0.18	0.1	0.14	0.1	0.14	0.14	0.05
Permeability (m^2) x	1.97E-15	2.81E-12	6.51E-13	1.78E-12	3.55E-14	2.81E-12	2.81E-12	2.81E-12	2.81E-12	6.51E-13	3.55E-14	2.81E-12	6.51E-13	2.81E-12	3.55E-14	6.51E-13	3.55E-14	6.51E-13	6.51E-13	9.87E-16
Permeability (m^2) y	1.97E-15	2.81E-12	6.51E-13	1.78E-12	3.55E-14	2.81E-12	2.81E-12	2.81E-12	2.81E-12	6.51E-13	3.55E-14	2.81E-12	6.51E-13	2.81E-12	3.55E-14	6.51E-13	3.55E-14	6.51E-13	6.51E-13	9.87E-16
Permeability (m^2) z	9.87E-17	7.31E-13	8.47E-14	3.91E-13	1.78E-14	7.31E-13	7.31E-13	7.31E-13	7.31E-13	8.47E-14	1.78E-14	7.31E-13	8.47E-14	7.31E-13	1.78E-14	8.47E-14	1.78E-14	8.47E-14	8.47E-14	4.93E-17
*Permeability (mD) x	2	1600	260	1500	120	1100	2843	1800	3000	660	4	2200	360	1600	10	650	30	750	500	1
*Permeability (m^2) x	1.97E-15	1.58E-12	2.57E-13	1.48E-12	1.18E-13	1.09E-12	2.81E-12	1.78E-12	2.96E-12	6.51E-13	3.55E-15	2.17E-12	3.55E-13	1.58E-12	9.87E-15	6.41E-13	2.96E-14	7.40E-13	4.93E-13	9.87E-16
*Permeability (m^2) z	9.87E-17	3.16E-13	2.31E-14	2.66E-13	1.18E-14	1.74E-13	7.30E-13	3.91E-13	7.70E-13	8.47E-14	1.78E-16	5.21E-13	3.55E-14	3.16E-13	4.93E-16	8.34E-14	2.37E-15	1.04E-13	5.92E-14	4.93E-17
van Genuchten λ	0.53	0.4	0.5	0.457	0.53	0.4	0.4	0.4	0.4	0.5	0.53	0.4	0.5	0.4	0.53	0.5	0.53	0.5	0.5	0.53
liquid residual saturation	0.26	0.26	0.14	0.26	0.26	0.26	0.26	0.26	0.26	0.14	0.26	0.26	0.14	0.26	0.26	0.14	0.26	0.14	0.14	0.26
gas residual saturation	0.10	0.1	0.1	0.1	0.10	0.1	0.1	0.1	0.1	0.1	0.10	0.1	0.1	0.1	0.10	0.1	0.10	0.1	0.1	0.10
capillary entry pressure (Pa)	200000	1727	1724	1721	20000	1727	1727	1727	1727	1724	20000	1727	1724	1727	20000	1724	20000	1724	1724	200000

1. Horizontal permeabilities are the average measured (for each HSU) whereas vertical permeability estimates are from the CTSCo injection and flow model. Precipice Sandstone relative permeability and capillary properties derived from FEI-Lithicon Technical Report for ANLEC Project 7-0311-0128.

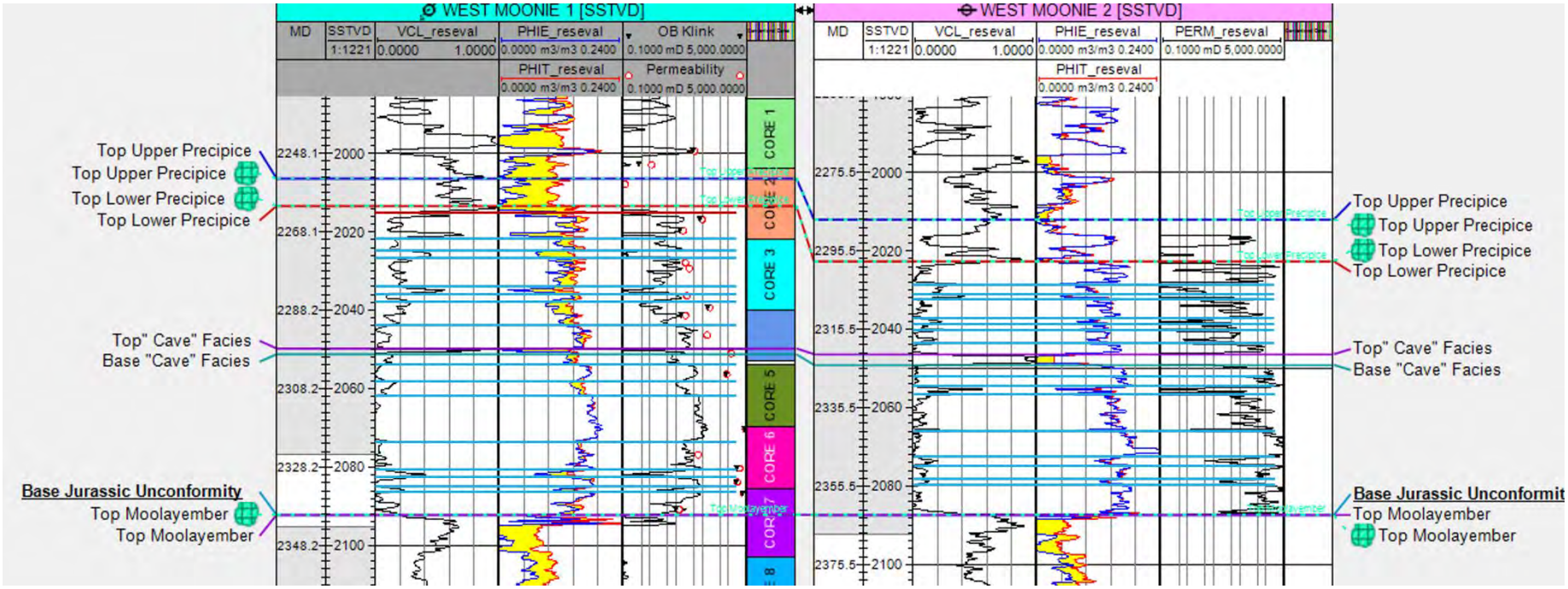

Figure 58: West Moonie 1 and 2 geophysical well logs showing the formation tops and the blue lines show the different HSU used in the reactive transport models (bottom to top, 1 is top Moolayember Formation, 2 – 18 are lower Precipice Sandstone, and 20 is upper Precipice Sandstone/lower Evergreen Formation).

Table 22: Mineralogy used in the model set up in volume %.

Core depth (SSTVD)	2098.5	2091.1	2082.5	2080.6	2074.7	2059.2	2040.6	2036.2	2026.1	2015.7	2007	1994.5
(mRT)	2346.40-.51	2339.00-.17	2330.41-.55	2328.54-.59	2322.61-.73	2307.08-.20	2288.49-.61	2284.13-.24	2274.10-.20	2263.61-.77	2254.94-2255	2245.44-.54
Sample ID	477	481	483	484	485	486	489	490	492	495	497	500
Quartz	45.9	76	94.7	44	94.6	94.4	85.2	79.4	69.3	61.8	67.9	62.5
Siderite 1	0.39	0	0.174	0	0	0	0	0	0	0	0	0
Siderite 2	0	0.123	0	0.125	0.19	0.144	0.11	0.1	0.247	0.165	0.303	0.9
Ankerite	0	0	0	0	0	0	0	0	0.01	0	0	0
Calcite 1	0.031	0	0	0	0	0	0	0	0	0	0.15	0.07
K-feldspar	15.7	0	1.47	0	0.66	0	1.48	0.95	8.94	4.74	9.35	5.43
Kaolinite	14.3	19.2	1.8	25.9	1.43	1	5.27	8.57	7.59	5.9	15.8	21.9
Illite	9.2	1.38	0	27.6	1.69	0.45	4.39	8.29	9.4	8.16	0	7.57
Chlorite	3.51	0.9	0.064	0.032	0.079	0.06	0.052	0.06	0.65	0.108	2.64	1.64
Fe(OH)3	5.00E-06	5.00E-06	5.00E-06	5.00E-05	5.00E-06	5.00E-06	5.00E-06	5.00E-06	5.00E-06	5.00E-06	5.00E-05	5.00E-05

For all of the simulations, relative permeability of the aqueous phase was set through the van Genuchten-Mualem model and the gas phase through Corey's curves, and capillary pressures were calculated using the van Genuchten function (Pruess et al., 1999). Changes in porosity during simulations were used to calculate permeability changes using the cubic law (Xu et al., 2014). This formulation may not reflect the complexity of natural geologic media in terms of porosity-permeability relationships, especially with respect to the role of factors such as pore size distribution, pore shape and connectivity, but does allow for an estimation of permeability reduction through pore throat closure at finite porosity. Changes in permeability depend on the changes in porosity and also on how the pore space geometry evolves, in particular where dissolution and precipitation occur within the pore space. The process is media dependent and is very difficult to simulate accurately.

The mineralogy for each of the HSU is based on that established in the reaction path modelling section. The formation major and minor element water chemistry is calculated by reacting the mineralogy with the initial water chemistry (based on the batch experiments and a drill mud contaminated water sample collected from West Moonie 1) for 1000 years. A previous modelling study established that the initial formation water composition used in the modelling had little influence on model outcomes for the range of potential formation water composition in the region (Haese et al., 2016). The initial formation water trace element content used in the models (Table 17) is within a few ppb of the sampled groundwater. While the trace element content of adsorption sites can be partially deduced from the sequential extraction data there is some ambiguity in the method used regarding weakly adsorbed species and trace elements associated with carbonates. This makes the adsorption site occupation the most difficult to establish and one of the parameters with the highest uncertainty. Upper limits for trace element content on the absorption sites are constrained by the bulk chemistry. The site occupancy is set by the formation water composition using the adsorption constants in the thermodynamic database. The adsorption constants of Dzombak and Morel (1990) were modified to history match the experiments accounting for the higher temperature (80°C vs 25°C of the database). However, no other adsorption site types were used in the modelling and adsorption to clay mineral surfaces and other oxides may be important in the more clay-rich HSU.

Details of the chemical component of the reactive transport models are provided in Appendix D. Calcite, siderite, and ankerite used in the models are of mixed composition and contain varying amounts of trace elements (including As, Ba, Cd, Co, Cu, Mn, Ni, Pb, Sr and Zn) as described in the reaction path modelling section. Dissolution of these minerals results in the addition of the trace elements in proportions defined by the mineral stoichiometry. In addition, trace elements are associated with adsorption sites linked to the surface of the hydrous ferric oxide ($Fe(OH)_3$). The total amounts of sites are dependent on the amount of $Fe(OH)_3$, therefore the

amount of sites can vary depending on changes, either through dissolution or precipitation, to the volume fraction of $Fe(OH)_3$. Thus, the adsorption sites can be described in terms of sites per kg of rock which relates only to the volume fraction of $Fe(OH)_3$ or sites per kg of water which takes into account the porosity and reflects how many sites are available to interact with a volume or mass of the formation water. The adsorption sites include both strong and weak sites and have a pH dependent charge that is dominated by a positive charge at lower pH (hfo_woh2+), a neutral or no charge composition (hfo_woh) at moderate pH and negative charge at higher pH (hfo_wo-) leading to changes in surface attraction to the ions in solution as the pH changes (Dzombak and Morel, 1990). In these models, the carbonates act largely as sources of trace elements while adsorption can be a source or a sink.

Table 23: Reactive transport initial water composition for each of the HSU in ppm and trace metals in ppb. Adsorption sites are reported as mol sites per kg water.

	Moolayember	HSU 1	HSU 2	HSU 3	HSU 4	HSU 5	HSU 6	HSU 7	HSU 8	HSU 9	HSU 10	HSU 11	HSU 12	HSU 13	HSU 14	HSU 15	HSU 16	HSU 17	HSU 18	U. Precipice
Mineralogy	477	483	484	483	484	485	485	486	485	489	484	486	489	490	484	495	492	495	495	497
pH	7.34	7.14	7.23	7.29	7.24	7.16	7.19	7.18	7.17	7.34	7.24	7.13	7.34	7.24	7.24	7.34	7.23	7.34	7.34	7.44
Na	571	545	473	573	467	541	548	552	545	571	467	548	571	545	467	571	527	571	571	578
K	14.58	10.03	17.53	8.81	17.27	11.47	10.85	8.87	11.15	14.58	17.28	9.16	14.58	15.28	17.28	14.58	18.05	14.58	14.58	10.57
Ca	1.15	1.85	1.64	1.34	1.63	1.82	1.72	1.76	1.77	1.15	1.63	2.00	1.15	1.48	1.63	1.15	1.51	1.15	1.15	1.18
Mg	0.31	0.37	0.47	0.24	0.47	0.41	0.38	0.36	0.39	0.31	0.47	0.38	0.31	0.39	0.47	0.31	0.43	0.31	0.31	1.07
Fe	0.069	0.093	0.082	0.079	0.082	0.084	0.082	0.082	0.083	0.069	0.082	0.087	0.069	0.077	0.082	0.069	0.078	0.069	0.069	0.057
HCO_3^-	1284	1258	1038	1295	1018	1244	1256	1265	1250	1284	1018	1259	1284	1239	1018	1284	1193	1284	1284	1329
Cl	187	187	187	187	187	187	187	187	187	187	187	187	187	187	187	187	187	187	187	187
SO_4^{-2}	10.8	10.8	10.8	10.8	10.8	10.8	10.8	10.8	10.8	10.8	10.8	10.8	10.8	10.8	10.8	10.8	10.8	10.8	10.8	10.8
HS^-	4.00E-14	5.78E-13	3.32E-14	2.64E-13	2.52E-14	2.12E-13	1.73E-13	9.07E-14	1.88E-13	4.00E-14	2.53E-14	3.65E-13	4.00E-14	5.81E-13	2.53E-14	4.00E-14	3.09E-13	4.00E-14	4.00E-14	5.05E-12
NO_2^-	4.60E-06	4.60E-06	4.60E-06	4.60E-06	4.60E-06	4.60E-06	4.60E-06	4.60E-06	4.60E-06	4.60E-06	4.60E-06	4.60E-06	4.60E-06	4.60E-06	4.60E-06	4.60E-06	4.60E-06	4.60E-06	4.60E-06	4.60E-06
NO_3^-	6.33E-46	6.45E-46	6.42E-46	6.36E-46	6.42E-46	6.37E-46	6.36E-46	6.34E-46	6.36E-46	6.33E-46	6.42E-46	5.14E-48	6.33E-46	6.37E-46	6.42E-46	6.33E-46	6.37E-46	6.33E-46	6.33E-46	6.40E-46
NO(aq)	3.00E-26	3.00E-26	3.00E-26	3.00E-26	3.00E-26	3.00E-26	3.00E-26	3.00E-26	3.00E-26	3.00E-26	3.00E-26	3.00E-26	3.00E-26	3.00E-26	3.00E-26	3.00E-26	3.00E-26	3.00E-26	3.00E-26	3.00E-26
O_2(aq)	2.18E-37	7.09E-37	2.31E-37	2.36E-37	2.00E-37	8.14E-37	6.90E-37	7.43E-37	7.49E-37	2.18E-37	2.01E-37	1.07E-36	2.18E-37	4.37E-37	2.01E-37	2.18E-37	4.00E-37	2.18E-37	2.18E-37	1.75E-37
SO_2 (aq)	6.40E-06	6.40E-06	6.40E-06	6.40E-06	6.40E-06	6.40E-06	6.40E-06	6.40E-06	6.40E-06	6.40E-06	6.40E-06	6.40E-06	6.40E-06	6.40E-06	6.40E-06	6.40E-06	6.40E-06	6.40E-06	6.40E-06	6.40E-06
SiO_2(aq)	58.4	57.8	58.0	58.2	58.0	57.9	57.9	57.9	57.9	58.4	58.0	57.8	58.4	58.1	58.0	58.4	58.0	58.4	58.4	58.8
Al	32.6	20.9	25.4	29.1	25.8	22.1	23.3	22.8	22.7	32.6	25.8	20.5	32.6	26.0	25.8	32.6	25.6	32.6	32.6	40.3
As	2.23	2.23	2.23	2.23	2.23	2.23	2.23	2.23	2.23	2.23	2.23	2.23	2.23	2.23	2.23	2.23	2.23	2.23	2.23	2.23
Ba	445	445	445	445	445	445	445	445	445	445	445	445	445	445	445	445	445	445	445	445
Cd	0.1	0.1	0.1	0.1	0.1	0.1	0.1	0.1	0.1	0.1	0.1	0.1	0.1	0.1	0.1	0.1	0.1	0.1	0.1	0.10
Co	14.6	14.6	14.6	14.6	14.6	14.6	14.6	14.6	14.6	14.6	14.6	14.6	14.6	14.6	14.6	14.6	14.6	14.6	14.6	14.6
Cu	28.8	28.8	28.8	28.8	28.8	28.8	28.8	28.8	28.8	28.8	28.8	28.8	28.8	28.8	28.8	28.8	28.8	28.8	28.8	28.8
Mn	54.3	54.3	54.3	54.3	54.3	54.3	54.3	54.3	54.3	54.3	54.3	54.3	54.3	54.3	54.3	54.3	54.3	54.3	54.3	54.3
Ni	1	1	1	1	1	1	1	1	1	1	1	1	1	1	1	1	1	1	1	1
Pb	0.07	0.07	0.07	0.07	0.07	0.07	0.07	0.07	0.07	0.07	0.07	0.07	0.07	0.07	0.07	0.07	0.07	0.07	0.07	0.07
Sr	384	384	384	384	384	384	384	384	384	384	384	384	384	384	384	384	384	384	384	384
Zn	14.8	14.8	14.8	14.8	14.8	14.8	14.8	14.8	14.8	14.8	14.8	14.8	14.8	14.8	14.8	14.8	14.8	14.8	14.8	15
Adsorption sites strong	1.31E-06	8.54E-07	1.31E-05	9.73E-07	1.92E-05	8.54E-07	8.54E-07	8.54E-07	8.54E-07	1.31E-06	1.92E-05	8.54E-07	1.31E-06	8.54E-07	1.92E-05	1.31E-06	1.92E-05	1.31E-06	1.31E-06	8.70E-05
Adsorption sites weak	5.26E-04	3.43E-04	5.26E-03	3.90E-04	7.71E-03	3.43E-04	3.43E-04	3.43E-04	3.43E-04	5.26E-04	7.71E-03	3.43E-04	5.26E-04	3.43E-04	7.71E-03	5.26E-04	7.71E-03	5.26E-04	5.26E-04	1.10E-03

5.2.2. 3D Model Setup

The 3D model structure and gridding were initiated using data provided from the CTSCo Petrel™ model of the West Moonie EPQ10 site. The data provided was a 2 km by 2 km grid at 25 m spacing of the depths of the base of the lower Precipice Sandstone (top of the Moolayember Formation), base of the Cave facies, top of the Cave facies, top of the lower Precipice Sandstone and top of the upper Precipice. These were used to define the bottoms and tops of HSU based on the thickness of each of the HSU at West Moonie 1 and their fractional thickness for the lower Precipice C Sandstone above the Cave facies to the top of the lower Precipice Sandstone and the lower Precipice A Sandstone below the Cave facies to the bottom of the unit. The 3D model was set up as a 1.6 km by 1.6 km section centred on the proposed injection well location (Figures 59 and 60). The area was chosen based on the extent of CO_2 impacted water (super critical and dissolved) in the radial models. Grid refinement around the well and layers within each of the HSU is shown in Figures 59 and 60. The maximum area of the polygons close to the well was set at 0.25 m^2 and the maximum area for any polygons was set to 1600 m^2. The gridding resulted in 47,125 elements and 182,960 connections (interfaces) for the model. The Windows™ compiled edition of TOUGHREACT V 3.0 is constrained by the maximum amount of memory that is assigned by the OS which limits the number of elements to 60,000 and connections to 225,000. The limits are set in order to allow for large enough arrays to handle the chemical data (numbers of components, species, minerals, adsorption sites etc). Thus, in addition to the length of processing time the large reactive transport models require in order to run, a limiting factor on the domain size was the compiled code itself (unfortunately the authors did not have the source code for this version of TOUGHREACT so could not recompile with larger limits that conformed with the actual memory demand). No flow boundary conditions were imposed on the top and bottom and the sides of the model domain were assigned a fixed pressure. An analytical model (Warner et al., 1979) was applied to determine the radius of pressure influence and it was determined that for a 2 Darcy 35 m thick interval, the maximum pressure increase at 800 m was 0.24 bar at the chosen injection rate and, even for a 660 mD unit, the pressure would not exceed 0.64 bar above ambient at 800 m. The fixed pressure boundary at 800 m will thus have a minor effect on the pressure gradient and hence the flow rate but it appears to be limited. Injection of 110,000 tonnes per year for 3 years of CO_2 with 400 ppm O_2, 15 ppm NO and 5 ppm SO_2 was simulated, and the model was run until 10 years of a 100-year simulation (the simulation was halted due to a power outage after running for 2 weeks and there was not sufficient time to rerun the simulation from the beginning). Mineralogy, water chemistry and adsorption site composition were the same as those used in the radial models.

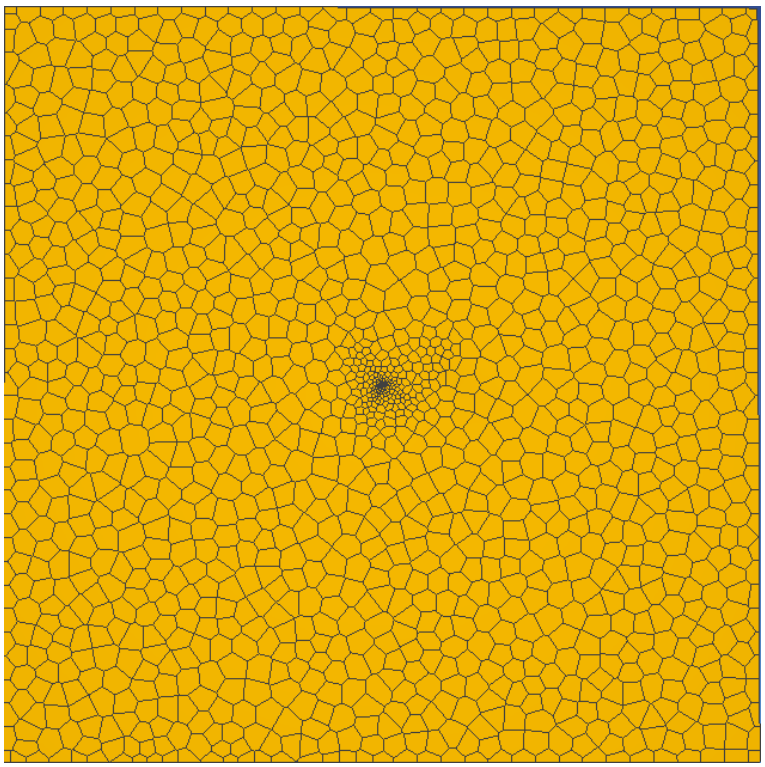

Figure 59: Top view of the model showing the 1.6 km x 1.6 km distribution of the polygonal cells with grid refinement centred on the injection well.

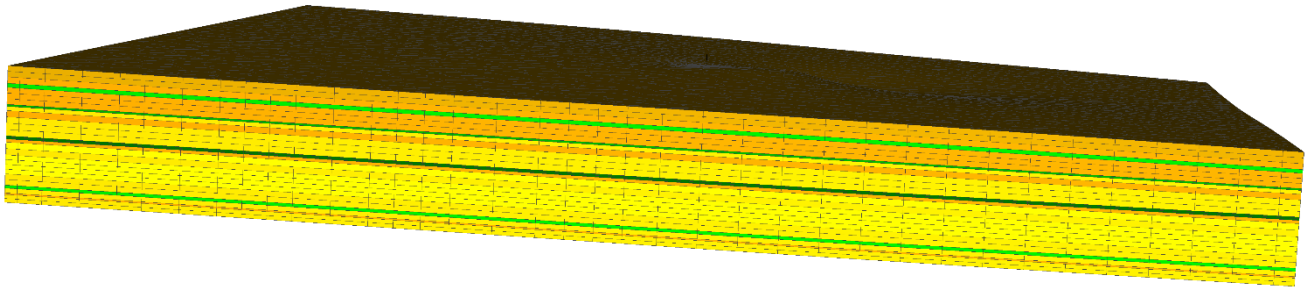

Figure 60: Side view of the 3D model showing the 17 lower Precipice Sandstone Precipice HSU and the subtle topography of the layering. The yellow-coloured HSU have the highest porosity and permeabilities, the brown HSU have intermediate porosities and permeabilities and the green have low porosities and permeabilities. The thickness is 70 m and width is 1600 m with 2X vertical exaggeration. The view is tilted to display the upper surface.

5.2.3. Uncertainty

In numerical modelling one of the difficulties lies in determining the sources and extent of uncertainty in the model outputs. The uncertainty can be attributed to the physical set up of the model that includes the dimensions, the discretisation and the boundary conditions, and the parameterisation of the model in terms of flow, transport, and chemistry. The HSU in the radial and 3D models consist of series of homogeneous anisotropic layers that have a consistent mineralogy and initial formation water composition. There is no lateral heterogeneity either in the flow related properties (porosity, permeability, relative permeability, capillary pressure) or the chemistry (mineralogy, water chemistry) of the individual HSU. Computational limitations restrict how fine the gridding could be, so the domain is more finely discretised proximal to the well where the greatest variations in pressure and fluid composition occur. Further from the well the gridding is coarser, which limits the finer scale flow and transport features that may be important in longer term CO_2 storage simulations. The largest grid size for any of the radial or 3D models where CO_2 migrated to was ~40 m.

Using the equations of Riaz et al. (2006), the critical time for the onset of instabilities and density driven fingering and critical wavelength which defines the maximum grid spacing required for those instabilities to develop were calculated for the models. The critical time ranges from ~3 to 20 years while the critical wavelength is ~5 to 10 m. Gridding larger than the critical wavelength will result in a delayed onset of the density driven flow in the model (Riaz et al., 2006). The parameters used in the flow related properties were derived from the Lithicon Special Core Analysis Report for the Glenhaven site (Golab et al., 2015) so it is unknown how applicable they are to the West Moonie site. However, the porosity and permeabilities are reasonably well constrained. Some higher values for λ, residual water saturation and residual gas saturation were tested, but these commonly lead to non-convergence after 0-5 years simulation for both the radial and 3D models.

Uncertainty in the geochemical model output is associated with factors such as heterogeneity but also how reactions are modelled and rates that are used for kinetically controlled reactions. The dissolution of CO_2 into the formation water is treated as an equilibrium reaction in TOUGHREACT; however, Guo et al. (2016) determined that this assumption was typically valid in modelling when appropriate gridding was employed. Kinetically controlled aqueous phase reactions were employed for the main redox associated reactions for the trace gas related solutes. This was required in order for the models to run with the widely ranging redox states that are introduced when very reducing (SO_2, NO) and very oxidizing (O_2) gases are dissolved simultaneously. The rates of these reactions are relatively rapid and were constrained by observations from the batch experiments conducted in this and previous studies (Dawson et al., 2021; Golding et al., 2019; Pearce et al., 2015; Pearce et al., 2019b). The reaction rate parameters of mineral dissolution and precipitation were derived from literature and the rates were modelled in the batch reaction history matching. The carbonate dissolution reactions and the $Fe(OH)_3$ precipitation reaction rates used in the radial and 3D models were the same as those derived from the experiments with no upscaling since these were rapid reactions and tend to be unaffected by variable reaction rates associated with proximity to equilibrium (Kampman et al., 2014). Simulations examining the sensitivity to the reactive surface area assigned to the mineral phases show that there is a corresponding change to the time scale for the reactions to occur and the numbers used in these models are consistent with those in other modelling studies (Kharaka et al., 2010; Viswanathan et al., 2012; Xu et al., 2007; Zheng et al., 2012; Zheng et al; 2016). Adsorption and exchange reactions tend to be fast relative to mineral dissolution and precipitation reactions and typically do not require kinetics to be applied (Varadharajan et al., 2013; Zheng et al., 2016). In previous batch experiments equilibrium modelling of adsorption during precipitation of $Fe(OH)_3$ provided suitable history matching of trace element decreases (Golding et al., 2019; Dawson et al., 2021).

The use of fixed pressure boundaries provides for some pressure relief when injection occurs in order to simulate reservoir/aquifer systems that are hydraulically connected to regional flow systems. The radial models apply a fixed pressure boundary at 5 km and there does not appear to be an influence of the boundary conditions on migration of the CO_2. The same radial models with domains size of 10 km resulted in similar CO_2 migration distances and applying the fixed pressure condition to single cells or multiple cells along the distal edge had no impact. The 3D model fixed pressure boundary condition results in a decrease of pressure of approximately 0.24 bar at 800 m, according to the analytical solution of Warner et al. (1979), leading to a small increase in the pressure gradient imposed by the injection. That small increase may result in slightly higher flow rates and interception of the migrating CO_2 with the boundary. The 2D modelling of Spycher et al. (2019) showed lateral CO_2 migration of 800 to 1000 m along a dipping surface at the West Wandoan site. The Spycher et al. (2019) model contained an elevation change of ~30 m while that in West Moonie site is ~5-6 m suggesting that the West Moonie migration should be at a lower rate.

5.3. Results and Discussion

5.3.1. Radial Models

The radial models were run for a 100-year simulation time. Injection of CO_2 with trace gases was in the bottom left-hand side of the figures. The distribution of porosity is shown in Figure 61 and the proportions of the slice are typical for the majority of the figures (Z from the base of the lower Precipice Sandstone to the top of the lower Precipice Sandstone transition facies; X for the injector at 0 m to 1000 m). The evolution of CO_2 saturation for the model with injection from the base of the lower Precipice Sandstone to 30 m above the model base is shown in Figure 62 and the model with injection in the 20 m interval with a base at 2082 m is shown in Figure 63. The supercritical CO_2 migrates vertically within the higher porosity/permeability units and then is deflected laterally when lower permeability HSU are encountered. The CO_2 never reaches the top of the lower precipice Sandstone for the model with the long injection interval as the lower permeability HSU near the base of the model domain decreases the amount of CO_2 that reaches the base of the "cave facies". The CO_2 in the shorter injection interval scenario does migrate to the top of the lower Precipice Sandstone but only a very limited amount makes it past the lower permeability HSU. The maximum extent of the supercritical CO_2 plume migration laterally was ~575 m for the longer injection interval simulation and ~600 m for the shorter injection interval simulation. Dissolution of the CO_2 decreases the pH of the water and the development of density driven convection currents over time leads to increased dissolution and significantly extends the vertical extent of lower pH (Figure 62 e - h; Figure 63 e - h). The density driven cells manifest by 10 years in the simulations. At 100 years there are some slight pH variations between the two simulations but the volumes of CO_2 impacted formation water appear to be quite similar. The redistribution of CO_2 by dissolution and increased density of the formation water and the resultant lower pH are the main drivers of reactions leading to fluid chemistry changes.

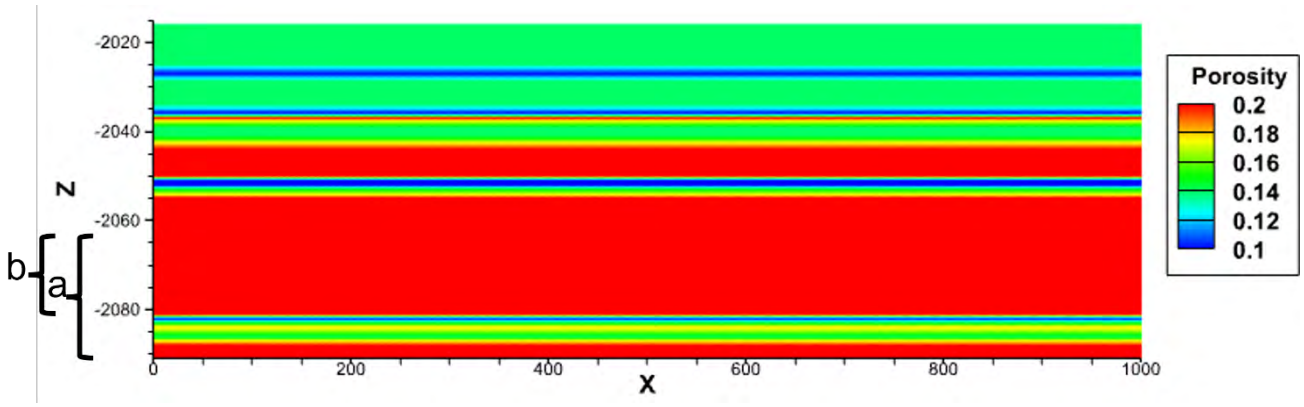

Figure 61: Porosity distribution of the lower Precipice Sandstone HSU used in the radial model showing the different injection intervals a) long interval and b) short interval. Z is depth (m) and X is metres from well.

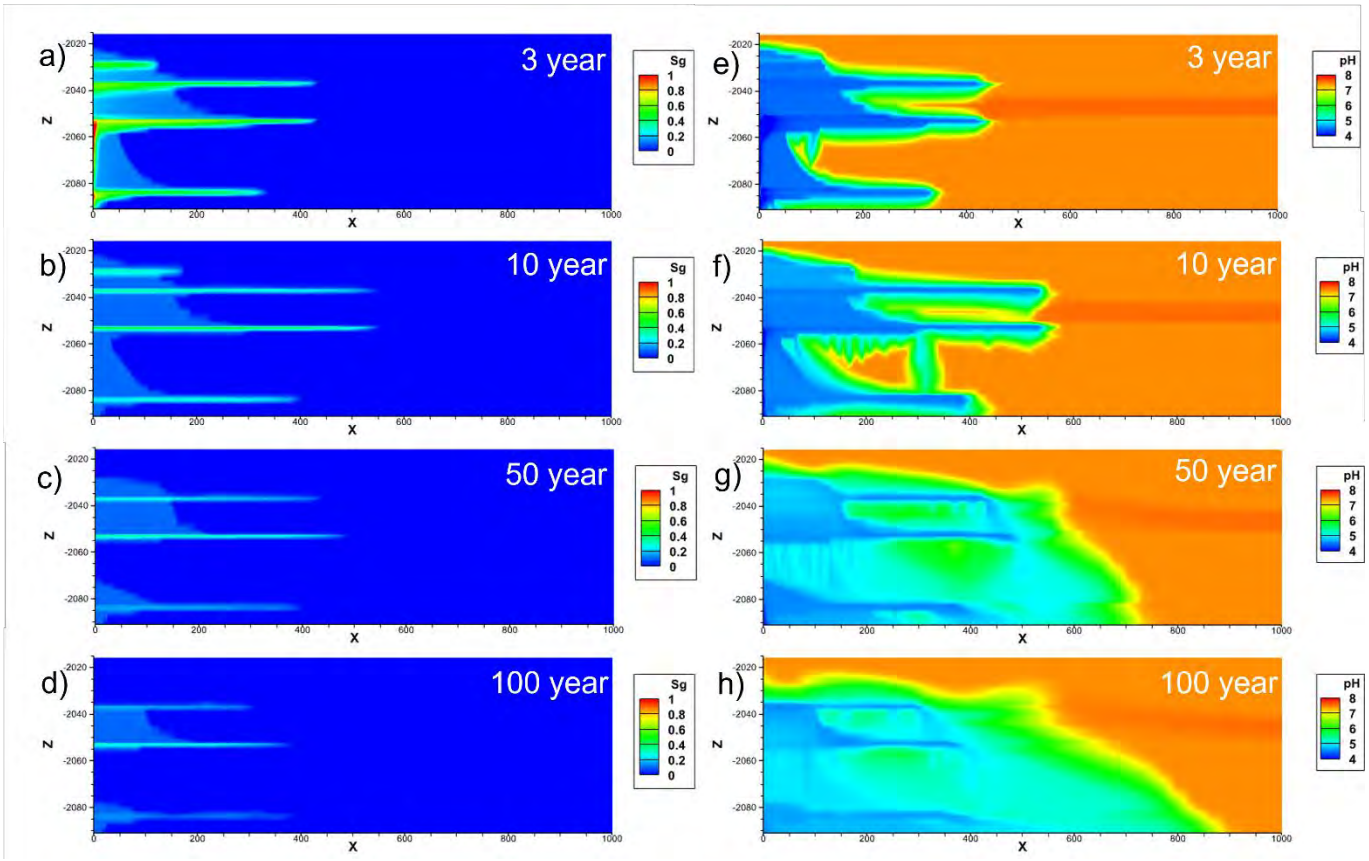

Figure 62: Supercritical CO_2 saturation (a - d) and pH (e - h) distribution over time at 3, 10, 50, and 100 years for the simulation with the longer injection interval.

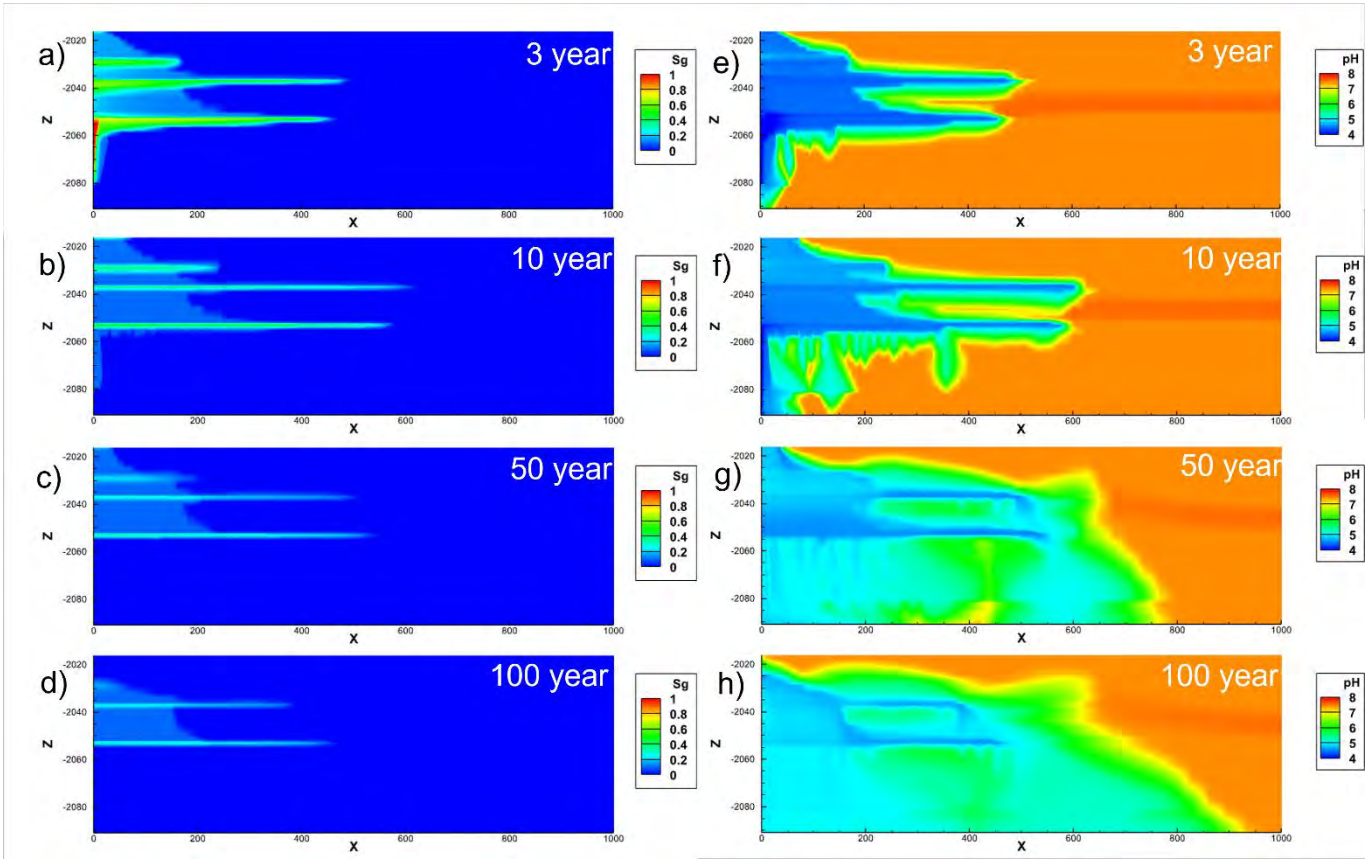

Figure 63: Supercritical CO_2 saturation (a - d) and pH (e - h) distribution over time at 3, 10, 50, and 100 years for the simulation with the shorter injection interval.

The distribution of the trace gases is dominated by their solubility, initial concentration, and rate of reaction. O_2, NO and SO_2 dissolve in the water and react according to the equations 1-3 in Appendix D. O_2(g) shows the widest distribution at 3 years although by 8 years it is largely depleted (Figure 64). The high initial concentration of O_2(g) (400 ppm) in the CO_2 and low solubility lead to the greater extent of migration. While the O_2(aq) reacts both with the HS^- and the NO(aq) near the injector, the majority of the O_2(aq) reacts with Fe mobilized from chlorite and siderite dissolution to precipitate $Fe(OH)_3$ leading to the very low and limited extent of concentrations at 8 years (Figures 64 and 65). The O_2(aq) is completely reacted prior to the onset of density driven convective flow. SO_2(g) is the most soluble (although at the lowest concentration in the CO_2 - 5 ppm) with most very rapidly dissolving in the formation water whereupon it undergoes disproportionation to produce HS^- and SO_4^{-2}. The HS^- reacts with O_2(aq) to produce SO_4^{-2} and H^+ leading to a zone of very low pH water that extends approximately 2 m beyond the volume where complete displacement of water occurs (dryout zone) proximal to the injector (Figure 65 f, g). NO(g) which is less soluble than SO_2(g), and at a higher concentration (15 ppm) in the CO_2, occupies a larger volume than SO_2(g) at 3 years (Figure 65). The gas phase concentration of NO(g) is significantly reduced by 8 years through dissolution and reaction with O_2(aq) to produce nitric acid (Figure 65 d, e). The pH in the volume of reservoir where of SO_2(aq) and NO(aq) oxidation dominates drops to as low as 1 and values as low as 2-3 extend to approximately 10 m outwards and up to the bottom of the Cave facies at 3 years (not shown). Very high SO_4^{-2} and NO_3^- concentrations occur in that volume with SO_4^{-2} in excess of 50,000 mg/kg and NO_3^- greater than 20,000 mg/kg predicted in extremely small volumes near the injector. The low pH water is rapidly buffered to pH 2-3 and by 10 years is the same as the CO_2 impacted formation water (pH ~4-5).

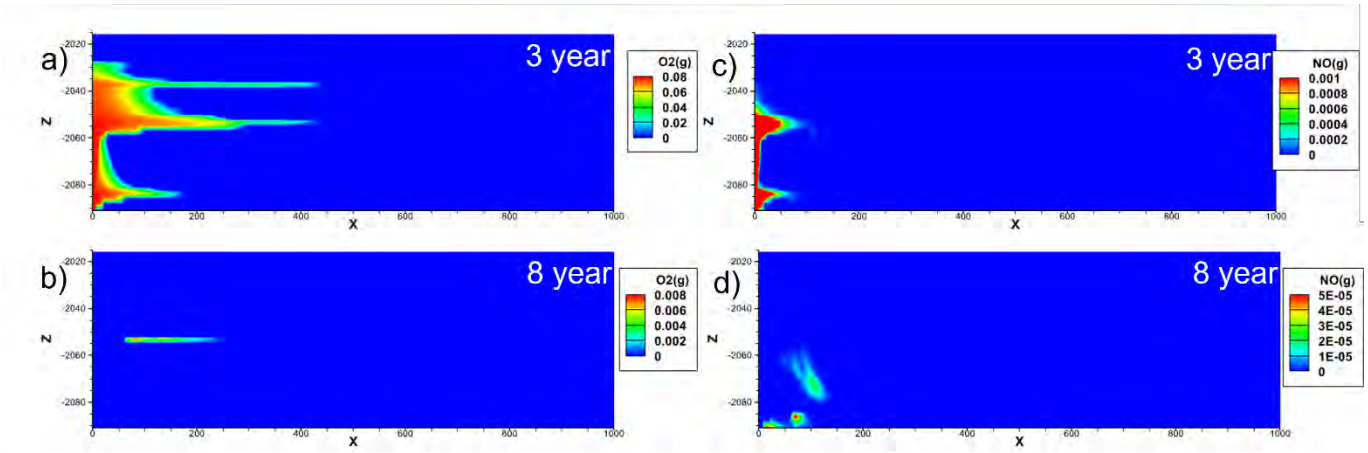

Figure 64: Distribution of O_2(g) (a, b) and NO(g) (c, d) at 3 and 8 years. SO_2(g) has very high solubility and nearly all dissolves on contact with the formation water. Units are in partial pressure of the gas phase and note the 2 orders of magnitude drop in the scale for NO(g) at 8 years.

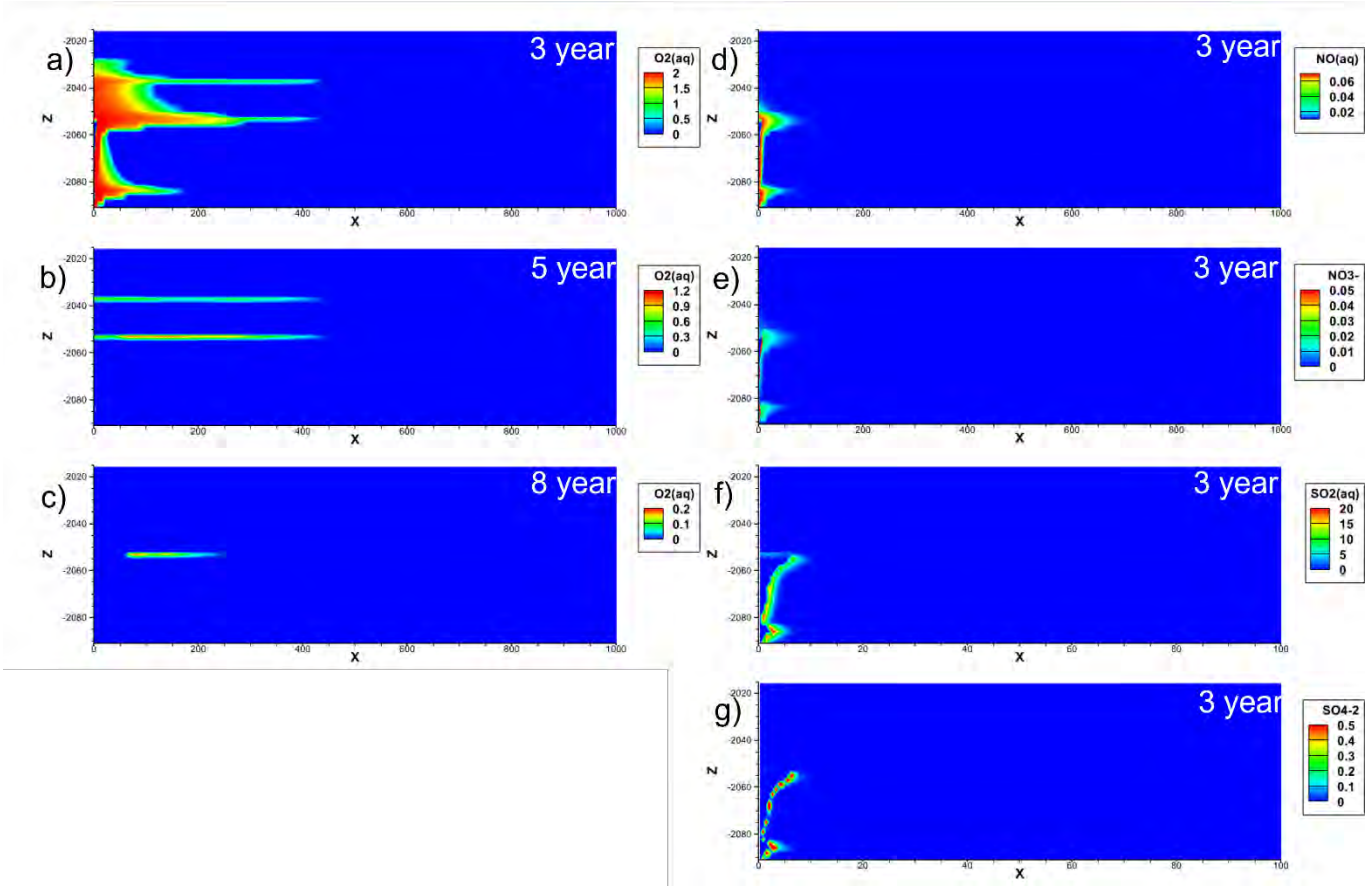

Figure 65: Dissolved O_2(aq) (a - c), NO(aq) (d), NO_3^- (e), SO_2(aq) (f), and SO_4^{-2} (g) in mol/kg. Note the X axis for the SO_2(aq) and SO_4^{-2} is set to within 100 m of the injector. The red areas for the NO_3^- and SO_2(aq) distributions represent concentrations significantly greater than the legends maximums. Units are in mg/kg.

Carbonate minerals were identified as major sources of trace elements of concern. The dissolution of carbonate minerals in the batch experiments led to increases in most trace elements (Golding et al., 2019; Dawson et al., 2021: this study). Two slightly different composition siderite minerals were incorporated in the model with Siderite 1 occurring in the HSU 1 and 3 and Siderite 2 in the rest of the HSU in the model. None of the various Lower Precipice Sandstone HSU contained calcite but number 16 did contain some ankerite. Siderite dissolution in the lower Precipice Sandstone is dominated by the volumes where an Fe containing mineral precipitates, in this case $Fe(OH)_3$ (Figures 66 and 67). The dissolution of siderite and chlorite contribute Fe and HCO_3^- to solution leading to saturation with respect to siderite unless there is a sink for Fe or HCO_3^-. Chlorite dissolution in the CO_2 impacted volume results in little or no siderite dissolving outside the volume where O_2(g) and O_2(aq) were transported with the CO_2. This is shown in Figures 66 and 67 when comparing the distribution of siderite dissolution with $Fe(OH)_3$ precipitation. Outside of that volume the primary source of any mobilised trace element must be from desorption due to the change in pH and solution chemistry. Ankerite dissolution occurred in hydrostatic unit 16 (not shown).

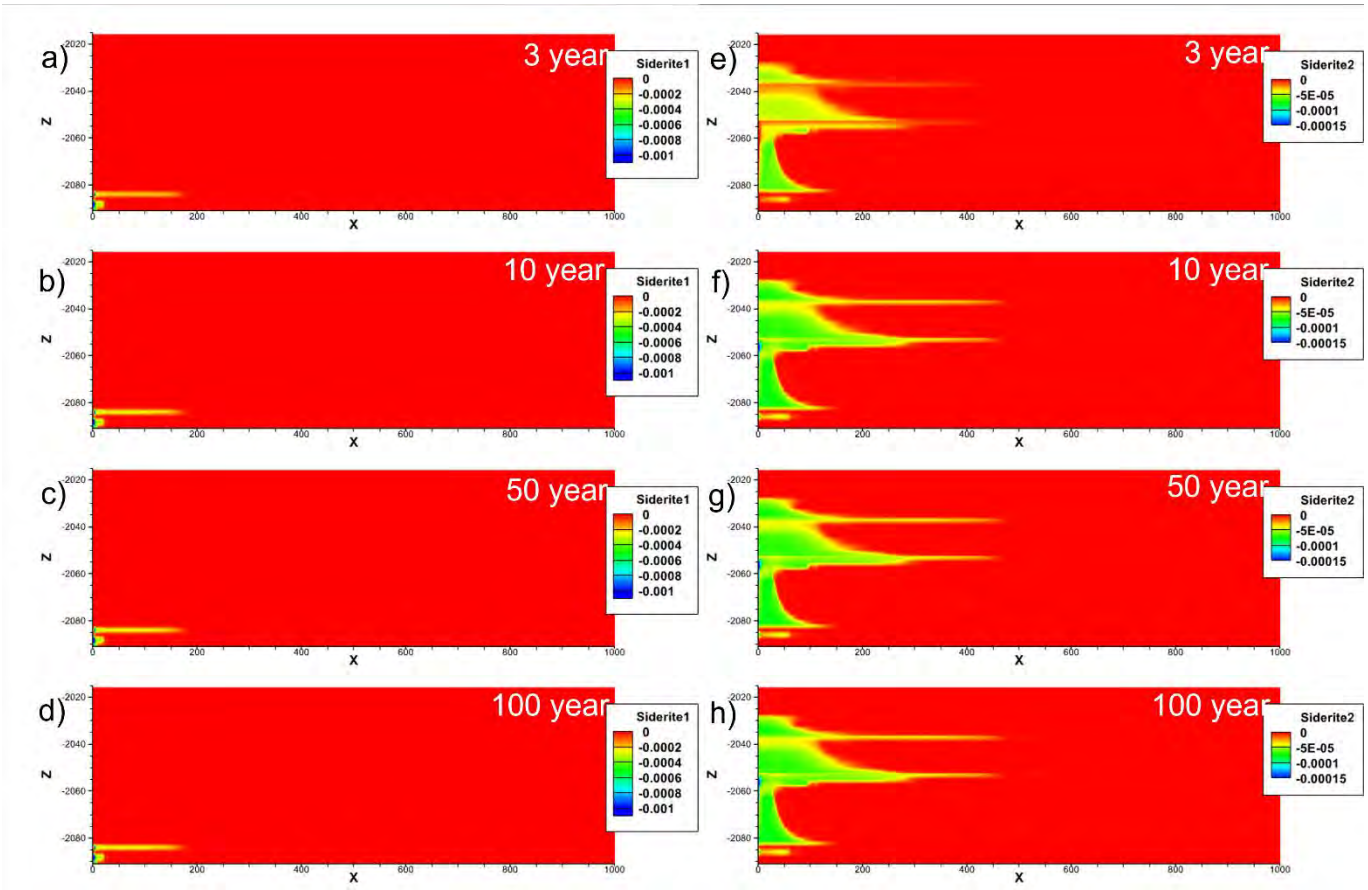

Figure 66: Siderite 1 (a - d) and Siderite 2 (e - h) dissolution at 3, 10, 50, and 100 years. Units are as change in volume fraction. Note the change in scale which increases by at least one order of magnitude from the 3 year to the post 3 year values.

Model outputs for dissolution of chlorite and precipitation of $Fe(OH)_3$ are shown in Figure 67. Chlorite reacted in the lower pH water containing CO_2 and the dissolution pattern follows that of the low pH water in Figure 62. In the batch modelling the chlorite dissolution was the primary source of Si and Al and also contributed both Fe and Mg to solution. The precipitation of smectite and kaolinite mimics the pattern of chlorite dissolution shown in Figure 67. In the batch reactors with mixed gas, Fe was precipitated as $Fe(OH)_3$ similar to what the models show. The amount of $Fe(OH)_3$ that formed was constrained by the availability of O_2 and it can be seen in Figure 67 that after 10 years no additional $Fe(OH)_3$ precipitation occurred.

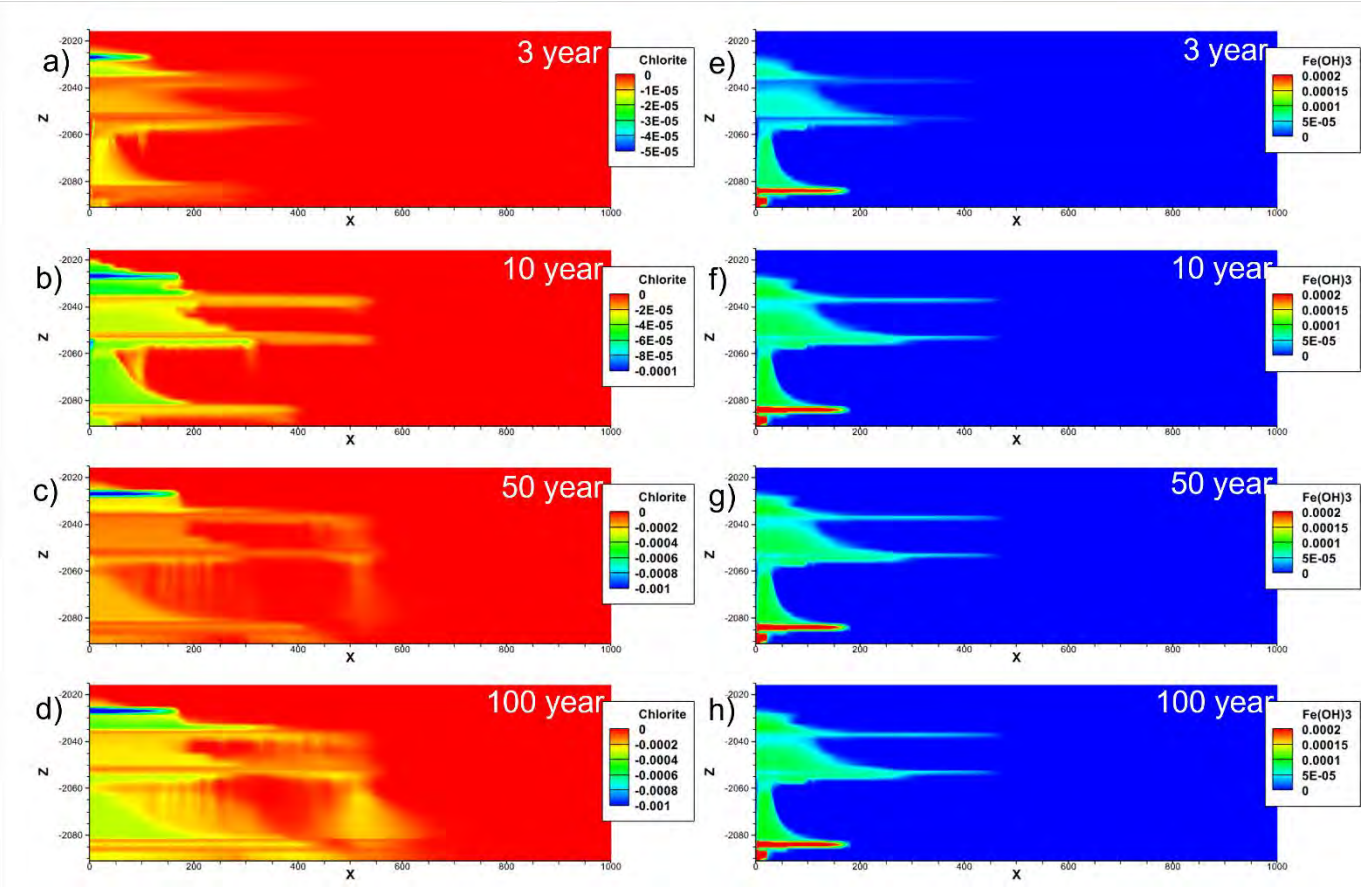

Figure 67: Chlorite dissolution (a-d) and Fe(OH)3 precipitation (e - h) as change in volume fraction at 3, 10, 50, and 100 years. Note the change in scale of the chlorite dissolution from 3 years to 10 years (4 times), and 10 years to 50 years (10 times).

The precipitated $Fe(OH)_3$ is the source of new adsorption sites in the model (Figure 68). The initial distribution of the weak and strong adsorption sites in mol sites per kg water (Figure 68 a and e) was dependant on the volume fraction of $Fe(OH)_3$ and the porosity initially assigned to each of the HSU. The highest number of sites in mol per kg formation water were in the lower porosity HSU as these have a higher proportion of rock mass to water. The precipitation of the $Fe(OH)_3$ resulted in approximately an order of magnitude increases in adsorption sites for all of the HSU within 10 years of the start of injection, with most new sites formed by year 7 (not shown).

The batch experiments showed that the sources of trace elements include carbonate minerals and adsorption sites. Dissolution of carbonate minerals and/or desorption result in mobilisation, and one of the primary mechanisms of dissolution and desorption is pH change. The lower pH of the CO_2 impacted formation water drives both of these processes while precipitation of carbonate minerals and minerals that are capable of providing adsorption sites can act as sinks for the trace elements. Arsenic and lead are trace elements of concern, and their mobilisation and demobilisation are important to understand in the context of subsurface carbon storage.

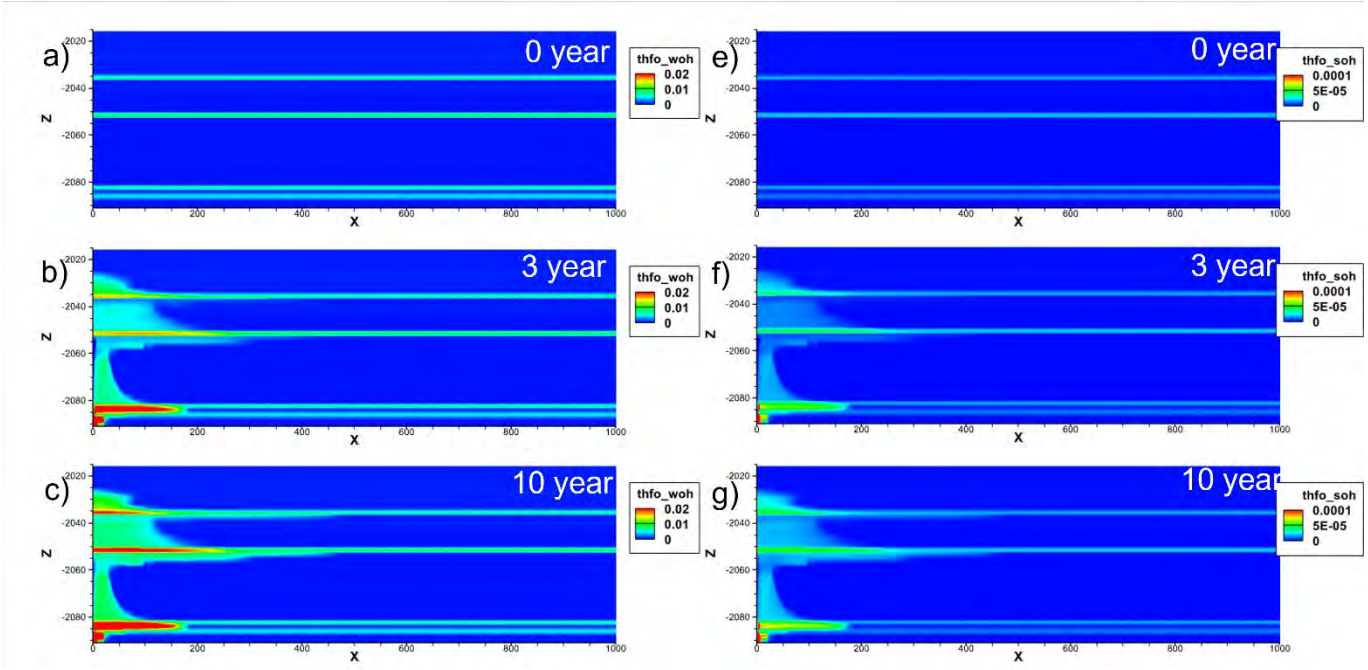

Figure 68: Weak (a - c) and strong (d - f) adsorption site densities shown in mol sites per kg formation water at 0, 3, and 10 years. Distribution of new sites reflects the $Fe(OH)_3$ precipitation.

Figure 69 shows the distribution of As and Pb at 3, 10, 50 and 100 years of the simulation. Arsenic mobilisation is dominated by desorption, with the highest concentrations in formation water (Figure 69) occurring along the edges of the CO_2 impacted volume (Figure 68) and low concentrations occur within the volume where $Fe(OH)_3$ precipitation takes place. This indicates that mobilised As is demobilised where there are increases in adsorption sites. Since there is little to no carbonate mineral dissolution outside of the volume where $Fe(OH)_3$ precipitation occurs then the distribution of As must reflect mobilisation by desorption and As transported by advection from areas of higher concentrations. Arsenic adsorption in the Dzombak and Morel (1990) model involves 3 different types of sites that include strong and weak adsorption with adsorption complexes between hfo_wo-, hfo_woh and hfo_wh2+ and hfo_so-, hfo_soh and hfo_sh2+ with arsenate and a single set of sites for arsenite adsorption. The relative abundance of the different types of sites is pH dependant with the hfo_wh2+ and hfo_sh2+ sites dominating at lower pH and the hfo_wo- and hfo_so- sites dominating at higher pH. In the model, As is desorbed from the hfo_wohAsO4 sites and re-adsorbed on the other sites (including the new sites formed during $Fe(OH)_3$ precipitation) as the pH drops. In addition, As occupancy of the hfo_h2+ sites decreases after 3 years due to the slow buffering of pH and changes in the amounts of the associated strong and weak sites since their relative abundance is very pH dependant.

Lead displays a very different evolution of distribution than As (Figure 69 e - h). Initially the highest Pb concentrations are where carbonate mineral dissolution dominates and then advective dispersion becomes the main process affecting Pb distribution. Adsorption of Pb plays an important role in controlling the concentration and adsorption sites, particularly in the volume of $Fe(OH)_3$ precipitation act as a sink for Pb. However, some of the Pb from adsorption sites is remobilised as the Pb concentrations drop.

The other trace elements considered in this study displayed behaviour similar to Pb (Figure 70). The Cd, Co, Cu, Mn, Ni and Zn all have high concentrations in the zone of greatest carbonate mineral dissolution, and like Pb display elevated adsorption site occupancy in that volume. The higher concentrations in the density driven plumes are the result of both carbonate mineral dissolution and transport within those density currents. Desorption occurs as the concentrations drop through advective transport through density driven convection.

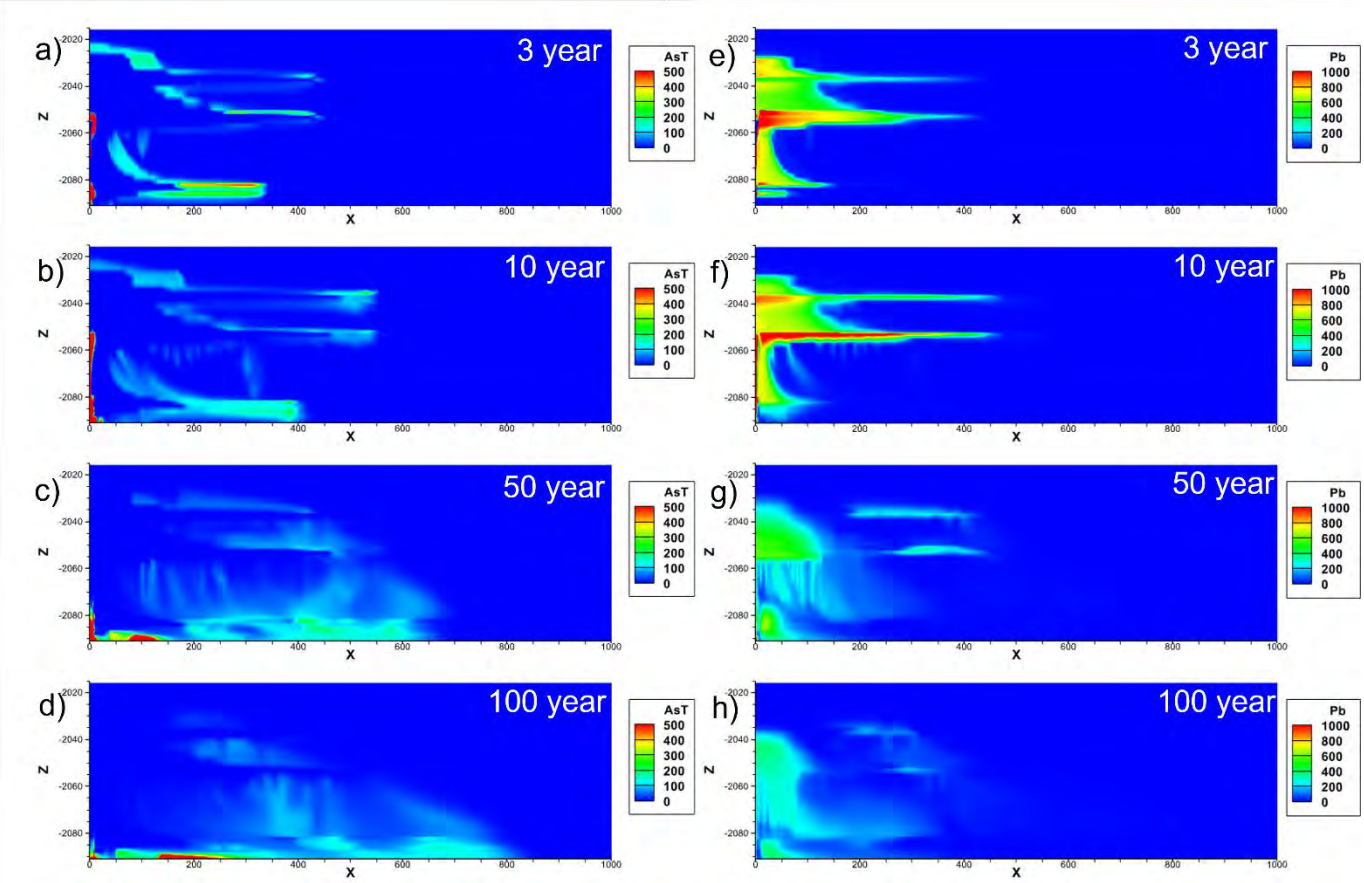

Figure 69: As (a - d) and Pb (e - h) formation water concentration (ppb) distributions with time at 3, 10, 50 and 100 years.

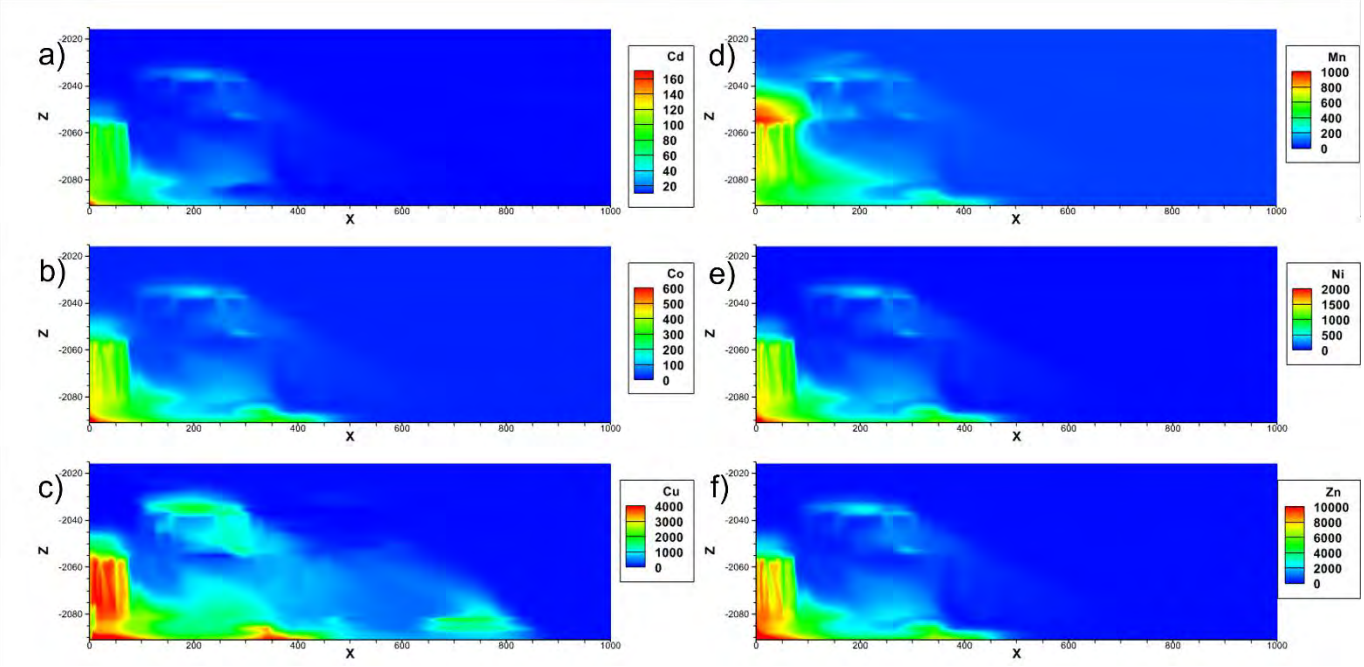

Figure 70: Formation water trace element concentrations in ppb of Cd (a), Cu (b), Co (c), Mn (d), Ni (e), and Zn (f) at 100 years. The different behaviour of Cd and Cu is illustrated in the volume near the injector and locations at the edges of the density driven plumes.

The potential for monitoring the evolution of CO_2 migration and formation water chemistry is possible with the presence of monitoring wells. Reactive transport modelling enables predictive modelling of the chemical evolution at any location in the site and thus can provide a guide to monitoring strategies, model validation and defining expectations regarding concentrations. Five locations were selected within the model volume, to

evaluate the changes in formation water chemistry over time. The temporal evolution of pH, Fe, K, Mg and HCO_3^- were selected because they were observed to vary in the batch reactor experiments (Mg, Fe), or are expected to show changes related to the CO_2 migration (pH), or reflect water rock interactions and were not measurable in the batch reactors (HCO_3^-) or, in the case of K, are measures of the reaction of phases that occur in higher amounts in the lower Precipice Sandstone HSU but have relatively slow reaction rates. In addition, As and Pb concentration variations are provided for each location because they are elements of concern and serve as proxies for other trace metals. Four of those locations are at 200 m from the injector, approximately coinciding with the location of the West Moonie 2 well while the other is more distal and is an indicator of the density driven component of the storage system. The locations are shown in Figure 71 overlain on the porosity and pH distribution. Location 1 is just below the "cave facies" at a depth of 2054.5 m (SSTVD) within the interval targeted for injection, location 2 is just below at a depth of 2065 m (SSTVD) within hydrostatic unit 6, specifically targeted for injection, location 3 is just above the "cave facies" at a depth of 2043 m (SSTVD) in the high porosity and permeability material of hydrostatic unit 11, location 4 is at a depth of 2031 m (SSTVD) just below the low porosity and permeability hydrostatic unit 16 and location 5 is at a depth of 2088 m (SSTVD) in HSU 1 700 m from the injector.

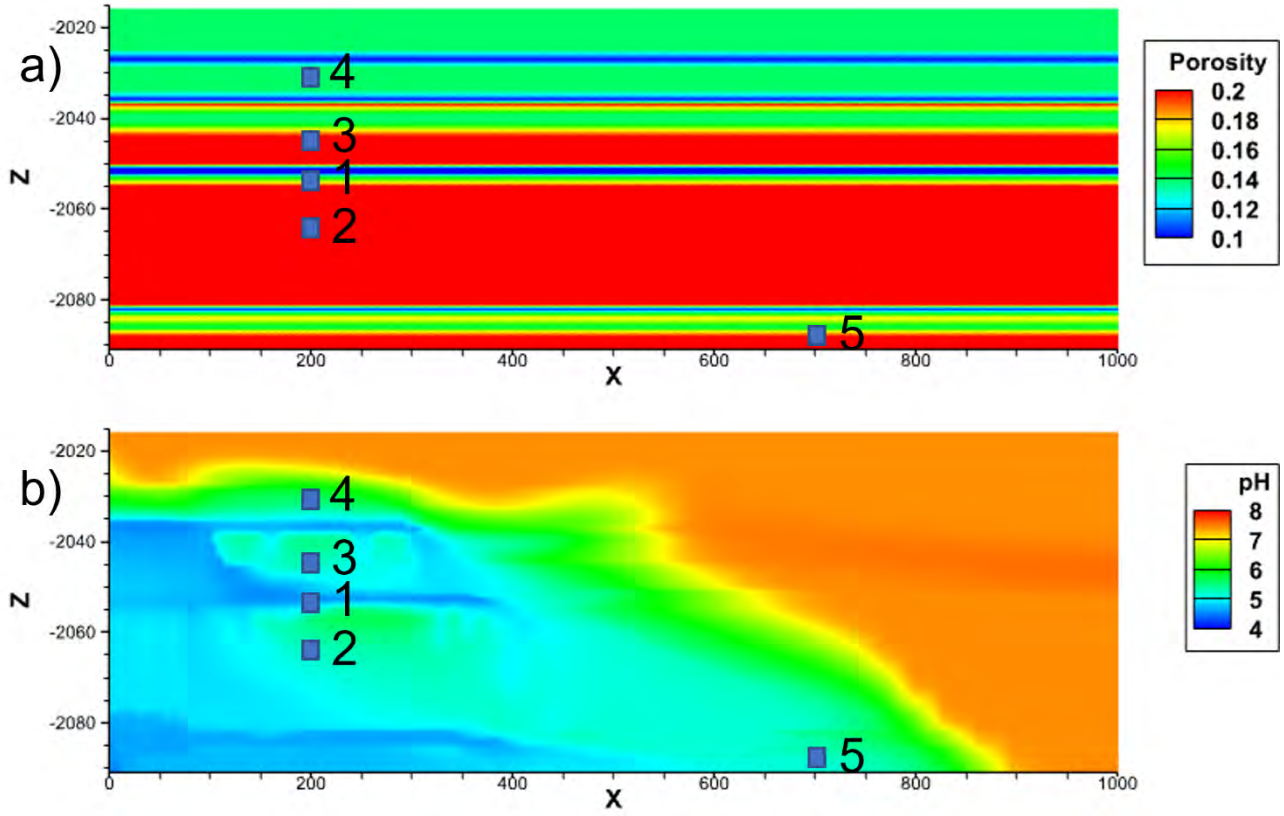

Figure 71: Locations of the X-Y plots from different parts of the CO_2 impacted part of the reservoir overlain on a) the initial porosity distribution and b) the pH at 100 years. The X and Z coordinates for location 1 (200m, 2054.5m), 2 (200m, 2065m), 3 (200m, 2043m), 4 (200m, 2031m), and location 5 (700m, 2088m).

The changes in concentration of pH, Fe, Mg, K and HCO_3^- for location 1 are shown in Figure 72. The pH begins to decrease at just before 0.5 years with a coinciding small increase in HCO_3^- and Fe. Shortly thereafter the Mg increases and by 5 years there are some significant increases in concentrations of all the elements. Mineral dissolution and precipitation reactions can result in increases or decreases in concentrations. Similarly, advective transport both during formation water displacement as the super critical CO_2 migrates and through density driven convective flow can result in increases or decreases in concentrations. Siderite dissolution and $Fe(OH)_3$ precipitation dominate in the first 5 years as indicated by the increases in HCO_3^- and Mg and the

initial small increase in Fe then decrease as $Fe(OH)_3$ precipitates. At 5 years the O_2 is exhausted and Fe increases, largely through siderite dissolution. Dissolution of the trace element containing Siderite1 stops at 10 years although siderite (without trace elements) precipitation initiates at 5 years. The increase in Fe from 10 years to 15 years is largely through advective transport through density driven convection. After approximately 15 years, the Fe, along with the other elements begin to decrease through increasing siderite precipitation and advective transport. At 25 years there is another shift in the flow dynamics, possibly through a reduction in the convective drive and chlorite and K-feldspar dissolution becomes dominant resulting in increases in K, Mg and HCO_3^-.

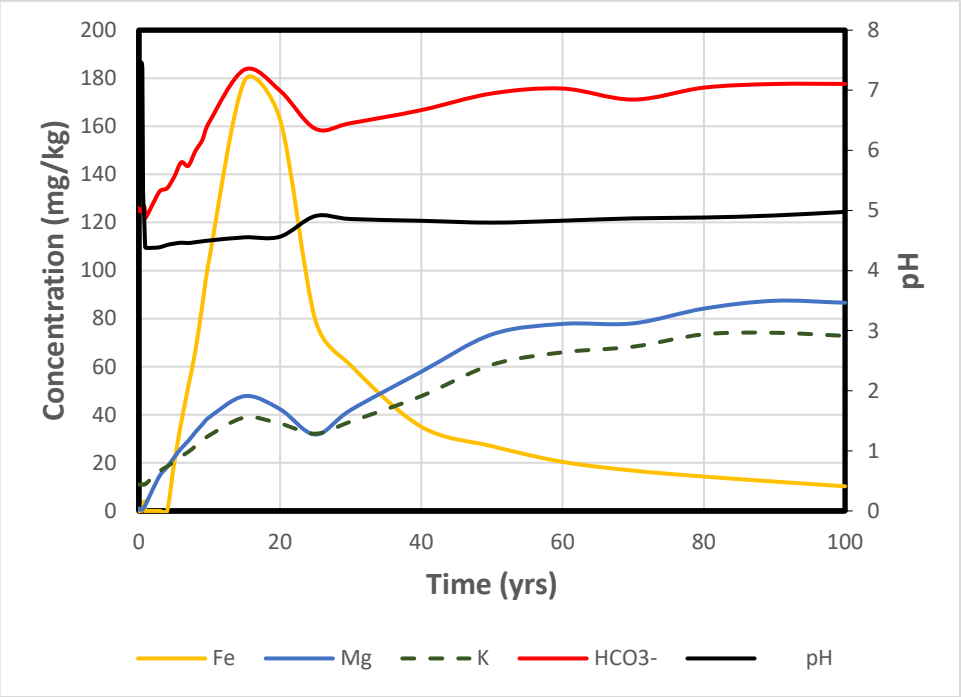

Figure 72: Major components Fe, Mg, K, HCO_3^- and pH at location 1 (X 200m, Z -2054.5 m). Concentrations in mg/kg water with HCO_3^- total decreased by an order of magnitude.

The As and Pb concentrations over time for location 1 are shown in Figure 73. Although not clear on this plot, As initially increases, coinciding with the decrease in pH, to a value of 19 ppb, then decrease to below 1 ppb for the remainder of the simulation time. At the same time Pb increases rapidly then there is a decrease in the rate of increase followed by a decrease in the concentration at approximately 9 years. The initial rapid increase reflects siderite dissolution and the drop in rate is when O_2 is depleted and $Fe(OH)_3$ is no longer precipitating so the rate of siderite dissolution slows and hence the Pb increase slows. At location 1 most of the As is adsorbed onto the newly formed $Fe(OH)_3$ adsorption sites so there is little to transport from the volume where siderite 1 dissolution is occurring. Density driven convective flow also begins to have an impact and by 9 years the Pb is being transported away. Similar to the major elements in Figure 72, at 25 years there is a change in the flow dynamics and Pb shows a slight increase then decreases until the end of the simulation with concentrations of less than 50 ppb for the last 30 years.

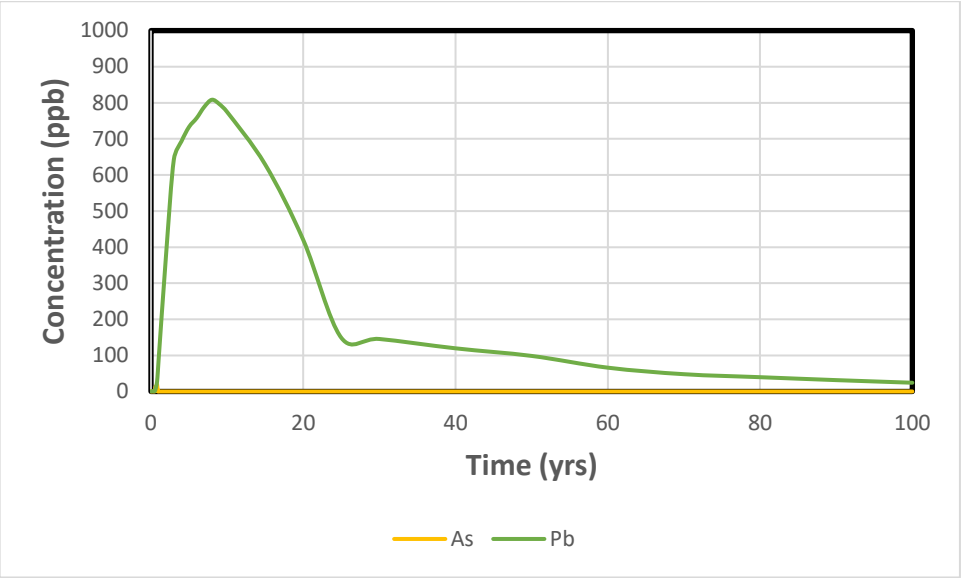

Figure 73: Location 1 (X 200m, Z -2054.5 m) As and Pb concentrations in ppb. Maximum drinking water quality concentration for both As and Pb is 10 ppb.

The plot of the major components at location 2 is shown in Figure 74. This location is just below location 1 and is largely impacted by the density driven convection flow as opposed to CO_2 migration. The pH begins to decrease at 9 years, coinciding with the observation at location 1 of Pb decrease through advective transport. At 9 years the other elements begin to increase with subdued Fe, Mg and HCO_3^- peaks at 25 years and then a Fe decrease and continued increase in the other elements. The peaks at 25 years mimic that of location 1 at 15 years and the subsequent decrease in Fe while the other elements increase is the result of authigenic siderite precipitation and continuing chlorite and K-feldspar dissolution.

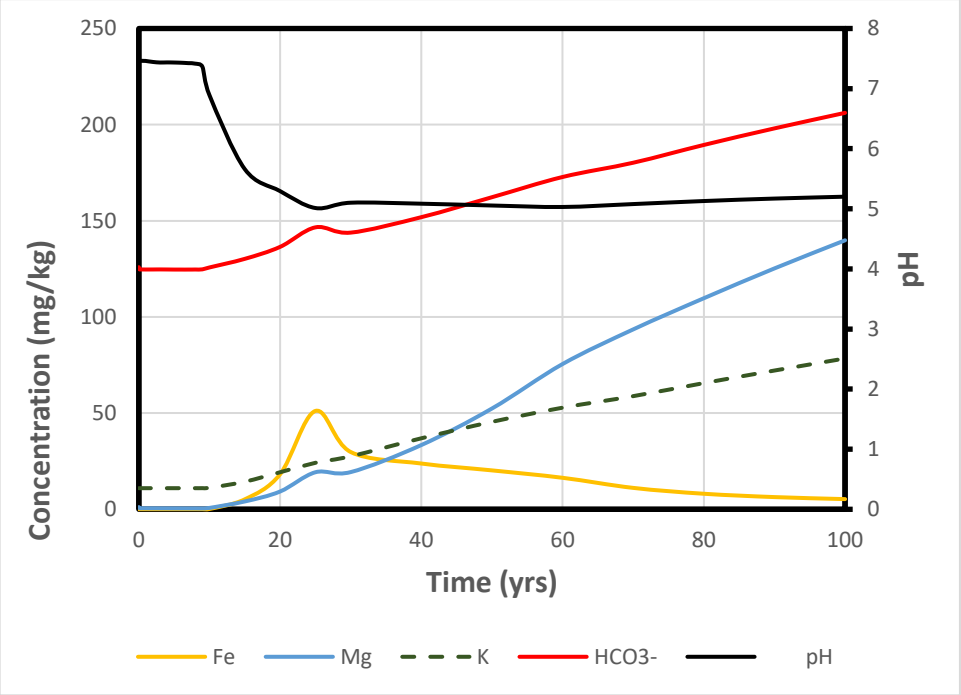

Figure 74: Major components Fe, Mg, HCO_3^- and pH at location 2 (X 200m, Z -2065 m). Concentrations in mg/kg water with HCO_3^- total decreased by an order of magnitude.

Concentration changes with time for As and Pb for location 2 are shown in Figure 75. Arsenic and Pb arrive at 10 years, slightly later than the major elements in Figure 74. The As concentration increases until approximately 20 years then decreases. The As peak does not coincide with the major elements because the

As is mobilized through desorption as the front of CO_2 impacted water migrates through the reservoir. The low pH of the CO_2 impacted formation water results in As desorption from the hfo_wohAsO4 sites and while some re-adsorption on the other sites occur, As concentrations increase. The Pb concentration increases until 25 years and then decreases, coinciding with the arrival of the major elements peak, indicating that advective transport is the primary mechanism controlling the Pb at this location. Additional changes in As and Pb reflect the dynamics of the density driven flow as the concentrations follow approximately parallel paths on the plot.

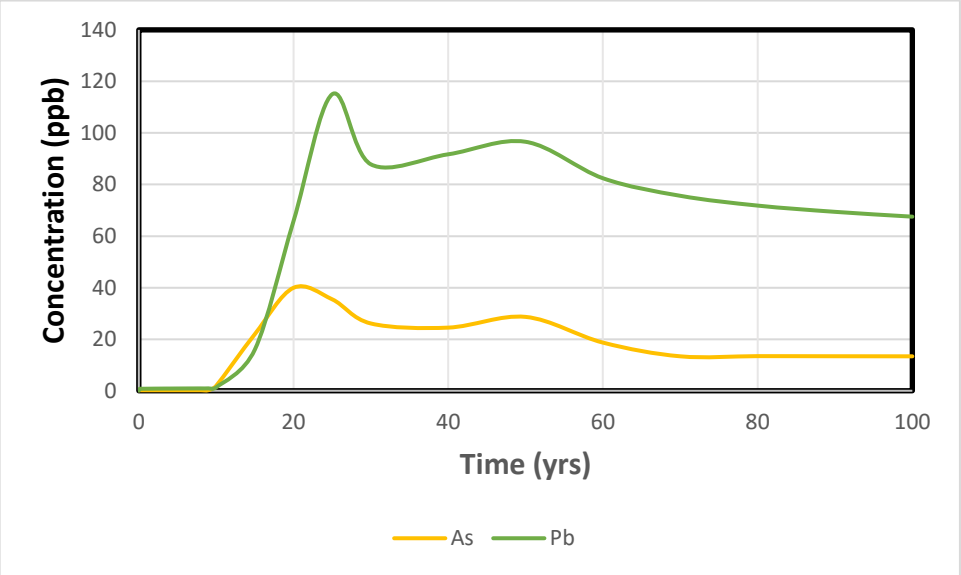

Figure 75: Location 2 (X 200m, Z -2065 m) As and Pb concentrations in ppb. Maximum drinking water quality concentration for both As and Pb is 10 ppb.

The major component concentrations for location 3 are shown in Figure 76. Location 3 sits just above location 1 and the chemical evolution is similar. Supercritical CO_2 does not migrate to the cells at this depth, the CO_2 plume sits just above in the cells at 2037 m and 2039 m; however, CO_2 impacted formation water does. The arrival of the CO_2 impacted water is marked by a decrease in pH at 0.9 years. The Fe begins to slowly increase and then significantly increases by year 5. Iron concentration peaks at 9 years then decreases slightly, then increases and begins to decrease at 15 years. Unlike location 1, the initial increase is due to Fe transported along with the migrating CO_2 impacted water. Density driven advective transport becomes more significant after 10 years and authigenic siderite precipitation becomes increasingly important in controlling the Fe concentration. The K, Mg and HCO3- increase similar to the Fe and show the same decrease and then increase resulting from advective transport to the location. At approximately 25 years, dissolution of chlorite and K-feldspar becomes significant dominate although the density driven flow continues to be dominant as the pH shows a decline rather than the increase expected if mineral dissolution reactions dominate.

The location 3 As and Pb concentrations with time are shown in Figure 77. Arsenic and Pb concentrations increase as the pH decreases with As showing a more rapid and larger increase. Arsenic displays 3 peaks, one at 6 years, then at 9 and again at 15 years while lead has 2 peaks, one at 9 years and the other at 15. The 9 and 15 year peaks correspond to the major element behaviour and reflect the migration of CO_2 impacted water that has dissolved siderite and advective transport results in the As and Pb concentrations. The earlier peak at 6 years and the more rapid increase for As is the result of desorption as the pH decreases in the migrating front. The increases after ~ 80 years reflect the influx of the lower pH formation water that has reacted up gradient from the location.

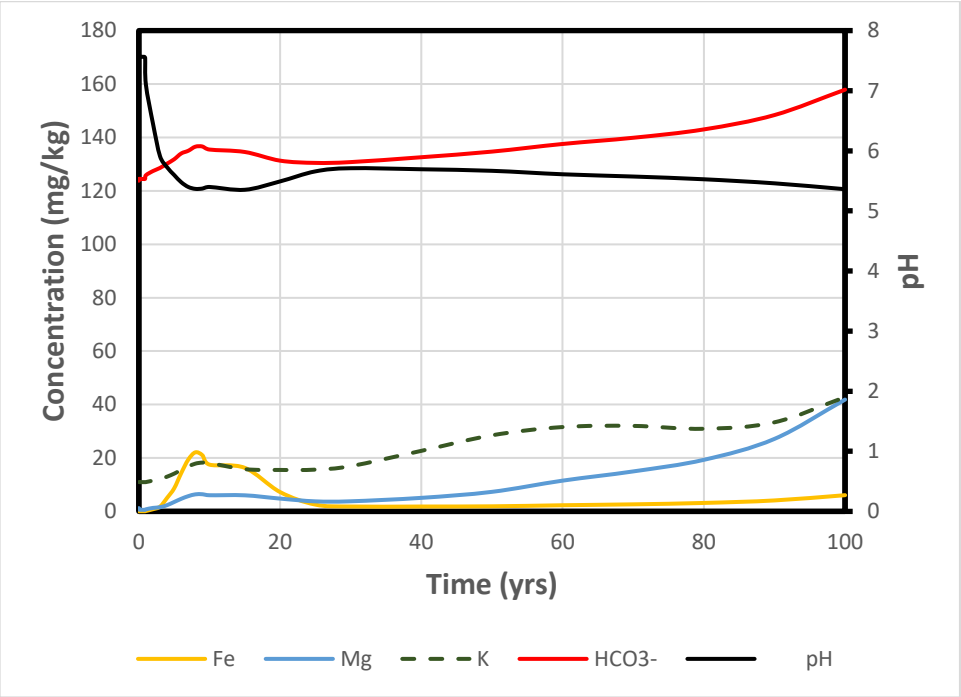

Figure 76: Major components Fe, Mg, K, HCO_3^- and pH at location 3 (X 200m, Z -2043 m). Concentrations in mg/kg water with HCO_3^- total decreased by an order of magnitude.

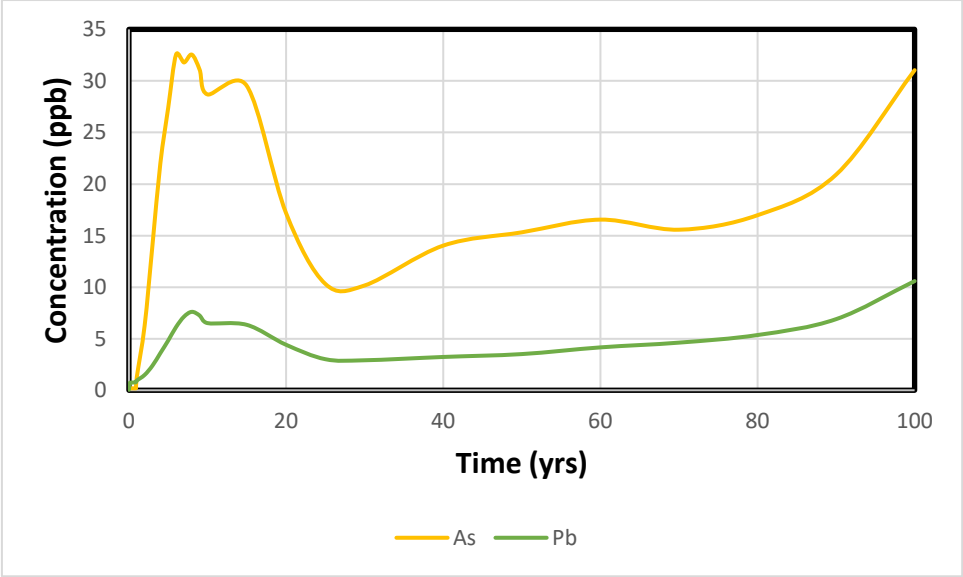

Figure 77: Location 3 (X 200m, Z -2043 m) As and Pb concentrations in ppb. Maximum drinking water quality concentration for both As and Pb is 10 ppb.

The major components at location 4 are shown in Figure 78. Location 4 is just below a low permeability barrier in the lower Precipice Sandstone. The pH decreases at 0.9 years marking arrival of the CO_2 impacted water; however, the pH only decreases to 6.5 initially and then slowly decreases to 5.5 at 10 years. Like location 3, no supercritical CO_2 migrates to the cells at this location, rather it is CO_2 charged formation water. With that formation water, K and HCO_3^- increase until 10 years and then Fe and Mg increase. K-feldspar as well as a small amount of illite dissolution initiates at 1 year and chlorite dissolution does not begin until year 15. Siderite precipitation starts around 1 year but does not increase until the onset of chlorite dissolution.

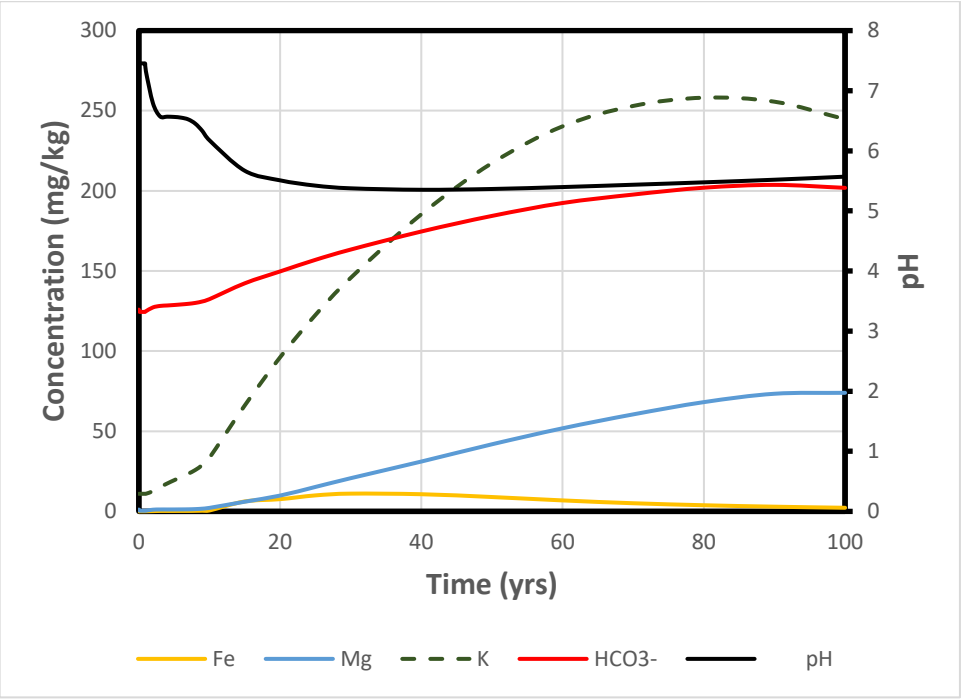

Figure 78: Major components Fe, Mg, K, HCO_3^- and pH at location 4 (X 200m, Z -2031 m). Concentrations in mg/kg water with HCO_3^- total decreased by an order of magnitude.

The concentrations of As and Pb for location 4 are shown in Figure 79. There is a small increase in As that coincides with the initial drop in pH and then As concentration increases significantly until 40 years after which it decreases. Lead displays similar behaviour with a smaller initial increase and delayed rise compared to As, it peaks just prior to 60 years followed by a decline. Since there is no siderite with trace elements dissolving at this location, the As and Pb content is changing due to transport in and out. The more rapid increase in As reflects the source from desorption compared to Pb sourced entirely from siderite dissolution. The As desorption is contributed to locally through transport and Pb is primarily transported.

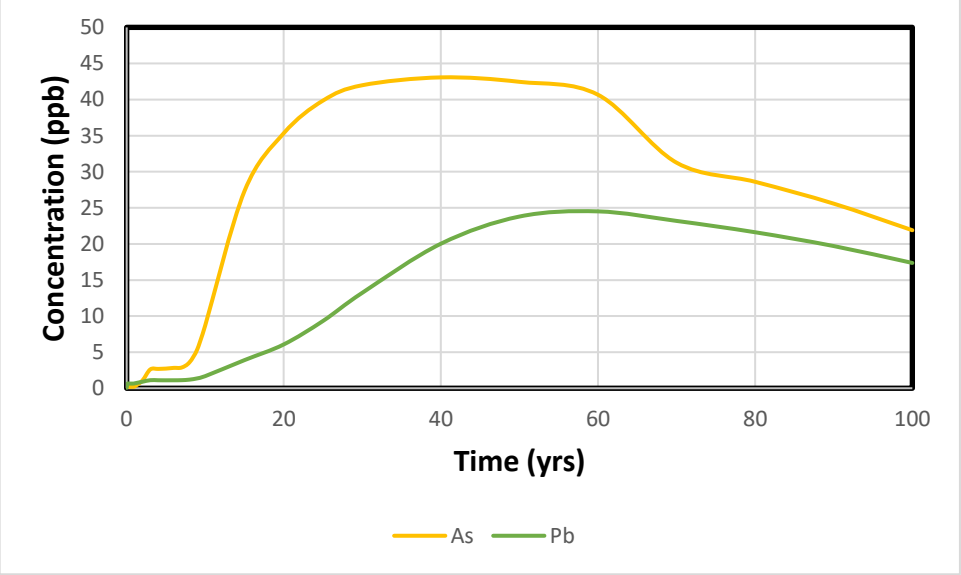

Figure 79: Location 4 (X 200m, Z -2031 m) As and Pb concentrations in ppb. Maximum drinking water quality concentration for both As and Pb is 10 ppb.

The major components at location 5 are shown in Figure 80. Location 5 is near the bottom of the lower Precipice Sandstone at a distance of 700 m from the injector. The pH declines slowly, beginning at 40 years, marking the arrival of the CO_2 impacted water. The rate of change reflects the declining of fluid flow velocity in combination with increased mineral reactions buffering the pH along the flow path. K-feldspar and chlorite

dissolution dominate with kaolinite and siderite precipitation also occurring. The siderite precipitation keeps the Fe low compared to the other components in Figure 80. The increases in K, Mg, Fe and HCO3- are the result of transport and local dissolution, with transport being the dominant source.

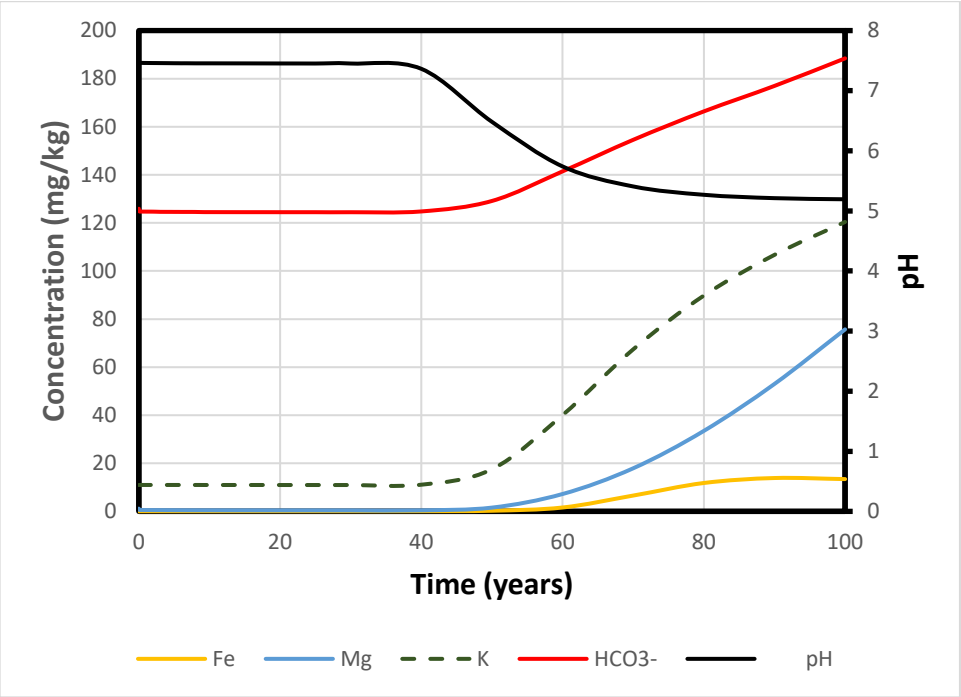

Figure 80: Major components Fe, Mg, K, HCO_3^- and pH at location 5 (X 700m, Z -2088 m). Concentrations in mg/kg water with HCO_3^- total decreased by an order of magnitude.

The location 5 As and Pb concentrations with time are shown in Figure 81. Arsenic concentrations increase at year 50 and rapidly rise while Pb shows only a small increase. Similar to locations 3 and 4, the As is sourced through desorption and the increase reflects local and as well transported As. The Pb is entirely derived from Siderite 2 dissolution and advective dispersion has resulted in the very low concentrations as no Siderite 2 was dissolved outside of the volume where O_2 concentrations were sufficiently high to drive $Fe(OH)_3$ precipitation.

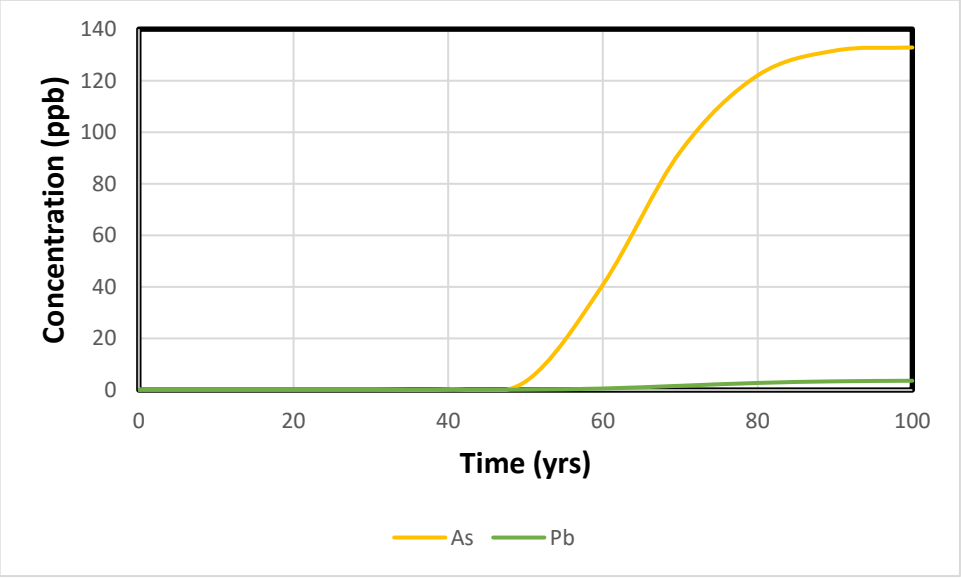

Figure 81: Location 5 (X 700m, Z -2088 m) As and Pb concentrations in ppb. Maximum drinking water quality concentration for both As and Pb is 10 ppb.

The mobility of trace elements in the lower Precipice Sandstone at West Moonie is strongly dependent on adsorption/desorption and carbonate mineral sources. The models demonstrate that As mobilisation is largely controlled by desorption from pre-existing adsorption sites. The primary mechanism is desorption along the low pH front of the CO_2 charged formation water. In the volume of reservoir where O_2 migrates along with the CO_2, the precipitation of $Fe(OH)_3$ leads to the production of new adsorption sites and the As is rapidly adsorbed leaving very low concentrations. The modelling indicates that the strong As adsorption affinity means that a much lower concentration was available for transport through density driven advection. The other trace elements investigated in this study, Pb, Cd, Co, Cu, Mn, Ni and Zn, were mobilized predominantly by dissolution of carbonate minerals containing these elements in their crystal structure as well as some mobilisation through desorption. In the volume where $Fe(OH)_3$ precipitation occurs, a proportion of these trace elements was adsorbed on newly formed adsorption sites; however, concentrations in the formation water where carbonate mineral dissolution occurred remained high and advective transport became important in their redistribution. In this modelling, carbonate mineral dissolution only took place in volumes where $Fe(OH)_3$ precipitation occurred. The iron oxyhydroxides acting as sinks for Fe and undersaturation with respect to the carbonate minerals was maintained as long as precipitation took place. Once the O_2 was depleted, $Fe(OH)_3$ precipitation ceased and carbonate mineral dissolution also stopped.

The distribution of the trace elements through time was dependent on the sources/sinks and the development of the density driven convection within the volume of reservoir impacted by the migration of CO_2. Desorption at the migrating front of As resulted in higher concentrations in the front, and the subsequent adsorption where new $Fe(OH)_3$ precipitated meant low concentrations occurred behind the front. Once the O_2 was depleted then migration of the front continued to increase As content so the concentrations remained elevated. Ongoing adsorption on the existing strong and weak sites resulted in As concentrations reaching maximums in the 100's of ppb. The re-adsorption behind that front and dispersion through mixing with the CO_2 charged formation water that continued to be mobilised by the density convection resulted in decreasing As concentrations with time. Pb, Cd, Co, Cu, Mn, Ni and Zn were transported by the density driven migrating formation fluids, along those pathways it appears that adsorption and dispersion at the mixing front resulted in the highest concentrations proximal to the volume where carbonate mineral dissolution occurred with a rapid decrease in concentrations away from that volume. The source volumes for the density driven fluids, those areas where some residual super critical CO_2 remained, are eventually depleted in the trace elements and the resulting CO_2 charged fluids appear to have low trace element concentrations resulting in decreasing concentrations with time along the flow paths.

5.3.2. 3D Reactive Transport Models

The 3D RTM simulation only ran for 10 years before the program was unexpectedly shut down due to a power outage. However, the results of the 10 years simulation will be presented and compared with the results of the radial modelling. The implications for future 3D modelling of plume behaviour are also discussed as the results showed that a different approach is required for 3D modelling at EPQ10 than employed in the current study. Unlike the radial models, the 3D simulation provides some indication of how the injected super critical CO_2 buoyancy migration and CO_2 charged fluid migration could be affected as a result of the topography and porosity/permeability characteristics of the HSU. The general structure of the lower Precipice Sandstone is dipping towards the north-north-west with the various HSU of the lower Precipice thinning in that direction as well. The 3D model was run with 400 ppm O_2(g), 15 ppm NO(g) and 5 ppm SO_2(g) in the injection stream. The model viewer was set up to provide fence diagrams with 3 perpendicular slices oriented north-south and 1 slice east-west (Figure 82). The orientation of viewing is from the southeast towards northwest (Figure 82).

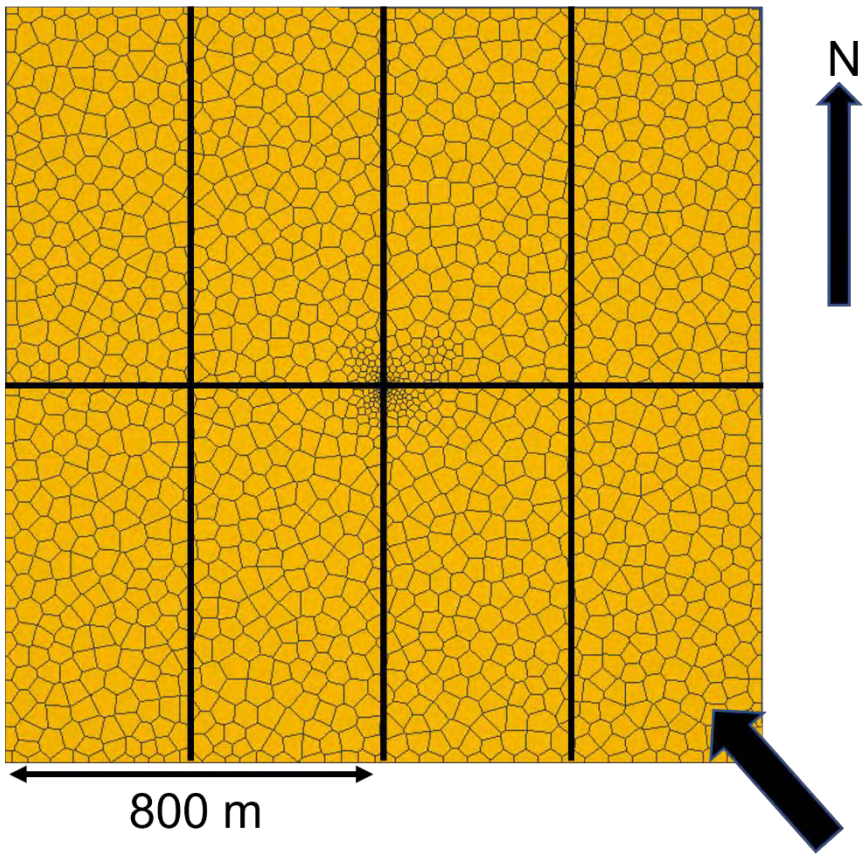

Figure 82: Plan view of model showing the orientation of the fences and angle of view (arrow in the bottom right).

Injection over 3 years into the bottom 30 m of the reservoir and the subsequent migration of the supercritical CO_2 was controlled by buoyancy. The topography of the lower surfaces of the low permeability HSU (4, 10, 14 and 16) was the main factor impacting the orientation of the plume and the direction of migration (Figure 83). Like the radial models with injection from the base of the lower Precipice Sandstone, the super critical CO_2 never reaches the top of the lower Precipice Sandstone/base of the upper Precipice. The isosurface in Figure 83 shows the areas where CO_2 content was above residual saturation at 1, 2, 3, 4, 5, 6, 7, 8 and 10 years. The surfaces of the HSU dip towards the northwest thus the supercritical CO_2 plume migrated towards the south-south-east of the model domain and also followed a structural high towards the east-northeast. By year 5 the CO_2 had reached the model boundary in the south. The fixed pressure boundary resulted in the migration of CO_2 out of the model domain.

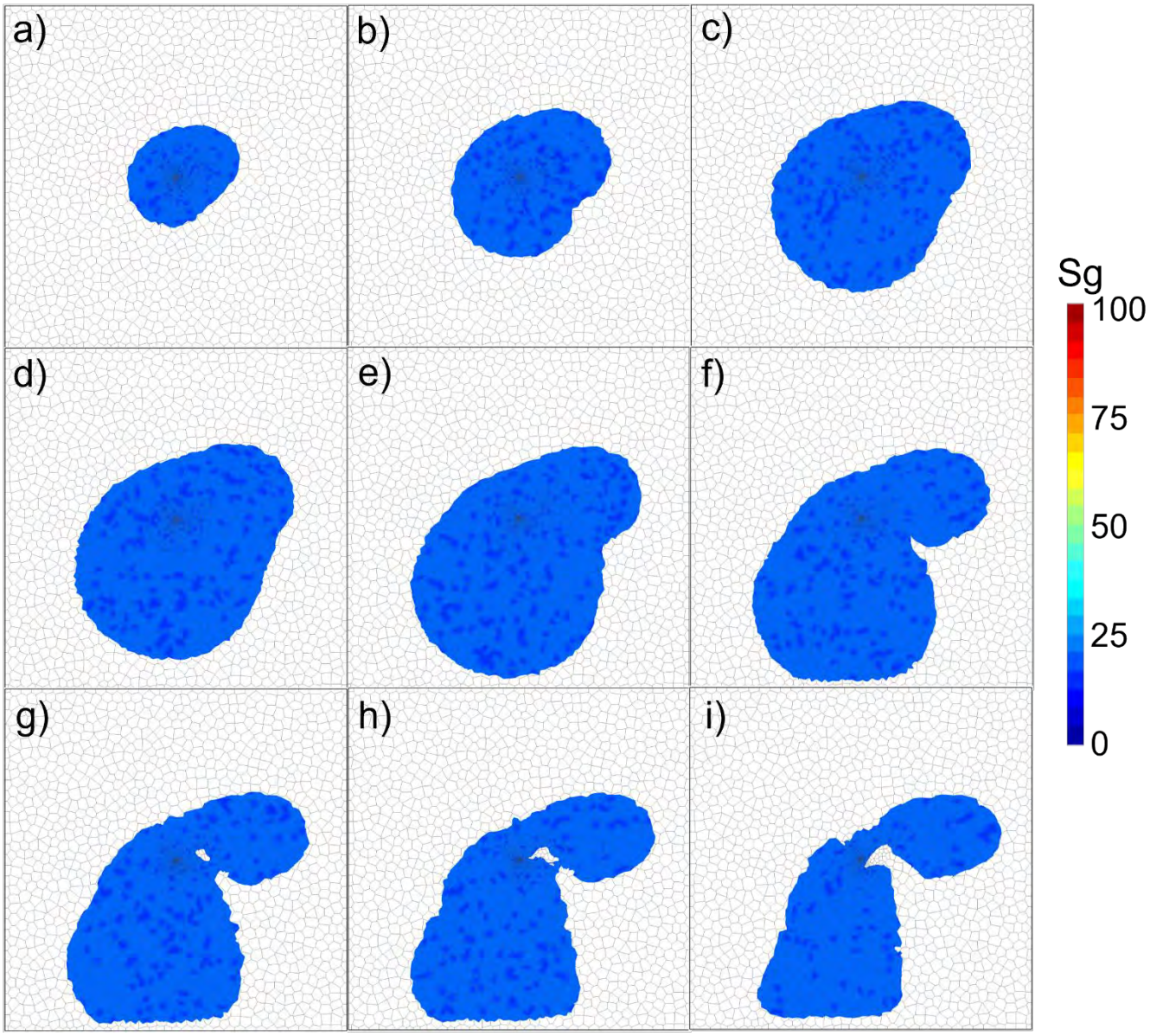

Figure 83: Supercritical CO_2 saturation isosurface at a) 1, b) 2, c) 3, d) 4, e) 5, f) 6, g) 7, H) 8, and i) 10 years. The isosurface in shows only the areas with greater than ~20% saturation.

The cross-section fence diagram of the porosity distribution is shown in Figure 84. Figure 85 shows the supercritical CO_2 saturation. The CO_2 migration was dominated by the 4 lower permeability HSU resulting in 4 zones where lateral migration dominated. After the end of injection, migration of super critical CO_2 towards the east and south, especially below hydrostatic unit 14 occurred. As the plume expanded the gas saturation decreased, and this reduced the potential of the buoyancy driven flow.

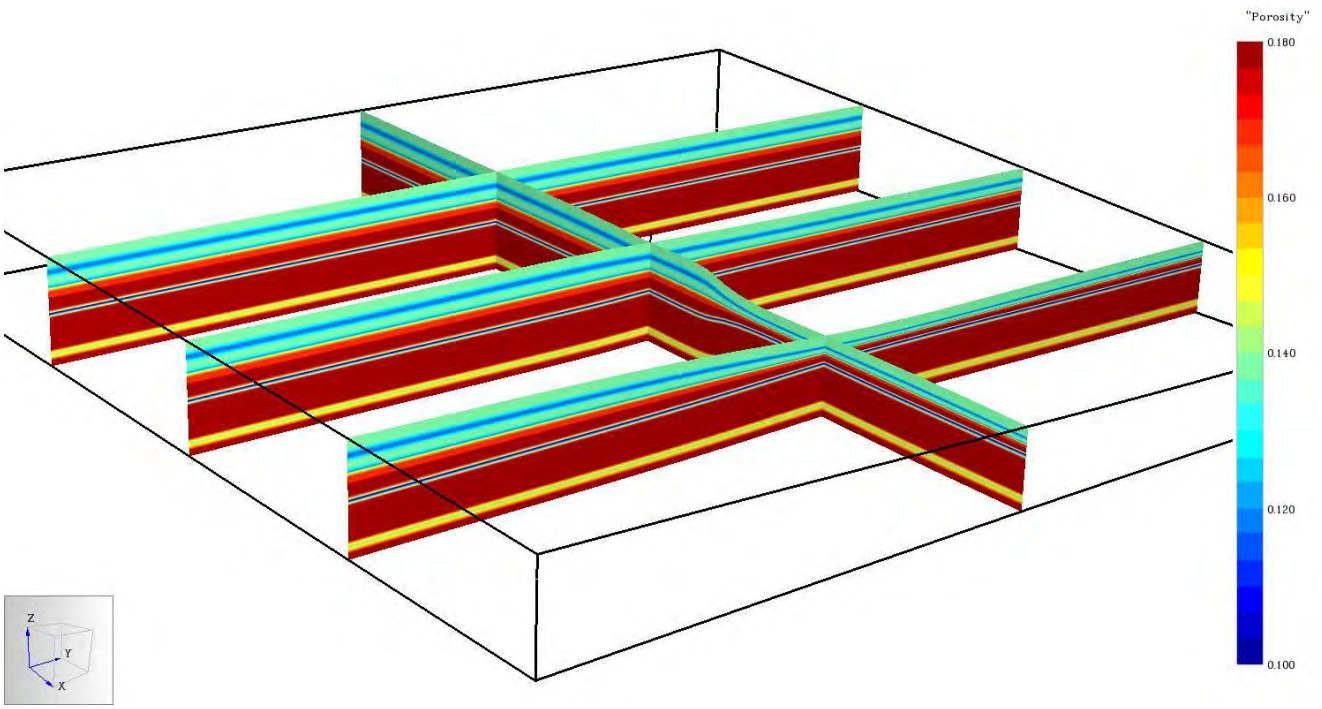

Figure 84: Porosity distribution in the 3D model. Each section of the fence diagrams is 1600 m.

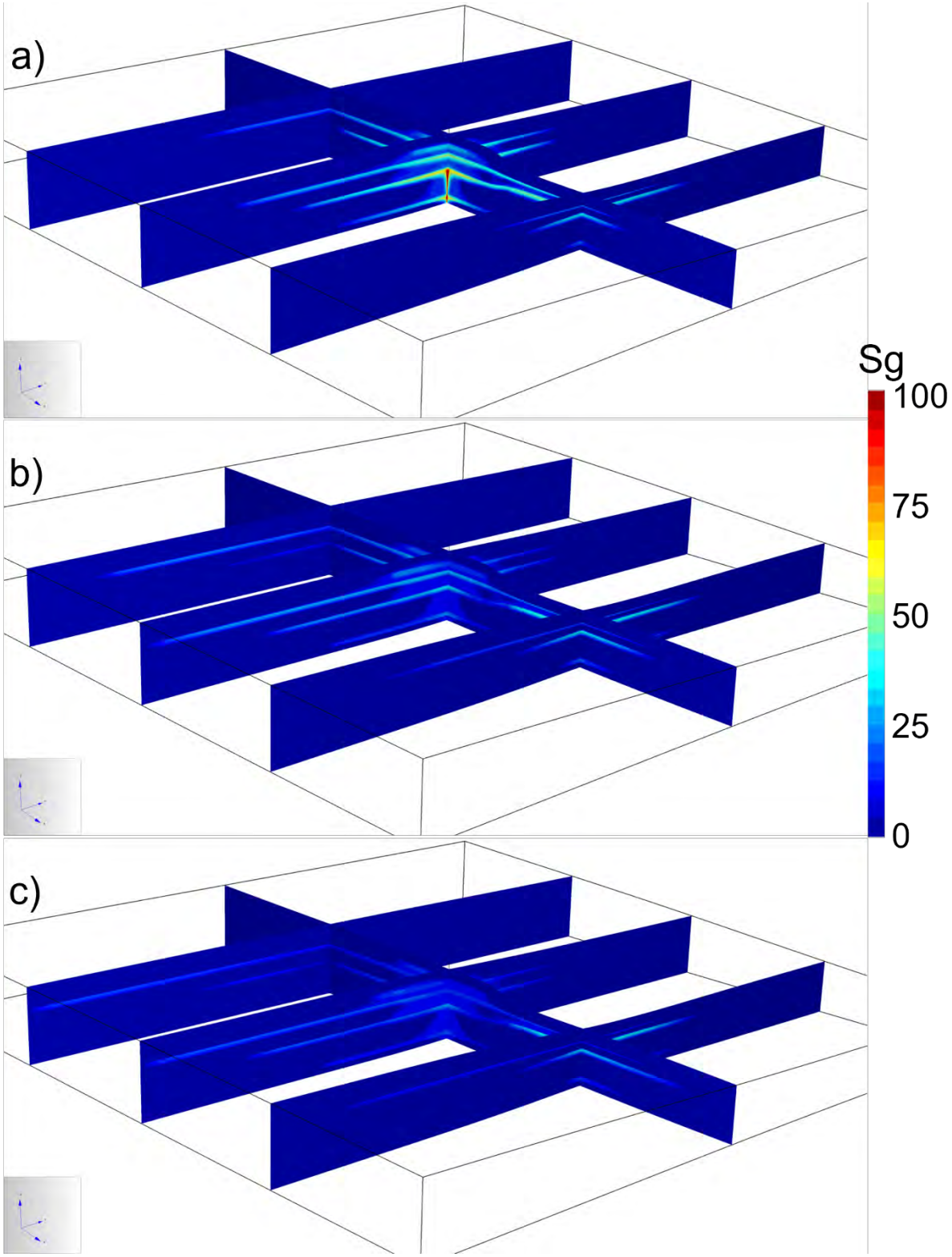

Figure 85: Supercritical CO_2 saturation at 3, 5, and 10 years. Each section of the fence diagrams is 1600 m.

The distribution of pH coincides with the supercritical CO_2 migration (Figure 86). The lowest pH is nearest the injector and over time, mineral buffering, largely through carbonate mineral dissolution, increases the pH. The pH remaining below 5 in most of the CO_2 impacted volume. Density driven migration of the CO_2-rich formation water initiates after ~7 years and affects the volume within 400 m of the injector especially below the "cave facies". The pH distribution is consistent with that of the radial models. Like the radial model, very low pH occurred proximal to the injector, with values as low as 1 in the < 2 m zone around the volume of dryout. The low pH corresponds to elevated SO_4^{-2} and NO_3^- from the production of nitric and sulfuric acid.

Outside of this volume the pH is initially controlled by the CO_2 content and later by buffering from the carbonate minerals.

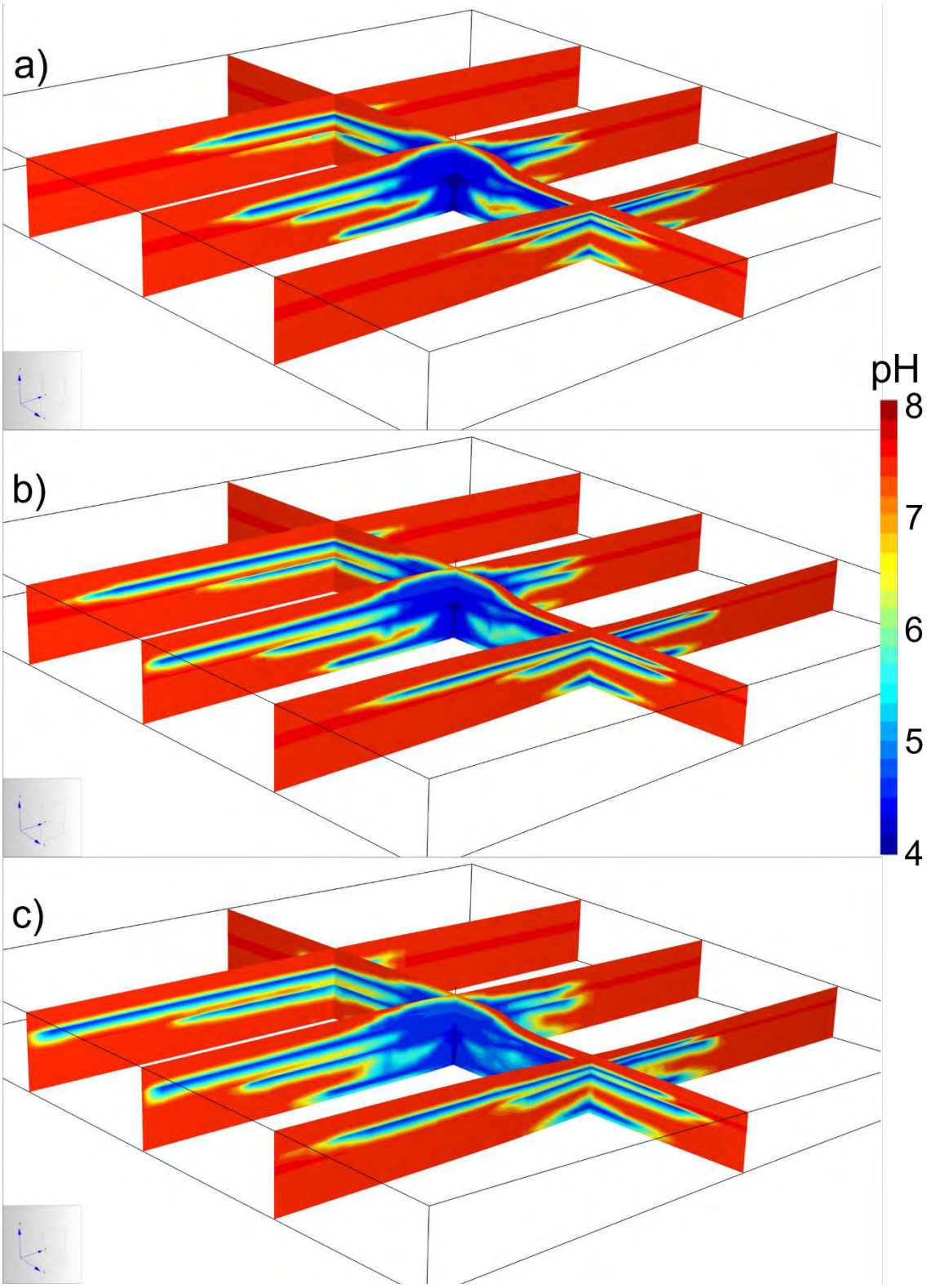

Figure 86: Distribution of pH at 3, 5, and 10 years. Each section of the fence diagrams is 1600 m.

The low pH drives the dissolution of the carbonate minerals that contain trace elements (Siderite 1, Siderite 2, and ankerite; Figure 87 shows Siderite 2 only). Near complete dissolution of siderite only occurs within 2 m of the injector. The siderite and ankerite in the models release trace metals on dissolution and they act as one of the sources of elevated trace element concentrations in the experiments and the models. Siderite is also a

significant source of Fe for the precipitation of $Fe(OH)_3$ and therefore the production of additional adsorption sites (Figure 88). The other source of Fe for iron oxyhydroxide precipitation is chlorite (not shown) but the amount of Fe from chlorite is relatively small initially. Authigenic siderite (not shown) precipitates along the migrating low pH fronts in the zones where O_2 is depleted, and that supersaturation inhibits further Siderite 1 or Siderite 2 dissolution. The volume where the $Fe(OH)_3$ precipitates is entirely controlled by O_2(aq) availability and by approximately 8 years no more $Fe(OH)_3$ precipitation occurs.

The main sinks for carbon in the models are siderite, magnesite and ankerite (not shown). The precipitating minerals are the pure endmembers so contain no trace metals. Very limited precipitation of trace metal end member carbonate minerals (cerussite, malachite, $NiCO_3$, otavite, rhodochrosite, smithsonite, sphaerocobaltite and strontianite) occurred in the modelling of the lower Precipice Sandstone as Glenhaven (Dawson et al., 2021) so these minerals were not incorporated in this study. Other minerals that precipitate in the models include kaolinite, illite, smectite and chalcedony and there is minor K-feldspar dissolution consistent with the radial modelling and previous modelling (Dawson et al., 2021; Golding et al., 2019; Pearce et al., 2015).

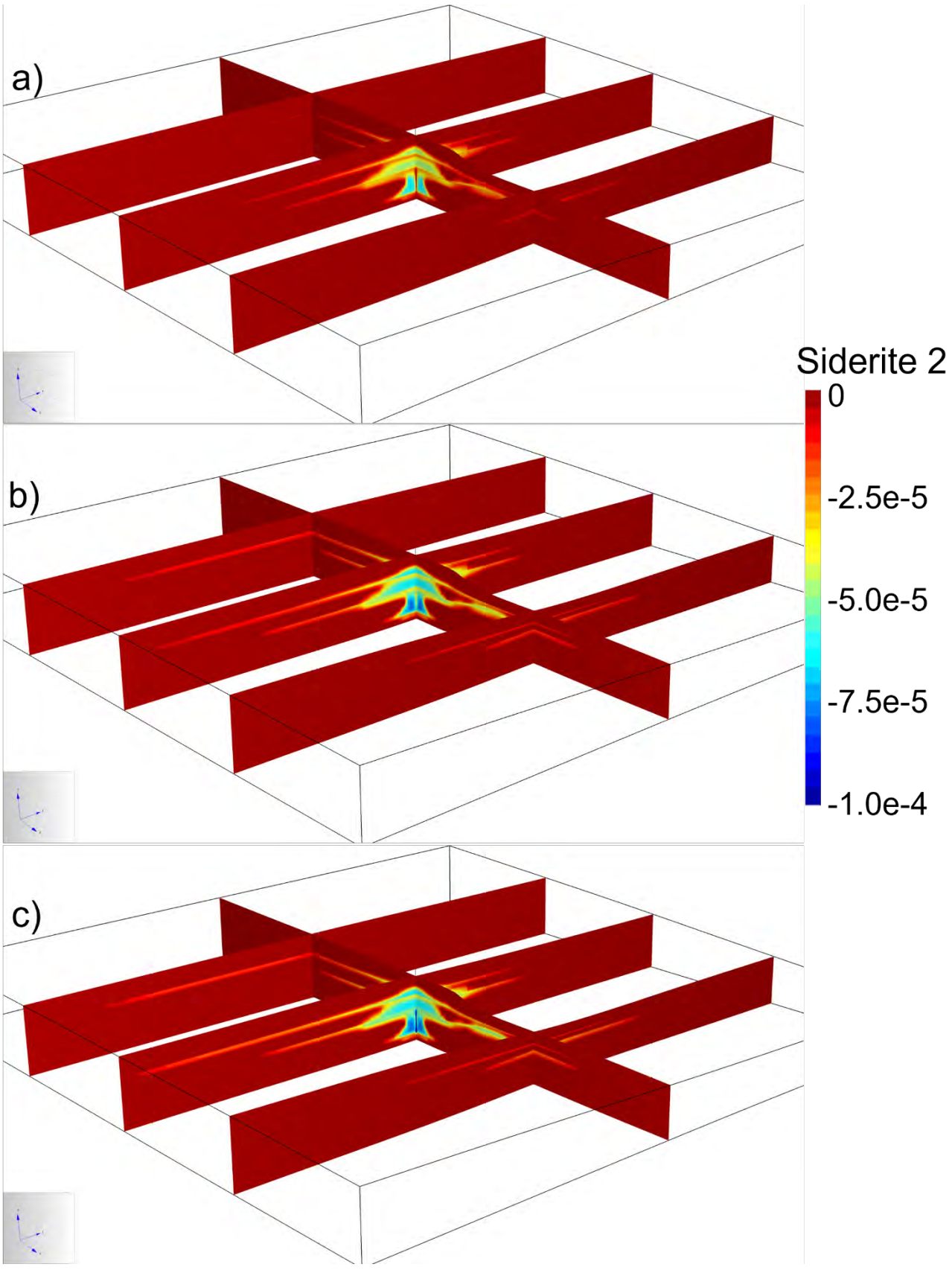

Figure 87: Siderite 2 dissolution (negative values) in volume fraction at 3, 5, and 10 years. Each section of the fence diagrams is 1600 m.

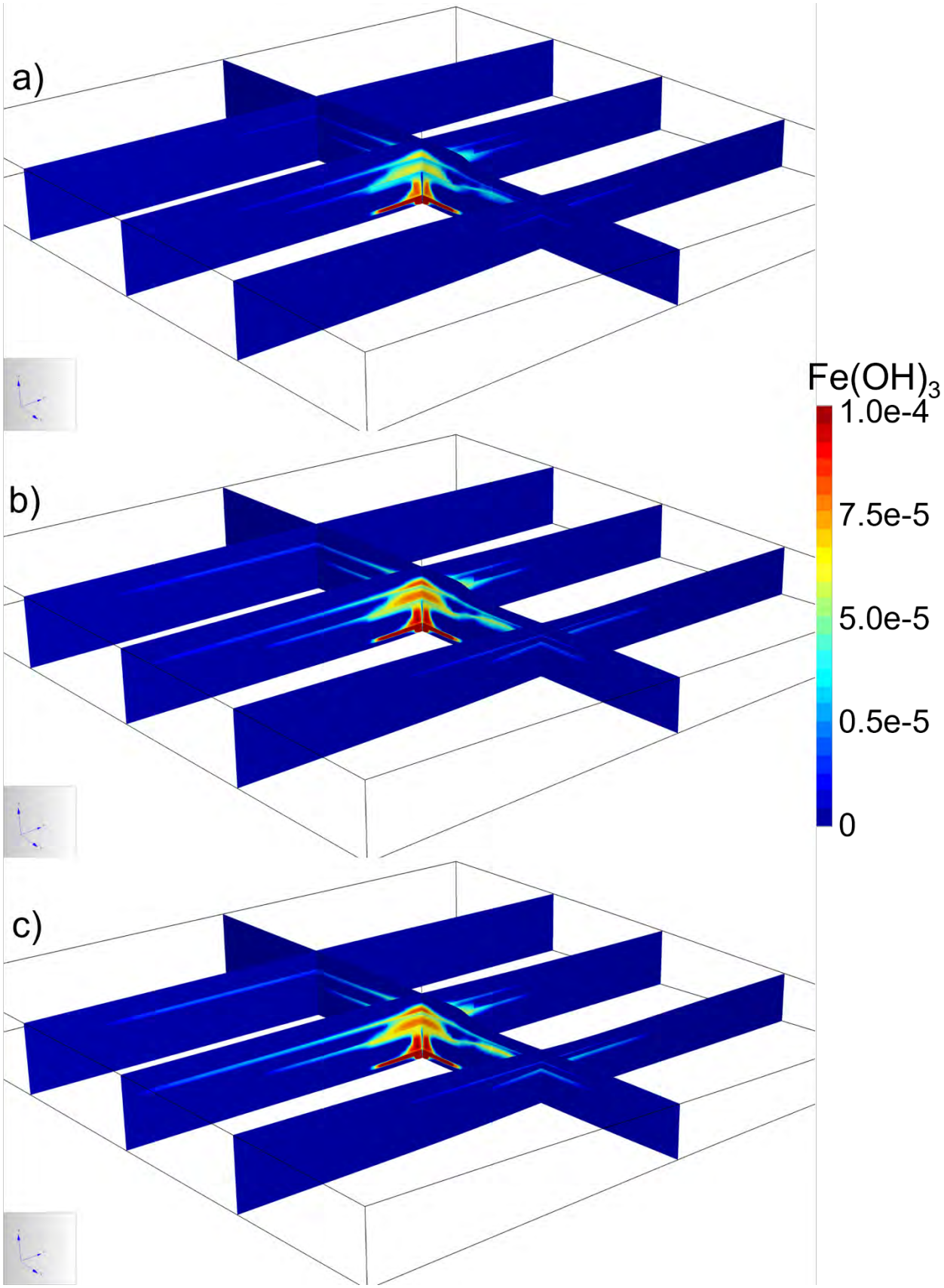

Figure 88: $Fe(OH)_3$ precipitation in volume fraction at 3, 5, and 10 years. Each limb of the fence diagrams is 500 m.

Changes in the As concentration with time are shown in Figure 89. Similar to the radial models, the As concentrations are the highest at the edges of the volume containing the CO_2 impacted lower pH water and low in the volume where $Fe(OH)_3$ precipitation occurs. The low As concentration reflects the role of the new adsorption sites in controlling the As mobility.

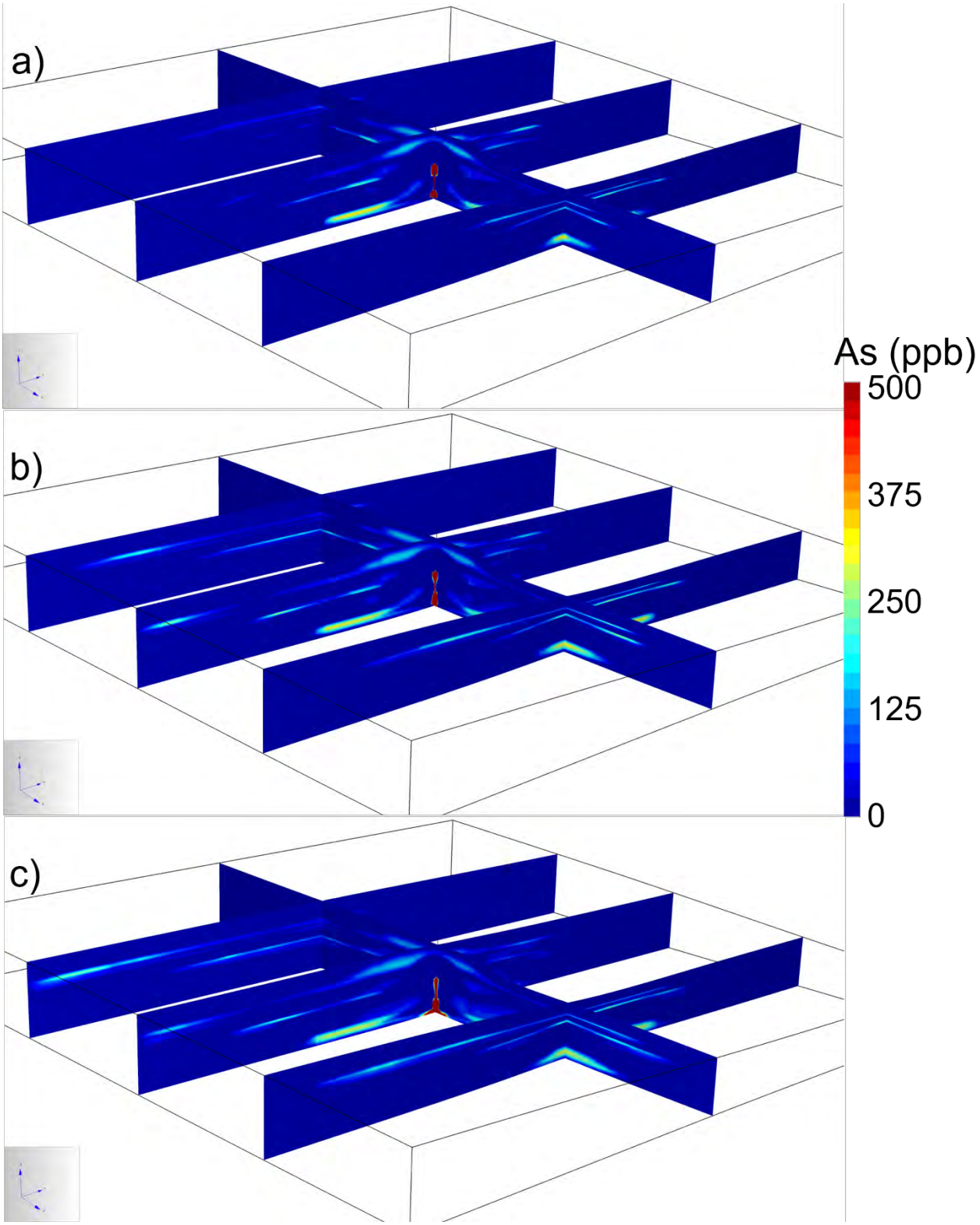

Figure 89: Dissolved arsenic distribution in ppb at 3, 5, and 10 years. Each section of the fence diagrams is 1600 m.

Lead concentrations are higher in the volume where siderite dissolution dominates (Figure 90). The Pb concentrations show trends that were observed in the radial models including the increase largely through dissolution of carbonate minerals and then decrease via advective transport and redistribution along with adsorption.

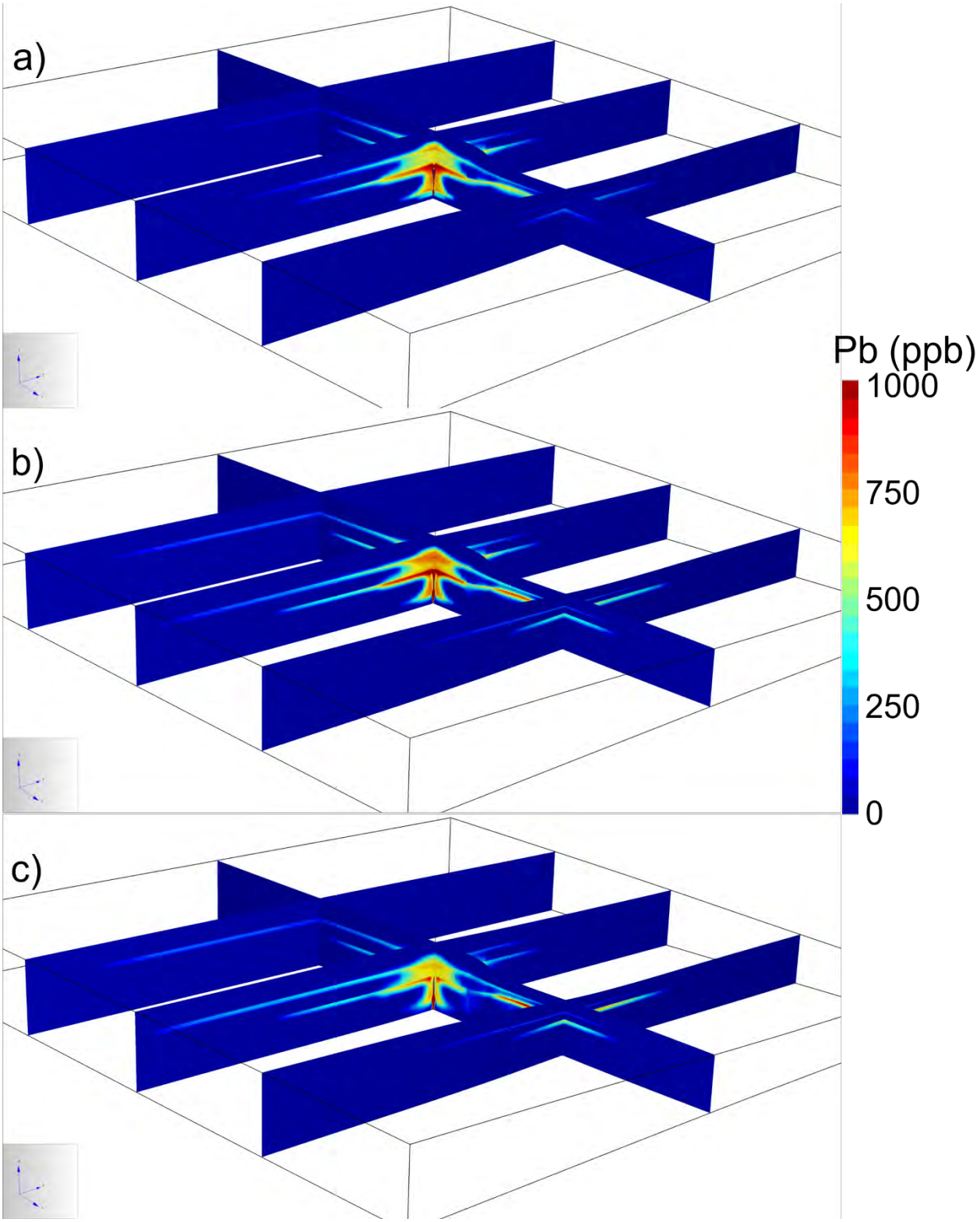

Figure 90: Dissolved lead distribution in ppb at 3, 5, and 10 years. Each section of the fence diagrams is 1600 m.

The concentrations of the other trace elements modelled in the RTM at 10 years are shown in Figures 91 and 92. The concentration evolution of Cd, Co, Cu, Mn, Ni, and Zn are similar to that of Pb, with carbonate mineral dissolution dominating and advective transport and minor adsorption producing distributions that decrease with time.

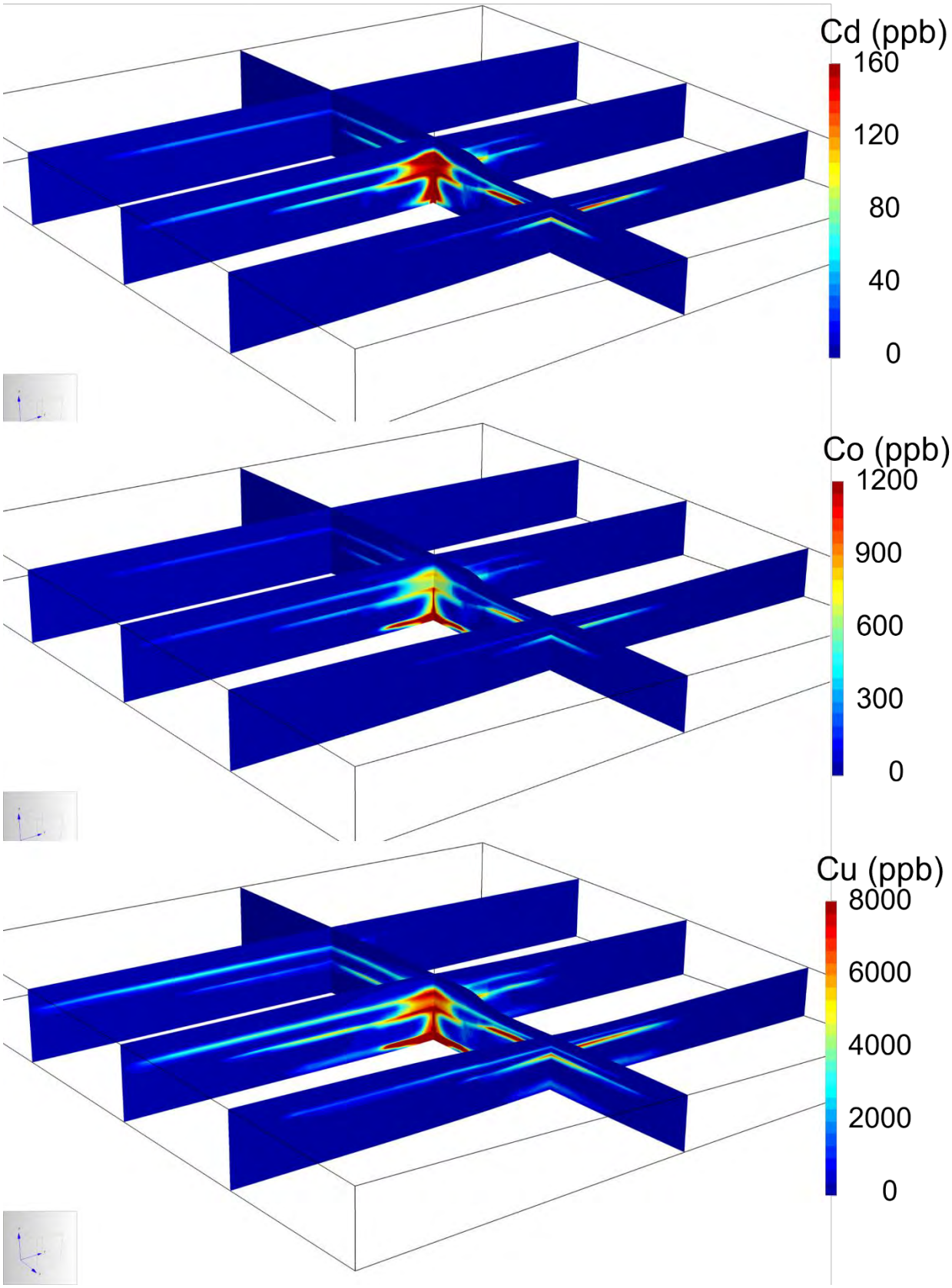

Figure 91: Trace element concentrations at 10 years for Cd (a), Cu (b), Co (c) in ppb. Each section of the fence diagrams is 1600 m.

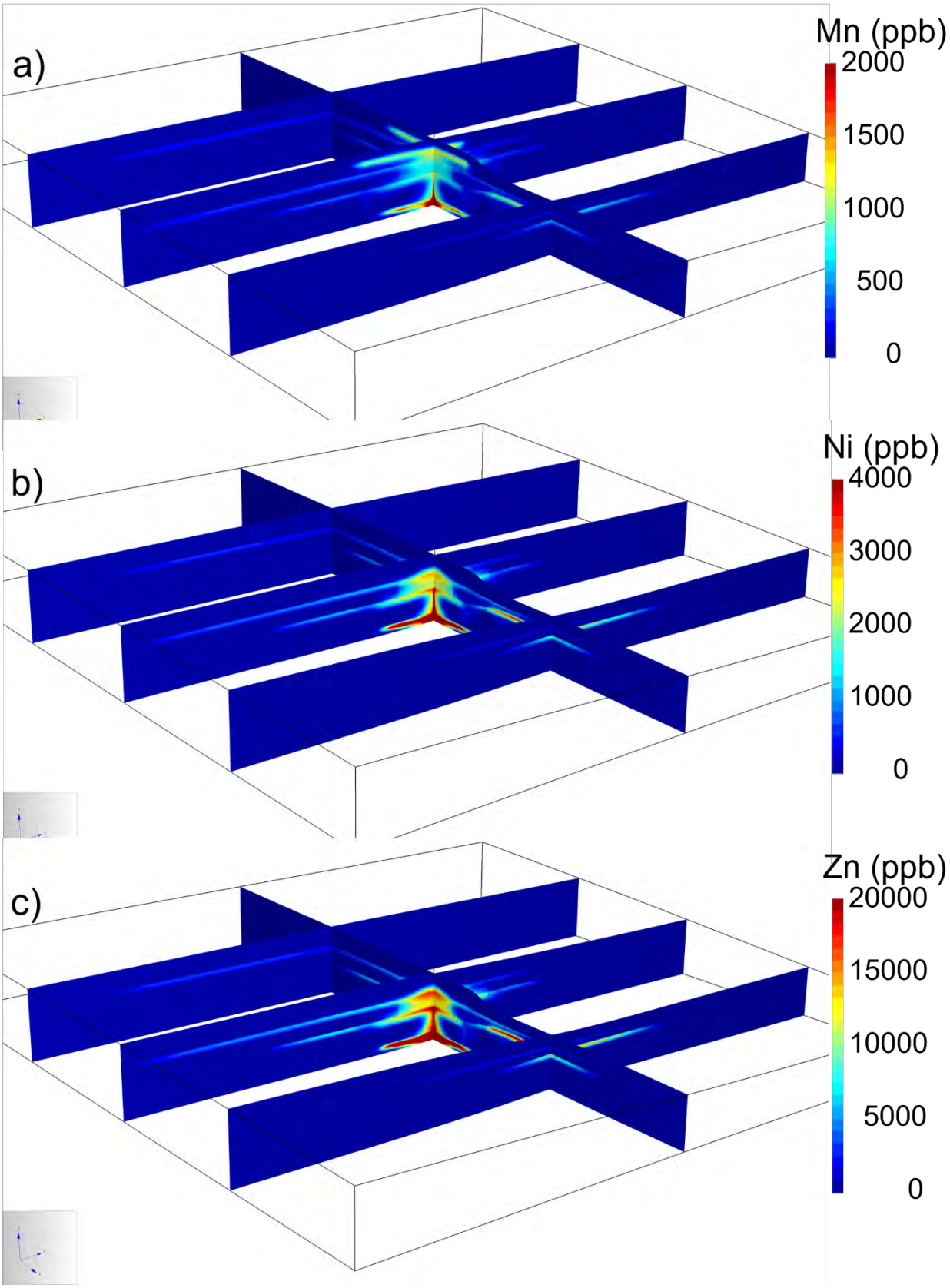

Figure 92: Trace element concentrations at 10 years for Mn (a), Ni (b), Zn (c) in ppb. Each section of the fence diagrams is 1600 m.

The 3D model as set up was not adequate to capture the migrating supercritical CO_2. The dimensions were reduced to 1600 m x 1600 m to fit to limitations on TOUGHREACT compiled for Windows where the number of elements and number of connections are limited by the maximum amount of memory Windows assigns.

Future models can be run using Linux executables which have a higher limit. The 1600 x 1600 m dimensions saw CO_2 migrating to the boundary where the boundary conditions led to CO_2 migrating out of the model. An increase to 2000 m x 2000 m is likely sufficient for the additional cells to pin the supercritical CO_2 migration through capillary forces. While this degree of migration does not fit with that predicted by the tNavigator™ modelling of the site done by others (not publicly available), the model gives some indication of the potential for migration in a high permeability medium.

5.3.4. Summary of radial and 3D reactive transport modelling

Despite the many uncertainties, assumptions, and simplifications that must be made in any numerical modelling exercise of complex geological and fluid systems, the results shed light on some fundamental characteristics of the dynamic hydrochemistry and multiphase flow behaviour in the proposed CO_2 injection into the Lower Precipice Sandstone of EPQ10. The radial and 3D reactive transport modelling shows that the temporal chemical evolution of the formation water is dominated by two components. The first is the migration of the supercritical CO_2 (with trace gases) and the second is the development of density driven flow of CO_2 saturated formation water. Both are the result of density contrasts that lead to pressure differentials driving fluid flow. Multiphase flow in the case of supercritical CO_2 means that physical factors of the HSU that control relative permeability and capillary response characterise the migration. Density contrast in the aqueous phase is largely subject to permeability variations in the HSU for determining the migration. The different HSU in the model resulted in supercritical CO_2 migration that was dominated by lateral flow below each of the low permeability HSU encountered at shallower depths, with vertical migration occurring only where the thickness of the migrating CO_2 front was greatest, and this was primarily close to the injector in these models.

As the supercritical CO_2 migrates, some CO_2 partitions to the formation water because of its high solubility. The dissolved CO_2 acts as a weak acid, lowering the pH and this drives the water-rock interactions that lead to changes in formation water composition. Those interactions are strongly coupled, as the lower pH drives dissolution of mineral phases like siderite, chlorite and K-feldspar, resulting in increases in pH and the concentrations of major components like Fe, K, Mg, HCO_3- and SiO_2 as well as the trace elements including As, Ba, Cd, Co, Cu, Mn, Ni, Pb, Sr and Zn. The changes in pH and water composition lead to adsorption/desorption of the elements being mobilised from the mineral dissolution reactions. In addition, the presence of O_2 in the supercritical stream drives precipitation of iron oxyhydroxide minerals generating new adsorption sites and even greater reduction in the mobile trace elements.

The extent of migration of trace gases injected with the supercritical CO_2 was primarily controlled by their solubility in the formation water. $SO_2(g)$ concentrations were only present close to the injector as it is the most soluble and rapidly partitioned into the formation water. The aqueous disproportionation reaction of $SO_2(aq)$ going to HS^- and SO_4^{-2} was kinetically controlled with the HS^- and dissolved oxygen additionally reacting to produce sulfuric acid. The high solubility of $SO_2(g)$ and these reactions resulted in high SO_4^{-2} concentrations within a few meters of the dryout volume. Evaporation near the zone of dryout, as water partitioned into the supercritical CO_2, also increased the concentration of the solutes in the formation water near the wellbore as the injection proceeded. High dissolved concentrations of SO_4^{-2} near the injector also occurred. NO(aq) underwent similar increases in concentration near the dryout volume due to relatively high solubility and the kinetically controlled reaction with dissolved O_2 lead to the production of nitric acid. The $SO_2(aq)$ and NO(aq) oxidation reactions created a zone of very low pH near the injector. Within 10's of meters of the dryout zone, the $SO_2(g)$ and NO(g) concentrations in the supercritical CO_2 were depleted and $O_2(g)$ was the only remaining trace gas transporting with the supercritical CO_2. The $O_2(aq)$ reacted with Fe mobilised from the dissolution of carbonate minerals and chlorite to produce $Fe(OH)_3$. This resulted in the depletion of the $O_2(aq)$ and the generation of new adsorption sites. The P-T-X experiments conducted as part of previous work on the Precipice Sandstone (Dawson et al., 2021; Golding et al., 2019; Pearce et al., 2015) demonstrate the rapid dissolution and reaction of $SO_2(g)$ and the slower reaction of NO(g) to produce strong acids. At the low trace gas concentrations used in this study and earlier experiments (Dawson et al., 2021; Golding et al.,

2019) there was little effect on the pH; however, in experiments when the concentrations were high in the supercritical phase (up to ~1% SO_2(g)) the pH was very low (<2) (Pearce et al., 2015). The different solubilities of the trace gases leads to chromatographic concentration variations away from the injector and the impact on pH of the formation water in the models is consistent with the results of the experiments and field observations (Boreham et al., 2011; Underschultz et al., 2011). The experiments also confirm the formation of the Fe oxyhydroxides was after the SO_2(g) and NO(g) oxidation reactions indicating the slower kinetic rate.

The models show that at the migrating supercritical CO_2 front there is formation water that is saturated with CO_2 being displaced ahead of the supercritical CO_2. This CO_2 impacted formation water dissolves some of the siderite and chlorite and drives desorption of As from the type of adsorption site that is most abundant at neutral pH. When O_2 is present, $Fe(OH)_3$ precipitation reduces the Fe concentration and more siderite can dissolve. In the volume at the migrating front where the O_2 has been entirely consumed, siderite 1 and 2 (modelled containing trace elements) dissolution ceases, and siderite (no trace elements) precipitation initiates as the Fe content and pH increase from the chlorite dissolution. The As mobilised from desorption is partially re-adsorbed on the low pH dominant adsorption sites, and, in the volume where $Fe(OH)_3$ precipitates, the As concentration is lowered even more through adsorption on the new sites. Behind the migrating front, the siderite 1 and 2 continues to dissolve as the O_2 is consumed in the precipitation of $Fe(OH)_3$. This mobilises the trace elements that are incorporated in the siderite 1 and 2 crystal structure and also leads to some adsorption of those trace elements as the concentrations increase. By 8 years, all of the O_2 is consumed, and the dissolution of siderite 1 and 2 stops. As this was the primary source of trace elements in the volume of reservoir impacted by CO_2, the fate of the trace elements becomes predominantly controlled by adsorption/desorption and transport.

Around this time, the onset of downward directed convection initiates as the higher density of the CO_2 impacted formation begins to overcome the static forces. The density driven flow continues migrating in a downward and outward direction, with the CO_2 impacted formation water from within the volume where siderite 1 and 2 dissolution occurred that contains elevated concentrations of the trace elements, dominating the water composition. Through dispersion and larger scale mixing the concentrations of the major, minor and trace elements decrease; however, the water is still CO_2 charged and drives chlorite and K-feldspar dissolution and As desorption. This leads to the differences in the evolving water chemistry at the locations 1-5 and is important for understanding how the elements are being mobilised and transported. Flow initiated by the density contrast between the CO_2 impacted formation water and initial formation water is downwardly directed and drives additional CO_2 dissolution. This occurs largely within the thicker sections of accumulated CO_2 that coincide with the volume where siderite 1 and 2 dissolution and $Fe(OH)_3$ precipitation took place.

Arsenic and lead concentrations displayed very different behaviour. The As was primarily mobilised as the pH decreased from pH dependent adsorption sites. Concentrations reached as high as ~500 ppb with most areas displaying maximum concentrations of <250 ppb. Lead concentrations in the models were as high as ~1000 ppb. In both cases, and for the remaining trace elements, the high concentrations decreased significantly as dispersion and adsorption became dominant through convective flow. In the batch experiments, trace element concentration changes of approximately 1-5 ppb were at the lower end, when accounting for the water to rock ratio of the experiments, the rock density and porosity, the equivalent total concentrations mobilised are ~200 to 1000 ppb for the higher porosity HSU and ~390 to 1950 ppb for the lower porosity HSU. For those trace elements that displayed even higher concentration changes in the experiments, the numbers are proportionately higher with values ranging from 4000 to 40000 ppb. The reactive transport models show changes in the trace element concentrations that are similar to these amounts for the highest values in the zone of evaporation and transport from that zone though density driven convection redistributes these. The trace element concentrations in the models are not as high as those observed in the experiments because of the limitation on siderite 1 and 2 dissolution due to the O_2 availability and through adsorption.

The evolution of the spatial distribution of supercritical CO_2 was dominated by the vertical heterogeneity of the different HSU in the reactive transport modelling. The radial models consist of HSU that are flat lying, and the migration of supercritical CO_2 was controlled by a vertical component due to buoyancy and a horizontal component that was controlled by pressure. The injection creates elevated pressure that drives the CO_2 horizontally into the reservoir. The lower density of the supercritical CO_2 relative to the formation water results in an upwardly directed flow potential. The vertical drive is greater than the horizontal drive within 10's of meters of the injector and the supercritical CO_2 rises. Resistance to the vertical flow potential comes through lower vertical permeability of the HSU and capillary forces resulting from multiphase occupation of pore space. As the CO_2 migrates upward, when it encounters a lower permeability material, the flow rate is slowed and there is accumulation at that intersection. Capillary forces contribute to the reduction in flow as the water has to be displaced from the pore spaces by the supercritical CO_2. Once the pressure at this accumulation point exceeds the capillary forces in the horizontal direction, flow proceeds laterally, and, similarly, once the capillary forces are overcome in the vertical direction, flow will proceed vertically. The rate of that flow is controlled by the relative permeability so is a function of the saturation of the 2 phases. After approximately 7 years the relatively dense formation water that is saturated with CO_2 begins forming fingers of convective flow. This flow drives increased dissolution of supercritical CO_2 (Figure 93). The total amount of supercritical CO_2 shows an increase during injection and then rapidly decreases. There is no apparent difference between the pure CO_2 and the mixed gas models for the different injection intervals, and the mixed gas models had slightly higher CO_2 dissolution after approximately 50 years. The 3D model shows a much larger decline after 5 years which is when the supercritical CO_2 reached the boundary of the model. In the 3D models, the dipping surfaces result in flow orientated up dip and this combined with the hydraulic drive from injection leads to an even greater extent of lateral flow along that surface. In the 3D model the supercritical CO_2 reaches the model boundary and is essentially removed from the system by the fixed pressure boundary condition. The proximity of the fixed pressure boundary condition cells means that there is a steeper pressure gradient and that leads to increased flow as the supercritical CO_2 migrates along the dipping surfaces. The net result is CO_2 leaves the model. The main forces that stop the flow of the supercritical CO_2 are capillary and because the boundary cells are close to the injector, capillary forces do not slow and stop the migration. It is likely that even a small increase in the size of the model domain could provide enough flow resistance to stop the migration.

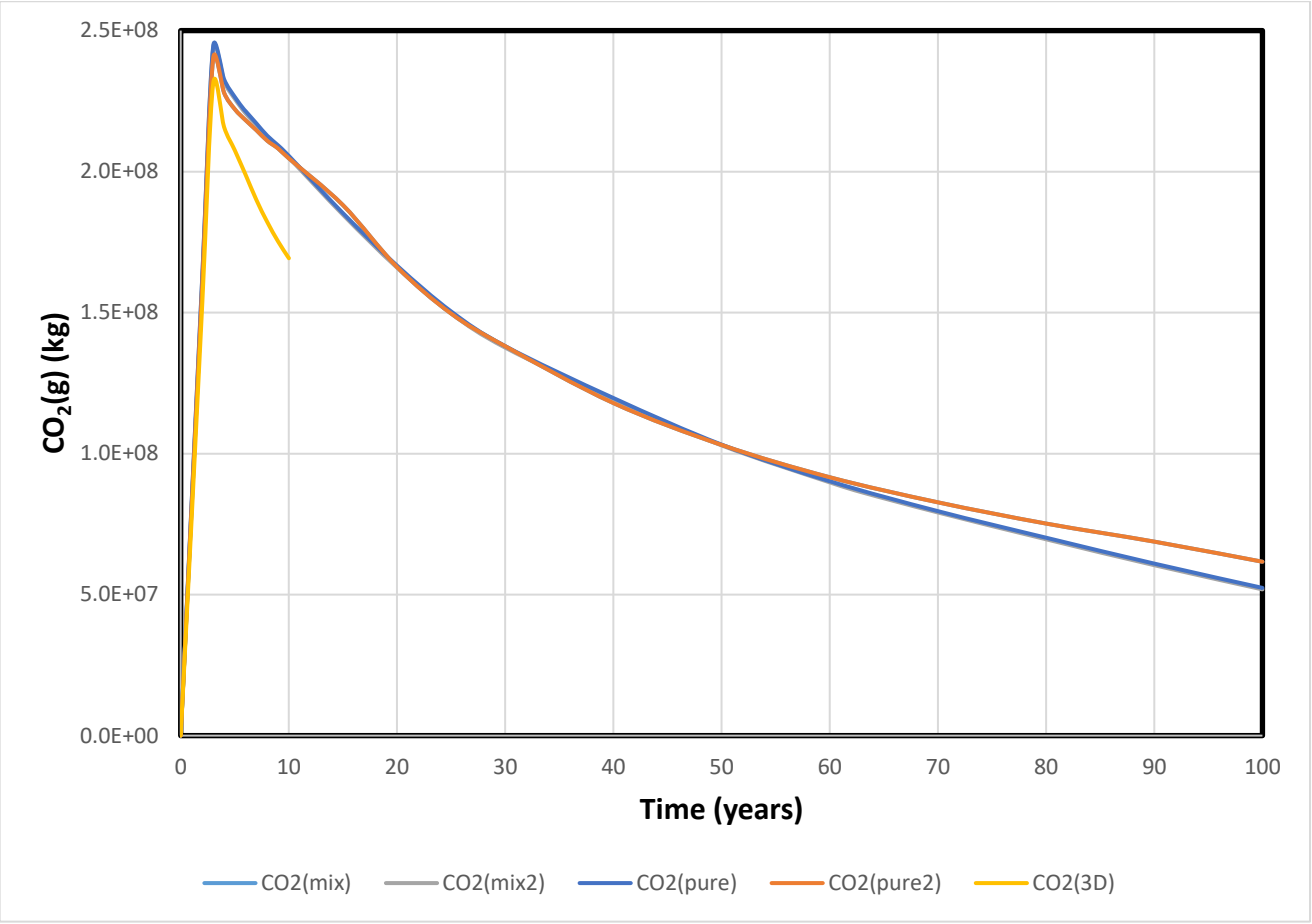

Figure 93: Total CO_2(g) in the radial and 3D models. The CO_2(mix) and CO_2(pure) models were for the 30 m injection interval and the CO_2(mix2) and CO_2(pure2) models had the 20 m injection interval. CO_2(3D) was from the 3D model that ran to 10 years).

The batch experiments and modelling are consistent with observations in other studies (Humez et al., 2014; Kirsch et al., 2014; Little & Jackson, 2010; Lawter et al., 2016; Lu et al., 2010; Varadharajan et al., 2013; Zheng et al., 2016). Zheng et al. (2016) show, in modelling column experiments that the amounts of adsorption sites and carbonate minerals play a vital role in how the different trace elements will mobilise and transport. Carbonates were commonly identified as sources of trace elements and adsorption/desorption as important processes controlling their mobility. The mechanisms of mobilisation, concentrations and sources of trace elements were commonly found to be strongly related to the sediment/rock being studied and there were some differences between studies that were conflicting. Field based studies often observed limited impacts of trace elements (Cahill and Jakobsen, 2013; Kharaka et al., 2010; Peter et al., 2012; Trautz et al., 2013). Many of the experimental and modelling studies focussed on the migration of CO_2 or CO_2 with brine into shallow formations (Lawter et al., 2016; Qafoku et al., 2017; Viswanathan et al., 2012; Xiao et al., 2020; Zheng et al., 2012, 2016). These were at lower pressure but still indicated that mobilisation and demobilisation processes along with advective dispersion are the primary factors leading to understanding the trace element behaviour.

In this study As behaved differently from the other trace elements. The primary controls included the initial concentration in the formation water, the total content in the modelled carbonate minerals and the adsorption site complexation constants used in the double layer model. Changes in any of these parameters could change As from adsorption/desorption dominated behaviour to the carbonate dissolution and advective transport dominated behaviour predicted for Pb, Co, Cu, Mn, Ni, Sr and Zn. The mechanisms of mobilisation and demobilisation remain the same, it is just the relative degree to which they apply to particular trace elements that controls how that trace element will distribute. The most sensitive parameter controlling how

the trace elements Pb, Co, Cu, Mn, Ni, Sr and Zn were mobilised and transported was the amount that was incorporated in the carbonate minerals in this study and where the carbonate minerals dissolved. The importance of a sink for Fe mobilised from siderite dissolution dictated where and how much siderite could dissolve and thus the extent to which trace element mobilisation could occur. Adsorption and desorption were important for all the trace elements with As showing a strong short term control and for the remainder of the traces in this study, the longer term distributions and concentrations were more heavily impacted.

The sources of uncertainty in the modelling include the lack of chemical and lateral physical heterogeneity in each of the HSU, the larger grid spacing away from the injector and the fixed trace element content of the carbonate minerals, both as sources and as sinks. Dawson et al. (2021) investigated the impact of changing adsorption site density and showed that there is a significant impact on the trace element behaviour. Additionally, the adsorption modelling is limited to just using sites associated with $Fe(OH)_3$ and there are several other minerals (illite, smectite, goethite, chlorite) which contribute to adsorption in the rocks that have slightly different adsorption behaviour from $Fe(OH)_3$ that could have an impact on the longer term transport. The experiments provide some constraints on the numbers associated with the Fe precipitation and give greater confidence to the model outputs in the areas where $Fe(OH)_3$ is modelled to precipitate; however in the rest of the reservoir the other minerals are also important. Similarly, the trace element content of the minerals and the exchange and adsorption sites used in the models is constrained by the bulk chemistry and the sequential extraction results and the similarity of the numbers for the samples from the different HSU indicates there is some consistency and the models at least do not exceed the real system. So, while chemical heterogeneity within HSU and between HSU is important, the fundamental processes and the chemical basis of HSU govern most of the chemical behaviour and capturing the heterogeneity may not be as critical as defining those processes. Preferential flow along higher permeability pathways can significantly impact how the CO_2 migrates. Navarre-Sitchler et al. (2013) demonstrated that lateral heterogeneity commonly decreased the water quality impacts when simulating a CO_2 leak into a shallow aquifer reactive transport modelling. In modelling two phase flow, the role of capillary forces is particularly important for constraining lateral flow (Tang et al., 2019) and the relative permeability impacts the distribution and rates at which the supercritical CO_2 migrates (Oostrom et al., 2016). The relative permeability terms and the capillary pressure terms used in this modelling largely came from the West Wandoan site, so, while broadly applicable, they add uncertainty and should be further refined in future studies. Density driven convection was important for the distribution of CO_2-rich formation water and the mobilisation of trace elements sourced from carbonate mineral dissolution. The models show that trace element mobilisation is significant within the convection cells and how and where the fingering develops is an important factor to consider when evaluating the potential impacts on the water quality. How and when density driven convection initiates in porous media is a vital area of knowledge that still is uncertain.

6. Conclusions

Carbonate minerals, followed by weak acid-reactive aluminosilicates, phosphates, and sulfur-bearing minerals, were the main hosts of elements extracted during the weak acid (pH 5 and pH 3) steps of the sequential extraction procedure. Based upon both absolute amounts and proportions that were acid-extracted, the trace elements that should be most closely monitored in lower Precipice Sandstone groundwater at EPQ10 include As, Co, Cu, Ni, Pb, and Sb. At pH 3, acid-extractable Pb correlates with extractable Cd and Zn, and extracted Cu correlates with Cs and Rb. Occurrence and extraction of the elements Co and Ni are closely correlated with each other under all tested conditions. There was similar median acid extraction of Ca, Pb and Sb, higher Cd (albeit very low magnitude), P, and S, and lower As, Ba, Co, Cu, Fe, Mg, Mn, Ni, Sr, and Zn from WM1 lower Precipice Sandstone samples compared with the median values for previously studied sites.

Eight lower Precipice Sandstone samples, one upper Precipice Sandstone, one lower Evergreen Formation, and two Moolayember Formation samples from the West Moonie 1 well have been reacted with a mixed gas stream (CO_2 O_2 SO_2 NO). Dissolved elements such as Ca, Mg, Mn, Sr, and Ba increased from the reaction of trace amounts of carbonates in lower Evergreen Formation and upper Precipice Sandstone samples as well as one Moolayember Formation sample, and a clay-rich lower Precipice, with stabilising trends in other lower Precipice Sandstone experiments. Dissolved elements such as K, Al, Si, and Li generally increased or stabilised indicating some silicate mineral reaction in all experiments. Dissolved Fe, Pb, Mo, Cr, Se mainly increased and subsequently decreased indicating subsequent adsorption or precipitation processes in the majority of West Moonie 1 core experiments. However, Cr, and other elements including As and Pb increased in concentrations from two lower Precipice Sandstone samples and a Moolayember sample. Overall, the concentrations of As and Pb at the end of mixed gas experiments were below 30 µg/kg. Four pure CO_2 experiments were also run with lower Precipice Sandstone core. Dissolved As and Pb were initially slightly higher in two pure CO_2 experiments with lower Precipice Sandstone core (than mixed gas); however, concentrations also decreased below 10 µg/kg by the end of reactions. The Fe-hydroxyoxides precipitated in mixed gas stream experiments may sequester more trace metals and maintain lower dissolved concentrations. It should be noted, however, that no West Moonie 1 lower Precipice Sandstone samples from the injection zone have batch reactions performed, and no samples of the mudstone layer (lower Precipice Sandstone B baffle unit) from West Moonie 1 have been reacted as these were not available to the project. Such work may be completed in the future as a supplement to the current study, but in the meantime proxy data from other locations (previous studies) help inform the current modelling.

Mixed gas experiment comparison of EPQ10 and previous EPQ7 core experiments: Variation in results of experiments and models for the different sites is to be expected, given the natural stratigraphic and regional geological variation and the distances between the wells. The dissolved concentration of elements such as Pb, Cu, Mo, and Cd during EPQ 10 West Moonie 1 core lower Precipice Sandstone reactions with mixed gas (CO_2 O_2 SO_2 NO) are lower than or comparable with EPQ 7 (West Wandoan 1 and Woleebee Creek core) lower Precipice Sandstone experiments where increasing or stabilisation trends were observed (Golding et al., 2019). Mainly EPQ10 West Moonie 1 samples show initial increases and subsequent decreases in Pb concentrations. Whereas lower Precipice Sandstones 2284.13 m and 2288.51 m have a slightly increasing trend (along with a Moolayember sample). The Pb concentrations are overall lower or comparable to EPQ7 experiments where increasing and decreasing or stabilisation trends were observed. Mo concentrations are higher from West Moonie 1 core (compared to EPQ7); however, the initial increases trend to subsequent decreases in concentration. Cd concentrations are generally lower in West Moonie 1 experiments than West Wandoan 1 experiments. The concentration of U in West Moonie 1 EPQ 10 experiments was overall almost an order of magnitude lower than EPQ 7 core experiments, especially from quartz rich sandstones. In general, dissolved U was low overall, below 1.6 and 6 µg/kg respectively in EPQ10 and EPQ7 experiments. The West Moonie 1 experimental dissolved As trend was an initial increase and subsequent decrease or stabilisation in

the majority of experiments, with an increasing concentration from one lower Precipice Sandstone 2284.13 m (and two Moolayember). However, As concentrations remain low, below 30 µg/kg in West Moonie 1 mixed gas experiments, and similar to EPQ7 experiments. EPQ 7 experiments had As concentrations with initial increases and subsequent decreases likely from adsorption to precipitated Fe-oxide/hydroxide, concentrations also remained below 30 µg/kg. Dissolved Cr, Cu and Zn have increasing or stabilising trends in West Moonie 1 lower Precipice Sandstone experiments but have comparable concentrations to those from EPQ 7 experiments (Golding et al., 2019). The mineral dissolution reactions are similar between the Glenhaven and West Moonie models, with the main difference being that at the higher temperatures of the West Moonie site siderite solubility is lower and its dissolution is largely controlled by the extent of Fe mineral precipitation. Trace metal mobility was somewhat different between the two sites. At Glenhaven, As, Cd, and Cu were primarily controlled by adsorption/desorption with the Pb, Co, Mn, Ni, Sr and Zn mobilised through carbonate mineral dissolution, whereas at West Moonie, As was the only trace element that was under adsorption/desorption control.

Reaction path modelling of the experiments provided an understanding of the reactions occurring under the pressure-temperature-composition conditions of 12 different HSU. The batch experiments all showed varying degrees of carbonate and silicate mineral dissolution as well as Fe and Al mineral precipitation. History matching modelling of the experiments identified chlorite, calcite, siderite, ankerite and some K-feldspar as the reacting mineral phases and $Fe(OH)_3$ and $Al(OH)_3$ as the precipitating phases. Mineral dissolution of calcite, 2 different siderite compositions and an ankerite enabled the development of mixed composition carbonate minerals that could be incorporated in the models. The experiments and modelling were supported by sequential extraction, XRD, SEM-EDS and micro-XRF to generate the mixed composition carbonates and also establish some information on exchange/adsorption site content and occupancy. The reactions mobilised major, minor and trace elements and the rate of the mobilisation and the mineral sources and sinks were incorporated into the geochemical models. These provided constraints on the models that significantly reduce the uncertainty of the model outcomes. In most cases the carbonate and chlorite mineral content was below detection of the XRD. Thermodynamic modelling of mixed composition carbonate minerals was utilised to generate stoichiometric minerals that would, on dissolution, mobilise the trace elements As, Ba, Cd, Co, Cu, Mn, Ni, Pb, Sr and Zn. Adsorption was incorporated by assigning strong and weak adsorption sites to the mineral $Fe(OH)_3$. Initial adsorption site densities and occupation were assigned based on the amounts of $Fe(OH)_3$ present and the starting water composition and new sites could be generated by the precipitation of $Fe(OH)_3$ or lost by dissolution of $Fe(OH)_3$.

Based on the well logs and examination of the core, 20 HSU were identified. These included 18 HSU making up the lower Precipice Sandstone and 1 each for the Moolayember Formation and the upper Precipice Sandstone. The lower Precipice A Sandstone was modelled as 40 m thick and contained 9 HSU with one lower permeability hydrostatic unit at 5 m above the base and the low permeability lower Precipice B Sandstone ("cave facies") at the top. Above the "cave facies" the lower Precipice C Sandstone was 29 m thick and consisted of 7 HSU, with two low permeability HSU at 15 m and 23 m above the base of the lower Precipice C Sandstone. The lower Precipice B Sandstone was 7 m thick and directly underlies the upper Precipice Sandstone. Radial reactive transport models were generated that were populated by physical and chemical data obtained for the HSU. Two different injection scenarios were simulated. The first had a 28 m injection interval that extended from the base of the lower Precipice A Sandstone and the second had a 18 m interval from 10 m above the base of the lower Precipice A Sandstone. Injection over 3 years of 310,000 tonnes of pure CO_2 and CO_2 with 400ppm O_2, 15 ppm NO and 5 ppm SO_2 was simulated. A radial model and a 3D model were constructed. The radial models are not able to represent stratigraphic structure that is dipping but require fewer cells and are thus less computationally demanding. The 3D models allow the incorporation of structural features including the topography of surfaces and regional dip or depth variations that can play an

important role in the dynamics of multiphase and density dependent flow and transport. From the preliminary radial modelling that incorporated all of the HSU, it was determined that there was limited interaction with the underlying Moolayember and the overlying upper Precipice Sandstone due to their very low permeabilities, so these were not included in the final models in order to improve computational efficiency and reduce run times. In addition, the 3D model run was terminated at just over 10 years simulation time and the abrupt termination made it incapable of a restart and there was not sufficient time to rerun the simulation from the beginning.

Supercritical CO_2 migration was dominated by buoyancy, moving upward until encountering lower permeability HSU at which point lateral migration dominated. This is a reason for the difference in the modelled distribution of the supercritical CO_2 plume in the lower Precipice Sandstone at West Moonie 1 compared with the Glenhaven site models that included fewer low-permeability HSU. The 4 lower permeability HSU in the lower Precipice Sandstone at West Moonie acted to divert the upward migration and led to horizontal accumulation and flow below those units. The trace gases SO_2, NO and O_2 were sequentially stripped out of the migrating supercritical CO_2 based on the trace gas solubility in the formation water. Rapid oxidation of SO_2 and NO to sulfuric and nitric acid lead to very low pH proximal to the injector. The migration of O_2 was considerably more extensive and contributed to the oxidation of Fe and precipitation of $Fe(OH)_3$. The primary control of the pH in and adjacent to the migrating supercritical CO_2 was the CO_2 content of the formation water. The highest concentrations occurred where either migrating supercritical CO_2 or residual trapped CO_2 were present and maintained high dissolved CO_2 concentrations. Dissolution of CO_2 into the formation water also led to increases in the formation water density and the onset of density driven convection. The low pH drove mineral dissolution reactions including carbonate mineral, chlorite and K-feldspar dissolution. In the volume where O_2 migrated, dissolution of siderite and chlorite released Fe and precipitation of $Fe(OH)_3$ occurred. That precipitation maintained undersaturation with respect to the siderite and dissolution continued. Where O_2 was depleted within the volume where CO_2 migrated, siderite dissolution was very minor and saturation with respect to the carbonate mineral resulted in little to no more dissolution. This had important implications for the mobilising of trace elements. The primary mechanism of trace element mobilisation was from carbonate mineral dissolution. In the volume where O_2 migrated, that dissolution led to elevated trace element concentrations; however, once the O_2 was depleted and, in any CO_2 impacted formation water where O_2 had not migrated, this mechanism was no longer operating significantly enough to cause elevated trace element concentrations. The mobility of As, however, followed a different pattern. The low pH of the CO_2 impacted water caused As desorption from sites that were dominant in neutral pH, this resulted in an increase in As concentrations. Where the O_2 migrated, As was mobilised from the carbonate mineral dissolution; however, the newly formed $Fe(OH)_3$ provided additional adsorption capacity and the As, along with a proportion of the other trace elements was adsorbed. The As concentrations were very low (< 10 ppb); however, the concentrations of the other trace elements, Pb, Ba, Cd, Co, Cu, Mn, Ni, Sr and Zn, remained elevated but not as high as those observed in the experiments because of the limitation on siderite 1 and 2 dissolution due to the O_2 availability and through adsorption.

The onset of density driven convection at approximately 7 years resulted in increased dissolution of supercritical CO_2, as formation water with low CO_2 content came into contact with migrated and residually trapped CO_2. In the volume where O_2 did not migrate with the supercritical CO_2, as the dense formation water migrated, As was liberated from the existing adsorption sites but few of the other trace elements showed increases in concentration. For CO_2 impacted formation water migrating from within the volume where O_2 had migrated, the concentrations of the other trace elements were high and As was low. This contrast led to differences in the concentration profiles of As versus the other trace elements. Arsenic displayed elevated concentrations along the migrating front of the density driven convection cells especially those more distant from the injection zone. The other trace elements had the highest concentrations closer to the injector and

those concentrations decreased as migration away from the source volumes progressed. In all cases, the important factors that contributed to decreasing concentrations of the trace elements were depletion in the source volumes, adsorption and advective mixing. The potential for monitoring locations was investigated and it was determined monitoring of EC, pH, Fe, K, Mg and HCO3- in addition to minor and trace elements would make useful tools for identifying migration and processes occurring along the migration pathway.

In the radial models, lateral migration of supercritical CO_2 was controlled by the presence of lower permeability HSU. The greatest extent of lateral migration occurred in the lower part of the Precipice C Sandstone and the upper part of the Precipice A Sandstone. The maximum extent of migration was ~575 m in the lower Precipice A and ~550 m in the lower Precipice C Sandstone. The main difference between the two injection interval simulations was that very little supercritical CO_2 migrated up to the base of the Upper Precipice Sandstone seal in the longer injection interval simulation while a small proportion of the injected supercritical CO_2 arrived at the base of the upper Precipice Sandstone seal and underwent lateral migration in the shorter injection interval simulation. After approximately 20 years' the supercritical CO_2 plumes began to shrink as the CO_2 was increasingly dissolved and transported through density driven convection currents.

The 3D model was limited in size due to constraints imposed on the TOUGHREACT code by the Windows operating system. Chemically the results of the 3D model matched those of the radial models with similar reactions dominating and the mineral dissolution and precipitation patterns as well as the mobilisation of trace elements showing consistency between the two. The migration of supercritical CO_2 in the 3D models was influenced by the dip of the HSU with migration of the supercritical phase orienting towards the south-southwest. The smaller model size 1600 m x 1600 m resulted in boundary affects influencing the supercritical CO_2 migration and a larger model that is run to the 100-year simulation time would provide additional understanding of the potential for trace element migration over time.

References

ANZECC and ARMCANZ. (2000). Australian Water Quality Guidelines for Fresh and Marine Waters, National Water Quality Management Strategy. Australian and New Zealand Environment and Conservation Council, Agriculture and Resource Management Council of Australia and New Zealand, Canberra, ACT, Australia.

Appelo, C. and Postma, D. (2005) Geochemistry, Groundwater and Pollution. 2nd Edition, Balkema, Rotterdam. http://dx.doi.org/10.1201/9781439833544

Bethke, C. M., Farrell, B., and Yeakel, S. (2022). The Geochemist's Workbench. Release 12. Aqueous Solutions, LLC. Champaign, Illinois, USA.

Blanc, P., Vieillard, P., Gailhanou, H., Gaboreau, S., Gaucher, E., Fialips, C. I., Made, B., and Giffaut, E. (2015). A generalized model for predicting the thermodynamic properties of clay minerals. American Journal of Science 315 (8), 734-780.

Boreham, C., Underschultz, J., Stalker, L., Kirste, D., Freifeld, B., Jenkins, C., and Ennis-King, J. (2011). Monitoring of CO_2 storage in a depleted natural gas reservoir: Gas geochemistry from the CO2CRC Otway Project, Australia. International Journal of Greenhouse Gas Control 5(4), 1039-1054.

Burton, W. K., Cabrera, N., and Frank, F. C. (1951). The Growth of Crystals and the Equilibrium Structure of their Surfaces. Philosophical Transactions of the Royal Society of London. Series A, Mathematical and Physical Sciences 243, 299-358.

Cahill, A. G. and Jakobsen, R. (2013). Hydro-geochemical impact of CO_2 leakage from geological storage on shallow potable aquifers: A field scale pilot experiment. International Journal of Greenhouse Gas Control, 19, 678–688. https://doi.org/10.1016/J.IJGGC.2013.03.015

Darcy, H. (1856). Les Fontaines Publiques de la Ville de Dijon, Dalmont, Paris.

Dawson, G. K. W., Biddle, D., Farquhar, S. M., Gao, J.-F., Golding, S. D., Jiang, X., Keck, R., Khan, C., Law, A. C. K., Li, Q., Pearce, J. K., Rudolph, V., Watson, A., and Xing, H. (2015). Achieving Risk and Cost Reductions in CO_2 Geosequestration through 4D Characterisation of Host Formations. Project 7-1110-0101. Final Report for ANLEC R&D., Manuka, ACT, Australia.

Dawson, G. K. W., Pearce, J. K., Biddle, D., and Golding, S. D. (2019). ANLEC Project 7-1116-0295: Interaction of CO_2 saturated groundwater with Moolayember Formation lithologies, Report for ANLEC R&D.

Dawson, G. K. W., Pearce, J., Kirste, D., Biddle, D., and Golding, S. D. (2020). ANLEC Project 7-0919-0320 Progress Report: Groundwater Geochemistry of the Moolayember Formation, Report for ANLEC R&D.

Dawson, G. K. W., Pearce, J. K., Kirste, D. M., and Golding, S. D. (2021). Groundwater geochemistry of the Moolayember Formation, Final Report for ANLEC R&D.

Derkowski, A. and Bristow, T. (2012). On the Problems of Total Specific Surface Area and Cation Exchange Capacity Measurements in Organic-Rich Sedimentary Rocks. Clays and Clay Minerals, 60. https://doi.org/10.1346/CCMN.2012.0600402

Dzombak, D. A. and Morel, F. M. M. (1990). Surface complexation modeling: hydrous ferric oxide. Wiley and Sons.

Garnett, A., Underschultz, J., and Ashworth, P. (2019). Scoping study for material carbon abatement via carbon capture and storage: Executive summary. The University of Queensland Surat Deep Aquifer Appraisal Project (UQ-SDAAP). Brisbane, Australia: The University of Queensland. https://natural-gas.centre.uq.edu.au/ccs/final-project-reports

Glynn, P. (2000). Solid-Solution Solubilities and Thermodynamics: Sulfates, Carbonates and Halides. Reviews in Mineralogy and Geochemistry 40, 481-511.

Golab, A., Arena, A., Sommacal, S., Goodwin, C., Rajan, P., Dodd, N., Khor, J., Deakin, L., Zhang, J., Young, B., and Carnerup, A. (2015). Milestone 2.9: Final report of digital core analysis results for plug samples from West Wandoan-1 Well. FEI-Lithicon, Report for ANLEC R&D.

Golding, S. D., Pearce, J. K., Dawson, G. K. W., and Kirste, D. M. (2019) ANLEC Project 7-1115-0236: Mobilisation and Fate of Heavy Metals Released by the GHG Stream, Final Report for ANLEC R&D.

Guo, B., Bandilla, K. W., Nordbotten, J. M., Celia, M. A., Keilegavlen, E., and Doster, F. (2016). A multiscale multilayer vertically integrated model with vertical dynamics for CO_2 sequestration in layered geological formations. Water Resources Research, 52 (8), 6490-6505.

Haese, R., Frank, A., Grigorescu, M., Horner, K., Kirste, D., Schacht, U., and Tenthorey, E. (2016). Geochemical Impacts and Monitoring of CO_2 Storage in Low Salinity Aquifers. ANLEC R&D Project 3-1110-088 Final Report. CO2CRC Report No.: RPT15-5328. 65 p.

Hellevang, H., Pham, V. T. H., and Aagaard, P. (2013). Kinetic modelling of CO_2–water–rock interactions. International Journal of Greenhouse Gas Control 15, 3-15.

Hofmann, H., Pearce, J. K., Rodger, I., Golding, S. D., and Hayes, P. (2021). Hydrogeology of the Southern Surat Basin, ANLEC R&D Final report.

Humez, P., Négrel, P., Lagneau, V., Lions, J., Kloppmann, W., Gal, F., Millot, R., Guerrot, C., Flehoc, C., Widory, D., and Girard, J.-F. (2014). CO_2–water–mineral reactions during CO_2 leakage: Geochemical and isotopic monitoring of a CO_2 injection field test. Chemical Geology, 368 (0), 11-30. https://doi.org/http://dx.doi.org/10.1016/j.chemgeo.2014.01.001

Kampman, N., Bickle, M., Wigley, M., and Dubacq, B. (2014). Fluid flow and CO_2–fluid–mineral interactions during CO_2-storage in sedimentary basins. Chemical Geology, 369 (0), 22-50. https://doi.org/http://dx.doi.org/10.1016/j.chemgeo.2013.11.012

Kharaka, Y. K., Thordsen, J. J., Kakouros, E., Ambats, G., Herkelrath, W. N., Beers, S. R., Birkholzer, J. T., Apps, J. A., Spycher, N. F., Zheng, L., Trautz, R. C., Rauch, H. W., and Gullickson, K. S. (2010). Changes in the chemistry of shallow groundwater related to the 2008 injection of CO_2 at the ZERT field site, Bozeman, Montana. Environmental Earth Sciences, 60 (2), 273-284. https://doi.org/10.1007/S12665-009-0401-1

Kirsch, K., Navarre-Sitchler, A. K., Wunsch, A., and McCray, J. E. (2014). Metal Release from Sandstones under Experimentally and Numerically Simulated CO_2 Leakage Conditions. Environmental Science & Technology, 48 (3), 1436–1442. https://doi.org/10.1021/es403077b

Köhler, S.J., Dufaud, F., and Oelkers, E.H., (2003). An experimental study of illite dissolution kinetics as a function of ph from 1.4 to 12.4 and temperature from 5 to 50°C. *Geochimica et Cosmochimica Acta* 67, 3583-3594.

Lasaga, A. C. (1995). Fundamental approaches in describing mineral dissolution and precipitation rates. In A. F. White and S. L. Brantley (Eds.), Chemical weathering rates of silicate minerals (Vol. 31, pp. 23-86). Mineralogical Society of America, Reviews in Mineralogy.

Lawter, A., Qafoku, N. P., Wang, G., Shao, H., and Brown, C. F. (2016). Evaluating impacts of CO_2 intrusion into an unconsolidated aquifer: I. Experimental data. International Journal of Greenhouse Gas Control, 44, 323-333. https://doi.org/10.1016/j.ijggc.2015.07.009

Little, M. G. and Jackson, R. B. (2010). Potential impacts of leakage from deep CO_2 geosequestration on overlying freshwater aquifers. Environmental Science and Technology, 44 (23), 9225–9232. https://doi.org/10.1021/ES102235W

Lowson R. T., Brown P. L., Comarmond M. J., and Rajaratnam G. (2007). The kinetics of chlorite dissolution. Geochimica et Cosmochimica Acta 71, 1431-1447.

Lu, J. M., Partin, J. W., Hovorka, S. D., and Wong, C. (2010). Potential risks to freshwater resources as a result of leakage from CO_2 geological storage: a batch-reaction experiment. Environmental Earth Sciences, 60 (2), 335-348. https://doi.org/10.1007/s12665-009-0382-0

Navarre-Sitchler, A. K., Maxwell, R. M., Siirila, E. R., Hammond, G. E., and Lichtner, P. C. (2013). Elucidating geochemical response of shallow heterogeneous aquifers to CO_2 leakage using high-performance computing: Implications for monitoring of CO_2 sequestration. Advances in Water Resources, 53. https://doi.org/10.1016/j.advwatres.2012.10.005

NHMRC, 2011. Australian Drinking Water Guidelines Paper 6 National Water Quality Management Strategy, National Health and Medical Research Council, National Resource Management Ministerial Council, Commonwealth of Australia, Canberra.

Nielsen, A. E. (1983). Precipitates: formation, coprecipitation, and aging. Wiley.

Oostrom, M., White, M. D., Porse, S. L., Krevor, S. C. M., and Mathias, S. A. (2016). Comparison of relative permeability–saturation–capillary pressure models for simulation of reservoir CO_2 injection. International Journal of Greenhouse Gas Control, 45, 70–85. https://doi.org/10.1016/J.IJGGC.2015.12.013

Palandri, J. L. and Kharaka, Y. K. (2004). A compilation of rate parameters of water-mineral interaction kinetics for application to geochemical modeling. In Open-File Report - U.S. Geological Survey: Reston, VA, United States.

Pearce, J. K., Kirste, D. M., Dawson, G. K. W., Farquhar, S. M., Biddle, D., Golding, S. and Rudolph, V. (2015). SO_2 Impurity Impacts on Experimental and Simulated CO_2-Water-Reservoir Rock Reactions at Carbon Storage Conditions. Chem. Geol. 399, 65-86.

Pearce, J. K., Kirste, D. M., Dawson, G. K. W., Rudolph, V., and Golding, S. D. (2019b). Geochemical modelling of experimental $O_2/SO_2/CO_2$ reactions of reservoir, cap-rock, and overlying cores. Applied Geochemistry, 109. https://doi.org/10.1016/j.apgeochem.2019.104400

Pearce, J., Underschultz, J. and La Croix, A. (2019a). Mineralogy, geochemical CO_2-water-rock reactions and associated characterisation. The University of Queensland Surat Deep Aquifer Appraisal Project (UQ-SDAAP) Brisbane, Australia: The University of Queensland, 978-1-74272-251-1. https://espace.library.uq.edu.au/view/UQ:734565/UQ_SDAAP_F10.pdf?dsi_version=b884746b13e4bb6fd4ce e7f1fb393d8b

Peter, A., Lamert, H., Beyer, M., Hornbruch, G., Heinrich, B., Schulz, A., Geistlinger, H., Schreiber, B., Dietrich, P., Werban, U., Vogt, C., Richnow, H. H., Großmann, J., and Dahmke, A. (2012). Investigation of the geochemical impact of CO_2 on shallow groundwater: Design and implementation of a CO_2 injection test in Northeast Germany. Environmental Earth Sciences, 67 (2), 335-349. https://doi.org/10.1007/S12665-012-1700-5

Pham V. T. H., Lu P., Aagaard P., Zhu C., and Hellevang H. (2011). On the potential of CO_2–water–rock interactions for CO_2 storage using a modified kinetic model. International Journal of Greenhouse Gas Control 5, 1002-1015.

Pruess, K. and Spycher, N. (2007). ECO2N – a Fluid property module for the TOUGH2 code for studies of CO_2 storage in saline aquifers. Energy Convers. Manage. 48 (6), 1761-1767.

Pruess, K. Faybishenko, B., and Bodvarsson, G. S. (1999). Alternative concepts and approaches for modeling flow and transport in thick unsaturated zones of fractured rocks. Journal of Contaminant Hydrology, 38, 281-322.

Pueyo, M., Mateu, J., Rigol, A., Vidal, M., López-Sánchez, and J. F., Rauret, G. (2008). Use of the modified BCR three-step sequential extraction procedure for the study of trace element dynamics in contaminated soils. Environmental Pollution 152, 330-341.

Qafoku, N. P., Lawter, A. R., Bacon, D. H., Zheng, L., Kyle, J., and Brown, C. F. (2017). Review of the impacts of leaking CO_2 gas and brine on groundwater quality. Earth-Science Reviews, 169, 69-84. https://doi.org/10.1016/j.earscirev.2017.04.010

Revil, A. and Leroy, P. (2004). Constitutive equations for ionic transport in porous shales [Article]. Journal of Geophysical Research: Solid Earth, 109 (B3), B03208-n/a.

Riaz, A., Hesse, M., Tchelepi, H. A., and Orr Jr, F. M. (2006). Onset of convection in a gravitationally unstable diffusive boundary layer in porous media. Journal of Fluid Mechanics, 548, 87-111. https://doi.org/10.1017/S0022112005007494

Rodger, I., Pearce, J.K., Hofmann, H., Golding, S.D., and Hayes, P. (2020). Hydrogeology of the Southern Surat Basin, ANLEC R&D Memo Report 2.

Sonnenthal, E., Spycher, N., Xu, T., Zheng, L., Miller, N., and Pruess, K. (2014). TOUGHREACT V3.0-OMP Reference Manual: a Parallel Simulation Program for Non-isothermal Multiphase Geochemical Reactive Transport. Lawrence Berkeley National Laboratory, Berkeley, CA.

Spycher, N., Llanos, E. M., Vu, H. P., and Haese, R. R. (2019). Reservoir scale reactive-transport modeling of a buoyancy-controlled CO_2 plume with impurities (SO_2, NO_2, O_2). International Journal of Greenhouse Gas Control. 89, 40-51. https://doi.org/10.1016/j.ijggc.2019.06.026

Steefel, C. I. (2001). GIMRT, version 1.2: Software for modeling multicomponent, multidimensional reactive transport. User's Guide, UCRL-MA-143182, Livermore, California: Lawrence Livermore National Laboratory.

Tang, Y., Li, Z., Wang, R., Cui, M., Wang, X., Lun, Z., and Lu, Y. (2019). Experimental Study on the Density-Driven Carbon Dioxide Convective Diffusion in Formation Water at Reservoir Conditions. ACS Omega, 4 (6), 11082-11092. https://doi.org/10.1021/acsomega.9b00627

Trautz, R. C., Pugh, J. D., Varadharajan, C., Zheng, L., Bianchi, M., Nico, P. S., Spycher, N. F., Newell, D. L., Esposito, R. A., Wu, Y., Dafflon, B., Hubbard, S. S., and Birkholzer, J. T. (2013). Effect of dissolved CO_2 on a shallow groundwater system: a controlled release field experiment. Environmental Science & Technology, 47 (1), 298-305. https://doi.org/10.1021/es301280t

Underschultz, J., Boreham, C., Dance, T., Stalker, L., Freifeld, B., Kirste, D., and Ennis-King, J. (2011). CO_2 storage in a depleted gas field: An overview of the CO2CRC Otway Project initial results. International Journal of Greenhouse Gas Control, 5 (4), 922-932.

US EPA (2007). Drinking water standards and health advisories table. San Francisco, CA, USA, 30 p.

US EPA (2017). Accessed 05/08/2017 from, URL: https://safewater.zendesk.com/hc/en-us/articles

Varadharajan, C., Tinnacher, R. M., Pugh, J. D., Trautz, R. C., Zheng, L., Spycher, N. F., Birkholzer, J. T., Castillo-Michel, H., Esposito, R. A., and Nico, P. S. (2013). A laboratory study of the initial effects of dissolved carbon

dioxide (CO_2) on metal release from shallow sediments. International Journal of Greenhouse Gas Control, 19, 183-211.

Viswanathan, H., Dai, Z., Lopano, C., Keating, E., Hakala, J. A., Scheckel, K. G., Zheng, L., Guthrie, G. D., and Pawar, R. (2012). Developing a robust geochemical and reactive transport model to evaluate possible sources of arsenic at the CO_2 sequestration natural analog site in Chimayo, New Mexico. International Journal of Greenhouse Gas Control, 10, 199-214.

Walton, A. G. (1967). The Formation and Properties of Precipitates. Interscience Publ, New York.

Warner, D., L. Koederitz, A. Simon, and M. Yow. (1979). Radius of pressure influence of injection wells. U.S. Environmental Protection Agency, Washington, D.C., EPA/600/2-79/170 (NTIS PB80100498).

Wolery, T. J. (1992). EQ3/6: Software package for geochemical modeling of aqueous systems: package overview and installation guide (Version 8.0. Lawrence Livermore National Laboratory Report UCRL-MA-10662 PT 1, Livermore CA.

Xiao, T., McPherson, B., Esser, R., Jia, W., Dai, Z., Chu, S., Pan, F., and Viswanathan, H. (2020). Chemical Impacts of Potential CO_2 and Brine Leakage on Groundwater Quality with Quantitative Risk Assessment: A Case Study of the Farnsworth Unit. Energies, 13 (24). https://doi.org/10.3390/en13246574

Xu, T. F., Apps, J. A., Pruess, K., and Yamamoto, H. (2007). Numerical modeling of injection and mineral trapping Of CO_2 with H_2S and SO_2 in a sandstone formation. Chemical Geology, 242 (3-4), 319-346.

Xu T., Sonnenthal E., Spycher N., and Pruess K. (2014). TOUGHREACT V3.0-OMP Reference Manual: A simulation program for non-isothermal multiphase reactive geochemical transport in variably saturated geologic media. Lawrence Berkeley National Laboratory Draft Report, Berkeley, CA.

Zheng, L., Apps, J. A., Spycher, N., Birkholzer, J. T., Kharaka, Y. K., Thordsen, J., Beers, S. R., Herkelrath, W. N., Kakouros, E., and Trautz, R. C. (2012). Geochemical modeling of changes in shallow groundwater chemistry observed during the MSU-ZERT CO_2 injection experiment. International Journal of Greenhouse Gas Control, 7, 202-217. https://doi.org/10.1016/j.ijggc.2011.10.003

Zheng, L., Apps, J. A., Zhang, Y., Xu, T., and Birkholzer, J. T. (2009). On mobilization of lead and arsenic in groundwater in response to CO_2 leakage from deep geological storage. Chemical Geology, 268, 281–297.

Zheng, L., Qafoku, N. P., Lawter, A., Wang, G., Shao, H., and Brown, C. F. (2016). Evaluating impacts of CO_2 intrusion into an unconsolidated aquifer: II. Modeling results. International Journal of Greenhouse Gas Control, 44, 300-309. https://doi.org/10.1016/j.ijggc.2015.07.001

Zhu, C., Veblen, D. R., Blum, A. E., and Chipera, S. J. (2006). Naturally weathered feldspar surfaces in the Navajo Sandstone aquifer, Black Mesa, Arizona: Electron microscopic characterization. Geochimica et Cosmochimica Acta, 70, 4600-461.

Appendix A – Geochemistry supplement

Table A1: Table of element names and symbols used in this report[1].

Symbol	Element	Atomic #	Symbol	Element	Atomic #	Symbol	Element	Atomic #
Ag	Silver	47	Ge	Germanium	32	Sc	Scandium	21
Al	Aluminium	13	Hf	Hafnium	72	Se	Selenium	34
As	Arsenic	33	Ho	Holmium	67	Si	Silicon	14
B	Boron	5	K	Potassium	19	Sm	Samarium	62
Ba	Barium	56	La	Lanthanum	57	Sn	Tin	50
Be	Beryllium	4	Li	Lithium	3	Sr	Strontium	38
Ca	Calcium	20	Lu	Lutetium	71	Ta	Tantalum	73
Cd	Cadmium	48	Mg	Magnesium	12	Tb	Terbium	65
Ce	Cerium	58	Mn	Manganese	25	Th	Thorium	90
Cl	Chlorine	17	Mo	Molybdenum	42	Ti	Titanium	22
Co	Cobalt	27	Na	Sodium	11	Tl	Thallium	81
Cr	Chromium	24	Nb	Niobium	41	Tm	Thulium	69
Cs	Cesium	55	Nd	Neodymium	60	U	Uranium	92
Cu	Copper	29	Ni	Nickel	28	V	Vanadium	23
Dy	Dysprosium	66	P	Phosphorus	15	W	Tungsten	74
Er	Erbium	68	Pb	Lead	82	Y	Yttrium	39
Eu	Europium	63	Pr	Praseodymium	59	Yb	Ytterbium	70
Fe	Iron	26	Rb	Rubidium	37	Zn	Zinc	30
Ga	Gallium	31	S	Sulfur	16	Zr	Zirconium	40
Gd	Gadolinium	64	Sb	Antimony	51			

[1] Not a complete list of the elements of the periodic table. Grey highlighted elements are Total REEs or REE (total rare earth elements) in this report. Light REEs (LREE) are La, Ce, Pr, Nd (and Pm but it is always <DL). Middle REEs (MREE) are Sm, Eu, Gd, Tb, and Dy. Heavy REEs (HREE) are Ho, Er, Tm, Yb, and Lu.

Table A2: Concentrations of rare earth elements (REE) within WM1 core samples (mg element per kg rock).

Unit		Depth (mRT)	LREE				MREE					HREE					REE	LREE	MREE	HREE
			La	Ce	Pr	Nd	Sm	Eu	Gd	Tb	Dy	Ho	Er	Tm	Yb	Lu				
Lower Evergreen Formation		2235.81-2235.94	36	74	8.2	30	5.5	0.9	5.6	0.7	3.7	0.7	2.0	0.3	1.9	0.3	170	149	16	5.3
		2242.25	59	132	15	58	12	2.9	13	1.9	11	2.1	5.9	0.9	5.7	0.8	320	263	41	15
		2242.44-2242.54	43	93	11	40	8.0	1.9	8.4	1.2	6.5	1.3	3.7	0.5	3.6	0.5	222	187	26	10
Upper Precipice Sandstone		2246.14-2246.25	9.1	20	2.3	8.7	1.8	0.5	1.8	0.2	1.4	0.3	0.8	0.1	0.8	0.1	48	40	5.7	2.1
		2254.94-2255.10	24	57	6.4	26	5.1	1.7	5.4	0.6	3.4	0.6	1.7	0.2	1.6	0.2	134	113	16	4.4
Lower Precipice Sandstone D		2263.61-2263.77	5.2	10	1.2	4.4	1.0	0.3	1.1	0.2	1.2	0.3	0.8	0.1	0.8	0.1	26	20	3.7	2.1
		2267.71-2267.84	38	81	9.3	37	7.4	1.4	7.2	1.0	6.4	1.3	4.1	0.6	4.4	0.7	199	165	23	11
		2267.84-2267.90	20	42	5.0	21	4.7	1.0	4.4	0.6	3.8	0.8	2.5	0.4	2.6	0.4	109	88	15	6.7
Lower Precipice Sandstone C		2274.10-2274.18	5.4	11	1.2	4.5	1.0	0.3	1.1	0.2	1.0	0.2	0.7	0.1	0.7	0.1	27	22	3.5	1.7
		2281.82-2281.92	24	54	6.4	25	5.4	1.2	6.1	1.0	5.9	1.2	3.7	0.5	3.5	0.5	139	110	20	10
		2284.13-2284.24	6.0	11	1.4	5.2	1.1	0.3	1.3	0.2	1.1	0.2	0.6	0.1	0.6	0.1	30	24	4.0	1.7
		2285.05	42	87	10	39	7.4	1.7	8.1	1.1	6.5	1.3	3.9	0.6	4.1	0.6	213	178	25	11
		2288.49-2288.61	7.1	14	1.4	5.1	1.0	0.2	1.1	0.2	0.9	0.2	0.5	0.08	0.5	0.08	32	27	3.4	1.4
		2294	20	40	4.3	16	2.8	0.3	3.0	0.4	1.8	0.3	0.9	0.1	0.9	0.2	91	80	8.2	2.4
		2296.97-2297.13	62	130	15	55	11	1.0	10	1.2	5.4	0.9	2.0	0.3	1.6	0.2	294	261	28	5.0
Lower Precipice Sandstone B		2297.13-2297.19	61	120	14	57	12	2.0	10	1.3	7.3	1.3	3.9	0.5	3.8	0.6	294	252	32	10
		2298.92	9.1	17	1.8	6.1	1.0	0.2	1.2	0.1	0.6	0.1	0.3	0.05	0.3	0.05	38	34	3.2	0.9
Lower Precipice Sandstone A	2	2307.20	6.4	13	1.3	4.8	0.9	0.1	0.9	0.1	0.6	0.1	0.3	0.04	0.3	0.05	29	25	2.6	0.8
		2315.77	4.5	9	0.9	3.2	0.5	0.1	0.6	0.06	0.3	0.06	0.2	0.03	0.2	0.03	20	18	1.7	0.5
		2322.61-2322.73	7.5	15	1.6	5.6	1.1	0.1	1.1	0.1	0.8	0.2	0.5	0.07	0.5	0.08	34	30	3.2	1.3
		2323.25	4.2	8	0.9	3.2	0.6	0.1	0.6	0.07	0.4	0.07	0.2	0.03	0.2	0.03	19	17	1.7	0.5
	1	2328.54-2328.59	64	119	13	46	8.1	1.5	8.8	1.2	6.8	1.4	4.0	0.6	4.0	0.6	279	242	26	11
		2328.59-2328.68	17	32	3.6	13	2.3	0.4	2.2	0.3	1.5	0.3	0.9	0.1	0.9	0.1	75	66	6.6	2.4
		2330.41-2330.55	4.6	9	1.0	3.4	0.6	0.1	0.7	0.09	0.5	0.1	0.3	0.05	0.3	0.05	21	18	2.0	0.9
		2338.75-2338.85	9.0	18	2.1	8.0	1.6	0.3	1.5	0.2	0.9	0.2	0.5	0.07	0.5	0.07	43	37	4.5	1.2
Moolayember Formation		2339.00-2339.17	25	51	6.6	25	5.1	1.1	5.2	0.7	4.3	0.9	2.8	0.4	2.9	0.4	132	108	16	7.4
		2340.54-2340.62	29	56	6.8	26	5.2	1.2	5.6	0.8	4.7	1.0	3.0	0.4	2.9	0.4	143	118	18	7.7
		2346.40-2346.51	28	55	6.7	25	5.0	1.3	5.6	0.8	4.9	1.0	3.1	0.5	3.2	0.5	141	115	18	8.3
		2348.16-2348.30	24	46	5.5	21	4.0	1.0	4.4	0.6	3.4	0.7	2.0	0.3	2.0	0.3	114	96	13	5.4
		2356.94-2357.06	22	43	5.2	20	3.9	1.1	4.4	0.6	3.8	0.8	2.4	0.4	2.5	0.4	110	90	14	6.5
		2362.90-2363.00	31	66	7.5	29	6.0	1.5	6.9	1.0	5.5	1.1	3.2	0.5	3.1	0.5	162	133	21	8.3
		2366.50-2366.61	29	61	7.1	27	5.6	1.3	6.2	0.9	5.2	1.1	3.2	0.5	3.2	0.5	152	124	19	8.6
		2373.89-2373.99	20	39	4.8	18	3.6	0.9	4.0	0.6	3.3	0.7	2.0	0.3	2.1	0.3	99	81	12	5.4
		2427.52-2427.74	19	39	4.8	19	4.3	1.3	5.4	0.8	4.6	0.9	2.3	0.3	2.0	0.3	104	82	16	5.8
Unit Medians	Upper Precipice Sandstone	WM1	24	57	6.4	26	5.1	1.7	5.4	0.6	3.4	0.6	1.7	0.2	1.6	0.2	134	113	16	4.4
		C4, T153, WCG4, WW1	30	61	7.1	27	5.3	1.5	5.4	0.7	4.0	0.8	2.3	0.3	2.2	0.3	147	124	17	5.9
	Lower Precipice Sandstone	WM1	7.8	16	1.7	5.9	1.1	0.3	1.3	0.2	1.0	0.2	0.6	0.09	0.6	0.1	36	32	3.8	1.6
		C4, T153, WCG4, WW1	8.5	17	1.9	6.6	1.2	0.2	1.2	0.1	0.8	0.2	0.4	0.06	0.4	0.07	38	34	3.5	1.2
	Moolayember Formation	WM1	27	54	6.6	25	5.0	1.2	5.4	0.8	4.6	0.9	2.8	0.4	2.9	0.4	134	111	16	7.4
		WCG4, WW1	25	53	6.2	24	5.0	1.3	5.5	0.7	4.5	0.9	2.7	0.4	2.7	0.4	134	109	17	7.2
Legend	Trace	Ultra-Trace	100 - 1,000		10 - 100		< 10													

Table A3: Elements extracted by pH 7 water (mg element per kg rock powder).

		Element Set	Alkali metals					Alkaline earth metals					Lanthanoids	Actinoids		Transition metals																						Post transition metals								Metalloids					Nonmetals		
		Element Group	1					2					3	3		3		4		5		6			7	8	9	10	11		12		13					14			15	13	14				15	16		
Unit		Depth (m)	Li	Na	K	Rb	Cs	Be	Mg	Ca	Sr	Ba	REE	Th	U	Sc	Y	Ti	Zr	Hf	V	Nb	Ta	Cr	Mo	W	Mn	Fe	Co	Ni	Cu	Ag	Zn	Cd	Al	Ga	Tl	Sn	Pb	Bi	B	Si	Ge	As	Sb	P	S	Se
Lower Evergreen Formation		2235.81-2235.94	0.2	166	146	0.5	0.06	<DL	9.0	64	6.4	8.0	0.003	<DL	<DL	0.003	< 0.0001	0.002	<DL	<DL	0.003	<DL	<DL	<DL	0.08	<DL	0.2	<DL	1.5	1.5	0.03	<DL	2.4	0.001	<DL	0.0005	0.02	<DL	0.005	<DL	<DL	17	0.003	0.01	0.004	<DL	47	0.03
		2242.25	0.4	274	482	1.5	0.2	<DL	13	107	11	13	0.005	<DL	<DL	0.004	0.0001	0.003	<DL	<DL	0.004	<DL	<DL	<DL	0.1	<DL	0.1	<DL	0.4	0.4	0.03	<DL	0.5	<DL	<DL	0.0005	0.04	<DL	0.003	0.03	0.008	<DL	119	0.02
		2242.44-2242.54	0.5	363	194	2.1	0.3	<DL	15	106	11	8.6	0.003	<DL	<DL	0.007	0.0001	<DL	<DL	<DL	0.01	<DL	<DL	0.0002	0.3	0.2	<DL	<DL	0.4	1.3	0.006	<DL	0.02	<DL	<DL	0.001	0.04	<DL	0.004	<DL	0.1	49	0.003	0.05	0.02	<DL	31	0.01
Upper Precipice Sandstone		2246.14-2246.25	0.08	105	242	0.2	0.02	<DL	14	34	2.6	4.1	0.002	<DL	<DL	0.001	< 0.0001	<DL	<DL	<DL	0.0004	<DL	<DL	< 0.0001	0.008	0.01	0.7	<DL	0.5	0.8	0.07	<DL	3.5	0.003	<DL	0.0003	0.03	<DL	0.04	<DL	<DL	8.4	0.0005	0.006	0.006	<DL	67	0.006
		2254.94-2255.10	0.2	148	206	0.4	0.04	0.001	13	47	4.3	5.8	0.002	<DL	<DL	0.002	0.0001	<DL	<DL	<DL	0.002	<DL	<DL	<DL	0.02	<DL	0.8	<DL	1.5	0.7	0.003	<DL	2.5	0.003	<DL	0.0005	0.05	<DL	0.004	<DL	<DL	15	0.0009	0.006	0.007	<DL	61	0.006
Lower Precipice Sandstone D		2263.61-2263.77	0.03	39	176	0.2	0.02	<DL	4.3	11	0.7	2.3	0.001	<DL	<DL	0.0008	0.0001	0.003	<DL	<DL	0.0003	<DL	<DL	<DL	0.005	<DL	0.9	<DL	1.2	1.9	0.8	<DL	3.0	0.002	<DL	0.0005	0.02	<DL	0.06	<DL	<DL	5.1	0.0004	0.01	0.005	<DL	44	0.002
		2267.71-2267.84	0.2	208	268	0.6	0.1	<DL	10	76	6.4	7.8	0.002	<DL	< 0.0001	<DL	<DL	<DL	<DL	0.0002	0.005	<DL	<DL	<DL	0.2	<DL	<DL	<DL	1.7	2.8	<DL	<DL	0.6	<DL	<DL	<DL	0.02	<DL	0.001	<DL	<DL	27	<DL	0.02	0.01	<DL	19	0.02
		2267.84-2267.90	0.6	466	347	1.8	0.3	<DL	18	122	12	11	0.003	0.0002	< 0.0001	<DL	0.0001	<DL	0.0004	0.001	0.01	0.003	<DL	<DL	0.4	<DL	<DL	<DL	2.3	3.9	<DL	<DL	<DL	<DL	<DL	<DL	0.02	<DL	<DL	<DL	<DL	64	<DL	0.02	0.02	<DL	28	0.02
Lower Precipice Sandstone C		2274.10-2274.18	0.03	26	136	0.1	0.02	0.002	4.0	11	0.5	2.0	0.0008	<DL	<DL	0.0008	< 0.0001	0.003	<DL	<DL	<DL	<DL	<DL	<DL	0.002	0.001	2.9	<DL	1.0	1.7	0.8	<DL	2.7	0.002	<DL	0.0004	0.01	<DL	0.02	<DL	<DL	5.0	0.0005	0.01	0.01	<DL	42	0.001
		2281.82-2281.92	0.1	114	124	0.6	0.1	0.002	6.9	48	4.1	6.0	0.002	<DL	<DL	0.002	< 0.0001	<DL	<DL	<DL	0.004	<DL	<DL	0.0008	0.1	0.006	<DL	<DL	2.0	2.3	0.05	<DL	2.8	0.006	<DL	0.0005	0.02	<DL	0.01	<DL	<DL	15	0.001	0.02	0.02	<DL	46	0.02
		2284.13-2284.24	0.06	39	153	0.1	0.02	0.0008	1.5	10	0.6	2.5	0.001	<DL	<DL	0.001	< 0.0001	<DL	<DL	<DL	0.004	<DL	<DL	< 0.0001	0.04	<DL	<DL	<DL	0.8	0.8	0.1	<DL	2.1	0.004	<DL	0.0006	0.01	<DL	0.1	<DL	<DL	8.1	0.0006	0.04	0.02	<DL	10	0.004
		2285.05	0.5	250	293	1.9	0.3	0.003	14	84	7.7	8.5	0.003	<DL	<DL	0.003	0.0001	0.002	0.001	<DL	0.006	<DL	<DL	0.0004	0.3	<DL	0.08	<DL	1.7	2.6	0.006	<DL	0.4	<DL	<DL	0.0002	0.03	<DL	0.002	<DL	0.1	24	0.002	0.02	0.02	<DL	108	0.03
		2288.49-2288.61	0.04	22	152	0.1	0.02	<DL	1.0	9.7	0.4	1.5	0.0006	<DL	<DL	0.0008	<DL	<DL	<DL	<DL	0.003	<DL	<DL	<DL	0.01	<DL	<DL	<DL	0.2	0.6	0.4	<DL	0.6	<DL	<DL	0.0006	0.003	<DL	0.08	<DL	<DL	6.3	0.0004	0.01	0.008	<DL	7.0	0.003
		2294	0.04	150	1,389	0.3	0.005	0.001	4.7	48	1.9	1.7	0.07	0.01	0.005	0.003	0.004	2.6	0.02	<DL	0.05	0.02	0.004	0.02	0.09	0.009	<DL	0.09	0.2	0.4	0.05	<DL	0.5	<DL	<DL	0.003	0.005	0.007	0.12	<DL	<DL	6.3	0.001	0.05	0.01	<DL	38	0.007
		2296.97-2297.13	<DL	<DL	44	0.0004	<DL	<DL	<DL	<DL	<DL	<DL	0.002	0.0004	< 0.0001	<DL	<DL	<DL	0.0004	0.0002	<DL	<DL	<DL	<DL	<DL	<DL	<DL	<DL	<DL	<DL	<DL	<DL	<DL	<DL	<DL	<DL	<DL	<DL	<DL	<DL	<DL	3.2	<DL	<DL	<DL	<DL	<DL	<DL
Lower Precipice Sandstone B		2297.13-2297.19	0.02	<DL	302	0.2	0.02	0.0009	3.1	25	1.5	3.9	0.02	0.002	0.003	<DL	0.001	0.05	0.004	0.0005	0.02	<DL	<DL	<DL	0.1	<DL	<DL	<DL	0.2	0.2	<DL	<DL	0.07	<DL	4.8	0.003	0.003	<DL	0.002	<DL	<DL	24	0.0005	0.01	0.01	<DL	<DL	0.02
		2298.92	0.06	89	1,004	0.2	0.008	0.001	2.7	31	1.2	1.3	0.03	0.002	0.001	0.002	0.001	0.1	0.007	<DL	0.02	<DL	<DL	0.006	0.04	0.03	0.1	<DL	0.05	0.1	0.04	<DL	0.8	<DL	<DL	0.002	0.003	0.0006	0.06	<DL	<DL	9.2	0.0004	0.02	0.006	<DL	17	0.004
Lower Precipice Sandstone A	2	2307.2	0.1	120	1,515	0.3	0.01	0.0008	6.6	68	2.0	3.7	0.03	0.002	0.0007	0.003	0.002	0.2	0.008	<DL	0.01	0.002	<DL	0.005	0.05	0.003	0.7	0.2	0.05	0.1	0.2	<DL	0.4	<DL	<DL	0.002	0.004	0.002	0.02	<DL	0.1	20	0.0006	0.01	0.005	<DL	22	0.003
		2315.77	0.03	104	1,095	0.2	0.004	<DL	3.9	67	1.7	1.2	0.02	0.002	0.0009	0.002	0.001	0.2	0.008	<DL	0.01	0.002	<DL	0.009	0.06	0.005	0.5	0.2	0.03	0.09	0.03	<DL	0.2	<DL	<DL	0.001	0.003	0.0009	0.01	<DL	<DL	7.2	0.0004	0.03	0.006	<DL	22	0.001
		2322.61-2322.73	0.03	76	393	0.1	0.01	<DL	3.4	27	0.9	3.2	0.07	0.009	0.002	0.004	0.004	0.9	0.03	<DL	0.03	0.007	0.002	0.02	0.05	0.007	0.3	0.2	0.2	0.1	1.8	<DL	0.4	<DL	<DL	0.004	0.001	0.02	0.05	<DL	<DL	16	0.001	0.02	0.005	<DL	10	0.004
		2323.25	0.03	110	1,253	0.2	0.005	<DL	3.9	71	1.6	1.7	0.02	0.001	0.001	0.002	0.002	0.2	0.007	<DL	0.01	0.001	<DL	0.008	0.05	0.001	0.6	0.1	0.02	0.06	0.04	<DL	0.3	<DL	<DL	0.001	0.002	0.0009	0.01	<DL	<DL	9.0	0.0004	0.01	0.003	<DL	15	0.001
	1	2328.54-2328.59	0.4	298	250	2.2	0.3	0.001	23	100	8.2	10	0.003	<DL	< 0.0001	0.007	< 0.0001	<DL	<DL	<DL	0.02	<DL	<DL	<DL	0.07	<DL	<DL	<DL	0.1	0.4	0.04	<DL	<DL	<DL	<DL	0.001	0.02	<DL	0.0007	<DL	0.1	48	0.002	0.04	0.06	<DL	23	0.007
		2328.59-2328.68	0.08	42	171	0.2	0.04	0.0009	2.4	13	0.8	3.5	0.001	<DL	0.0001	0.001	<DL	<DL	<DL	<DL	0.009	<DL	<DL	0.0009	0.02	0.2	<DL	<DL	0.2	0.3	0.06	<DL	0.7	0.002	<DL	0.0007	0.004	<DL	0.02	<DL	<DL	9.2	0.001	0.004	0.007	<DL	8.9	0.009
		2330.41-2330.54	0.02	29	112	0.06	0.007	<DL	1.2	16	0.4	2.6	0.02	0.002	0.0006	0.002	0.001	0.1	0.01	<DL	0.02	<DL	<DL	0.004	0.01	<DL	0.09	<DL	0.2	0.1	4.4	<DL	0.2	<DL	<DL	0.002	0.001	0.007	0.04	<DL	<DL	7.4	0.0005	0.02	0.004	<DL	5.4	0.004
		2338.75-2338.85	0.04	53	189	0.1	0.02	0.0008	1.8	7.8	0.4	2.4	0.001	<DL	< 0.0001	0.001	< 0.0001	<DL	<DL	<DL	0.006	<DL	<DL	0.0002	0.02	<DL	<DL	<DL	0.1	0.09	1.0	<DL	2.0	0.001	<DL	0.0006	0.004	<DL	0.009	<DL	<DL	6.3	0.001	0.005	0.007	<DL	8.5	0.006
Moolayember Formation		2339.00-2339.17	0.4	167	137	1.0	0.1	0.002	19	66	5.8	8.5	0.004	<DL	< 0.0001	0.003	0.0002	0.004	<DL	<DL	0.002	<DL	<DL	<DL	0.03	<DL	0.1	<DL	4.6	4.1	0.07	<DL	9.1	0.01	<DL	0.0004	0.04	<DL	0.05	<DL	<DL	20	0.001	0.02	0.02	<DL	192	0.05
		2340.54-2340.62	0.4	381	312	2.4	0.3	<DL	24	94	8.4	8.3	0.003	<DL	<DL	0.006	< 0.0001	<DL	<DL	<DL	0.008	<DL	<DL	<DL	0.03	<DL	0.1	<DL	0.02	0.06	0.0006	<DL	0.03	<DL	<DL	0.0009	0.008	<DL	0.0007	<DL	0.1	40	0.004	0.08	0.01	<DL	24	0.02
		2346.40-2346.51	0.4	280	262	1.3	0.2	<DL	24	75	11	10	0.004	<DL	<DL	0.004	0.0002	0.005	<DL	<DL	0.003	<DL	<DL	<DL	0.8	<DL	0.2	<DL	0.7	0.5	0.003	<DL	0.2	<DL	<DL	0.0004	0.02	<DL	0.002	<DL	0.2	26	0.001	0.03	0.04	<DL	62	0.02
		2348.16-2348.30	0.2	104	175	0.7	0.1	<DL	117	259	8.9	6.7	0.002	<DL	< 0.0001	0.003	0.0001	0.01	<DL	<DL	0.0003	<DL	<DL	<DL	0.3	0.003	3.8	<DL	0.6	0.6	0.002	<DL	0.07	<DL	0.4	0.0004	0.02	<DL	0.003	<DL	0.09	10	0.0002	0.004	0.03	<DL	350	0.007
		2356.94-2357.06	0.3	228	264	1.0	0.2	<DL	30	78	10	9.2	0.003	<DL	<DL	0.003	0.0002	<DL	<DL	<DL	0.002	<DL	<DL	<DL	0.04	0.009	0.4	<DL	0.03	0.04	0.001	<DL	0.05	<DL	<DL	0.0004	0.004	<DL	0.001	<DL	0.2	20	0.0005	0.004	0.006	<DL	13	0.01
		2362.90-2363.00	0.8	453	464	2.4	0.5	<DL	22	85	14	11	0.004	<DL	< 0.0001	0.005	0.0002	0.007	0.002	<DL	0.009	<DL	<DL	<DL	0.1	0.08	<DL	<DL	0.02	0.03	0.003	<DL	0.02	<DL	<DL	0.001	0.01	<DL	0.003	<DL	0.3	36	0.0008	0.02	0.03	<DL	18	0.04
		2366.50-2366.61	0.6	333	363	1.8	0.3	0.0009	28	87	13	11	0.004	<DL	< 0.0001	0.005	0.0002	<DL	0.001	<DL	0.003	<DL	<DL	<DL	0.09	0.002	0.3	<DL	0.02	0.03	0.0006	<DL	0.01	<DL	<DL	0.001	0.008	<DL	<DL	<DL	0.2	31	0.0008	0.008	0.01	<DL	16	0.03
		2373.89-2373.99	0.2	167	358	0.8	0.1	<DL	61	222	8.7	8.3	0.003	<DL	< 0.0001	0.003	0.0001	0.004	0.001	<DL	0.002	<DL	<DL	<DL	0.05	0.03	0.8	<DL	0.02	0.03	0.002	<DL	0.002	<DL	<DL	0.002	0.006	<DL	0.0009	<DL	0.1	13	0.0002	0.005	0.01	<DL	23	0.01
		2427.52-2427.74	0.07	123	460	0.4	0.07	<DL	14	1,038	11	7.5	0.005	<DL	0.0009	0.006	0.003	0.007	0.003	0.002	0.007	<DL	<DL	0.0003	0.07	0.1	10	<DL	0.2	0.06	0.009	<DL	0.004	<DL	<DL	0.002	0.02	<DL	0.001	<DL	0.09	12	0.0003	0.3	0.04	2.2	76	0.01
Unit Medians	Upper Precipice Sandstone	WM1	0.1	127	224	0.3	0.03	0.001	13	40	3.4	5.0	0.002	<DL	<DL	0.002	0.0001	<DL	<DL	<DL	0.001	<DL	<DL	<DL	0.02	0.01	0.8	<DL	1.0	0.8	0.04	<DL	3.0	0.003	<DL	0.0004	0.04	<DL	0.02	<DL	<DL	12	0.001	0.01	0.01	<DL	64	0.01
		C4, T153, WCG4, WW1	0.3	16	21	0.2	0.1	0.09	93	343	11	20	3	0.2	0.06	0.4	0.3	0.4	0.05	0.001	0.8	<DL	<DL	0.4	0.01	<DL	12	375	1	1	1	<DL	14	0.007	370	0.1	0.01	<DL	6	0.04	<DL	131	0.04	0.7	0.02	<DL	<DL	0.1
	Lower Precipice Sandstone	WM1	0.04	83	259	0.2	0.02	0.001	3.9	29	1.3	2.5	0.003	0.0001	<DL	0.002	0.0001	0.003	0.0004	<DL	0.01	<DL	<DL	0.0003	0.05	<DL	<DL	<DL	0.2	0.3	0.05	<DL	0.5	<DL	<DL	0.001	0.004	<DL	0.02	<DL	<DL	9.1	0.001	0.02	0.01	<DL	18	0.004
		C4, T153, WCG4, WW1	<DL	4	10	0.03	0.006	0.01	3	8	0.4	3	0.5	0.07	0.03	0.04	0.06	0.6	0.03	<DL	0.2	<DL	<DL	0.2	0.02	0.01	0.5	54	0.9	0.9	6	<DL	3	<DL	278	0.03	0.001	0.03	2	0.01	<DL	96	0.007	0.5	0.02	<DL	<DL	<DL
	Moolayember Formation	WM1	0.4	228	312	1.0	0.2	<DL	24	87	10	8.5	0.004	<DL	<DL	0.004	0.0002	0.004	<DL	<DL	0.003	<DL	<DL	<DL	0.07	0.003	0.3	<DL	0.03	0.06	0.002	<DL	0.03	<DL	<DL	0.001	0.01	<DL	0.001	<DL	0.1	20	0.001	0.02	0.02	<DL	24	0.02
		WCG4, WW1	0.2	0.7	2	0.3	0.1	0.05	10	234	1	1	2	0.2	0.03	0.6	0.7	0.2	0.03	<DL	1	<DL	<DL	0.3	0.02	<DL	9	75	2	4	6	<DL	7	<DL	221	0.02	0.008	<DL	5	0.08	<DL	4	0.05	0.5	0.05	<DL	1	0.06

Legend	Major	Minor	Trace	Ultra-Trace	1,000 - 100,00	100 - 1,000	10 - 100	< 10

Table A4: Elements extracted by pH 7 water (percentage of total amount in rock powder).

		Element Set	Alkali metals					Alkaline earth metals					Lanthanoids	Actinoids		Transition metals																						Post transition metals						Metalloids					Nonmetals		
		Element Group	1					2					3	3		3		4			5			6			7	8	9	10	11		12			13					14		15		13	14		15		15	16	
Unit		Depth (m)	Li	Na	K	Rb	Cs	Be	Mg	Ca	Sr	Ba	REE	Th	U	Sc	Y	Ti	Zr	Hf	V	Nb	Ta	Cr	Mo	W	Mn	Fe	Co	Ni	Cu	Ag	Zn	Cd	Al	Ga	Tl	Sn	Pb	Bi	B	Si	Ge	As	Sb	P	S	Se
Lower Evergreen Formation		2235.81-2235.94	0.8	27.2	1.4	0.9	2.5	<DL	0.9	29.0	16.3	3.9	0.0	<DL	<DL	0.0	0.0	0.0	<DL	<DL	0.0	<DL	<DL	<DL	9.4	<DL	0.6	<DL	10.5	5.7	0.1	<DL	3.5	0.2	<DL	0.0	7.8	<DL	0.0	<DL	<DL	0.0	0.2	0.4	1.0	<DL	34.4	4.8
		2242.25	0.9	27.2	1.9	1.0	1.3	<DL	0.6	27.5	13.1	3.1	0.0	<DL	<DL	0.0	0.0	0.0	<DL	<DL	0.0	<DL	<DL	<DL	7.1	<DL	0.4	<DL	3.2	2.0	0.1	<DL	0.5	<DL	<DL	0.0	4.6	<DL	0.0	<DL	0.1	0.0	0.1	0.3	1.0	<DL	18.3	1.2
		2242.44-2242.54	0.5	28.9	0.9	1.5	1.5	<DL	0.5	25.8	13.7	2.2	0.0	<DL	<DL	0.0	0.0	<DL	<DL	<DL	0.0	<DL	<DL	0.0	10.9	2.8	<DL	<DL	1.2	2.1	0.0	<DL	0.0	<DL	<DL	0.0	4.4	<DL	0.0	<DL	0.2	0.0	0.1	0.8	2.9	<DL	6.0	1.3
Upper Precipice Sandstone		2246.14-2246.25	0.5	17.1	2.3	0.5	1.5	<DL	3.8	20.7	8.4	2.0	0.0	<DL	<DL	0.0	0.0	<DL	<DL	<DL	0.0	<DL	<DL	0.0	1.6	1.4	3.2	<DL	10.9	11.2	1.5	<DL	11.7	1.8	<DL	0.0	10.6	<DL	0.3	<DL	<DL	0.0	0.1	0.2	1.6	<DL	20.8	3.0
		2254.94-2255.10	1.2	17.5	0.8	0.5	3.8	0.1	1.2	6.4	6.8	1.3	0.0	<DL	<DL	0.0	0.0	<DL	<DL	<DL	0.0	<DL	<DL	<DL	7.5	<DL	0.5	<DL	13.3	8.8	0.0	<DL	3.4	0.8	<DL	0.0	8.2	<DL	0.0	<DL	<DL	0.0	0.1	0.1	2.2	<DL	15.1	0.8
Lower Precipice Sandstone D		2263.61-2263.77	0.4	5.8	1.2	0.3	1.3	<DL	1.9	12.3	3.4	1.4	0.0	<DL	<DL	0.0	0.0	0.0	<DL	<DL	0.0	<DL	<DL	<DL	1.9	<DL	7.0	<DL	25.1	34.1	10.5	<DL	20.7	1.1	<DL	0.0	5.8	<DL	0.6	<DL	<DL	0.0	0.2	0.3	1.2	<DL	23.7	1.6
		2267.71-2267.84	0.7	47.9	1.8	1.6	1.4	<DL	1.3	30.2	15.7	2.9	0.0	0.0	0.0	<DL	0.0	<DL	0.0	0.0	0.0	0.0	<DL	<DL	14.1	<DL	<DL	<DL	5.8	4.9	<DL	<DL	<DL	<DL	<DL	<DL	3.4	<DL	<DL	0.3	<DL	0.0	<DL	0.3	2.2	<DL	5.5	2.5
		2267.84-2267.90	0.6	23.8	1.4	0.7	1.6	<DL	1.3	28.4	9.4	2.5	0.0	<DL	0.0	<DL	<DL	<DL	<DL	0.0	0.0	<DL	0.0	<DL	19.0	<DL	<DL	<DL	14.4	12.1	<DL	<DL	0.8	<DL	<DL	<DL	2.8	<DL	0.0	<DL	<DL	0.0	<DL	0.5	1.9	<DL	6.8	4.6
Lower Precipice Sandstone C		2274.10-2274.18	0.4	5.6	1.1	0.3	1.1	0.3	2.1	8.6	1.8	1.3	0.0	<DL	<DL	0.1	0.0	0.0	<DL	<DL	<DL	<DL	<DL	<DL	0.4	0.2	3.6	<DL	22.6	21.3	9.3	<DL	13.9	1.9	<DL	0.0	3.0	<DL	0.2	<DL	<DL	0.0	0.1	0.2	2.3	<DL	3.4	0.9
		2281.82-2281.92	0.6	17.8	0.8	0.8	2.1	0.1	1.0	31.1	7.9	2.6	0.0	<DL	<DL	0.0	0.0	<DL	<DL	<DL	0.0	<DL	<DL	0.0	13.0	0.2	<DL	<DL	16.3	11.3	0.3	<DL	5.1	1.0	<DL	0.0	4.0	<DL	0.1	<DL	<DL	0.0	0.1	0.5	2.6	<DL	14.0	3.3
		2284.13-2284.24	0.7	30.3	6.9	1.4	3.3	0.2	0.9	20.9	2.9	5.6	0.0	<DL	<DL	0.1	0.0	<DL	<DL	<DL	0.0	<DL	<DL	0.0	13.9	<DL	<DL	<DL	11.0	7.2	0.6	<DL	10	4.8	<DL	0.0	9.8	<DL	1.5	<DL	<DL	0.0	0.2	1.5	4.6	<DL	11.3	2.7
		2285.05	0.9	15.3	1.4	1.5	1.8	0.0	0.7	24.3	9.9	2.6	0.0	<DL	<DL	0.0	0.0	0.0	0.0	<DL	0.0	<DL	<DL	0.0	12.1	<DL	0.4	<DL	6.4	5.5	0.0	<DL	0.3	<DL	<DL	0.0	4.3	<DL	0.0	<DL	0.2	0.0	0.1	0.3	1.7	<DL	13.4	2.4
		2288.49-2288.61	0.5	25.1	7.7	0.9	2.1	<DL	0.4	15.9	2.9	4.1	0.0	<DL	<DL	0.0	<DL	<DL	<DL	<DL	0.0	<DL	<DL	<DL	10.2	<DL	<DL	<DL	11.0	8.8	5.7	<DL	7.3	<DL	<DL	0.0	3.6	<DL	1.1	<DL	<DL	0.0	0.2	1.7	4.0	<DL	8.9	2.6
		2294	1.2	39.5	43.8	6.1	2.1	0.5	4.4	40.1	7.7	3.7	0.1	0.1	0.3	0.1	0.0	0.1	0.0	<DL	0.4	0.1	2.8	0.2	29.3	0.3	<DL	0.0	12.3	6.7	2.0	<DL	5.9	<DL	<DL	0.1	8.2	0.3	1.3	<DL	<DL	0.0	0.2	3.7	6.2	<DL	22.5	1.4
		2296.97-2297.13	0.5	<DL	18.1	2.5	4.4	0.2	2.0	14.5	2.6	5.9	0.0	0.0	0.1	<DL	0.0	0.0	0.0	0.0	0.2	<DL	<DL	<DL	25.3	<DL	<DL	<DL	8.9	7.7	<DL	<DL	0.5	<DL	0.0	0.0	4.3	<DL	0.0	<DL	<DL	0.0	0.0	0.6	2.3	<DL	<DL	1.8
Lower Precipice Sandstone B		2297.13-2297.19	<DL	<DL	0.2	0.0	<DL	<DL	<DL	<DL	<DL	<DL	0.0	0.0	0.0	<DL	<DL	<DL	0.0	0.0	<DL	<DL	<DL	<DL	<DL	<DL	<DL	<DL	<DL	<DL	<DL	<DL	<DL	<DL	<DL	<DL	<DL	<DL	<DL	<DL	<DL	0.0	<DL	<DL	<DL	<DL	<DL	<DL
		2298.92	0.8	17.8	33.2	2.3	1.7	0.3	2.0	32.6	6.4	2.5	0.1	0.1	0.2	0.1	0.0	0.0	0.0	<DL	0.2	<DL	<DL	0.0	10.1	3.7	3.3	<DL	5.2	2.9	1.0	<DL	6.3	<DL	<DL	0.0	5.5	0.0	0.9	<DL	<DL	0.0	0.1	2.9	3.9	<DL	18.3	2.0
Lower Precipice Sandstone A	2	2307.2	3.3	36.4	51.7	7.8	4.9	0.5	6.1	47.4	18.6	8.3	0.1	0.1	0.1	0.4	0.1	0.0	0.0	<DL	0.2	0.1	<DL	0.1	21.3	0.4	2.4	0.0	5.0	3.4	0.7	<DL	3.6	<DL	<DL	0.1	14.5	0.2	0.4	<DL	1.4	0.0	0.2	2.0	3.3	<DL	31.8	1.6
		2315.77	1.0	32.9	47.9	10.8	2.4	<DL	2.3	42.5	16.0	2.6	0.1	0.2	0.3	0.5	0.1	0.1	0.0	<DL	0.5	0.1	<DL	0.4	56.8	1.5	7.5	0.0	5.7	4.0	2.1	<DL	4.4	<DL	<DL	0.1	18.5	0.3	0.3	<DL	<DL	0.0	0.3	5.5	5.7	<DL	23.7	2.0
		2322.61-2322.73	0.9	57.9	32.7	3.7	3.6	<DL	4.8	32.8	7.5	6.2	0.2	0.3	0.3	0.4	0.1	0.1	0.0	<DL	0.6	0.2	0.3	0.2	38.3	0.8	3.3	0.0	38.7	9.4	14.7	<DL	18.2	<DL	<DL	0.2	3.0	0.7	1.3	<DL	<DL	0.0	0.3	5.4	4.0	<DL	34.3	3.4
		2323.25	1.1	20.5	59.9	9.3	2.7	<DL	6.4	47.0	16.8	3.9	0.1	0.1	0.4	0.4	0.1	0.1	0.0	<DL	0.4	0.1	<DL	0.3	28.5	0.2	6.0	0.0	4.6	2.5	3.2	<DL	4.4	<DL	<DL	0.1	12.7	0.0	0.4	<DL	<DL	0.0	0.2	3.4	3.1	<DL	30.7	1.9
	1	2328.54-2328.59	0.5	32.0	1.4	1.6	1.5	0.0	1.1	31.9	6.5	2.6	0.0	<DL	0.0	0.0	0.0	<DL	<DL	<DL	0.0	<DL	<DL	<DL	8.4	<DL	<DL	<DL	0.6	1.0	0.1	<DL	<DL	<DL	<DL	0.0	3.4	<DL	0.0	<DL	0.2	0.0	0.1	0.9	8.2	<DL	6.2	0.8
		2328.59-2328.68	0.7	18.7	4.9	1.2	2.2	0.1	0.9	23.6	3.0	3.6	0.0	<DL	0.0	0.0	<DL	<DL	<DL	<DL	0.0	<DL	<DL	0.0	13.1	6.2	<DL	<DL	7.9	6.3	1.3	<DL	4.3	0.5	<DL	0.0	3.8	<DL	0.2	<DL	<DL	0.0	0.3	0.5	4.1	<DL	15.4	3.7
		2330.41-2330.54	0.6	4.5	11.7	1.6	2.4	<DL	2.2	32.0	4.2	3.9	0.1	0.1	0.1	0.2	0.0	0.0	0.0	<DL	0.4	<DL	<DL	0.1	21.6	<DL	3.4	<DL	19.9	7.6	20.0	<DL	6.9	<DL	<DL	0.1	3.9	0.2	0.8	<DL	<DL	0.0	0.3	4.7	3.1	<DL	11.6	6.4
		2338.75-2338.85	0.8	31.8	12.4	2.1	3.3	0.2	1.5	17.6	2.6	4.9	0.0	<DL	0.0	0.1	0.0	<DL	<DL	0.1	<DL	<DL	<DL	0.0	15.7	<DL	<DL	<DL	10.2	3.0	8.9	<DL	24.5	1.1	<DL	0.0	6.0	<DL	0.2	<DL	<DL	0.0	0.2	0.7	3.9	<DL	22.0	3.9
Moolayember Formation		2339.00-2339.17	0.9	38.2	1.5	2.1	6.3	0.1	1.9	39.4	8.9	7.5	0.0	<DL	0.0	0.0	0.0	0.0	<DL	<DL	0.0	<DL	<DL	<DL	4.0	<DL	0.9	<DL	29.8	22.3	0.5	<DL	5.0	2.0	<DL	0.0	10	<DL	0.2	<DL	<DL	0.0	0.1	0.2	1.7	<DL	36.8	8.6
		2340.54-2340.62	0.9	40.3	1.4	1.9	1.9	<DL	0.7	15.3	15.1	2.5	0.0	<DL	<DL	0.0	0.0	<DL	<DL	<DL	0.0	<DL	<DL	<DL	7.4	<DL	0.1	<DL	0.1	0.2	0.0	<DL	0.0	<DL	<DL	0.0	1.3	<DL	0.0	<DL	0.4	0.0	0.4	1.3	1.9	<DL	8.6	2.8
		2346.40-2346.51	1.1	17.1	0.8	0.9	3.6	<DL	0.6	6.8	15.0	1.7	0.0	<DL	<DL	0.0	0.0	0.0	<DL	<DL	0.0	<DL	<DL	<DL	30.0	<DL	0.1	<DL	3.1	2.3	0.0	<DL	0.2	<DL	<DL	0.0	2.2	<DL	0.0	<DL	0.8	0.0	0.1	0.4	2.3	<DL	22.2	3.1
		2348.16-2348.30	0.9	7.6	0.6	0.6	4.1	<DL	2.8	10.3	11.6	1.4	0.0	<DL	0.0	0.0	0.0	0.0	<DL	<DL	0.0	<DL	<DL	<DL	4.6	0.1	0.6	<DL	5.1	3.1	0.0	<DL	0.1	<DL	0.0	0.0	2.0	<DL	0.0	<DL	0.6	0.0	0.0	0.0	1.1	<DL	3.2	1.0
		2356.94-2357.06	1.1	13.0	0.9	0.7	4.3	<DL	0.6	4.5	14.0	1.6	0.0	<DL	<DL	0.0	0.0	<DL	<DL	<DL	0.0	<DL	<DL	<DL	10.9	0.4	0.1	<DL	0.5	0.4	0.0	<DL	0.1	<DL	<DL	0.0	0.6	<DL	0.0	<DL	0.9	0.0	0.0	0.2	0.9	<DL	12.2	2.0
		2362.90-2363.00	0.9	25.7	1.6	1.5	2.4	<DL	0.3	10.7	17.5	2.0	0.0	<DL	0.0	0.0	0.0	0.0	<DL	<DL	0.0	<DL	<DL	<DL	22.1	2.0	<DL	<DL	0.2	0.2	0.0	<DL	0.0	<DL	<DL	0.0	1.5	<DL	0.0	<DL	0.8	0.0	0.0	0.7	2.7	<DL	14.3	3.0
		2366.50-2366.61	1.1	6.9	1.3	1.2	3.5	0.0	0.3	3.1	16.6	2.1	0.0	<DL	0.0	0.0	0.0	<DL	0.0	<DL	0.0	<DL	<DL	<DL	16.2	0.1	0.0	<DL	0.2	0.2	0.0	<DL	0.0	<DL	<DL	0.0	1.1	<DL	<DL	<DL	1.1	0.0	0.0	0.3	1.1	<DL	9.2	3.2
		2373.89-2373.99	0.8	2.1	1.1	0.6	3.2	<DL	1.2	8.3	13.8	1.5	0.0	<DL	0.0	0.0	0.0	0.0	0.0	<DL	0.0	<DL	<DL	<DL	15.5	1.4	0.3	<DL	0.3	0.3	0.0	<DL	0.0	<DL	<DL	0.0	0.9	<DL	0.0	<DL	0.7	0.0	0.0	0.1	1.2	<DL	23.6	1.9
		2427.52-2427.74	0.5	2.2	2.0	0.4	2.6	<DL	0.6	3.2	6.5	1.6	0.0	<DL	0.1	0.1	0.0	0.0	0.0	0.1	0.0	<DL	<DL	0.0	17.5	6.9	1.4	<DL	1.1	0.5	0.2	<DL	0.0	<DL	<DL	0.0	3.7	<DL	0.0	<DL	0.7	0.0	0.0	2.7	3.8	1.5	31.2	1.6
Unit Medians	Upper Precipice Sandstone	WM1	0.9	17.3	1.6	0.5	2.6	0.1	2.5	13.5	7.6	1.7	0.0	<DL	<DL	0.0	0.0	<DL	<DL	<DL	0.0	<DL	<DL	0.0	4.5	0.7	1.8	<DL	12.1	10	0.7	<DL	7.6	1.3	<DL	0.0	9.4	<DL	0.2	<DL	<DL	0.0	0.1	0.1	1.9	<DL	17.9	1.9
		C4, T153, WCG4, WW1	<DL	17	1	2	4	<DL	2	6	4	1	0.0	<DL	<DL	<DL	<DL	<DL	<DL	<DL	0.0	<DL	<DL	<DL	6	<DL	0.2	<DL	0.1	0.2	<DL	<DL	<DL	0.1	0.0	0.0	4	<DL	0.0	<DL	0.1	0.0	<DL	0.2	2	0.8	19	<DL
	Lower Precipice Sandstone	WM1	0.7	22.1	7.3	1.6	2.1	0.0	1.7	29.3	6.5	3.2	0.0	0.0	0.0	0.1	0.0	0.0	0.0	<DL	0.0	<DL	<DL	0.0	14.0	<DL	<DL	<DL	9.6	6.5	1.1	<DL	4.8	<DL	<DL	0.0	4.1	<DL	0.3	<DL	<DL	0.0	0.2	0.8	3.2	<DL	13.7	2.2
		C4, T153, WCG4, WW1	<DL	18	14	8	6	<DL	4	7	6	2	0.0	<DL	<DL	<DL	<DL	<DL	<DL	<DL	0.1	<DL	<DL	<DL	9	<DL	0.4	<DL	3	2	<DL	<DL	0.1	0.1	0.0	0.0	14	<DL	0.0	<DL	<DL	0.0	<DL	<DL	3	2	38	<DL
	Moolayember Formation	WM1	0.9	13.0	1.3	0.9	3.5	<DL	0.6	8.3	14.0	1.7	0.0	<DL	0.0	0.0	0.0	0.0	<DL	<DL	0.0	<DL	<DL	<DL	15.5	0.1	0.1	<DL	0.5	0.4	0.0	<DL	0.0	<DL	<DL	0.0	1.5	<DL	0.0	<DL	0.7	0.0	0.0	0.3	1.7	<DL	14.3	2.8
		WCG4, WW1	0.3	23	2	1	3	<DL	2	10	15	2	0.0	<DL	<DL	<DL	0.0	<DL	<DL	<DL	0.0	<DL	<DL	<DL	11	<DL	0.1	<DL	0.0	<DL	0.0	<DL	0.0	<DL	0.0	0.0	2	<DL	<DL	<DL	<DL	0.0	<DL	0.2	2	<DL	23	1

Legend	Major	Minor	Trace	Ultra-Trace	> 75	50 – 75	25 – 50	5 – 25	< 5

(0.0 indicates < 0.05 %).

Table A5: Elements extracted by pH 5 acid (mg element per kg rock powder).

		Element Set	Alkali metals					Alkaline earth metals					Lanthan-oids	Actinoids		Transition metals															Post transition metals						Metalloids					Nonmetals		
		Element Group	1					2					3	3		3		4		5		6		7	8	9	10	11	12		13			14		15	13	14		15		15	16	
Unit		Depth (m)	Li	Na	K	Rb	Cs	Be	Mg	Ca	Sr	Ba	REE	Th	U	Sc	Y	Ti	Zr	Hf	V	Nb	Ta	Cr	Mo	W	Mn	Fe	Co	Ni	Cu	Ag	Zn	Cd	Al	Ga	Tl	Sn	Pb	Bi	B	Si	Ge	As	Sb	P	S	Se
Lower Evergreen Formation		2235.81-2235.94	0.2	0.5	<DL	0.09	0.04	0.07	14	50	3.7	8.1	0.3	0.09	0.04	0.09	0.06	0.1	<DL	<DL	0.2	<DL	<DL	0.1	0.001	0.08	1.9	121	5.5	11	4.6	<DL	19	0.3	39	0.009	0.007	<DL	9.2	0.1	0.2	53	0.006	0.5	0.04	<DL	<DL	0.02
		2242.25	0.4	<DL	<DL	0.6	0.4	0.2	13	110	11	28	0.4	0.09	0.07	0.3	0.2	0.1	<DL	<DL	0.05	<DL	<DL	0.2	<DL	<DL	0.6	57	3.9	4.9	7.5	<DL	22	0.3	65	0.009	0.05	<DL	22	0.5	2.4	75	0.008	1.5	0.07	<DL	9	0.009
		2242.44-2242.54	1.2	10	<DL	1.4	0.9	0.2	25	156	17	41	0.6	0.09	0.04	0.2	0.1	0.3	<DL	<DL	0.1	<DL	<DL	0.4	0.06	<DL	<DL	56	14	27	5.6	<DL	14	0.3	253	0.02	0.07	<DL	12	0.5	1.0	257	0.01	1.0	0.07	3.3	38	0.03
Upper Precipice Sandstone		2246.14-2246.25	0.02	<DL	<DL	0.03	0.006	0.02	13	29	0.8	2.0	0.2	0.03	0.009	0.08	0.08	0.2	<DL	<DL	0.09	<DL	<DL	0.09	<DL	<DL	1.7	137	0.6	1.1	2.2	<DL	4.6	0.3	19	0.005	0.002	0.007	4.5	0.02	<DL	21	0.005	0.9	0.05	<DL	<DL	<DL
		2254.94-2255.10	0.1	<DL	<DL	0.08	0.02	0.1	22	51	2.7	5.8	0.7	0.07	0.02	0.4	0.3	0.1	<DL	<DL	0.3	<DL	<DL	0.2	0.002	<DL	5.6	329	3.2	2.3	0.8	<DL	15	0.3	34	0.01	0.01	0.001	5.8	0.04	2.2	34	0.014	1.0	0.04	0.9	<DL	0.003
Lower Precipice Sandstone D		2263.61-2263.77	0.02	<DL	<DL	0.03	0.005	0.02	1.6	18	0.2	0.8	0.2	0.06	0.009	0.02	0.06	0.1	<DL	<DL	0.02	<DL	<DL	0.02	<DL	<DL	<DL	29	0.7	1.0	3.6	<DL	1.4	0.004	13	0.006	0.001	0.09	3.0	0.01	<DL	34	0.003	0.8	0.03	28	17	<DL
		2267.71-2267.84	<DL	<DL	<DL	<DL	<DL	0.3	<DL	<DL	<DL	<DL	0.1	0.03	0.02	0.07	0.05	0.1	0.02	<DL	0.07	<DL	0.0006	0.07	<DL	<DL	<DL	11	2.2	5.2	1.5	<DL	7.4	0.08	48	0.005	<DL	0.008	6.9	0.1	1.0	<DL	0.001	0.9	<DL	<DL	<DL	<DL
		2267.84-2267.90	0.1	<DL	<DL	<DL	0.2	0.7	4.8	81	6.3	39	0.2	0.1	0.04	0.2	0.09	0.3	0.03	<DL	0.2	<DL	0.0003	0.2	0.05	<DL	0.7	47	15	30	3.3	<DL	7.0	0.08	329	0.01	<DL	0.004	14	0.4	1.1	156	0.004	0.6	<DL	<DL	<DL	0.01
Lower Precipice Sandstone C		2274.10-2274.18	0.02	<DL	<DL	0.03	0.006	0.03	1.4	6.8	0.2	0.9	0.2	0.02	0.009	0.004	0.06	0.2	<DL	<DL	0.03	<DL	<DL	0.03	<DL	0.06	1.5	58	0.7	1.0	4.7	<DL	1.8	0.004	11	0.007	0.001	0.09	2.6	0.08	0.4	27	0.003	1.1	0.07	12	47	<DL
		2281.82-2281.92	0.06	<DL	<DL	0.09	0.05	0.2	3.5	23	1.8	5.1	0.08	0.01	0.02	0.01	0.03	0.09	<DL	<DL	0.06	<DL	<DL	0.03	0.03	<DL	<DL	16	3.0	5.4	2.4	<DL	7.3	0.02	35	0.004	0.003	<DL	4.3	0.08	<DL	47	0.003	0.7	0.05	12	10	0.005
		2284.13-2284.24	0.03	0.06	<DL	0.02	0.005	0.04	0.9	3.2	0.2	1.0	0.05	<DL	0.008	<DL	0.01	0.08	<DL	<DL	0.03	<DL	<DL	0.02	0.05	<DL	<DL	7.6	1.3	2.9	1.8	<DL	2.7	0.006	17	0.003	<DL	0.02	4.8	0.03	<DL	35	0.002	1.2	0.04	8.2	<DL	<DL
		2285.05	0.5	<DL	<DL	0.8	0.5	0.8	12	88	8.8	23	0.2	0.04	0.05	0.1	0.07	0.2	<DL	<DL	0.07	<DL	<DL	0.2	0.05	<DL	<DL	31	9.3	17	4.0	<DL	19	0.3	88	0.008	0.03	<DL	18	0.3	0.5	89	0.005	1.1	0.1	<DL	10	0.02
		2288.49-2288.61	0.02	<DL	<DL	0.02	0.004	0.03	0.9	1.3	0.1	0.4	0.05	<DL	0.008	<DL	0.008	0.1	<DL	<DL	0.03	<DL	<DL	0.02	<DL	<DL	<DL	4.5	0.6	2.0	4.1	<DL	0.7	0.003	12	0.002	<DL	0.06	3.3	0.03	<DL	17	0.002	0.4	0.01	4.5	4	<DL
		2294	<DL	<DL	<DL	<DL	<DL	0.007	0.7	3.6	0.1	0.5	0.04	0.006	0.03	<DL	0.009	0.2	<DL	<DL	0.05	<DL	<DL	0.01	0.07	<DL	<DL	9.5	0.2	0.5	0.4	<DL	0.4	0.001	<DL	0.001	<DL	<DL	3.0	0.01	<DL	<DL	0.003	0.2	0.02	6.7	7	<DL
		2296.97-2297.13	0.2	<DL	<DL	<DL	0.5	0.7	<DL	<DL	1.3	14	0.3	0.09	0.06	0.2	0.07	0.3	0.03	<DL	0.2	<DL	0.0	0.3	<DL	<DL	0.3	51	6.2	7.4	6.7	<DL	9.0	0.09	241	0.02	<DL	0.004	10	0.2	1.1	72	0.004	3.3	0.1	<DL	<DL	0.009
Lower Precipice Sandstone B		2297.13-2297.19	<DL	<DL	<DL	<DL	<DL	0.03	<DL	<DL	<DL	<DL	0.4	0.04	0.05	0.03	0.1	0.5	0.02	<DL	0.1	< 0.0001	0.0	0.07	<DL	0.001	0.8	28	<DL	<DL	2.0	<DL	2.0	0.06	6.8	0.009	<DL	0.03	4.2	0.08	1.0	<DL	0.004	0.05	<DL	<DL	<DL	<DL
		2298.92	0.03	<DL	<DL	0.01	0.002	0.02	0.7	2.1	0.2	0.7	0.04	<DL	0.009	<DL	0.008	0.04	<DL	<DL	0.04	<DL	<DL	0.02	0.04	<DL	<DL	6.4	0.2	0.5	0.6	<DL	2.4	0.001	6.3	0.003	<DL	<DL	2.3	0.02	<DL	<DL	0.002	0.09	0.008	15	2	<DL
Lower Precipice Sandstone A	2	2307.2	0.03	<DL	<DL	0.02	0.003	0.01	5.6	12	0.4	2.9	0.2	0.01	0.01	0.003	0.04	0.3	<DL	<DL	0.07	<DL	<DL	0.07	0.01	<DL	2.8	99	0.2	0.5	3.0	<DL	2.5	0.004	29	0.007	<DL	0.03	1.6	0.02	<DL	42	0.004	0.1	0.01	20	<DL	<DL
		2315.77	0.02	<DL	<DL	<DL	<DL	<DL	2.1	7.1	0.2	0.7	0.06	<DL	0.003	<DL	0.01	0.1	<DL	<DL	0.02	<DL	<DL	0.03	<DL	<DL	<DL	28	0.2	0.3	0.3	<DL	0.9	0.006	<DL	0.0008	<DL	<DL	0.6	0.008	2.1	16	0.004	0.1	0.01	11	<DL	<DL
		2322.61-2322.73	0.02	<DL	<DL	0.01	0.002	0.008	2.0	3.8	0.1	1.5	0.09	0.008	0.01	<DL	0.02	0.2	<DL	<DL	0.04	<DL	<DL	0.03	<DL	<DL	1.3	48	0.1	0.2	8.0	<DL	0.3	0.002	4.3	0.003	<DL	0.29	1.2	0.01	<DL	14	0.003	0.06	0.005	14	3	<DL
		2323.25	0.02	<DL	<DL	<DL	<DL	<DL	1.5	8.2	0.2	1.1	0.06	<DL	0.004	<DL	0.01	0.1	<DL	<DL	0.02	<DL	<DL	0.03	<DL	<DL	0.6	27	0.07	0.2	0.4	<DL	1.5	0.005	1.7	0.002	<DL	<DL	0.6	<DL	<DL	8	0.002	0.05	0.004	1.7	5.7	<DL
	1	2328.54-2328.59	1.0	4.0	<DL	1.1	0.8	0.6	22	110	9.5	25	0.2	0.05	0.08	0.1	0.05	0.2	<DL	<DL	0.1	<DL	<DL	0.2	0.007	<DL	<DL	33	5.1	8.6	11	<DL	2.1	0.2	202	0.01	0.03	0.01	7.8	0.3	1.7	195	0.007	0.5	0.1	<DL	19	0.01
		2328.59-2328.68	0.06	<DL	<DL	0.03	0.01	0.05	1.8	9.7	0.2	1.6	0.04	0.006	0.03	0.001	0.01	0.1	<DL	<DL	0.07	<DL	<DL	0.09	<DL	<DL	<DL	6.7	0.4	0.9	2.0	<DL	2.8	0.3	26	0.004	<DL	0.01	4.3	0.03	1.1	30	0.002	0.1	0.01	3.7	<DL	0.0008
		2330.41-2330.54	0.01	<DL	<DL	0.006	0.002	0.008	0.9	5.2	0.07	0.9	0.04	<DL	0.008	<DL	0.008	0.2	<DL	<DL	0.03	<DL	<DL	0.01	<DL	0.02	<DL	3.1	0.2	0.3	13	<DL	0.1	0.002	3.0	0.002	<DL	0.68	1.2	0.009	<DL	17	0.002	0.07	0.005	5.3	<DL	<DL
		2338.75-2338.85	0.03	0.3	<DL	0.03	0.006	0.03	1.6	4.7	0.1	1.1	0.09	0.005	0.01	<DL	0.01	0.4	<DL	<DL	0.05	<DL	<DL	0.03	<DL	<DL	<DL	4.5	0.2	0.3	7.1	<DL	1.9	0.004	9.4	0.004	<DL	0.08	2.0	0.06	<DL	35	0.004	0.1	0.01	10	<DL	<DL
Moolayember Formation		2339.00-2339.17	0.2	<DL	<DL	0.2	0.09	0.4	11	49	4.1	12	0.1	0.04	0.04	0.1	0.06	0.09	<DL	<DL	0.06	<DL	<DL	0.1	0.005	<DL	<DL	47	4.8	5.4	4.0	<DL	36	0.3	96	0.01	0.01	<DL	14	0.1	<DL	95	0.003	3.3	0.1	<DL	12	0.01
		2340.54-2340.62	0.7	7.7	<DL	1.3	0.8	0.2	76	173	16	39	0.3	0.06	0.03	0.3	0.09	0.1	<DL	<DL	0.4	<DL	<DL	0.2	<DL	<DL	9.4	673	1.3	2.7	8.7	<DL	16	0.3	157	0.01	0.01	<DL	11	0.3	1.3	184	0.01	0.7	0.05	<DL	<DL	0.03
		2346.40-2346.51	0.4	7.1	<DL	0.4	0.3	0.2	178	124	14	30	0.5	0.09	0.03	0.3	0.1	0.08	<DL	<DL	0.8	<DL	<DL	0.4	0.3	1.6	15	1,101	9.7	8.6	3.4	<DL	12	0.3	70	0.02	0.01	<DL	9.8	0.2	0.2	108	0.02	1.7	0.3	<DL	3	0.02
		2348.16-2348.30	0.1	3.2	<DL	0.1	0.06	0.1	275	834	7.3	11	0.7	0.09	0.02	0.3	0.5	0.07	<DL	<DL	0.2	<DL	<DL	0.2	0.2	<DL	20	734	3.3	3.5	1.3	<DL	4.3	0.4	26	0.01	0.008	<DL	6.8	0.07	1.6	51	0.01	1.1	0.2	11	34	0.003
		2356.94-2357.06	0.2	5.7	<DL	0.2	0.1	0.2	227	141	9.2	19	0.7	0.1	0.02	0.3	0.2	0.07	<DL	<DL	0.8	<DL	<DL	0.3	<DL	<DL	21	1,497	0.8	1.2	2.3	<DL	6.7	0.4	42	0.02	< 0.0001	<DL	9.2	0.1	1.5	71	0.03	0.4	0.03	5.1	1	0.02
		2362.90-2363.00	1.0	12	59	1.5	1.3	0.3	162	200	29	61	0.5	0.07	0.02	0.3	0.1	0.1	<DL	<DL	0.7	<DL	<DL	0.2	0.003	<DL	11	1,125	3.9	3.1	4.7	<DL	8.1	0.3	122	0.01	0.01	<DL	11	0.3	2.1	155	0.01	0.2	0.09	<DL	<DL	0.05
		2366.50-2366.61	0.7	13	<DL	0.8	0.6	0.2	248	249	20	44	1.5	0.1	0.03	0.4	0.4	0.1	<DL	<DL	1.1	<DL	<DL	0.4	0.009	<DL	39	2,227	1.9	1.8	4.0	<DL	9.3	0.4	106	0.03	0.007	<DL	11	0.3	1.0	146	0.04	0.2	0.05	19	7	0.06
		2373.89-2373.99	0.1	<DL	<DL	0.1	0.08	0.1	226	659	5.7	12	1.3	0.08	0.01	0.7	0.5	0.1	<DL	<DL	0.6	<DL	<DL	0.3	<DL	<DL	19	1,182	1.3	1.4	1.5	<DL	4.7	0.4	47	0.02	0.0009	<DL	7.7	0.09	<DL	52	0.02	0.8	0.06	12	13	0.02
		2427.52-2427.74	0.07	5.4	<DL	0.06	0.02	0.05	92	18,515	100	7.4	19	0.2	0.01	0.9	9.6	0.08	<DL	<DL	0.2	<DL	<DL	0.1	0.02	0.02	338	677	7.2	4.1	1.0	<DL	3.1	0.3	19	0.3	0.007	0.003	4.2	0.05	2.2	32	0.2	4.8	0.2	5.1	118	0.2
Unit Medians	Upper Precipice Sandstone	WM1	0.1	<DL	<DL	0.1	0.01	0.07	17	40	1.7	3.9	0.5	0.05	0.01	0.2	0.2	0.1	<DL	<DL	0.2	<DL	<DL	0.1	0.001	<DL	3.6	233	1.9	1.7	1.5	<DL	9.6	0.3	26	0.01	0.01	0.004	5.2	0.03	1.1	28	0.01	1.0	0.05	0.5	<DL	0.002
		C4, T153, WCG4, WW1	0.3	16	21	0.2	0.1	0.09	93	343	11	20	3	0.2	0.06	0.4	0.3	0.4	0.05	0.001	0.8	<DL	<DL	0.4	0.01	<DL	12	375	1	1	1	<DL	14	0.007	370	0.1	0.01	<DL	6	0.04	<DL	131	0.04	0.7	0.02	<DL	<DL	0.1
	Lower Precipice Sandstone	WM1	0.03	<DL	<DL	0.01	0.004	0.03	1.6	6.0	0.2	1.1	0.09	0.01	0.01	0.002	0.03	0.2	<DL	<DL	0.05	<DL	<DL	0.03	<DL	<DL	<DL	27	0.5	1.0	3.2	<DL	2.0	0.01	12	0.004	<DL	0.01	3.1	0.03	<DL	28	0.003	0.3	0.01	6.0	1.2	<DL
		C4, T153, WCG4, WW1	<DL	4	10	0.03	0.006	0.01	3	8	0.4	3	0.5	0.07	0.03	0.04	0.06	0.6	0.03	<DL	0.2	<DL	<DL	0.2	0.02	0.01	0.5	54	0.9	0.9	6	<DL	3	<DL	278	0.03	0.001	0.03	2	0.01	<DL	96	0.007	0.5	0.02	<DL	<DL	<DL
	Moolayember Formation	WM1	0.2	5.7	<DL	0.2	0.1	0.2	178	200	14	19	0.7	0.09	0.02	0.3	0.2	0.09	<DL	<DL	0.6	<DL	<DL	0.2	0.005	<DL	19	1,101	3.3	3.1	3.4	<DL	8.1	0.3	70	0.02	0.01	<DL	10	0.1	1.3	95	0.02	0.8	0.09	5.1	7.3	0.02
		WCG4, WW1	0.2	0.7	2	0.3	0.1	0.05	10	234	1	1	2	0.2	0.03	0.6	0.7	0.2	0.03	<DL	1	<DL	<DL	0.3	0.02	<DL	9	75	2	4	6	<DL	7	<DL	221	0.02	0.008	<DL	5	0.08	<DL	4	0.05	0.5	0.05	<DL	1	0.06

Legend	Major	Minor	Trace	Ultra-Trace	1,000 - 100,00	100 - 1,000	10 - 100	< 10

Table A6: Elements extracted by pH 5 acid (percentage of total amount in rock powder).

		Element Set	Alkali metals					Alkaline earth metals					Lanthan-oids	Actinoids	Transition metals												Post transition metals						Metalloids						Nonmetals		
		Element Group	1					2					3	3	3	4		5		6		7	8	9	10	11	12	13			14		15	13	14		15		15	16	
Unit		Depth (m)	Li	Na	K	Rb	Cs	Be	Mg	Ca	Sr	Ba	REE	Th	U	Sc	Y	Ti	Zr	Hf	V	Nb	Ta	Cr	Mo	W	Mn	Fe	Co	Ni	Cu	Ag	Zn	Cd	Al	Ga	Tl	Sn	Pb	Bi	B	Si	Ge	As	Sb	P	S	Se
Lower Evergreen Formation		2235.81-2235.94	0.6	0.1	<DL	0.2	1.8	5.9	1.4	22.7	9.5	4.0	0.1	0.5	1.5	0.8	0.3	0.0	<DL	<DL	0.2	<DL	<DL	0.2	0.1	1.5	4.9	2.8	39.1	40.8	19.7	<DL	28.0	42.7	0.1	0.1	2.3	<DL	44.6	59.9	0.7	0.0	0.5	14.5	7.5	<DL	<DL	3.4
		2242.25	0.7	<DL	<DL	0.4	2.1	6.5	0.6	28.4	13.7	6.4	0.1	0.4	1.0	1.1	0.3	0.0	<DL	<DL	0.0	<DL	<DL	0.2	<DL	<DL	2.0	0.8	30.2	23.3	17.0	<DL	20.2	18.9	0.1	0.0	5.5	<DL	52.8	56.1	4.1	0.0	0.2	17.3	8.5	<DL	1.4	0.5
		2242.44-2242.54	1.4	0.8	<DL	1.0	4.4	6.1	0.9	38.3	21.6	10.4	0.3	0.5	0.9	1.1	0.4	0.0	<DL	<DL	0.1	<DL	<DL	0.4	2.4	<DL	<DL	0.6	47.6	42.5	16.0	<DL	11.2	34.2	0.2	0.1	8.6	<DL	36.2	60.8	2.5	0.1	0.5	16.4	9.1	1.5	7.4	2.9
Upper Precipice Sandstone		2246.14-2246.25	0.1	<DL	<DL	0.1	0.4	4.9	3.4	17.8	2.6	1.0	0.4	0.7	0.9	2.4	1.1	0.0	<DL	<DL	0.3	<DL	<DL	0.7	<DL	<DL	7.4	5.9	12.1	15.4	42.9	<DL	15.3	100	0.1	0.1	0.6	0.4	34.5	31.7	<DL	0.0	1.3	23.8	14.1	<DL	<DL	<DL
		2254.94-2255.10	0.9	<DL	<DL	0.1	1.9	13.1	2.2	7.1	4.3	1.3	0.5	1.1	1.9	5.4	1.8	0.0	<DL	<DL	0.8	<DL	<DL	0.9	0.7	<DL	3.7	3.1	28.4	28.1	5.5	<DL	19.9	91.5	0.1	0.1	2.1	0.0	35.7	59.9	29.5	0.0	0.9	22.0	14.0	0.4	<DL	0.4
Lower Precipice Sandstone D		2263.61-2263.77	0.3	<DL	<DL	0.1	0.3	6.7	0.7	20.5	0.9	0.5	0.8	2.4	1.2	0.9	0.8	0.0	<DL	<DL	0.2	<DL	<DL	0.2	<DL	<DL	2.3	15.0	18.0	45.3	<DL	10.0	2.4	0.1	0.1	0.3	3.4	32.7	34.8	<DL	0.0	1.3	26.2	7.1	WR<DL	9.1	<DL
		2267.71-2267.84	0.1	<DL	<DL	<DL	1.2	10.7	0.3	20.2	8.1	10.1	0.1	0.6	0.8	1.1	0.3	0.0	0.0	<DL	0.2	<DL	0.0	0.3	1.5	<DL	2.8	0.9	37.8	37.3	16.3	<DL	6.5	13.0	0.3	0.0	<DL	0.1	39.9	38.0	4.9	0.1	0.1	11.2	<DL	<DL	<DL	1.5
		2267.84-2267.90	<DL	<DL	<DL	<DL	<DL	11.7	<DL	<DL	<DL	<DL	0.1	0.4	1.0	1.0	0.2	0.0	0.0	<DL	0.1	<DL	0.0	0.2	<DL	<DL	<DL	0.4	18.0	22.4	19.3	<DL	9.2	21.2	0.1	0.0	<DL	0.2	34.7	43.2	9.2	<DL	0.0	19.7	<DL	<DL	<DL	<DL
Lower Precipice Sandstone C		2274.10-2274.18	0.3	<DL	<DL	0.1	0.4	7.1	0.7	5.3	0.7	0.6	0.6	0.8	1.5	0.3	1.0	0.0	<DL	<DL	0.2	<DL	<DL	0.3	<DL	8.1	1.8	1.5	15.7	13.4	52.1	<DL	9.0	4.4	0.1	0.2	0.3	4.0	24.6	69.4	5.4	0.0	0.6	27.5	16.6	31.8	3.8	<DL
		2281.82-2281.92	0.3	<DL	<DL	0.1	1.1	6.9	0.5	15.0	3.4	2.2	0.1	0.1	0.7	0.1	0.1	0.0	<DL	<DL	0.1	<DL	<DL	0.1	3.9	<DL	<DL	0.7	23.8	26.5	16.2	<DL	13.7	2.8	0.1	0.0	0.6	<DL	28.6	37.0	<DL	0.0	0.2	18.9	8.9	12.1	2.9	0.9
		2284.13-2284.24	0.4	0.0	<DL	0.2	0.8	11.0	0.5	6.5	0.8	2.3	0.2	<DL	1.5	<DL	0.2	0.0	<DL	<DL	0.3	<DL	<DL	0.2	17.3	<DL	<DL	1.2	19.3	25.5	10.2	<DL	12.5	7.9	0.1	0.1	<DL	0.5	61.4	22.6	<DL	0.0	0.8	41.0	9.5	WR<DL	<DL	<DL
		2285.05	0.9	<DL	<DL	0.6	2.8	13.2	0.6	25.4	11.3	7.0	0.1	0.2	1.0	0.6	0.2	0.0	<DL	<DL	0.0	<DL	<DL	0.2	2.0	<DL	<DL	0.5	36.1	36.3	9.0	<DL	11.6	23.5	0.1	0.0	4.2	<DL	43.3	48.8	1.2	0.0	0.2	19.3	9.6	<DL	1.3	1.6
		2288.49-2288.61	0.2	<DL	<DL	0.1	0.5	9.1	0.4	2.2	0.8	1.1	0.1	<DL	0.9	<DL	0.2	0.0	<DL	<DL	0.3	<DL	<DL	0.2	<DL	<DL	<DL	0.6	29.4	29.2	58.1	<DL	8.3	2.9	0.1	0.0	<DL	2.7	43.0	48.3	<DL	0.0	0.9	42.0	7.1	13.3	4.9	<DL
		2294	<DL	<DL	<DL	<DL	<DL	3.3	0.7	3.0	0.5	1.0	0.0	0.1	1.9	<DL	0.1	0.0	<DL	<DL	0.4	<DL	<DL	0.1	20.9	<DL	<DL	1.9	19.6	10.3	13.5	<DL	5.4	0.2	<DL	0.0	<DL	<DL	31.4	32.7	<DL	<DL	0.3	12.9	7.7	WR<DL	3.8	<DL
		2296.97-2297.13	<DL	<DL	<DL	<DL	<DL	6.4	<DL	<DL	<DL	<DL	0.1	0.2	1.7	1.3	0.5	0.0	0.0	<DL	0.6	0.0	0.0	0.5	<DL	0.1	2.0	1.5	<DL	<DL	40.4	<DL	14.3	13.8	0.0	0.1	<DL	0.9	30.4	65.6	7.5	<DL	0.1	2.2	<DL	<DL	<DL	<DL
Lower Precipice Sandstone B		2297.13-2297.19	0.2	<DL	<DL	<DL	1.9	9.5	<DL	<DL	0.7	3.6	0.1	0.3	1.0	1.1	0.2	0.0	0.0	<DL	0.1	<DL	0.0	0.2	<DL	<DL	1.1	0.7	18.7	10.1	16.1	<DL	6.7	10.3	0.2	0.0	<DL	0.1	27.2	32.0	2.5	0.0	0.2	18.4	5.1	<DL	<DL	0.7
		2298.92	0.3	<DL	<DL	0.1	0.5	5.3	0.5	2.1	1.0	1.3	0.1	<DL	1.9	<DL	0.3	0.0	<DL	<DL	0.3	<DL	<DL	0.2	8.8	<DL	<DL	1.2	16.7	9.2	14.5	<DL	18.3	0.9	0.0	0.1	<DL	<DL	32.8	33.9	<DL	<DL	0.6	13.3	4.6	4.5	2.5	<DL
Lower Precipice Sandstone A	2	2307.2	1.1	<DL	<DL	0.5	1.2	6.7	5.2	8.4	3.8	6.7	0.7	0.5	2.3	0.4	1.3	0.0	<DL	<DL	1.6	<DL	<DL	1.7	4.1	<DL	10.0	7.4	23.9	18.0	13.8	<DL	22.3	3.2	0.6	0.4	<DL	3.2	31.2	55.7	<DL	0.0	1.4	18.8	6.5	WR<DL	<DL	<DL
		2315.77	0.8	<DL	<DL	<DL	<DL	<DL	1.3	4.5	1.6	1.5	0.3	<DL	0.9	<DL	0.8	0.0	<DL	<DL	0.7	<DL	<DL	1.6	<DL	<DL	<DL	6.4	24.6	14.5	24.9	<DL	21.1	8.3	<DL	0.1	<DL	<DL	18.1	30.7	46.1	0.0	2.3	20.4	12.8	WR<DL	<DL	<DL
		2322.61-2322.73	0.5	<DL	<DL	0.3	0.7	5.2	2.8	4.6	1.1	3.0	0.3	0.3	1.6	<DL	0.4	0.0	<DL	<DL	0.7	<DL	<DL	0.4	<DL	<DL	14.8	9.1	22.4	18.3	64.6	<DL	14.9	1.2	0.1	0.2	<DL	12.5	32.8	41.6	<DL	0.0	0.8	14.9	3.6	WR<DL	11.6	<DL
		2323.25	0.5	<DL	<DL	<DL	<DL	<DL	2.5	5.5	1.8	2.5	0.3	<DL	1.2	<DL	0.8	0.0	<DL	<DL	0.7	<DL	<DL	1.1	<DL	<DL	6.4	4.5	20.6	8.5	27.2	<DL	21.5	4.8	0.0	0.2	<DL	<DL	18.8	<DL	<DL	0.0	1.0	12.1	3.9	0.5	11.7	<DL
	1	2328.54-2328.59	1.1	0.4	<DL	0.8	3.4	9.6	1.1	34.9	7.6	6.8	0.1	0.1	1.1	0.8	0.1	0.0	<DL	<DL	0.1	<DL	<DL	0.2	0.9	<DL	<DL	0.5	23.2	20.1	26.6	<DL	7.5	22.6	0.1	0.0	3.9	0.2	24.8	55.5	3.1	0.1	0.2	13.0	15.2	<DL	5.3	1.0
		2328.59-2328.68	0.5	<DL	<DL	0.2	0.7	7.7	0.7	17.7	0.9	1.6	0.1	0.1	2.0	0.0	0.1	0.0	<DL	<DL	0.3	<DL	<DL	0.5	<DL	<DL	0.8	21.1	20.0	44.7	<DL	18.0	81.5	0.1	0.1	<DL	0.6	39.4	42.5	6.4	0.0	0.5	13.8	7.6	6.5	<DL	0.4
		2330.41-2330.54	0.4	<DL	<DL	0.2	0.5	4.5	1.6	10.1	0.7	1.4	0.2	<DL	1.6	<DL	0.3	0.0	<DL	<DL	0.5	<DL	<DL	0.3	<DL	3.1	<DL	1.2	15.8	21.1	58.8	<DL	3.5	2.1	0.0	0.1	<DL	19.7	26.1	46.0	<DL	0.0	1.1	18.2	3.3	22.5	<DL	<DL
		2338.75-2338.85	0.7	0.2	<DL	0.4	1.1	7.0	1.3	10.5	0.9	2.2	0.2	0.2	2.4	<DL	0.3	0.0	<DL	<DL	0.5	<DL	<DL	0.3	<DL	<DL	<DL	1.0	15.8	11.2	65.5	<DL	23.4	3.9	0.1	0.1	<DL	3.8	36.5	69.2	<DL	0.0	0.9	17.8	7.3	2.9	<DL	<DL
Moolayember Formation		2339.00-2339.17	0.5	<DL	<DL	0.4	4.3	16.8	1.1	29.2	6.2	10.5	0.1	0.3	1.1	0.9	0.2	0.0	<DL	<DL	0.1	<DL	<DL	0.3	0.6	<DL	<DL	1.4	31.2	29.7	31.5	<DL	19.9	53.2	0.1	0.0	3.8	<DL	64.9	58.8	<DL	0.0	0.2	32.7	14.0	<DL	2.2	2.5
		2340.54-2340.62	1.6	0.8	<DL	1.0	4.6	10.7	2.3	28.3	28.0	12.0	0.2	0.4	0.8	1.7	0.3	0.0	<DL	<DL	0.4	<DL	<DL	0.5	<DL	<DL	5.1	3.6	6.9	10.2	26.8	<DL	16.3	51.8	0.2	0.0	1.5	<DL	48.6	52.1	4.7	0.1	1.0	12.2	7.2	<DL	<DL	4.3
		2346.40-2346.51	1.0	0.4	<DL	0.3	4.6	10.9	4.2	11.2	19.4	5.1	0.4	0.7	0.8	2.0	0.5	0.0	<DL	<DL	0.8	<DL	<DL	0.9	9.5	38.2	6.4	5.9	43.3	36.7	21.0	<DL	13.4	49.5	0.1	0.1	1.3	<DL	45.9	59.2	0.9	0.0	1.1	26.0	16.8	<DL	0.9	2.7
		2348.16-2348.30	0.6	0.2	<DL	0.1	2.0	9.5	6.6	33.1	9.5	2.3	0.6	0.9	0.7	4.8	2.6	0.0	<DL	<DL	0.5	<DL	<DL	1.0	2.9	<DL	3.0	1.8	27.5	19.6	17.7	<DL	8.5	54.6	0.0	0.1	0.8	<DL	46.8	53.2	10.0	0.0	0.9	2.6	9.2	1.2	0.3	0.4
		2356.94-2357.06	0.8	0.3	<DL	0.2	3.6	10.5	4.4	8.1	12.8	3.5	0.6	1.4	0.8	2.9	0.9	0.0	<DL	<DL	1.3	<DL	<DL	1.2	<DL	<DL	6.0	5.8	12.9	11.1	21.2	<DL	9.1	82.6	0.1	0.1	0.0	<DL	54.0	53.8	7.9	0.0	2.1	16.4	5.3	0.6	1.3	3.3
		2362.90-2363.00	1.2	0.7	0.2	0.9	7.0	11.4	2.5	25.3	36.8	11.1	0.3	0.5	0.7	2.1	0.5	0.0	<DL	<DL	0.7	<DL	<DL	0.6	0.6	<DL	3.8	4.4	32.6	16.8	20.6	<DL	8.5	48.8	0.1	0.1	1.8	<DL	39.9	51.2	6.6	0.1	0.7	6.7	9.1	<DL	<DL	4.5
		2366.50-2366.61	1.4	0.3	<DL	0.6	6.6	8.2	3.0	8.8	25.7	8.5	1.0	0.9	0.9	2.9	1.4	0.0	<DL	<DL	1.2	<DL	<DL	0.9	1.5	<DL	4.2	4.6	19.0	11.0	17.5	<DL	9.4	54.0	0.1	0.2	1.0	<DL	44.0	53.5	4.8	0.1	1.9	8.9	5.0	1.7	4.1	7.2
		2373.89-2373.99	0.6	<DL	<DL	0.1	1.9	7.8	4.3	24.8	9.0	2.2	1.3	0.9	0.7	7.7	2.8	0.0	<DL	<DL	1.2	<DL	<DL	1.3	<DL	<DL	6.2	5.2	18.0	13.3	16.0	<DL	6.8	100	0.1	0.2	0.1	<DL	45.3	57.1	<DL	0.0	1.9	23.1	8.0	4.3	13.2	3.7
		2427.52-2427.74	0.5	0.1	<DL	0.1	0.9	6.3	3.9	57.8	59.5	1.6	18.6	2.7	0.6	17.3	39.9	0.0	<DL	<DL	0.7	<DL	<DL	1.0	5.5	1.1	46.2	6.1	42.4	33.3	17.9	<DL	10.7	100	0.1	3.0	1.2	0.2	29.9	50.6	18.0	0.0	16.6	42.0	18.9	3.6	48.6	24.9
Unit Medians	Upper Precipice Sandstone	WM1	0.5	<DL	<DL	0.1	1.1	9.0	2.8	12.4	3.4	1.1	0.5	0.9	1.4	3.9	1.5	0.0	<DL	<DL	0.6	<DL	<DL	0.8	0.4	<DL	5.5	4.5	20.2	21.7	24.2	<DL	17.6	100	0.1	0.1	1.3	0.2	35.1	45.8	14.7	0.0	1.1	22.9	14.1	0.2	<DL	0.2
		C4, T153, WCG4, WW1	1	1	0.3	0.6	5	10	4	21	9	4	1	3	2	3	1	0.0	0.0	0.0	1	<DL	<DL	1	2	<DL	5	3	14	8	17	<DL	18	3	0.3	0.7	4	<DL	36	34	<DL	0.0	2	16	7	<DL	<DL	9
	Lower Precipice Sandstone	WM1	0.3	<DL	<DL	0.1	0.6	7.0	0.7	6.0	0.9	1.9	0.1	0.1	1.4	0.1	0.3	0.0	<DL	<DL	0.3	<DL	<DL	0.3	<DL	<DL	1.2	20.1	18.2	25.7	<DL	12.1	4.6	0.1	0.1	<DL	0.3	32.1	42.0	<DL	0.0	0.6	18.3	7.1	<DL	0.6	<DL
		C4, T153, WCG4, WW1	<DL	0.3	0.5	0.5	2	2	1	3	3	6	1	2	1	2	1	0.1	0.0	<DL	2	<DL	<DL	2	8	<DL	2	5	28	10	35	<DL	19	<DL	1	1	3	1	31	14	<DL	0.0	2	1	6	<DL	<DL	<DL
	Moolayember Formation	WM1	0.8	0.3	<DL	0.3	4.3	10.5	3.9	25.3	19.4	5.1	0.6	0.9	0.8	2.9	0.9	0.0	<DL	<DL	0.7	<DL	<DL	0.9	0.6	<DL	5.1	4.6	27.5	16.8	20.6	<DL	9.4	54.0	0.1	0.1	1.2	<DL	45.9	53.5	4.8	0.0	1.1	16.4	9.1	0.6	1.3	3.7
		WCG4, WW1	0.7	0.0	0.0	0.5	4	5	0.1	2	1	0.4	2	2	2	5	3	0.0	0.0	<DL	0.7	<DL	<DL	0.6	2	<DL	0.5	0.1	15	12	20	<DL	8	<DL	0.3	0.1	2	<DL	32	36	<DL	0.0	2	7	17	<DL	0.1	4

Legend	Major	Minor	Trace	Ultra-Trace	> 75	50 – 75	25 – 50	5 – 25	< 5

(0.0 indicates < 0.05 %).

Table A7: Elements extracted by pH 3 acid (percentage of total amount in rock powder).

		Element Set	Alkali metals					Alkaline earth metals					Lanthan-oids	Actinoids		Transition metals																		Post transition metals						Metalloids					Nonmetals		
		Element Group	1					2					3	3		3		4		5		6		7	8	9	10	11		12		13			14		15	13	14		15		15	16	
Unit		Depth (m)	Li	Na	K	Rb	Cs	Be	Mg	Ca	Sr	Ba	REE	Th	U	Sc	Y	Ti	Zr	Hf	V	Nb	Ta	Cr	Mo	W	Mn	Fe	Co	Ni	Cu	Ag	Zn	Cd	Al	Ga	Tl	Sn	Pb	Bi	B	Si	Ge	As	Sb	P	S	Se
Lower Evergreen Formation		2235.81-2235.94	0.1	<DL	<DL	0.05	0.01	0.07	51	16	0.1	0.3	0.2	0.07	0.01	0.2	0.05	0.06	<DL	<DL	0.6	<DL	<DL	0.2	0.08	0.008	9.6	813	1.3	2.1	0.6	<DL	6.1	0.02	28	0.02	0.002	<DL	0.8	0.01	0.06	40	0.01	0.09	0.003	<DL	5.6	0.006
		2242.25	0.2	<DL	<DL	0.2	0.06	0.2	4.1	15	0.2	0.7	0.2	0.04	0.02	0.3	0.06	0.02	<DL	<DL	0.2	<DL	<DL	0.1	<DL	0.01	<DL	62	1.6	1.5	1.5	<DL	12	0.01	36	0.01	0.02	<DL	2.0	0.04	<DL	92	0.008	0.6	0.004	<DL	25	0.008
		2242.44-2242.54	0.4	0.7	<DL	0.4	0.1	0.1	9.1	0.8	0.4	1.7	0.3	0.06	0.01	0.2	0.06	0.06	<DL	<DL	0.3	<DL	<DL	0.2	<DL	<DL	<DL	80	4.7	6.3	2.0	<DL	12	0.01	127	0.02	0.02	<DL	2.4	0.06	0.1	203	0.01	0.2	0.004	<DL	22	0.01
Upper Precipice Sandstone		2246.14-2246.25	0.1	0.5	<DL	0.03	0.003	0.02	31	31	0.09	0.1	0.3	0.04	0.004	0.1	0.08	0.1	<DL	<DL	0.3	<DL	<DL	0.08	<DL	<DL	6.9	452	0.3	0.5	0.2	<DL	1.5	0.003	17	0.01	0.001	<DL	0.5	<DL	<DL	22	0.008	0.2	0.006	<DL	2.2	<DL
		2254.94-2255.10	0.1	1.2	<DL	0.06	0.005	0.1	70	163	0.4	0.6	2.7	0.1	0.01	0.5	0.6	0.03	<DL	<DL	1.0	<DL	<DL	0.3	<DL	0.03	19	1,263	1.0	0.6	0.2	<DL	6.6	0.01	34	0.06	0.004	<DL	0.5	<DL	<DL	39	0.05	0.3	0.006	124	4.7	0.02
Lower Precipice Sandstone D		2263.61-2263.77	<DL	0.005	<DL	0.01	<DL	<DL	1.6	5.6	0.0	<DL	0.04	0.01	0.002	0.01	0.01	<DL	<DL	<DL	0.02	<DL	<DL	0.02	<DL	<DL	<DL	32	0.06	0.09	0.3	<DL	0.2	<DL	6.1	0.003	<DL	0.01	0.2	<DL	<DL	1.7	0.001	0.09	0.004	<DL	1.3	<DL
		2267.71-2267.84	0.06	<DL	<DL	0.2	0.05	0.2	1.0	<DL	0.3	0.8	0.03	0.02	0.01	0.07	0.009	0.04	< 0.0001	<DL	0.2	<DL	<DL	0.06	0.001	<DL	<DL	14	1.6	1.7	1.4	<DL	3.1	0.007	31	0.02	0.009	0.0004	0.9	0.05	0.06	29	0.004	0.5	0.02	<DL	<DL	0.007
		2267.84-2267.90	<DL	<DL	<DL	0.008	0.002	0.03	4.2	1.7	0.05	3.0	0.1	0.01	0.01	0.02	0.04	0.2	0.0009	<DL	0.08	<DL	<DL	0.02	0.0004	<DL	0.5	51	0.07	0.1	0.2	<DL	0.2	0.002	153	0.006	<DL	0.002	0.2	0.006	0.2	138	0.005	0.02	0.003	<DL	5.6	0.005
Lower Precipice Sandstone C		2274.10-2274.18	<DL	0.1	<DL	0.009	<DL	0.009	1.0	6.6	0.02	0.01	0.04	0.009	0.003	0.004	0.02	<DL	<DL	<DL	0.02	<DL	<DL	0.01	<DL	<DL	1.1	53	0.05	0.06	0.3	<DL	0.2	<DL	6.2	0.004	<DL	0.009	0.3	<DL	<DL	1.7	0.001	0.09	0.006	<DL	<DL	<DL
		2281.82-2281.92	0.08	<DL	<DL	0.03	0.004	0.09	0.5	2.2	0.03	<DL	0.01	<DL	0.003	0.009	0.004	0.05	<DL	<DL	0.06	<DL	<DL	0.03	0.005	<DL	<DL	4.4	0.3	0.5	0.2	<DL	0.9	0.001	9.6	0.004	0.0004	<DL	0.2	<DL	<DL	13	0.001	0.07	0.002	<DL	1.1	<DL
		2284.13-2284.24	0.08	<DL	<DL	<DL	<DL	0.01	<DL	3.4	0.01	<DL	0.007	<DL	0.001	0.004	0.002	0.03	<DL	<DL	0.01	<DL	<DL	0.01	<DL	<DL	<DL	1.6	0.1	0.2	0.1	<DL	0.3	<DL	5.8	0.004	<DL	<DL	0.1	<DL	<DL	4.1	<DL	0.07	0.005	<DL	5.4	<DL
		2285.05	0.2	<DL	<DL	0.3	0.07	0.4	2.2	1.7	0.2	1.1	0.07	0.03	0.02	0.1	0.03	0.05	<DL	<DL	0.3	<DL	<DL	0.1	<DL	<DL	<DL	41	3.4	4.3	1.2	<DL	12	0.02	58	0.02	0.01	<DL	3.1	0.05	<DL	107	0.005	0.3	0.009	<DL	20	0.009
		2288.49-2288.61	<DL	<DL	<DL	<DL	<DL	0.009	0.2	2.4	0.009	<DL	0.005	<DL	0.0009	0.003	0.002	<DL	<DL	<DL	0.02	<DL	<DL	0.01	<DL	<DL	<DL	1.4	0.05	0.2	0.2	<DL	0.1	<DL	3.5	0.002	<DL	0.01	0.1	<DL	<DL	3.5	<DL	0.03	0.002	<DL	<DL	<DL
		2294	0.08	<DL	<DL	<DL	<DL	<DL	0.3	<DL	0.02	<DL	0.008	<DL	0.005	0.0006	0.003	<DL	<DL	<DL	0.03	<DL	<DL	0.01	<DL	0.03	<DL	2.5	0.04	0.09	0.04	<DL	0.2	<DL	<DL	0.001	<DL	<DL	0.1	<DL	<DL	<DL	0.001	0.02	0.003	<DL	2.6	<DL
		2296.97-2297.13	<DL	<DL	<DL	<DL	< 0.0001	<DL	1.4	<DL	<DL	2.3	0.0002	<DL	<DL	<DL	0.0002	<DL	0.0001	<DL	<DL	<DL	<DL	<DL	<DL	<DL	<DL	40	<DL	0.0004	0.0003	<DL	<DL	<DL	85	<DL	<DL	0.0007	<DL	<DL	0.09	70	<DL	<DL	<DL	<DL	1.8	0.0002
Lower Precipice Sandstone B		2297.13-2297.19	0.02	<DL	<DL	<DL	0.0001	0.005	5.3	3.6	0.003	1.2	0.0002	<DL	<DL	0.007	< 0.0001	<DL	< 0.0001	<DL	<DL	<DL	<DL	0.002	<DL	0.0009	8.1	315	<DL	0.03	0.002	<DL	<DL	0.0002	31	<DL	0.002	0.001	0.001	0.0002	0.3	22	<DL	<DL	<DL	<DL	15	0.003
		2298.92	0.08	<DL	<DL	<DL	<DL	<DL	0.4	<DL	0.01	<DL	0.006	<DL	0.002	0.001	0.002	<DL	<DL	<DL	0.02	<DL	<DL	0.02	<DL	<DL	<DL	2.9	0.02	0.07	0.04	<DL	0.2	<DL	<DL	0.002	<DL	<DL	0.07	<DL	<DL	2.1	<DL	0.008	0.002	<DL	<DL	<DL
Lower Precipice Sandstone A	2	2307.2	<DL	0.3	<DL	0.01	0.002	0.008	2.0	4.9	0.03	<DL	0.06	<DL	0.003	0.004	0.01	0.05	<DL	<DL	0.03	<DL	<DL	0.02	<DL	<DL	0.7	38	0.03	0.09	0.2	<DL	0.2	<DL	25	0.007	0.001	<DL	0.07	<DL	<DL	13	0.001	0.01	0.002	57	<DL	<DL
		2315.77	<DL	<DL	<DL	<DL	<DL	0.008	1.3	3.7	0.007	<DL	0.007	<DL	0.0006	0.001	0.002	<DL	<DL	<DL	0.01	<DL	<DL	0.01	<DL	<DL	<DL	24	0.05	0.09	0.05	<DL	0.2	<DL	<DL	0.002	<DL	<DL	0.03	<DL	<DL	3.1	0.002	0.02	0.003	<DL	0.8	<DL
		2322.61-2322.73	0.06	0.4	<DL	<DL	<DL	<DL	1.3	3.1	0.01	<DL	0.02	<DL	0.002	0.002	0.006	0.03	<DL	<DL	0.02	<DL	<DL	0.02	<DL	<DL	<DL	24	0.01	0.04	0.2	<DL	0.1	<DL	3.9	0.003	<DL	0.04	0.04	<DL	<DL	2.6	0.001	0.007	0.002	<DL	0.6	<DL
		2323.25	0.07	0.1	<DL	<DL	<DL	<DL	1.3	6.5	0.01	<DL	0.006	<DL	0.001	0.002	0.002	0.04	<DL	<DL	0.01	<DL	<DL	0.01	<DL	<DL	<DL	22	0.02	0.07	0.04	<DL	0.3	0.0008	<DL	0.0009	<DL	<DL	0.03	<DL	<DL	4.3	0.002	0.007	0.002	<DL	7.3	<DL
	1	2328.54-2328.59	0.3	1.4	<DL	0.4	0.1	0.3	3.2	5.2	0.3	1.2	0.09	0.02	0.04	0.1	0.05	0.06	<DL	<DL	0.2	<DL	<DL	0.1	<DL	<DL	<DL	29	2.8	2.3	2.2	<DL	1.6	0.005	112	0.02	0.009	<DL	0.8	0.02	<DL	162	0.006	0.1	0.006	51	14	0.004
		2328.59-2328.68	0.08	0.7	<DL	0.03	0.01	0.03	0.8	3.0	0.04	0.1	0.04	0.01	0.02	0.02	0.02	0.1	<DL	<DL	0.09	<DL	<DL	0.03	<DL	0.01	<DL	3.9	0.1	0.2	0.2	<DL	0.6	0.007	20	0.009	<DL	<DL	0.3	<DL	<DL	21	0.004	0.01	0.003	53	<DL	<DL
		2330.41-2330.54	<DL	0.9	<DL	<DL	<DL	<DL	0.4	3.9	0.007	0.004	0.007	<DL	0.001	0.002	0.002	0.02	<DL	<DL	0.01	<DL	<DL	0.007	<DL	0.01	<DL	1.4	0.02	0.04	0.3	<DL	0.08	<DL	<DL	0.002	<DL	0.08	0.05	<DL	<DL	0.6	0.0008	0.007	0.001	<DL	4.5	<DL
		2338.75-2338.85	0.06	<DL	<DL	0.005	<DL	0.02	0.7	1.2	0.01	<DL	0.01	<DL	0.002	0.005	0.003	0.04	<DL	<DL	0.04	<DL	<DL	0.008	<DL	<DL	<DL	2.0	0.02	0.03	0.3	<DL	0.2	0.0006	4.5	0.003	<DL	0.02	0.08	<DL	<DL	3.0	0.002	0.01	0.002	<DL	1.2	<DL
Moolayember Formation		2339.00-2339.17	0.2	1.9	<DL	0.09	0.01	0.2	1.5	2.1	0.07	0.3	0.05	0.02	0.01	0.08	0.02	0.04	<DL	<DL	0.2	<DL	<DL	0.04	<DL	<DL	<DL	48	1.0	0.8	1.1	<DL	20	0.03	57	0.02	0.008	<DL	2.9	0.02	<DL	75	0.005	1.1	0.02	<DL	19	0.01
		2340.54-2340.62	0.2	4.9	<DL	0.4	0.08	0.2	304	83	0.5	2.1	0.3	0.06	0.01	1.3	0.09	0.03	<DL	<DL	3.3	<DL	<DL	0.7	<DL	<DL	57	4,449	1.2	2.0	2.9	<DL	11	0.02	107	0.03	0.003	<DL	1.6	0.05	<DL	155	0.05	0.2	0.006	<DL	2.5	0.02
		2346.40-2346.51	0.2	4.1	<DL	0.1	0.04	0.2	410	113	0.7	1.8	1.0	0.1	0.01	0.6	0.2	0.02	<DL	<DL	2.4	<DL	<DL	0.7	0.04	0.01	37	2,762	2.7	2.6	0.8	<DL	6.4	0.01	63	0.03	0.003	<DL	0.9	0.02	0.05	77	0.04	0.8	0.06	60	11	0.01
		2348.16-2348.30	0.1	3.2	<DL	0.09	0.02	0.09	230	162	0.7	1.4	2.2	0.2	0.02	0.2	0.4	0.02	<DL	<DL	1.1	<DL	<DL	0.3	0.02	<DL	36	2,084	1.1	1.1	0.4	<DL	2.7	0.008	37	0.05	0.007	<DL	0.3	0.007	<DL	42	0.05	0.6	0.07	68	87	0.02
		2356.94-2357.06	0.2	2.3	<DL	0.1	0.03	0.2	590	289	1.2	1.7	2.3	0.2	0.02	0.6	0.6	<DL	<DL	<DL	2.1	<DL	<DL	0.5	<DL	<DL	62	4,258	1.1	1.4	0.7	<DL	4.4	0.007	60	0.05	0.0001	<DL	0.5	0.009	<DL	66	0.06	0.1	0.008	98	6.7	0.02
		2362.90-2363.00	0.6	4.1	<DL	0.4	0.1	0.2	333	86	0.9	2.5	0.4	0.1	0.007	0.8	0.1	0.04	<DL	<DL	1.8	<DL	<DL	0.3	<DL	<DL	33	3,251	2.1	2.0	2.9	<DL	4.8	0.01	109	0.02	0.004	<DL	1.8	0.06	<DL	164	0.04	0.1	0.01	<DL	7.9	0.02
		2366.50-2366.61	0.5	7.2	<DL	0.2	0.06	0.2	493	432	1.9	2.7	3.6	0.2	0.02	0.9	1.0	<DL	<DL	<DL	2.4	<DL	<DL	0.5	<DL	<DL	88	5,382	0.9	1.1	2.3	<DL	3.6	0.01	116	0.08	0.002	<DL	0.8	0.02	<DL	132	0.08	0.08	0.009	71	<DL	0.03
		2373.89-2373.99	0.2	6.6	<DL	0.1	0.03	0.1	378	313	1.4	1.4	3.1	0.2	0.01	0.5	0.8	<DL	<DL	<DL	1.4	<DL	<DL	0.5	<DL	<DL	39	3,015	0.9	1.1	0.4	<DL	2.2	0.008	88	0.07	0.0006	<DL	0.4	0.006	0.05	87	0.07	0.3	0.02	88	6.3	0.02
		2427.52-2427.74	0.2	7.0	<DL	0.06	0.01	0.05	174	251	1.1	1.2	2.2	0.2	0.006	0.3	0.5	0.04	<DL	<DL	1.1	<DL	<DL	0.3	0.003	<DL	45	1,626	1.7	1.0	0.2	<DL	1.1	0.006	47	0.05	0.003	<DL	0.4	<DL	0.1	49	0.03	1.5	0.04	71	15	0.02
Unit Medians	Upper Precipice Sandstone	WM1	0.1	0.9	<DL	0.04	0.004	0.06	50	97	0.2	0.3	1.5	0.07	0.01	0.3	0.3	0.09	<DL	<DL	0.6	<DL	<DL	0.2	<DL	0.02	13	857	0.6	0.5	0.2	<DL	4.1	0.01	26	0.03	0.002	<DL	0.5	<DL	<DL	30	0.03	0.3	0.01	62	3.5	0.01
		C4, T153, WCG4, WW1	<DL	8	14	0.09	0.02	0.1	134	261	1	2	4	0.4	0.05	0.5	0.7	0.03	0.0005	0.0003	1	<DL	<DL	0.3	0.0004	<DL	35	1,849	1	1	0.7	<DL	6	0.004	415	0.1	0.005	0.002	2	0.02	<DL	190	0.09	0.6	0.01	23	<DL	0.2
	Lower Precipice Sandstone	WM1	0.06	<DL	<DL	0.002	<DL	0.01	1.2	3.0	0.02	<DL	0.01	<DL	0.002	0.004	0.004	0.03	<DL	<DL	0.02	<DL	<DL	0.01	<DL	<DL	<DL	23	0.05	0.09	0.2	<DL	0.2	<DL	6.2	0.003	<DL	0.0002	0.1	<DL	<DL	4.2	0.001	0.02	0.003	<DL	1.3	<DL
		C4, T153, WCG4, WW1	<DL	6	7	0.03	0.006	0.01	3	2	0.09	0.3	0.09	0.01	0.005	0.06	0.02	0.1	<DL	<DL	0.3	<DL	<DL	0.1	<DL	<DL	0.2	29	0.3	0.6	1	<DL	1	0.002	211	0.03	0.002	0.003	0.6	0.009	<DL	57	0.002	0.04	0.003	<DL	<DL	<DL
	Moolayember Formation	WM1	0.2	4.1	<DL	0.1	0.03	0.2	333	162	0.9	1.7	2.2	0.2	0.01	0.6	0.4	0.02	<DL	<DL	1.8	<DL	<DL	0.5	<DL	<DL	39	3,015	1.1	1.1	0.8	<DL	4.4	0.01	63	0.05	0.003	<DL	0.8	0.02	<DL	77	0.05	0.3	0.02	68	7.9	0.02
		WCG4, WW1	0.2	42	15	0.1	0.02	0.08	164	730	2	2	4	0.2	<DL	0.3	0.8	0.2	<DL	<DL	2	<DL	<DL	0.6	0.006	<DL	29	1,490	1	2	3	<DL	3	0.005	214	0.04	<DL	<DL	0.7	0.01	<DL	123	0.1	0.3	0.01	<DL	<DL	0.2

Legend: Major | Minor | Trace | Ultra-Trace | 1,000 - 100,00 | 100 - 1,000 | 10 - 100 | < 10

Table A8: Elements extracted by pH 3 acid (percentage of total amount in rock powder).

		Element Set	Alkali metals					Alkaline earth metals					Lanthan-oids	Actinoids		Transition metals															Post transition metals						Metalloids					Nonmetals		
		Element Group	1					2					3	3		3	4		5		6		7	8	9	10	11	12		13		14		15	13	14		15	15	16		
Unit		Depth (m)	Li	Na	K	Rb	Cs	Be	Mg	Ca	Sr	Ba	REE	Th	U	Sc	Y	Ti	Zr	Hf	V	Nb	Ta	Cr	Mo	W	Mn	Fe	Co	Ni	Cu	Ag	Zn	Cd	Al	Ga	Tl	Sn	Pb	Bi	B	Si	Ge	As	Sb	P	S	Se
Lower Evergreen Formation		2235.81-2235.94	0.4	<DL	<DL	0.1	0.4	5.6	5.2	7.3	0.3	0.1	0.1	0.4	0.4	1.8	0.3	0.0	<DL	<DL	0.7	<DL	<DL	0.2	9.8	0.1	25.0	18.8	9.6	7.9	2.5	<DL	8.9	2.6	0.0	0.1	0.7	<DL	3.9	5.5	0.3	0.0	1.0	2.9	0.6	<DL	4.1	0.9
		2242.25	0.4	<DL	<DL	0.2	0.4	5.0	0.2	3.8	0.3	0.2	0.1	0.2	0.4	1.2	0.1	0.0	<DL	<DL	0.1	<DL	<DL	0.1	<DL	0.1	<DL	0.9	12.1	7.2	3.5	<DL	11.0	0.8	0.0	0.0	2.1	<DL	5.0	4.7	<DL	0.0	0.3	6.7	0.5	<DL	3.8	0.5
		2242.44-2242.54	0.5	0.1	<DL	0.3	0.6	3.1	0.3	0.2	0.5	0.4	0.1	0.3	0.3	0.9	0.2	0.0	<DL	<DL	0.2	<DL	<DL	0.2	<DL	<DL	<DL	0.9	16.2	10.0	5.7	<DL	9.6	1.6	0.1	0.1	2.7	<DL	7.0	7.9	0.3	0.1	0.5	3.9	0.5	<DL	4.4	1.3
Upper Precipice Sandstone		2246.14-2246.25	0.6	0.1	<DL	0.1	0.2	3.3	8.3	19.1	0.3	0.0	0.6	1.1	0.4	3.9	1.1	0.0	<DL	<DL	1.0	<DL	<DL	0.5	<DL	<DL	29.6	19.4	6.1	6.3	4.4	<DL	5.0	2.3	0.0	0.1	0.3	<DL	4.1	<DL	<DL	0.0	1.9	6.2	1.7	<DL	0.7	<DL
		2254.94-2255.10	0.8	0.1	<DL	0.1	0.5	11.2	6.9	22.5	0.7	0.1	2.0	1.7	1.1	6.6	4.0	0.0	<DL	<DL	2.6	<DL	<DL	1.6	<DL	2.2	12.8	12.0	8.9	7.5	1.8	<DL	9.1	3.4	0.1	0.4	0.7	<DL	3.2	<DL	<DL	0.0	2.9	7.1	2.1	50.7	1.2	2.7
Lower Precipice Sandstone D		2263.61-2263.77	<DL	0.0	<DL	0.0	<DL	<DL	0.7	6.3	0.1	<DL	0.2	0.5	0.3	0.5	0.2	<DL	<DL	<DL	0.2	<DL	<DL	0.2	<DL	<DL	<DL	2.5	1.3	1.6	3.3	<DL	1.1	<DL	0.0	0.1	<DL	0.4	2.8	<DL	<DL	0.0	0.6	3.0	1.1	<DL	0.7	<DL
		2267.71-2267.84	<DL	<DL	<DL	0.0	0.0	0.4	0.3	0.4	0.1	0.8	0.1	0.1	0.2	0.1	0.1	0.0	0.0	<DL	0.1	<DL	<DL	0.0	0.0	<DL	2.2	0.9	0.2	0.2	1.0	<DL	0.2	0.4	0.1	0.0	<DL	0.0	0.6	0.6	0.7	0.0	0.2	0.3	0.4	<DL	1.1	0.5
		2267.84-2267.90	0.2	<DL	<DL	0.2	0.7	7.4	0.1	<DL	0.4	0.2	0.0	0.2	0.5	0.9	0.0	0.0	0.0	<DL	0.3	<DL	<DL	0.2	0.1	<DL	<DL	0.5	13.5	7.5	17.1	<DL	3.9	1.8	0.0	0.1	1.6	0.0	4.4	16.6	0.6	0.0	0.2	11.9	3.6	<DL	<DL	1.4
Lower Precipice Sandstone C		2274.10-2274.18	<DL	0.0	<DL	0.0	<DL	2.0	0.5	5.1	0.1	0.0	0.2	0.4	0.4	0.3	0.3	<DL	<DL	<DL	0.1	<DL	<DL	0.1	<DL	<DL	1.4	1.3	1.1	0.8	3.1	<DL	0.8	<DL	0.0	0.1	<DL	0.4	3.3	<DL	<DL	0.0	0.2	2.2	1.3	<DL	<DL	<DL
		2281.82-2281.92	0.3	<DL	<DL	0.0	0.1	3.8	0.1	1.5	0.1	<DL	0.0	<DL	0.1	0.1	0.0	0.0	<DL	<DL	0.1	<DL	<DL	0.1	0.6	<DL	<DL	0.2	2.7	2.3	1.4	<DL	1.6	0.2	0.0	0.0	0.1	<DL	1.1	<DL	<DL	0.0	0.1	1.9	0.4	<DL	0.4	<DL
		2284.13-2284.24	0.9	<DL	<DL	<DL	<DL	3.8	<DL	6.9	0.1	<DL	0.0	<DL	0.2	0.2	0.0	0.0	<DL	<DL	0.1	<DL	<DL	0.1	<DL	<DL	0.3	1.6	1.7	0.5	<DL	<DL	1.6	<DL	0.0	0.1	<DL	<DL	1.7	<DL	<DL	0.0	0.1	2.3	1.0	<DL	6.2	<DL
		2285.05	0.4	<DL	<DL	0.2	0.4	7.3	0.1	0.5	0.3	0.3	0.0	0.2	0.5	0.6	0.1	0.0	<DL	<DL	0.2	<DL	<DL	0.1	<DL	<DL	<DL	0.7	13.3	9.2	2.6	<DL	7.3	1.4	0.1	0.1	1.8	<DL	7.7	8.2	<DL	0.0	0.2	5.7	0.8	<DL	2.4	0.6
		2288.49-2288.61	<DL	<DL	<DL	<DL	<DL	2.4	0.1	4.0	0.1	<DL	0.0	<DL	0.1	0.2	0.0	<DL	<DL	<DL	0.2	<DL	<DL	0.1	<DL	<DL	<DL	0.2	2.7	2.6	2.7	<DL	1.3	<DL	0.0	0.1	<DL	0.5	1.5	<DL	<DL	0.0	<DL	3.2	0.9	<DL	<DL	<DL
		2294	2.1	<DL	<DL	<DL	<DL	<DL	0.3	<DL	0.1	<DL	0.0	<DL	0.3	0.0	0.0	<DL	<DL	<DL	0.3	<DL	<DL	0.1	<DL	1.3	<DL	0.5	3.3	1.8	1.5	<DL	2.3	<DL	<DL	0.0	<DL	<DL	1.1	<DL	<DL	<DL	0.2	1.3	1.2	<DL	1.5	<DL
		2296.97-2297.13	0.3	<DL	<DL	<DL	0.0	1.0	3.4	2.1	0.0	1.8	0.0	<DL	<DL	0.3	0.0	<DL	0.0	<DL	<DL	<DL	<DL	0.0	<DL	0.0	20.6	16.4	<DL	1.4	0.0	<DL	<DL	0.0	0.2	<DL	3.1	0.0	0.0	0.1	2.1	0.0	<DL	<DL	<DL	<DL	14.7	0.4
Lower Precipice Sandstone B		2297.13-2297.19	<DL	<DL	<DL	<DL	0.0	<DL	0.1	<DL	<DL	0.6	0.0	<DL	<DL	<DL	0.0	<DL	0.0	<DL	<DL	<DL	<DL	<DL	<DL	0.5	<DL	0.0	0.0	<DL	<DL	<DL	0.1	<DL	<DL	0.2	0.0	<DL	<DL	<DL	<DL	0.1	0.0
		2298.92	1.0	<DL	<DL	<DL	<DL	<DL	0.3	<DL	0.1	<DL	0.0	<DL	0.3	0.1	0.1	<DL	<DL	<DL	0.1	<DL	<DL	0.1	<DL	<DL	0.5	1.9	1.5	1.1	<DL	1.5	<DL	<DL	0.0	<DL	<DL	1.0	<DL	<DL	0.0	<DL	1.3	1.4	<DL	<DL	<DL
Lower Precipice Sandstone A	2	2307.2	<DL	0.1	<DL	0.3	0.8	5.1	1.8	3.4	0.3	<DL	0.2	<DL	0.5	0.5	0.5	0.0	<DL	<DL	0.8	<DL	<DL	0.6	<DL	<DL	2.6	2.8	3.2	3.2	1.0	<DL	2.1	<DL	0.5	0.4	3.7	<DL	1.4	<DL	<DL	0.0	0.4	2.1	1.5	WR<DL	<DL	<DL
		2315.77	<DL	<DL	<DL	<DL	<DL	7.4	0.7	2.3	0.1	<DL	0.0	<DL	0.2	0.2	0.1	<DL	<DL	<DL	0.4	<DL	<DL	0.6	<DL	<DL	5.4	7.5	4.2	3.5	<DL	4.0	<DL	<DL	0.1	<DL	<DL	0.9	<DL	<DL	0.0	1.0	2.8	3.0	<DL	0.9	<DL
		2322.61-2322.73	2.1	0.3	<DL	<DL	<DL	<DL	1.8	3.8	0.1	<DL	0.1	<DL	0.3	0.2	0.1	0.0	<DL	<DL	0.3	<DL	<DL	0.2	<DL	<DL	4.6	2.2	4.0	1.5	<DL	4.4	<DL	0.1	0.1	<DL	1.6	1.1	<DL	<DL	0.0	0.4	1.7	1.5	<DL	2.1	<DL
		2323.25	2.2	0.0	<DL	<DL	<DL	<DL	2.1	4.3	0.1	<DL	0.0	<DL	0.3	0.3	0.1	0.0	<DL	<DL	0.3	<DL	<DL	0.5	<DL	<DL	3.8	4.3	2.7	3.1	<DL	3.8	0.7	<DL	0.1	<DL	<DL	0.9	<DL	<DL	0.0	1.0	1.8	2.1	<DL	15.0	<DL
	1	2328.54-2328.59	0.3	0.2	<DL	0.3	0.5	4.2	0.2	1.6	0.2	0.3	0.0	0.1	0.5	0.6	0.1	0.0	<DL	<DL	0.2	<DL	<DL	0.1	<DL	<DL	0.4	12.6	5.4	5.3	<DL	5.7	0.4	0.1	0.1	1.3	<DL	2.6	4.3	<DL	0.1	0.2	2.9	0.8	18.2	3.9	0.4
		2328.59-2328.68	0.7	0.3	<DL	0.2	0.6	3.9	0.3	5.4	0.1	0.1	0.1	0.2	1.1	0.5	0.2	0.0	<DL	<DL	0.4	<DL	<DL	0.2	<DL	0.4	<DL	0.5	7.8	5.3	4.7	<DL	3.7	2.0	0.1	0.1	<DL	<DL	2.9	<DL	<DL	0.0	0.7	1.3	1.8	93.9	<DL	<DL
		2330.41-2330.54	<DL	0.1	<DL	<DL	<DL	<DL	0.8	7.6	0.1	0.0	0.0	<DL	0.3	0.2	0.1	0.0	<DL	<DL	0.2	<DL	<DL	0.2	<DL	1.8	<DL	0.5	1.6	2.4	1.4	<DL	2.7	<DL	<DL	0.1	<DL	2.4	1.0	<DL	<DL	0.0	0.6	1.7	1.0	<DL	9.6	<DL
		2338.75-2338.85	1.3	<DL	<DL	0.1	<DL	3.6	0.5	2.7	0.1	<DL	0.0	<DL	0.3	0.3	0.1	0.0	<DL	<DL	0.3	<DL	<DL	0.1	<DL	<DL	0.5	1.6	1.2	3.2	<DL	2.4	0.5	0.0	0.1	<DL	0.8	1.5	<DL	<DL	0.0	0.4	1.5	1.2	<DL	3.2	<DL
Moolayember Formation		2339.00-2339.17	0.4	0.4	<DL	0.2	0.6	5.9	0.1	1.2	0.1	0.3	0.0	0.1	0.4	0.7	0.1	0.0	<DL	<DL	0.2	<DL	<DL	0.1	<DL	<DL	<DL	1.5	6.8	4.2	8.7	<DL	11.0	4.6	0.1	0.1	2.1	<DL	13.3	10.4	<DL	0.0	0.3	11.1	1.6	<DL	3.6	1.7
		2340.54-2340.62	0.5	0.5	<DL	0.3	0.5	8.8	9.0	13.5	1.0	0.6	0.2	0.4	0.3	7.3	0.3	0.0	<DL	<DL	3.2	<DL	<DL	1.5	<DL	<DL	31.1	23.8	6.4	7.5	9.1	<DL	11.6	3.0	0.1	0.1	0.5	<DL	6.9	8.6	<DL	0.0	0.4	3.4	0.9	<DL	0.9	2.4
		2346.40-2346.51	0.4	0.2	<DL	0.1	0.6	7.9	9.6	10.2	1.0	0.3	0.7	0.8	0.4	4.3	0.8	0.0	<DL	<DL	2.7	<DL	<DL	1.9	1.5	0.3	16.2	14.7	12.2	11.2	4.8	<DL	7.3	2.3	0.1	0.1	0.4	<DL	4.3	4.9	0.2	0.0	2.6	12.2	3.4	21.0	4.1	1.8
		2348.16-2348.30	0.6	0.2	<DL	0.1	0.6	8.1	5.6	6.4	0.9	0.3	1.9	1.9	0.8	2.8	2.5	0.0	<DL	<DL	2.3	<DL	<DL	1.4	0.3	<DL	5.6	5.0	8.8	6.3	5.2	<DL	5.2	1.2	0.1	0.4	0.7	<DL	1.9	4.7	<DL	0.0	3.4	1.4	2.8	7.9	0.8	2.6
		2356.94-2357.06	0.6	0.1	<DL	0.1	0.7	8.6	11.3	16.7	1.6	0.3	2.0	2.2	0.7	6.0	2.7	<DL	<DL	<DL	3.3	<DL	<DL	1.9	<DL	<DL	17.5	16.5	15.9	13.1	6.7	<DL	5.9	1.6	0.1	0.3	0.0	<DL	3.0	4.6	<DL	0.0	5.2	5.3	1.3	11.5	6.2	3.0
		2362.90-2363.00	0.7	0.2	<DL	0.2	0.6	8.2	5.1	10.9	1.2	0.5	0.2	0.8	0.2	5.6	0.4	0.0	<DL	<DL	1.8	<DL	<DL	0.9	<DL	<DL	11.7	12.8	17.5	10.9	12.5	<DL	5.1	1.7	0.1	0.1	0.5	<DL	6.3	10.1	<DL	0.1	2.0	4.6	1.3	<DL	6.2	1.6
		2366.50-2366.61	0.9	0.1	<DL	0.1	0.7	8.7	6.0	15.3	2.5	0.5	2.4	1.4	0.6	6.3	3.7	<DL	<DL	<DL	2.7	<DL	<DL	1.4	<DL	<DL	9.4	11.2	9.0	6.7	10.2	<DL	3.6	1.6	0.1	0.4	0.2	<DL	3.2	4.4	<DL	0.0	4.3	3.7	1.0	6.4	<DL	3.3
		2373.89-2373.99	1.1	0.1	<DL	0.1	0.6	7.3	7.2	11.8	2.2	0.3	3.1	2.0	0.5	5.6	4.6	<DL	<DL	<DL	2.8	<DL	<DL	2.1	<DL	<DL	13.1	13.3	12.6	10.3	3.8	<DL	3.3	2.1	0.1	0.4	0.1	<DL	2.5	3.7	0.2	0.0	5.7	7.5	2.1	32.3	6.4	4.2
		2427.52-2427.74	1.5	0.1	<DL	0.1	0.5	6.0	7.3	0.8	0.7	0.3	2.1	2.3	0.4	6.5	2.2	0.0	<DL	<DL	3.3	<DL	<DL	2.2	0.8	<DL	6.1	14.6	10.0	8.1	4.2	<DL	3.8	2.3	0.1	0.4	0.6	<DL	2.8	<DL	1.0	0.0	3.1	13.5	4.4	49.8	6.3	2.6
Unit Medians	Upper Precipice Sandstone	WM1	0.7	0.1	<DL	0.1	0.3	7.3	7.6	20.8	0.5	0.1	1.3	1.4	0.7	5.2	2.5	0.0	<DL	<DL	1.8	<DL	<DL	1.1	<DL	1.1	21.2	15.7	7.5	6.9	3.1	<DL	7.1	2.9	0.0	0.3	0.5	<DL	3.7	<DL	<DL	0.0	2.4	6.7	1.9	25.3	0.9	1.4
		C4, T153, WCG4, WW1	<DL	0.6	0.2	0.2	0.6	11	6	8	0.9	0.6	2	2	2	5	2	0.001	0.0004	0.005	2	<DL	<DL	1	0.05	<DL	11	9	10	6	7	<DL	8	2	0.4	0.6	1	0.1	8	12	<DL	0.1	6	11	2	6	<DL	13
	Lower Precipice Sandstone	WM1	0.3	<DL	<DL	0.0	<DL	2.2	0.3	2.5	0.1	<DL	0.0	<DL	0.3	0.3	0.1	0.0	<DL	<DL	0.2	<DL	<DL	0.1	<DL	<DL	<DL	0.5	2.5	2.4	2.1	<DL	2.2	<DL	0.0	0.1	<DL	0.0	1.3	<DL	<DL	0.0	0.2	1.8	1.1	<DL	1.0	<DL
		C4, T153, WCG4, WW1	<DL	0.9	0.3	0.5	0.3	0.8	1	0.1	0.5	0.8	0.2	0.2	0.3	0.7	0.3	0.01	<DL	<DL	2	<DL	<DL	1	<DL	<DL	<DL	5	8	6	7	<DL	5	0.9	2	0.8	1	0.08	7	6	<DL	0.0	0.3	<DL	0.9	<DL	<DL	<DL
	Moolayember Formation	WM1	0.6	0.2	<DL	0.1	0.6	8.1	7.2	10.9	1.0	0.3	1.9	1.4	0.4	5.6	2.2	0.0	<DL	<DL	2.7	<DL	<DL	1.5	<DL	<DL	11.7	13.3	10.0	8.1	6.7	<DL	5.2	2.1	0.1	0.3	0.5	<DL	3.2	4.7	<DL	0.0	3.4	5.3	1.6	7.9	4.1	2.6
		WCG4, WW1	0.5	4	0.1	0.1	0.4	9	3	10	2	0.7	5	2	<DL	2	7	0.004	<DL	<DL	1	<DL	<DL	0.9	0.7	<DL	4	3	10	7	8	<DL	4	2	0.3	0.2	<DL	<DL	5	5	<DL	0.1	6	7	3	<DL	<DL	9

Legend	Major	Minor	Trace	Ultra-Trace	> 75	50 – 75	25 – 50	5 – 25	< 5

(0.0 indicates < 0.05 %).

Table A9: Cumulative weak-acid extraction of elements (mg element per kg rock powder).

		Element Set	Alkali metals					Alkaline earth metals					Lanthan-oids	Actinoids		Transition metals														Post transition metals						Metalloids					Nonmetals		
		Element Group	1					2					3	3		3		4		5		6		7	8	9	10	11		12	13			14		15	13	14			15	15	16	
Unit		Depth (m)	Li	Na	K	Rb	Cs	Be	Mg	Ca	Sr	Ba	REE	Th	U	Sc	Y	Ti	Zr	Hf	V	Nb	Ta	Cr	Mo	W	Mn	Fe	Co	Ni	Cu	Ag	Zn	Cd	Al	Ga	Tl	Sn	Pb	Bi	B	Si	Ge	As	Sb	P	S	Se
Lower Evergreen Formation		2235.81-2235.94	0.3	0.5	<DL	0.1	0.05	0.1	65	66	3.9	8.4	0.4	0.2	0.05	0.3	0.1	0.2	<DL	<DL	0.8	<DL	<DL	0.3	0.08	0.09	12	934	6.8	13	5.2	<DL	25	0.3	66	0.02	0.009	<DL	10	0.2	0.2	94	0.02	0.5	0.04	<DL	5.6	0.03
		2242.25	0.6	<DL	<DL	0.8	0.4	0.4	17	125	11	28	0.6	0.1	0.09	0.6	0.2	0.1	<DL	<DL	0.3	<DL	<DL	0.3	<DL	0.01	0.6	119	5.5	6.4	9.1	<DL	34	0.3	102	0.02	0.07	<DL	24	0.5	2.4	167	0.02	2.1	0.07	<DL	34	0.02
		2242.44-2242.54	1.7	11	<DL	1.8	1.0	0.4	34	157	17	43	0.9	0.2	0.05	0.4	0.2	0.3	<DL	<DL	0.4	<DL	<DL	0.5	0.06	<DL	<DL	137	18	33	7.6	<DL	27	0.3	380	0.04	0.09	<DL	15	0.5	1.1	460	0.02	1.2	0.07	3.3	60	0.04
Upper Precipice Sandstone		2246.14-2246.25	0.1	0.5	<DL	0.06	0.009	0.04	43	61	0.9	2.1	0.5	0.07	0.01	0.2	0.2	0.3	<DL	<DL	0.3	<DL	<DL	0.2	<DL	<DL	8.6	588	0.8	1.6	2.4	<DL	6.2	0.3	36	0.01	0.003	0.007	5.1	0.02	<DL	42	0.01	1.2	0.06	<DL	2.2	<DL
		2254.94-2255.10	0.2	1.2	<DL	0.1	0.03	0.2	92	215	3.1	6.3	3.4	0.2	0.03	0.8	0.9	0.1	<DL	<DL	1.3	<DL	<DL	0.4	0.002	0.03	25	1,592	4.2	2.9	1.0	<DL	21	0.3	69	0.07	0.02	0.001	6.3	0.04	2.2	74	0.06	1.3	0.05	125	4.7	0.02
Lower Precipice Sandstone D		2263.61-2263.77	0.02	0.005	<DL	0.04	0.005	0.02	3.2	24	0.2	0.8	0.2	0.07	0.01	0.03	0.07	0.1	<DL	<DL	0.05	<DL	<DL	0.04	<DL	<DL	<DL	61	0.7	1.1	3.8	<DL	1.6	0.004	19	0.009	0.001	0.1	3.2	0.01	<DL	35	0.004	0.9	0.03	28	18	<DL
		2267.71-2267.84	0.06	<DL	<DL	0.2	0.05	0.5	1.0	<DL	0.3	0.8	0.2	0.05	0.03	0.1	0.06	0.2	0.02	<DL	0.2	<DL	0.0006	0.1	0.001	<DL	<DL	25	3.8	7.0	2.9	<DL	11	0.09	78	0.02	0.009	0.008	7.7	0.2	1.0	29	0.005	1.4	0.02	<DL	<DL	0.007
		2267.84-2267.90	0.1	<DL	<DL	0.008	0.2	0.7	9.0	83	6.3	42	0.4	0.1	0.05	0.2	0.1	0.6	0.03	<DL	0.3	<DL	0.0003	0.2	0.05	<DL	1.2	98	15	30	3.5	<DL	7.3	0.09	482	0.02	<DL	0.006	14	0.4	1.3	294	0.009	0.6	0.003	<DL	5.6	0.02
Lower Precipice Sandstone C		2274.10-2274.18	0.02	0.1	<DL	0.04	0.006	0.04	2.5	13	0.2	0.9	0.2	0.03	0.01	0.008	0.08	0.2	<DL	<DL	0.04	<DL	<DL	0.04	<DL	0.06	2.6	111	0.8	1.1	5.0	<DL	1.9	0.004	18	0.01	0.001	0.1	2.9	0.08	0.4	28	0.004	1.2	0.08	12	47	<DL
		2281.82-2281.92	0.1	<DL	<DL	0.1	0.05	0.3	3.9	25	1.8	5.1	0.09	0.01	0.02	0.02	0.04	0.1	<DL	<DL	0.1	<DL	<DL	0.06	0.04	<DL	<DL	20	3.3	5.9	2.6	<DL	8.2	0.02	45	0.008	0.003	<DL	4.5	0.08	<DL	60	0.004	0.8	0.05	12	11	0.005
		2284.13-2284.24	0.1	0.06	<DL	0.02	0.005	0.06	0.9	6.5	0.2	1.0	0.06	<DL	0.009	0.004	0.02	0.1	<DL	<DL	0.05	<DL	<DL	0.03	0.05	<DL	<DL	9.2	1.4	3.1	1.9	<DL	3.0	0.006	23	0.007	<DL	0.02	4.9	0.03	<DL	39	0.002	1.3	0.05	8.2	5.4	<DL
		2285.05	0.7	<DL	<DL	1.1	0.6	1.2	14	90	9.0	24	0.2	0.07	0.07	0.2	0.1	0.2	<DL	<DL	0.3	<DL	<DL	0.3	0.05	<DL	<DL	72	13	21	5.2	<DL	30	0.3	147	0.03	0.04	<DL	21	0.3	0.5	195	0.01	1.4	0.1	<DL	30	0.03
		2288.49-2288.61	0.02	<DL	<DL	0.02	0.004	0.04	1.1	3.8	0.1	0.4	0.05	<DL	0.009	0.003	0.01	0.1	<DL	<DL	0.05	<DL	<DL	0.04	<DL	<DL	<DL	6.0	0.6	2.1	4.3	<DL	0.8	0.003	15	0.004	<DL	0.07	3.4	0.03	<DL	20	0.002	0.4	0.02	4.5	3.9	<DL
		2294	0.08	<DL	<DL	<DL	<DL	0.007	1.0	3.6	0.2	0.5	0.05	0.006	0.04	0.0006	0.01	0.2	<DL	<DL	0.08	<DL	<DL	0.03	0.07	0.03	<DL	12	0.3	0.6	0.4	<DL	0.6	0.001	<DL	0.002	<DL	<DL	3.1	0.01	<DL	<DL	0.004	0.2	0.02	6.7	9.1	<DL
		2296.97-2297.13	0.2	<DL	<DL	<DL	0.5	0.7	1.4	<DL	1.3	17	0.3	0.09	0.06	0.2	0.07	0.3	0.03	<DL	0.2	<DL	0.0009	0.3	<DL	<DL	0.3	91	6.2	7.4	6.7	<DL	9.0	0.09	326	0.02	<DL	0.005	10	0.2	1.2	142	0.004	3.3	0.1	<DL	1.8	0.009
Lower Precipice Sandstone B		2297.13-2297.19	0.02	<DL	<DL	<DL	0.0001	0.03	5.3	3.6	0.003	1.2	0.4	0.04	0.05	0.04	0.1	0.5	0.02	<DL	0.1	<DL	0.0007	0.07	<DL	0.002	8.9	343	<DL	0.03	2.0	<DL	2.0	0.06	38	0.009	0.002	0.03	4.2	0.08	1.3	22	0.004	0.05	<DL	<DL	15	0.003
		2298.92	0.1	<DL	<DL	0.01	0.002	0.02	1.1	2.1	0.2	0.7	0.04	<DL	0.01	0.001	0.009	0.04	<DL	<DL	0.05	<DL	<DL	0.04	0.04	<DL	<DL	9.2	0.2	0.5	0.6	<DL	2.6	0.001	6.3	0.004	<DL	<DL	2.4	0.02	<DL	2.1	0.002	0.09	0.01	15	2.3	<DL
Lower Precipice Sandstone A	2	2307.2	0.03	0.3	<DL	0.03	0.005	0.02	7.6	17	0.5	2.9	0.3	0.01	0.01	0.007	0.05	0.3	<DL	<DL	0.1	<DL	<DL	0.09	0.01	<DL	3.6	137	0.3	0.6	3.2	<DL	2.7	0.004	53	0.01	0.001	0.03	1.7	0.02	<DL	55	0.006	0.1	0.01	77	<DL	<DL
		2315.77	0.02	<DL	<DL	<DL	<DL	0.008	3.4	11	0.2	0.7	0.07	<DL	0.003	0.001	0.01	0.1	<DL	<DL	0.03	<DL	<DL	0.05	<DL	<DL	<DL	52	0.2	0.4	0.4	<DL	1.1	0.006	<DL	0.002	<DL	<DL	0.6	0.008	2.1	19	0.005	0.1	0.02	11	0.8	<DL
		2322.61-2322.73	0.07	0.4	<DL	0.01	0.002	0.008	3.2	6.9	0.1	1.5	0.1	0.008	0.01	0.002	0.02	0.2	<DL	<DL	0.05	<DL	<DL	0.05	<DL	<DL	1.3	72	0.2	0.2	8.2	<DL	0.5	0.002	8.2	0.006	<DL	0.3	1.3	0.01	<DL	16	0.004	0.07	0.007	14	3.9	<DL
		2323.25	0.08	0.1	<DL	<DL	<DL	<DL	2.8	15	0.2	1.1	0.07	<DL	0.005	0.002	0.01	0.2	<DL	<DL	0.03	<DL	<DL	0.05	<DL	<DL	0.6	49	0.09	0.3	0.4	<DL	1.7	0.006	1.7	0.003	<DL	<DL	0.7	<DL	<DL	12	0.004	0.05	0.006	1.7	13	<DL
	1	2328.54-2328.59	1.3	5.4	<DL	1.5	0.9	0.9	26	115	9.8	27	0.3	0.07	0.1	0.3	0.09	0.2	<DL	<DL	0.3	<DL	<DL	0.3	0.007	<DL	<DL	62	7.8	11	13	<DL	3.7	0.3	314	0.03	0.04	0.01	8.6	0.3	1.7	357	0.01	0.7	0.12	51	34	0.01
		2328.59-2328.68	0.1	0.7	<DL	0.06	0.02	0.07	2.5	13	0.3	1.7	0.09	0.02	0.05	0.02	0.03	0.2	<DL	<DL	0.2	<DL	<DL	0.1	<DL	0.01	<DL	11	0.6	1.2	2.2	<DL	3.3	0.3	47	0.01	<DL	0.01	4.7	0.03	1.1	51	0.006	0.1	0.02	57	<DL	0.0008
		2330.41-2330.54	0.01	0.9	<DL	0.006	0.002	0.008	1.3	9.0	0.08	0.9	0.05	<DL	0.009	0.002	0.01	0.2	<DL	<DL	0.04	<DL	<DL	0.02	<DL	0.04	<DL	4.5	0.2	0.4	13	<DL	0.2	0.002	3.0	0.004	<DL	0.8	1.3	0.009	<DL	17	0.002	0.08	0.006	5.3	4.5	<DL
		2338.75-2338.85	0.09	0.3	<DL	0.03	0.006	0.04	2.2	5.9	0.2	1.1	0.1	0.005	0.02	0.005	0.02	0.4	<DL	<DL	0.09	<DL	<DL	0.03	<DL	<DL	<DL	6.5	0.3	0.4	7.4	<DL	2.1	0.005	14	0.007	<DL	0.1	2.1	0.06	<DL	38	0.005	0.1	0.01	10	1.2	<DL
Moolayember Formation		2339.00-2339.17	0.4	1.9	<DL	0.3	0.1	0.6	13	51	4.1	12	0.2	0.05	0.05	0.2	0.07	0.1	<DL	<DL	0.2	<DL	<DL	0.1	0.005	<DL	<DL	95	5.8	6.2	5.1	<DL	56	0.3	153	0.03	0.02	<DL	17	0.2	<DL	171	0.008	4.5	0.2	<DL	30	0.02
		2340.54-2340.62	1.0	13	<DL	1.7	0.9	0.4	381	256	16	41	0.7	0.1	0.04	1.6	0.2	0.2	<DL	<DL	3.7	<DL	<DL	0.9	<DL	<DL	67	5,122	2.5	4.7	12	<DL	27	0.3	265	0.04	0.01	<DL	13	0.3	1.3	339	0.07	1.0	0.06	<DL	2.5	0.05
		2346.40-2346.51	0.5	11	<DL	0.6	0.3	0.4	587	237	15	32	1.5	0.2	0.04	0.8	0.3	0.1	<DL	<DL	3.2	<DL	<DL	1.1	0.3	1.7	52	3,863	12	11	4.2	<DL	18	0.3	134	0.05	0.01	<DL	11	0.2	0.3	185	0.06	2.5	0.3	60	14	0.04
		2348.16-2348.30	0.2	6.4	<DL	0.2	0.08	0.2	504	996	8.0	12	2.9	0.3	0.03	0.6	0.9	0.09	<DL	<DL	1.3	<DL	<DL	0.6	0.2	<DL	56	2,818	4.4	4.6	1.7	<DL	7.0	0.4	64	0.06	0.01	<DL	7.1	0.08	1.6	94	0.06	1.7	0.3	78	121	0.02
		2356.94-2357.06	0.4	8.1	<DL	0.4	0.2	0.3	816	431	10	21	3.0	0.4	0.04	0.9	0.7	0.07	<DL	<DL	3.0	<DL	<DL	0.8	<DL	<DL	83	5,754	1.9	2.5	3.0	<DL	11	0.4	102	0.07	0.0001	<DL	9.7	0.1	1.5	137	0.09	0.5	0.04	103	8.1	0.04
		2362.90-2363.00	1.7	16	59	1.9	1.5	0.5	494	287	30	64	0.9	0.2	0.03	1.1	0.3	0.1	<DL	<DL	2.4	<DL	<DL	0.6	0.003	<DL	44	4,376	5.9	5.1	7.6	<DL	13	0.3	232	0.03	0.02	<DL	13	0.4	2.1	319	0.05	0.3	0.1	<DL	7.9	0.07
		2366.50-2366.61	1.1	20	<DL	1.0	0.7	0.4	741	681	22	46	5.1	0.3	0.05	1.3	1.4	0.1	<DL	<DL	3.5	<DL	<DL	0.9	0.009	<DL	127	7,609	2.9	2.9	6.3	<DL	13	0.4	222	0.1	0.009	<DL	11	0.3	1.0	279	0.1	0.3	0.05	90	7.3	0.09
		2373.89-2373.99	0.4	6.6	<DL	0.2	0.1	0.2	604	972	7.1	13	4.4	0.3	0.03	1.2	1.3	0.1	<DL	<DL	2.1	<DL	<DL	0.7	<DL	<DL	58	4,197	2.2	2.5	1.9	<DL	6.9	0.4	134	0.09	0.001	<DL	8.1	0.1	0.05	139	0.09	1.1	0.08	100	19	0.04
		2427.52-2427.74	0.3	12	<DL	0.1	0.04	0.1	266	18,765	101	8.6	22	0.4	0.02	1.3	10	0.1	<DL	<DL	1.3	<DL	<DL	0.4	0.03	0.02	382	2,303	8.9	5.1	1.2	<DL	4.1	0.4	66	0.4	0.01	0.003	4.6	0.05	2.3	80	0.2	6.3	0.2	76	134	0.2
Unit Medians	Upper Precipice Sandstone	WM1	0.2	0.9	<DL	0.1	0.02	0.1	68	138	2.0	4.2	1.9	0.1	0.02	0.5	0.5	0.2	<DL	<DL	0.8	<DL	<DL	0.3	0.001	0.02	17	1,090	2.5	2.2	1.7	<DL	14	0.3	52	0.04	0.01	0.004	5.7	0.03	1.1	58	0.04	1.3	0.05	62	3.5	0.01
		C4, T153, WCG4, WW1	0.4	27	35	0.3	0.1	0.2	226	604	12	22	7	0.6	0.1	0.9	1	0.5	0.05	0.001	2	<DL	<DL	0.7	0.01	<DL	47	2,688	3	2	2	<DL	20	0.02	786	0.3	0.02	0.003	9	0.06	<DL	328	0.1	1	0.03	23	<DL	0.3
	Lower Precipice Sandstone	WM1	0.08	0.002	<DL	0.02	0.01	0.04	2.7	9.9	0.2	1.1	0.1	0.01	0.02	0.01	0.03	0.2	<DL	<DL	0.09	<DL	<DL	0.05	<DL	<DL	<DL	51	0.6	1.1	3.4	<DL	2.4	0.01	21	0.01	<DL	0.01	3.3	0.03	<DL	32	0.004	0.3	0.02	9.2	5.0	<DL
		C4, T153, WCG4, WW1	<DL	10	12	0.1	0.02	0.02	7	14	0.5	3	0.7	0.08	0.04	0.1	0.09	0.8	0.03	<DL	0.6	<DL	<DL	0.4	0.02	0.01	0.6	89	1	2	9	<DL	5	0.003	547	0.06	0.006	0.04	3	0.02	<DL	148	0.01	0.6	0.02	1	<DL	<DL
	Moolayember Formation	WM1	0.4	11	<DL	0.4	0.2	0.4	504	431	15	21	2.9	0.3	0.04	1.1	0.7	0.1	<DL	<DL	2.4	<DL	<DL	0.7	0.00	<DL	58	4,197	4.4	4.7	4.2	<DL	13	0.4	134	0.06	0.01	<DL	11	0.2	1.3	171	0.07	1.1	0.1	76	14	0.04
		WCG4, WW1	0.5	33	15	0.5	0.3	0.1	185	856	3	3	10	0.3	0.03	2	3	0.4	0.03	<DL	3	<DL	0.04	1	0.03	0.005	36	1,511	4	5	10	<DL	11	0.008	460	0.04	0.006	<DL	7	0.1	<DL	185	0.2	1	0.06	190	0.3	0.4

Legend	Major	Minor	Trace	Ultra-Trace	1,000 - 100,00	100 - 1,000	10 - 100	< 10

Table A10: Cumulative weak-acid extraction of elements (percentage of total amount in rock powder).

			Element Set	Alkali metals					Alkaline earth metals					Lanthanoids	Actinoids	Transition metals																							Post transition metals							Metalloids					Nonmetals		
			Element Group	1					2					3	3	4			5		6			7	8	9	10	11		12			13				14		15	13	14		15		15	16	
Unit			Depth (m)	Li	Na	K	Rb	Cs	Be	Mg	Ca	Sr	Ba	REE	Th	U	Sc	Y	Ti	Zr	Hf	V	Nb	Ta	Cr	Mo	W	Mn	Fe	Co	Ni	Cu	Ag	Zn	Cd	Al	Ga	Tl	Sn	Pb	Bi	B	Si	Ge	As	Sb	P	S	Se
Lower Evergreen Formation			2235.81-2235.94	1.0	0.1	<DL	0.3	2.2	11.5	6.5	30.0	9.9	4.2	0.2	0.9	1.9	2.6	0.6	0.0	<DL	<DL	0.8	<DL	<DL	0.4	9.9	1.6	29.9	21.7	48.7	48.7	22.2	<DL	37.0	45.3	0.1	0.2	3.0	<DL	48.5	65.4	1.0	0.0	1.5	17.4	8.1	<DL	4.1	4.3
			2242.25	1.1	<DL	<DL	0.5	2.4	11.4	0.7	32.2	13.9	6.6	0.2	0.6	1.4	2.3	0.4	0.0	<DL	<DL	0.2	<DL	<DL	0.2	<DL	0.1	2.0	1.8	42.3	30.5	20.5	<DL	31.2	19.7	0.1	0.1	7.6	<DL	57.8	60.8	4.1	0.1	0.5	24.0	8.9	<DL	5.2	0.9
			2242.44-2242.54	1.9	0.9	<DL	1.3	4.9	9.1	1.2	38.5	22.1	10.8	0.4	0.8	1.2	2.0	0.6	0.0	<DL	<DL	0.2	<DL	<DL	0.5	2.4	<DL	<DL	1.5	63.9	52.4	21.7	<DL	20.9	35.8	0.3	0.1	11.3	<DL	43.2	68.7	2.8	0.2	1.0	20.3	9.6	1.5	11.9	4.2
Upper Precipice Sandstone			2246.14-2246.25	0.8	0.1	<DL	0.1	0.7	8.3	11.7	36.8	2.8	1.0	1.0	1.8	1.3	6.3	2.2	0.0	<DL	<DL	1.3	<DL	<DL	1.2	<DL	<DL	37.0	25.3	18.2	21.7	47.3	<DL	20.4	100	0.1	0.2	0.9	0.4	38.6	31.7	<DL	0.0	3.1	30.1	15.9	<DL	0.7	<DL
			2254.94-2255.10	1.7	0.1	<DL	0.2	2.3	24.3	9.0	29.5	5.0	1.4	2.5	2.8	2.9	12.0	5.7	0.0	<DL	<DL	3.3	<DL	<DL	2.5	0.7	2.2	16.4	15.1	37.2	35.6	7.3	<DL	29.0	94.9	0.1	0.5	2.7	0.0	38.9	59.9	29.5	0.0	3.8	29.2	16.1	51.1	1.2	3.1
Lower Precipice Sandstone D			2263.61-2263.77	0.3	0.0	<DL	0.1	0.3	6.7	1.4	26.8	1.0	0.5	0.9	2.9	1.6	1.3	1.0	0.0	<DL	<DL	0.5	<DL	<DL	0.4	<DL	<DL	<DL	4.9	16.2	19.6	48.6	<DL	11.2	2.4	0.1	0.2	0.3	3.8	35.5	34.8	<DL	0.0	1.9	29.2	8.1	WR<DL	9.8	<DL
			2267.71-2267.84	0.1	<DL	<DL	0.0	1.2	11.1	0.6	20.6	8.2	10.9	0.2	0.6	1.1	1.2	0.4	0.0	0.0	<DL	0.2	<DL	0.0	0.3	1.5	<DL	5.0	1.8	37.9	37.5	17.3	<DL	6.8	13.3	0.4	0.1	<DL	0.1	40.6	38.6	5.6	0.1	0.3	11.5	0.4	<DL	1.1	2.0
			2267.84-2267.90	0.2	<DL	<DL	0.2	0.7	19.1	0.1	<DL	0.4	0.2	0.1	0.6	1.4	1.8	0.3	0.0	0.0	<DL	0.4	<DL	0.0	0.4	0.1	<DL	<DL	1.0	31.6	29.9	36.4	<DL	13.1	22.9	0.1	0.1	1.6	0.2	39.1	59.9	9.8	0.0	0.2	31.6	3.6	<DL	<DL	1.4
Lower Precipice Sandstone C			2274.10-2274.18	0.3	0.0	<DL	0.1	0.4	9.2	1.3	10.4	0.7	0.6	0.7	1.2	1.9	0.6	1.3	0.0	<DL	<DL	0.4	<DL	<DL	0.4	<DL	8.1	3.2	2.8	16.9	14.2	55.2	<DL	9.8	4.4	0.1	0.3	0.3	4.4	27.9	69.4	5.4	0.0	0.9	29.8	17.9	31.8	3.8	<DL
			2281.82-2281.92	0.6	<DL	<DL	0.2	1.1	10.7	0.5	16.5	3.4	2.2	0.1	0.1	0.9	0.2	0.1	0.0	<DL	<DL	0.2	<DL	<DL	0.1	4.5	<DL	<DL	0.9	26.4	28.8	17.6	<DL	15.3	3.1	0.1	0.1	0.7	<DL	29.7	37.0	<DL	0.0	0.2	20.7	9.3	12.1	3.3	0.9
			2284.13-2284.24	1.3	0.0	<DL	0.2	0.8	14.8	0.5	13.4	0.8	2.3	0.2	<DL	1.7	0.2	0.3	0.0	<DL	<DL	0.4	<DL	<DL	0.3	17.3	<DL	<DL	1.5	20.9	27.2	10.8	<DL	14.2	7.9	0.1	0.1	<DL	0.5	63.1	22.6	<DL	0.0	0.8	43.3	10.5	WR<DL	6.2	<DL
			2285.05	1.3	<DL	<DL	0.8	3.2	20.5	0.7	25.9	11.6	7.4	0.1	0.4	1.5	1.3	0.3	0.0	<DL	<DL	0.2	<DL	<DL	0.3	2.0	<DL	<DL	1.2	49.4	45.5	11.6	<DL	19.0	24.8	0.2	0.1	6.0	<DL	50.9	57.0	1.2	0.1	0.4	25.0	10.4	<DL	3.7	2.2
			2288.49-2288.61	0.2	<DL	<DL	0.1	0.5	11.5	0.5	6.2	0.8	1.1	0.2	<DL	1.1	0.2	0.2	0.0	<DL	<DL	0.4	<DL	<DL	0.3	<DL	<DL	<DL	0.8	32.1	31.8	60.8	<DL	9.6	2.9	0.1	0.1	<DL	3.2	44.5	48.3	<DL	0.0	0.9	45.2	8.0	13.3	4.9	<DL
			2294	2.1	<DL	<DL	<DL	<DL	3.3	0.9	3.0	0.6	1.0	0.1	0.1	2.1	0.0	0.1	0.0	<DL	<DL	0.7	<DL	<DL	0.3	20.9	1.3	<DL	2.4	22.9	12.1	15.0	<DL	7.7	0.2	<DL	0.1	<DL	<DL	32.5	32.7	<DL	<DL	0.5	14.2	8.9	WR<DL	5.3	<DL
			2296.97-2297.13	0.3	<DL	<DL	<DL	0.0	7.4	3.4	2.1	0.0	1.8	0.1	0.2	1.7	1.6	0.5	0.0	0.0	<DL	0.6	0.0	0.0	0.5	<DL	0.1	22.5	17.8	<DL	1.4	40.4	<DL	14.3	13.9	0.2	0.1	3.1	0.9	30.5	65.7	9.6	0.0	0.1	2.2	<DL	<DL	14.7	0.4
Lower Precipice Sandstone B			2297.13-2297.19	0.2	<DL	<DL	<DL	1.9	9.5	0.1	<DL	0.7	4.2	0.1	0.3	1.0	1.1	0.2	0.0	0.0	<DL	0.1	<DL	0.0	0.2	<DL	<DL	1.1	1.2	18.7	10.1	16.1	<DL	6.7	10.3	0.2	0.0	<DL	0.1	27.2	32.0	2.7	0.1	0.2	18.4	5.1	<DL	0.1	0.7
			2298.92	1.3	<DL	<DL	0.1	0.5	5.3	0.8	2.1	1.1	1.3	0.1	<DL	2.2	0.1	0.3	0.0	<DL	<DL	0.5	<DL	<DL	0.3	8.8	<DL	<DL	1.7	18.6	10.7	15.7	<DL	19.8	0.9	0.0	0.1	<DL	<DL	33.7	33.9	<DL	0.0	0.6	14.6	6.1	4.5	2.5	<DL
Lower Precipice Sandstone A		2	2307.2	1.1	0.1	<DL	0.8	2.0	11.8	7.0	11.8	4.1	6.7	0.9	0.5	2.8	0.8	1.8	0.1	<DL	<DL	2.4	<DL	<DL	2.3	4.1	<DL	12.6	10.3	27.1	21.3	14.8	<DL	24.4	3.2	1.1	0.7	3.7	3.2	32.6	55.7	<DL	0.0	1.8	20.9	8.0	WR<DL	<DL	<DL
			2315.77	0.8	<DL	<DL	<DL	<DL	7.4	2.0	6.8	1.7	1.5	0.3	<DL	1.1	0.2	0.9	0.0	<DL	<DL	1.1	<DL	<DL	2.2	<DL	<DL	<DL	11.8	32.1	18.7	28.4	<DL	25.1	8.3	<DL	0.2	<DL	<DL	19.0	30.7	46.1	0.0	3.3	23.2	15.8	WR<DL	0.9	<DL
			2322.61-2322.73	2.7	0.3	<DL	0.3	0.7	5.2	4.5	8.4	1.2	3.0	0.3	0.3	1.8	0.2	0.6	0.0	<DL	<DL	1.1	<DL	<DL	0.6	<DL	<DL	14.8	13.6	24.7	22.3	66.1	<DL	19.2	1.2	0.2	0.3	<DL	14.1	33.9	41.6	<DL	0.0	1.1	16.6	5.1	WR<DL	13.7	<DL
			2323.25	2.7	0.0	<DL	<DL	<DL	<DL	4.6	9.7	1.9	2.5	0.3	<DL	1.5	0.3	0.9	0.0	<DL	<DL	1.0	<DL	<DL	1.6	<DL	<DL	6.4	8.3	24.9	11.2	30.3	<DL	25.3	5.6	0.0	0.2	<DL	<DL	19.8	<DL	<DL	0.0	2.1	13.9	6.0	0.5	26.7	<DL
		1	2328.54-2328.59	1.4	0.6	<DL	1.1	3.9	13.8	1.3	36.6	7.8	7.1	0.1	0.2	1.6	1.4	0.3	0.0	<DL	<DL	0.3	<DL	<DL	0.3	0.9	<DL	<DL	0.9	35.8	25.5	31.9	<DL	13.2	23.1	0.2	0.1	5.2	0.2	27.4	59.8	3.1	0.1	0.5	15.9	16.0	18.2	9.2	1.5
			2328.59-2328.68	1.2	0.3	<DL	0.4	1.3	11.7	0.9	23.2	1.0	1.7	0.1	0.3	3.0	0.5	0.3	0.0	<DL	<DL	0.7	<DL	<DL	0.7	<DL	0.4	<DL	1.2	28.9	25.3	49.4	<DL	21.6	83.5	0.1	0.2	<DL	0.6	42.2	42.5	6.4	0.0	1.2	15.1	9.4	100	<DL	0.4
			2330.41-2330.54	0.4	0.1	<DL	0.2	0.5	4.5	2.4	17.6	0.7	1.4	0.2	<DL	1.8	0.2	0.4	0.0	<DL	<DL	0.7	<DL	<DL	0.5	<DL	4.9	<DL	1.7	17.4	23.5	60.2	<DL	6.1	2.1	0.0	0.2	<DL	22.0	27.1	46.0	<DL	0.0	1.7	20.0	4.3	22.5	9.6	<DL
			2338.75-2338.85	2.0	0.2	<DL	0.5	1.1	10.7	1.8	13.2	0.9	2.2	0.3	0.2	2.7	0.3	0.4	0.0	<DL	<DL	0.8	<DL	<DL	0.4	<DL	<DL	<DL	1.5	17.4	12.5	68.7	<DL	25.7	4.5	0.1	0.2	<DL	4.5	38.0	69.2	<DL	0.0	1.3	19.3	8.5	2.9	3.2	<DL
Moolayember Formation			2339.00-2339.17	1.0	0.4	<DL	0.6	4.9	22.6	1.2	30.5	6.3	10.7	0.1	0.4	1.5	1.6	0.3	0.0	<DL	<DL	0.3	<DL	<DL	0.4	0.6	<DL	<DL	2.9	38.0	33.9	40.1	<DL	30.9	57.8	0.2	0.2	5.9	<DL	78.2	69.2	<DL	0.0	0.5	43.8	15.6	<DL	5.8	4.3
			2340.54-2340.62	2.1	1.3	<DL	1.3	5.0	19.6	11.3	41.9	29.0	12.7	0.5	0.8	1.1	8.9	0.7	0.0	<DL	<DL	3.6	<DL	<DL	2.0	<DL	<DL	36.2	27.4	13.3	17.8	35.9	<DL	27.9	54.8	0.3	0.2	2.1	<DL	55.5	60.7	4.7	0.1	5.3	15.6	8.1	<DL	0.9	6.7
			2346.40-2346.51	1.4	0.7	<DL	0.4	5.2	18.9	13.8	21.4	20.4	5.4	1.1	1.5	1.2	6.3	1.3	0.0	<DL	<DL	3.5	<DL	<DL	2.8	11.0	38.5	22.6	20.6	55.5	48.0	25.8	<DL	20.7	51.8	0.2	0.2	1.7	<DL	50.2	64.1	1.1	0.1	3.7	38.3	20.2	21.0	5.0	4.6
			2348.16-2348.30	1.1	0.5	<DL	0.2	2.7	17.6	12.2	39.6	10.4	2.6	2.5	2.8	1.5	7.6	5.0	0.0	<DL	<DL	2.8	<DL	<DL	2.4	3.2	<DL	8.6	6.7	36.3	25.8	22.9	<DL	13.7	55.8	0.1	0.5	1.6	<DL	48.7	57.9	10.0	0.0	4.3	4.0	12.0	9.2	1.1	3.0
			2356.94-2357.06	1.3	0.5	<DL	0.3	4.3	19.1	15.7	24.8	14.4	3.8	2.7	3.5	1.5	8.9	3.6	0.0	<DL	<DL	4.5	<DL	<DL	3.1	<DL	<DL	23.5	22.3	28.8	24.2	27.9	<DL	15.1	84.2	0.1	0.4	0.0	<DL	57.0	58.4	7.9	0.0	7.2	21.7	6.6	12.1	7.4	6.3
			2362.90-2363.00	1.9	0.9	0.2	1.2	7.6	19.7	7.6	36.2	37.9	11.6	0.5	1.3	0.9	7.7	0.9	0.0	<DL	<DL	2.5	<DL	<DL	1.5	0.6	<DL	15.5	17.2	50.1	27.8	33.1	<DL	13.6	50.5	0.3	0.1	2.3	<DL	46.3	61.3	6.6	0.1	2.7	11.3	10.4	<DL	6.2	6.1
			2366.50-2366.61	2.3	0.4	<DL	0.7	7.3	16.9	9.0	24.1	28.2	9.0	3.3	2.3	1.5	9.2	5.0	0.0	<DL	<DL	4.0	<DL	<DL	2.3	1.5	<DL	13.6	15.8	28.1	17.7	27.6	<DL	13.0	55.6	0.3	0.5	1.2	<DL	47.2	57.9	4.8	0.1	6.3	12.6	6.0	8.1	4.1	10.5
			2373.89-2373.99	1.7	0.1	<DL	0.2	2.5	15.1	11.5	36.5	11.3	2.4	4.5	2.9	1.2	13.3	7.5	0.0	<DL	<DL	3.9	<DL	<DL	3.3	<DL	<DL	19.3	18.5	30.6	23.6	19.7	<DL	10.1	100	0.2	0.6	0.2	<DL	47.8	60.8	0.2	0.0	7.6	30.6	10.1	36.7	19.6	7.9
			2427.52-2427.74	2.0	0.2	<DL	0.1	1.4	12.2	11.2	58.6	60.2	1.8	20.8	5.0	1.0	23.8	42.1	0.0	<DL	<DL	4.0	<DL	<DL	3.3	6.3	1.1	52.3	20.7	52.4	41.4	22.1	<DL	14.4	100	0.2	3.4	1.8	0.2	32.6	50.6	19.0	0.0	19.7	55.5	23.3	53.4	54.9	27.4
Unit Medians	Upper Precipice Sandstone		WM1	1.2	0.1	<DL	0.1	1.5	16.3	10.4	33.2	3.9	1.2	1.8	2.3	2.1	9.2	4.0	0.0	<DL	<DL	2.3	<DL	<DL	1.9	0.4	1.1	26.7	20.2	27.7	28.6	27.3	<DL	24.7	100	0.1	0.3	1.8	0.2	38.8	45.8	14.7	0.0	3.4	29.6	16.0	25.5	0.9	1.6
			C4, T153, WCG4, WW1	2	2	0.4	1	6	25	10	32	10	5	3	5	4	8	3	0.009	0.03	0.02	3	<DL	<DL	2	2	<DL	16	12	23	14	25	<DL	26	6	0.7	2	5	0.1	47	50	<DL	0.1	7	29	9	6	<DL	22
	Lower Precipice Sandstone		WM1	0.9	0.0	<DL	0.2	0.7	10.1	1.1	11.1	1.0	2.0	0.2	0.2	1.6	0.4	0.3	0.0	<DL	<DL	0.5	<DL	<DL	0.4	<DL	<DL	1.7	24.8	21.8	31.1	<DL	14.2	5.0	0.1	0.1	<DL	0.3	33.2	42.0	<DL	0.0	0.8	19.6	8.1	<DL	3.7	<DL
			C4, T153, WCG4, WW1	<DL	2	1	1	3	4	3	5	4	8	2	2	2	4	2	0.1	0.04	<DL	4	<DL	<DL	4	8	<DL	3	10	37	15	42	<DL	25	2	3	2	5	1	38	28	<DL	0.0	3	1	7	<DL	<DL	<DL
	Moolayember Formation		WM1	1.7	0.5	<DL	0.4	4.9	18.9	11.3	36.2	20.4	5.4	2.5	2.3	1.2	8.9	3.6	0.0	<DL	<DL	3.6	<DL	<DL	2.4	0.6	<DL	19.3	18.5	36.3	25.8	27.6	<DL	14.4	55.8	0.2	0.4	1.7	<DL	48.7	60.7	4.8	0.0	5.3	21.7	10.4	9.2	5.8	6.3
			WCG4, WW1	1	4	0.2	0.7	4	14	4	18	3	2	8	4	2	8	11	0.008	0.03	<DL	2	<DL	<DL	2	3	<DL	5	4	25	20	29	<DL	12	3	0.5	0.4	2	<DL	39	43	<DL	0.1	9	13	20	<DL	0.2	13

Legend	Major	Minor	Trace	Ultra-Trace	> 75	50 – 75	25 – 50	5 – 25	< 5

(0.0 indicates < 0.05 %).

Comparison between element extraction during batch and sequential experiments

This is an attempt to directly compare blank-corrected element extraction from the same sample intervals during each incremental batch reaction sampling step with total sequential element extraction (all three steps). Averaged nitrogen-step water chemistry for blank batch reactor experiments with the chosen artificial formation water composition (but no rock samples) has been subtracted from incremental batch reactor sample experiments, to help negate the background contribution of elements from reactors as well as the initial water chemistry. Then water chemistry was converted to mass of elements extracted per mass of rock sample reacted, which involved estimating the total fluid volume remaining within Parr reactors just prior to each incremental fluid sample being taken. Batch reactor element extraction was then divided by blank-corrected total sequential element extraction (the sum of the three steps).

Differences in reactive surface area and fluid rock ratio have not been accounted for, however, which could help to account for why there was comparatively much lower extraction of several elements (Tables A11, A12, A13, A14) during the batch reactor experiments with intact rock samples as opposed to powders used for sequential extractions. Another factor is the precipitation of iron phase/s during batch reactions, that may both directly incorporate other elements like Mn and provide adsorption sites for a host of other elements. Some elements had greater apparent extraction during batch reactor experiments through. Sodium (Na) and tungsten (W) extraction was persistently higher. For Na, this could be due to ion exchange from clays because of fluid-rock disequilibrium. Whereas elevated W could be due to either an additional contribution from Parr reactors not captured by the blank experiments, or else rocks are simply more likely to release W during the batch reactor conditions than during sequential extractions. Most (but not all) batch reactor experiment incremental analyses found greater apparent extraction of Ca, Cr, K, Li, Mg, Mn, Mo, and S. The Ca, Mg, and Mn, probably mostly come from carbonate mineral dissolution. The Li and K could have come from cation exchange and/or, together with Cr, from aluminosilicate dissolution. The Mo and S could be from a variety of sources, which for S includes the gas mix used in most experiments. Some batch reactor experiments also had comparatively more extraction of Al, B, Cd, Co, Cu, Ni, Se, Si, Tl, and Zn than sequential extractions. There was more Mg extraction into the fluid phase during three of the CO_2-only experiments compared with mixed gas experiments, probably due to differences in amounts of Mg-phase/s precipitation, whereas more Cu, Cr, Mn, Ni, S (as expected), and Si were extracted during mixed-gas experiments.

Table A11: Blank-corrected batch reaction incremental element extraction normalised to total sequential element extraction for selected elements[1], uppermost units.

		Element Set		Alkali metals					Alkaline earth metals		Actinoids	Transition metals											Post transition metals		Metalloids			Nonmetals	
		Element Group		1					2		3	3	5	6			7	8	9	10	11	12	13		13	14		16	
Unit	Core Depth (mRT)	Gas	Day #	Li	Na	K	Rb	Cs	Mg	Ca	U	Sc	Nb	Cr	Mo	W	Mn	Fe	Co	Ni	Cu	Zn	Cd	Al	Tl	B	Si	Ge	S	Se
Lower Evergreen Formation	2242.44-2242.54	N_2 (1st)	0	0.8	14	1.3	0.2	0.1	0.1	0.1	0.0	0.0	SE<DL	0.5	1.7	11	SE<DL	0.0	0.0	0.0	0.1	0.0	0.0	0.0	0.1	0.2	0.1	0.1	1.0	0.1
		Mixed (1st)	7	1.3	12	1.2	0.2	0.1	0.2	0.1	0.0	0.0	SE<DL	1.5	0.5	11	SE<DL	0.1	0.0	0.1	0.1	0.0	0.0	0.0	0.2	0.3	0.2	0.3	1.4	0.1
			21	1.8	12	1.3	0.2	0.1	0.3	0.2	0.0	0.0	SE<DL	0.6	0.2	0.8	SE<DL	0.0	0.0	0.5	0.0	0.0	0.0	0.0	0.2	0.4	0.2	0.6	1.3	0.1
			28	1.2	8.8	1.0	0.2	0.1	0.2	0.1	0.0	0.0	SE<DL	6.7	4.6	31	SE<DL	0.1	0.0	0.2	0.2	0.1	0.0	0.0	0.1	0.4	0.2	0.3	1.0	0.1
		N_2 (2nd)	0	0.5	13	1.0	0.2	0.1	0.3	0.2	0.0	0.0	SE<DL	0.3	1.0	8.2	SE<DL	0.0	0.0	0.0	0.0	0.0	0.0	BR<DL	0.1	0.1	0.0	0.1	0.9	0.0
		Mixed (2nd)	20	1.2	9.4	0.8	0.2	0.1	0.5	0.2	0.0	0.0	SE<DL	1.0	0.1	11	SE<DL	0.0	0.0	0.5	0.1	0.0	0.0	0.0	0.1	0.2	0.2	0.3	1.2	0.0
			55	1.9	12	1.2	0.3	0.1	0.9	0.4	0.0	0.0	SE<DL	0.5	0.3	5.7	SE<DL	0.0	0.0	0.1	0.0	0.0	0.0	0.0	0.2	0.2	0.3	0.5	1.2	0.0
			62	1.9	11	1.1	0.3	0.1	0.9	0.3	0.0	0.0	SE<DL	0.4	0.3	5.5	SE<DL	0.0	0.0	0.0	0.0	0.0	0.0	0.0	0.2	0.2	0.3	0.6	1.1	0.0
Upper Precipice Sandstone	2254.94-2255.10	N_2	0	2.1	43	2.3	0.5	0.4	1.3	0.6	0.0	0.0	SE<DL	2.7	9.6	60	0.4	0.0	0.1	0.5	0.8	0.1	0.0	0.0	1.0	0.1	1.0	0.0	2.8	0.3
		CO_2	1	2.4	47	2.5	0.5	0.4	1.5	0.7	0.0	0.0	SE<DL	0.2	7.6	40	0.5	0.0	0.2	1.3	1.3	0.1	0.1	0.0	1.0	0.1	1.1	BR<DL	2.9	0.3
			3	2.2	42	2.2	0.5	0.4	1.5	0.6	0.0	0.0	SE<DL	0.2	11	99	0.5	0.0	0.2	0.6	0.8	0.1	0.0	0.0	0.8	0.1	1.1	BR<DL	2.6	0.2
			5	2.4	41	2.2	0.5	0.4	1.5	0.7	0.0	0.0	SE<DL	0.3	7.7	85	0.7	0.0	0.2	0.5	0.7	0.2	0.0	0.0	0.9	0.1	1.2	BR<DL	2.6	0.2
			9	2.8	36	1.9	0.5	0.4	1.6	0.7	0.0	0.0	SE<DL	0.2	3.8	46	0.8	0.0	0.3	1.0	0.5	0.2	0.0	0.0	0.9	0.1	1.3	0.0	2.4	0.2
			21	2.9	34	1.9	0.5	0.4	1.8	0.8	0.0	0.0	SE<DL	0.2	3.9	60	1.1	0.0	0.2	0.4	0.5	0.3	0.0	0.0	0.9	0.1	1.8	0.0	2.7	0.1
			25	2.9	31	1.8	0.5	0.4	1.8	0.8	0.0	0.0	SE<DL	0.1	-0.6	9.1	1.2	0.0	0.3	0.7	0.4	0.3	0.0	0.0	0.9	0.1	1.9	0.0	2.5	0.1
			30	2.7	28	1.7	0.5	0.3	1.7	0.7	0.0	0.0	SE<DL	0.1	0.0	10	1.1	0.0	0.2	0.6	0.3	0.3	0.0	0.0	0.8	0.1	1.8	0.0	2.6	0.1
		N_2	0	1.8	85	6.0	0.6	0.5	0.9	1.0	0.0	BR<DL	ALL<DL	2.1	7.6	51	1.0	0.0	0.2	0.9	2.5	0.1	0.2	0.0	1.0	BR<DL	1.0	BR<DL	4.2	BR<DL
		Mixed	7	2.1	70	4.8	0.4	0.4	1.4	1.0	0.1	0.0	ALL<DL	4.9	171	273	1.5	0.0	0.3	1.6	3.1	0.3	0.1	0.0	0.7	BR<DL	1.8	BR<DL	3.6	BR<DL
			14	1.9	69	4.6	0.5	0.3	1.4	1.0	0.1	0.0	ALL<DL	3.9	168	257	1.2	0.0	0.2	1.0	2.9	0.3	0.0	0.0	0.6	BR<DL	1.7	BR<DL	3.2	BR<DL
			21	2.0	52	3.7	0.5	0.4	1.3	0.9	0.0	0.0	ALL<DL	2.3	81	154	1.1	0.0	0.3	0.7	1.8	0.3	0.1	BR<DL	0.7	BR<DL	1.5	BR<DL	2.6	BR<DL
			42	2.0	61	4.3	0.5	0.4	1.7	1.2	0.0	0.0	ALL<DL	2.5	32	12	2.1	0.0	0.3	3.0	0.7	0.4	0.1	0.0	0.7	BR<DL	2.3	BR<DL	3.0	BR<DL
			71	2.8	68	4.9	0.7	0.4	2.4	1.4	0.1	0.0	ALL<DL	2.6	46	213	2.3	0.0	0.3	0.4	2.0	0.4	0.0	0.0	1.0	BR<DL	3.3	BR<DL	4.0	BR<DL
			84	2.8	64	4.8	0.6	0.4	2.3	1.3	0.1	0.0	ALL<DL	2.4	47	276	2.1	0.0	0.3	0.5	1.4	0.4	0.0	0.0	0.9	BR<DL	3.2	BR<DL	3.7	BR<DL
			105	3.5	68	5.3	0.8	0.4	2.5	1.6	0.1	0.0	ALL<DL	2.3	27	174	2.6	0.0	0.4	0.8	6.4	0.5	0.1	0.0	1.1	BR<DL	3.9	0.1	4.3	BR<DL
Lower Precipice Sandstone D	2263.61-2263.77	N_2	0	2.8	209	1.6	0.4	0.6	17	4.5	0.2	0.1	SE<DL	49.1	38	SE<DL	2.6	2.8	0.6	0.7	1.9	0.8	13	0.2	0.6	SE<DL	0.9	1.2	1.7	0.9
		CO_2	1	7.4	209	1.6	0.4	0.6	17	4.4	0.1	0.0	SE<DL	6.2	83	SE<DL	3.0	0.0	0.6	1.0	1.2	0.6	25	0.0	0.6	SE<DL	0.8	BR<DL	1.6	1.9
			3	1.7	208	1.5	0.4	0.6	16	3.8	0.2	0.1	SE<DL	2.4	217	SE<DL	1.9	0.0	0.6	0.4	1.1	0.7	12	0.0	0.5	SE<DL	0.7	BR<DL	1.6	1.1
			5	4.0	182	1.3	0.3	0.6	15	3.9	0.1	0.1	SE<DL	2.4	63	SE<DL	2.7	0.0	0.6	0.6	1.0	0.7	8.2	0.0	0.5	SE<DL	0.7	BR<DL	1.4	0.7
			9	1.8	175	1.3	0.3	0.6	15	3.7	0.1	0.1	SE<DL	1.6	122	SE<DL	3.0	0.0	0.6	0.5	0.9	0.7	5.4	0.0	0.5	SE<DL	0.8	BR<DL	1.4	0.8
			21	3.1	157	1.2	0.3	0.5	14	3.4	0.1	0.2	SE<DL	2.1	13	SE<DL	4.5	0.0	0.6	1.0	0.9	0.8	8.9	0.0	0.5	SE<DL	1.0	BR<DL	1.3	0.8
			25	1.5	143	1.1	0.3	0.5	12	3.0	0.1	0.1	SE<DL	1.2	45	SE<DL	3.5	0.0	0.5	0.4	0.7	0.7	4.6	0.0	0.4	SE<DL	1.0	BR<DL	1.2	0.9
			30	1.7	139	1.1	0.3	0.5	12	3.0	0.1	0.2	SE<DL	1.0	10	SE<DL	4.1	0.0	0.5	0.4	0.7	0.8	3.9	0.0	0.5	SE<DL	1.0	BR<DL	1.2	0.3
		N_2	0	2.8	177	1.6	0.3	0.6	2.4	1.6	0.1	0.1	ALL<DL	4.7	57	SE<DL	3.8	0.3	0.4	1.5	1.4	0.3	0.2	0.1	0.7	SE<DL	1.1	0.3	2.3	1.7
		Mixed	6	3.1	164	1.5	0.4	0.7	2.9	1.6	0.2	0.2	ALL<DL	16	39	SE<DL	9.9	0.1	0.6	1.8	2.2	0.7	9.3	0.0	0.7	SE<DL	1.4	0.4	3.6	1.4
			21	2.0	143	1.4	0.4	0.6	3.5	4.3	0.2	0.1	SE<DL	20	256	SE<DL	23	0.0	0.4	0.5	0.4	0.4	15	0.0	0.5	SE<DL	1.0	0.1	5.1	2.1
			41	4.6	157	1.5	0.6	0.7	2.9	1.6	0.3	0.5	ALL<DL	4.0	38	SE<DL	3.8	0.0	0.6	0.4	2.4	0.7	-0.1	0.1	0.8	SE<DL	2.9	0.5	2.5	2.8
			55	3.5	128	1.3	0.5	0.6	2.5	1.4	0.2	0.4	ALL<DL	4.0	20	SE<DL	3.7	0.0	0.5	1.8	2.5	0.6	0.1	0.0	0.7	SE<DL	2.8	0.4	2.2	2.4
			62	3.4	132	1.3	0.6	0.7	2.5	1.4	0.3	0.4	SE<DL	7.2	39	SE<DL	4.9	0.0	0.6	4.0	2.6	1.0	3.1	0.0	0.7	SE<DL	2.7	0.3	2.2	1.9
			97	3.5	118	1.2	0.6	0.6	2.3	1.3	0.2	0.4	SE<DL	3.5	28	SE<DL	4.5	0.0	0.6	5.1	2.5	0.7	1.8	0.0	0.7	SE<DL	2.9	0.3	2.0	2.4

Colour Legend	Major	Minor	Trace	Ultra-Trace	>10x	2x – 10x	1.5x – 2x	1.1x – 1.5x	0.9x – 1.1x (BR approx. = SE)	0.5x – 0.9x	0.1x – 0.5x	-0.1x – 0.1x	< -0.1x (< average BR background)

1. Only elements with > 0.5x median apparent element extraction for one batch reactor cycle, compared with sequential extractions, are included here.

Table A12: Blank-corrected batch reaction incremental element extraction normalised to total sequential element extraction for selected elements[1], lower Precipice Sandstone C.

		Element Set		Alkali metals					Alkaline earth metals		Actinoids	Transition metals											Post transition metals		Metalloids			Nonmetals	
		Element Group		1					2		3	3	5	6			7	8	9	10	11	12	13		13	14		16	
Unit	Core Depth (mRT)	Gas	Day #	Li	Na	K	Rb	Cs	Mg	Ca	U	Sc	Nb	Cr	Mo	W	Mn	Fe	Co	Ni	Cu	Zn	Cd	Al	Tl	B	Si	Ge	S	Se
Lower Precipice Sandstone C	2274.10-2274.18	N_2	0	2.2	233	2.0	0.3	0.5	2.4	6.5	0.0	0.2	ALL<DL	3.1	52	4.3	1.3	0.1	0.3	0.5	0.3	0.2	142	BR<DL	0.6	0.4	0.9	BR<DL	2.4	3.3
		Mixed	6	2.3	257	2.1	0.4	0.6	3.6	7.2	0.1	0.4	ALL<DL	12	406	7.2	2.6	0.0	0.5	0.6	0.4	0.4	16	0.0	0.8	0.0	1.0	0.1	3.8	3.5
			21	4.4	216	1.8	0.5	0.6	3.2	2.2	0.2	1.0	ALL<DL	9.8	64	6.4	0.6	0.0	0.5	0.7	1.8	0.6	0.7	0.1	1.0	0.1	2.5	0.3	1.8	2.1
			41	2.3	235	2.0	0.4	0.7	4.5	7.0	0.2	0.6	SE<DL	15	587	21	4.3	0.0	0.5	0.5	0.3	0.8	15	0.0	1.0	0.1	1.5	0.1	4.1	3.6
			55	2.0	227	2.0	0.5	0.7	4.6	6.9	0.2	0.5	SE<DL	14	742	38	4.4	0.0	0.5	0.5	0.3	0.6	16	0.1	1.0	0.1	1.7	BR<DL	4.3	3.1
			62	2.1	237	2.1	0.5	0.7	4.7	7.3	0.2	0.6	SE<DL	17	304	70	4.9	0.0	0.5	0.6	0.4	0.9	14	0.0	1.1	0.1	1.8	0.1	4.6	4.5
			97	2.0	209	1.9	0.5	0.6	4.5	6.4	0.2	0.7	ALL<DL	19	608	31	4.5	0.0	0.5	0.6	2.3	0.8	14	0.1	1.2	0.1	2.0	0.1	4.7	4.2
	2284.13-2284.24	N_2	0	0.4	166	2.6	0.5	0.6	5.6	6.8	0.1	BR<DL	ALL<DL	9.3	13	SE<DL	SE<DL	0.2	0.6	0.8	0.8	0.2	20	BR<DL	1.2	ALL<DL	0.5	0.8	7.3	BR<DL
		Mixed	7	0.5	141	2.3	0.5	0.6	4.9	6.1	0.3	BR<DL	ALL<DL	14	18	SE<DL	SE<DL	0.1	0.8	0.8	1.9	0.5	11	0.0	1.2	ALL<DL	0.5	BR<DL	11	BR<DL
			14	0.8	134	2.2	0.5	0.7	4.7	5.5	0.3	BR<DL	ALL<DL	11	17	SE<DL	SE<DL	0.0	0.7	0.9	1.8	0.4	11	0.1	1.2	ALL<DL	0.6	BR<DL	7.8	BR<DL
			21	0.8	102	1.6	0.5	0.6	3.4	4.1	0.3	BR<DL	ALL<DL	11	17	SE<DL	SE<DL	0.0	0.7	0.9	1.8	0.5	9.1	0.0	BR<DL	ALL<DL	0.5	BR<DL	6.1	BR<DL
			42	0.4	99	1.6	0.3	0.5	3.5	4.0	0.3	BR<DL	ALL<DL	15	34	SE<DL	SE<DL	0.1	0.5	0.6	1.5	0.4	6.9	0.1	1.0	ALL<DL	0.6	BR<DL	6.8	BR<DL
			71	0.7	99	1.6	0.3	0.5	3.6	4.2	0.3	BR<DL	ALL<DL	22	37	SE<DL	SE<DL	0.2	0.5	0.7	1.6	0.5	7.4	0.1	1.0	ALL<DL	0.8	BR<DL	7.7	BR<DL
			84	0.8	108	1.8	0.4	0.5	3.9	4.4	0.4	1.2	ALL<DL	31	18	SE<DL	SE<DL	0.2	0.6	0.8	1.9	0.5	7.4	0.1	1.1	ALL<DL	0.9	BR<DL	8.7	BR<DL
			105	1.0	100	1.7	0.4	0.5	4.0	4.4	0.4	1.0	ALL<DL	31	15	SE<DL	SE<DL	0.2	0.6	0.9	1.9	0.5	7.6	0.2	1.2	ALL<DL	1.0	BR<DL	8.9	BR<DL
	2288.49-2288.61	N_2	0	3.8	335	1.9	0.7	1.1	55	10	0.3	0.4	SE<DL	107	28	SE<DL	SE<DL	14	0.9	1.2	2.1	1.8	8.2	0.1	1.1	SE<DL	1.3	0.9	8.1	1.3
		CO_2	1	5.2	297	1.7	0.7	0.9	50	9.4	0.2	0.5	SE<DL	8.1	30	SE<DL	SE<DL	0.5	0.9	1.1	1.8	2.0	5.5	0.0	1.0	SE<DL	1.8	0.2	7.4	1.2
			3	2.9	293	1.7	0.6	1.0	51	9.8	0.2	BR<DL	SE<DL	3.5	8.7	SE<DL	SE<DL	0.3	1.1	1.5	1.9	2.7	3.1	BR<DL	1.2	SE<DL	1.6	BR<DL	7.3	1.0
			5	2.1	271	1.4	0.6	1.0	43	7.6	0.3	0.5	SE<DL	17	80	SE<DL	SE<DL	0.2	0.9	0.8	1.3	1.5	0.1	0.0	0.9	SE<DL	1.1	BR<DL	7.1	1.3
			9	2.7	234	1.4	0.5	0.8	36	6.2	0.2	0.2	SE<DL	7.6	113	SE<DL	SE<DL	0.2	0.7	0.6	0.9	1.1	-1.8	0.0	0.8	SE<DL	1.1	0.0	6.1	1.2
			21	3.1	204	1.1	0.5	0.8	32	5.8	0.2	0.3	SE<DL	3.9	56	SE<DL	SE<DL	0.1	0.7	0.6	0.7	1.1	-0.6	0.0	0.8	SE<DL	1.2	0.1	5.6	1.2
			25	2.5	164	0.9	0.4	0.7	28	4.9	0.2	0.3	SE<DL	2.8	37	SE<DL	SE<DL	0.1	0.6	0.5	0.6	1.1	-0.9	0.0	0.8	SE<DL	1.0	BR<DL	4.4	0.9
			30	2.8	136	0.8	0.4	0.7	22	4.2	0.2	0.3	SE<DL	2.3	19	SE<DL	SE<DL	0.0	0.6	0.6	0.6	1.1	0.2	0.0	0.8	SE<DL	0.9	0.1	3.9	0.6
		N_2	0	1.9	314	1.8	0.7	0.9	8.2	4.1	0.1	0.6	SE<DL	10	-7.4	SE<DL	SE<DL	0.6	1.3	2.1	2.2	1.1	103	BR<DL	2.1	SE<DL	1.2	0.5	12	0.0
		Mixed	7	2.2	304	1.8	0.8	1.1	8.3	3.6	0.6	1.5	SE<DL	24	47	SE<DL	SE<DL	0.4	1.2	1.7	1.6	1.3	57	0.1	1.6	SE<DL	1.3	0.7	18	0.5
			21	2.3	273	1.6	0.7	1.1	7.5	3.4	0.7	1.0	SE<DL	13	66	SE<DL	SE<DL	0.3	1.1	1.3	1.5	1.5	24	0.2	1.9	SE<DL	1.4	0.9	15	0.7
			28	3.3	267	1.6	0.7	1.2	8.4	3.4	0.7	1.5	SE<DL	13	71	SE<DL	SE<DL	0.2	1.2	1.5	1.6	1.9	27	0.2	2.0	SE<DL	1.5	1.0	16	0.5
			49	3.6	245	1.4	0.7	1.1	7.1	3.1	0.8	1.5	SE<DL	17	107	SE<DL	SE<DL	0.3	1.1	1.4	1.6	1.9	27	0.3	2.2	SE<DL	1.7	0.8	16	1.1
			84	4.1	240	1.4	0.7	1.1	7.5	3.0	0.9	1.6	SE<DL	27	87	SE<DL	SE<DL	0.2	1.1	1.5	1.7	2.0	17	0.4	2.5	SE<DL	2.1	0.7	17	0.5
			91	4.3	231	1.4	0.7	1.1	6.8	2.9	0.8	1.6	SE<DL	24	64	SE<DL	SE<DL	0.2	1.1	1.6	1.6	2.0	21	0.4	2.6	SE<DL	2.1	0.9	16	0.6

Colour Legend	Major	Minor	Trace	Ultra-Trace	>10x	2x – 10x	1.5x – 2x	1.1x – 1.5x	0.9x – 1.1x (BR approx. = SE)	0.5x – 0.9x	0.1x – 0.5x	-0.1x – 0.1x	< -0.1x (< average BR background)

1. Only elements with > 0.5x median apparent element extraction for one batch reactor cycle, compared with sequential extractions, are included here.

Table A13: Blank-corrected batch reaction incremental element extraction normalised to total sequential element extraction for selected elements[1], lower Precipice Sandstone A.

		Element Set		Alkali metals					Alkaline earth metals		Actinoids	Transition metals												Post transition metals		Metalloids			Nonmetals	
		Element Group		1					2		3	3	5	6			7	8	9	10	11	12		13		13	14		16	
Unit	Core Depth (mRT)	Gas	Day #	Li	Na	K	Rb	Cs	Mg	Ca	U	Sc	Nb	Cr	Mo	W	Mn	Fe	Co	Ni	Cu	Zn	Cd	Al	Tl	B	Si	Ge	S	Se
Lower Precipice Sandstone A	2307.2	N_2	0	0.8	60	0.2	0.2	0.9	8.6	1.7	0.2	0.1	3.1	33	4.3	34	1.2	0.2	0.8	3.8	1.0	0.9	15	0.0	0.4	1.8	0.4	0.2	3.9	1.6
		CO_2	1	0.8	60	0.2	0.2	0.8	8.6	1.8	0.3	0.2	1.2	2.5	4.8	1850	1.3	0.0	1.0	4.1	1.3	1.2	38	0.0	0.7	1.7	0.4	0.0	3.8	2.7
			3	1.1	57	0.2	0.2	0.7	8.2	1.5	0.4	0.0	2.8	30	12	791	1.4	0.1	0.7	3.3	1.4	0.8	24	0.0	0.6	1.4	0.4	BR<DL	3.8	2.0
			5	1.8	53	0.2	0.2	0.7	7.3	1.4	0.3	0.2	0.5	2.2	9.0	944	1.5	0.0	0.6	1.7	1.3	0.6	11	0.0	0.5	1.4	0.4	BR<DL	3.7	2.2
			9	0.6	49	0.2	0.1	0.5	6.3	1.3	0.3	0.1	0.1	1.5	9.7	906	1.6	0.0	0.6	0.9	1.2	0.5	11	0.0	0.5	0.8	0.4	BR<DL	3.6	2.0
			21	0.7	43	0.2	0.2	0.5	6.3	1.2	0.3	0.2	0.4	1.4	9.7	1266	1.7	0.0	0.6	1.0	1.2	0.5	7.9	0.0	0.4	1.3	0.4	BR<DL	3.4	1.9
			25	0.5	41	0.2	0.2	0.5	6.0	1.1	0.2	0.2	0.4	0.9	3.2	152	1.6	0.0	0.6	0.9	1.3	0.5	11	0.0	0.3	1.4	0.4	BR<DL	3.0	1.4
			30	0.9	40	0.2	0.1	0.4	5.6	1.1	0.2	0.2	0.3	1.2	1.8	234	1.7	0.0	0.6	1.2	1.2	0.5	9.4	0.0	0.3	1.4	0.4	BR<DL	2.8	1.4
		N_2	0	0.2	74	0.5	0.2	0.5	1.5	2.1	0.2	BR<DL	BR<DL	7.8	3.0	-56.1	0.3	0.2	0.5	2.7	1.0	0.1	3.6	0.0	BR<DL	BR<DL	0.3	BR<DL	4.2	BR<DL
		Mixed	7	0.6	66	0.5	0.2	BR<DL	1.5	1.8	0.2	BR<DL	BR<DL	13	88	345	0.9	0.1	0.7	2.6	2.0	0.4	13	0.0	BR<DL	BR<DL	0.3	BR<DL	7.7	BR<DL
			14	0.2	61	0.4	0.2	BR<DL	1.4	1.6	0.2	BR<DL	BR<DL	11	92	741	1.1	0.1	0.7	3.4	1.9	0.5	11	0.1	BR<DL	BR<DL	0.4	BR<DL	5.0	BR<DL
			21	BR<DL	59	0.4	0.2	BR<DL	1.5	1.6	0.2	BR<DL	BR<DL	5.9	39	325	1.3	0.1	0.6	3.0	1.7	0.4	4.9	0.0	BR<DL	BR<DL	0.4	BR<DL	4.5	BR<DL
			42	BR<DL	52	0.4	0.1	BR<DL	1.3	1.3	0.2	BR<DL	BR<DL	10	141	1132	0.9	0.3	0.5	1.4	1.1	0.3	5.7	0.0	BR<DL	BR<DL	0.5	BR<DL	5.2	BR<DL
			71	BR<DL	65	0.5	0.2	0.5	1.7	1.8	0.2	BR<DL	BR<DL	12	111	1037	1.4	0.3	0.6	2.7	1.6	0.6	13	0.1	BR<DL	BR<DL	0.6	0.5	5.1	BR<DL
			84	BR<DL	47	0.3	0.1	BR<DL	1.3	1.4	0.2	BR<DL	BR<DL	9.3	57	474	1.1	0.2	0.5	2.5	1.2	0.5	6.7	0.1	BR<DL	BR<DL	0.5	BR<DL	3.9	BR<DL
			105	BR<DL	52	0.4	0.2	BR<DL	1.4	1.5	0.2	BR<DL	BR<DL	9.9	44	263	1.2	0.2	0.6	3.9	1.9	0.5	8.0	0.1	BR<DL	BR<DL	0.6	BR<DL	4.0	BR<DL
	2322.61-2322.73	N_2	0	0.4	75	0.9	0.3	0.4	2.1	5.2	0.1	0.4	BR<DL	2.3	-1.4	-33.7	0.5	0.9	0.3	0.5	3.5	3.5	1.9	0.2	BR<DL	SE<DL	0.8	0.4	4.9	1.0
		Mixed	6	0.9	71	0.9	0.4	0.7	2.8	4.4	0.3	0.8	BR<DL	3.8	15	303	4.0	0.0	0.5	3.5	6.5	14	8.9	0.1	BR<DL	SE<DL	1.5	0.2	8.6	1.3
			21	1.2	59	0.7	0.3	0.7	3.7	4.2	0.2	1.1	1.4	11	21	786	7.8	0.2	0.8	14	4.5	48	14	0.1	BR<DL	SE<DL	1.8	0.3	7.3	1.1
			41	0.7	61	0.7	0.3	0.5	2.2	4.2	0.2	0.6	1.9	5.3	18	98	2.3	0.0	0.3	2.5	3.6	14	17	0.1	BR<DL	SE<DL	1.2	0.2	5.9	0.9
			55	19	69	0.7	7.1	17	2.1	2.3	0.8	1.2	BR<DL	5.7	14	1175	-0.1	0.0	1.6	3.7	0.0	3.0	24	0.1	14	SE<DL	2.5	1.0	7.8	1.5
			62	3.2	57	0.7	0.2	0.4	1.8	3.8	0.2	0.5	2.0	5.0	19	107	2.0	0.0	0.3	2.9	3.5	8.4	12	0.0	BR<DL	SE<DL	1.3	0.2	5.4	0.7
			97	0.3	48	0.6	0.2	0.3	1.7	3.4	0.2	0.6	1.2	5.6	24	103	1.8	0.0	0.3	2.7	6.0	5.8	11	0.1	BR<DL	SE<DL	1.4	0.2	4.6	0.7
	2328.54-2328.59	N_2	0	0.8	30	1.8	0.4	0.2	0.4	0.7	0.0	0.0	ALL<DL	1.1	-0.1	SE<DL	SE<DL	0.3	0.1	0.2	0.7	0.1	0.3	0.0	0.4	0.1	0.2	0.4	2.4	0.4
		Mixed	6	1.3	31	1.8	0.4	0.3	0.5	0.7	0.1	0.0	ALL<DL	1.7	16	SE<DL	SE<DL	0.1	0.1	0.2	0.1	3.3	0.6	0.0	0.5	0.2	0.2	0.3	4.7	0.5
			21	1.4	28	1.8	0.5	0.3	0.4	0.6	0.1	0.0	ALL<DL	2.2	10	SE<DL	SE<DL	0.1	0.1	0.2	0.1	4.2	0.6	0.0	0.4	0.1	0.2	0.6	3.1	0.4
			41	1.6	27	1.8	0.5	0.3	0.5	0.6	0.2	0.0	ALL<DL	2.1	7.8	SE<DL	SE<DL	0.0	0.1	0.2	0.1	2.1	0.5	0.0	0.5	0.2	0.3	0.7	3.0	0.4
			55	0.1	27	1.8	0.0	0.0	0.3	1.0	0.0	0.0	SE<DL	1.9	43	SE<DL	SE<DL	0.2	0.0	0.1	4.2	4.5	0.2	0.0	BR<DL	0.0	0.2	0.1	2.6	0.5
			62	2.0	27	1.7	0.5	0.3	0.5	0.6	0.2	0.0	ALL<DL	1.5	11	SE<DL	SE<DL	0.0	0.1	0.2	0.1	1.0	0.3	0.0	0.5	0.2	0.3	0.7	3.0	0.5
			97	2.0	24	1.6	0.5	0.3	0.5	0.6	0.2	0.0	ALL<DL	0.9	8.9	SE<DL	SE<DL	0.0	0.2	0.2	0.2	0.9	0.3	0.0	0.5	0.2	0.3	0.8	2.9	0.4
	2330.41-2330.54	N_2	0	1.8	249	3.8	0.9	0.6	9.6	5.2	0.2	1.1	SE<DL	105	-7.8	-8.7	36	7.1	1.5	18	0.8	4.3	85	0.4	1.5	SE<DL	1.5	0.5	12	1.4
		Mixed	7	-0.4	258	3.9	0.8	0.8	9.8	4.5	0.3	1.2	SE<DL	200	64	4.9	12	20	0.9	9.8	1.2	4.5	26	1.0	0.3	SE<DL	1.1	0.7	18	0.3
			21	0.5	262	3.8	0.9	0.9	9.2	4.1	0.3	1.1	SE<DL	88	280	58	3.7	5.1	0.5	2.5	1.0	3.5	2.5	1.3	0.5	SE<DL	1.1	0.5	16	0.3
			28	2.0	351	5.2	1.4	1.4	12	5.3	0.4	1.7	SE<DL	108	486	51	7.5	3.3	0.8	6.2	1.2	6.4	14	2.1	1.3	SE<DL	1.7	1.1	21	0.9
			49	0.9	235	3.4	0.8	0.9	8.6	4.1	0.3	1.1	SE<DL	50	125	21	3.4	1.0	0.5	2.3	0.9	4.0	6.7	2.0	0.6	SE<DL	1.4	0.5	13	0.4
			84	1.4	229	3.2	0.8	1.0	7.4	3.8	0.4	1.2	SE<DL	66	321	57	3.2	0.7	0.5	2.5	0.9	3.8	3.3	2.4	0.6	SE<DL	1.7	0.2	13	0.3
			91	1.7	252	3.8	1.1	1.1	10	4.4	0.3	1.4	SE<DL	66	39	5.9	9.6	0.8	0.8	7.4	0.9	5.3	7.5	2.7	1.0	SE<DL	2.1	0.2	13	0.7

Colour Legend	Major	Minor	Trace	Ultra-Trace	>10x	2x – 10x	1.5x – 2x	1.1x – 1.5x	0.9x – 1.1x (BR approx. = SE)	0.5x – 0.9x	0.1x – 0.5x	-0.1x – 0.1x	< -0.1x (< average BR background)

1. Only elements with > 0.5x median apparent element extraction for one batch reactor cycle, compared with sequential extractions, are included here.

Table A14: Blank-corrected batch reaction incremental element extraction normalised to total sequential element extraction for selected elements[1], Moolayember Formation.

			Element Set	Alkali metals					Alkaline earth metals		Actinoids	Transition metals											Post transition metals		Metalloids			Nonmetals	
			Element Group	1					2		3	3	5	6			7	8	9	10	11	12	13		13	14		16	
Unit	Core Depth (mRT)		Gas	Day #	Li	Na	K	Rb	Cs	Mg	Ca	U	Sc	Nb	Cr	Mo	W	Mn	Fe	Co	Ni	Cu	Zn	Cd	Al	Tl	B	Si	Ge	S	Se
Moolayember Formation	2339.00-2339.17		N_2	0	3.6	36	3.7	1.0	0.5	0.9	0.5	0.0	0.1	SE<DL	10	-2.1	SE<DL	8.5	0.2	0.3	0.8	0.3	0.1	1.5	BR<DL	1.1	SE<DL	0.6	0.9	2.6	2.3
			Mixed	7	1.6	35	2.3	0.5	0.3	0.6	0.4	0.0	0.0	SE<DL	20	42	SE<DL	3.2	0.2	0.2	0.4	0.2	0.1	0.5	0.0	0.5	SE<DL	0.3	0.4	1.3	0.6
				21	1.8	31	1.6	0.4	0.3	0.6	0.4	0.1	0.1	SE<DL	7.0	22	SE<DL	2.1	0.1	0.3	0.4	0.0	0.2	0.4	0.0	0.5	SE<DL	0.4	0.5	0.9	0.4
				28	1.9	29	1.7	0.4	0.2	0.6	0.4	0.1	0.1	SE<DL	4.3	23	SE<DL	2.3	0.0	0.2	0.4	0.0	0.2	0.3	0.0	0.5	SE<DL	0.4	0.5	0.9	0.4
				49	2.3	29	1.6	0.4	0.3	0.6	0.4	0.1	0.1	SE<DL	3.8	19	SE<DL	2.3	0.0	0.3	0.4	0.0	0.2	0.3	0.0	0.6	SE<DL	0.5	0.9	1.0	0.4
				84	2.7	31	1.8	0.5	0.3	0.7	0.4	0.1	0.1	SE<DL	5.1	39	SE<DL	3.8	0.0	0.3	0.5	0.7	0.3	0.3	0.0	0.6	SE<DL	0.6	1.2	1.2	0.4
				91	2.8	33	1.9	0.5	0.3	0.7	0.4	0.1	0.1	SE<DL	6.1	16	SE<DL	4.5	0.0	0.3	0.6	1.2	0.4	0.3	0.0	0.6	SE<DL	0.6	1.0	1.2	0.4
	2346.40-2346.51		N_2	0	1.3	28	1.7	0.5	0.2	0.0	0.2	0.0	BR<DL	ALL<DL	0.8	0.5	-0.1	0.0	0.0	0.0	0.3	0.8	0.0	0.8	0.0	BR<DL	BR<DL	0.2	0.1	1.1	BR<DL
			Mixed	7	1.8	26	1.7	0.6	0.2	0.1	0.3	0.0	BR<DL	ALL<DL	0.6	2.8	6.6	0.0	0.0	0.0	0.2	0.4	0.0	0.3	BR<DL	BR<DL	BR<DL	0.3	0.1	1.9	BR<DL
				14	2.0	24	1.6	0.5	0.2	0.1	0.3	0.1	BR<DL	ALL<DL	0.4	3.4	5.8	0.0	0.0	0.0	0.1	0.2	0.0	0.3	0.0	BR<DL	BR<DL	0.3	0.0	1.4	BR<DL
				21	2.0	25	1.7	0.5	0.2	0.1	0.4	0.1	BR<DL	ALL<DL	0.2	1.9	3.0	0.0	0.0	0.0	0.1	0.1	0.0	0.5	0.0	BR<DL	BR<DL	0.4	0.2	1.3	BR<DL
				42	2.2	21	1.5	0.5	0.2	0.1	0.3	0.1	BR<DL	ALL<DL	1.1	2.6	5.2	0.0	0.0	0.0	0.1	0.1	0.0	0.3	0.0	BR<DL	BR<DL	0.4	0.2	1.1	BR<DL
				71	2.2	18	1.3	0.4	0.2	0.1	0.3	0.1	BR<DL	ALL<DL	0.9	1.2	2.5	0.0	0.0	0.0	0.1	0.1	0.0	0.3	BR<DL	BR<DL	BR<DL	0.5	0.1	0.9	BR<DL
				84	2.6	19	1.4	0.5	0.2	0.1	0.4	0.1	0.0	ALL<DL	0.4	1.0	3.7	0.0	0.0	0.0	0.1	0.4	0.1	0.4	BR<DL	BR<DL	BR<DL	0.6	0.1	1.0	BR<DL
				105	3.2	21	1.6	0.6	0.3	0.1	0.4	0.1	0.0	ALL<DL	0.3	0.7	0.8	0.0	0.0	0.1	0.2	0.5	0.1	0.4	BR<DL	BR<DL	BR<DL	0.7	0.1	1.1	BR<DL
Colour Legend	Major	Minor	Trace	Ultra-Trace			>10 x	2x – 10x		1.5x – 2x		1.1x – 1.5x	0.9x – 1.1x (BR approx. = SE)				0.5x – 0.9x		0.1x – 0.5x		-0.1x – 0.1x			< -0.1x (< average BR background)						

1. Only elements with > 0.5x median apparent element extraction for one batch reactor cycle, compared with sequential extractions, are included here.

Appendix B – Literature Water Quality Data

Table B1: Water quality guideline values for human health and aesthetics, and threshold values for livestock and irrigation, for metals, non-metals, and other parameters predominantly from ANZECC & ARMCANZ (2000) and NHMRC (2011), supplemented with data from the US EPA (2007, 2017). Concentrations are in mg/l, EC is µS/cm.

	Ag	Al	As	B	Ba	Be	Ca	Cd	Co	Cr	Cu	Fe	Hg	Li	Mg	Mn	Mo	Na	Ni	P	Pb	Sb	Se	SiO_2	Sr [1]	Tl [2]	U	V	Zn	pH	TDS [3]	EC
Human health	0.1		0.01	4	0.7 – 2	0.06		0.002		0.05	2		0.001			0.5	0.05		0.02		0.01	0.003	0.01		17	0.002	0.017					
Cattle							1000				1				600																7,000 – 10,000	
Sheep							1000				0.4				600																13,000	
Stock		5	As(V) 0.5 – 5	5			1000	0.01		Cr(VI) 1	0.4 – 5		0.002		2000		0.15		1		0.1		0.02				0.2		20			2,985 – 7,463
Irrigation		5	0.1	0.5				0.01	0.05	0.1	0.2	0.2	0.002	0.075 – 2.5		0.2	0.01	115	0.2	0.05 – 0.8	2		0.02				0.01	0.1	2			
Aesthetic		0.2									1	0.3				0.1		180						80					3	6.5-8.5 (9.2 tolerated)	1,200 (<600 good quality)	

[1] US EPA (2007). Drinking water standards and health advisories table. San Francisco, CA, USA, 30 p.

[2] US EPA (2017). Accessed 05/08/2017 from, URL: https://safewater.zendesk.com/hc/en-us/articles

[3] Tolerated for short periods only. TDS with no adverse effects is 4000 mg/l for Beef cattle, 2500 mg/l for dairy cattle, and 5000 mg/l for sheep.

Appendix C – Mineralogy and Geochemist's Workbench (GWB) modelling supplement

Table C1: XRD estimated mineralogy (%) of WM1 core samples.

Unit or Formation	Core depth (mRT)	Quartz	Siderite	(Fe-Mg/Ca/Mn)-carbonate	Calcite	Albite	K-feldspar	Kaolinite	Muscovite	I/S	Smectite	Chlorite	Anatase	Pyrite	Sylvite
Lower Evergreen Formation	2235.81-2235.94	73.4		0.6			2.6	11.4	7.3			4	0.7		
	2242.25	63.2		0.4			3.4	13.7	15.9			2.5	0.9		
	2242.44-2242.54	28.6		0.7	1.2		4.1	38	17.8		7.9		1.7		
Upper Precipice Sandstone	2246.14-2246.25	60.7		1.4			7.1	16.8	11.1			2.9			
	2254.94-2255.10	58.7	1.1	1.8			14.2	16.6	4.6		0.8		0.5		
	2254.95	63.4		0.9			10.9	20.5	2			1.9	0.4		
Lower Precipice Sandstone D	2263.61-2263.77	85.5		1.2	0.4		6.4	3.8	2.4		0.3				
	2267.71-2267.84	57.3					9.4	20.7	12.6						
	2267.84-2267.90	80.2			0.9		5.6	7.9	4.7			0.7			
Lower Precipice Sandstone C	2274.10-2274.18	84.3	0.5	1.6			6.8	3.8	2.4		0.3				
	2281.82-2281.92	64		0.7			4	16	13.5			1.3	0.5		
	2284.13-2284.24	88.2		0.7	0.2			7.4	3.2		0.4				
	2285.05	49		0.8			5	14.4	30.1				0.7		
	2288.49-2288.61	89.9		0.3				6.2	3.3		0.3				
	2288.9	76.3	0.7	1			2.5	13.3	5			1.2			
	2294	92.1			0.4	2.3	0.8	2.5	0.4			1.3	0.2		
	2296.97-2297.13	85.8		0.5				13.3				0.5			
Lower Precipice Sandstone B (baffle)	2297.13-2297.19	37.1						23.4	39.6						
	2298.92	89.2		0.5				5.6	3.9			0.3	0.3	0.2	
Lower Precipice Sandstone A	2301.09	85.9		0.5			1.9	5.3	5.6			0.5	0.3		
	2307.2	97.7						1.3	0.7		0.1				0.2
	2315.77	80.6		0.4	0.2	1.8	0.8	3.2	12.1			0.9			
	2322.61-2322.73	96.9		0.2				1.1	1.4		0.1		0.3		
	2323.25	85.9		0.4		3.6	1.6	3.6	3			1.4	0.5		
	2328.54-2328.59	25.6		1.5			0.7	43.9	19.5		7.4		1.3		
	2328.59-2328.68	84.2		0.6	0.2			9.4	4.8		0.2		0.7		
	2330.41-2330.55	95.7		0.2	0.3			2	1.4		0.4				
	2338.75-2338.85	89.1		0.4				5.7	3.4			1	0.4		
Moolayember Formation	2339.00-2339.17	55.6		0.7	0.0		0.8	33.6	7.5		1.1		0.7		
	2340.54-2340.62	43	3		0.7		3.4	21.4	18	5.7	3.6		1.2		
	2346.40-2346.51	43.6	3.4	0.4	0.6		17	16.3	13.7	4.3	0.2		0.5		
	2348.16-2348.30	52.4	3.4	6.2			15	10.2	9.2		2		0.3	1.3	
	2356.94-2357.06	46.3	1.4	6.2			15.4	13.3	11.9	2.9	2.3		0.3		
	2362.90-2363.00	38.8	2.2		0.6		11.7	12.1	16.7	5.7	6.3	4.6	1.3		
	2366.50-2366.61	34.6	3.9	6.8	0.1	3.5	13.3	13.8	14.4	5.3	0.5	3.8			
	2373.89-2373.99	50.3	1.6	1.9	0.1	8.6	16.2	7.3	9.6	2	0.7	1.7			
	2427.52-2427.74	62.2	1.2		6.3	5.9	12.7	3.8	5.1		1.3	1.5			

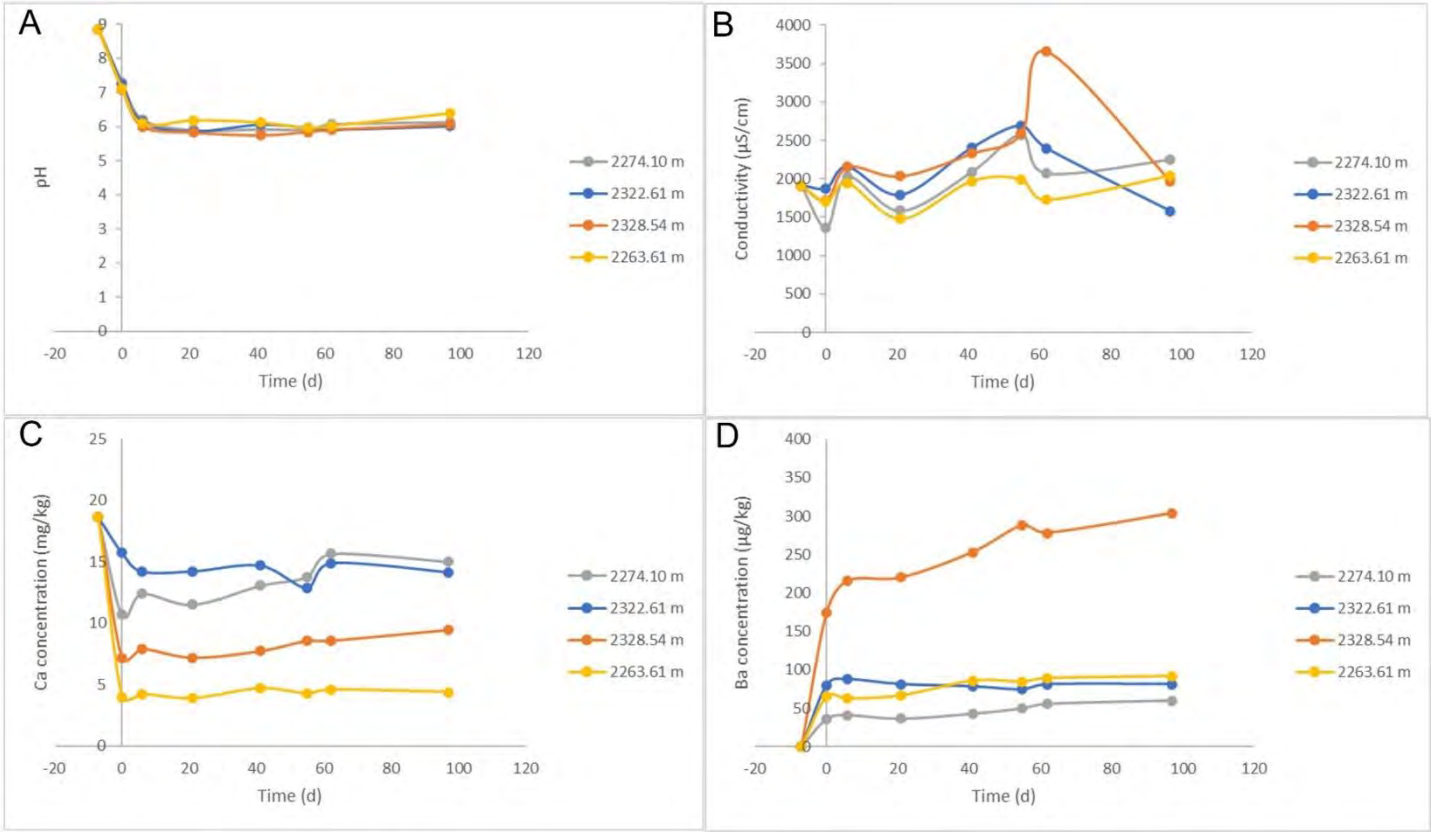

Figure C1: EPQ 10 West Moonie 1 core: a) Ex situ pH, b) electrical conductivity, c) dissolved Ca (mg/kg), and d) dissolved Ba concentration (µg/kg) during batch reaction of lower Precipice Sandstone, lower Evergreen Formation and Moolayember Formation samples with O_2-NO-SO_2-CO_2. Negative time is the initial water composition and N_2 rock soak, after time zero mixed gas was added. The core samples are all from the lower Precipice Sandstone.

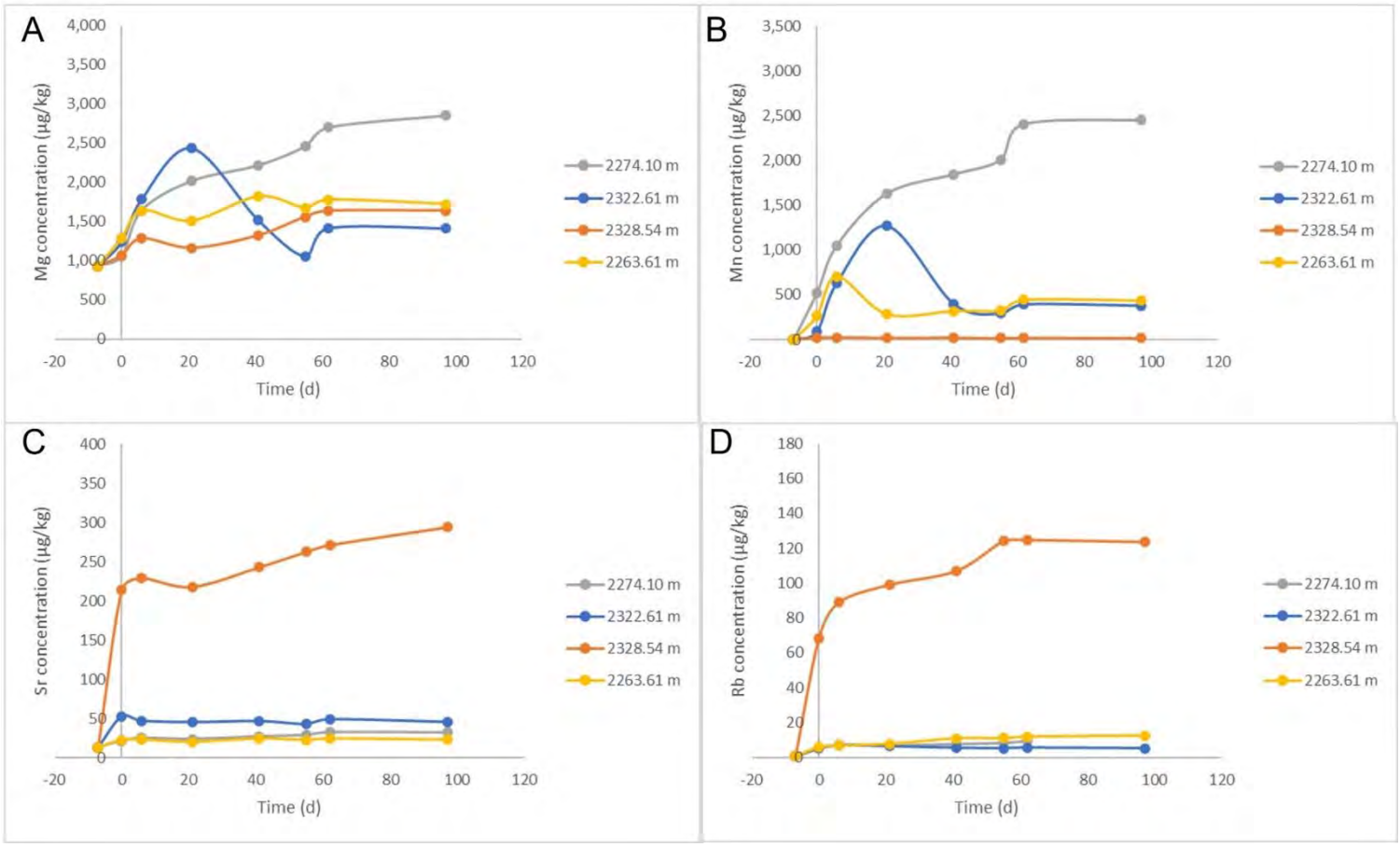

Figure C2: EPQ 10 West Moonie 1 core: Concentrations of a) dissolved Mg (µg/kg), b) dissolved Mn (µg/kg), c) dissolved Sr (µg /kg), and d) dissolved Rb concentration (µg/kg) during batch reaction of lower Precipice Sandstone, lower Evergreen Formation and Moolayember Formation samples with O_2-NO-SO_2-CO_2. Negative time is the initial water composition and N_2 rock soak, after time zero mixed gas was added. The core samples are all from the lower Precipice Sandstone.

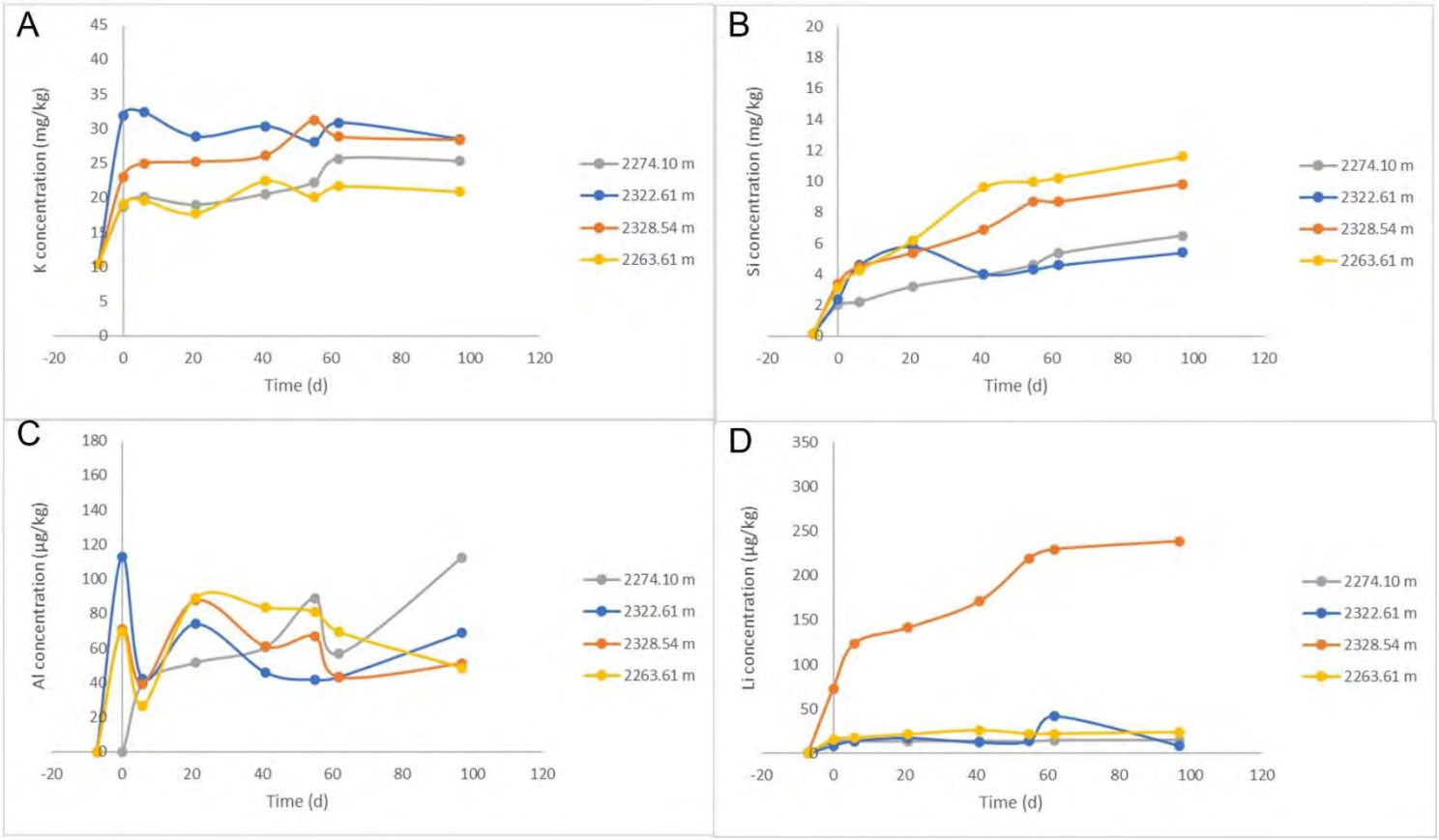

Figure C3: EPQ 10 West Moonie 1 core: Concentrations of a) dissolved K (mg/kg), b) dissolved Si (mg/kg), c) dissolved Al (µg /kg), and d) dissolved Li concentration (µg/kg) during batch reaction of lower Precipice Sandstone, upper Precipice Sandstone and Moolayember Formation with O_2-NO-SO_2-CO_2. Negative time is the initial water composition and N_2 rock soak, after time zero mixed gas was added. The core samples are all from the lower Precipice Sandstone.

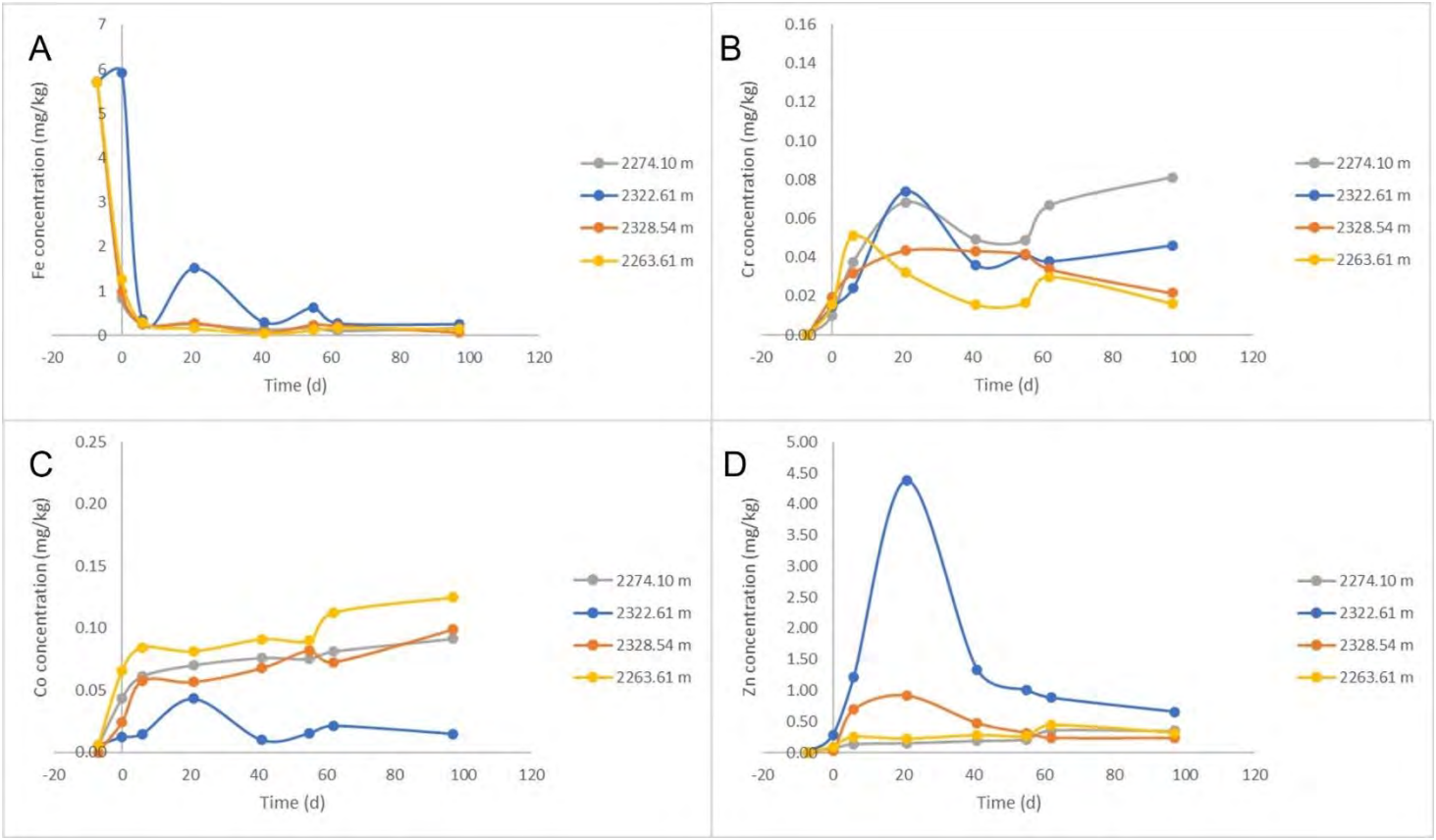

Figure C4: EPQ 10 West Moonie 1 core: Concentrations of a) dissolved Fe (mg/kg), b) dissolved Cr (mg/kg), c) dissolved Co (mg/kg), d) dissolved Zn (mg/kg) during batch reaction of lower Precipice Sandstone, lower Evergreen Formation and Moolayember Formation samples with O_2-NO-SO_2-CO_2. Negative time is the initial water composition and N_2 rock soak, after time zero mixed gas was added. The core samples are all from the lower Precipice Sandstone.

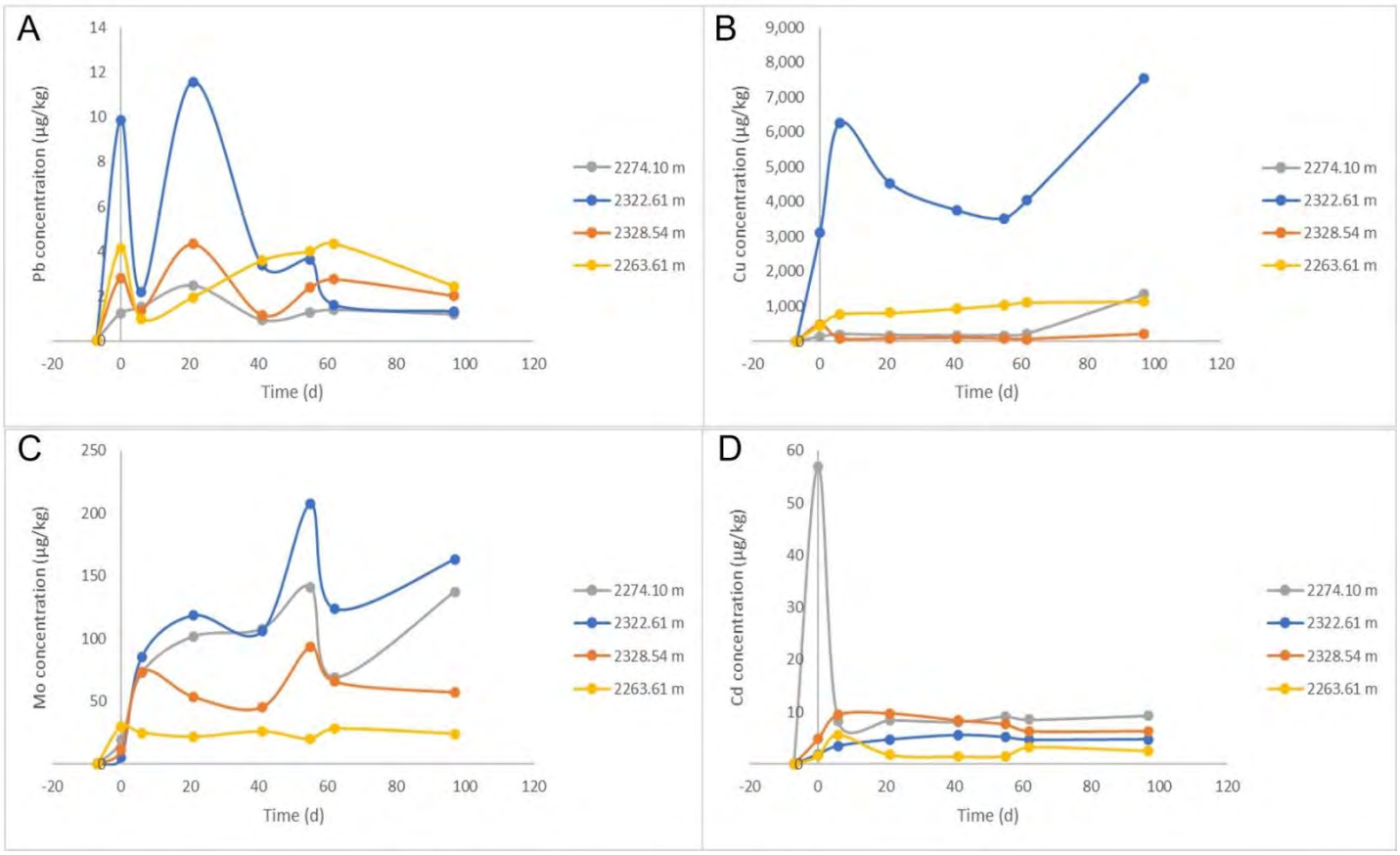

Figure C5: EPQ 10 West Moonie 1 core: Concentrations of a) dissolved Pb (µg/kg), b) dissolved Cu (µg/kg), c) dissolved Mo (µg/kg), d) dissolved Cd (µg/kg), during batch reaction of lower Precipice Sandstone, upper Precipice Sandstone and Moolayember Formation with O_2-NO-SO_2-CO_2. Negative time is the initial water composition and N_2 rock soak, after time zero mixed gas was added. The core samples are all from the lower Precipice Sandstone.

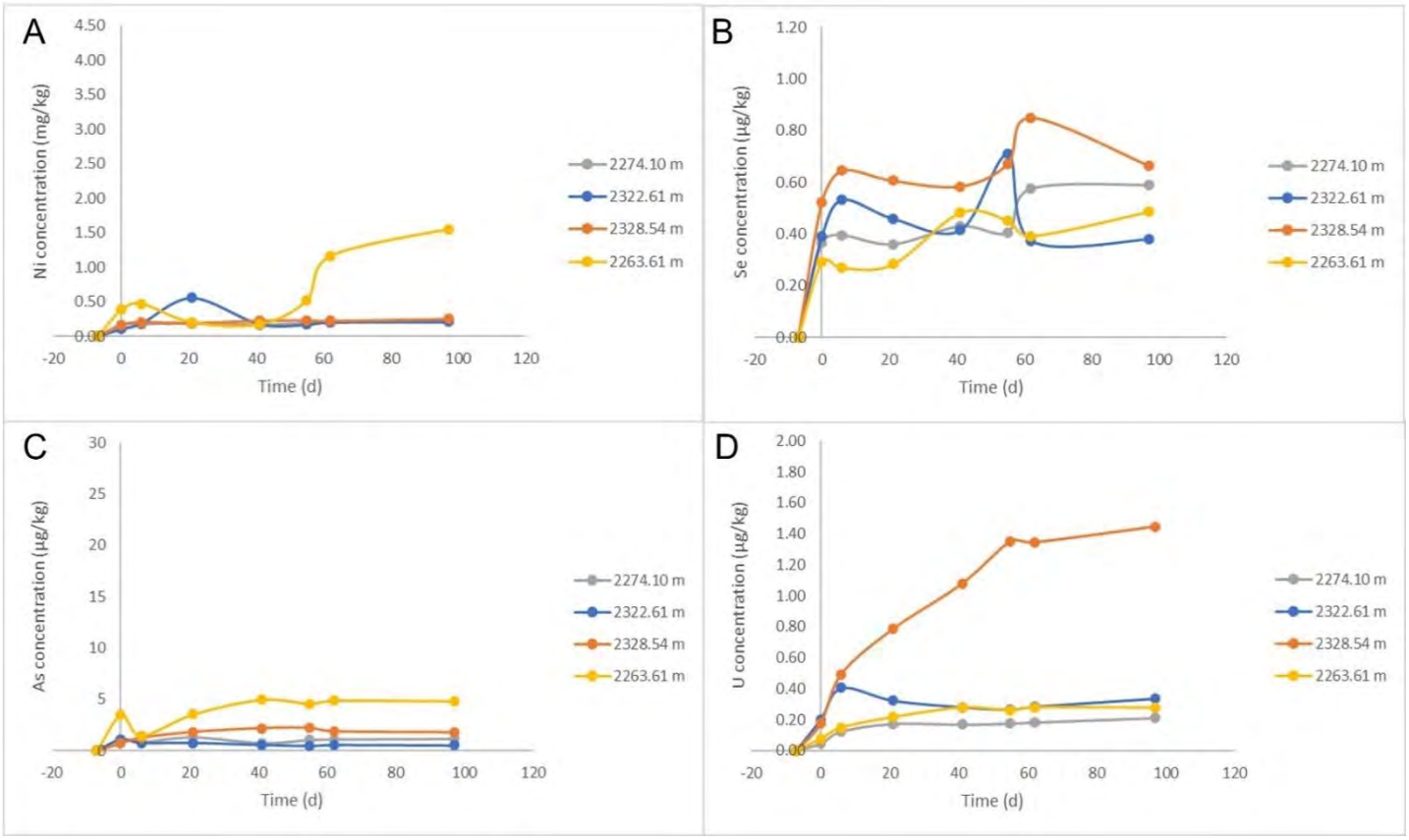

Figure C6: EPQ 10 West Moonie 1 core: Concentrations of a) dissolved Ni (mg/kg), b) dissolved Se (µg/kg), c) dissolved As (µg/kg), d) dissolved U (µg/kg), during batch reaction of lower Precipice Sandstone, upper Precipice Sandstone and Moolayember Formation with O_2-NO-SO_2-CO_2. Negative time is the initial water composition and N_2 rock soak, after time zero mixed gas was added. The core samples are all from the lower Precipice Sandstone.

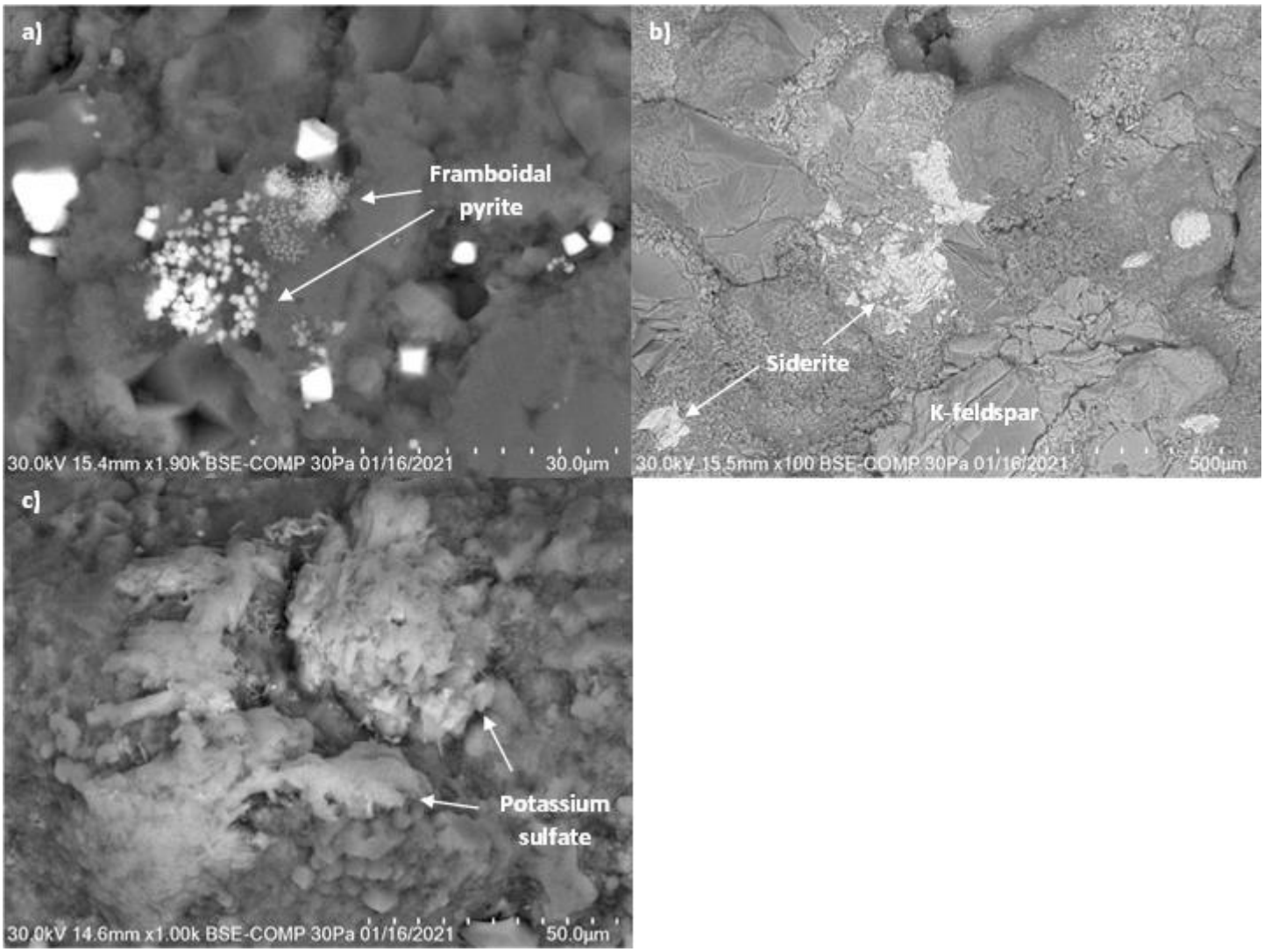

Figure C7: WM1 upper Precipice Sandstone 2254.94 – 2255.10 m sandstone core backscatter electron (BSE) images; a) framboidal pyrite, b) siderite cement (white) in between quartz and K-feldspar, c) potassium sulfate (probably from drilling fluid).

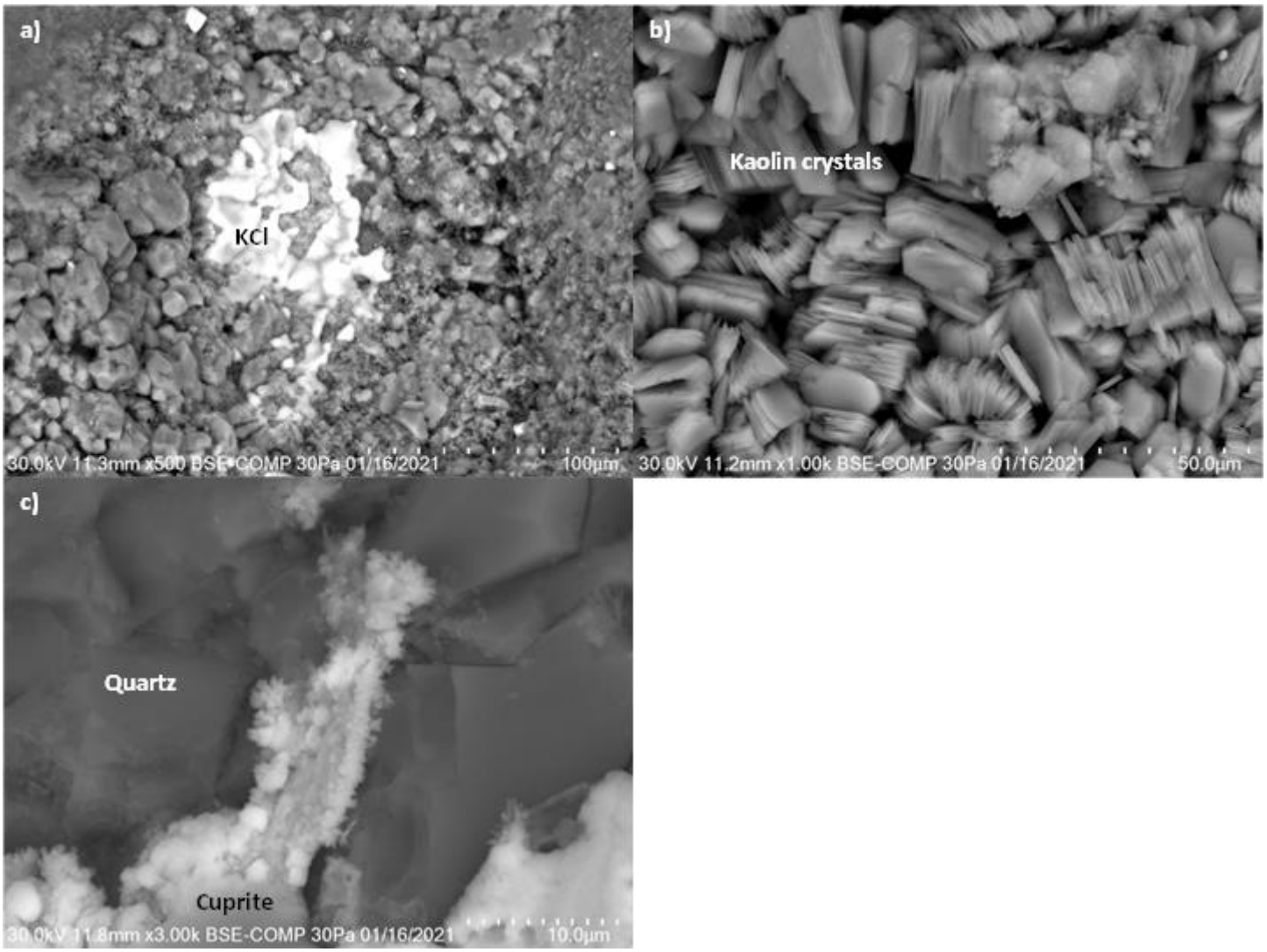

Figure C8: WM1 lower Precipice Sandstone C 2284.13 – 2284.24 m sandstone core BSE images; a) KCl from drilling fluid, b) kaolin, c) cuprite (copper oxide) precipitation between quartz grains.

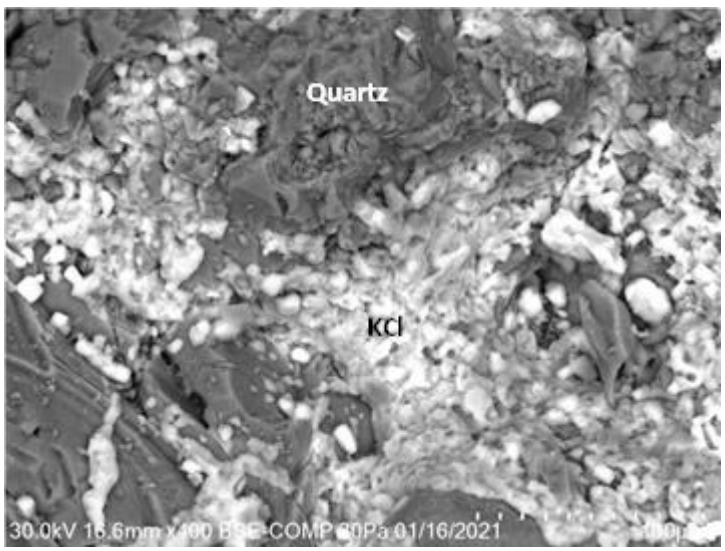

Figure C9: WM1 lower Precipice Sandstone A 2307.20 m sandstone core BSE image showing KCl precipitation (from drilling fluid) between quartz grains.

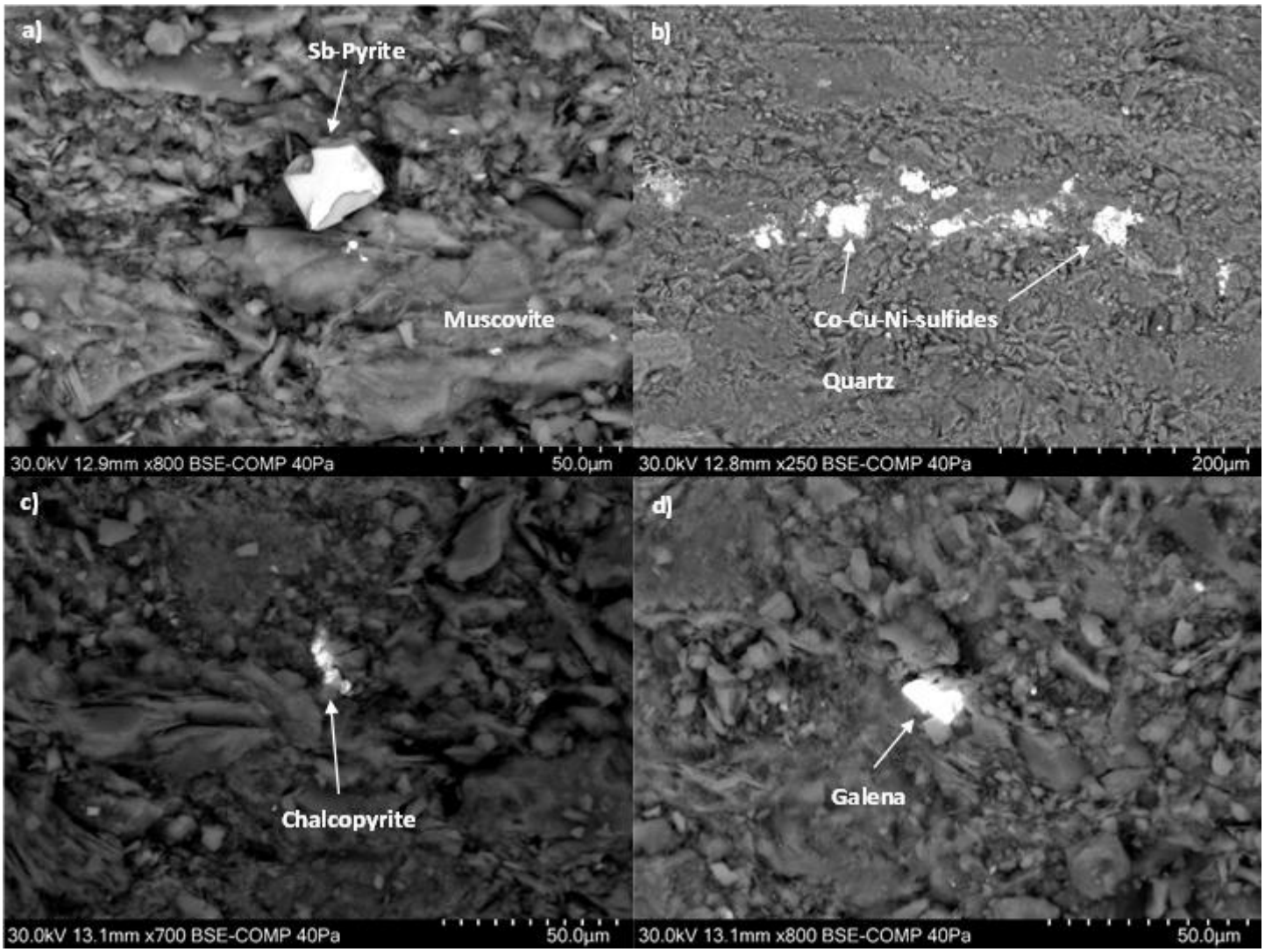

Figure C10: WM1 lower Precipice Sandstone A 2328.54 – 2328.59 m sandy siltstone core BSE images; a) pyrite with minor antimony (Sb), b) mixed Co, Cu, Ni sulfides, c) chalcopyrite, d) galena.

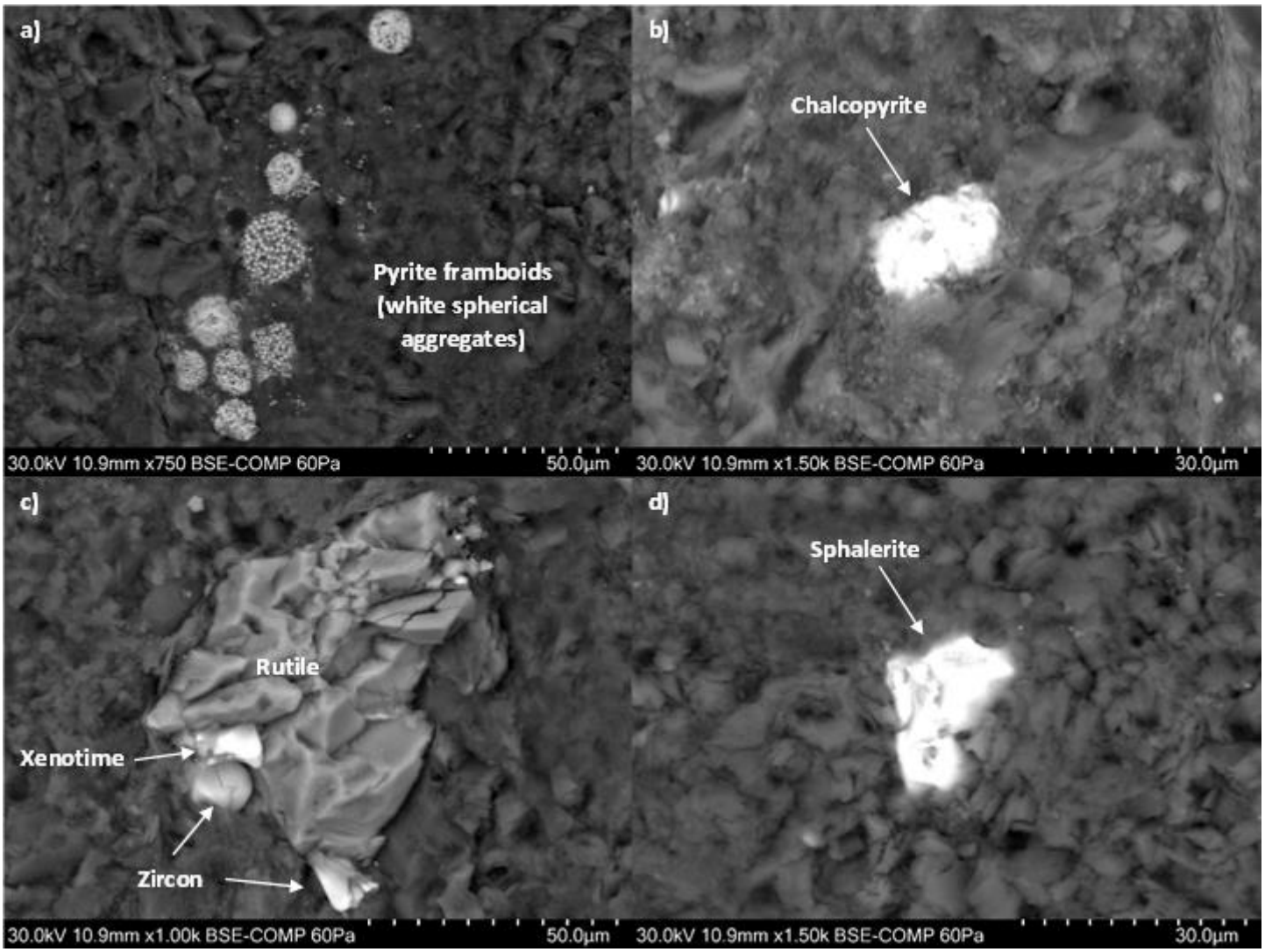

Figure C11: WM1 Moolayember Formation 2339.00 – 2339.17 m sandstone core BSE images; a) microbial pyrite, b) chalcopyrite, c) rutile with Xenotime (HREE-phosphate) and zircons, d) sphalerite.

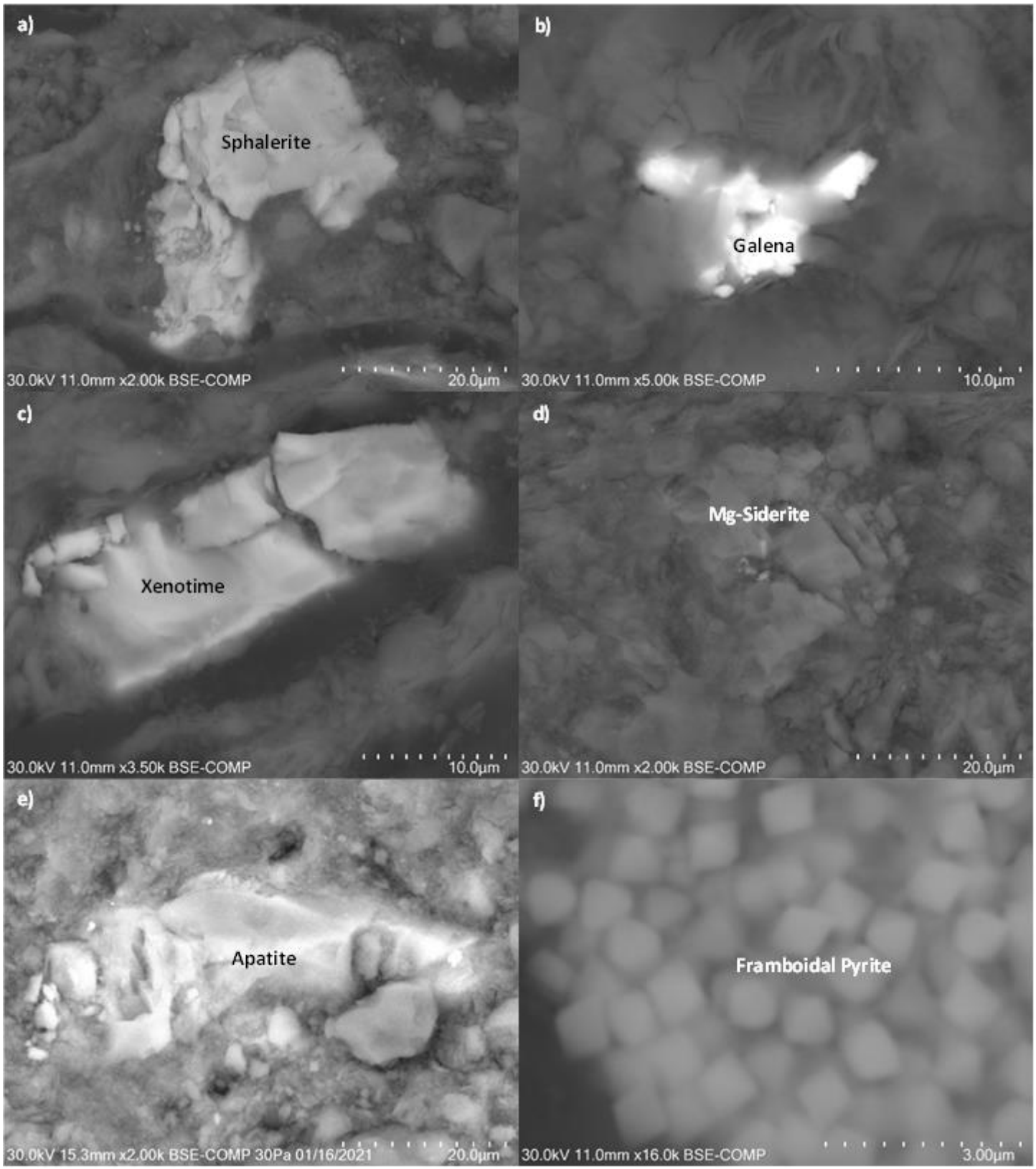

Figure C12: WM1 Moolayember Formation 2346.40 – 2346.51 m sandstone core BSE images; a) sphalerite, b) galena, c) xenotime, d) Mg-siderite, e) apatite, f) framboidal pyrite.

CTSCo

Carbon Transport & Storage

A GLENCORE Company

300 George Street · Brisbane · QLD 4000 · Australia
Tel 1300 119 786 · Web www.ctsco.com.au

Carbon Transport and Storage Corporation (CTSCo) Pty Limited ABN 12 143 012 971